UNIVERSITÀ DI PARMA

UNIVERSITA' DEGLI STUDI DI PARMA

DOTTORATO DI RICERCA IN
"*Scienze Chimiche*"

CICLO XXXVIII

Dispersion Interactions and EnT relay: Novel Strategies in Visible Light-promoted Processes

Coordinatore:
Chiar.mo Prof. Maestri Giovanni

Tutore:
Chiar.mo Prof. Maestri Giovanni

Dottorando: Sparascio Sara

Anni Accademici 2022/2023 – 2024/2025

Index

General Abstract

Together with most employed Ir-based photocatalysts, the original use of a poly-naphthalene (poly-NP) co-catalyst has allowed us to enhance the efficiency of previously reported photocatalytic synthetic methods, to develop new strategies with a low-effort optimization study, and, eventually, to promote reactivities that would have been otherwise unattainable. The beneficial effect of those additives was addressed to the stabilization of triplet reaction intermediates with radical-π dispersion interactions between mono-occupied molecular orbitals and the π-clouds of the poly-NP additive. In addition to the positive "dispersion interactions effect" of the co-catalyst, we unveiled an unprecedented behavior: in our visible light-mediated synthesis of densely functionalized azetidines from allenamides, the "triplet-state relay" phenomenon provides a more efficient substrate activation by relaying two EnT cycles, and replacing a slower EnT with two faster ones, as demonstrated by experimental and computational evidence. Eventually, we anticipate that these findings will allow us to elaborate even more far-fetched reactivities: preliminary results show an original intermolecular HAT reactivity from a typically inert unactivated -OH site - the reactive vinylic radical originated from the photosensitization of an allenamide in presence of a poly-NP co-catalyst could be the key to unlock the extremely challenging conventional direct HAT from aliphatic O-H bonds.

Chapter I

General Introduction

1.1 *Unactivated C-H bonds Functionalization*

Selective functionalization of inert C-H bonds is a constant need for synthetic organic chemists. The topic of "C-H functionalization" - or "C-H activation" - has recently gathered greater emphasis as an ideal method to access previously unfeasible substitutions, as well as diversification and late-stage functionalization of complex natural products.[1] Since this approach has emerged as an atom- and step-economic methodology for carbon-carbon and carbon-heteroatom bond formation, this field has received increasing attention from various branches of the Chemical research (Figure 1).

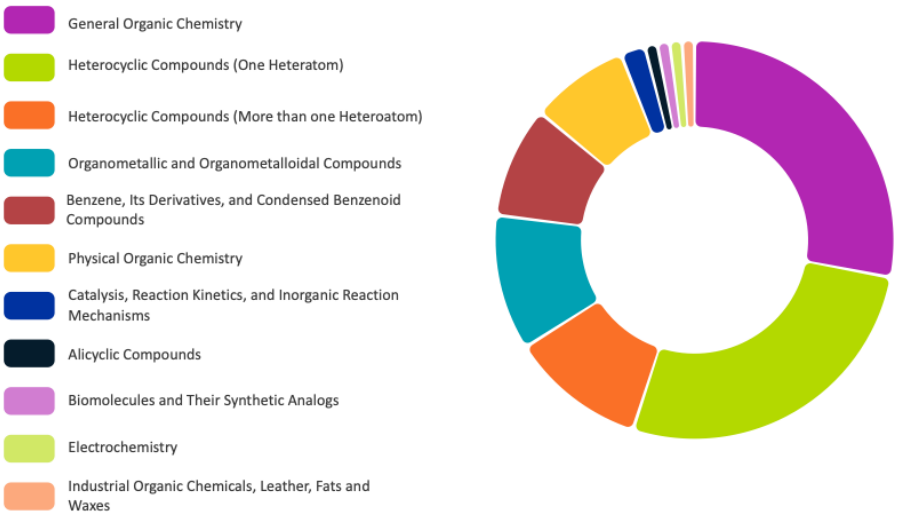

Figure 1. Top CA (subject areas) involved in "C-H functionalization". From scifinder-n.cas.org

Nevertheless, although almost every organic molecule is extensively decorated with aliphatic C-H bonds, these are undoubtedly among the least reactive in organic chemistry, making their efficient activation - without using harsh conditions - very challenging, and thus often resulting in a lack of selectivity among other similar C–H bonds available for functionalization.

While in the past decades synthetic organic chemists took tremendous interest in the functionalization of C(sp^2)-H bonds, thus ensuring remarkable progress in this area, remote C(sp^3)-H activation has been perceived as trickier and potentially problematic, since C(sp^3)-H bonds are ubiquitous in organic molecules, thus jeopardizing the selectivity of any possible transformation.[2]

Over the past decades, transition metal-catalyzed C(sp^3)–H activation reactions have been extensively developed (Scheme 1).

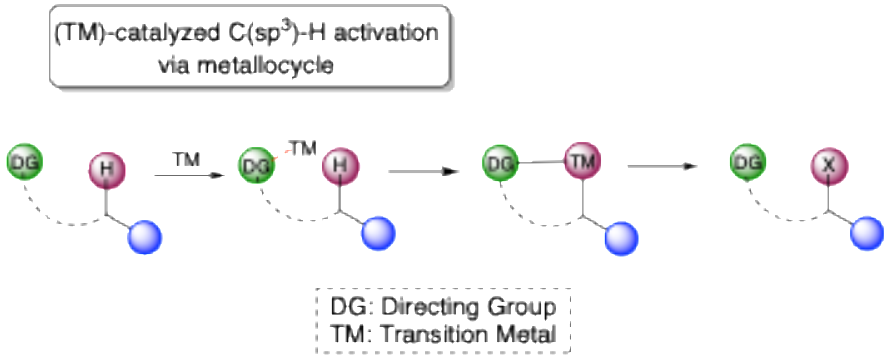

Scheme 1. Transition-metal-catalyzed reactions for remote C(sp^3)-H activation.

These strategies usually require harsh conditions (high temperature), and the use of often non-removable *directing groups* to address the selectivity problem – the presence of the directing group results in a reduction of the energy barrier for the cleavage of the C-H bond and enables specificity toward a particular C-H bond trough the formation of a cyclic transition state. In these examples, the selectivity strongly depends on the thermodynamic stability of the carbon-transition metal species which is formed in the transition state (Scheme 2).[3]

M	Ru	Rh	Pd	H	
M–C(H)(H)–H	48.5	52.0	41.6	102.7	kcal/mol
M–C(H_3)(H)–H	46.5	50.3	40.9	99.8	kcal/mol
M–C(H_3)(CH_3)–H	45.7	50.3	41.1	98.2	kcal/mol

Scheme 2. Metal-Alkyl Bond energies (kcal/mol) for Ru, Rh, and Pd.

Thus, the functionalization *via* a transition metal-catalyzed approach of a tertiary C-H site is quite rare, while secondary and especially primary C-H bonds are easier to activate.

Focusing more on transition metal catalyzed reactions resulting in the formation of $C(sp^3)$-$C(sp^3)$ bonds, the examples are scarce and they are limited by the use of an appropriate specific reaction partner, that is used as a trapper of the alkyl-palladium intermediate.[2a] For instance, Chen and co-workers achieved the formation of a $C(sp^3)$-$C(sp^3)$ bond using **1**, an amine functionalized with a permanent electron-withdrawing group (bidentate picolinamide) that has the role of the directing group for C-H activation and an alkyl iodide as the reaction partner (Scheme 3).[4]

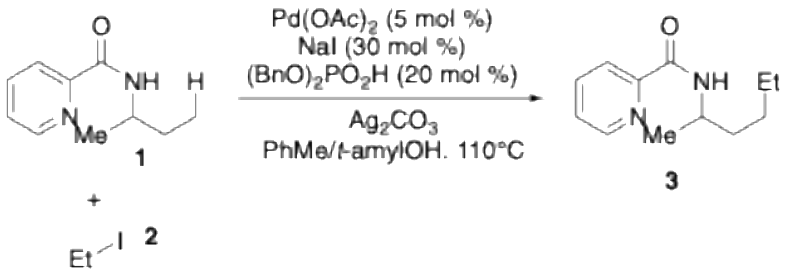

Scheme 3. Picolinamides for amine functionalization and $C(sp^3)$-$C(sp^3)$ bond formation.

Another notable example in $C(sp^3)$-$C(sp^3)$ bond formation making use of transition metal-catalysis was brought by Yu and co-workers.[5] In this case a perfluorinated amide was used as the directing group for the C-H functionalization in the β-position of carbonyl compounds. The electrophilic benzyl acrylate (**5**) is used as the reaction partner, allowing the formation of a nitrogen heterocycle through an olefination of the C-H bond in the substrate, followed by an aza-Michael addition (Scheme 4).

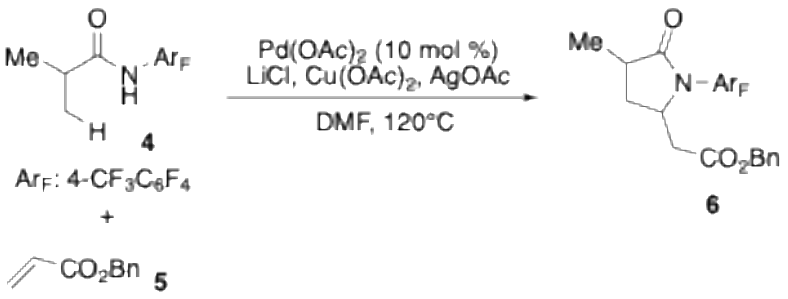

Scheme 4. Synthesis of nitrogen heterocycles from perfluorinated amides.

On the other hand, carbene/nitrene insertion reactions also represented an alternative route to the cleavage of unactivated C(sp^3)-H bonds.[2a] Indeed, carbenes and nitrenes only possess six electrons in their valence electron shell, making them greatly unstable. Nowadays the generation of such unstable species occurs again via transition-metal catalysis, with the formation of new species called carbenoids/nitrenoids (Scheme 5).

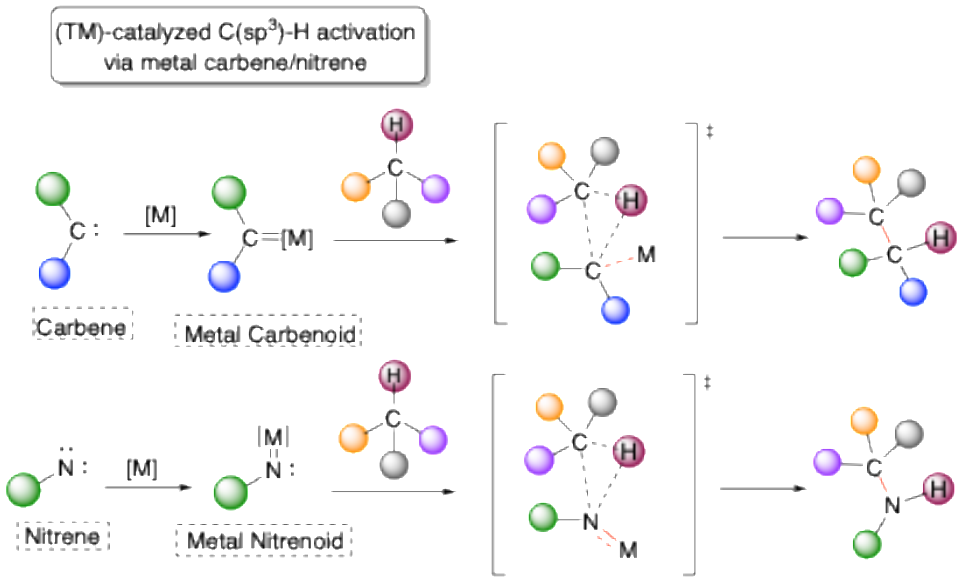

Scheme 5. Transition metal-catalyzed via carbenoid/nitrenoid for remote C(sp^3)-H activation.

However, in this approach a diazo functionality is required as this is usually the precursor of the metal carbenoid. For this very reason, an electron-withdrawing group (i.e. α-diazo ester)[1a] is necessary to simplify the placement of the diazo group, as well as to increase the stability - and thus the safety at handling - of this type of compounds.[2a] In contrast to the previously mentioned transition metal catalyzed strategies, carbene or nitrene insertion reactions occur preferentially at the most electron-rich C-H bonds, thus showing an opposite rank order of reactivity among different C-H bond substitution pattern – tertiary C-H bonds are the most reactive, while reactivity decreases for secondary and primary C-H bonds.[2a]

For instance, Petty developed an intramolecular cyclization to form a cyclopentanone (**8**) through carbene insertion starting from an α-diazo-β-keto ester (Scheme 6).[6]

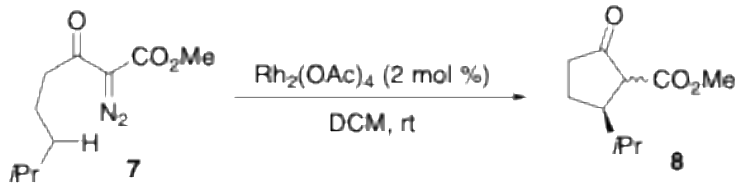

Scheme 6. Rh^{II}-catalyzed intramolecular C−H insertion via carbenoid.

A nitrogen containing five-member ring was synthesized by Du Bois and co-workers through metal nitrenoid intramolecular insertion, using a carbamate as the precursor of the reactive nitrene species (Scheme 7).[7]

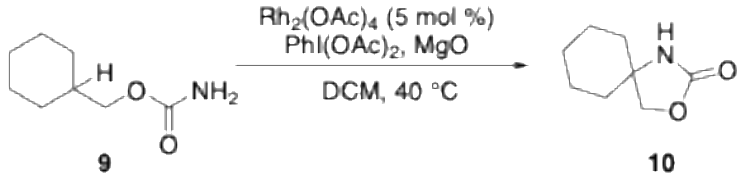

Scheme 7. Rh^{II}-catalyzed intramolecular C−H amination via nitrenoid.

1.2 The Hydrogen Atom Transfer strategy

When referring to radical chemistry, it should be noted that the Hydrogen Atom Transfer (HAT) strategy brought an extensive update in the field of selective remote functionalization of ubiquitous inert C-H bonds. Since the diffusion of mild approaches toward the generation of radicals, the HAT strategy has witnessed a tremendous interest from synthetic organic chemists as it is generally recognized as a smart tool for the functionalization of unactivated C-H bonds under mild conditions. Indeed, methods relying on HAT often show a wider scope, higher functional group tolerance, and sometimes allow transformations which would be very challenging to access with the traditional transition metal catalysis routes.[1] Historically, the first examples of HAT were showcased in the Hofmann–Löffler–Freytag reaction and Barton's nitrite photolysis,[8] in which the Hydrogen abstraction was initiated by nitrogen and oxygen-centered radicals, and since then the number of HAT protocols relying on a heteroatom-based radical have kept growing and growing. On the other hand, the limited number of synthetic methodologies involving a HAT process mediated by carbon-centered radicals was probably due to the lack of mild methods known for the generation of those carbon-based radical species. However, since in the most recent decades new strategies to generate those radicals have emerged numerously, HAT is now considered as one of the methods of choice when willing to achieve selective and efficient remote C(sp^3)-H functionalization along with C-C bond formation.

HAT is based on the homolytic cleavage of weak C-H bonds, thus the entire process is strongly influenced by the BDE[1] (Bond Dissociation Energy) of the C-H bond that gets cleaved and the one that is formed after the Hydrogen abstraction; since HAT has an exothermic nature, the process usually works *via* an early transition state, meaning its energy is much more similar to that of the reactant. Therefore, there must exist a significant difference between the BDEs of the two C-H bonds involved in the HAT mechanism, otherwise the process could be ideally reversible, and show selectivity issues. Indeed, typically aryl, vinyl or primary alkyl radicals trigger HAT, because of their much higher BDEs compared to that of alkyl C-H bonds (Scheme 8).

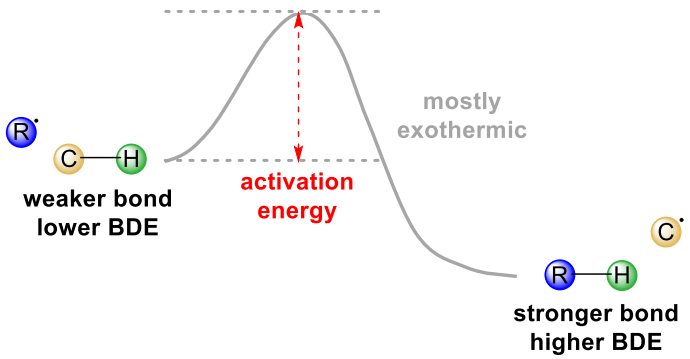

Scheme 8. Influence of the BDE on HATs.

Another important factor determining efficiency and selectivity of a HAT process is radical philicity. The radical philicity is determined by the electrophilicity or nucleophilicity index, which in turn can be quantified from the electron affinity (EA) and ionization potential (IP) of free radicals.[9] A nucleophilic radical (i.e. *t*-Bu·) is expected to abstract Hydrogen preferentially from a more protic site while an electrophilic radical (i.e. *t*-BuO·) would undergo HAT preferentially from a more hydridic site (Scheme 9).[10]

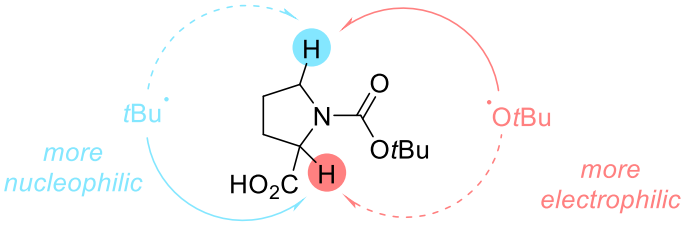

Scheme 9. The effect of radical philicity on HAT selectivity.

However, in case of polarity mismatch, the issue could be addressed by employing a catalytic amount of another partner as the source of an appropriate philicity radical, performing the polarity reversal catalysis.[11]

The rate of HAT is mostly controlled by enthalpic factors; however, in intramolecular HAT reactions the Thorpe–Ingold effect can also have a significant role.[12] On an intramolecular level, C-based radicals can abstract hydrogen typically *via* 1,*n*-HAT, where *n* is a number between 4 and 8. Moreover, the initial radical and the Hydrogen atom that gets abstracted must be allocated in a precise orientation and at a certain distance toward one another – the optimal orientation is linear to

moderately distorted from linear (≤35°) and the distance should not be higher than 3 Å.[13] The most common type of intramolecular HAT mediated by C-centered radicals is the 1,5-HAT - with some exceptions if the optimal geometry is altered by heteroatoms.[1] Indeed, higher order HATs usually have a higher entropic barrier; moreover in 1,5-HAT the transition state forms a sort of six-member cycle that resembles the "chair" conformation of cyclohexane, contributing at lowering the activation energy barrier (Scheme 10).

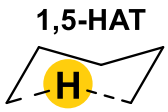

Scheme 10. Preferred TS conformation in 1,5-HAT.

It is well known that olefinic C-H bonds are much stronger than aliphatic C-H bonds. This means that typically aryl or vinyl radicals abstract hydrogen from alkyl C-H sites, because the former have higher BDEs[3] (Scheme 11).

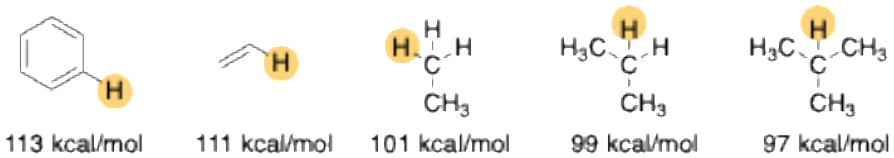

Scheme 11. BDE values for different types of C-H bonds.

The first studies on vinyl radical mediated intramolecular 1,5-HAT were reported by Parsons and co-workers in the late 80s (Scheme 12).[14] In this study, the strategy used to generate the vinyl radical is the halogen abstraction/single electron reduction of vinyl iodide **11**. The vinyl radical mediated intramolecular 1,5-HAT takes place, followed by a *5-exo-trig* cyclization and reduction of the resulting intermediate, affording an elegant and complex pyrrolizidine ring system.

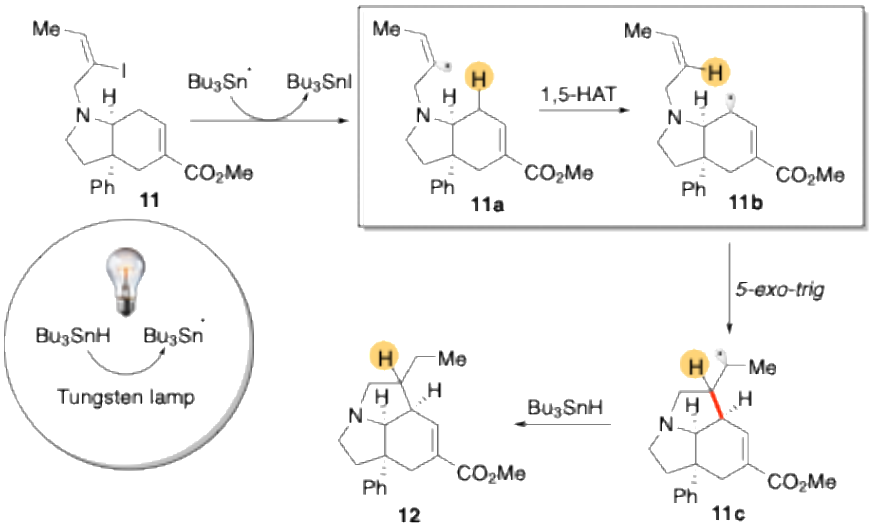

Scheme 12. Synthesis of a 3-member ring system *via* vinyl radical mediated intramolecular 1,5-HAT.

This pioneering work opened the path to the development of several strategies involving 1,5-HAT/cyclization sequences to selectively and efficiently target aliphatic weak C-H bonds and build complex molecules, showing the robustness and extensive versatility of the 1,5-HAT strategy.

Another expedient commonly used to generate vinyl radicals is radical addition to alkynes. Indeed, in 1993 Bachi and co-workers reported the synthesis of a bicyclic β-lactam *via* 1,5-HAT/cyclization cascade (Scheme 13).[15] In this example, the tributyltin radical performs the addition to the alkyne group of **13**, triggering intramolecular 1,5-HAT, then a *6-endo-trig* cyclization and eventually β-tin elimination occur. It is interesting to notice that the isomerization of the double bond of the bicyclic β-lactam **13c** allows the formation of **15**, whose structure resembles the *Cephem* ring, one of the most common Nitrogen containing heterocycles found in approved small molecules drugs.[16]

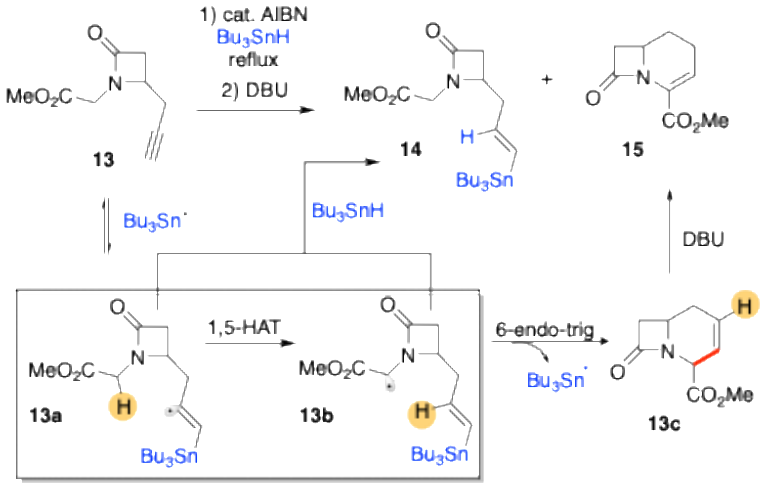

Scheme 13. Synthesis of a bicyclic β-lactam *via* vinyl radical mediated intramolecular 1,5-HAT.

A few years later, in 1999, Malacria and co-workers developed the diastereoselctive synthesis of densely substituted cyclopentanes *via XAT/5-exo-trig* and *1,5-HAT/5-exo-trig* double cascade (Scheme 14).[17] XAT from substrate **16** forms an α-silyl radical which undergoes cyclization to give vinyl radical intermediate **16a**. The latter undergoes 1,5-HAT towards the unactivated primary C-H bond followed by an interestingly rare *5-endo-trig* cyclization.

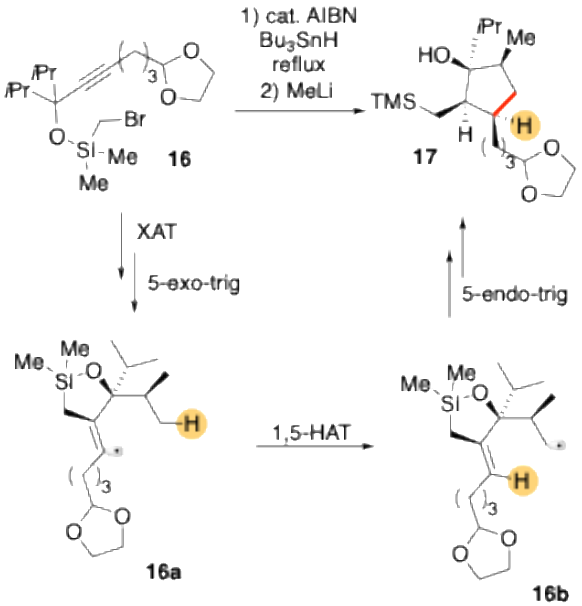

Scheme 14. Diastereoselective cyclization/1,5-HAT/cyclization cascade.

Concerning *intermolecular* HAT mediated by Carbon-centered radicals, only a few protocols are reported in literature. This is due to the low efficiency of C-radicals toward this process, compared to O-centered radicals.[18] These few examples are limited to alkyl and aryl radical mediated HAT toward activated C-H sites and/or using a solvent-amount of the C-H source.

In this regard, very recently, Shi and co-workers reported a cross-dehydrogenative coupling of C(sp^3)-H/C(sp^3)-H and C(sp^3)-H/C(sp^2)-H via intermolecular HAT (Scheme 15).[19] In this protocol, an in situ generated sacrificial aryl radical plays the role of the Hydrogen abstractor, generating an alkyl or an alkenyl radical, that eventually undergoes radical-radical cross-coupling to form new C(sp^3)-C(sp^3) and C(sp^3)-C(sp^2) bonds.

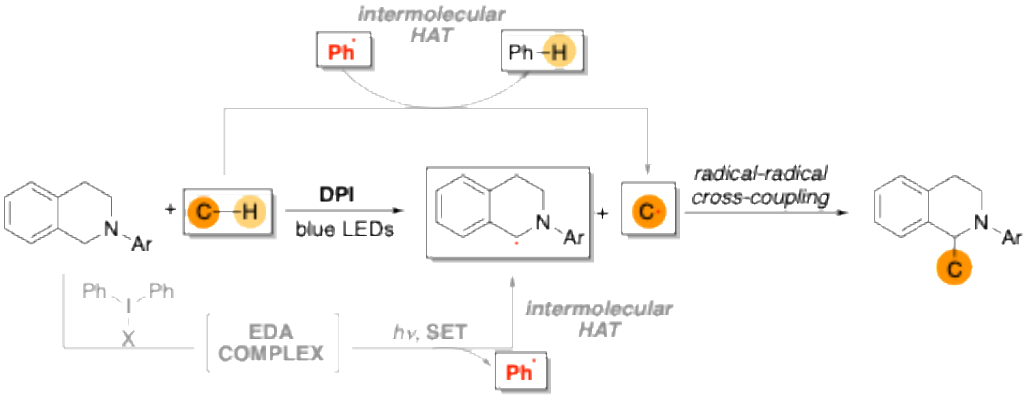

Scheme 15. Intermolecular HAT mediated by aryl radicals.

Another noticeable example of intermolecular HAT used to activate inert C-H bonds is the photoinduced Palladium catalysis for the direct alkylation of Glycine derivatives (Scheme 16).[20] In this work, an alkyl bromide is used as a precursor of the Hydrogen abstractor: a peculiar Pd(I)/alkyl radical hybrid species.[21] After the HAT event of that hybrid species on a glycine derivative, a radical addition on an imine intermediate occurs forming a new C(sp^3)-C(sp^3) bond.

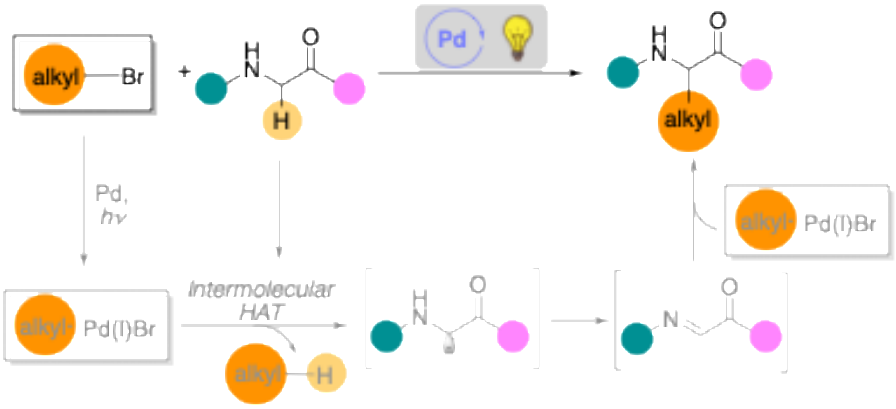

Scheme 16. Intermolecular HAT mediated by alkyl radicals.

These example, along with many others, proved the ample versatility and the key advantages that the HAT strategy brings to synthetic organic chemistry: the direct and selective activation of unactivated and ubiquitous C-H sites - opening route for late-stage functionalization of complex molecules and natural products. Moreover, HAT protocols can be performed under benign conditions, thus widening the scope of classical transition metal-catalyzed approaches. Eventually, HAT is a versatile method as it tolerates the use of every type of strategy for the mild generation of reactive species such as radicals.

1.3 Visible-light Photocatalysis

One of the main goals of the XXI century is to solve the rapidly rising issue of global warming, as well as to find another energy source to efficiently replace the traditional carbon fuels, which will be almost exhausted by 2060-2070 approximately. When the day comes, what will fulfill our energy demand? Experts from all around the globe agree to identify one and only one option: sustainable sources – mainly solar energy storage, but also nuclear fusion, sea tide, and wind and geothermic energy.[22] Great efforts to increase the efficiency of these new technologies will have to be made, but visible light-driven processes are the main strategy to reach a low-carbon economy in the near future. Indeed, nature inspired us with the ultimate sustainable process: *photosynthesis* (Figure 2), the source of fossil fuel.

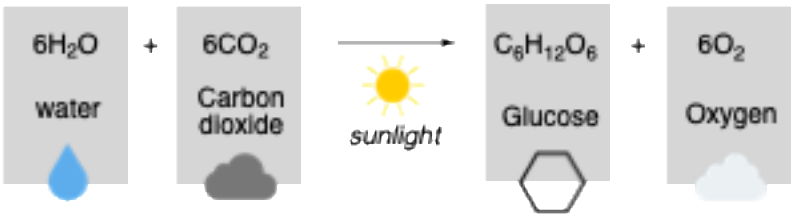

Figure 2. The Photosynthesis equation.

On a cloudless day, a fully grown tree transforms about 10 m^3 of carbon dioxide in the same amount of oxygen and 12 kg of carbohydrates. Approximately 2 x 10^{12} tons of CO_2 are stored in biomass *via* photosynthesis per year, which is the equivalent of 2 x 10^{19} kJ in terms of energy production.[22] This natural process inspired the prophetic statement of the pioneering chemist Giacomo Ciamician[23] "not harmful to progress and to human happiness", referring to a solar energy-based economy of the future.

Nevertheless, photosynthesis is a process that remains unrivaled by any man-made attempt to emulate it so far. Indeed, the synthesis of organic molecules with a photochemical approach encounters several issues – typically, organic molecules tend not to absorb in the visible-light but rather in the ultraviolet (UV) region of the spectra, which is only a small percentage of the solar radiation that reaches the Earth's surface trough the atmosphere. In the past, this has limited the application of photochemical synthesis in industries since efficient UV-sources instruments have only

recently become available.[24] In addition, due to the high energy of its photons, UV light can cause decomposition of the reagents, as well as selectivity issues, since any potential undesired side reaction could also be catalyzed, affecting the overall outcome of the reaction. These issues were solved when chemists realized that some transition metal complexes could be used as *photocatalysts* to promote visible light-initiated reactions.[25] In the recent decades, photocatalysis received an extraordinary interest from all the synthetic organic chemistry community, as demonstrated by the impressive increase in the number of publications in this research area (Figure 3).

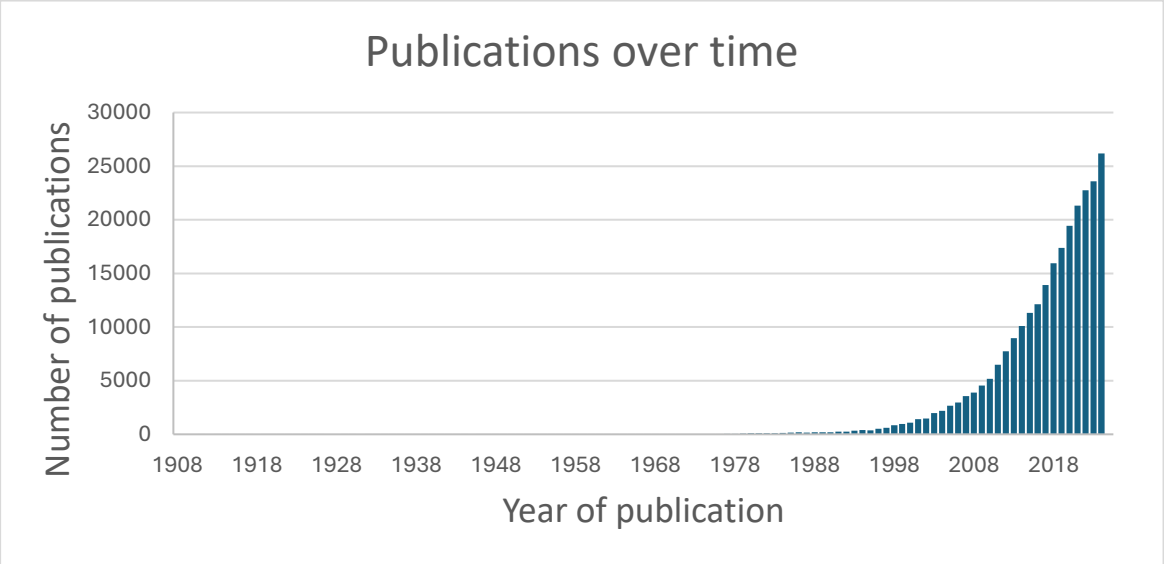

Figure 3. The number of publications on the topic of Photocatalysis (blue bars) between 1908 and 2024. Data for the bar chart were obtained by a SciFinder search run in September 2025.

Photocatalysis enables the generation of highly reactive intermediates and excited state species under very mild conditions, and, since the reactivity of excited state species is often incredibly different from that of the ground-state, in many cases, photocatalysis opens the route for completely new reactivities and chemical disconnections, which would be unachievable by the traditional ground-chemistry. In addition to that, photocatalysis usually requires relatively inexpensive equipment. In figure 4, a typical setup for photocatalytic reactions performed in our laboratory is shown – we use a simple and very cheap (about 10-20 €) blue or violet household LED stripe as the light source, placed into a glass becker and a fan recovered by outdated computers to dissipate the heat generated by the LEDs.

Figure 4. Typical set-up for photocatalytic reactions in our lab.

Photocatalysis usually employs safer and benign reagents and very mild reaction conditions, thus making it applicable to late-stage functionalization of complex natural products.[26] Moreover, nowadays the number of commercially available metal - and organic - photocatalysts is impressive, but many of the most used are polypyridyl complexes of Ruthenium and Iridium (Figure 5).

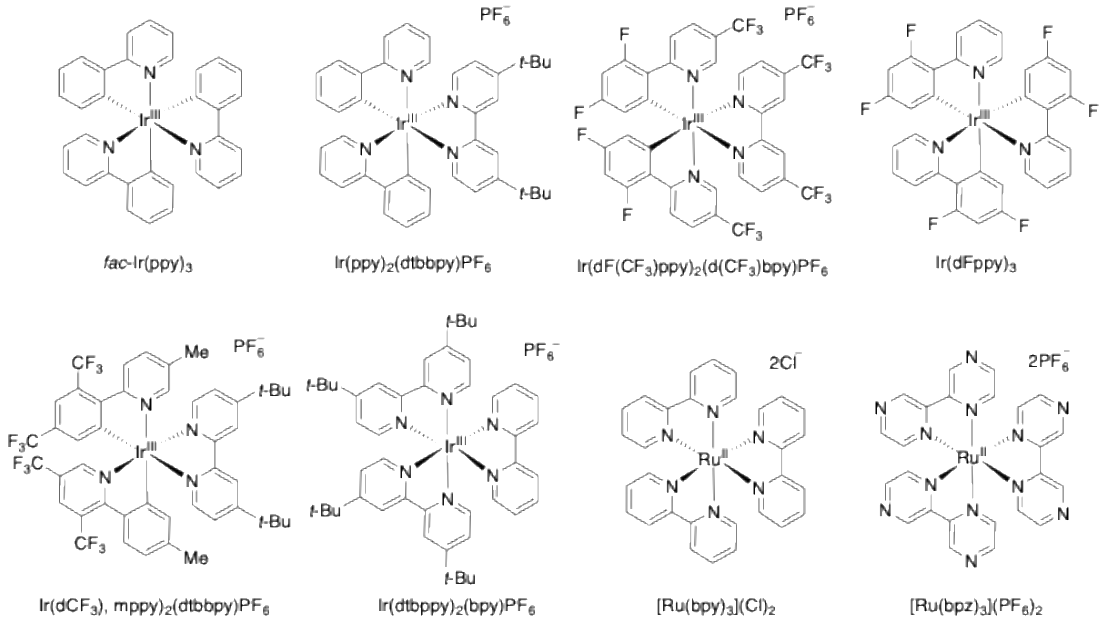

Figure 5. Some of the most common employed Ir- and Ru-based photocatalysts.

Each photocatalyst has its own characteristic properties – UV-vis absorption maximum, reduction/oxidation potentials and quantum yield, energy and lifetime of the excited triplet state – and each of them should be singularly evaluated in the choice of the appropriate candidate for the desired photochemical transformation.[26]

There are two main mechanisms with whom a photocatalyst (**PC**) can participate in a visible light-induced reaction: *photoredox catalysis* and *photosensitization*. Visible light excites the photocatalyst from its ground state to its excited singlet state (^{1}**PC***), then intersystem crossing (**ISC**) occurs to generate the excited triplet state of the photocatalyst (^{3}**PC***).

In photoredox catalysis (Scheme 17), the excited state of the photocatalyst can go through single electron transfer (SET) to the reductive or oxidative quenching cycle whether it receives/donates an electron from/to the substrate. Alternatively, a sacrificial electron donor/electron acceptor can quench the photocatalyst, giving the corresponding reduced/oxidized photocatalyst that can oxidize/reduce the substrate.[27]

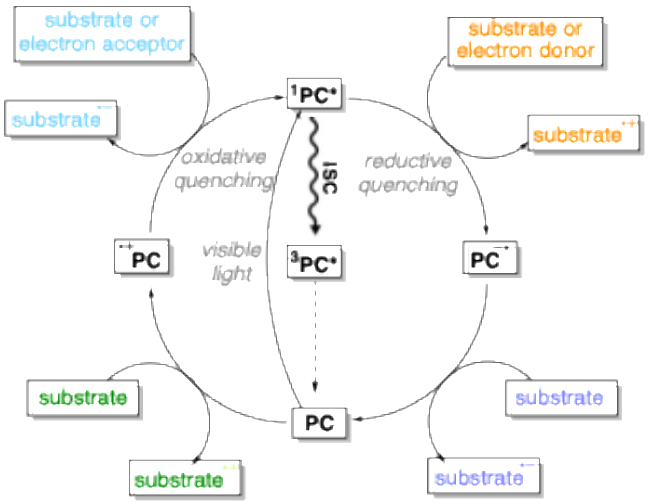

Scheme 17. General mechanisms of photoredox catalysis.

In photosensitization (Energy Transfer), the excited photocatalyst transfers its triplet-state energy to a substrate which would not otherwise be able to absorb light in the visible region, returning to its ground-state, and thus closing the catalytic cycle (Scheme 18).[27]

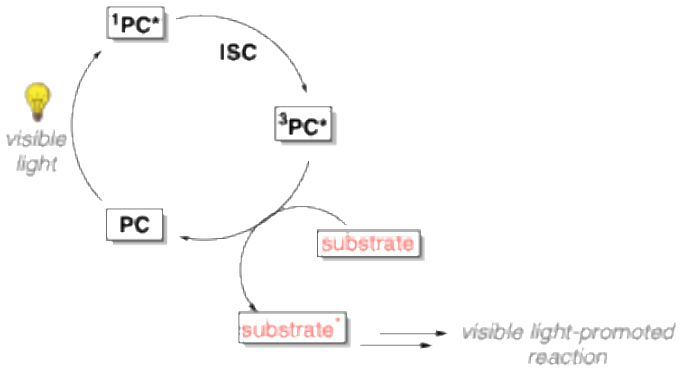

Scheme 18. General mechanisms of photosensitization.

1.4 HAT & Photocatalysis

Photocatalysis induced-HAT reactions are a smart way to merge the advantages of both photocatalysis and HAT: the selective, efficient and atom-economic functionalization of inert C-H sites through mild and environmental-friendly activation of the reactants, and generation of very reactive radical intermediates. Hereinafter are reported some noteworthy examples of visible light-promoted reactions proceeding *via* one or more HAT steps. Although photoredox catalyzed/HAT procedures were extensively developed in the recent decades,[1a,28] the following selected examples only include reactions that proceed *via* photosensitization (energy-transfer catalysis), since the synthetic methodologies that will be discussed in the following chapters are promoted by an *EnT* event. Furthermore, most of the photocatalyzed approaches developed by our research group that will be discussed in the next chapters of this thesis lead to the formation of interesting four-, five- or six-membered rings. Thus, the following examples are focused on the synthesis of four- or five-membered rings *via* olefin photoactivation, as this is one of the most developed strategies to access benzo- and naphtocyclobutanes, indolines, β-lactams, oxetanes, and azetidines, which all are valuable products in small bioactive molecules and pharmaceuticals. As the result of a π-bond photoactivation, a C-C-centered biradical species is generated, which efficiently undergoes the HAT process, eventually followed by radical-radical recombination to access the desired cyclization product.

In 1977, Aoyama and co-workers[29] reported the synthesis of β-lactams, which are known to be very important structural motifs in pharmaceuticals,[16] employing acrylamide derivatives to generate a C-C-centered biradical species, which is responsible for an intramolecular 1,5-HAT event (Scheme 19).

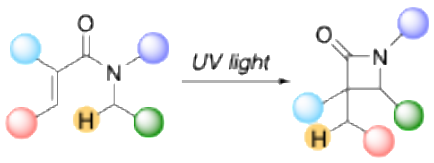

Scheme 19. UV-light triggered 1,5-HAT for the synthesis of β-lactams.

Since at that time the knowledge in the field of photocatalysis was quite limited, strong ultraviolet (UV) light was required to directly activate olefins. This resulted in decomposition of reactants and

products, causing low reaction yields, low functional-group tolerance as well as the formation of various by-products.

More recently, Koert's group reported the photocatalytic activation of the olefin of naphtyl acrylates employing an Ir-based photocatalyst and blue LEDs as the light source.[30] The olefin of **18** is sensitized to its triplet state by the excited triplet of the photocatalyst, generating a C-C-centered biradical species which easily undergoes intramolecular 1,5-HAT, followed by radical recombination to afford naphtocyclobutanes **19** (Scheme 20).

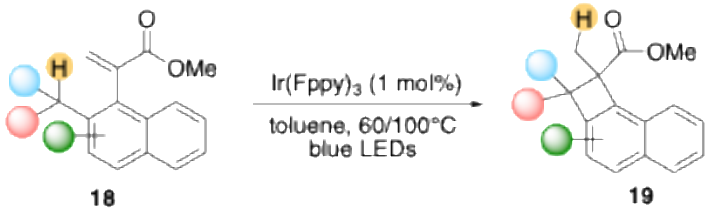

Scheme 20. Photocatalysis and visible light-enabled 1,5-HAT.

In 2022, Wei's group[31] reported a protocol to build benzocyclobutane scaffolds **21** from diarylethylene (DAE) systems **20**, through visible light-induced, photocatalyzed activation of DAEs (Scheme 21).

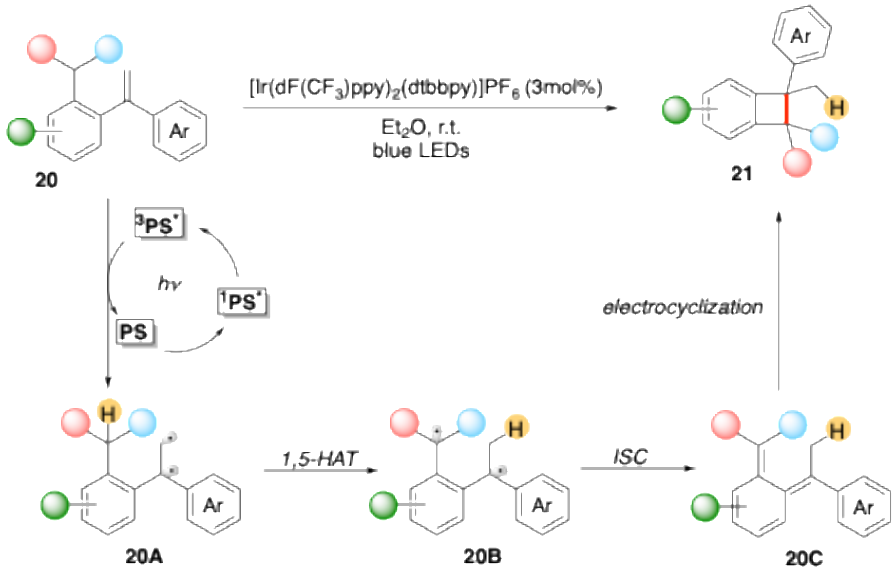

Scheme 21. EnT-mediated 1,5-HAT in DAE systems for benzocyclobutene construction.

This methodology afforded benzocyclobutanol and benzocyclobutylamine derivatives in good to excellent yields and low to moderate d.r. Moreover, deuterium-labeling experiments confirmed the participation of an intermolecular 1,5-HAT event.[31] In this approach, diaryl-substituted olefins are required, while simple styrene substrates were unsuccessful. Indeed, in styrene derivatives the 1,5-HAT event generates a 1,4-biradical species, which eventually decomposes via Norrish Type-II cleavage.[32]

Similarly, Xiong's group[33] reported the synthesis of benzocyclobutanes **23** using arylvinylpiridines **22** (Scheme 22). In this EnT-mediated 1,5-HAT strategy a Lewis acid (LA) is required to facilitate the reaction, as it can coordinate the pyridine ring of the substrate, promoting the cyclization step leading to the desired products in good to excellent yields.

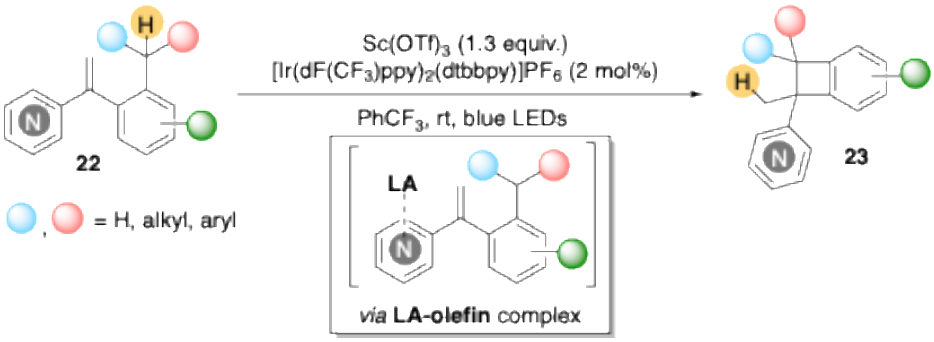

Scheme 22. EnT-mediated 1,5-HAT promoted by Lewis acid.

Wei's group also employed DAE systems for the synthesis of indoline derivatives *via* EnT-mediated 1,6-HAT route.[34] The mechanism is analogous to the one reported for the synthesis of benzocyclobutanes: the primary alkyl radical of the excited triplet state of DAE **24** abstracts a hydrogen from the C-H bond adjacent to the Nitrogen atom. The radical recombination of the resulting biradical species allows the formation of indolines **25** (Scheme 23).

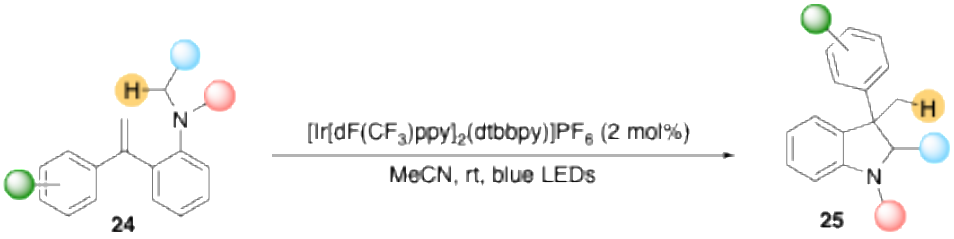

Scheme 23. Synthesis of indolines *via* En-T mediated 1,6-HAT.

To overcome the previously mentioned limitation to the only photoactivation of diaryl substituted olefins to induce the 1,5-HAT/cyclization sequence (Scheme 21),[31] the same group reported the synthesis of azetidines and oxetanes from styrene derivatives, simply introducing heteroatoms in the alkyl chain (Scheme24).[33] This strategy gave access to various azetidines and oxetanes **27** with moderate to good yields through the photoactivation of styrene derivatives **26** tethered with an amine or an ether moiety respectively.

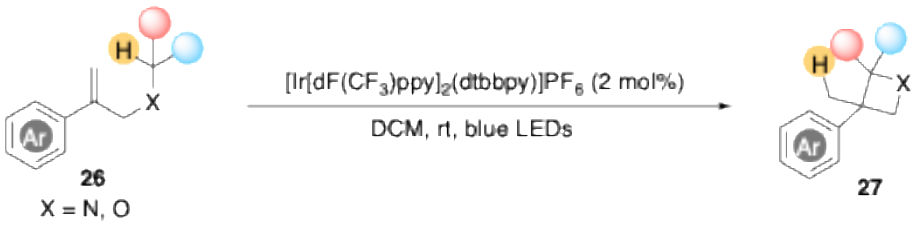

Scheme 24. EnT-mediated 1,5-HAT in styrenes for azetidine/oxetane construction.

Similarly to the above-mentioned styrene derivatives, acrylamide moieties have also been used for the synthesis of β-lactam skeletons. The photoactivation of the acrylamide moiety triggers the remote hydrogen abstraction, mediated by the primary alkyl radical of the excited triplet state of the acrylamide derivative, generating a biradical species. Eventually radical-radical cyclization occurs to give the desired β-lactam product.

In 2022, Bach and co-workers[35] employed indole-3-carboxamides **28** to synthesize the spiro[azetidine-3,3'-indoline] skeleton **29** (Scheme 25a). The same chemistry employed by Aoyama[29] for the synthesis of β-lactams though direct UV-activation of acrylamides (Scheme 19) was exploited by Petersen's group[36] for the synthesis of β-lactam **31**, except for in this work the employment of a photosensitizer enabled the use of visible light as a milder light source for the EnT-mediated activation of readily available acrilamides **30** (Sheme 25b). More recently, Yang's group[37] improved this synthetic protocol by lowering the catalyst loading and widening the substrate scope (Scheme 25c).

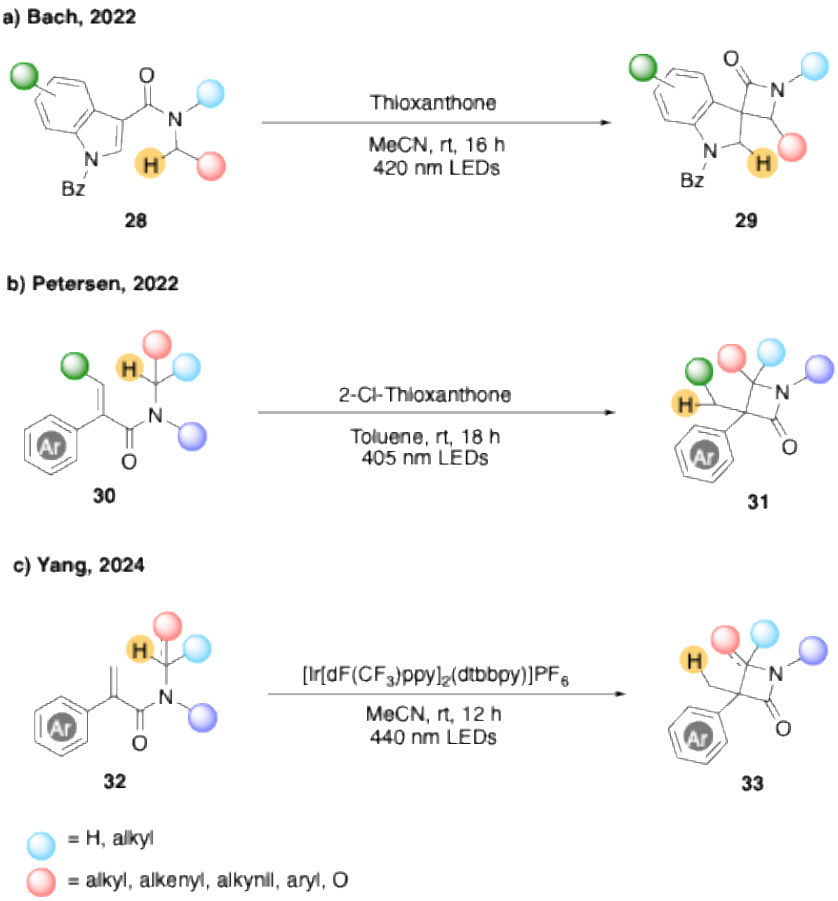

Scheme 25. Synthesis of β-lactams *via* EnT-mediated 1,5-HAT from acrylamides.

As a demonstration of the ample versatility and power of the HAT strategy, the last very recent examples are two surprisingly efficient visible light-promoted dearomatization reactions of (hetero)arenes in which one or more HAT steps play a key role. Indeed, dearomatization strategies have emerged numerously in the recent decades, since the awareness of how increasing the three-dimensionality and architectural complexity of potential small molecule drugs could improve some of their pharmacokinetic and pharmacodynamic properties, such as their water solubility and the number of positive interactions with the active site of the target protein.[38] However, the dearomatization of (hetero)aromatics is intrinsically challenging; indeed, the overcoming of high kinetic energy barriers is usually necessary to "break" the aromaticity of those compounds,[39] thus requiring the use of harsh reaction conditions. This generally results in poor selectivity, low yields and very limited substrate scope. In this scenario, a photocatalysis-enabled HAT approach could offer some great advancements in terms of reaction efficiency and selectivity.

The first example is a highly chemoselective dearomative reduction of quinolines and isoquinolines *via* selective Energy Transfer catalysis-enabled HAT.[40] In this protocol, the highly selective activation of the heteroarene via EnT prevents the reduction of an alkene moiety, which is known to be more readily reduced than aromatics - when employing traditional reduction protocols, such as the Birch reduction reaction[41] - reversing the conventional higher reactivity of the alkene over the arene. In addition, the high chemoselectivity of this approach allowed the authors to perform late-stage modification of drugs. The reaction starts with the EnT event from the excited Iridium-photosensitizer (**PS**) to **quinoline-BF_3**, which undergoes the first HAT step with γ-terpinene, followed by the second HAT event, generating the reduced quinoline product and *p*-cymene (Scheme 26).

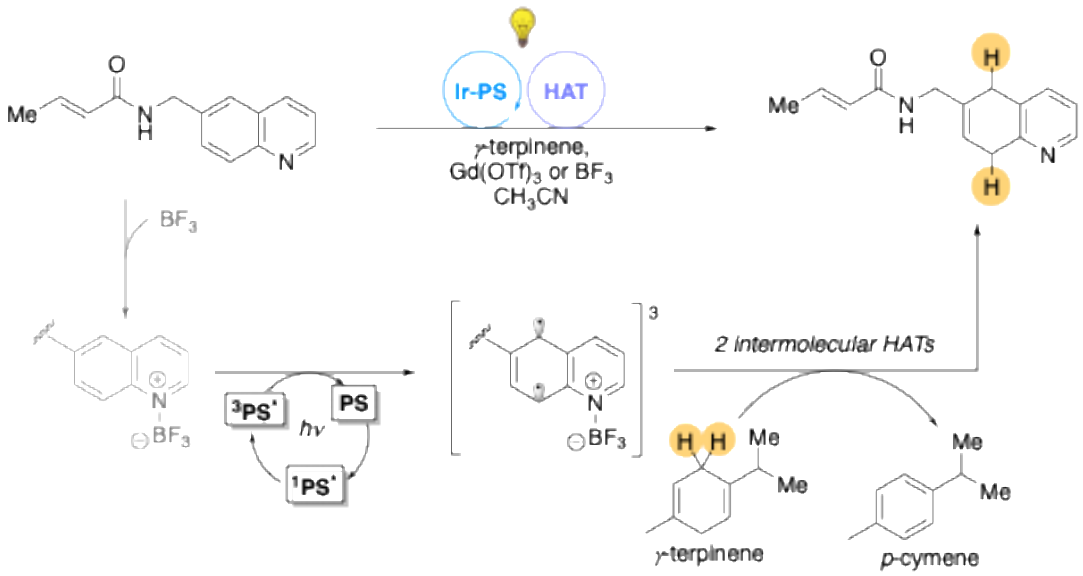

Scheme 26. Quinoline and Isoquinoline Reduction by Energy Transfer Catalysis Enabled Hydrogen Atom Transfer.

Similarly, in 2025 Shi and co-workers[42] reported a visible light-induced intramolecular dearomative reaction to form bicyclo[4.1.1] frameworks through (1,3)-cyclization of bicyclo[1.1.0]butanes (BCBs). Furthermore, the unprecedented (1,2,3)-cyclization of BCBs through 1,4-HAT process was also observed.[42] First of all, **34** is excited to its triplet state by the excited photosensitizer (**PS**), followed by C-C bond formation between C1 position of naphthalene and the bridgehead position of BCBs, with consequent formation of intermediate **34A**. The 1,4-HAT of **34A** allows the formation of intermediate **34B**, which is rapidly re-excited by the excited photocatalyst. Eventually, the intramolecular cyclization of **34B** gives the final HAT product **35** which is the thermodynamically favorite (Scheme 27).

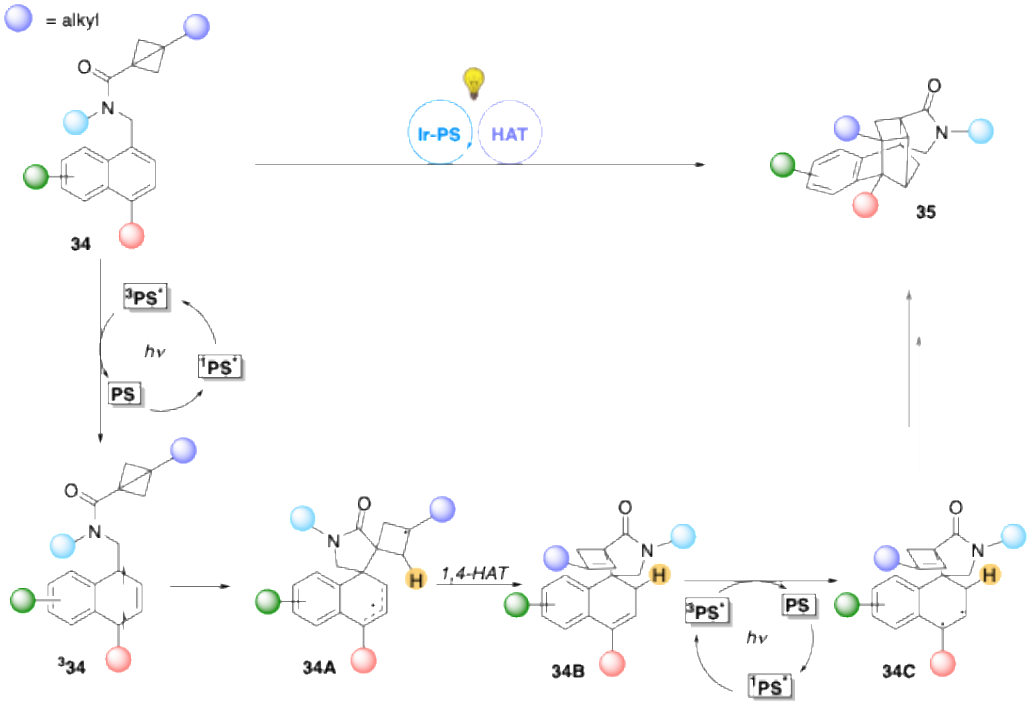

Scheme 27. Visible light-mediated Intramolecular dearomatization of Naphthalene and Anthracene.

1.6 Dispersion interactions in Chemistry and Biology

According to the IUPAC Gold Book definition,[43] Van der Waals interactions are "The attractive or repulsive forces between molecular entities (or between groups within the same molecular entity) other than those due to bond formation or to the electrostatic interaction of ions or of ionic groups with one another or with neutral molecules". The attractive component of vdW interactions are London dispersion forces (LDF or LD interactions) which are described as "quantum-mechanical fluctuations of the electron density leading to induced-dipole-induced-dipole interactions".[44] If we stick to these definitions, we cannot help but admit that vdW and LD interactions are the fundament of any chemical process – the precondition for two molecules to interact is that they must be close to each other, thus they must attract each other. These forces are the basis for the explanation of any (bio)chemical reaction mechanism, catalytic activity or tridimensional structure of molecules and matter in general. Indeed, these *weak* but powerful interactions can dictate the favorite molecule conformation or the most stabilized transition intermediate, even the folding of peptides, catalyst-substrate interaction and the disposition of molecules in the crystal lattice.[44] While theoretical chemists as well as protein scientists have already acknowledged the importance of LD interactions in their research field, most synthetic organic chemists have long been stuck on the simplistic assumption that all non-bonded atoms repel each other, only taking into account Pauli exchange repulsion, often called steric hindrance.[44]

Historically, LD interactions had been mostly disregarded for large systems, such as peptides, enzymes, catalysts or medium to large chemical entities in general, since these forces are significantly weaker than other forces that exist both on an intra- and inter-molecular level (i.e. Coulomb interactions and Pauli repulsion).[44] This is true if we only consider a single pairwise interaction between two entities or two groups of the same entity, but LD interactions are ubiquitous and much more numerous in larger and complex systems and therefore can significantly alter their chemical and physical properties.[44] This concept culminated in the introduction of "bulky" and highly polarizable substituents, called "dispersion energy donors" (DEDs), capable of increasing the number of LD interactions in any chemical entity.[44] DEDs have been recently employed to stabilize otherwise unstable structures, through a protecting "LD shell" of bulky substituents around a reactive center, for whom the term "corset effect" was coined.[44] A remarkable example demonstrating how LD forces

play a dominant role in structure stabilization is the case of hexaphenylethane (HPE).[45] The Gomberg's unsubstituted HPE[45a] is quite unstable as it rapidly dissociates into triphenyl methyl radical monomers. This phenomenon could be explained by the traditional steric hindrance model, since the repulsive interactions between the phenyl rings is responsible for the very low stability of dimeric HPE. However, the traditional steric model could not explain why the much bulkier all-*meta tert*-butyl HPE can be isolated[45b] (Figure 6).

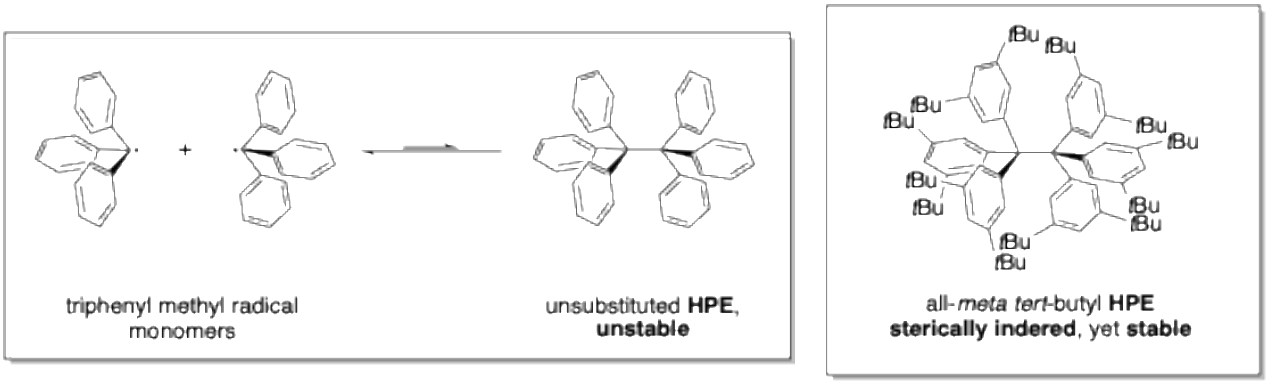

Figure 6. Stability of unsubstituted HPE vs. all-*meta tert*-butyl HPE.

While in unsubstituted HPE Pauli repulsion between the phenyl rings is responsible for the dissociation of HPE, in all-*meta tert*-butyl HPE the LD interactions between the *tert*-butyl groups around the weak C-C bond compensate repulsive interactions. The same effect was observed in unsubstituted HPE congeners with longer central C-C bond chains: extending the central bond increases the LD interactions between phenyl groups, counteracting their Pauli exchange repulsion.[45c] On this wave, much more recently, Suzuki and co-workers[46] synthesized a hexaphenylethane-like compound with a longer central C-C bond (1.77 Å vs. ≈ 1.70 Å). They observed a significant C-C bond contraction when bulky *tert*-butyl groups were used as substituents. This case demonstrates how LD forces are strong enough to "pull" the two poles of the molecule closer toward one another, instead of playing the expected role of the steric hindrance. LD interactions also play a main role in the stabilization of much larger biological entities, such as the double helix of DNA.[47]

The development of DEDs brought great innovation also to synthetic chemistry, as they can be employed as an innovative tool to *control* chemical reactivity – increase stereo- and

enantioselectivity, stabilize substrates or intermediates or facilitate a single reaction pathway.[44] A striking example of how the clever use of DED groups can boost the selectivity of a chemical reaction is the enantioselective version of the traditionally non-enantioselective Dakin-West reaction,[48] reported in 2016 by Schreiner's group.[49] The traditional Dakin-West reaction enables the synthesis of α-acylamido ketones from primary α-amino acids,[48] but the chiral information of the starting natural α-amino acid gets lost during the reaction mechanism due to the formation of two achiral intermediates, thus generating a racemic mixture of the α-acylamido ketone product (Scheme 28).

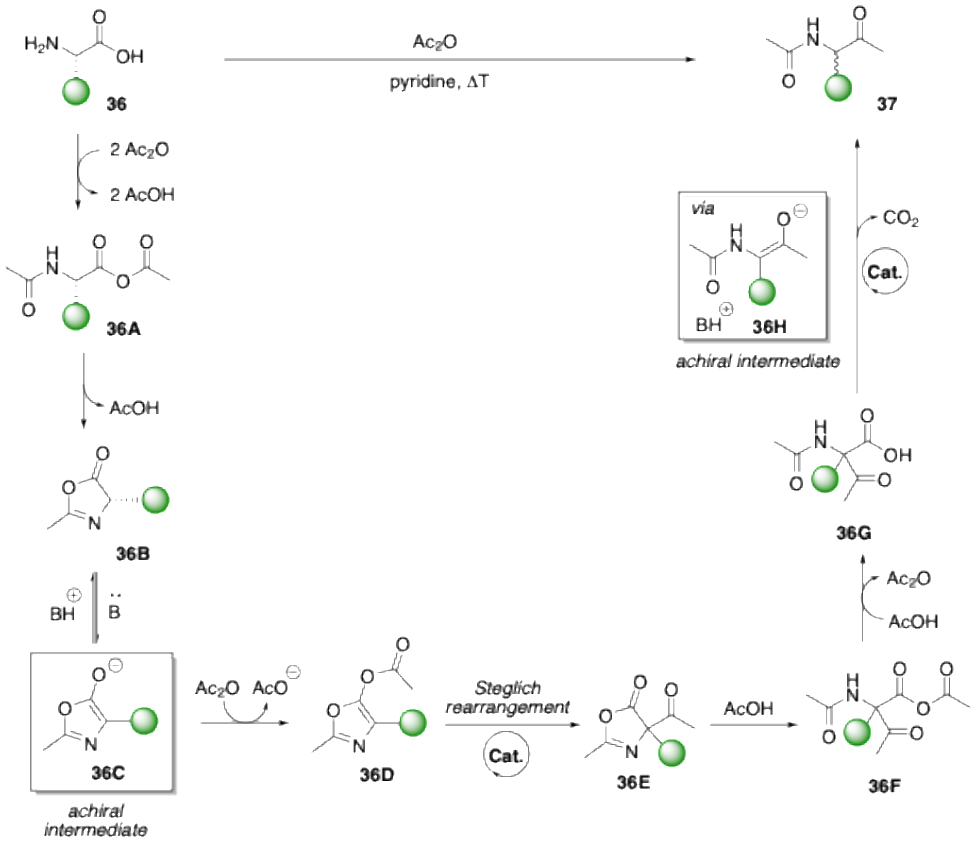

Scheme 28. Mechanism of the Dakin-West reaction.

Schreiner et al.[49] realized that it was possible to develop an enantioselective version of this process acting on the final decarboxylative protonation step, by adding a synthetic oligopeptide as acylation catalyst. The stereoselectivity was achieved through a final *enantioselective* re-protonation of the terminal enol **36H**. The enantioselectivity was ascribed to the formation of both enolate binding and LD interactions between the catalyst and intermediate enolate, immobilizing the latter in its position for the re-protonation step (Scheme29).

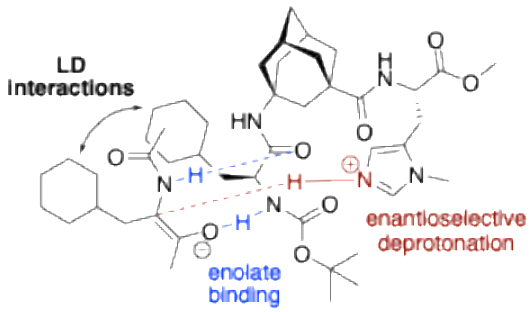

Scheme 29. Interaction between catalyst and substrate in enantioselective Dakin-West reaction.

LD interactions were also found to stabilize reaction intermediates, as in the CuH-catalyzed hydroamination of unactivated olefins reported by Liu et al.[50] In this work, the authors attribute the enhanced reactivity of copper catalysts to the presence of bulky bidentate phosphine ligands. Indeed, these ligands are responsible for stabilizing ligand-substrate dispersion interactions (Scheme 30), as demonstrated by experimental and computational data.

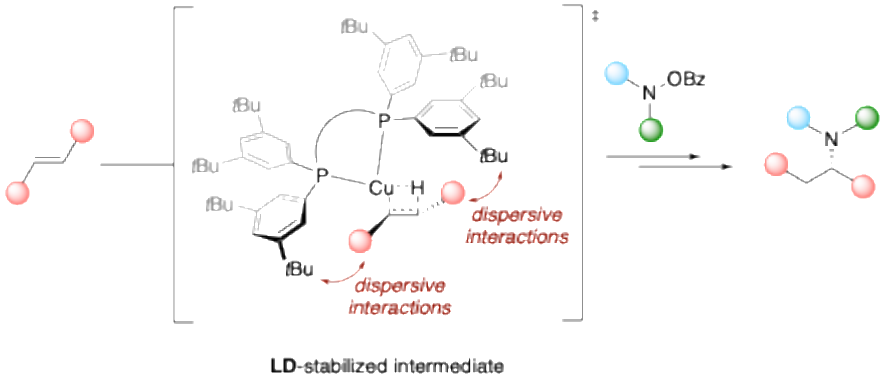

Scheme 30. Dispersion effect-enabled hydroamination of unactivated olefins.

A striking example demonstrating how steric hindrance is not the only type of interaction dictating selectivity in a reaction mechanism is the [4+3] cycloaddition of chiral oxyallyls with substituted furans.[51] The original intent of the authors was to protect one of the two faces of the oxalyl substrate, so that of the two possible transition states, **TS-I** (Scheme 31) would have been disfavored due to steric hindrance. Indeed, for most of the monosubstituted furans the *endo-I* stereochemistry – *via* **TS-I** – was the favored reaction pathway. In contrast to the steric hindrance model, DFT calculations proved that **TS-I** is favored over **TS-II** due to stabilizing CH-π dispersive interactions between the furan and the phenyl ring of the oxyallyl fragment.

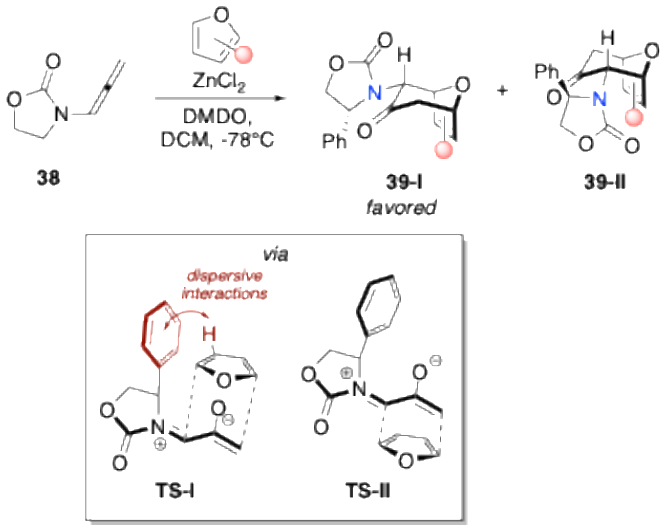

Scheme 31. Dispersive interactions dictated-stereoselectivity of [4+3] cycloadditions.

The last example reported in this chapter is an enantioselective protocol[52] in which hydrogen-bonding along with π-π stacking, and LD interactions are accounted for substrate recognition and enantioinduction (Scheme 32).

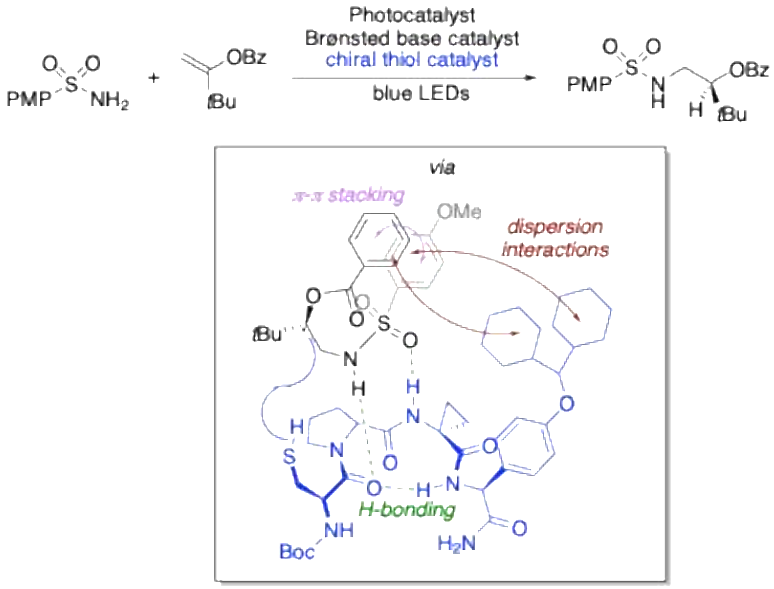

Scheme 32. Hydrogen-bonding, π-π stacking, and LD interactions induce asymmetric HAT.

This hydroamination of enol esters with sulfonamides proceeds *via* radical intermediates and an asymmetric HAT step, which owes its enantioselectivity to a combination of non-covalent interactions among the substrates and a cysteine-bearing tetrapeptide catalyst.[52]

Chapter II

Synthesis of Vinyl-Azetidines from Allenamides via Energy-Transfer Relay

From this chapter:

Sparascio, S.; Scarica, G.; Cerveri, A.; Russo, G.; Spataro, D.; Marchiò, L.; Lanzi M.; Maestri, G. Synthesis of Vinyl Azetidines and β-Lactams from Allenamides via Energy-Transfer Relay. *ACS Catal.* **2025**, 15, 16, 13799–13809.

2.1 Azetidine: the importance in small-molecule drugs and their synthesis

Azetidines already are a key structural feature in bioactive molecules and pharmaceuticals (Scheme 33).[53]

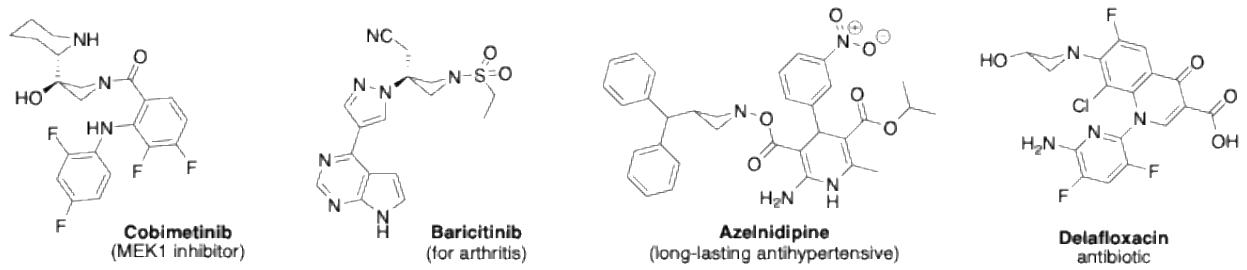

Scheme 33. Examples of relevant azetidines in SM drugs.

Incorporating an azetidine core in a small molecule (SM) drug candidate can enhance its chemical and pharmacokinetic properties. Indeed, one of the most employed strategies to slow down a drug's metabolism is to reduce its overall hydrophobicity, and since azetidines are among the least lipophilic saturated heterocyclic compounds,[54] a bioactive molecule could find great benefits from the incorporation of its tridimensional core.

Few catalytic methods to synthesize densely functionalized monocyclic azetidines were reported. Nucleophilic substitution has been widely used to create these strained rings (Scheme 34),[55] but the synthesis of functionalized precursors is an open issue.

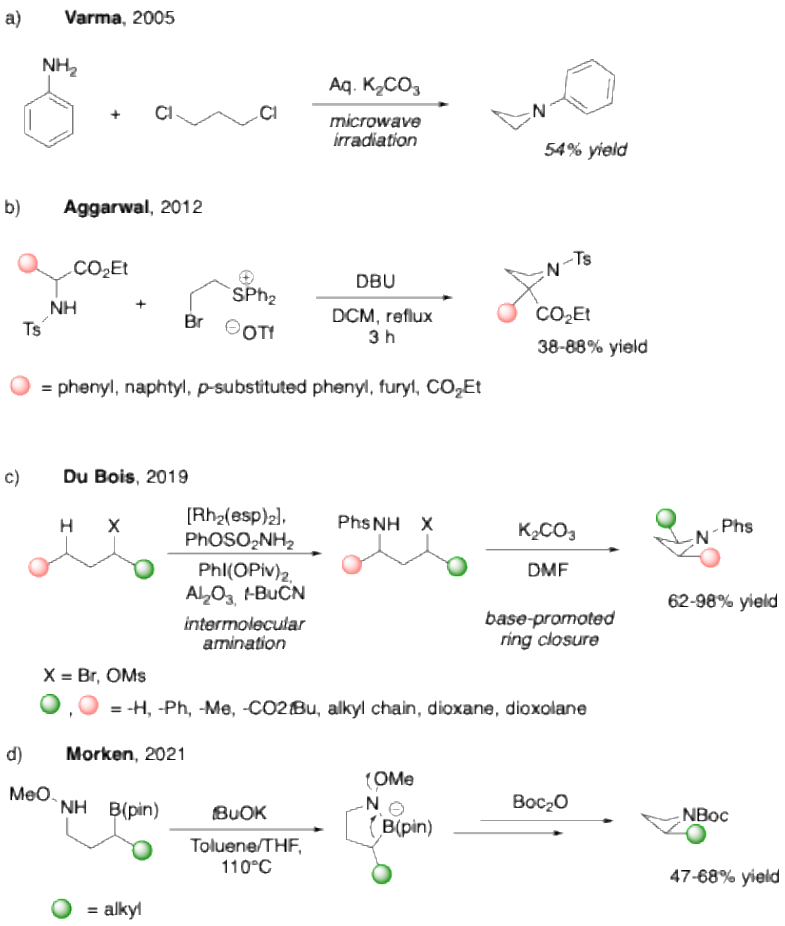

Scheme 34. Traditional synthesis of azetidines *via* nucleophilic substitution.

For instance, Varma and Ju[55a] reported the synthesis of various nitrogen-containing heterocycles through double alkylation of amines or hydrazine by alkyl dihalides or ditosylates under microwave irradiation in aqueous media, in presence of K_2CO_3 (Scheme 34a). Aggarwal and co-workers[55b] reported the synthesis of azetidines through an annulation reaction of aryl glycines with (2-bromoethyl)sulfonium triflate (Scheme 34b). Du Bois and co-workers[55c] developed an intermolecular Rh-catalyzed C(sp^3)-H amination of alkyl bromide derivatives; the reaction proceeds *via* C-H amination of the alkyl halide and subsequent sulfamate base promoted-alkylation and ring closure (Scheme 34c). Azacycles were also accessed through intramolecular amination of organoboronates[55d] *via* a 1,2 metalate shift of an aminoboronate complex (Scheme 34d).

An elegant method which was recently abundantly employed for the synthesis of azetidines is the catalytic ring strain release strategy.[56] The Aggarwal's group firstly exploited the high ring strain associated with azabicyclo[1.1.0]butanes (ABBs), for the synthesis of monocyclic azetidines (Scheme

35).[56a] In this protocol, the *in-situ* generation of an azabicyclo[1.1.0]butyl lithium reactive species **43** is followed by its trapping with a boronic ester, giving an intermediate boronate complex **43A**; the latter undergoes N-protonation by acetic acid and subsequently 1,2-migration occurs, with cleavage of the central C-N bond, releasing the desired azetidine product **46**. Although it seems a quite convenient approach for the synthesis of monocyclic azetidines, the protocol operates at very low temperatures (-78 °C), as it requires the use of the very hazardous reagent *t*-butyl lithium. In addition to this, the azabicyclo[1.1.0]butyl lithium initiating species requires an operationally demanding and elaborate synthetic protocol: the treatment of ammonium salt **41** with phenyl lithium at -78 °C, generates azabicylo[1.1.0]butane **42** *in situ*; the latter is lithiated using *s*-butyl litium/TMEDA at -78 °C, affording azabicyclo[1.1.0]butyl lithium **43**. Eventually, since **43** is a very unstable starting material, the authors used methyl 4-methylbenzenesulfinate **44** to trap the lithiated species as a sulfoxide (**45)**, which is used as a stable precursor of **43**.

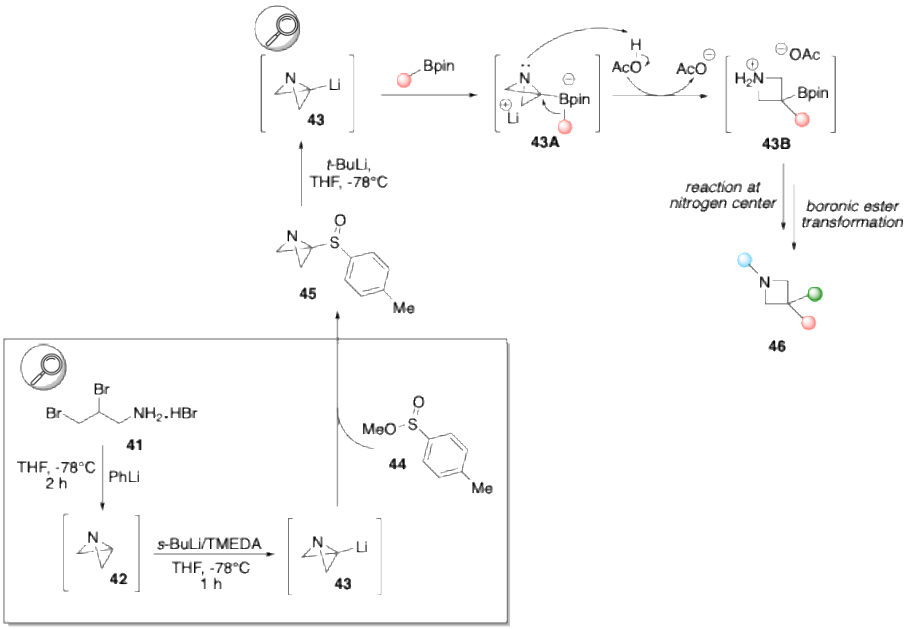

Scheme 35. ABBs for the synthesis of monocyclic azetidines.

In 2021, the same group reported the synthesis of spirocyclic azetidines using similarly synthesized ABB-ketones.[56b] The spirocyclization-desilylation reaction of **51** is induced by an electrophilic species, such as trifluoroacetic or trifluoromethanesulfonic anhydride.

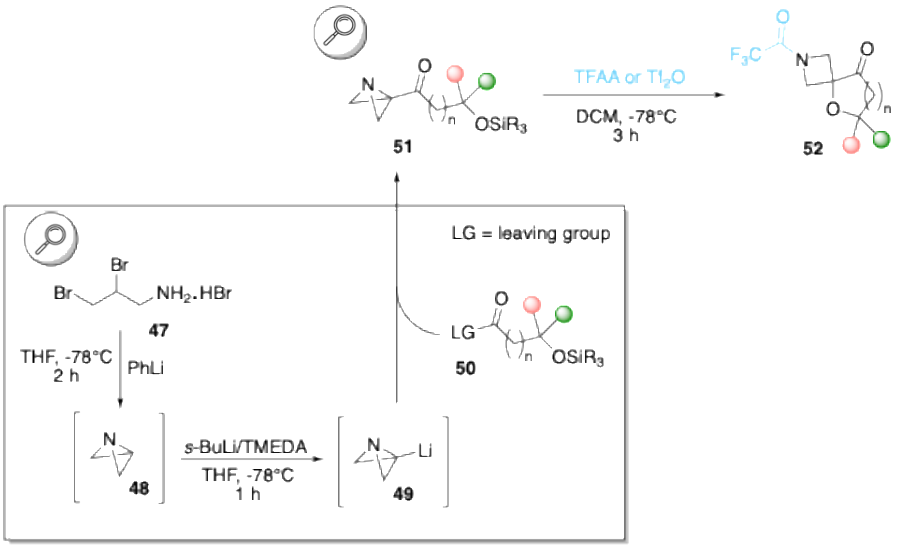

Scheme 36. ABB-ketones for the synthesis of spirocyclic azetidines.

In 2023, Saha's group employed C3-substituted ABBs to synthesize N-substituted azetidines through a tandem N/C3-functionalization/rearrangement *via* a cationic activation of ABBs.[56c] A α-halohydroxamate **54** (a proelectrophile) precursor is employed to generate *in situ* the reactive (aza)oxyallyl cation (**54A**), which is responsible for the N-activation of ABB **53** (Scheme 37). Still, the N-activation of ABBs remains limited to the use of appropriate electrophiles.

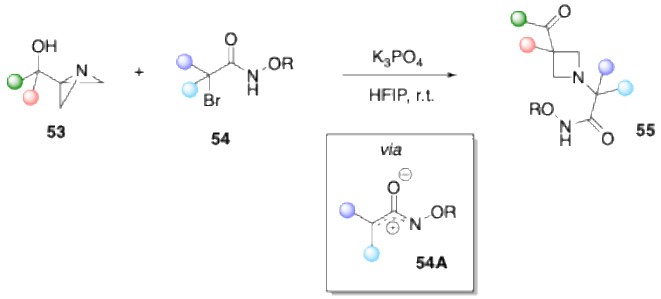

Scheme 37. Cation-promoted strain-release of ABBs for the synthesis of N-functionalized Azetidines.

ABBs were also employed in a nickel-catalyzed Suzuki C(sp^2)-C(sp^3) cross-coupling with aryl and alkenyl boronic acids.[55d] In this protocol, Benzoyl-ABBs are synthesized from the same 2,3-dibromopropan-1-ammonium salt employed by Aggarwal,[56a,b] with a similar synthetic route (Scheme 38). Similarly to the previous works,[56a-c] the N-activation of ABBs occurs *via* electrophile (Boc-anhydride, in this case), generating a Boc-activated benzoyl ABB **57A**. In the catalytic cycle

(Scheme 38), the reductive elimination of the $Ni^{(II)}$ precatalyst generates a $Ni^{(0)}$ species, whose comproportionation with $Ni^{(II)}$ species, forms the active $Ni^{(I)}$-Br complex **I**. Then, an aryl-$Ni^{(I)}$ complex **II** is generated through transmetalation of aryl boronic acid **58** with $Ni^{(I)}$-Br complex **I**. In parallel, Boc-activated benzoyl ABB **57A** relieves its ring strain *via* polar pathway, forming *in situ* the actual redox-active species **57B**, thanks to a catalytic amount of bromide. The reduction of this intermediate by aryl-$Ni^{(I)}$ complex **II**, leads to the formation of an azetidinyl radical **57C** and a $Ni^{(II)}$-bromide complex **III**. Eventually, the recombination of these last two species (**57C** and **III**) liberates the last $Ni^{(III)}$ intermediate **IV**, which easily decomposes *via* reductive elimination, affording the desired azetidine product **59**, and regenerating the $Ni^{(I)}$ species **I**, thereby closing the catalytic cycle.

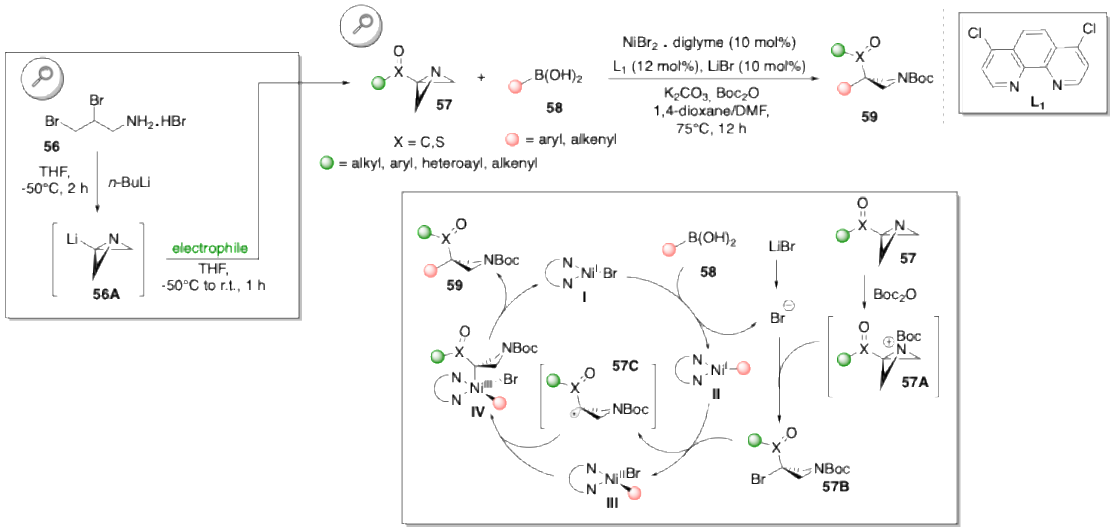

Scheme 38. Cross-Coupling type arylation/alkenylation of ABBs for the synthesis of azetidines.

The aforementioned approaches require the use of sacrificial group, which is associated to low atom-economy.

Higher atom economy has been achieved by a few energy-transfer (EnT)-based methods. Very recently, a radical strain-release photocatalytic approach for the synthesis of N-sulfonyl azetidines was developed, employing [1.1.0]-azabicyclobutanes and *N*-sulfonyl diarylimines.[57] In this work, visible light and a photosensitizer are employed to promote the homolytic cleavage of N-sulfonyl imines, resulting in the formation of two radical intermediates. These radicals can directly activate ABBs, promoting a radical ring strain release, which eventually results in the incorporation of the two radical fragments in the azetidine core (Scheme 39).

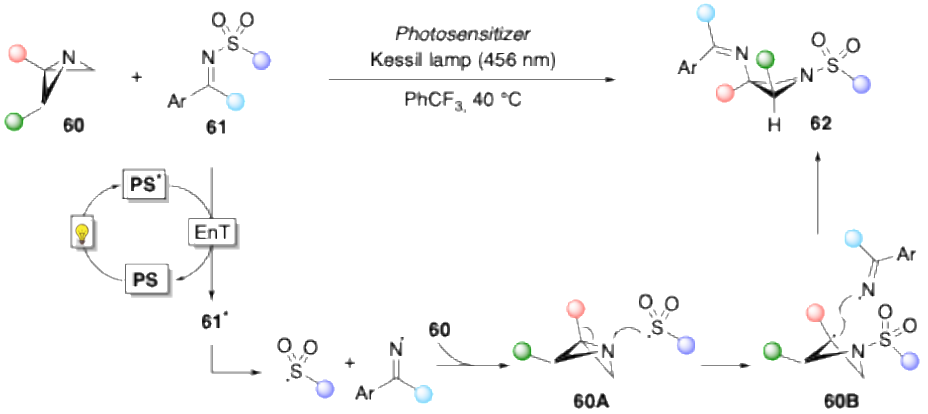

Scheme 39. Radical strain-release photocatalysis of ABBs for the synthesis of N-sulfonyl azetidines.

An intermolecular visible light-promoted aza Paternò-Büchi reaction ([2+2]-cycloaddition) of β-carboxy oxime with a styryl fragment to prepare monocyclic azetidines was very recently reported (Scheme 40).[58]

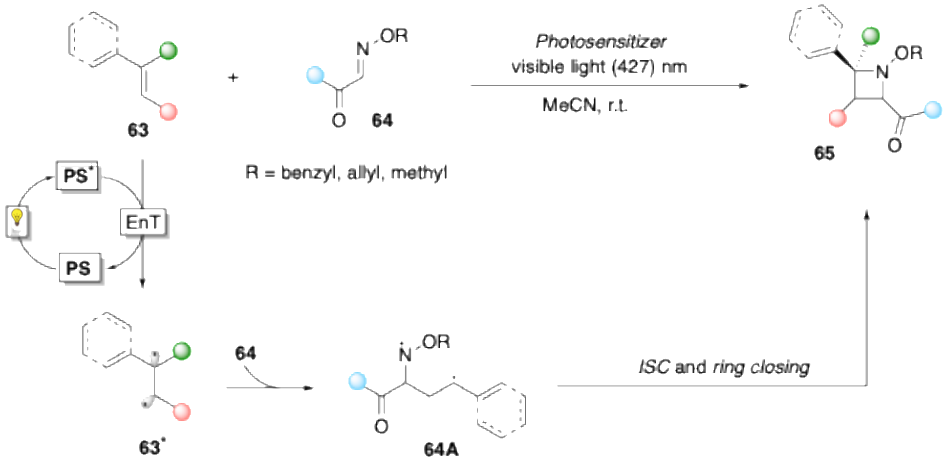

Scheme 40. Visible light-promoted [2+2]-cycloaddition of β-carboxy oxime with a styryl fragment to prepare monocyclic azetidines.

α-vinyl azetidine is a highly versatile species, as demonstrated by numerous applications in photocatalysis with metal-carbene complexes,[59a] catalyst-free ring expansion with benzyne,[59b] and ring expansion as azetidinium salts,[59c] as well as in Pd-catalysis.[59d] Altough, only a few methodologies are available for their construction (Scheme 41).[60]

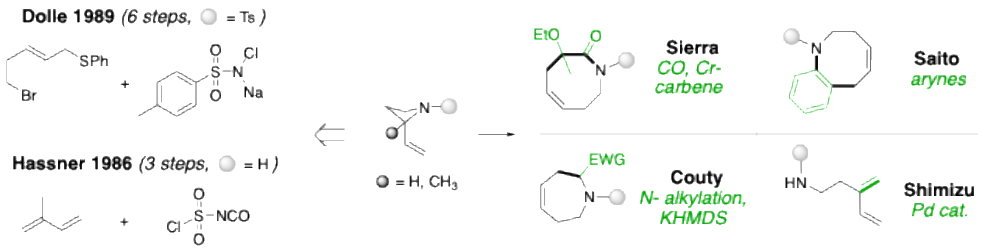

Scheme 41. Synthesis and applications of α-Vinyl Azetidines.

So-far, EnT strategies have been grounded on the activation of conjugated π-bonds, and the need for auxochromes, such as aryl-rings and carbonyl groups (Scheme 42, highlighted in orange), limits the chemical space that can be accessed through these methodologies. [57,58]

Scheme 42. EnT approaches activating conjugated π-bonds.

We targeted instead a cumulated π-system. A few reported examples prove that the EnT-mediated activation of an allene can give access to reactive species with a vinyl-radical site.[61] We wanted to find appropriate conditions to activate unbiased allenyl substrates, aiming to prepare strained 4-membered heterocycles, via 1,5-HAT/radical recombination cascade. This outline is challenging, as very few precedents that employ mono-substituted allenamides in EnT approaches were reported,[61b,c] none of them involving a HAT step. Nevertheless, the concept would bring valualble advantages: the sequence would provide α-vinyl azetidines and, at present, no general catalytic method has been reported[56-58,62] to synthesize these heterocycles, which present a synthetically useful allylamine unit;[59,63] additionally, in contrast to the conventional generation of vinyl radicals,[1,64,65] the EnT on an allene is atom-economical, and it would both trigger the desired HAT and provide the vinyl function to the product.

2.2 Results and Discussion

In this chapter, the first synthesis of monocyclic α-vinyl azetidines *via* photocatalytic activation of allenamides is reported. The visible-light-promoted HAT cascade demonstrated wide functional-group tolerance, giving access to strained products with a congested all-carbon quaternary center and an exocyclic vinyl group (Scheme 43).

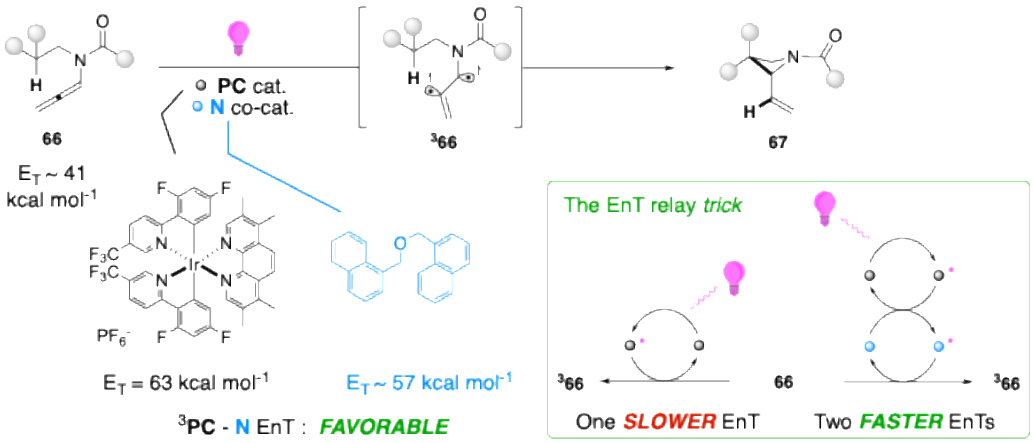

Scheme 43. EnT-relay activation of unbiased allenes for the synthesis of α-vinyl azetidines.

Our protocol combines a tailored Ir(III) complex with high triplet energy (E_T) and long lifetime (τ) and a bi-naphthyl co-catalyst, which proved itself to be beneficial for the reaction outcome. Indeed, in this mechanism the co-catalyst plays a dual role: the bi-naphthyl (bi-NP) stabilizes the bi-radical intermediate *via* dispersion interactions (LD forces), and provides a more efficient substrate activation thanks to a "triplet-state relay" phenomenon: the co-catalyst relays two EnT cycles, replacing a slower EnT with two faster ones (Scheme 43); this is an unprecedented behavior, since the triplet-state relay concept has been so far reserved to reagents - rather than (co-)catalysts - that incorporate an internal antenna in their skeleton, such as an acyl-naphthalene group.[66]

In figure 7, the photocatalysts and **N** co-catalysts tested for the synthesis of azetidine **67a** in the optimization study are depicted.

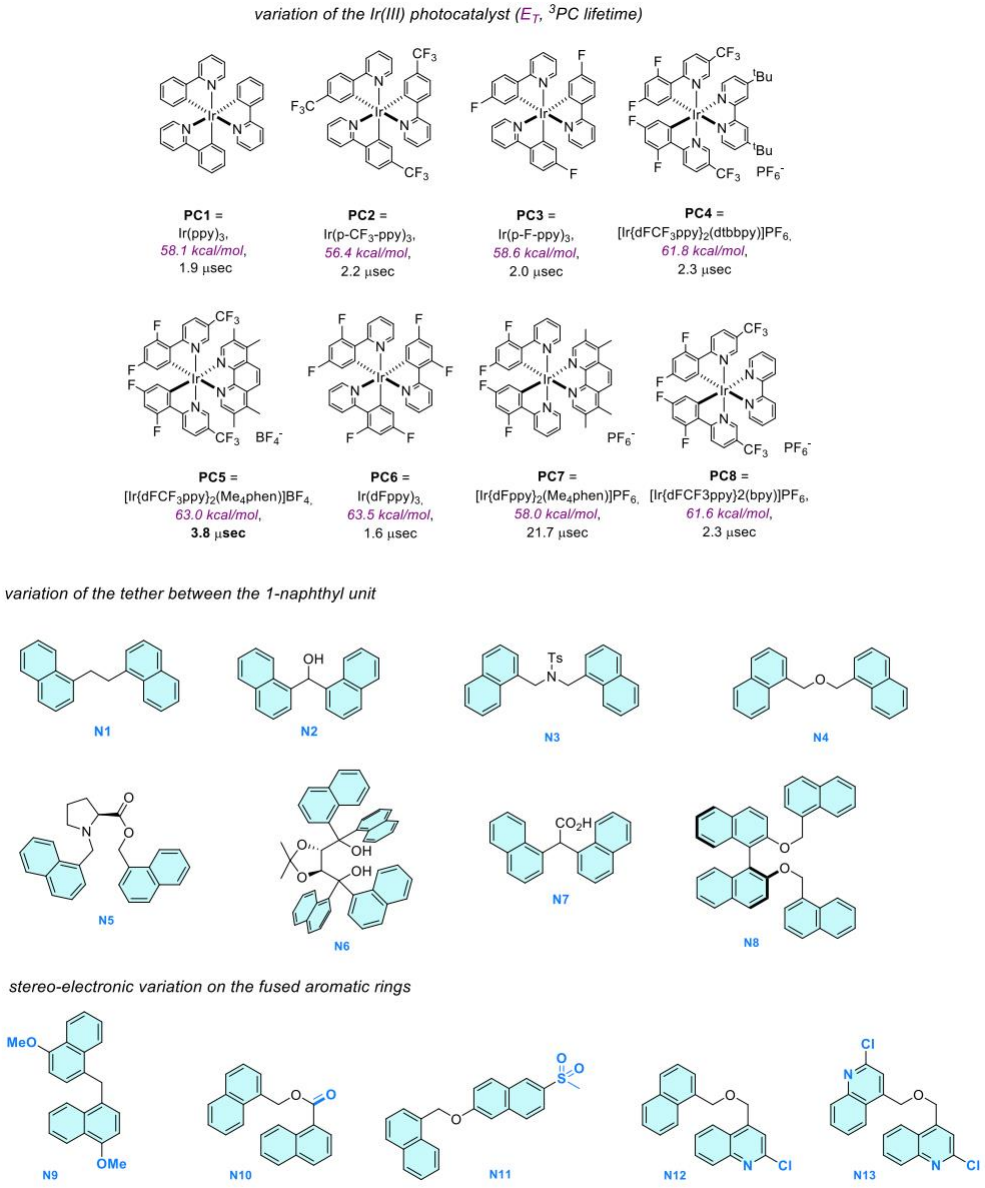

Figure 7. Chart of the photocatalysts and N co-catalysts tested for the synthesis of azetidine **67a.**

In our first experiment, a 0.1 M solution of **66a** in DMF and 1 mol% of $Ir(ppy)_3$ (**PC1**) were added into a 5-mm NMR tube (Table 1a). The mixture was degassed twice by freezing-thaw and then irradiated with a household blue LED strip. A low 22% yield of azetidine **67a** was observed upon 168 hours of irradiation (entry 1). We observed partial decomposition of both product and substrate through time in the presence of light and photosensitizer, lowering the final yield.

In our previous work,[61c] naphthalene was firstly used as an additive (20 equiv.) to significantly increase the rate of a visible light-promoted intramolecular dearomatization reaction on allenamides. According to DFT calculations, this positive effect was ascribed to stabilizing π-radical

LD interactions between naphthalene and the bi-radical intermediate originated by EnT-activation of allenamides.[61] For our synthetic route to azetidines, we suspected that the addition of simple naphthalene would have caused a competitive intermolecular dearomatization side reaction - which we already reported[68] - most probably hindering the 1,5-HAT/cyclization sequence of the allenamide substrate. We thus tested bi-naphthyls as additives, hoping to observe a minor competition with the desired intramolecular reactivity of our allenamide substrate compared to the use of simple naphthalene, but with a similar stabilizing effect of the transient biradical species. We thus performed a second experiment with identical reaction conditions to entry 1, but adding bi-naphthyl additive **N3** (30 mol%). Luckily, entry 2 gave a significantly faster conversion (ca. four-fold rate increase) of **66a**, and a higher yield of **67a**. This suggested that those additives really had a beneficial effect on the reaction rate. This loading of **N** was then kept for the following steps of the optimization.

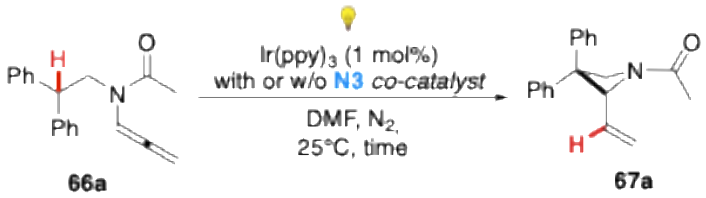

Entry	N co-cat.	Time (h)	Conversion of **66a** [%][a]	Yield of **67a** [%][a]
1	--	168	30	22
2	**N3** (30 mol%)	84	75	61

Table 1a. Preliminary experiments on the role of N3 on rate; [a] by ^{1}H NMR using 2,2'-dipyridine as internal standard. Reactions performed with blue LEDs.

Blank experiments confirmed that no reaction occurred without either the **PC** or the visible light source (Table 1b).

Entry	Variation	N co-cat.	Time (h)	Conversion of **66a**[a] [%]	Yield of **67a**[a] [%]
3	No **PC**	**N3** (30 mol%)	84	--	--
4	No light	**N3** (30 mol%)	84	--	--

Table 1b. Blank experiments; [a] by ^{1}H NMR using 2,2'-dipyridine as internal standard.

Different Ir(III) photocatalysts were initially tested using blue LEDs as the light source (Table 1c). In this conditions, **PC1**-**3** were competent species for the activation of **66a** in combination with **N3** as co-catalyst. Indeed, a higher conversion of substrate **66a** was observed using either **PC2** (entry 6) or

PC3 (entry 7) compared to **PC1** (entry 2); however, the yield of **67a** was slightly worse in both cases. Both **PC2** and **PC3** have triplet energies and triplet state lifetimes comparable to those of **PC1**. Under these conditions, a slower conversion of **66a** was observed using **PC4** (entry 8). An increased rate for the conversion of **66a** was observed when we increased the loading of **N3** from 30 mol% up to 100 mol% (entry 5). In this entry, we observed a full conversion of the substrate upon 66 hours of irradiation, but at the same time the yield of **67a** did not increase because of the concomitant formation of byproducts, due to a parasitic intermolecular para-cycloaddition of the allene on one of the naphthyl arm of **N3** (see *Tetrahedron Chem* **2023**, *8*, 100053). Under these conditions no traces of **67a** were observed performing the reaction using thioxanthone as photosensitizer (entry 9). These results led us to keep the conditions used in entry 2 and move on to the evaluation of the effect of the solvent on our reaction.

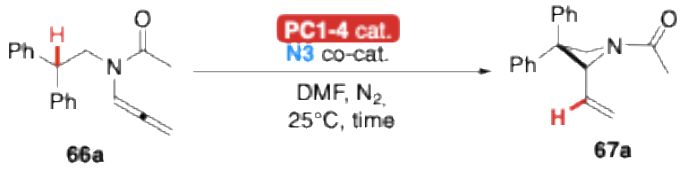

Entry	**PC** cat. (1 mol %)	Time (h)	Conversion of **66a** [%][a]	Yield of **67a** [%][a]
2	**PC1**, $Ir(ppy)_3$	84	75	61
5[b]	**PC1**, $Ir(ppy)_3$	66	>99	62
6	**PC2**, $Ir(p\text{-}CF_3\text{-}ppy)_3$	84	92	52
7	**PC3**, $Ir(p\text{-}F\text{-}ppy)_3$	84	87	54
8	**PC4**, $[Ir\{dFCF_3ppy\}_2(dtbbpy)]PF_6$	84	33	14
9	Thioxanthone (20 mol%)	84	/	Traces

Table 1c. Initial comparison of different Ir(III) PCs. [a] by ^1H NMR using 2,2'-dipyridine as internal standard. [b] with 100 mol% of **N3**. Reactions performed with blue LEDs.

Several solvents, and combinations thereof, were tested (table 1d, notice that, when using acetonitrile as solvent, a small amount of DCM was required to solubilize both the photosensitizer and the additive, which would have otherwise remained as precipitate; higher but not complete solubilization of the reagents was also observed when using pure toluene as solvent). Overall, no direct correlation between the polarity of the medium and the rate of conversion of **66a**, or the yield of **67a**, was observed. Nonetheless, this series of results showed a slightly faster substrate

conversion, and a moderate increase in the yield of azetidine **67a** when performing the reaction in a 8:2 toluene:DCM mixture (entry 13). Variation of the concentration of the substrate, either increasing it up to 0.2 M (entry 14), or diluting the mixture down to 0.05 M (entry 15) on **66a**, provided worse results. Therefore, we kept the solvent, and the concentration employed in entry 13 for the rest of the optimization effort.

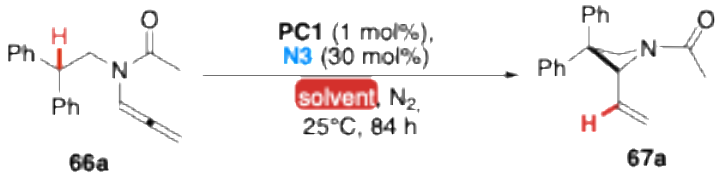

Entry	Solvent (0.1 M)	Conversion of **66a** [%][a]	Yield of **67a** [%][a]
2	DMF	75	61
10	CH_3CN:DCM 8:2	84	57
11	toluene	93	62
12	DCM	82	43
13	Tol:DCM 8:2	91	68
14[c]	Tol:DCM 8:2	93	53
15[d]	Tol:DCM 8:2	87	54

Table 1d. Evaluation of the effect of the solvent. [a] by ^{1}H NMR using 2,2'-dipyridine as internal standard. [c] 0.2 M on **66a**. [d] 0.05 M on **66a**. Reactions performed with purple LEDs, entry 2 performed with blue LEDs.

Seven different poly-naphthyl derivatives were tested (table 1e), varying mainly the length and the rigidity of the tether between the two naphthyl units, because these structural properties proved to be crucial for the efficacy of the additive in a recent study on alkene-alkene [2+2] photocycloadditions (see *Photochem. Photobio. Sci.* **2024**, *23*, 1543). In all cases, the rate of the reaction in the presence of the **N** additives is significantly higher than that performed without a co-catalyst (entry 16). Among the tested **N** species, **N5** provided the highest substrate conversion, followed by **N7** (entries 20 and 22, respectively). However, the highest yield of **67a** was observed in the reaction performed in the presence of **N4** (entry 19). This derivative was thus adopted for the following optimization experiments.

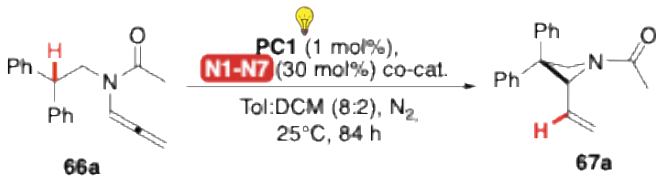

Entry	N Co-cat. (30 mol%)	Conversion of **66a**[a] [%]	Yield of **67a**[a] [%]
16	--	18	11
17	**N1**	87	61
18	**N2**	65	41
13	**N3**	91	68
19	**N4**	84	70
20	**N5**	95	42
21	**N6**	73	46
22	**N7**	90	61

Table 1e. Evaluation of the effect of the different N co-catalysts N1-N7. [a] by ^{1}H NMR using 2,2'-dipyridine as internal standard. Reactions performed with purple LEDs.

Although **67a** was obtained in a good yield (70%), we wanted to shorten the irradiation times, with the purpose of increasing the practical viability of our synthetic method. Therefore, we performed a second-generation analysis on the role of the **PC**. Once established the optimal reaction medium and N co-catalyst, we re-evaluated seven model Iridium (III) complexes (Table 1f). The highest yield of **67a** was observed using the heteroleptic complex **PC5** (entry 26); in this case, the full consumption of the substrate required 24 hours of irradiation. The efficiency of this photosensitizer can be attributed to an overall good balance between a high E_T and long-lived triplet state lifetime (63.0 kcal/mol and 3.8 msec, respectively). The fastest conversion of the allenyl reagent was observed using either homoleptic complex **PC6** (entry 27) or heteroleptic complex **PC7** (entry 28); in both cases, however, the yield of **67a** was lower than that obtained in entry 26. These results highlight that there is no linear correlation between the triplet energy of the photocatalyst and the rate of the substrate activation. Indeed, the fastest consumption of the starting material was observed using **PC6**, which has the higher E_T of the series, as well as **PC7**, which has one of the lowest one (63.5 and 58.0 kcal/mol, respectively). It is also worth noting that the latter has an excited state lifetime that dwarfs the former (21.7 vs 1.6 msec, respectively), and that both species could in principle sensitize the co-catalyst **N4** (56.1 and 57.0 kcal/mol for the experimental and calculated E_T, respectively).

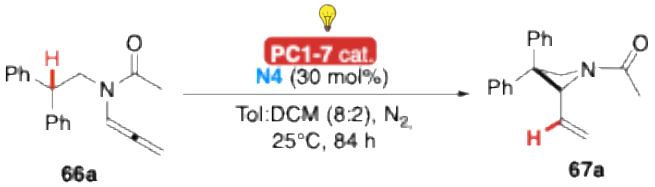

Entry[a]	**PC** cat. (1 mol%)	Time (h)[b,c]	Yield of **67a** [c] [%]
19	**PC1**, $Ir(ppy)_3$	84	70
23	**PC2**, $Ir(pCF_3ppy)_3$	72	62
24	**PC3**, $Ir(pFppy)_3$	72	69
25	**PC4**, $[Ir\{dFCF_3ppy\}_2(dtbbpy)]PF_6$	36	71
26	**PC5**, $[Ir[dF(CF_3)ppy]_2(Me_4phen)]BF_4$	24	76
27	**PC6**, $Ir(dFppy)_3$	14	74
28	**PC7**, $[Ir[dFppy]_2(Me_4phen)]PF_6$	14	50

Table 1f. Second comparison of different Ir(III) PCs. [a] reactions performed using purple LEDs; [b] irradiation time required to reach full conversion of **66a**; [c] by ^1H NMR using 2,2'-dipyridine as internal standard. Best result (highest yield of **67a**) highlighted in pale orange; best result (fastest conversion of **66a**) highlighted in pale green. Reactions performed with purple LEDs.

To further confirm the catalytic effect of the **N** co-catalyst, we performed additional experiments comparing four different Iridium photosensitizers, with and without **N4** (Table 1g). For the latter series of experiments, table 1g shows the irradiation times required to achieve a full conversion of the substrate. The four corresponding entries (29-32) showing reactions performed without **N4** were monitored by TLC and kept under light irradiation for a significantly longer period. Nonetheless, the achieved conversion of **66a**, as measured by ^1H NMR, was invariably much lower. These results are consistent with the trend previously observed using **PC1**, (see entries 1-2, Table 1a, and entries 16-17, Table 1e). Overall, among 12 parallel experiments, a significantly faster rate of conversion of **66a** was observed. Furthermore, the series of results presented in Table 1g show that the beneficial effect of **N4** is general, and it is not limited to the use of a particular Iridium (III) photocatalyst.

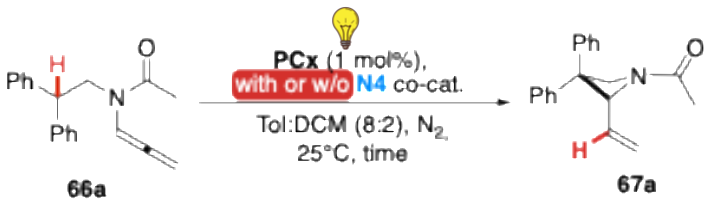

Entry[a]	**PC** cat. (1 mol%)	Co-cat. (30 mol%)	Time (h)	Conversion of **66a** [b] [%]	Yield of **67a** [b] [%]
25	**PC4**, $[Ir\{dFCF_3ppy\}_2(dtbbpy)]PF_6$	**N4**	36	>99	71
29	**PC4**, $[Ir\{dFCF_3ppy\}_2(dtbbpy)]PF_6$	--	80	41	25
26	**PC5**, $[Ir[dF(CF_3)ppy]_2(Me_4phen)]BF_4$	**N4**	24	>99	76
30	**PC5**, $[Ir[dF(CF_3)ppy]_2(Me_4phen)]BF_4$	--	80	48	27
27	**PC6**, $Ir(d\text{-}F\text{-}ppy)_3$	**N4**	14	>99	74
31	**PC6**, $Ir(d\text{-}F\text{-}ppy)_3$	--	24	65	46
28	**PC7**, $[Ir[dFppy]_2(Me_4phen)]PF_6$	**N4**	14	>99	50
32	**PC7**, $[Ir[dFppy]_2(Me_4phen)]PF_6$	--	14	67	11

Table 1g. Additional experiments confirming the co-catalytic role of N4. [a] reactions performed using purple LEDs. [b] by ^1H NMR using 2,2'-dipyridine as internal standard. Best result (highest yield of **67a**) highlighted in pale orange; best results (fastest conversion of **66a**) highlighted in pale green. Reactions performed with purple LEDs.

A representative series of five bi-naphthyls derivatives with electron-donating or electron-withdrawing groups on the aromatic rings of the **N** co-catalyst were prepared, to assess the role of electronic factors on its efficiency (**N9**-**N13**). These compounds were tested with the optimized conditions in the model reaction for the synthesis of **67a** (Table 1h). Overall, all of them ensured a faster conversion of the starting material **66a** compared to the experiment performed without an **N** co-catalyst. In particular, the reagent was fully consumed upon 24 hours of irradiation using both **N12** and **N13**, which have one and two 2-chloro-quinoline fragments, respectively (entries 37-38). However, in both cases, the selectivity towards **67a** was reduced. Reactions performed using **N10** and **N11**, which feature two electron-withdrawing groups conjugated with a naphthyl arm (the carbonyl of an ester and a sulfone substituent, respectively), did not achieve the full consumption of the substrate **66a** and afforded **67a** in moderate yields (entries 35-36). A relatively better result was achieved in the presence of **N9**, in which each naphthyl fragment is decorated by a methoxy group (entry 33). The conversion of the substrate was lower than that achieved using **N4**, but the yield of **67a** was promising. However, by repeating the experiment and leaving the mixture for a

longer irradiation time we observed that the conversion of **66a** became progressively slower, and the final yield did not improve significantly. It is worth noting that a linear correlation between the electronic properties of the co-catalyst and the outcome of the reaction is likely not possible because the substituents on the aromatic rings of **N** could play several different roles, which overcome the positive effect ascribed to the formation of bimolecular adducts driven by dispersion interactions. In addition, the presence of conjugated auxochromes on the system could alter the E_T of the **N** derivative, making one or both the EnT involved in the reaction less favorable; this may be especially relevant for Dexter-type EnT steps which require, beside a net thermodynamic convenience, an orbital overlap between the two SOMOs of the donor and the frontier MOs of the acceptor. The substituent on the **N** species could alter its overall steric demands, potentially disfavoring the formation of adducts with the substrate and/or the transient triplets of the reaction, regardless of the net electronic effect of the substituent itself. Additionally, strongly polarized derivatives may no longer be redox neutral in the presence of Iridium photocatalysts. Similarly, π-systems with strong quadrupolar moments could lead to the formation of Electron Donor-Acceptor (EDA) complexes, which may no longer be suitable for the desired HAT sequence.

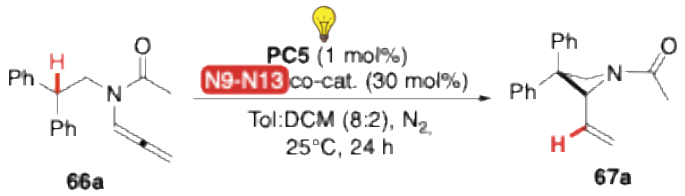

Entry[a]	N Co-cat. (30 mol%)	Conversion of **66a** [b] [%]	Yield of **67a** [b] [%]
30[c]	--	41	25
25	**N4**	>99	76
33	**N9**	78	64
34[c]	**N9**	>99	67
35	**N10**	72	46
36	**N11**	88	41
37	**N12**	>99	55
38	**N13**	>99	traces

Table 1h. Evaluation of the effect of stereo-electronic factors on the N co-catalysts N9-N13. [a] reactions performed using purple LEDs. [b] by ^{1}H NMR using 2,2'-dipyridine as internal standard. [c] reaction irradiated for 80 hours. Reactions performed with purple LEDs.

Two additional experiments using **PC5** and **PC6** were performed (Table 1i), but during their setup we did not perform the freeze-pump-thaw. The irradiation time required to consume **66a** was not affected by this modification when using **PC5** (entry 39, 24 hours required in both cases, monitored by TLC). On the contrary, a slower conversion of **66a** was observed using **PC6** (entry 40), suggesting that this complex is more sensitive to the presence of O_2 than **PC5**.

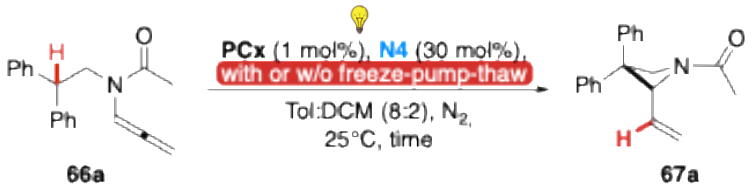

Entry[a]	**PC** cat. (1 mol%)	Time (h)	Conversion of **66a** [b] [%]	Yield of **67a** [b] [%]
26	**PC5**, $[Ir[dF(CF_3)ppy]_2(Me_4phen)]BF_4$	24	>99	76
39[c]	**PC5**, $[Ir[dF(CF_3)ppy]_2(Me_4phen)]BF_4$	24	>99	60
27	**PC6**, $Ir(d\text{-}F\text{-}ppy)_3$	14	>99	74
40[c]	**PC6**, $Ir(d\text{-}F\text{-}ppy)_3$	24	91	44

Table 1i. Evaluation of the effect of the freeze-pump-thaw step. [a] reactions performed using purple LEDs. [b] by ^1H NMR using 2,2'-dipyridine as internal standard. [c] without the freeze-pump-thaw step.

Note that for experiments performed with commercial Ir(III) complexes, whose E_T are too low (i.e. $E_{T(\mathbf{PC1})}$ = 58 kcal/mol) for the efficient sensitization of bi-naphthyl derivatives (i.e. $E_{T(\mathbf{N4})}$ = 57 kcal/mol), only the stabilizing LD interactions effect of the additive can be confirmed. While, for higher triplet-energy **PC**s (i.e. $E_{T(\mathbf{PC5})}$ = 63 kcal/mol, or $E_{T(\mathbf{PC6})}$ = 63.5 kcal/mol), the additional co-catalytic role of the **N4** bi-naphthyl additive could be addressed. The highest yield of **2a** was achieved combining **N4** and **PC5**, under purple LEDs irradiation for 24 hours (Table 1e, entry 16). The **PC5** complex has not been previously used in EnT methods despite its high E_T (63.0 kcal/mol),[67a] and long-lived triplet state (τ = 3.8 msec in MeCN).[67b]

With the optimized conditions in our hands, we then tested the scope of our reaction. Allenamides were prepared by sequential reductive amination, acylation and isomerization reactions. A large panel of azetidines **67a-v** could was efficiently synthesized. The scope of the reaction is depicted in Scheme 44.

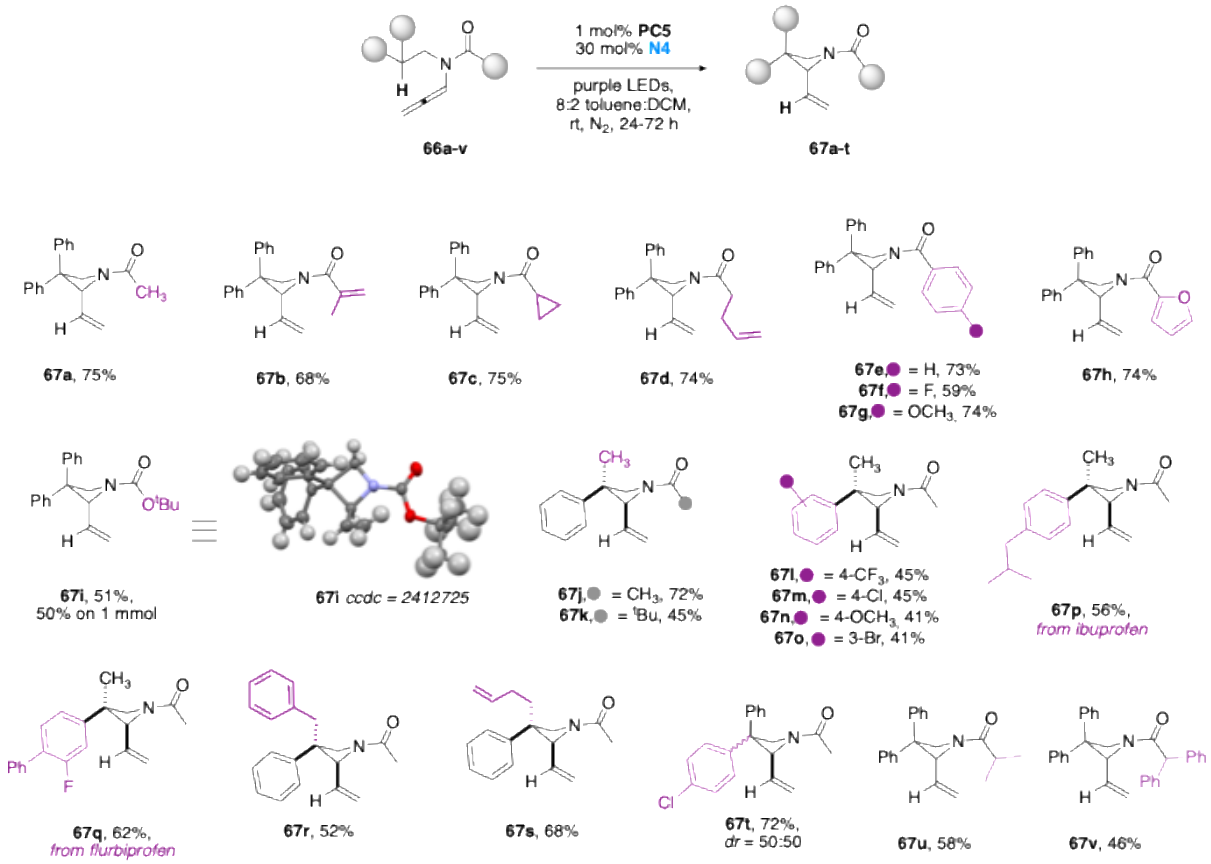

Scheme 44. Scope for the synthesis of α-vinyl azetidines.

When we replaced the acetyl unit of **67a** with a methacryloyl fragment, the azetidine product was accessed (**67b**) in a very slightly lower yield, but no polymerization was observed in our reaction conditions. The reaction also well tolerated a strained cyclopropyl substituent (**67c)** and terminal α-olefins (**67d**). Replacing the aliphatic amido- group with an (hetero)arylamide also did not hamper the reaction (**67e**-**h**). Higher yields were obtained with electron -neutral and -rich (hetero)aryl groups, and a slightly lower yield was observed with electron-poor systems. Our reaction still works when the amido group is replaced by a Boc-carbamate (**67i**); this product was then easily deprotected, delivering a versatile N-H azetidine. The product was isolated in a synthetically useful yield, and we also performed the same reaction scaling it up to 1 mmol. We then evaluated the variation at the position of the abstraction site. A tertiary C(sp^3)-H site, bearing one aryl substituent can still afford the desired product (**67j**) despite a higher BDE.[65] Indeed, in these cases, a bit longer irradiation times were required to reach full conversion of the starting material, and the steric hindrance of the acyl group seemed to play a more relevant role (**67k**). Products with substituents

on the aryl ring were obtained in moderate yields (**67l**-**67o**). Interestingly, with this approach we were also able to prepare an azetidine product with an Ar-Br group (**67o**), which could be useful for further functionalization. Substrates derived from ibuprofen and flurbiprofen delivered the desired products **67p**-**q** in good yields. Pendant benzyl groups and alkenes were also well tolerated (**67r**-**s**). A single diastereomer of products **67j**-**67s** was isolated, possibly due to the low stability of the other diastereomer during the purification procedures. We were also able to synthesize an azetidine product with two different aryls at the quaternary carbon (**67t**). Representative substrates **66b**, **c**, and **h** were also tested in the presence of **PC6** instead of **PC5**. As observed with **66a** (see Table 1f, entry 27), the irradiation time required to reach full conversion of the reagent was reduced, but a slight erosion of the yield occurred. Substrates with a secondary C(sp^3)-H did not afford the desired product, possibly due to their higher BDE, thus inevitably hampering the HAT step (limitations in the experimental section).[68]

To give proof of our mechanistic proposal, we performed Deuterium-labeling experiments. Irradiation of allenamide **66v**-*d* employing **PC5** and co-catalyst **N1**, allowed the formation of the deuterated azetidine **67v**-*d*. We observed the Deuterium shifting from the di-benzylic position of substrate **66v**-*d* to the vinylic site of product **67v**-*d*, in accordance with the proposed intramolecular 1,5-HAT event (Scheme 45).

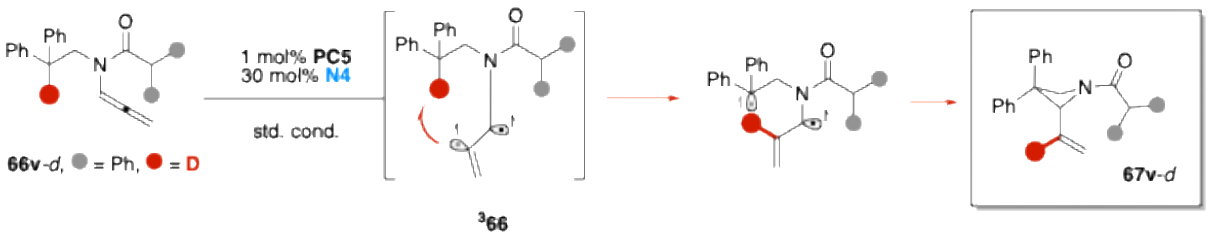

Scheme 45. Deuterium-labeling experiment.

We then demonstrated the catalytic role of **N4** by monitoring two parallel reactions through time by ^{1}H NMR (Scheme 46). The reaction rate for the formation of azetidine **67i** was clearly lower without **N4**.

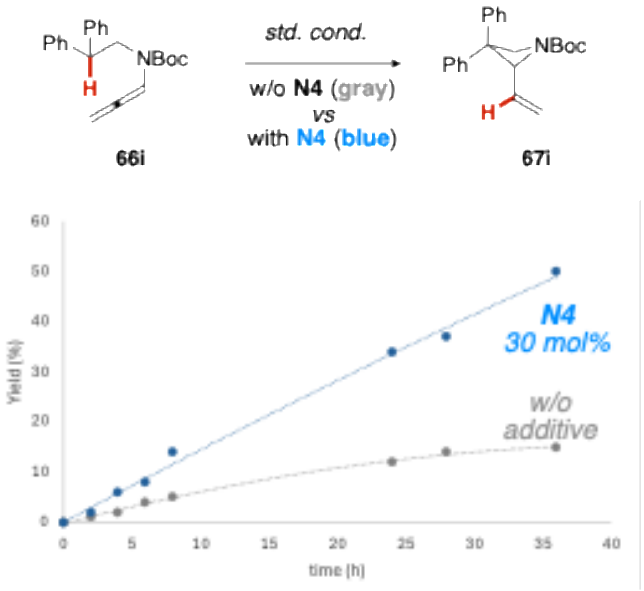

Scheme 46. Kinetic study proving the co-catalytic effect.

This effect can be explained by the proposed mechanism depicted in Scheme 47.

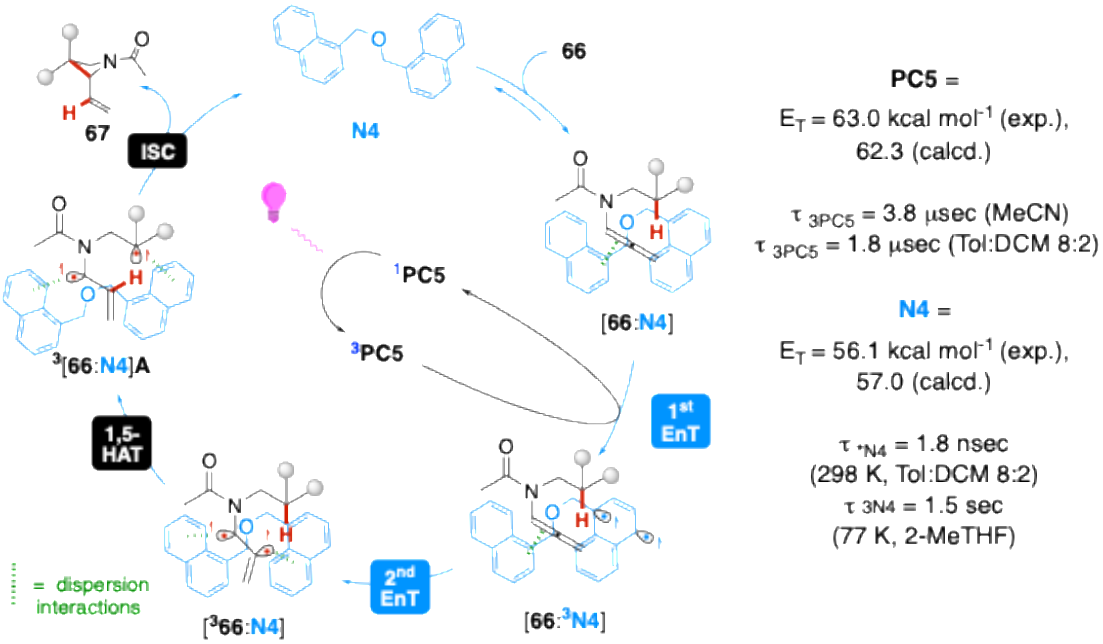

Scheme 47. Proposed mechanistic rationale.

Stabilizing π-π and C-H-π dispersion interactions[69,70] enable the formation of the ground state **[66:N4]** adduct. After that, two sequential EnTs would follow. The first EnT event is intermolecular, occurring between the photoexcited ^{3}**PC5** and ground state co-catalyst **N4**, giving **[66:^{3}N4]** intermediate. The second EnT is an intramolecular process, happening in the same adduct, between

^{3}**N4** and **66**, affording **[^{3}66:N4]** intermediate, that has a delocalized allylic mono-occupied molecular orbital and a reactive vinyl-radical site. This intermediate can efficiently undergo the 1,5-HAT process, delivering a more stable tertiary benzylic radical site intermediate **[^{3}66:N4]A** - in agreement with the results of the labelled substrate **66u**-*d* (Scheme 45). The azetidine ring is finally accessed through intersystem crossing *via* radical-radical recombination, allowing co-catalyst **N4** to turnover.

This rationale is supported by experimental and computational evidence; co-catalyst **N4** quenches ^{3}**PC5** much more efficiently than allenamide **66a** (K_{SV} = 5120 vs 346 mol^{-1}, respectively, Figure 8).

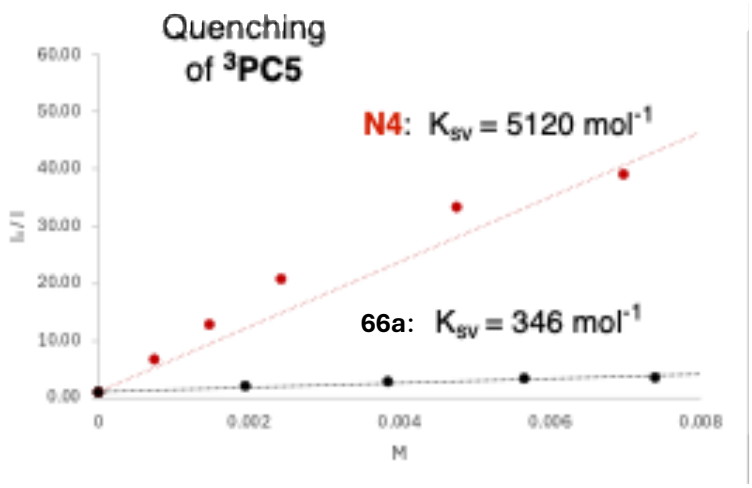

Figure 8. Phosphorescence quenching studies on **^{3}PC5.**

We measured the lifetime (τ) of ^{3}**PC5** in an 8:2 toluene/DCM solution at room temperature, and we found a value of 1.8 msec. Therefore, the calculated **PC5**-**66a** bimolecular quenching constant (k_q) is significantly smaller than that of **PC5**-**N4** (2.2 x 10^8 vs 3.2 x 10^9 L mol^{-1} sec^{-1}, respectively). These results suggest that an initial EnT may occur between the ^{3}**PC5** and the co-catalyst **N4**, and according to DFT data, this step is exergonic by 5.3 kcal mol^{-1}. The same trend was observed when quenching the luminescence of ^{3}**PC6**, for which we experimentally measured τ = 0.75 msec in an 8:2 toluene/DCM solution at room temperature. The **PC6**-**66a** bimolecular quenching constant (k_q) is more than one order of magnitude smaller than that of **PC6**-**N4** (3.9 x 10^8 vs 5.0 x 10^9 L mol^{-1} sec^{-1}, respectively).

^{3}**N4** and **66** would then undergo the second EnT process, affording the sensitized allenamide substrate. The phosphorescence of ^{3}**N4** was registered, employing 2-MeTHF as solvent at 77 K, and

we measured an E_T (0-0 band) of 56.1 kcal mol^{-1}, which is quite close to the calculated value of 57.0 kcal mol^{-1}. These results confirm that the EnT between **^{3}N4** and **66** is possible, and this step is also exergonic (the calculated E_T of substrates **66** were ca. 41 kcal mol^{-1} according to DFT data acquired at the M06/Def2-TZVP level, using toluene as implicit solvent and considering dispersion interactions *via* G3 corrections).

At 77 K, the lifetime of **^{3}N4** is very long (τ = 1.5 sec), suggesting that this additive acts as a powerful triplet-state reservoir.[71] Unfortunately, we were not able to directly measure the **^{3}N4-1a** EnT step *via* Stern-Volmer titration because we did not observe the phosphorescence decay of **^{3}N4** at room temperature (RT), in any solvent we tested. At RT, the emission spectrum of **N4** presents two fluorescence bands, with maxima at around 330 and 410 nm (Figure 9).

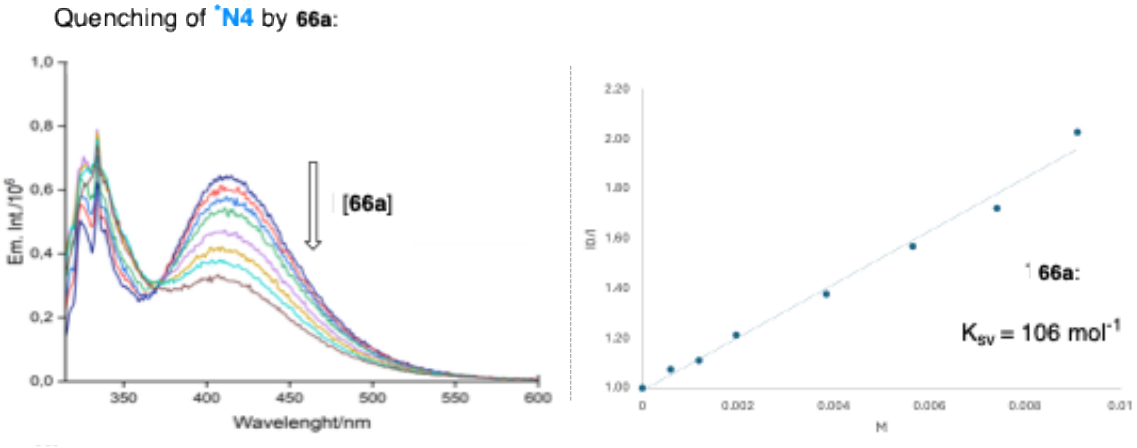

Figure 9. Luminescence quenching studies on **N4**.

The lifetimes at RT of these two emitting species were 6.7 and 1.8 nsec, respectively. The first luminescence band is characteristic of isolated 1-naphthyl groups while the second band was attributed to the emission of an excimer of **N4** in which the two aryl groups are in a closer interaction.[72] As observable in figure 9, the intensity of this band was linearly dependent on the addition of **66a** (K_{SV} = 106 mol^{-1}). We excluded static luminescence quenching between the chromophore and the substrate, as we did not observe shifts in the corresponding absorption and emission UV-vis spectra (spectra in the experimental section). For this reason, the linear correlation observed between the intensity of the excimer luminescence and the concentration of **66a** is an indication of a dynamic quenching. This, in turn, implies that the rate of decay of the excimer is slower than the ^{3}**N4-66a** EnT.[73] Having measured the lifetime of the **N4** excimer (τ = 1.8 nsec), the

calculated bimolecular ^{3}**N4-66a** quenching constant (k_q) is higher than 1.6 x 10^{10} L mol^{-1} sec^{-1}. The k_q values calculated for ^{3}**PC5-N4**, ^{3}**PC6-N4**, and ^{3}**N4-66a** EnTs are close to diffusion (10^9-10^{10} L mol^{-1} sec^{-1}), which is most often the ceiling rate of homogeneous chemical events.[74] These results strongly indicate that these reactions involve a first EnT between the **PC** and the **N** co-catalyst, followed by a second EnT event between the latter and the substrate **66** (Figure 10 summarizes the proposed kinetic scenario involving **PC5**, **N4** and **66a**).

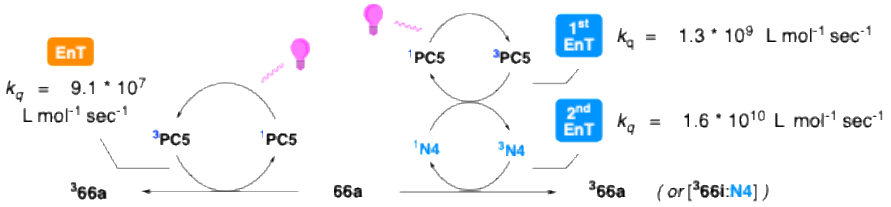

Figure 10. Comparison of the kinetic quenching constants supporting the EnT relay scenario.

A more efficient activation of challenging substrates - such as terminal allenamides - is ensured by this "triplet state relay" phenomenon, replacing a slower EnT (Scheme 43) with two faster EnT events. The ^{3}**N4-66** intramolecular EnT can occur *via* an encounter complex formation between ^{3}**N4** and the ground state substrate, taking advantage of the long lifetime of the former, acting as a EnT-reservoir. Alternatively, a supramolecular adduct **[66j:N4]** can form at the ground state, followed by the two aforementioned EnTs (Figure 10); the first one is an intermolecular event while the second becomes intramolecular in this case, bypassing concentration issues. Anyway, both cases lead to the formation of the key biradical intermediate of our reaction. According to DFT modeling data (Figure 11), the sensitization of the adduct **[66j:N4]** appears to be more likely because a stabilization of 4.1 kcal mol^{-1} in ΔG of the adduct compared to the corresponding isolated species (**66j** and **N4**) was calculated. This putative complexation was also confirmed by ^{1}H-NMR titration (spectra in the experimental section).

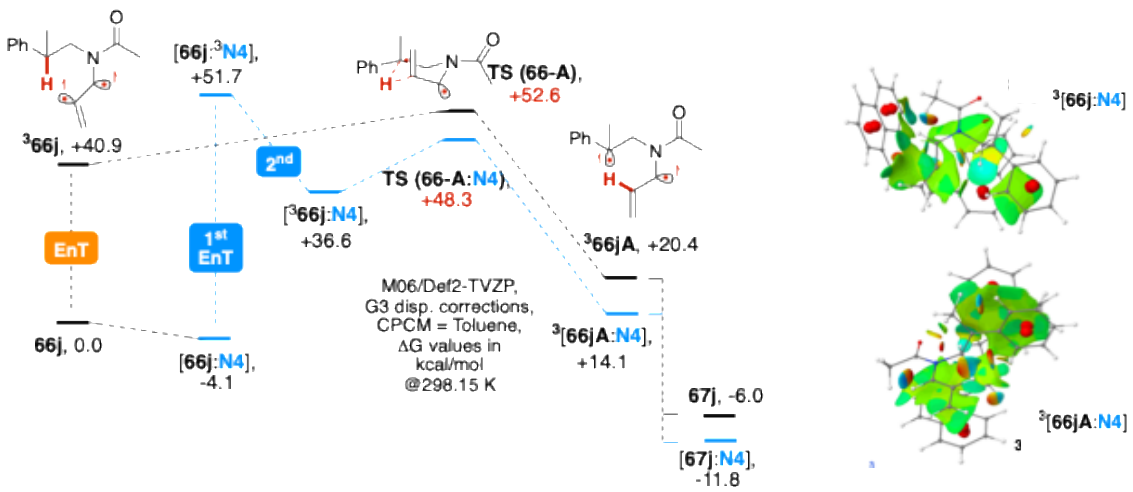

Figure 11. DFT modeling data with NCI plot of key intermediates, color code: green basins for dispersion interactions, red spheres for ring critical points, orange/blue lobes for destabilizing steric interactions.

In addition to the described role in the more efficient substrate activation, the **N** co-catalysts allows the formation of products through energetically favored pathways (blue vs black paths for the complexed vs isolated manifolds, respectively, Figure 11). For **67j**, a stabilization of 4.3 kcal mol^{-1} for the transition state was calculated, and **^{3}[66j:N4]A** is more stable than 6.3 kcal mol^{-1} compared to the separate species **^{3}66jA** and **N4**. This stabilizing effect is ensured by the formation of dispersion interactions between the π-clouds of co-catalyst **N4** and the mono-occupied molecular orbitals (green basins in the Non-Covalent-Interactions plots[75]).

The role of dispersion interactions between mono-occupied orbitals and the π-clouds of naphthyl groups has been described by recent DFT studies on alkene-alkene [2+2][76] and dearomative [4+2] cycloadditions.[61c] In this reactivity, the formation of adducts with the **N** co-catalyst finds an additional experimental support.

The derivatization of α-vinyl azetidines[59] **67** was used to extend the accessible chemical space with our methodology (Scheme 48).

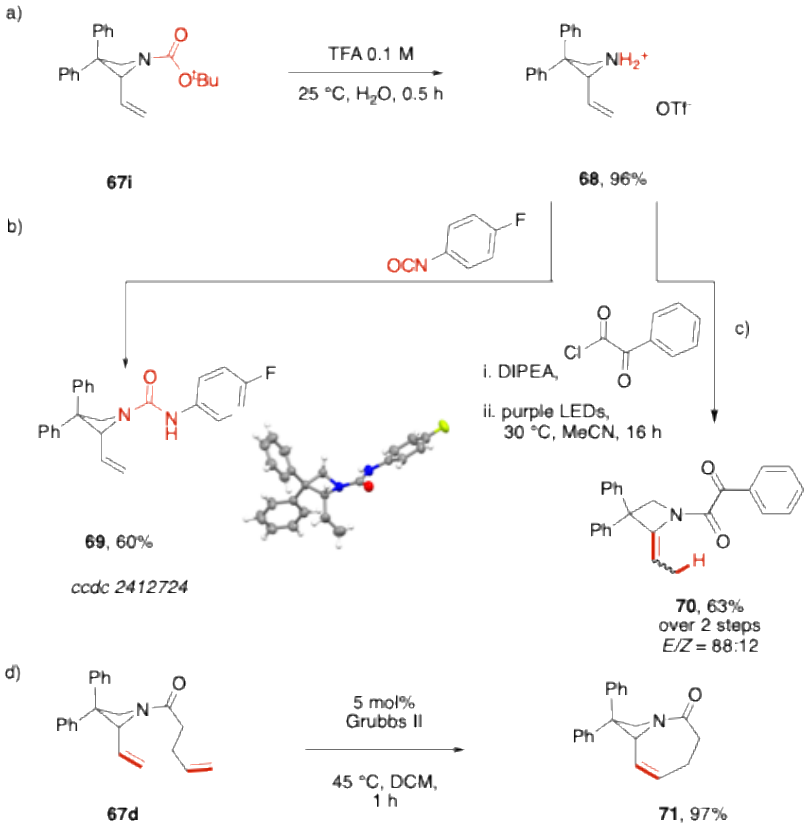

Scheme 48. Representative model derivatizations of vinyl-azetidines.

The carbamate group of **67i** could be easily deprotected, delivering the NH-free azetidine **68** with an excellent yield (Scheme 48a), which has many further applications (Scheme 41)[59] as it can be derivatized with electrophiles. For instance, the treatment with an isocyanate gives urea **69** (Scheme 48b); the treatment with phenylglyoxyl chloride allowed us to perform an additional a visible-light-promoted reaction, which is a formal allylic isomerization[77] (Scheme 48c) to afford a valuable[62b] vinylidene-azetidine with two contiguous quaternary carbons (**70**). Finally, ring-closing methathesis on azetidine **67d** gave access to a fused bicyclic product **71**, featuring a prized headbridging nitrogen nucleus[53b] in an excellent yield (Scheme 48d).

2.3 Conclusions

In this chapter, a simple visible light-promoted preparation of densely functionalized monocyclic azetidines with a valuable allylamine unit from allenamides was described. A double EnT mechanism gives access to these strained saturated heterocycles at room temperature and with wide functional group tolerance. This original 1,5-HAT/cyclization sequence exploits the reactivity of a vinyl-radical site, which was photo-generated with an atom-economical strategy. The method combines a high triplet-energy Ir(III) photosensitizer - which was not previously employed in EnT-promoted reactions - with a binaphthyl co-catalyst, which has a dual role of stabilizing the reaction intermediates with its π-clouds, as well as providing a more efficient substrate activation by relaying two EnT cycles.

2.4 Experimental section

General remarks

All the chemicals whereby the syntheses are not reported here after were purchased from commercial sources and used as received. Solvents were dried passing through alumina columns using an Inert® system and were stored under nitrogen. Chromatographic purifications were performed under gradient using a Combiflash® system and prepacked disposable silica cartridges or through isocratic flash chromatography using commercial 60 Å silica gel. All reactions that required heating were performed with the use of high-vacuum grade silicon oil.

Present visible light promoted reactions required the use of degassed solvents as the presence of molecular oxygen exerts a negative effect on their rate. Reactions promoted by visible light were performed into standard 5 mm NMR tubes, which were placed inside a 500 mL glass beaker equipped with a commercial strip of 300 RGB household LEDs (12V, 14W) on its internal surface. The temperature of the tubes was checked with a thermometer. During warmer seasons, cooling was ensured by two fans recovered by outdated PCs to avoid overheating due to LEDs emission.

^{1}H and ^{13}C NMR spectra were recorded at 300 K on a Bruker 400 MHz or a Jeol 600 MHz spectrometers using residual non-deuterated solvents as internal standards (7.26 ppm for ^{1}H NMR and 77.00 ppm for ^{13}C-NMR for $CDCl_3$, 2.05 ppm for ^{1}H NMR and 29.84 ppm for ^{13}C NMR for acetone-d6). ^{19}F-NMR spectra were recorded in $CDCl_3$ at 298 K on a Jeol 600 spectrometer fitted with a BBFO probe head at 565 MHz. The terms m, s, d, t, q and quint represent multiplet, singlet, doublet, triplet, quadruplet and quintuplet respectively, and the term br and h mean respectively a broad signal and a heptuplet. Reported assignments were based on decoupling, COSY, NOESY, HSQC and HMBC correlation experiments.

Mass analyses were recorded on an Infusion Water Acquity Ultra Performance LC HO6UPS-823M instrument equipped with a SQ detector (Electrospray source); high-resolution mass analyses were recorded on a LTQ ORBITRAP XL Thermo Mass Spectrometer (Electrospray source).

Single crystal Data were collected with a Bruker D8 diffractometer equipped with PhotonII area detector, using a CuKα or a MoKα microfocus 4 radiation source. The data collection strategy covered

the sphere of reciprocal space. Absorption corrections were applied using the program SADABS. The structure was solved with the SHELXT code. Fourier analysis and refinement were performed by the full-matrix least-squares methods based on F2 using SHELXL-2014 as implemented in Olex2. All the nonH atoms were refined with anisotropic displacement parameters.

CCDC 2412724 and 2412725 contain supplementary crystallographic data for compounds **69** and **67i**.

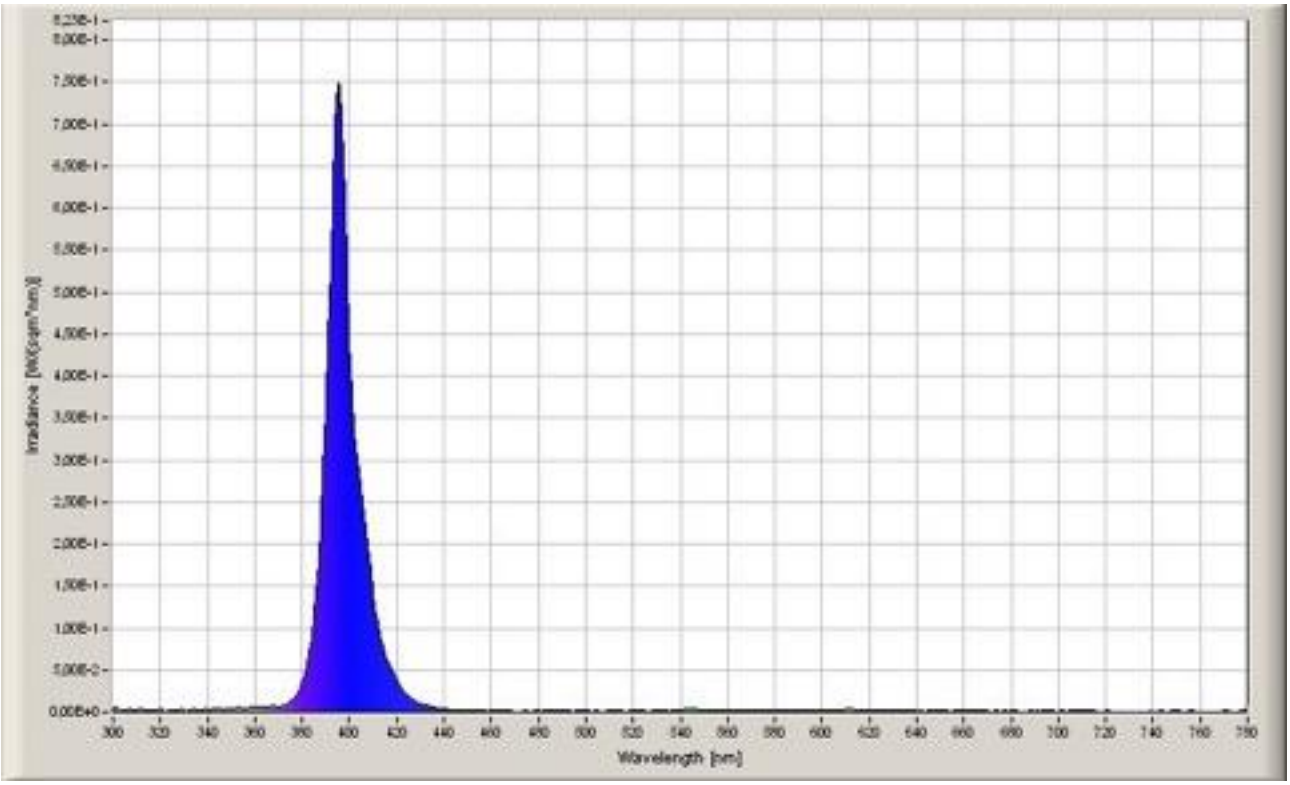

Measured emission spectrum of the purple LEDs used in this study.

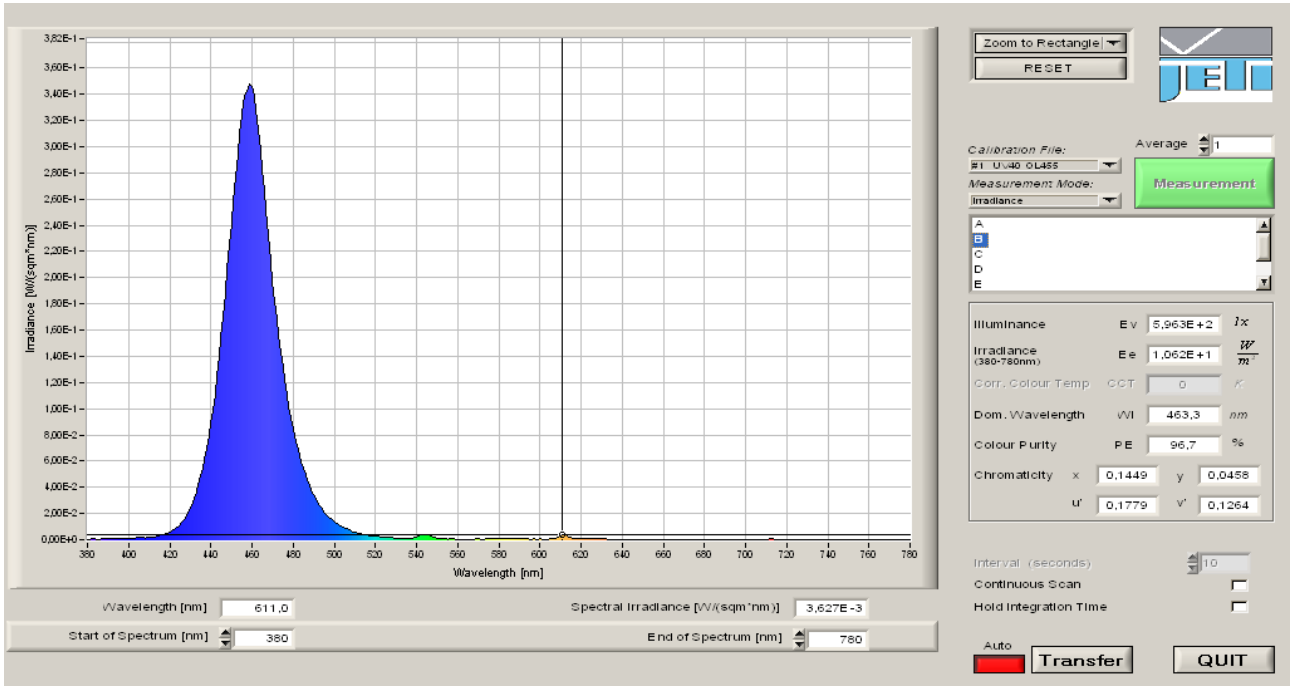

Measured emission spectrum of the blue LEDs used in this study.

Left: representative setup using blue LEDs; right: setup using purple LEDs.

Synthesis of substrates and photocatalysts

General procedure A:

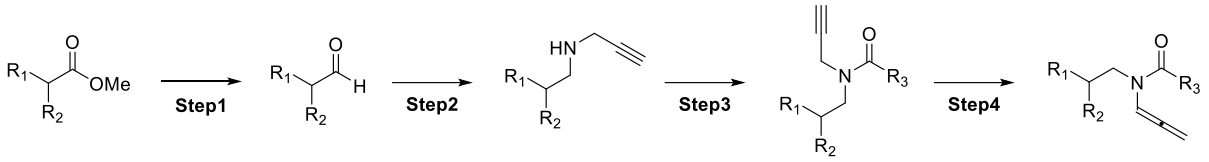

Step 1: To a solution of methyl diphenylacetate (1 equiv.) in dry DCM (0.2 M) at -78 °C, a DIBAL-H solution (1.0 M in toluene, 1 equiv.) was added dropwise over 15 minutes. The resulting solution was stirred for one hour at the same temperature and then the reaction was quenched with a Rochelle salt saturated aqueous solution. The resulting biphasic mixture was kept under vigorous stirring and allowed to warm to room temperature, then separated and the aqueous phase was extracted three times with DCM. The organic phase was then dried over Na_2SO_4, filtered and concentrated in vacuo. The crude product was used without further purification for **Step 2**.

Step 2: To the solution of the crude aldehyde (1 equiv.) in MeOH (0.1 M), freshly distilled propargyl amine (1 equiv.) was added. The resulting mixture was stirred for 3 hours at room temperature, after which $NaBH_4$ (2.5 equiv.) was added portion wise at 0 °C. The reaction was stirred for one hour at room temperature and then quenched with water. The organic solvent was removed under reduced pressure, and the residue was extracted three times with DCM. The organic phase was then dried over Na_2SO_4, filtered and concentrated under reduced pressure. The crude product was used without further purification for **Step 3**.

Step 3: To the solution of the crude amine (1 equiv.) in dry DCM (0.25 M) TEA (1.5 equiv.) and DMAP (0.02 equiv.) were added, then the correspondent acyl chloride was added dropwise (1.1 equiv.) at 0 °C. The resulting solution was kept under vigorous stirring overnight at rt. The reaction was then quenched with a saturated NH_4Cl aqueous solution and then extracted three times with DCM. The organic phase was then dried over Na_2SO_4, filtered and concentrated under reduced pressure. The crude product was purified by chromatography on silica gel (*n*-hexane/EtOAc gradient) to afford the correspondent propargyl amide.

Step 4: The desired propargyl amide (1 equiv.) was dissolved in dry toluene (0.20 M) in a round-bottom two-necked flask equipped with a magnetic stirring bar. Then under N_2 atmosphere, *t*-BuOK (0.2 equiv.) was added, and the resulting mixture was stirred at room temperature for 10 - 15

minutes. After complete conversion as monitored by TLC, 5 mL of saturated NH_4Cl aqueous solution was added. The mixture was sequentially extracted with EtOAc (3 x 15 mL), the organic layers separated and dried over Na_2SO_4. The solution was concentrated under reduced pressure and the crude purified by chromatography on silica gel (*n*-hexane/EtOAc gradient) to afford the corresponding allenamide.

Note: sometimes 0.2 equiv. of t-BuOK were not sufficient to achieve full conversion of the starting material. In these cases, additional portions of the base were added until complete isomerization occurred, as monitored by TLC.

Synthesis of PC5

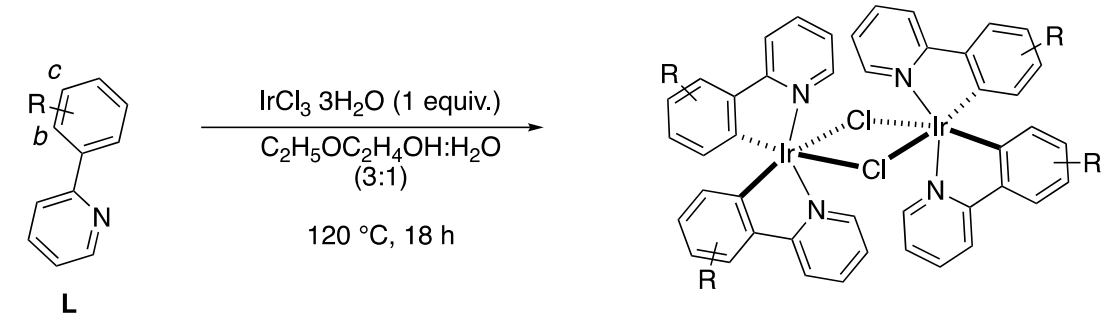

L = 2-(2,4-difluorophenyl)-5-(trifluoromethyl)pyridine

The Iridium dimer was synthetized adapting a literature procedure by Sun (*RSC Adv.* ***2016****, 6, 41214*). Iridium (III) chloride hydrate (200 mg, 0.63 mmol, 1 equiv.) and **L** (334 mg, 1.30 mmol, 2.05 equiv.) were placed in a sealed Schlenk, equipped with a stirring bar, under a nitrogen atmosphere. A degassed 2:1 solution of 2-ethoxyethanol and water (12 mL) was added, the mixture was stirred at 120 °C for 48 h and then cooled to room temperature. Water was added (10 mL) and the resulting mixture stirred for 0.5 h. The resulting yellow precipitate was filtered under vacuum, washed with water and hexane, and finally dried under reduced pressure affording the pure dimer as a yellow solid (341 mg, 0.23 mmol, 72% yield), which was used without further purification.

^{1}H NMR (600 MHz, $CDCl_3$) δ 9.51 (s, 4H), 8.46 (dd, *J* = 8.7, 2.9 Hz, 4H), 8.04 (dd, *J* = 8.7, 2.2 Hz, 4H), 6.43 (ddd, *J* = 12.4, 8.8, 2.3 Hz, 4H), 5.07 (dd, *J* = 8.8, 2.3 Hz, 4H). *Data consistent with the literature.*

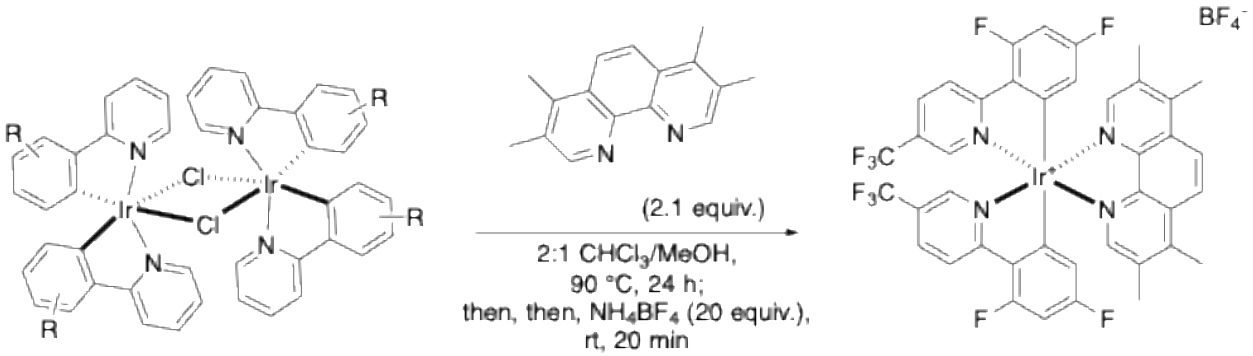

L = 2-(2,4-difluorophenyl)-5-(trifluoromethyl)pyridine

PC5

The heteroleptic Iridium complex **PC5** was synthetized adapting a literature procedure by Böttcher (*Inorg. Chim. Acta* ***2021****, 527, 120554*). To a vial equipped with a stirring bar, the Iridium dimer (1 equiv.) and the desired bidentate *N-N'* ligand (2.2 equiv.) were charged under nitrogen. A degassed

solution of $CHCl_3$ and MeOH (0.005 M, 2:1 v/v) was added, and the resulting mixture was stirred at 90 °C for 24 hours. After cooling the solution to room temperature, NH_4BF_4 (20 equiv.) was added. The mixture was stirred for further 20 minutes. Solvents were removed under reduced pressure and the crude product was purified by chromatography on silica gel (DCM:MeOH 30:1 to 9:1). Yellow crystalline solid (70 mg, 86% yield).

^{1}H NMR (400 MHz, CD_2Cl_2) δ 8.56 (dd, *J* = 8.8, 3.1 Hz, 2H), 8.45 (s, 2H), 8.15 – 8.05 (m, 2H), 8.04 (s, 2H), 7.54 – 7.44 (m, 2H), 6.76 (ddd, *J* = 12.5, 9.1, 2.3 Hz, 2H), 5.86 (dd, *J* = 8.1, 2.3 Hz, 3H), 2.93 (s, 6H), 2.51 (s, 6H). **^{13}C NMR** (101 MHz, CD_2Cl_2) δ 168.1 (d, *J* = 7.3 Hz), 166.2 (d, *J* = 12.6 Hz), 164.0 (d, *J* = 12.9 Hz), 163.6 (d, *J* = 12.7 Hz), 161.4 (d, *J* = 13.2 Hz), 154.4 (d, *J* = 7.1 Hz), 151.3, 148.4, 145.0 (d, *J* = 4.8 Hz), 144.8, 136.4 (d, *J* = 37.6 Hz), 130.5, 126.6, 125.8, 125.5, 124.9, 123.9 (d, *J* = 21.0 Hz), 123.0, 120.3, 114.5 (dd, *J* = 17.8, 3.1 Hz), 99.9 (t, *J* = 26.8 Hz), 18.0, 15.2. **^{19}F NMR** (565 MHz, CD_2Cl_2) δ -63.2, -99.2 – -104.1 (m), -106.2 (td, *J* = 12.4, 3.3 Hz), -153.2. **ESI-HRMS** calcd for $C_{40}H_{26}F_{10}IrN_4^+$ [M-BF_4]$^+$ 945.1621, found 945.1630. *Data consistent with the literature (Inorganica Chim. Acta, **2021**, 527, 120554).*

Synthesis of PC6

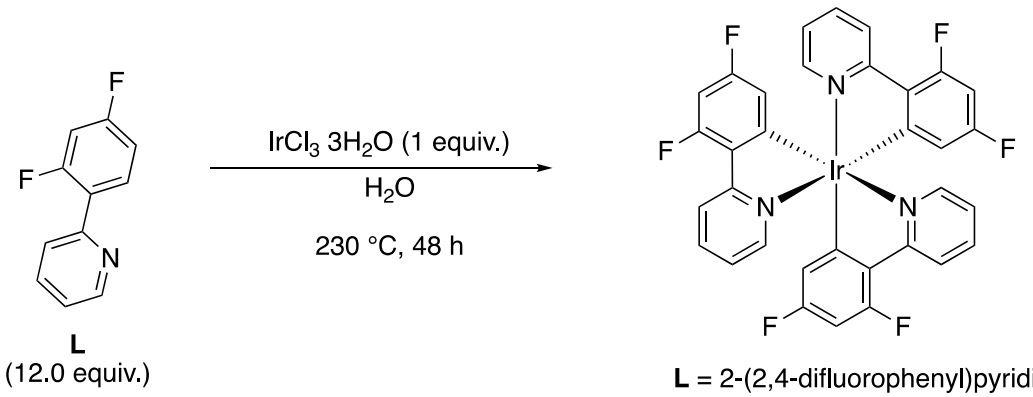

The homoleptic Iridium complex **PC6** was synthetized adapting a literature procedure (Organic Synth. **2018**, 95, 29-45). Iridium (III) chloride hydrate (65 mg, 0.20 mmol, 1.0 equiv.) and **L** (466 mg, 2.44 mmol, 12.0 equiv.) were added to a 45 mL autoclave. Distilled water (42 mL, 0.005 M) was bubbled with nitrogen for 15 minutes and then was added to the autoclave, which was immediately sealed. The reaction mixture was heated at 230 °C for 48 hours. The reactor was then allowed to cool to room temperature. After cooling, the reactor was opened revealing an insoluble yellow solid

that was dispersed on the surfaces and in the aqueous phase. The content of the autoclave was transferred to a separatory funnel. The interior of the reactor was mechanically scraped to extract the yellow solid, with metal tongs, cotton balls and drops of dichloromethane; all the recovered contents were added to the separatory funnel. The aqueous phase was extracted with DCM (3 x 20 mL). The combined organic layers were washed with HCl 1M (3 x 20 mL), dried over Na_2SO_4 and concentrated under reduced pressure. The crude was purified by column chromatography on silica gel (DCM) to afford the Iridium complex **PC6** as a bright yellow solid (85 mg, 0.11 mmol, 56% yield).

^{1}H NMR (600 MHz, $CDCl_3$) δ 8.32 – 8.29 (m, 3H), 7.70 – 7.67 (m, 3H), 7.46 – 7.45 (m, 3H), 6.93 (ddd, *J* = 7.1, 5.6, 1.1 Hz, 3H), 6.40 (ddd, *J* = 12.9, 9.0, 2.4 Hz, 3H), 6.26 (dd, *J* = 9.1, 2.4 Hz, 3H). *Data consistent with the literature*.

Synthesis of PC7

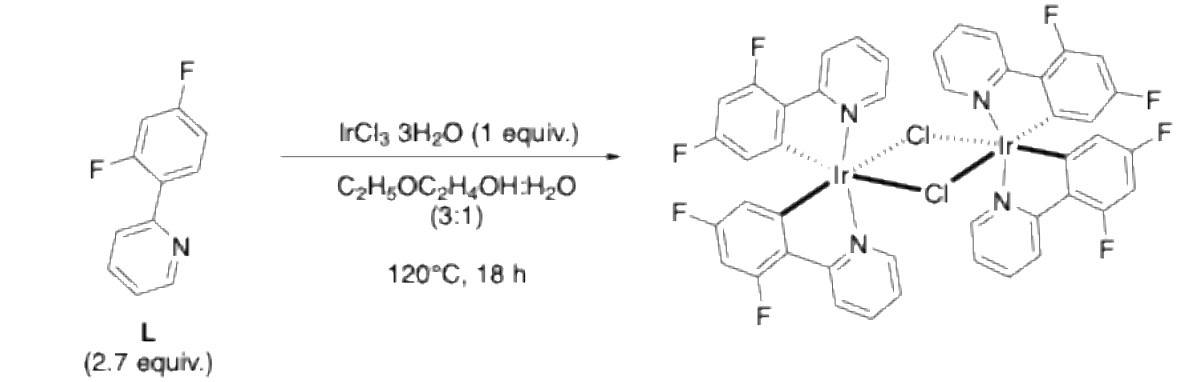

L = 2-(2,4-difluorophenyl)pyridine

The Iridium dimer was synthetized following a literature procedure (*Chem. Eur. J.* **2025**, 31, e202403309). Iridium (III) chloride hydrate (200 mg, 0.63 mmol, 1.0 equiv.) and **L** (325 mg, 1.70 mmol, 2.7 equiv.) were placed in a sealed Schlenk, equipped with a magnetic stirring bar, under nitrogen atmosphere. A degassed 3:1 solution of 2-ethoxyethanol and water (12 mL) was added, the mixture was stirred at 120 °C for 18 hours, and then let cool down to room temperature. Water was added (10 mL) and the resulting mixture was stirred for 30 minutes, during which a yellow solid started to precipitate. The yellow precipitate was filtered under vacuum, washed with water and hexane, and eventually dried under reduced pressure affording the pure dimeric complex (280 mg, 0.23 mmol, 72% yield), which was used without further purification.

^{1}H NMR (600 MHz, $CDCl_3$) δ 9.12 (d, *J* = 5.6 Hz, 1H), 8.31 (d, *J* = 8.0 Hz, 1H), 7.83 (t, *J* = 7.9 Hz, 1H), 6.83 (t, *J* = 6.5 Hz, 1H), 6.34 (t, *J* = 10.5 Hz, 1H), 5.29 (d, *J* = 10.2 Hz, 1H). *Data consistent with literature.*

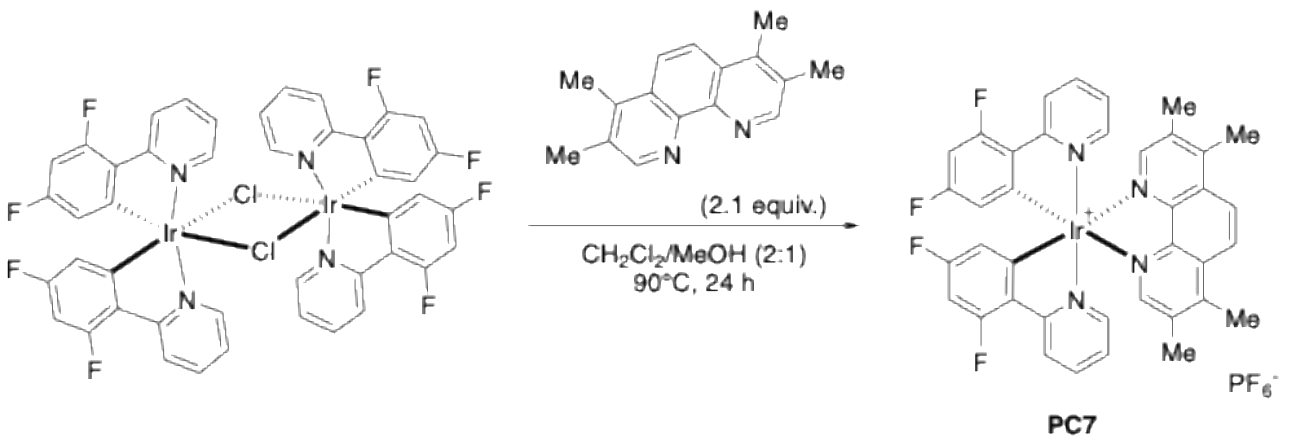

PC7

The heteroleptic iridium complex **PC7** was synthesized adapting a reported literature procedure (*Chem. Eur. J.* **2025**, 31, e202403309). The Iridium dimer (1.0 equiv.) and the bidentate *N*,*N'* ligand 3,4,7,8-tetramethyl-1,10-phenanthroline (2.1 equiv.) were placed in a sealed vial, equipped with a stirring bar, under nitrogen atmosphere. A mixture of $CHCl_3$ and MeOH (2:1, 0.005M), previously degassed by bubbling nitrogen for ca 15 minutes was added, and the resulting solution was stirred at 90 °C for 24 hours. The solution was let cool down to room temperature, NH_4PF_6 (20 equiv.) was added, and the mixture was kept under stirring for 1 hour. Solvents were removed under reduced pressure and the crude product was purified by column chromatography on silica gel (DCM/MeOH 30:1 to 9:1) affording **PC7** as a yellow solid (61 mg, 86% yield).

^{1}H NMR (600 MHz, ACN-d_3) δ 8.35 (s, 2H), 8.28 (d, *J* = 8.4 Hz, 2H), 8.00 (s, 2H), 7.83 – 7.78 (m, 2H), 7.42 – 7.38 (m, 2H), 6.90 – 6.84 (m, 2H), 6.68 (ddd, *J* = 12.0, 9.5, 2.3 Hz, 2H), 5.79 (dd, *J* = 8.6, 2.3 Hz, 2H), 2.79 (s, 6H), 2.36 (s, 6H). *Data consistent with literature* (*Inorg. Chim. Act.,* **2021**, 527, 120554).

Characterization of substrates for the synthesis of azetidines

N-(2,2-diphenylethyl)-*N*-(propa-1,2-dien-1-yl)acetamide

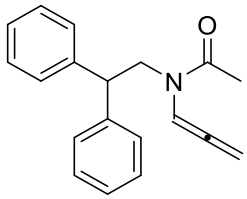

Allene **66a** was prepared following general procedure **GP-A** from the corresponding propargyl amide (277 mg, 1 mmol). White solid (205 mg, 74% yield). Two rotamers were observed due to the dynamic amide group (54:46 mixture of rotamers).

^{1}H NMR (400 MHz, $CDCl_3$) δ 7.58 (t, *J* = 6.5 Hz, 1H RotB), 7.33 – 7.19 (m, 10H RotA, 10H RotB), 6.45 (t, *J* = 6.2 Hz, 1H RotA), 5.32 (t, *J* = 6.2 Hz, 2H RotA, 2H RotB), 4.50 (t, *J* = 8.2 Hz, 1H RotA), 4.36 (t, *J* = 7.4 Hz, 1H RotB), 4.15 (d, *J* = 8.1 Hz, 2H RotA), 4.02 – 4.00 (m, 2H RotB), 2.05 (s, 3H RotA), 1.50 (s, 3H RotB). **^{13}C NMR** (101 MHz, $CDCl_3$) δ 202.2 (RotB), 201.5 (RotA), 169.3 (RotB), 168.7 (RotA), 142.0 (2C RotA), 141.6 (2C RotB), 128.8 (4C RotB), 128.54 (4C RotA), 128.46 (4C RotB), 128.4 (4C RotA), 127.2 (2C RotB), 126.7 (2C RotA), 101.1 (RotA), 98.1 (RotB), 87.2 (RotB), 86.8 (RotA), 52.2 (RotB), 48.4 (RotA), 48.2 (RotA), 48.1 (RotB), 22.1 (RotA), 21.2 (RotB). **ESI-HRMS** calcd for $C_{19}H_{20}NO$ $[M+H]^+$ 278.1467, found 278.1473.

N-(2,2-diphenylethyl)-*N*-(propa-1,2-dien-1-yl)methacrylamide

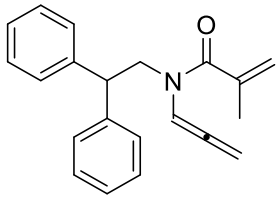

Allene **66b** was prepared following general procedure **GP-A** from the corresponding propargyl amide (303 mg, 1 mmol). Vanilla solid (152 mg, 50% yield).

^{1}H NMR (400 MHz, $CDCl_3$) δ 7.33 – 7.29 (m, 8H), 7.27 – 7.22 (m, 2H), 6.79 (br, 1H), 5.42 (d, *J* = 6.3 Hz, 2H), 5.17 (s, 1H), 4.80 (s, 1H), 4.62 – 4.58 (m, 1H), 4.25 (d, *J* = 8.3 Hz, 2H), 1.82 (s, 3H). **^{13}C NMR** (101 MHz, $CDCl_3$) δ 200.3, 170.6, 141.6 (2C), 139.9, 128.6 (4C), 128.4 (4C), 126.8 (2C), 117.4, 101.9, 87.1, 48.2, 47.3, 20.1. **ESI-HRMS** calcd for $C_{21}H_{21}NO$ $[M+H]^+$ 304.1701, found 304.1706.

***N*-(2,2-diphenylethyl)-*N*-(propa-1,2-dien-1-yl)cyclopropanecarboxamide**

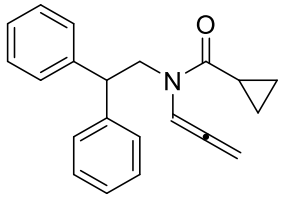

Allene **66c** was prepared following general procedure **GP-A** from the corresponding propargyl amide (303 mg, 1 mmol). Pale yellow oil (212 mg, 70% yield). Two rotamers were observed due to the dynamic amide group (53:47 mixture of rotamers).

^{1}H NMR (400 MHz, $CDCl_3$) δ 7.58 (t, *J* = 6.5 Hz, 1H RotA), 7.36 – 7.23 (m, 10H RotA. 10H RotB), 6.85 (t, *J* = 6.2 Hz, 1H RotB), 5.36 (d, *J* = 6.2 Hz, 2H RotB), 5.32 (d, *J* = 6.5 Hz, 2H RotA), 4.56 (t, *J* = 8.1 Hz, 1H RotB), 4.46 (t, *J* = 7.5 Hz, 1H RotA), 4.27 (d, *J* = 7.5 Hz, 2H RotA), 4.22 (d, *J* = 8.2 Hz, 2H RotB), 1.74 (tt, *J* = 8.3, 4.7 Hz, 1H RotB), 1.34 (tt, *J* = 8.2, 4.6 Hz, 1H RotA), 0.93 (dd, *J* = 4.6, 2.8 Hz, 2H RotB), 0.83 – 0.81 (m, 2H RotA), 0.77 (dd, *J* = 7.9, 3.2 Hz, 2H RotB), 0.52 (dt, *J* = 7.7, 3.5 Hz, 2H RotA). **^{13}C NMR** (101 MHz, $CDCl_3$) δ 202.1 (RotB), 202.0 (RotA), 172.2 (RotA), 171.7 (RotB), 142.0 (2C RotB), 141.7 (2C RotA), 128.7 (4C RotA), 128.53 (4C RotB), 128.46 (4C RotA), 128.3 (4C RotB), 127.0 (2C RotA), 126.6 (2C RotB), 100.5 (RotB), 99.0 (RotA), 87.1 (RotA), 86.4 (RotB), 50.9 (RotA), 48.9 (RotB), 48.8 (RotA), 48.5 (RotB), 12.0 (RotB), 11.6 (RotA), 8.6 (2C RotA), 7.8 (2C RotB). **ESI-HRMS** calcd for $C_{21}H_{21}NO$ M+H]$^+$ 304.1701, found 304.1705.

***N*-(2,2-diphenylethyl)-*N*-(propa-1,2-dien-1-yl)pent-4-enamide**

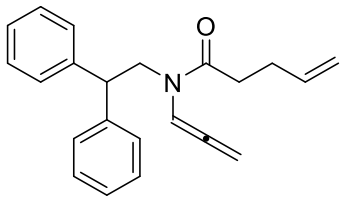

Allene **66d** was prepared following general procedure **GP-A** from the corresponding propargyl amide (317 mg, 1 mmol). Light-yellow oil (155 mg, 49% yield). Two rotamers were observed due to the dynamic amide group (61:39 mixture of rotamers).

^{1}H NMR (600 MHz, $CDCl_3$) δ 7.60 (t, *J* = 6.5 Hz, 1H RotB), 7.30 (t, *J* = 7.5 Hz, 3H RotA, 3H RotB), 7.25 – 7.16 (m, 7H RotA, 7H RotB), 6.48 (t, *J* = 6.2 Hz, 1H RotB), 5.73 (ddt, *J* = 16.8, 10.2, 6.4 Hz, 1H RotA), 5.56 (ddt, *J* = 16.9, 10.3, 6.6 Hz, 1H RotB), 5.32 – 5.31 (m, 2H RotA, 2H RotB), 4.99 – 4.93 (m, 2H RotA), 4.88 – 4.83 (m, 2H RotB), 4.49 (t, *J* = 8.2 Hz, 1H RotA), 4.35 (t, *J* = 7.4 Hz, 1H RotB), 4.16 (d, *J* = 8.2 Hz, 2H RotA), 4.01 (d, *J* = 7.4 Hz, 2H RotB), 2.37 – 2.35 (m, 2H RotA), 2.28 – 2.24 (m, 2H RotA),

2.06 – 2.02 (m, 2H RotB), 1.75 – 1.73 (m, 2H RotB). **^{13}C NMR** (151 MHz, $CDCl_3$) δ 202.25 (RotB), 201.72 (RotA), 170.99 (RotB), 170.58 (RotA), 141.92 (2C RotB), 141.64 (2C RotA), 137.39 (RotA), 137.27 (RotB), 128.76 (4C RotB), 128.55 (4C RotA), 128.47 (4C RotB), 128.38 (4C RotA), 127.14 (2C RotB), 126.69 (2C RotA), 115.34 (RotA), 115.15 (RotB), 100.33 (RotA), 98.32 (RotB), 87.11 (RotB), 86.60 (RotA), 51.14 (RotB), 48.53 (RotA), 48.42 (RotA), 48.13 (RotB), 33.05 (RotA), 32.24 (RotB), 28.95 (RotA), 28.91 (RotB). **ESI-HRMS** calcd for $C_{22}H_{24}NO$ $[M+H]^+$ 318.1858, found 318.1856.

***N*-(2,2-diphenylethyl)-*N*-(propa-1,2-dien-1-yl)benzamide**

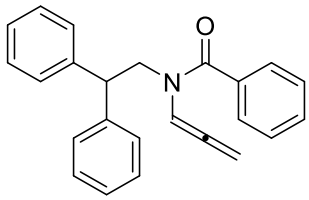

Allene **66e** was prepared following general procedure **GP-A** from the corresponding propargyl amide (339 mg, 1 mmol). Light-orange solid (173 mg, 51% yield).

^{1}H NMR (400 MHz, $CDCl_3$) δ 7.37 – 7.31 (m, 10H), 7.25 – 7.21 (m, 3H), 7.16 – 7.13 (m, 2H), 6.49 – 6.46 (m, 1H), 5.36 – 5.34 (m, 2H), 4.68 (t, *J* = 8.0 Hz, 1H), 4.35 (d, *J* = 8.4 Hz, 2H). **^{13}C NMR** (101 MHz, $CDCl_3$) δ 200.2, 169.7, 141.7 (2C), 135.2, 130.2, 128.6 (4C), 128.5 (4C), 127.7 (2C), 126.9 (4C), 102.7, 87.2, 67.2, 48.4. **ESI-HRMS** calcd for $C_{24}H_{21}NO$ $[M+H]^+$ 340.1623, found 340.1627.

***N*-(2,2-diphenylethyl)-4-fluoro-*N*-(propa-1,2-dien-1-yl)benzamide**

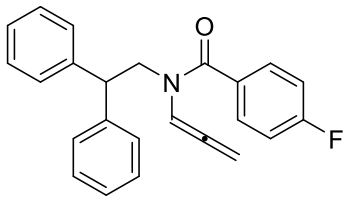

Allene **66f** was prepared following general procedure **GP-A** from the corresponding propargyl amide (357 mg, 1 mmol). Yellow oil (286 mg, 80% yield). Broad peaks observed due to the fluxionality of the allene observed.

^{1}H NMR (400 MHz, $CDCl_3$) δ 7.37 – 7.13 (m, 14H), 6.45 (br, 1H), 5.39 – 5.38 (m, 2H), 4.67 (br, 1H), 4.34 (br, 2H). **^{13}C NMR** (101 MHz, $CDCl_3$) δ 200.3, 168.8, 163.7 (d, *J* = 250.7 Hz), 141.6 (2C), 131.2 (d, *J* = 3.5 Hz, 2C), 130.1, 128.5 (8C), 126.9 (2C), 115.5 (d, *J* = 21.8 Hz, 2C), 102.6, 87.3,66.0, 48.4. **^{19}F NMR** (565 MHz, $CDCl_3$) δ -109.3. **ESI-HRMS** calcd for $C_{24}H_{21}FNO$ $[M+H]^+$ 358.1607, found 358.1615.

***N*-(2,2-diphenylethyl)-4-methoxy-*N*-(propa-1,2-dien-1-yl)benzamide**

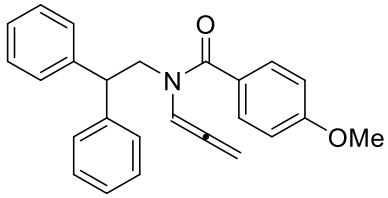

Allene **66g** was prepared following general procedure **GP-A** from the corresponding propargyl amide (369 mg, 1 mmol). Light-orange oil (203 mg, 55% yield).

^{1}H NMR (400 MHz, $CDCl_3$) δ 7.38 – 7.17 (m, 12H), 6.88 – 6.86 (m, 2H), 6.62 (br, 1H), 5.41 (d, *J* = 6.1 Hz, 2H), 4.71 (br, 1H), 4.36 (d, *J* = 8.3 Hz, 2H), 3.85 (s, 3H). **^{13}C NMR** (101 MHz, $CDCl_3$) δ 200.2, 169.6, 161.1, 141.7 (2C), 129.8, 128.6 (8C), 128.5, 127.2, 126.8 (4C), 113.7, 103.1, 87.1, 55.4, 48.4. **ESI-HRMS** calcd for $C_{25}H_{24}NO_2$ $[M+H]^+$ 370.1807, found 370.1811.

***N*-(2,2-diphenylethyl)-*N*-(propa-1,2-dien-1-yl)furan-2-carboxamide**

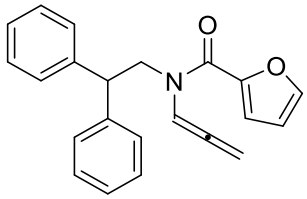

Allene **66h** was prepared following general procedure **GP-A** from the corresponding propargyl amide (329 mg, 1 mmol). Yellow solid (214 mg, 65% yield). Broad peaks observed due to the fluxionality of the allene observed.

^{1}H NMR (600 MHz, acetone-d^6) δ 7.68 (br, 1H), 7.40 – 7.21 (m, 9H), 7.20 – 7.16 (m, 2H), 6.89 (br, 1H), 6.54 – 6.53 (m, 1H), 5.45 (d, *J* = 6.4 Hz, 2H), 4.58 (br, 1H), 4.40 (br, 2H). ^{13}C NMR (151 MHz, acetone-d^6) δ 202.6, 172.0, 158.4, 148.1, 145.6, 142.9, 129.1 (8C), 127.4 (2C), 117.9, 112.2, 101.2, 87.5, 51.0, 49.7. **ESI-HRMS** calcd for $C_{22}H_{20}NO_2$ $[M+H]^+$ 330.4070, found 330.4075.

***tert*-butyl (2,2-diphenylethyl)(propa-1,2-dien-1-yl)carbamate**

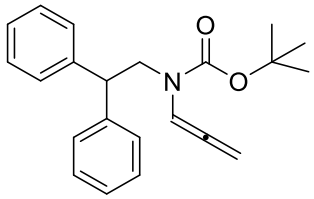

Allene **66i** was prepared following general procedure **GP-A** from the corresponding propargyl amide (335 mg, 1 mmol). White solid (201 mg, 60% yield). Two rotamers were observed due to the dynamic amide group (57:43 mixture of rotamers).

^{1}H NMR (400 MHz, $CDCl_3$) δ 7.32 – 7.18 (m, 11H RotA, 10H RotB), 6.89 (t, *J* = 6.4 Hz, 1H RotB), 5.35 (d, *J* = 6.4 Hz, 2H RotA, 2H RotB), 4.50 (t, *J* = 8.2 Hz, 1H RotB), 4.39 (t, *J* = 7.9 Hz, 1H RotA), 4.06 – 4.00 (m, 2H RotA, 2H RotB), 1.37 (s, 9H RotB), 1.28 (s, 9H RotA). **^{13}C NMR** (101 MHz, $CDCl_3$) δ 201.8 (RotA), 200.8 (RotB), 152.7 (RotA, RotB), 142.1 (2C RotA), 142.0 (2C RotB), 128.6 (4C RotA, 4C RotB), 128.5 (2C RotA), 128.3 (2C RotB), 126.7 (RotA), 126.6 (RotB), 100.5 (RotB), 100.1 (RotA), 87.3 (RotA), 86.8 (RotB), 81.1 (RotA, RotB), 49.9 (RotA), 48.7 (RotB), 48.4 (RotA, RotB), 28.2 (RotB), 28.1 (RotA). **ESI-HRMS** calcd for $C_{22}H_{25}NO_2$ $[M+H]^+$ 335.1885, found 335.1889.

***N*-(2-phenylpropyl)-*N*-(propa-1,2-dien-1-yl)acetamide**

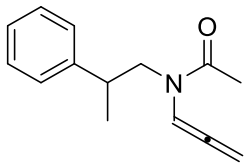

Allene **66j** was prepared following general procedure **GP-A** from the corresponding propargyl amide (215 mg, 1 mmol). Colorless oil (163 mg, 76% yield). Two rotamers were observed due to the dynamic amide group (51:49 mixture of rotamers).

^{1}H NMR (400 MHz, $CDCl_3$) δ 7.59 (t, *J* = 6.5 Hz, 1H RotB), 7.36 – 7.20 (m, 5H RotA, 5H RotB), 6.62 (t, *J* = 6.3 Hz, 1H RotA), 5.44 (qd, *J* = 9.9, 6.5 Hz, 1H RotA, 1H RotB), 5.36 (d, *J* = 2.5 Hz, 1H RotA), 5.35 (d, *J* = 2.4 Hz, 1H RotB), 3.84 (dd, *J* = 13.3, 8.5 Hz, 1H RotA), 3.53 – 3.48 (m, 1H RotA, 2H RotB), 3.25 – 3.18 (m, 1H RotA, 1H RotB), 2.17 (s, 3H RotA), 1.76 (s, 3H RotB), 1.34 (d, *J* = 7.1 Hz, 3H RotB), 1.27 (d, *J* = 7.0 Hz, 3H RotA). **^{13}C NMR** (101 MHz, $CDCl_3$) δ 202.5 (RotB), 201.3 (RotA), 169.1 (RotB), 168.7 (RotA), 144.3 (RotA), 143.5 (RotB), 128.8 (2C RotB), 128.3 (2C RotA), 127.5 (2C RotA), 127.3 (2C RotB), 127.1 (RotB), 126.6 (RotA), 101.3 (RotA), 98.4 (RotB), 86.9 (RotB), 86.6 (RotA), 54.3 (RotB), 50.6 (RotA), 37.8 (RotB), 37.7 (RotA), 22.0 (RotA), 21.5 (RotB), 18.4 (RotA), 17.5 (RotB). **ESI-HRMS** calcd for $C_{14}H_{18}NO$ $[M+H]^+$ 216.1388, found 216.1393.

***N*-(2-phenylpropyl)-*N*-(propa-1,2-dien-1-yl)pivalamide**

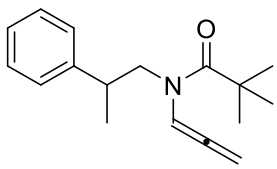

Allene **66k** was prepared following general procedure **GP-A** from the corresponding propargyl amide (257 mg, 1 mmol). Yellow oil (129 mg, 50% yield). **^{1}H NMR** (400 MHz, $CDCl_3$) δ 7.33 – 7.21 (m, 5H), 7.01 (t, *J* = 6.2 Hz, 1H), 5.33 (qd, *J* = 9.8, 6.2 Hz, 2H), 3.79 (dd, *J* = 13.3, 8.2 Hz, 1H), 3.60 (dd, *J* = 13.3,

7.5 Hz, 1H), 3.26 (h, *J* = 7.4 Hz, 1H), 1.30 (s, 9H). 1.27 (d, *J* = 7.1 Hz, 3H). **^{13}C NMR** (101 MHz, $CDCl_3$) δ 200.6, 176.0, 144.5, 128.3 (2C), 127.7 (2C), 126.5, 102.1, 86.2, 52.6, 39.4, 37.7, 28.5 (3C), 18.3. **ESI-HRMS** calcd for $C_{17}H_{24}NO$ $[M+H]^+$ 258.1858, found 258.1864.

***N*-(propa-1,2-dien-1-yl)-*N*-(2-(4-(trifluoromethyl)phenyl)propyl)acetamide**

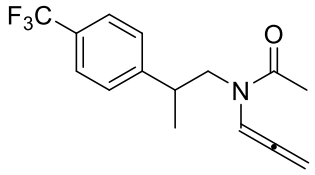

Allene **66l** was prepared following general procedure **GP-A** from the corresponding propargyl amide (283 mg, 1 mmol). Yellow oil (224 mg, 79% yield). Two rotamers were observed due to the dynamic amide group (59:41 mixture of rotamers).

^{1}H NMR (400 MHz, $CDCl_3$) δ 7.58 – 7.52 (m, 2H RotA, 3H RotB), 7.31 (t, *J* = 8.6 Hz, 2H RotA, 2H RotB), 6.58 (t, *J* = 6.2 Hz, 1H RotA), 5.45 – 5.27 (m, 2H RotA, 2H RotB), 3.76 (dd, *J* = 13.4, 8.2 Hz, 2H RotB), 3.57 – 3.45 (m, 2H RotA), 3.26 (qd, *J* = 7.2, 4.4 Hz, 1H RotA, 1H RotB), 2.13 (s, 3H RotA), 1.77 (s, 3H RotB), 1.33 (d, *J* = 7.1 Hz, 3H RotB), 1.24 (d, *J* = 7.0 Hz, 3H RotA). **^{13}C NMR** (101 MHz, $CDCl_3$) δ 202.4 (RotB), 201.2 (RotA), 168.9 (RotB), 168.8 (RotA), 148.4 (RotA), 147.6 (RotB), 130.3 – 128.3 (m, RotA, RotB), 127.9 (4C RotA), 127.8 (4C RotB), 125.85 – 125.47 (m, RotB), 125.3 (q, *J* = 4.0 Hz, RotA), 124.3 (q, *J* = 271.8 Hz, RotA, RotB), 101.3 (RotA), 98.4 (RotB), 87.1 (RotB), 86.8 (RotA), 53.9 (RotB), 50.3 (RotA), 37.8 (RotB), 37.7 (RotA), 22.0 (RotA), 21.6 (RotB), 18.4 (RotA), 17.5 (RotB). **^{19}F NMR** (565 MHz, $CDCl_3$) δ -62.3 (RotA), -62.4 (RotB). **ESI-HRMS** calcd for $C_{15}H_{17}F_3NO$ $[M+H]^+$ 284.1262, found 284.1267.

***N*-(2-(4-chlorophenyl)propyl)-*N*-(propa-1,2-dien-1-yl)acetamide**

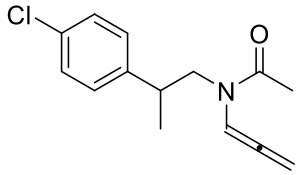

Allene **66m** was prepared following general procedure **GP-A** from the corresponding propargyl amide (250 mg, 1 mmol). Light-yellow oil (175 mg, 70% yield). Two rotamers were observed due to the dynamic amide group (60:40 mixture of rotamers).

^{1}H NMR (400 MHz, $CDCl_3$) δ 7.57 (t, *J* = 6.5 Hz, 1H RotB), 7.32 – 7.25 (m, 2H RotA, 2H RotB), 7.18 – 7.13 (m, 2H RotA, 2H RotB), 6.61 (t, *J* = 6.2 Hz, 1H RotA), 5.48 – 5.31 (m, 2H RotA, 2H RotB), 3.75 (dd,

J = 13.4, 8.2 Hz, 2H RotB), 3.55 – 3.43 (m, 2H RotA), 3.20 (hept, *J* = 7.0 Hz, 1H RotA, 1H RotB), 2.16 (s, 3H RotA), 1.80 (s, 3H RotB), 1.32 (d, *J* = 7.1 Hz, 3H RotB), 1.24 (d, *J* = 7.0 Hz, 3H RotA). **^{13}C NMR** (101 MHz, $CDCl_3$) δ 202.5 (RotB), 201.2 (RotA), 168.9 (RotB), 168.7 (RotA), 142.8 (RotA), 141.9 (RotB), 132.8 (RotB), 132.2 (RotA), 128.9 (2C RotA), 128.7 (2C RotB), 128.4 (2C RotA, 2C RotB), 101.3 (RotA), 98.4 (RotB), 87.0 (RotB), 86.8 (RotA), 54.1 (RotB), 50.4 (RotA), 37.2 (RotB), 37.2 (RotA), 22.0 (RotA), 21.6 (RotB), 18.5 (RotA), 17.5 (RotB). **ESI-HRMS** calcd for $C_{14}H_{17}ClNO$ $[M+H]^+$ 249.0920, found 249.0926.

***N*-(2-(4-methoxyphenyl)propyl)-*N*-(propa-1,2-dien-1-yl)acetamide**

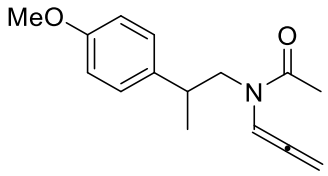

Allene **66n** was prepared following general procedure **GP-A** from the corresponding propargyl amide (245 mg, 1 mmol). Light-yellow oil (184 mg, 75% yield). Two rotamers were observed due to the dynamic amide group (59:41 mixture of rotamers).

^{1}H NMR (400 MHz, $CDCl_3$) δ 7.55 (t, *J* = 6.5 Hz, 1H RotA), 7.11 (dd, *J* = 18.4, 8.7 Hz, 2H RotA, 2H RotB), 6.83 (t, *J* = 8.4 Hz, 2H RotA, 2H RotB), 6.58 (t, *J* = 6.2 Hz, 1H RotB), 5.40 (qd, *J* = 9.9, 6.5 Hz, 1H RotA,1H RotB), 5.33 (dd, *J* = 6.2, 1.0 Hz, 1H RotA, 1H RotB), 3.78 – 3.77 (m, 3H RotA, 3H RotB), 3.50 – 3.39 (m, 2H RotA, 2H RotB), 3.17 – 3.09 (m, 1H RotA, 1H RotB), 2.14 (s, 3H RotA), 1.73 (s, 3H RotB), 1.28 (d, *J* = 7.1 Hz, 3H RotA), 1.22 – 1.18 (m, 3H RotB). **^{13}C NMR** (101 MHz, $CDCl_3$) δ 202.6 (RotA), 201.4 (RotB), 169.1 (RotA), 168.6 (RotB), 158.6 (RotA), 158.3 (RotB), 136.4 (RotB), 135.5 (RotA), 128.4 (2C RotB), 128.3 (2C RotA), 114.1 (2C RotA), 113.7 (2C RotB), 101.3 (RotA), 98.4 (RotB), 86.8 (RotA), 86.6 (RotB), 55.4 (RotA), 55.3 (RotB), 54.5 (RotA), 50.7 (RotB), 36.9 (RotA), 36.8 (RotB), 22.0 (RotB), 21.6 (RotA), 18.6 (RotB), 17.7 (RotA). **ESI-HRMS** calcd for $C_{15}H_{19}KNO_2$ $[M+K]^+$ 284.1053, found 284.1064.

***N*-(2-(3-bromophenyl)propyl)-*N*-(propa-1,2-dien-1-yl)acetamide**

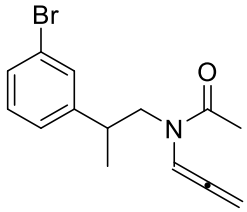

Allene **66o** was prepared following general procedure **GP-A** from the corresponding propargyl amide (294 mg, 1 mmol). Yellow oil (259 mg, 88% yield). Two rotamers were observed due to the dynamic amide group (63:37 mixture of rotamers).

^{1}H NMR (400 MHz, $CDCl_3$) δ 7.53 (t, *J* = 6.5 Hz, 1H RotB), 7.38 – 7.31 (m, 2H RotA, 2H RotB), 7.19 – 7.07 (m, 2H RotA, 2H RotB), 6.56 (t, *J* = 6.3 Hz, 1H RotA), 5.40 (qd, *J* = 10.0, 6.5 Hz, 1H RotA, 1H RotB), 5.33 (dd, *J* = 6.3, 1.4 Hz, 1H RotA, 1H RotB), 3.76 (dd, *J* = 13.3, 8.0 Hz, 2H RotB), 3.50 – 3.42 (m, 1H RotA), 3.16 (dq, *J* = 8.8, 7.2 Hz, 2H RotA, 1H RotB), 2.14 (s, 3H RotA), 1.83 (s, 3H RotB), 1.29 (d, *J* = 7.1 Hz, 3H RotB), 1.22 (d, *J* = 7.0 Hz, 3H RotA). **^{13}C NMR** (101 MHz, $CDCl_3$) δ 202.4 (RotB), 201.1 (RotA), 168.9 (RotB), 168.7 (RotA), 146.7 (RotA), 145.9 (RotB), 130.7 (RotA), 130.3 (RotB), 130.2 (RotA), 130.1 (RotB), 130.0 (RotA), 129.7 (RotB), 126.5 (RotB), 126.3 (RotA), 122.9 (RotB), 122.4 (RotA), 101.3 (RotA), 98.4 (RotB), 87.1 (RotB), 86.9 (RotA), 54.0 (RotB), 50.5 (RotA), 37.8 (RotB), 37.5 (RotA), 22.0 (RotA), 21.7 (RotB), 18.4 (RotA), 17.6 (RotB). **ESI-HRMS** calcd for $C_{14}H_{17}BrNO$ $[M+H]^+$ 294.0494, found 294.0499.

***N*-(2-(4-*iso*-butylphenyl)propyl)-*N*-(propa-1,2-dien-1-yl)acetamide**

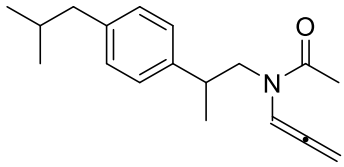

Allene **66p** was prepared following general procedure **GP-A** from the corresponding propargyl amide (271 mg, 1 mmol). Yellow oil (209 mg, 77% yield). Two rotamers were observed due to the dynamic amide group (54:46 mixture of rotamers).

^{1}H NMR (400 MHz, $CDCl_3$) δ 7.56 (t, *J* = 6.5 Hz, 1H RotA), 7.14 – 7.03 (m, 4H RotA, 4H RotB), 6.58 (t, *J* = 6.2 Hz, 1H RotB), 5.46 – 5.36 (m, 1H RotA, 1H RotB), 5.31 (dd, *J* = 6.3, 2.3 Hz, 1H RotA, 1H RotB), 3.84 – 3.78 (m, 1H RotB), 3.52 – 3.41 (m, 2H RotA, 1H RotB), 3.21 – 3.09 (m, 1H RotA, 1H RotB), 2.45 – 2.42 (m, 2H RotA, 2H RotB), 2.15 (s, 3H RotB), 1.83 (dp, *J* = 13.5, 6.8 Hz, 1H RotA, 1H RotB) , 1.69 (s, 3H RotA), 1.30 (d, *J* = 7.1 Hz, 3H RotA), 1.22 (d, *J* = 7.0 Hz, 3H RotB), 0.89 – 0.87 (m, 6H RotA, 6H RotB). **^{13}C NMR** (101 MHz, $CDCl_3$) δ 202.6 (RotA), 201.4 (RotB), 169.2 (RotA), 168.7 (RotB), 141.6

(RotB), 140.7 (RotA), 140.5 (RotA), 139.9 (RotB), 129.5 (2C RotA), 129.1 (2C RotB), 127.2 (2C RotB), 127.1 (2C RotA), 101.3 (RotB), 98.4 (RotA), 86.8 (RotA), 86.6 (RotB), 54.5 (RotA), 50.8 (RotB), 45.2 (RotB), 45.1 (RotA), 37.3 (RotA), 37.3 (RotB), 30.4 (RotA, RotB), 22.50 (2C RotA, 2C RotB), 22.47 (RotA), 22.4 (RotB), 22.0 (RotB), 21.5 (RotA), 18.4 (RotB), 17.5 (RotA). **ESI-HRMS** calcd for $C_{18}H_{26}NO$ $[M+H]^+$ 272.2014, found 272.2019.

***N*-(2-(2-fluoro-[1,1'-biphenyl]-4-yl)propyl)-*N*-(propa-1,2-dien-1-yl)acetamide**

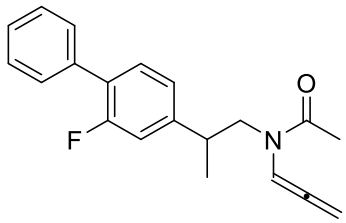

Allene **66q** was prepared following general procedure **GP-A** from the corresponding propargyl amide (309 mg, 1 mmol). Light-yellow oil (195 mg, 63% yield). Two rotamers were observed due to the dynamic amide group (60:40 mixture of rotamers).

^{1}H NMR (600 MHz, $CDCl_3$) δ 7.58 (t, *J* = 6.5 Hz, 1H RotB), 7.55 – 7.53 (m, 2H RotA, 2H RotB), 7.45 – 7.34 (m, 4H RotA, 4H RotB), 7.08 (dd, *J* = 7.9, 1.8 Hz, 1H RotA), 7.04 – 7.00 (m, 1H RotA, 2H RotB), 6.62 (t, *J* = 6.3 Hz, 1H RotA), 5.47 – 5.40 (m, 1H RotA, 1H RotB), 5.38 – 5.33 (m, 1H RotA, 1H RotB), 3.82 (dd, *J* = 13.4, 8.4 Hz, 1H RotA), 3.54 – 3.50 (m, 1H RotA, 2H RotB), 3.28 – 3.16 (m, 1H RotA, 1H RotB), 2.18 (s, 3H RotA), 1.88 (s, 3H RotB), 1.34 (d, *J* = 7.1 Hz, 3H RotB), 1.27 (d, *J* = 7.0 Hz, 3H RotA). **^{13}C NMR** (151 MHz, $CDCl_3$) δ 202.5 (RotB), 201.3 (RotA), 169.0 (RotB), 168.7 (RotA), 160.8 (d, *J* = 7.2 Hz, RotB), 159.7 (d, *J* = 7.2 Hz, RotA), 146.1 (d, *J* = 7.2 Hz, RotA), 145.2 (d, *J* = 7.1 Hz, RotB), 135.9 (RotA), 135.6 (RotB), 131.0 (d, *J* = 4.0 Hz, RotB), 130.5 (d, *J* = 3.9 Hz, RotA), 129.1 (RotB), 129.0 (RotA), 128.6 (2C RotA, 2C RotB), 128.5 (RotA, RotB), 127.8 (RotB), 127.6 (RotA), 127.1 (d, *J* = 13.4 Hz, RotA, RotB), 123.6 (d, *J* = 3.3 Hz, RotB), 123.5 (d, *J* = 3.2 Hz, RotA), 115.1 (d, *J* = 22.8 Hz, RotA), 114.8 (d, *J* = 22.9 Hz, RotB), 101.4 (RotA), 98.4 (RotB), 87.0 (RotB), 86.8 (RotA), 54.0 (RotB), 50.5 (RotA), 37.5 (RotB), 37.4 (RotA), 22.0 (RotA), 21.7 (RotB), 18.4 (RotA), 17.6 (RotB). **^{19}F NMR** (565 MHz, $CDCl_3$) δ -117.3 – -117.3 (m, RotB), -118.3 – -118.3 (m, RotA). **ESI-HRMS** calcd for $C_{20}H_{21}FNO$ $[M+H]^+$ 310.1607, found 310.1612.

***N*-(2-phenylhex-5-en-1-yl)-*N*-(propa-1,2-dien-1-yl)acetamide**

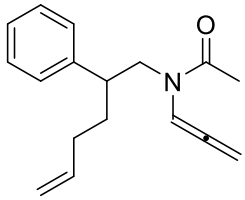

Allene **66r** was prepared following general procedure **GP-A** from the corresponding propargyl amide (255 mg, 1 mmol). Light-yellow oil (173 mg, 68% yield). Two rotamers were observed due to the dynamic amide group (53:47 mixture of rotamers).

^{1}H NMR (400 MHz, $CDCl_3$) δ 7.53 (t, *J* = 6.5 Hz, 1H RotB), 7.33 – 7.13 (m, 5H RotA, 5H RotB), 6.53 (t, *J* = 6.2 Hz, 1H RotA), 5.83 – 5.68 (m, 1H RotA, 1H RotB), 5.41 (qd, *J* = 9.9, 6.5 Hz, 1H RotA, 1H RotB), 5.30 (dt, *J* = 7.3, 3.7 Hz, 1H RotA, 1H RotB), 4.97 – 4.89 (m, 2H RotA, 2H RotB), 3.83 (dd, *J* = 13.3, 7.9 Hz, 1H RotA), 3.59 – 3.47 (m, 1H RotA, 2H RotB), 3.08 – 2.99 (m, 1H RotA, 1H RotB), 2.11 (s, 3H RotA), 1.96 – 1.72 (m, 4H RotA, 4H RotB), 1.71 (s, 3H RotB). **^{13}C NMR** (101 MHz, $CDCl_3$) δ 202.5 (RotB), 201.3 (RotA), 169.1 (RotB), 168.6 (RotA), 142.3 (RotA), 141.7 (RotB), 138.6 (RotA), 138.0 (RotB), 128.9 (2C RotB), 128.3 (2C RotA), 128.2 (2C RotA), 128.1 (2C RotB), 127.2 (RotB), 126.7 (RotA), 115.2 (RotB), 114.7 (RotA), 101.3 (RotB), 98.4 (RotA), 86.9 (RotB), 86.6 (RotA), 53.6 (RotB), 49.6 (RotA), 43.3 (RotB), 43.1 (RotA), 32.0 (RotB), 31.6 (RotA), 31.5 (RotA), 31.2 (RotB), 22.0 (RotA), 21.4 (RotB). **ESI-HRMS** calcd for $C_{17}H_{22}NO$ $[M+H]^+$ 256.1701, found 256.1705.

***N*-(2,3-diphenylpropyl)-*N*-(propa-1,2-dien-1-yl)acetamide**

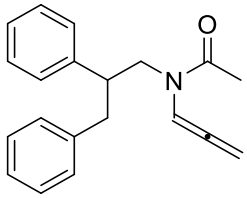

Allene **66s** was prepared following general procedure **GP-A** from the corresponding propargyl amide (291 mg, 1 mmol). Light-yellow oil (178 mg, 61% yield). Two rotamers were observed due to the dynamic amide group (57:43 mixture of rotamers).

^{1}H NMR (600 MHz, $CDCl_3$) δ 7.44 (t, *J* = 6.5 Hz, 1H RotB), 7.27 – 7.01 (m, 10H RotA, 10H RotB), 6.46 (t, *J* = 6.2 Hz, 1H RotA), 5.29 – 5.24 (m, 1H RotA, 1H RotB), 5.16 (dd, *J* = 10.1, 6.5 Hz, 1H RotA), 5.08 (dd, *J* = 10.1, 6.5 Hz, 1H RotB), 3.86 (dd, *J* = 13.5, 7.8 Hz, 1H RotA), 3.66 – 3.61 (m, 1H RotA, 1H RotB), 3.52 (dd, *J* = 14.4, 9.4 Hz, 1H RotB), 3.37 (p, *J* = 7.7 Hz, 1H RotA), 3.27 – 3.22 (m, 1H RotB), 3.03 (dd, *J* = 13.6, 7.7 Hz, 1H RotB), 2.98 – 2.84 (m, 2H RotA, 1H RotB), 2.01 (s, 3H RotA), 1.57 (s, 3H RotB). **^{13}C**

NMR (151 MHz, $CDCl_3$) δ 202.0 (RotB), 201.3 (RotA), 169.2 (RotB), 168.7 (RotA), 142.1 (RotA), 141.8 (RotB), 140.1 (RotA), 139.7 (RotB), 129.2 (RotB), 129.0 (RotA), 128.8 (2C RotA, 2C RotB), 128.4 (2C RotA, 2C RotB), 128.2 (2C RotA, 2C RotB), 128.14 (RotB), 128.13 (RotA), 127.3 (RotB), 126.7 (RotA), 126.4 (RotB), 125.9 (RotA), 101.1 (RotA), 98.3 (RotB), 86.9 (RotB), 86.7 (RotA), 52.7 (RotB), 49.0 (RotA), 45.8 (RotB), 45.1 (RotA), 39.9 (RotA), 39.0 (RotB), 21.9 (RotA), 21.3 (RotB). **ESI-HRMS** calcd for $C_{20}H_{21}NNaO$ $[M+Na]^+$ 314.1521, found 314.1522.

***N*-(2-(4-chlorophenyl)-2-phenylethyl)-*N*-(propa-1,2-dien-1-yl)acetamide**

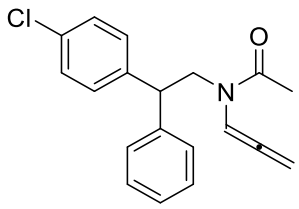

Allene **66t** was prepared following general procedure **GP-A** from the corresponding propargyl amide (312 mg, 1 mmol). Light-yellow oil (162 mg, 52% yield). Two rotamers were observed due to the dynamic amide group (66:34 mixture of rotamers).

^{1}H NMR (600 MHz, $CDCl_3$) δ 7.58 (t, *J* = 6.5 Hz, 1H RotB), 7.34 – 7.12 (m, 9H RotA, 9H RotB), 6.46 (t, *J* = 6.2 Hz, 1H RotA), 5.35 – 5.30 (m, 2H RotA, 2H RotB), 4.48 (t, *J* = 8.2 Hz, 1H RotA), 4.34 (t, *J* = 7.3 Hz, 1H RotB), 4.20 (dd, *J* = 13.4, 8.6 Hz, 1H RotB), 4.04 (dd, *J* = 13.4, 7.8 Hz, 1H RotB), 3.99 (d, *J* = 7.4 Hz, 2H RotA), 2.06 (s, 3H RotA), 1.54 (s, 3H RotB). **^{13}C NMR** (151 MHz, $CDCl_3$) δ 202.0 (RotB), 201.4 (RotA), 169.1 (RotB), 168.7 (RotA), 141.5 (RotA), 141.1 (RotA), 140.4 (RotB), 140.1 (RotB), 133.0 (RotA), 132.5 (RotA), 129.9 (RotA), 129.7 (RotB), 128.9 (2C RotA, 2C RotB), 128.50 (2C RotA, 2C RotB), 128.47 (2C RotA, 2C RotB), 128.3 (RotA, RotB), 127.4 (RotB), 126.9 (RotA), 101.0 (RotA), 98.1 (RotB), 87.2 (RotB), 86.8 (RotA) 52.0 (RotB), 48.0 (RotA), 47.8 (RotA), 47.5 (RotB), 22.0 (RotA), 21.2 (RotB). **ESI-HRMS** calcd for $C_{19}H_{18}ClNNaO$ $[M+Na]^+$ 334.0975, found 334.0973.

***N*-(2,2-diphenylethyl)-*N*-(propa-1,2-dien-1-yl)-*iso*-butyramide**

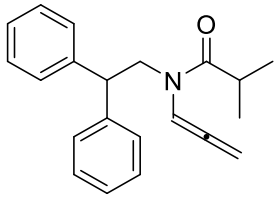

Allene **66u** was prepared following general procedure **GP-A** from the corresponding propargyl amide (305 mg, 1 mmol). Orange oil (220 mg, 72% yield). Two rotamers were observed due to the dynamic amide group (69:31 mixture of rotamers).

^{1}H NMR (600 MHz, $CDCl_3$) δ 7.60 (t, *J* = 6.5 Hz, 1H RotB), 7.31 – 7.15 (m, 10H RotA, 10H RotB), 6.55 (t, *J* = 6.2 Hz, 1H RotA), 5.32 – 5.30 (m, 2H RotA, 2H RotB), 4.51 (t, *J* = 8.3 Hz, 1H RotA), 4.36 (t, *J* = 7.4 Hz, 1H RotB), 4.17 (d, *J* = 8.3 Hz, 2H RotA), 4.05 (d, *J* = 7.5 Hz, 2H RotB), 2.72 (p, *J* = 6.7 Hz, 1H RotA), 2.19 (p, *J* = 6.7 Hz, 1H RotB), 0.97 (d, *J* = 6.8 Hz, 6H RotA), 0.77 (d, *J* = 6.7 Hz, 6H RotB). **^{13}C NMR** (151 MHz, $CDCl_3$) δ 202.4 (RotB), 201.7 (RotA), 175.9 (RotB), 175.3 (RotA), 141.8 (2C RotA), 141.5 (2C RotB), 128.7 (4C RotB), 128.5 (4C RotA), 128.4 (4C RotB), 128.3 (4C RotA), 127.0 (2C RotB), 126.6 (2C RotA), 100.2 (RotA), 98.4 (RotB), 86.9 (RotB), 86.5 (RotA), 50.6 (RotB), 48.5 (RotA), 48.3 (RotA, RotB), 30.7 (RotA), 30.7 (RotB), 19.2 (2C RotB), 19.1 (2C RotA). **ESI-HRMS** calcd for $C_{21}H_{23}NNaO$ $[M+Na]^+$ 328.1677, found 328.1685.

***N*-(2,2-diphenylethyl)-2,2-diphenyl-*N*-(propa-1,2-dien-1-yl)acetamide**

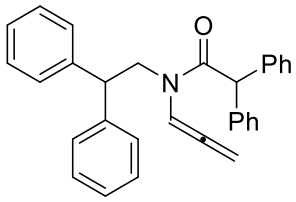

Allene **1v** was prepared following general procedure **GP-A** from the corresponding propargyl amide (430 mg, 1 mmol). Light-yellow oil (112 mg, 26% yield). Two rotamers were observed due to the dynamic amide group (70:30 mixture of rotamers).

^{1}H NMR (600 MHz, $CDCl_3$) δ 7.65 (t, *J* = 6.5 Hz, 1H RotB), 7.35 (dd, *J* = 8.2, 6.7 Hz, 1H RotA, 1H RotB), 7.31 – 7.19 (m, 16H RotA, 16H RotB), 6.94 – 6.93 (m, 3H RotA), 6.86 – 6.84 (m, 3H RotB), 6.51 (t, *J* = 6.2 Hz, 1H RotA), 5.30 (d, *J* = 6.2 Hz, 2H RotA, 3H RotB), 5.18 (s, 1H RotA), 4.52 – 4.48 (m, 1H RotA, 1H RotB), 4.28 (d, *J* = 8.2 Hz, 2H RotA), 3.95 (d, *J* = 7.3 Hz, 2H RotB). **^{13}C NMR** (151 MHz, $CDCl_3$) δ 202.38 (RotB), 202.21 (RotA), 170.47 (RotB), 170.34 (RotA), 141.97 (2C RotB), 141.76 (2C RotA),

139.05 (2C RotA), 138.97 (2C RotB), 129.10 (4C RotA), 129.02 (4C RotB), 128.98 (4C RotA, 4C RotB), 128.68 (RotA, RotB), 128.66 (4C RotA, 4C RotB), 128.53 (4C RotA, 4C RotB), 127.26 (RotB), 127.20 (RotB), 127.14 (2C RotA), 126.78 (2C RotA), 100.03 (RotA), 98.83 (RotB), 87.26 (RotB), 86.32 (RotA), 55.50 (RotA), 55.37 (RotB), 51.16 (RotB), 48.90 (RotA), 48.80 (RotA), 48.53 (RotB). **ESI-HRMS** calcd for $C_{31}H_{28}NO$ $[M+H]^+$ 430.2171, found 430.2175.

Synthesis of N derivatives

1,2-di(naphthalen-1-yl)ethane (N1)

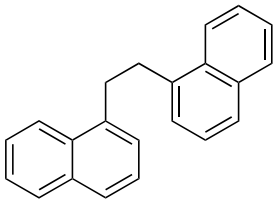

N1 was synthesized following a reported literature procedure (*Chem. Eur. J.* **2024**, 30, e202304010). From 1-chloro-methylnaphthalene (1.9 g, 11.1 mmol, 1 equiv.), **N1** was recovered as a white solid (1.3 g, 4.6 mmol, 82% yield).

^{1}HNMR (600 MHz, $CDCl_3$) δ 8.15 (dd, *J* = 8.4, 1.2 Hz, 2H), 7.95–7.86 (m, 2H), 7.79–7.74 (m, 2H), 7.59–7.48 (m, 4H), 7.42 (ddd, *J* = 8.3, 7.0, 2.6 Hz, 2H), 7.37 (dt, *J* = 7.1, 1.8 Hz, 2H), 3.54 (s, 4H). *Data consistent with literature*.

di(naphthalen-1-yl)methanol (N2)

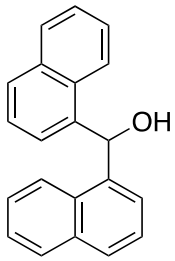

N2 was synthesized following a reported literature procedure (*Chem. Eur. J.* **2018**, *24*, 572). From 1-bromo-methyl-naphthalene (2.9 g, 14.4 mmol, 1.0 equiv.) **N2** was recovered as a white solid (1.5 g, 5.3 mmol, 81% yield).

^{1}H NMR (400 MHz, $CDCl_3$) δ 8.05 (d, J = 8.3 Hz, 2H), 7.92 (d, J = 7.9 Hz, 2H), 7.84 (d, J = 8.0 Hz, 2H), 7.55 – 7.37 (m, 8H), 7.29 (d, J = 3.9 Hz, 1H), 2.47 (d, J = 4.1 Hz, 1H). *Data consistent with literature.*

4-methyl-*N*,*N*-bis(naphthalen-1-ylmethyl)benzenesulfonamide (N3)

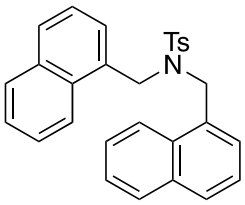

N3 was synthesized following a reported literature procedure (*Chem. Eur. J.* **2024**, 30, e202304010). From 4-methylbenzenesulfonamide (344 mg, 2.0 mmol, 1.0 equiv.) **N3** was recovered as a white solid (640 mg, 72% yield).

^{1}HNMR (400 MHz, $CDCl_3$) δ 7.90 (d, *J* = 8.5 Hz, 2H), 7.80 (d, *J* = 8.3 Hz, 2H), 7.68 (d, *J* = 8.2, 2H), 7.50 (d, *J* = 8.2 Hz, 2H), 7.35 (m, 6H), 7.12 (m, 2H), 7.03–6.96 (m, 2H), 4.83 (s, 4H), 2.46 (s, 3H). *Data consistent with literature.*

1,1'-(oxybis(methylene))dinaphthalene (N4)

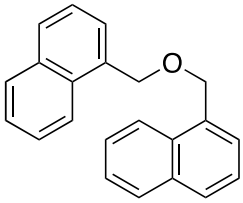

N4 was synthesized following a reported literature procedure (*Photochem. Photobiol. Sci.* **2024**, 23, 1543–1563). From 1-naphthalene methanol (2.0 mmol, 1.0 equiv.) **N4** was recovered as a white solid (283 mg, 0.9 mmol, 60% yield).

^{1}HNMR (400 MHz, $CDCl_3$) δ 8.26–8.17 (m, 2H), 8.00–7.93 (m, 2H), 7.93–7.87 (m, 2H), 7.69–7.49 (m, 8H), 5.14 (s, 4H). *Data consistent with literature*.

Naphthalen-1-ylmethyl (naphthalen-1-ylmethyl)-L-prolinate (N5)

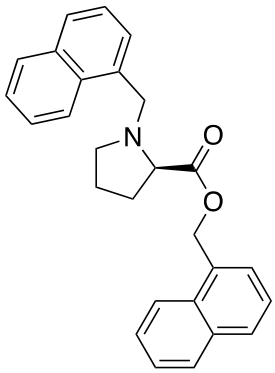

N5 was synthesized following a reported literature procedure (*Chem. Eur. J.* **2024**, 30, e202304010). From L-proline (345 mg, 3.0 mmol, 1.0 equiv.) **N5** was recovered as a colorless sticky oil (1.08 g, 91% yield).

^{1}H NMR (400 MHz, $CDCl_3$) δ 8.51 (d, J = 8.2 Hz, 1H), 8.10 – 8.04 (m, H), 7.94 – 7.88 (m, 3H), 7.82 (d, J = 7.9, 1H), 7.65 – 7.59 (m, 1H), 7.58 – 7.36 (m, 7H), 5.66 (s, 2H), 4.56 (d, J = 12.6 Hz, 1H), 3.90 (d, J = 12.6 Hz, 1H), 3.45 (dd, J = 8.9, 6.2 Hz, 1H), 2.98 (td, J = 7.8, 3.3 Hz, 1H), 2.48 (q, J = 8.4 Hz, 2H), 2.28 – 2.13 (m, 1H), 2.13 – 2.01 (m, 1H), 2.00 – 1.66 (m, 2H). *Data consistent with literature.*

2,2-di(naphthalen-1-yl)acetic acid (N7)

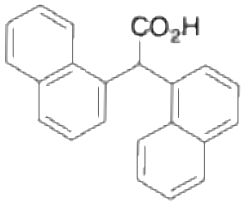

N7 was synthesized following a reported literature procedure (*Chem. Eur. J.* **2025**, 31, e202403309). From 1-bromo-methyl-naphthalene (2.9 g, 14.4 mmol, 1.0 equiv.), over 3 steps, **N7** was recovered as a white solid (160 mg, 0.4 mmol, 30% yield for the third step from di(naphthalen-1-yl)methane).

^{1}H NMR (400 MHz, $CDCl_3$) δ 12.64 (brs, 1H) 8.01 – 7.93 (m, 2H), 7.91 (dd, *J* = 7.4, 2.0 Hz, 2H), 7.83 (d, *J* = 8.1 Hz, 2H), 7.56 – 7.44 (m, 4H), 7.40 (t, *J* = 7.7 Hz, 2H), 7.33 (dd, *J* = 7.2, 1.2 Hz, 2H), 6.55 (s, 1H). *Data consistent with literature.*

(*S*)-2,2′-bis(naphthalen-1-ylmeth oxy)-1,1′-binaphthalene (N8)

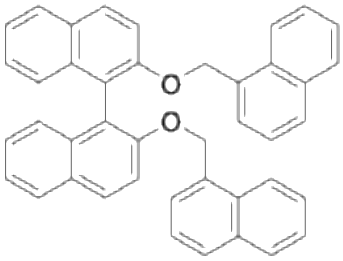

N8 was synthesized following a reported literature procedure (*Chem. Eur. J.* **2024**, 30, e202304010). From L-BINOL (280 mg, 1.0 mmol, 1.0 equiv.) **N8** was recovered as a white solide (270 mg, 0.5 mmol, 48% yield).

^{1}HNMR (400 MHz, $CDCl_3$) δ 7.92 (d, *J* = 9.0 Hz, 2H), 7.87 (d, *J* = 8.2 Hz, 2H), 7.77–7.72 (m, 2H), 7.61 (d, *J* = 8.1 Hz, 2H), 7.50 (d, *J* = 8.5 Hz, 2H), 7.45 (d, *J* = 9.0 Hz, 2H), 7.39–7.30 (m, 4H), 7.21 (d, *J* = 3.9 Hz, 4H), 7.12 (ddd, *J* = 8.3, 6.9, 1.3 Hz, 4H), 7.08–7.00 (m, 2H), 5.58–5.12 (m, 4H). *Data consistent with literature.*

bis(4-methoxynaphthalen-1-yl)methane (N9)

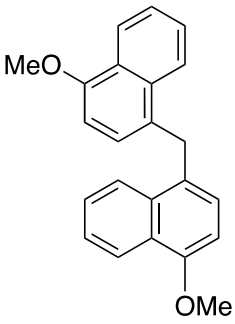

Step 1: 4-methoxy-1-naphthaldehyde (1.12 g, 6.0 mmol, 1.0 equiv.) was dissolved in MeOH (30 mL, 0.2 M) in a round bottom flask equipped with a magnetic stirring bar, then $NaBH_4$ (567 mg, 15.0 mmol, 2.5 equiv.) was added portion-wise at 0 °C. The resulting mixture was vigorously stirred at room temperature for 30 minutes, then quenched with distilled water. The solvent was removed in vacuo, the residue was suspended in water and extracted with EtOAc (3 x 15 mL), the organic phase was dried over Na_2SO_4, and the solvent was removed under reduced pressure. The crude product (4-methoxynaphthalen-1-yl)methanol was used without further purification for **Step 2**.

Step 2: (4-methoxynaphthalen-1-yl)methanol (753 mg, 4.0 mmol, 1.0 equiv.) in anhydrous DCM (30 mL, 0.13 M) was cooled to 0 °C and PBr_3 (0.8 mL, 8.5 mmol, 2.1 equiv.) was added dropwise. The

reaction was stirred at 0 °C for 1 h, quenched with a saturated $NaHCO_3$ aqueous solution and extracted with DCM (3 x 15 mL). Organic layers were collected, dried over Na_2SO_4, and concentrated under reduced pressure. The crude product 1-(bromomethyl)-4-methoxynaphthalene was used without further purification for **Step 3**.

Step 3: 1-(bromomethyl)-4-methoxynaphthalene (1.0 g, 4.0 mmol, 1.0 equiv.) was dissolved in THF (2.8 mL, 1.44 M) and slowly added to a stirred suspension of magnesium turnings (102 mg, 4.2 mmol, 1.05 equiv.) in THF (5.6 mL) in a two neck round bottom flask under nitrogen atmosphere. Two drops of di-bromo-ethane were added, and the resulting mixture was stirred at room temperature for 2 hours. Then, a solution of butyl formiate in THF (0.21 mL, 1.8 mmol, 0.45 equiv.) was slowly added to the mixture. The resulting solution was stirred overnight at room temperature. The reaction was quenched by the slow addition of a saturated NH_4Cl aqueous solution (10 mL). The resulting suspension was extracted with diethyl ether (15 mL × 3), dried with Na_2SO_4 and the solvent was removed under reduced pressure. The residue was purified by column chromatography on silica gel (*n*-hexane/EtOAc) affording bis(4-methoxynaphthalen-1-yl)methanol as a white solid (1.1 g, 3.2 mmol, 79% yield).

Step 4: bis(4-methoxynaphthalen-1-yl)methanol (1.1 g, 3.2 mmol, 1.0 equiv.) was dissolved in chloroform (20 mL, 0.16 M) and MsOH (0.23 mL, 3.52 mmol, 1.1 equiv.) was added at 0 °C. Then, Et_3SiH (0.82 mL, 5.12 mmol, 1.6 equiv.) was added dropwise under nitrogen atmosphere. The resulting solution was stirred at 60 °C for 1 hour, then quenched by the addition of a saturated $NaHCO_3$ aqueous solution and extracted with DCM (10 mL × 3). The organic phase was dried with Na_2SO_4, filtered and the solvent was removed under reduced pressure. The residue was purified by chromatography on silica gel (*n*-hexane/EtOAc). Recrystallization (DCM/*n*-hexane) of the purified product afforded **N9** as a white solid (347 mg, 1.1 mmol, 33% yield).

^{1}H NMR (600 MHz, $CDCl_3$) δ 8.40 – 8.32 (m, 2H), 8.03 – 7.94 (m, 2H), 7.51 (qd, *J* = 6.8, 3.4 Hz, 4H), 6.98 (d, *J* = 7.8 Hz, 2H), 6.68 (d, *J* = 7.9 Hz, 2H), 4.72 (s, 2H), 3.98 (s, 6H). **^{13}C NMR** (151 MHz, $CDCl_3$) δ 154.51, 133.17, 128.44, 126.99, 126.64, 126.04, 125.07, 124.00, 122.71, 103.63, 55.58, 34.91. **ESI-HRMS** calcd for $C_{23}H_{20}NaO_2$ $[M+Na]^+$ 351.1355, found 351.1364.

naphthalen-1-ylmethyl 1-naphthoate (N10)

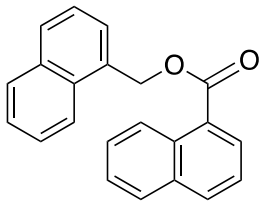

N10 was synthesized adapting a reported literature procedure (*Chem. Eur. J.* **2024**, 30, e202304010). 1-Naphthoic acid (344.4 mg, 2.0 mmol, 1.0 equiv.) and K_2CO_3 (560 mg, 4.0 mmol, 2.0 equiv.) were added to a round bottom flask equipped with a magnetic stirring bar. DMF (4 mL, 0.5 M) was added and the mixture was stirred at room temperature for 20 minutes, followed by the addition of (1-(chloromethyl)naphthalene (353 mg, 2.0 mmol, 1.0 equiv.). The reaction mixture was stirred at room temperature for 24 hours. After complete consumption of the starting material, 20 mL of distilled water were added, and the mixture was extracted with EtOAc (3x 15 mL). The organic layer was washed with distilled water (3x 15 mL) and brine (15 mL). It was then separated, dried over Na_2SO_4, and the solvent was removed under vacuum. The crude was purified by chromatography on silica gel (*n*-hexane/EtOAc) affording **N10** as a white solid (592 mg, 95% yield).

^{1}H NMR (400 MHz, $CDCl_3$) δ 9.00 (d, *J* = 8.7 Hz, 1H), 8.24 – 8.16 (m, 2H), 8.00 (d, *J* = 8.2 Hz, 1H), 7.90 (dd, *J* = 20.2, 9.3 Hz, 3H), 7.71 (d, *J* = 6.9 Hz, 1H), 7.64 – 7.56 (m, 2H), 7.56 – 7.48 (m, 3H), 7.47 – 7.40 (m, 1H), 5.93 (s, 2H). **^{13}C NMR** (101 MHz, $CDCl_3$) δ 167.45, 133.95, 133.65, 131.93, 131.70, 131.58, 130.63, 129.52, 128.92, 128.67, 127.95, 127.80, 126.97, 126.81, 126.34, 126.13, 125.95, 125.49, 124.62, 123.80, 65.33. **ESI-HRMS** calcd for $C_{22}H_{16}O_2$ $[M+H]^+$ 313.1223, found 313.1227.

2-(methylsulfonyl)-6-(naphthalen-1-ylmethoxy)naphthalene (N11)

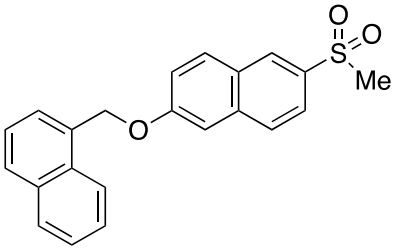

Step 1: 6,6'-disulfanediyldinaphthalen-2-ol (1.0 g, 2.85 mmol, 1.0 equiv.) and K_2CO_3 (1.6 g, 11.4 mmol, 4.0 equiv.) were added to a round bottom flask equipped with a magnetic stirring bar. DMF (6 mL, 0.5 M) was added and the mixture was stirred at room temperature for 20 minutes, followed by the addition of (1-(chloromethyl)naphthalene (1.5 g, 8.55 mmol, 3.0 equiv.). The reaction mixture was stirred at room temperature for 24 hours. After complete consumption of the starting material, 20 mL of distilled water were added, and the mixture was extracted with EtOAc (3x 15 mL). The organic layer was washed with distilled water (3x 15 mL) and brine (15 mL). It was then dried over Na_2SO_4, and the solvent was removed under vacuum. The crude product 1,2-bis(6-(naphthalen-1-ylmethoxy)naphthalen-2-yl)disulfane was used without further purification for **step 2**.

Step 2: 1,2-bis(6-(naphthalen-1-ylmethoxy)naphthalen-2-yl)disulfane (1.0 g, 2.8 mmol, 1.0 equiv.) was suspended in dry THF (11.2 mL, 0.25 M), then $NaBH_4$ (265 mg, 7.0 mmol, 2.5 equiv.) was added at room temperature. The resulting suspension was heated to reflux, and MeOH (1.12 mL) was added to the reaction mixture after 1 hour. The reaction was allowed to cool to room temperature, quenched with a 1 M HCl solution (5.6 mL), and then a 6 M HCl solution was added (8.4 mL). The organic layer was separated and the aqueous one was extracted with DCM (3 x 15 mL). The organic phase was dried over Na_2SO_4, and the solvent was removed under reduced pressure. The crude was purified by column chromatography on silica gel (*n*-hexane/EtOAc) affording 6-(naphthalen-2-ylmethoxy)naphthalene-2-thiol as a white solid (1.0 g, 56% yield over 2 steps).

Step 3: 6-(naphthalen-2-ylmethoxy)naphthalene-2-thiol (316 mg, 1.0 mmol, 1.0 equiv.) and K_2CO_3 (415 mg, 3.0 mmol, 3.0 equiv.) were added to a round bottom flask equipped with a magnetic stirring bar. DMF (2 mL, 0.5 M) was added, and the mixture was stirred at room temperature for 20 minutes, followed by the addition of iodomethane (69 μL, 1.1 mmol, 1.1 equiv.). The reaction mixture was stirred at room temperature for 24 hours. After complete consumption of the starting material, 5 mL of distilled water were added, and the mixture was extracted with EtOAc (3 x 10 mL). The organic layer was washed with distilled water (3 x 10 mL) and brine (15 mL). It was then and dried over

Na_2SO_4, and the solvent was removed under vacuum. The crude product was purified by column chromatography on silica gel (*n*-hexane/EtOAc) affording methyl(6-(naphthalen-2-ylmethoxy)naphthalen-2-yl)sulfane as a white solid (165 mg, 50% yield).

Step 4: To a solution of methyl(6-(naphthalen-2-ylmethoxy)naphthalen-2-yl)sulfane (165 mg, 0.5 mmol, 1.0 equiv.) in AcOH (230 μL, 2.2 M), a 30% aqueous H_2O_2 solution (130 μL) was added at room temperature. The mixture was cooled to 0 °C, H_2SO_4 (15 μL) was added, and the reaction was stirred at 0 °C for 30 minutes. The mixture was then heated at 70 °C for 1.5 hours. The reaction was allowed to cool to room temperature, then quenched with ice and vigorously stirred for 10 minutes. The precipitate was filtered and washed several times with distilled water, then dried under vacuum affording **N11** as a white solid (145 mg, 80% yield).

^{1}H NMR (400 MHz, $CDCl_3$) δ 8.45 (s, 1H), 8.07 (dd, *J* = 6.8, 2.5 Hz, 1H), 7.91 (ddd, *J* = 9.4, 6.1, 2.4 Hz, 5H), 7.66 (d, *J* = 6.9 Hz, 1H), 7.56 (dt, *J* = 6.2, 2.9 Hz, 2H), 7.52 – 7.47 (m, 1H), 7.43 (d, *J* = 2.2 Hz, 1H), 7.38 (dd, *J* = 9.0, 2.4 Hz, 1H), 5.66 (s, 2H), 3.12 (s, 3H). **^{13}C NMR** (101 MHz, $CDCl_3$) δ 159.60, 137.22, 135.38, 133.99, 131.65, 131.60, 131.24, 129.54, 128.99, 128.49, 127.87, 126.97, 126.80, 126.23, 125.49, 123.66, 123.09, 121.30, 107.32, 69.06, 44.85. **ESI-HRMS** calcd for $C_{22}H_{18}O_3S$ $[M+H]^+$ 363.1050, found 363.1058.

2-chloro-4-((naphthalen-1-ylmethoxy)methyl)quinoline (N12)

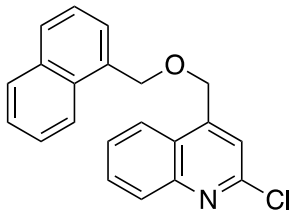

Step 1: 2-Chloroquinoline-4-carboxylic acid (1.2 g, 6.0 mmol, 1.0 equiv.) was dissolved in dry DCM (6.0 mL, 1.0 M) and the solution was cooled to 0 °C. Oxalyl chloride (0.76 mL, 9.0 mmol, 1.5 equiv.) and a few drops of dry DMF were added while stirring vigorously. The reaction was allowed to stir at room temperature until the evolution of gas had stopped (1 hour). The solvent was removed under reduced pressure, MeOH (2.6 mL) was added, and the solution was vigorously stirred for 30 minutes. The solvent was removed under reduced pressure and the residue was suspended in water. The aqueous phase was extracted with DCM (3 x 20 mL), washed with brine, dried over Na_2SO_4 and concentrated in *vacuo*. The crude product was dissolved in MeOH (30 mL, 0.2 M) and the solution

was cooled to 0 °C. $NaBH_4$ (568 mg, 15.0 mmol, 2.5 equiv.) was added portion-wise and the reaction was stirred at room temperature overnight. The solvent was removed in *vacuo*, the residue was suspended in water and extracted with EtOAc (3 x 20 mL). The organic layer was washed with brine (20 mL), dried over Na_2SO_4 and concentrated under reduced pressure. The crude product was purified by column chromatography on silica gel (*n*-hexane/EtOAc) affording (2-chloroquinolin-4-yl)methanol as a white solid (845 mg, 73% yield over 2 steps).

Step 2: (2-chloroquinolin-4-yl)methanol (194 mg, 1.0 mmol, 1.0 equiv.) was dissolved in dry DCM (5.0 mL, 0.2 M). The solution was cooled to 0 °C, $SOCl_2$ (0.15 mL, 2.0 mmol, 2.0 equiv.) was added dropwise and the reaction was kept under stirring at 0 °C for 2 hours. The solvent was removed under reduced pressure and the crude product 2-chloro-4-(chloromethyl)quinoline was used directly in **step 3**.

Step 3: In a 10 mL Schlenk, 1-naphthalene methanol (158 mg, 1.0 mmol, 1.0 equiv.) was dissolved in dry DMF (1.0 mL). The resulting solution was cooled to 0 °C and NaH (44 mg, 1.1 mmol, 1.1 equiv.) was added portion-wise. After 30 min, 2-chloro-4-(chloromethyl)quinoline (212 mg, 1.0 mmol, 1.0 equiv.) was added portion-wise. The reaction was stirred at room temperature for 36 hours, then distilled water was added to quench the reaction. The mixture was extracted with EtOAc (3 x 10 mL), the organic phase was washed with water (3 x 15 mL) and brine (15 mL), dried over Na_2SO_4, and the solvent was removed under reduced pressure. The solid residue was purified by column chromatography on silica gel (*n*-hexane/EtOAc) to afford **N12** as a white solid (234 mg, 0.7 mmol, 70% yield).

^{1}H NMR (600 MHz, $CDCl_3$) δ 9.00 (d, *J* = 8.7 Hz, 1H), 8.23 – 8.17 (m, 2H), 8.00 (d, *J* = 8.2 Hz, 1H), 7.96 – 7.85 (m, 3H), 7.71 (d, *J* = 6.9 Hz, 1H), 7.63 – 7.58 (m, 2H), 7.58 – 7.49 (m, 3H), 7.48 – 7.42 (m, 1H), 5.93 (s, 2H). **^{13}C NMR** (151 MHz, $CDCl_3$) δ 167.46, 133.97, 133.96, 133.64, 131.95, 131.72, 131.60, 130.63, 129.52, 128.93, 128.67, 127.95, 127.80, 127.00, 126.81, 126.35, 126.13, 125.97, 125.49, 124.62, 123.81, 65.32. **ESI-HRMS** calcd for $C_{21}H_{16}ClNO$ $[M+H]^+$ 334.0993, found 334.0981.

(2-chloroquinolin-4-yl)methyl 2-chloroquinoline-4-carboxylate (N13)

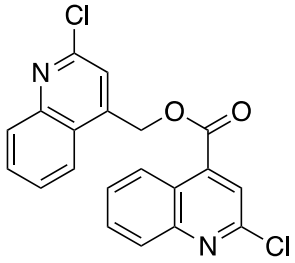

The advanced intermediate 2-chloroquinoline-4-carbonyl chloride was prepared in 2 steps from 2-chloroquinoline-4-carboxylic acid as described for the synthesis of **N12**. It was then directly used in **step 3**.

Step 3: (2-chloroquinolin-4-yl)methanol (823 mg, 4.2 mmol, 1.0 equiv.) was added to a solution of TEA (0.9 mL, 6.4 mmol, 1.5 equiv.), and DMAP (10 mg, 0.09 mmol, 0.02 equiv.) in dry DCM (17 mL, 0.25 M). The mixture was cooled to 0 °C and 2-chloroquinoline-4-carbonyl chloride (1.1 g, 4.7 mmol, 1.1 equiv.) was added portion-wise. The resulting solution was stirred at room temperature overnight, then a saturated NH_4Cl aqueous solution was used to quench the reaction. The mixture was extracted with DCM (3 x 20 mL), washed with brine (20 mL), dried over Na_2SO_4 and concentrated under reduced pressure. The crude product was purified by column chromatography on silica gel (*n*-hexane/EtOAc) affording **N13** as a white solid (1.2 g, 76% yield).

^{1}H NMR (400 MHz, $CDCl_3$) δ 8.76 – 8.69 (m, 1H), 8.14 – 8.06 (m, 2H), 8.06 – 7.99 (m, 1H), 7.92 (s, 1H), 7.80 (ddd, *J* = 8.4, 7.0, 1.3 Hz, 2H), 7.71 – 7.63 (m, 2H), 7.54 (d, *J* = 0.9 Hz, 1H), 5.91 (s, 2H). **^{13}C NMR** (101 MHz, $CDCl_3$) δ 164.38, 150.77, 150.19, 149.08, 148.20, 143.29, 136.73, 131.28, 131.02, 129.78, 129.42, 128.87, 127.86, 125.56, 124.75, 124.08, 123.95, 122.96, 121.51, 63.66. **ESI-HRMS** calcd for $C_{20}H_{12}Cl_2N_2O_2$ $[M+H]^+$ 383.0349, found 383.0350.

General procedure for the synthesis of azetidine 67a (GP-1)

A vial was charged with the allene **66a** (42 mg, 0.15 mmol, 1 equiv.), the desired photocatalyst (1 mol%), and the cocatalyst **N**. A freshly spilled dry solvent was added and the solution (0.1 M on substrate) was transferred into an NMR tube capped with a rubber septum. The mixture was degassed by freeze-pump-thaw (3 times) using a needle connected to a Schlenk line to pierce the septum, and then irradiated with either blue or purple LEDs. The reaction was monitored by TLC; once the conversion reached a plateau, the tube was recovered, the solvent removed under vacuum and 2,2'-dipyridine (11.7 mg, 0.075 mmol) was added as internal standard. A ^{1}H NMR was eventually collected to quantify the conversion **66a** and the yield of **67a**.

Unsuccessful substrates

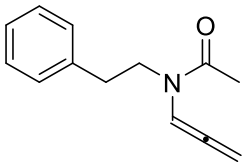

Traces + RSM

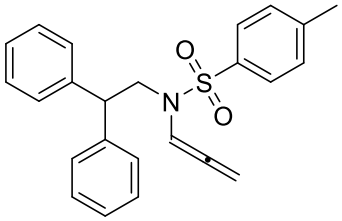

RSM

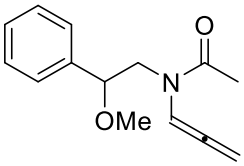

RSM

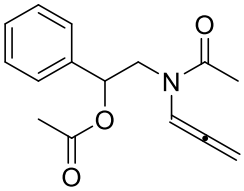

DEC + RSM

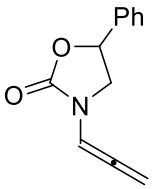

DEC + RSM

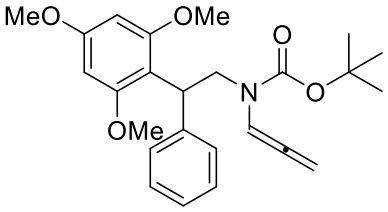

DEC + RSM

RSM: Recovery of starting material
DEC: Decomposition
SR: Side reaction

Characterization of azetidines

1-(3,3-diphenyl-2-vinylazetidin-1-yl)ethan-1-one

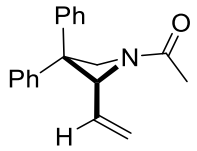

Product **67a** was prepared following general procedure **GP-1** in 24 hours from the corresponding allene (55.4 mg, 0.2 mmol). Light-yellow oil (41.6 mg, 75% yield). Two rotamers were observed due to the dynamic amide group (80:20 mixture of rotamers). Alternatively, the complete consumption of allene **66a** required 14 hours of irradiation performing the reaction in the presence of **PC6** instead of **PC5**; the experiment allowed us to isolate **67a** in 74% yield (41.0 mg).

^{1}H NMR (600 MHz, $CDCl_3$) δ 7.37 (t, *J* = 7.6 Hz, 2H RotA, 2H RotB), 7.29 (q, *J* = 7.0 Hz, 3H RotA, 3H RotB), 7.24 – 7.20 (m, 3H RotA, 3H RotB), 7.13 (d, *J* = 7.8 Hz, 2H RotA, 2H RotB), 5.62 – 5.56 (m, 1H RotA, 1H RotB), 5.49 (d, *J* = 7.1 Hz, 1H RotB), 5.40 (d, *J* = 17.1 Hz, 1H RotA, 1H RotB), 5.36 (d, *J* = 8.7 Hz, 1H RotA), 5.24 (d, *J* = 10.1 Hz, 1H RotA), 5.15 (d, *J* = 10.0 Hz, 1H RotB), 4.90 (d, *J* = 8.2 Hz, 1H RotB), 4.78 (d, *J* = 9.8 Hz, 1H RotA), 4.44 (d, *J* = 9.9 Hz, 1H RotA, 1H RotB), 1.99 (s, 3H RotB), 1.91 (s, 3H RotA). **^{13}C NMR** (151 MHz, $CDCl_3$) δ 172.3 (RotA), 171.8 (RotB), 146.5 (RotA), 146.4 (RotB), 141.5 (RotB), 141.3 (RotA), 135.8 (2C RotA), 134.9 (2C RotB), 128.9 (2C RotA, 2C RotB), 128.5 (3C RotA, 3C RotB), 128.3 (RotA, RotB), 127.1 (RotA, RotB), 127.0 (RotA, RotB), 126.8 (RotA, RotB), 120.0 (RotA), 118.6 (RotB), 75.0 (RotA), 72.2 (RotB), 61.3 (RotB), 58.4 (RotA), 50.7 (RotA), 50.6 (RotB), 20.5 (RotA), 19.9 (RotB). **ESI-HRMS** calcd for $C_{19}H_{19}KNO$ $[M+K]^+$ 316.1104, found 316.1108.

1-(3,3-diphenyl-2-vinylazetidin-1-yl)-2-methylprop-2-en-1-one

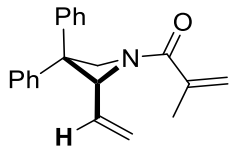

Product **67b** was prepared following general procedure **GP-1** in 36 hours from the corresponding allene (60.6 mg, 0.2 mmol). White solid (41.2 mg, 68% yield). Alternatively, the complete consumption of allene **66b** required 22 hours of irradiation performing the reaction in the presence of **PC6** instead of **PC5**; the experiment allowed us to isolate **67b** with the same yield (68%).

^{1}H NMR (600 MHz, $CDCl_3$) δ 7.38 – 7.35 (m, 2H), 7.32 – 7.27 (m, 3H), 7.24 – 7.21 (m, 3H), 7.13 – 7.11 (m, 2H), 5.57 – 5.49 (m, 2H), 5.40 – 5.30 (m, 3H), 5.15 (d, *J* = 9.8 Hz, 1H), 4.94 (d, *J* = 9.3 Hz, 1H), 4.48 (d, *J* = 9.4 Hz, 1H), 1.92 (s, 3H). **^{13}C NMR** (101 MHz, $CDCl_3$) δ 172.7, 146.7, 141.6, 139.2, 135.3, 128.9 (2C), 128.5 (2C), 128.3 (2C), 127.0 (2C), 126.9, 126.8, 119.7, 119.0, 60.0, 55.0, 51.1, 19.5. **ESI-HRMS** calcd for $C_{21}H_{22}NO$ $[M+H]^+$ 304.1701, found 304.1704.

cyclopropyl(3,3-diphenyl-2-vinylazetidin-1-yl)methanone

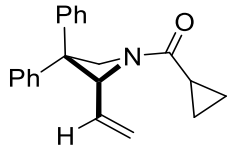

Product **67c** was prepared following general procedure **GP-2** in 24 hours from the corresponding allene (60.6 mg, 0.2 mmol). Light-yellow oil (45.5 mg, 75% yield). Two rotamers were observed due to the dynamic amide group (76:24 mixture of rotamers). Alternatively, the complete consumption of allene **66c** required 14 hours of irradiation performing the reaction in the presence of **PC6** instead of **PC5**; the experiment allowed us to isolate **67c** in 71% yield (43.1 mg).

^{1}H NMR (400 MHz, $CDCl_3$) δ 7.40 – 7.36 (m, 2H RotA, 2H RotB), 7.32 – 7.28 (m, 3H RotA, 3H RotB), 7.25 – 7.21 (m, 3H RotA, 3H RotB), 7.17 – 7.14 (m, 2H RotA, 2H RotB), 5.72 – 5.64 (m, 1H RotA), 5.55 – 5.40 (m, 2H RotA, 3H RotB), 5.22 (d, *J* = 10.1 Hz, 1H RotA, 1H RotB), 5.02 – 5.01 (m, 1H RotB), 4.76 (d, *J* = 9.7 Hz, 1H RotA), 4.62 – 4.61 (m, 1H RotB), 4.44 (d, *J* = 9.8 Hz, 1H RotA), 1.54 (tt, *J* = 7.9, 4.6 Hz, 1H RotA, 1H RotB), 1.01 – 0.88 (m, 2H RotA, 2H RotB), 0.73 – 0.71 (m, 2H RotA, 2H RotB). **^{13}C NMR** (101 MHz, $CDCl_3$) δ 176.1 (RotA, RotB), 146.6 (RotA, RotB), 142.1 (RotB), 141.6 (RotA), 136.7 (RotB), 136.6 (RotA), 128.8 (2C RotA, 2C RotB), 128.5 (2C RotA, 2C RotB), 128.2 (2C RotA, 2C RotB),

127.00 (2C RotA, 2C RotB), 126.95 (2C RotA), 126.9 (2C RotB), 119.4 (RotA), 119.0 (RotB), 74.3 (RotA, RotB), 60.7 (RotB), 58.8 (RotA), 51.0 (RotA, RotB), 11.5 (RotA), 11.0 (RotB), 7.9 (2C RotB), 7.7 (2C RotA). **ESI-HRMS** calcd for $C_{21}H_{21}NO$ $[M+H]^+$ 304.1701, found 304.1709.

1-(3,3-diphenyl-2-vinylazetidin-1-yl)pent-4-en-1-one

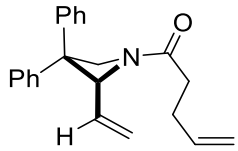

Product **67d** was prepared following general procedure **GP-1** in 24 hours from the corresponding allene (63.4 mg, 0.2 mmol). White solid (46.9 mg, 74% yield). Two rotamers are observed due to the dynamic amide group (74:26 mixture of rotamers).

^{1}H NMR (400 MHz, $CDCl_3$) δ 7.42 – 7.39 (m, 2H RotA, 2H RotB), 7.36 – 7.24 (m, 6H RotA, 6H RotB), 7.19 – 7.14 (m, 2H RotA, 2H RotB), 5.92 – 5.80 (m, 1H RotA, 1H RotB), 5.68 – 5.57 (m, 1H RotA, 1H RotB), 5.54 – 5.38 (m, 2H RotA, 2H RotB), 5.31 – 5.15 (m, 1H RotA, 1H RotB), 5.11 – 4.99 (m, 2H RotA, 2H RotB), 4.94 (d, *J* = 8.5 Hz, 1H RotB), 4.82 (d, *J* = 9.8 Hz, 1H RotA), 4.47 (d, *J* = 9.7 Hz, 1H RotA, 1H RotB), 2.47 – 2.25 (m, 4H RotA, 4H RotB). **^{13}C NMR** (101 MHz, $CDCl_3$) δ 174.2 (RotA), 173.6 (RotB), 146.5 (RotA), 146.4 (RotB), 141.4 (RotB), 141.3 (RotA), 137.4 (RotA, RotB), 136.0 (2C RotA), 134.9 (2C RotB), 128.8 (2C RotA, 2C RotB), 128.4 (2C RotA, 2C RotB), 128.3 (RotA, RotB), 127.0 (RotA, RotB), 126.9 (RotA), 126.8 (RotB), 126.7 (2C RotA, 2C RotB), 119.9 (RotA), 118.7 (RotB), 115.5 (RotB), 115.3 (RotA), 74.7 (RotA), 72.2 (RotB), 60.8 (RotB), 58.2 (RotA), 50.8 (RotA, RotB), 32.2 (RotA), 31.6 (RotB), 28.9 (RotA), 28.8 (RotB). **ESI-HRMS** calcd for $C_{22}H_{24}NO$ $[M+H]^+$ 318.1858, found 318.1862.

(3,3-diphenyl-2-vinylazetidin-1-yl)(phenyl)methanone

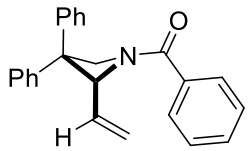

Product **67e** was prepared following general procedure **GP-1** in 36 hours from the corresponding allene (67.8 mg, 0.2 mmol). White solid (49.5 mg, 73% yield).

^{1}H NMR (400 MHz, $CDCl_3$) δ 7.69 (br, 2H), 7.46 – 7.27 (m, 8H), 7.24 – 7.16 (m, 5H), 5.63 (br, 3H), 5.09 (d, *J* = 9.1 Hz, 2H), 4.53 (d, *J* = 9.2 Hz, 1H). **^{13}C NMR** (101 MHz, $CDCl_3$) δ 171.9, 146.5, 141.6, 135.1,

133.8, 131.3, 128.9 (2C), 128.5 (4C), 128.4, 128.3 (2C), 128.2 (2C), 127.0, 126.9, 126.8, 118.9, 72.6, 64.1, 51.2. **ESI-HRMS** calcd for $C_{24}H_{22}NO$ $[M+H]^+$ 362.1521, found 362.1526.

(3,3-diphenyl-2-vinylazetidin-1-yl)(4-fluorophenyl)methanone

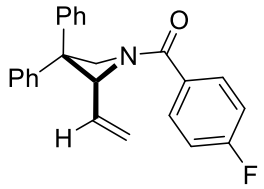

Product **67f** was prepared following general procedure **GP-1** in 36 hours from the corresponding allene (71.4 mg, 0.2 mmol). White solid (42.1 mg, 59% yield).

^{1}H NMR (400 MHz, $CDCl_3$) δ 7.71 (br, 2H), 7.39 – 7.07 (m, 12H), 5.62 (br, 3H), 5.09 (d, *J* = 9.2 Hz, 2H), 4.54 (d, *J* = 9.2 Hz, 1H). **^{13}C NMR** (101 MHz, $CDCl_3$) δ 170.8, 164.5 (d, *J* = 251.5 Hz), 146.4, 141.5, 135.0, 130.6 (d, *J* = 8.8 Hz, 2C), 128.9 (4C), 128.5, 128.3 (4C), 127.1, 127.0, 126.8, 119.2, 115.5 (d, *J* = 21.8 Hz), 72.5, 64.1, 51.2. **^{19}F NMR** (565 MHz, $CDCl_3$) δ -107.9 – -108.5 (m). **SI-HRMS** calcd for $C_{24}H_{21}FNO$ $[M+H]^+$ 358.1607, found 358.1601.

(3,3-diphenyl-2-vinylazetidin-1-yl)(4-methoxyphenyl)methanone

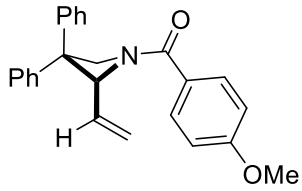

Product **67g** was prepared following general procedure **GP-1** in 36 hours from the corresponding allene (73.8 mg, 0.2 mmol). White solid (54.6 mg, 74% yield).

^{1}H NMR (400 MHz, $CDCl_3$) δ 7.71 – 7.68 (m, 2H), 7.38 – 7.17 (m, 10H), 6.91 (d, *J* = 8.3 Hz, 2H), 5.65 – 5.55 (m, 2H), 5.32 (br, 1H), 5.10 (d, *J* = 9.0 Hz, 2H), 4.54 (d, *J* = 9.0 Hz, 1H), 3.84 (s, 3H). **^{13}C NMR** (101 MHz, $CDCl_3$) δ 171.6, 162.0, 146.6, 141.7, 135.3, 130.3 (2C), 128.8 (2C), 128.5 (2C), 128.2 (2C), 127.0 (2C), 126.9 (2C), 125.9 (2C), 118.9, 113.6, 72.5, 64.0, 55.5, 51.1. **ESI-HRMS** calcd for $C_{25}H_{24}NO_2$ $[M+H]^+$ 370.1807, found 370.1817.

(3,3-diphenyl-2-vinylazetidin-1-yl)(furan-2-yl)methanone

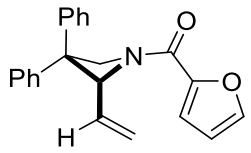

Product **67h** was prepared following general procedure **GP-1** in 36 hours from the corresponding allene (66.0 mg, 0.2 mmol). White solid (48.8 mg, 74% yield). Alternatively, the complete consumption of allene **66h** required 24 hours of irradiation performing the reaction in the presence of **PC6** instead of **PC5**; the experiment allowed us to isolate **67h** in 71% yield (46.8 mg).

^{1}H NMR (600 MHz, $CDCl_3$) δ 7.51 (s, 1H), 7.38 – 7.35 (m, 2H), 7.33 – 7.30 (m, 2H), 7.28 – 7.22 (m, 4H), 7.17 (d, *J* = 7.7 Hz, 2H), 7.12 (s, 1H), 6.49 (s, 1H), 5.73 (br, 1H), 5.61 (dt, *J* = 17.5, 9.1 Hz, 1H), 5.37 (br, 2H), 5.15 – 5.14 (m, 1H), 4.79 (br, 1H). **^{13}C NMR** (101 MHz, $CDCl_3$) δ 160.0, 146.6 (2C), 144.6, 141.5, 134.8, 128.8 (2C), 128.6 (2C), 128.2 (2C), 127.0 (2C), 126.9 (2C), 118.7, 116.1, 111.8, 72.6, 63.2, 51.7. **ESI-HRMS** calcd for $C_{22}H_{20}NO_2$ $[M+H]^+$ 330.1494, found 330.1500.

***tert*-butyl-(3,3-diphenyl-2-vinylazetidine-1-carboxylate)**

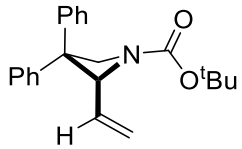

Product **67i** was prepared following general procedure **GP-1** in 24 hours from the corresponding allene (67.1 mg, 0.2 mmol). Colorless solid (34.2 mg, 51% yield).

^{1}H NMR (400 MHz, $CDCl_3$) δ 7.40 – 7.37 (m, 2H), 7.31 – 7.26 (m, 3H), 7.23 – 7.15 (m, 5H), 5.53 (ddd, *J* = 17.4, 10.1, 7.6 Hz, 1H), 5.35 (d, *J* = 17.0 Hz, 1H), 5.29 – 5.26 (m, 1H), 5.13 – 5.10 (m, 1H), 4.63 (d, *J* = 8.4 Hz, 1H), 4.35 (d, *J* = 8.4 Hz, 1H), 1.45 (s, 9H). **^{13}C NMR** (101 MHz, $CDCl_3$) δ 157.4, 146.7, 142.2, 135.9, 128.8 (2C), 128.5 (2C), 128.1, 127.1 (2C), 126.83 (2C), 126.75, 118.5, 80.1, 73.4, 60.1, 50.6, 28.5(3C). **ESI-HRMS** calcd for $C_{22}H_{24}NNaO_2$ $[M+Na]^+$ 358.1783, found 358.1789.

1-(3-methyl-3-phenyl-2-vinylazetidin-1-yl)ethan-1-one

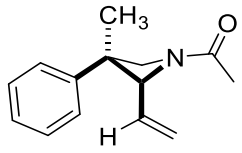

Product **67j** was prepared following general procedure **GP-1** in 72 hours from the corresponding allene (43.4 mg, 0.2 mmol). Only one diasteroisomer was isolated from the mixture as a colorless oil (31.2 mg, 72% yield). Two rotamers were observed due to the dynamic amide group (80:20 mixture of rotamers).

^{1}H NMR (600 MHz, $CDCl_3$) δ 7.33 (t, *J* = 7.7 Hz, 2H RotA, 2H RotB), 7.24 – 7.22 (m, 1H RotA, 1H RotB), 7.14 – 7.11 (m, 2H RotA, 2H RotB), 5.50 – 5.41 (m, 1H RotA, 1H RotB), 5.23 (d, *J* = 16.9 Hz, 1H RotA, 1H RotB), 5.14 (d, *J* = 11.6 Hz, 1H RotA), 5.09 (d, *J* = 10.3 Hz, 1H RotB), 4.68 (d, *J* = 7.5 Hz, 1H RotB), 4.62 (d, *J* = 8.2 Hz, 1H RotB), 4.57 (d, *J* = 8.4 Hz, 1H RotA), 4.45 (d, *J* = 9.6 Hz, 1H RotA), 3.92 – 3.89 (m, 1H RotA, 1H RotB), 1.98 (s, 3H RotB), 1.88 (s, 3H RotA), 1.70 (s, 3H RotA, 3H RotB). **^{13}C NMR** (151 MHz, $CDCl_3$) δ 171.7 (RotA), 170.9 (RotB), 142.0 (RotA, RotB), 135.6 (RotA), 134.7 (RotB), 128.4 (2C RotA, 2C RotB), 127.0 (2C RotA, 2C RotB), 126.7 (RotA, RotB), 118.9 (RotA), 118.1 (RotB), 76.0 (RotA), 73.2 (RotB), 59.4 (RotB), 56.2 (RotA), 43.1 (RotA, RotB), 30.5 (RotA), 30.3 (RotB), 20.1 (RotA), 19.7 (RotB). **ESI-HRMS** calcd for $C_{14}H_{18}NO$ $[M+H]^+$ 216.1388, found 216.1385.

2,2-dimethyl-1-(3-methyl-3-phenyl-2-vinylazetidin-1-yl)propan-1-one

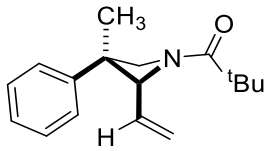

Product **67k** was prepared following general procedure **GP-1** in 160 hours from the corresponding allene (51.5 mg, 0.2 mmol). Only one diasteroisomer was isolated from the mixture as a colorless oil (23.2 mg, 45% yield).

^{1}H NMR (600 MHz, $CDCl_3$) δ 7.34 – 7.31 (m, 2H), 7.26 – 7.19 (m, 1H), 7.11 (d, *J* = 7.5 Hz, 2H), 5.46 (br, 1H), 5.20 (d, *J* = 16.8 Hz, 1H), 5.08 (d, *J* = 10.1 Hz, 1H), 4.73 (d, *J* = 7.6 Hz, 2H), 4.12 (br, 1H), 1.68 (s, 3H), 1.25 (s, 9H). **^{13}C NMR** (151 MHz, $CDCl_3$) δ 160.4, 142.4, 138.6, 128.4 (2C), 127.0 (2C), 126.5, 117.9, 58.7, 43.6, 42.0, 38.9, 30.5, 27.4 (3C). **ESI-HRMS** calcd for $C_{17}H_{24}NO$ $[M+H]^+$ 258.1858, found 258.1855.

1-(3-methyl-3-(4-(trifluoromethyl)phenyl)-2-vinylazetidin-1-yl)ethan-1-one

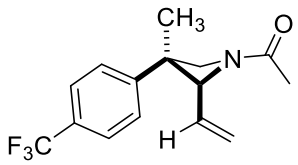

Product **67l** was prepared following general procedure **GP-1** in 72 hours from the corresponding allene (46.6 mg, 0.2 mmol). Only one diasteroisomer was isolated from the mixture as a light-yellow oil (21.0 mg, 45% yield). Two rotamers were observed due to the dynamic amide group (82:18 mixture of rotamers).

^{1}H NMR (600 MHz, $CDCl_3$) δ 7.59 (d, *J* = 8.1 Hz, 2H RotA, 2H RotB), 7.24 (d, *J* = 8.0 Hz, 2H RotA, 2H RotB), 5.46 – 5.40 (m, 1H RotA, 1H RotB), 5.27 (d, *J* = 15.7 Hz, 1H RotA, 1H RotB), 5.19 (d, *J* = 10.0 Hz, 1H RotA), 5.13 (d, *J* = 9.5 Hz, 1H RotB), 4.72 (br, 1H RotB), 4.61 (d, *J* = 8.3 Hz, 1H RotA, 1H RotB), 4.44 (d, *J* = 9.6 Hz, 1H RotA), 3.94 (d, *J* = 9.8 Hz, 1H RotA, 1H RotB), 1.99 (s, 3H RotB), 1.88 (s, 3H RotA), 1.71 (s, 3H RotA, 3H RotB). **^{13}C NMR** (151 MHz, $CDCl_3$) δ 171.7 (RotA), 170.9 (RotB), 146.1 (RotA, RotB), 135.2 (RotA, RotB), 129.1 (q, *J* = 32.6 Hz, RotA, RotB), 127.5 (2C RotA, 2C RotB), 125.4 (q, *J* = 4.0 Hz, 2C RotA, 2C RotB), 124.2 (q, *J* = 271.8 Hz, RotA, RotB), 119.6 (RotA, RotB), 75.8 (RotA), 73.1 (RotB), 59.3 (RotB), 56.1 (RotA), 43.2 (RotA, RotB), 30.3 (RotA), 29.8 (RotB), 20.1 (RotA, RotB). **^{19}F NMR** (565 MHz, $CDCl_3$) -62.4 (RotA, RotB). **ESI-HRMS** calcd for $C_{15}H_{16}F_3NNaO$ $[M+Na]^+$ 306.1082, found 306.1089.

1-(3-(4-chlorophenyl)-3-methyl-2-vinylazetidin-1-yl)ethan-1-one

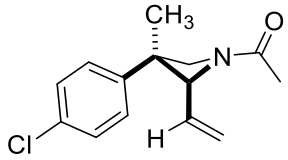

Product **67m** was prepared following general procedure **GP-1** in 72 hours from the corresponding allene (49.9 mg, 0.2 mmol). Only one diasteroisomer was isolated from the mixture as a light-yellow oil (22.4 mg, 45% yield). Two rotamers were observed due to the dynamic amide group (82:18 mixture of rotamers).

^{1}H NMR (400 MHz, $CDCl_3$) δ 7.31 – 7.29 (m, 2H RotA, 2H RotB), 7.14 – 7.04 (m, 2H RotA, 2H RotB), 5.47 – 5.35 (m, 1H RotA, 1H RotB), 5.23 (d, *J* = 16.8 Hz, 1H RotA, 1H RotB), 5.16 (d, *J* = 10.2 Hz, 1H RotA), 5.11 (d, *J* = 10.2 Hz, 1H RotB), 4.66 (d, *J* = 7.3 Hz, 1H RotB), 4.55 (d, *J* = 8.3 Hz, 1H RotA, 1H

RotB), 4.38 (d, *J* = 9.7 Hz, 1H RotA), 3.92 – 3.88 (m, 1H RotA, 1H RotB), 1.97 (s, 3H RotB), 1.87 (s, 3H RotA), 1.67 (s, 3H RotA, 3H RotB). **^{13}C NMR** (101 MHz, $CDCl_3$) δ 171.7 (RotA), 170.2 (RotB), 142.7 (RotB), 140.5 (RotA), 135.4 (RotA), 134.4 (RotB), 132.6 (RotA), 132.5 (RotB), 129.2 (RotB), 129.0 (RotA), 128.7 (RotB), 128.6 (RotA), 128.6 (2C RotB), 128.5 (2C RotA), 119.3 (RotA), 118.4 (RotB), 75.8 (RotA), 73.0 (RotB), 59.4 (RotB), 56.2 (RotA), 46.2 (RotB), 42.7 (RotA), 30.3 (RotA), 29.8 (RotB), 20.1 (RotA), 19.5 (RotB). **ESI-HRMS** calcd for $C_{14}H_{17}ClNO$ $[M+H]^+$ 250.0999, found 250.1008.

1-(3-(4-methoxyphenyl)-3-methyl-2-vinylazetidin-1-yl)ethan-1-one

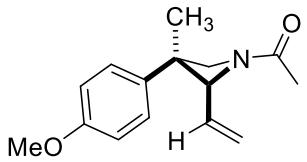

Product **67n** was prepared following general procedure **GP-1** in 72 hours from the corresponding allene (49.0 mg, 0.2 mmol). Only one diasteroisomer was isolated from the mixture as a light-yellow oil (20.1 mg, 41% yield). Two rotamers were observed due to the dynamic amide group (81:19 mixture of rotamers).

^{1}H NMR (600 MHz, $CDCl_3$) δ 7.07 – 7.04 (m, 2H RotA, 2H RotB), 6.87 – 6.85 (m, 2H RotA, 2H RotB), 5.49 – 5.40 (m, 1H RotA, 1H RotB), 5.23 – 5.19 (m, 1H RotA, 1H RotB), 5.14 (d, *J* = 10.2 Hz, 1H RotA), 5.09 (d, *J* = 10.2 Hz, 1H RotB), 4.65 (d, *J* = 7.3 Hz, 1H RotB), 4.57 (d, *J* = 8.2 Hz, 1H RotB), 4.53 (d, *J* = 8.4 Hz, 1H RotA), 4.41 (d, *J* = 9.7 Hz, 1H RotA), 3.90 – 3.87 (m, 1H RotA, 1H RotB), 3.80 (s, 3H RotA, 3H RotB), 1.97 (s, 3H RotB), 1.87 (s, 3H RotA), 1.67 (s, 3H RotA, 3H RotB). **^{13}C NMR** (151 MHz, $CDCl_3$) δ 171.7 (RotA), 171.0 (RotB), 158.3 (RotA, RotB), 135.8 (RotA), 134.9 (RotB), 134.0 (RotA, RotB), 128.1 (2C RotA, 2C RotB), 118.7 (RotA), 117.9 (RotB), 113.8 (2C RotA, 2C RotB), 76.0 (RotA), 73.2 (RotB), 59.7 (RotB), 56.4 (RotA), 55.4 (RotA, RotB), 43.7 (RotB), 42.5 (RotA), 30.4 (RotA), 30.2 (RotB), 20.1 (RotA), 19.7 (RotB). **ESI-HRMS** calcd for $C_{15}H_{20}NO_2$ $[M+H]^+$ 246.1494, found 246.1496.

1-(3-(3-bromophenyl)-3-methyl-2-vinylazetidin-1-yl)ethan-1-one

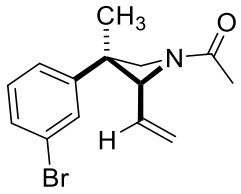

Product **67o** was prepared following general procedure **GP-1** in 72 hours from the corresponding allene (59.1 mg, 0.2 mmol). Only one diasteroisomer was isolated from the mixture as light-yellow oil (24.2 mg, 41% yield). Two rotamers were observed due to the dynamic amide group (80:20 mixture of rotamers).

^{1}H NMR (600 MHz, $CDCl_3$) δ 7.38 – 7.36 (m, 1H RotA, 1H RotB), 7.26 – 7.25 (m, 1H RotA, 1H RotB), 7.20 (t, *J* = 7.9 Hz, 1H RotA, 1H RotB), 7.06 – 7.05 (m, 1H RotA, 1H RotB), 5.48 – 5.41 (m, 1H RotA, 1H RotB), 5.25 (d, *J* = 17.0 Hz, 1H RotA, 1H RotB), 5.19 (d, *J* = 10.1 Hz, 1H RotA), 5.14 (d, *J* = 10.1 Hz, 1H RotB), 4.67 (d, *J* = 7.3 Hz, 1H RotB), 4.56 (d, *J* = 8.3 Hz, 1H RotA, 1H RotB), 4.39 (d, *J* = 9.7 Hz, 1H RotA), 3.90 (d, *J* = 9.8 Hz, 1H RotA, 1H RotB), 1.98 (s, 3H RotB), 1.87 (s, 3H RotA), 1.68 (s, 3H RotA, 3H RotB). **^{13}C NMR** (151 MHz, $CDCl_3$) δ 171.7 (RotA), 170.9 (RotB), 144.4 (RotA, RotB), 135.3 (RotA), 134.3 (RotB), 130.3 (RotA), 130.2 (RotB), 130.0 (RotA, RotB), 129.9 (RotA, RotB), 125.9 (RotB), 125.7 (RotA), 122.7 (RotA, RotB), 119.4 (RotA), 118.6 (RotB), 75.8 (RotA), 73.1 (RotB), 59.3 (RotB), 56.2 (RotA), 42.9 (RotA), 42.8 (RotB), 30.2 (RotA), 30.1 (RotB), 20.1 (RotA), 19.7 (RotB). **ESI-HRMS** calcd for $C_{14}H_{17}BrNO$ $[M+H]^+$ 295.2000, found 295.2015.

1-(3-(4-*iso*-butylphenyl)-3-methyl-2-vinylazetidin-1-yl)ethan-1-one

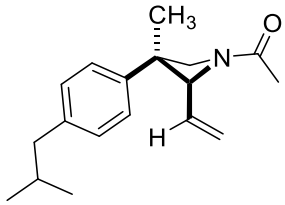

Product **67p** was prepared following general procedure **GP-1** in 72 hours from the corresponding allene (54.2 mg, 0.2 mmol). Only one diasteroisomer was isolated from the mixture as colorless oil (30.4 mg, 56% yield). Two rotamers were observed due to the dynamic amide group (82:18 mixture of rotamers).

^{1}H NMR (600 MHz, $CDCl_3$) δ 7.09 (d, *J* = 7.9 Hz, 2H RotA, 2H RotB), 7.04 – 7.02 (m, 2H RotA, 2H RotB), 5.50 – 5.41 (m, 1H RotA, 1H RotB), 5.23 – 5.19 (m, 1H RotA, 1H RotB), 5.13 (d, *J* = 10.3 Hz, 1H RotA),

5.08 (d, *J* = 10.3 Hz, 1H RotB), 4.66 (d, *J* = 7.4 Hz, 1H RotB), 4.59 (d, *J* = 8.1 Hz, 1H RotB), 4.54 (d, *J* = 8.3 Hz, 1H RotA), 4.43 (d, *J* = 9.6 Hz, 1H RotA), 3.90 – 3.87 (m, 1H RotA, 1H RotB), 2.45 – 2.44 (m, 2H RotA, 2H RotB), 1.97 (s, 3H RotB), 1.89 – 1.82 (m, 4H RotA, 1H RotB), 1.68 (s, 3H RotA, 3H RotB), 0.91 – 0.89 (m, 6H RotA, 6H RotB). **^{13}C NMR** (151 MHz, $CDCl_3$) δ 171.7 (RotA), 170.1 (RotB), 141.3 (RotB), 140.3 (RotB), 140.1 (RotA), 139.1 (RotA), 135.7 (RotA), 134.8 (RotB), 129.6 (2C RotB), 129.1 (2C RotA), 127.0 (2C RotB), 126.7 (2C RotA), 118.7 (RotA), 117.9 (RotB), 76.0 (RotA), 73.2 (RotB), 59.6 (RotB), 56.3 (RotA), 45.1 (RotA), 42.8 (RotB), 30.4 (RotA), 30.34 (RotB), 30.28 (RotA), 30.2 (RotB), 23.5 (RotB), 22.54 (3C RotB), 22.53 (RotA), 22.51 (3C RotA), 20.08 (RotA), 19.64 (RotB). **ESI-HRMS** calcd for $C_{18}H_{26}NO$ $[M+H]^+$ 272.2014, found 272.2010.

1-(3-(2-fluoro-[1,1'-biphenyl]-4-yl)-3-methyl-2-vinylazetidin-1-yl)ethan-1-one

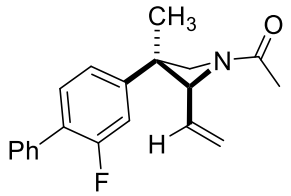

Product **67q** was prepared following general procedure **GP-1** in 72 hours from the corresponding allene (61.8 mg, 0.2 mmol). Only one diasteroisomer was isolated from the mixture as pale-yellow oil (38.3 mg, 62% yield). Two rotamers were observed due to the dynamic amide group (80:20 mixture of rotamers).

^{1}H NMR (600 MHz, $CDCl_3$) δ 7.55 – 7.54 (m, 2H RotA, 2H RotB), 7.46 – 7.36 (m, 4H RotA, 4H RotB), 7.07 – 7.06 (m, 1H RotB), 7.02 – 6.98 (m, 1H RotA, 1H RotB), 6.94 – 6.92 (m, 1H RotA), 5.56 – 5.49 (m, 1H RotA, 1H RotB), 5.28 (d, *J* = 17.0 Hz, 1H RotA, 1H RotB), 5.22 (d, *J* = 10.1 Hz, 1H RotA), 5.16 (d, *J* = 10.1 Hz, 1H RotB), 4.71 (d, *J* = 7.3 Hz, 1H RotB), 4.59 (d, *J* = 8.3 Hz, 1H RotA, 1H RotB), 4.43 (d, *J* = 9.7 Hz, 1H RotA), 3.94 (d, *J* = 9.8 Hz, 1H RotA, 1H RotB), 2.00 (s, 3H RotB), 1.89 (s, 3H RotA), 1.73 (s, 3H RotA, 3H RotB). **^{13}C NMR** (151 MHz, $CDCl_3$) δ 171.8 (RotA), 170.2 (RotB), 159.7 (d, *J* = 248.5 Hz, RotA, RotB), 143.6 (d, *J* = 7.2 Hz, RotA, RotB), 135.4 (d, *J* = 18.8 Hz, RotA, RotB), 131.1 (d, *J* = 3.9 Hz, RotB), 130.7 (d, *J* = 3.4 Hz, RotA), 129.08 (RotA, RotB), 129.06 (2C RotA, 2C RotB), 128.6 (2C RotA, 2C RotB), 127.9 (RotA), 127.8 (RotB), 127.3 (RotA, RotB), 123.4 (RotB), 123.0 (RotA), 119.4 (RotA), 118.5 (RotB), 115.2 – 114.8 (m, RotA, RotB), 75.9 (RotA), 73.1 (RotB), 57.7 (RotB), 56.3 (RotA), 46.2 (RotB), 42.9 (RotA), 30.1 (RotA), 29.8 (RotB), 20.1 (RotA), 19.4 (RotB). **^{19}F NMR** (565 MHz, $CDCl_3$) δ -117.41

(t, *J* = 10.2 Hz, RotA), -117.47 (t, *J* = 9.9 Hz, RotB). **ESI-HRMS** calcd for $C_{20}H_{21}FNO$ $[M+H]^+$ 310.1607, found 310.1604.

1-(3-benzyl-3-phenyl-2-vinylazetidin-1-yl)ethan-1-one

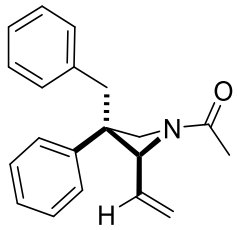

Product **67r** was prepared following general procedure **GP-1** in 72 hours from the corresponding allene (58.2 mg, 0.2 mmol). Only one diasteroisomer was isolated from the mixture as a light-yellow oil (30.3 mg, 52% yield). Two rotamers were observed due to the dynamic amide group (79:21 mixture of rotamers).

^{1}H NMR (600 MHz, $CDCl_3$) δ 7.24 – 7.09 (m, 6H RotA, 6H RotB), 6.84 (d, *J* = 7.2 Hz, 2H RotA, 2H RotB), 6.70 (d, *J* = 7.3 Hz, 2H RotA, 2H RotB), 5.58 – 5.49 (m, 1H RotA, 1H RotB), 5.29 (d, *J* = 17.0 Hz, 1H RotA, 1H RotB), 5.20 (d, *J* = 10.0, 1H RotA), 5.15 (d, *J* = 10.2 Hz, 1H RotB), 4.89 (d, *J* = 7.8 Hz, 1H RotB), 4.76 (d, *J* = 8.6 Hz, 1H RotA), 4.45 (d, *J* = 8.4 Hz, 1H RotB), 4.25 (d, *J* = 9.9 Hz, 1H RotA), 4.19 (d, *J* = 9.9 Hz, 1H RotA), 4.13 (d, *J* = 7.9 Hz, 1H RotB), 3.28 (d, *J* = 13.5 Hz, 1H RotA, 1H RotB), 3.22 (d, *J* = 13.4 Hz, 1H RotA, 1H RotB), 1.94 (s, 3H RotB), 1.86 (s, 3H RotA). **^{13}C NMR** (151 MHz, $CDCl_3$) δ 171.3 (RotA), 170.7 (RotB), 140.1 (RotB), 140.0 (RotA), 136.2 (RotA, RotB), 135.5 (RotA), 134.5 (RotB), 130.2 (2C RotA, 2C RotB), 128.4 (RotA, RotB), 128.1 (4C RotA, 4C RotB), 128.0 (RotA, RotB), 126.9 (RotA, RotB), 126.7 (RotA, RotB), 119.2 (RotA), 118.6 (RotB), 75.1 (RotA), 72.4 (RotB), 55.9 (RotB), 53.0 (RotA), 49.0 (RotA), 48.8 (RotB), 48.0 (RotA, RotB), 20.0 (RotA), 19.6 (RotB). **ESI-HRMS** calcd for $C_{20}H_{22}NO$ $[M+H]^+$ 292.1701, found 292.1695. *(Partial decomposition during the acquisition of NMR spectra was observed).*

1-(3-(but-3-en-1-yl)-3-phenyl-2-vinylazetidin-1-yl)ethan-1-one

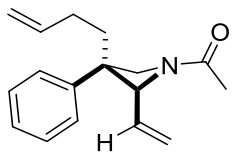

Product **67s** was prepared following general procedure **GP-1** in 72 hours from the corresponding allene (51.2 mg, 0.2 mmol). Only one diasteroisomer was isolated from the mixture as a light-yellow

oil (34.8 mg, 68% yield). Two rotamers were observed due to the dynamic amide group (81:19 mixture of rotamers).

^{1}H NMR (400 MHz, $CDCl_3$) δ 7.38 – 7.31 (m, 2H RotA, 2H RotB), 7.24 – 7.12 (m, 2H RotA, 2H RotB), 7.06 – 7.03 (m, 1H RotA, 1H RotB), 5.75 – 5.65 (m, 1H RotA, 1H RotB), 5.63 – 5.41 (m, 1H RotA, 1H RotB), 5.28 – 5.21 (m, 1H RotA, 1H RotB), 5.17 – 5.10 (m, 1H RotA, 1H RotB), 4.96 – 4.82 (m, 2H RotA, 2H RotB), 4.70 (d, *J* = 7.7 Hz, 1H RotB), 4.57 (d, *J* = 8.5 Hz, 1H RotA), 4.40 (d, *J* = 9.8 Hz, 1H RotA), 4.35 (d, *J* = 9.6 Hz, 1H RotB), 3.99 (d, *J* = 9.8 Hz, 1H RotA), 3.91 (d, *J* = 9.5 Hz, 1H RotB), 2.11 – 2.07 (m, 2H RotA, 2H RotB), 1.97 (s, 3H RotB), 1.87 (s, 3H RotA), 1.75 – 1.60 (m, 2H RotA, 2H RotB). **^{13}C NMR** (151 MHz, $CDCl_3$) δ 171.4 (RotA), 170.7 (RotB), 142.7 (RotB), 139.8 (RotA), 138.4 (RotB), 137.6 (RotA), 135.5 (RotA), 134.6 (RotB), 128.7 (RotB), 128.4 (RotA), 128.32 (RotA), 128.28 (RotB), 127.68 (RotA), 127.65 (RotB), 126.7 (RotA), 126.6 (RotB), 126.0 (RotA), 125.7 (RotB), 118.9 (RotA), 118.3 (RotB), 115.2 (RotA), 114.8 (RotB), 75.5 (RotA), 72.6 (RotB), 55.6 (RotB), 53.6 (RotA), 47.0 (RotA), 46.2 (RotB), 43.4 (RotB), 42.1 (RotA), 28.8 (RotA), 28.6 (RotB), 20.3 (RotB), 20.0 (RotA). **ESI-HRMS** calcd for $C_{17}H_{21}NNaO$ $[M+Na]^+$ 256.1521, found 278.1535. *(Partial decomposition during the acquisition of NMR spectra was observed).*

1-(3-(4-chlorophenyl)-3-phenyl-2-vinylazetidin-1-yl)ethan-1-one

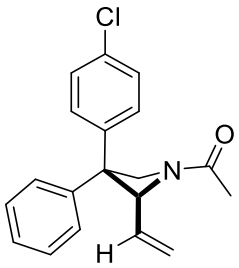

Product **67t** was prepared following general procedure **GP-1** in 36 hours, from the corresponding allene (62.3 mg, 0.2 mmol). A mixture of two diasteroisomers in 52:48 ratio was isolated as a light-yellow oil (46.4 mg, 75% yield). Two rotamers were observed due to the dynamic amide group (74:26 mixture of rotamers for Dia1, 81:19 mixture for Dia2).

^{1}H NMR (600 MHz, $CDCl_3$) δ 7.39 – 7.27 (m, 4H Dia1, RotA, RotB; 4H Dia2, RotA, RotB), 7.24 – 7.03 (m, 5H Dia1, RotA, RotB; 5H Dia2, RotA, RotB), 5.60 – 5.48 (m, 1H Dia1, RotA, RotB; 1H Dia2, RotA, RotB), 5.43 – 5.34 (m, 2H Dia1, RotA; 2H Dia2, RotA), 5.29 – 5.24 (m, 2H Dia1, RotA, 2RotB; 2H Dia2, RotA, RotB), 5.16 (t, *J* = 10.6 Hz, 1H Dia1, RotB), 4.90 (d, *J* = 8.2 Hz, 1H Dia2, RotB), 4.83 (d, *J* = 8.3 Hz,

1H Dia2, RotB), 4.76 (d, *J* = 9.8 Hz, 1H Dia2, RotA), 4.70 (d, *J* = 9.9 Hz, 1H Dia2, RotA), 4.45 (d, *J* = 8.2 Hz, 1H Dia 1, RotB), 4.42 (d, *J* = 9.9 Hz, 1H Dia1, RotA), 4.36 (d, *J* = 9.8 Hz, 1H Dia1, RotA, RotB), 1.98 (s, 3H Dia2, RotA, RotB), 1.90 (s, 3H Dia1, RotA, RotB). **^{13}C NMR** (151 MHz, $CDCl_3$) δ 172.4 (Dia2, RotA, RotB), 172.2 (Dia1, RotA, RotB), 145.9 (Dia2, RotA, RotB), 145.0 (Dia1, RotA, RotB), 140.7 (Dia1, RotA, RotB), 120.0 (Dia2, RotA, RotB), 135.6 (Dia1, Dia2, RotA, RotB), 134.7 (Dia2, RotB), 134.6 (Dia1, RotB), 133.03 (Dia2, RotA), 132.97 (Dia1, RotA), 129.8 (Dia1, Dia2, RotA; RotB) 129.0 (Dia1, Dia2, RotA, RotB), 128.48 (Dia2, RotA, RotB), 128.45 (Dia1, RotA, RotB), 128.2 (Dia1, Dia2, RotA, RotB), 127.3 (Dia1, Dia2, RotA, RotB), 127.2 (Dia1, RotA, RotB), 126.7 (Dia2, RotA, RotB), 120.3 (Dia1, Dia2, RotA, RotB), 120.2 (Dia2, RotA), 118.9 (Dia1, RotA), 75.01 (Dia1, Dia2, RotB), 74.7 (Dia1, RotA), 72.2 (Dia2, RotB), 71.9 (Dia1, RotB), 61.1 (Dia2, RotB), 60.5 (Dia2, RotB), 58.34 (Dia1, RotB), 58.19 (Dia1, RotA), 50.34 (Dia1, Dia2, RotA, RotB), 20.49 (Dia1, Dia2, RotA), 19.84 (Dia1, Dia2, RotB). **ESI-HRMS** calcd for $C_{19}H_{18}ClNO$ $[M+H]^+$ 311.1077, found 311.1073.

1-(3,3-diphenyl-2-vinylazetidin-1-yl)-2-methylpropan-1-one

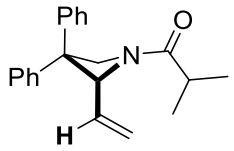

Product **67u** was prepared following general procedure **GP-1** in 24 hours from the corresponding allene (61.1 mg, 0.2 mmol). Light-yellow oil (35.4 mg, 58% yield). Two rotamers were observed due to the dynamic amide group (71:29 mixture of rotamers).

^{1}H NMR (400 MHz, $CDCl_3$) δ 7.38 – 7.35 (m, 2H RotA, 2H RotB), 7.32 – 7.20 (m, 6H RotA, 6H RotB), 7.13 (d, *J* = 7.7 Hz, 2H RotA, 2H RotB), 5.65 – 5.55 (m, 1H RotA, 1H RotB), 5.48 – 5.33 (m, 2H RotA, 2H RotB), 5.22 (d, *J* = 10.1 Hz, 1H RotA), 5.17 – 5.13 (m, 1H RotB), 4.93 (d, *J* = 8.2 Hz, 1H RotB), 4.77 (d, *J* = 9.9 Hz, 1H RotA), 4.47 – 4.40 (m, 1H RotA, 1H RotB), 2.52 (dt, *J* = 13.6, 7.2 Hz, 1H RotA, 1H RotB), 1.21 (d, *J* = 6.8 Hz, 3H RotB), 1.10 – 1.06 (m, 6H RotA, 3H RotB). **^{13}C NMR** (101 MHz, $CDCl_3$) δ 179.0 (RotA), 178.3 (RotB), 146.7 (RotA, RotB), 141.6 (RotB), 141.4 (RotA), 136.4 (RotA), 135.0 (RotB), 128.8 (2C RotA, 2C RotB), 128.5 (2C RotA, 2C RotB), 128.3 (RotA, RotB), 127.0 (2C RotA, 2C RotB), 126.9 (RotA, RotB), 126.8 (2C RotA, 2C RotB), 119.6 (RotA), 118.7 (RotB), 74.8 (RotA), 72.2 (RotB), 61.0 (RotB), 58.1 (RotA), 50.8 (RotA, RotB), 30.7 (RotA, RotB), 19.6 (RotB), 19.4 (RotA), 18.9 (RotA), 18.4 (RotB). **ESI-HRMS** calcd for $C_{21}H_{24}NO$ $[M+H]^+$ 306.1858, found 306.1868.

1-(3,3-diphenyl-2-vinylazetidin-1-yl)-2,2-diphenylethan-1-one

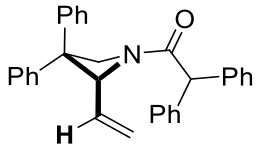

Product **67v** was prepared following general procedure **GP-1** in 24 hours from the corresponding allene (85.8 mg, 0.2 mmol). Light-yellow oil (39.5 mg, 46% yield). Two rotamers are observed due to the dynamic amide group (73:27 mixture of rotamers).

^{1}H NMR (400 MHz, $CDCl_3$) δ 7.41 – 7.17 (m, 17H RotA, 17H RotB), 7.10 (dd, *J* = 7.1, 1.8 Hz, 2H RotA, 2H RotB), 7.00 – 6.97 (m, 2H RotA), 6.95 – 6.93 (m, 2H RotB), 5.69 – 5.60 (m, 1H RotA), 5.53 – 5.48 (m, 1H RotB), 5.40 (d, *J* = 6.7 Hz, 2H RotB), 5.30 (dd, *J* = 10.1, 1.4 Hz, 1H RotA), 5.24 (d, *J* = 8.6 Hz, 1H RotA), 5.01 (s, 1H RotA), 4.95 (s, 1H RotB), 4.84 (d, *J* = 10.0 Hz, 1H RotA), 4.78 (d, *J* = 8.3 Hz, 1H RotB), 4.44 (d, *J* = 8.3 Hz, 1H RotB), 4.39 (d, *J* = 10.0 Hz, 1H RotA). **^{13}C NMR** (101 MHz, $CDCl_3$) δ 172.8 (RotA), 172.1 (RotB), 146.3 (RotA, RotB), 140.9 (RotA, RotB), 139.4 (RotA, RotB), 138.4 (RotA, RotB), 136.2 (RotA), 134.6 (RotB), 129.0 (2C RotA, 2C RotB), 128.9 (4C RotA), 128.83 (4C RotA), 128.75 (4C RotB), 128.7 (4C RotB), 128.6 (RotA), 128.51 (RotB), 128.47 (RotA), 128.3 (RotB), 128.3 (2C RotA, 2C RotB), 128.2 (RotA), 128.1 (RotB), 127.3 (RotA, RotB), 126.9 (RotA, RotB), 126.8 (RotA, RotB), 126.7 (2C RotB), 126.5 (2C RotA), 120.0 (RotA, RotB), 74.8 (RotA), 72.8 (RotB), 61.1 (RotB), 58.4 (RotA), 54.5 (RotB), 54.0 (RotA), 50.8 (RotA, RotB). **ESI-HRMS** calcd for $C_{31}H_{28}NO$ $[M+H]^+$ 430.2093, found 430.2098.

Scale-up syntheses

Synthesis of 2a on 1.0 mmol of starting material

To a flame-dried Schlenk tube equipped with magnetic stirring was charged allene **66i** (335 mg, 1.0 mmol, 1.0 equiv.), **PC5** (10.9 mg, 0.01 mmol, 1 mol%) and **N4** (119 mg, 0.3 mmol, 30 mol%). The mixture was then dissolved in 10 mL of a toluene:DCM 8:2 mixture (0.1 M). The Schlenk tube, capped with a rubber septum, was degassed by freeze-pump-thaw (3 times) and then irradiated with a purple LED strip for 5 days. Upon complete conversion, as determined by TLC, the mixture was diluted with DCM, transferred into a round-bottomed flask and concentrated under reduced pressure. The crude was purified by chromatography on silica gel (*n*-hexane/EtOAc, under gradient) to afford **67i** as a white solid (139 mg, 50%).

Valorization of the products

Deprotection of Boc-azetidine

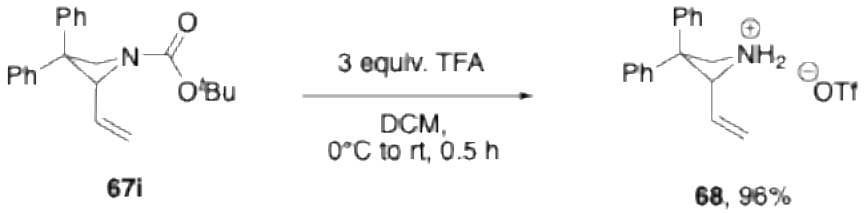

67i **68**, 96%

3,3-diphenyl-2-vinylazetidin-1-ium 2,2,2-trifluoroacetate 68

To a vial containing a solution of **67i** (34 mg, 0.1 mmol, 1 equiv.) in DCM (0.15 mL, 0.75 M), trifluoroacetic acid (23 mL, 0.3 mmol, 3 equiv.) was slowly added at 0 °C. The resulting mixture was stirred at room temperature until complete conversion of the starting material (30 minutes). The mixture was quenched with a saturated $NaHCO_3$ aqueous solution and extracted with DCM (3 x 15 mL). Upon evaporation of volatiles, the product **68** was obtained in 96% yield (33.6 mg) without further purification.

^{1}H NMR (600 MHz, D_2O) δ 7.47 – 7.41 (m, 4H), 7.38 – 7.33 (m, 6H), 5.80 – 5.70 (m, 3H), 5.51 – 5.49 (m, 1H), 5.06 (d, *J* = 11.3 Hz, 1H), 4.56 (d, *J* = 11.2 Hz, 1H). **^{13}C NMR** (151 MHz, D_2O) δ 163.0 (q, *J* = 35.55), 145.1, 138.9, 130.0, 129.3 (2C), 129.0 (2C), 127.8, 127.5, 127.4 (2C), 125.6 (2C), 124.1, 116.4 (q, *J* = 291.53), 69.8, 53.7, 52.2. **^{19}F NMR** (565 MHz, D_2O) δ -75.53. **ESI-HRMS** calcd for $C_{17}H_{18}N$ [M-($CF_3CO_2^-$)]$^+$ 236.1434, found 236.1426.

Synthesis of ureido-azetidine from 67i:

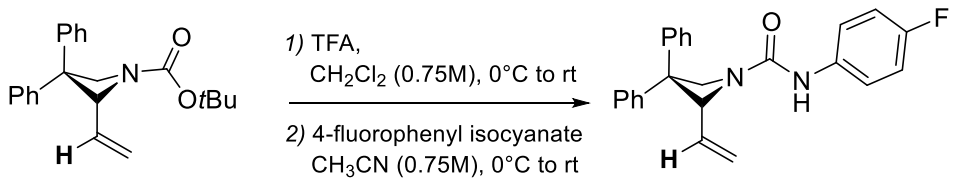

***N*-(4-fluorophenyl)-3,3-diphenyl-2-vinylazetidine-1-carboxamide 69**

To a vial containing a solution of **67i** (50 mg, 0.150 mmol, 1 equiv.) in DCM (0.2 mL, 0.75 M), trifluoroacetic acid (34 mL, 0.45 mmol, 3 equiv.) was slowly added at 0 °C. The resulting mixture was stirred at room temperature until complete conversion of the starting material (30 minutes). The

mixture was quenched with a saturated $NaHCO_3$ aqueous solution and sequentially extracted with DCM (3 x 15 mL). Product **68** was obtained in quantitative yield and directly used without further purification in the second step.

To a solution of **68** in dry CH_3CN (0.75M), 4-fluorophenyl isocyanate (25 mL, 0.225 mmol, 1.5 equiv.) was added at 0 °C. The mixture was stirred at room temperature for 12 hours, then the organic solvent was evaporated under reduced pressure, and the residue was purified by flash column chromatography (*n*-hexane/EtOAc 8:2) to afford the desired product **69** as a white solid (31.5 mg, 63%).

^{1}H NMR (600 MHz, $CDCl_3$) δ 7.39 (t, *J* = 7.7 Hz, 2H), 7.33 – 7.28 (m, 5H), 7.26 – 7.21 (m, 3H), 7.18 (dd, *J* = 8.2, 1.3 Hz, 2H), 6.96 (t, *J* = 8.7 Hz, 2H), 6.33 (br, 1H), 5.75 – 5.70 (m, 1H), 5.63 (dd, *J* = 17.2, 1.7 Hz, 1H), 5.37 – 5.33 (m, 2H), 4.67 (d, *J* = 8.3 Hz, 1H), 4.51 (d, *J* = 8.3 Hz, 1H). **^{13}C NMR** (151 MHz, $CDCl_3$) δ 158.9 (d, *J* = 241.9 Hz), 157.9, 146.0, 141.6, 136.8, 134.5 (d, *J* = 2.6 Hz), 128.9 (2C), 128.3 (8C), 127.1 (d, *J* = 6.1 Hz, 2C), 126.9, 121.0 – 120.9 (m, 2C), 115.7 (d, *J* = 22.5 Hz), 73.7, 59.2, 50.8. **^{19}F NMR** (565 MHz, $CDCl_3$) δ -119.8 (tt, *J* = 8.6, 4.8 Hz). **ESI-HRMS** calcd for $C_{24}H_{22}FN_2O$ $[M+H]^+$ 373.1716, found 373.1719.

Synthesis of ethylidene azetidine

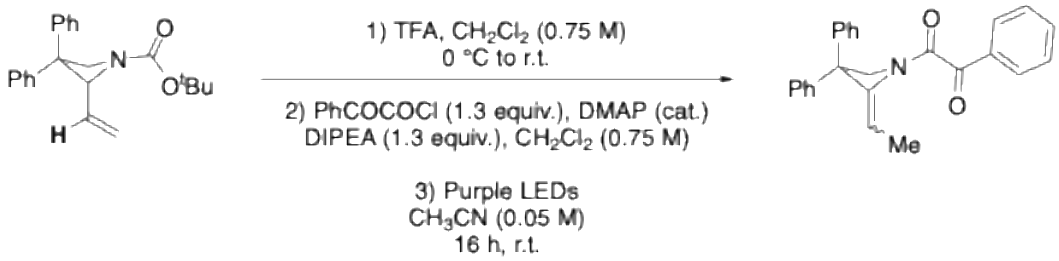

(*Z*)-1-(2-ethylidene-3,3-diphenylazetidin-1-yl)-2-phenylethane-1,2-dione 70

To a vial containing a solution of **67i** (34 mg, 0.1 mmol, 1 equiv.) in DCM (0.15 mL, 0.75 M), trifluoroacetic acid (23 mL, 0.3 mmol, 3 equiv.) was slowly added at 0 °C. The resulting mixture was stirred at room temperature until complete conversion of the starting material (30 minutes). The mixture was quenched with a saturated $NaHCO_3$ aqueous solution and sequentially extracted with DCM (3 x 15 mL). The crude product was obtained in quantitative yield and directly used without further purification in the second step.

To the solution of the crude amine (1 equiv.) in dry DCM (0.25 M), DIPEA (1.3 equiv.) and DMAP (0.02 equiv.) were added, then phenyl glyoxylic chloride (1.1 equiv.) was added dropwise at 0 °C. The resulting solution was allowed to stir at room temperature overnight. The reaction was then quenched with a saturated aqueous solution of NH_4Cl and then extracted with DCM three times. The organic phase was then dried over Na_2SO_4, filtered and concentrated under reduced pressure. The crude product was purified by chromatography on silica gel (*n*-hexane/EtOAc gradient) to afford the corresponding amide.

The phenyl glyoxylic azetidine (25 mg, 0.068 mmol) was dissolved in dry CH_3CN (680 mL, 0.05 M). The resulting solution was transferred into an NMR tube capped with a rubber septum, degassed by freeze-pump-thaw (3 times) and afterwards irradiated with a purple LED strip for 16 hours at room temperature. The solvent was then removed under reduced pressure, and the residue was purified by flash column chromatography (*n*-hexane/EtOAc 7:3) to afford the desired product **70** as pale-yellow solid (20 mg, 63% over two steps).

^{1}H NMR (600 MHz, $CDCl_3$) δ 8.15 (d, *J* = 7.5 Hz, 2H IsoB), 8.03 – 8.00 (m, 2H IsoA), 7.63 – 7.60 (m, 1H IsoA, 1H IsoB), 7.50 – 7.45 (m, 2H IsoA, 2H IsoB), 7.39 – 7.27 (m, 10H IsoA, 10H IsoB), 5.02 (q, *J* = 7.3 Hz, 1H IsoA), 4.89 (q, *J* = 7.3 Hz, 1H IsoB), 4.69 (s, 2H IsoB), 4.65 (s, 2H IsoA), 2.18 (d, *J* = 7.3 Hz, 3H IsoA), 1.47 (d, *J* = 7.5 Hz, 3H IsoB). **^{13}C NMR** (151 MHz, $CDCl_3$) δ 189.6 (IsoA, IsoB), 161.0 (IsoA, IsoB), 146.0 (IsoA), 143.4 (IsoB), 134.8 (IsoA, IsoB), 133.3 (IsoA, IsoB), 130.7 (IsoB), 130.4 (IsoA), 129.1 (IsoB), 129.0 (IsoA), 128.7 (IsoA, IsoB), 128.1 (IsoA, IsoB), 127.9 (IsoB), 127.7 (IsoA), 127.3 (IsoA, IsoB), 108.8 (IsoA, IsoB), 63.1 (IsoA), 62.2 (IsoB), 58.7 (IsoB), 56.8 (IsoA), 14.7 (IsoA), 12.24 (IsoB). **ESI-HRMS** calcd for $C_{25}H_{22}NO_2$ $[M+H]^+$ 368.1651, found 368.1655.

Ring closing metathesis on 67d

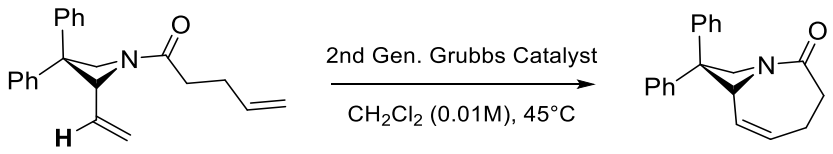

8,8-diphenyl-1-azabicyclo[5.2.0]non-5-en-2-one 71

To a solution of **67d** (30 mg, 0.095 mmol, 1 equiv.) in DCM (10 mL, 0.01 M) Grubbs 2nd generation catalyst was added (4 mg, 0.005 mmol, 5 mol%). The resulting mixture was stirred at reflux until complete conversion of the starting material (1 hour). The mixture was allowed to warm to room

temperature and the crude was directly purified through silica gel column (*n*-hexane/AcOEt gradient *8:2 to 1:1*) to give **71** as colorless oil in 97% yield (26.6 mg).[1]

^{1}H NMR (400 MHz, $CDCl_3$) δ 7.45 – 7.41 (m, 2H), 7.36 – 7.32 (m, 1H), 7.27 – 7.21 (m, 3H), 7.16 – 7.14 (m, 2H), 7.04 – 7.02 (m, 2H), 5.80 (br, 1H), 5.68 – 5.62 (m, 1H), 5.18 (dt, *J* = 11.8, 1.4 Hz, 1H), 4.71 (dd, *J* = 9.6, 1.5 Hz, 1H), 4.49 (d, *J* = 9.6 Hz, 1H), 2.81 – 2.73 (m, 1H), 2.54 – 2.44 (m, 1H), 2.42 – 2.36 (m, 1H), 2.35 – 2.26 (m, 1H). **^{13}C NMR** (101 MHz, $CDCl_3$) δ 173.1, 145.0, 142.0, 130.0, 128.9 (2C), 128.11 (2C), 128.08 (2C), 127.4, 127.2 (2C), 127.1, 126.8, 69.6, 59.9, 51.5, 34.8, 24.4. **ESI-HRMS** calcd for $C_{20}H_{19}NNaO$ $[M+Na]^+$ 312.1364, found 312.1369.

Synthesis of deuterated substrate *d*- 66v

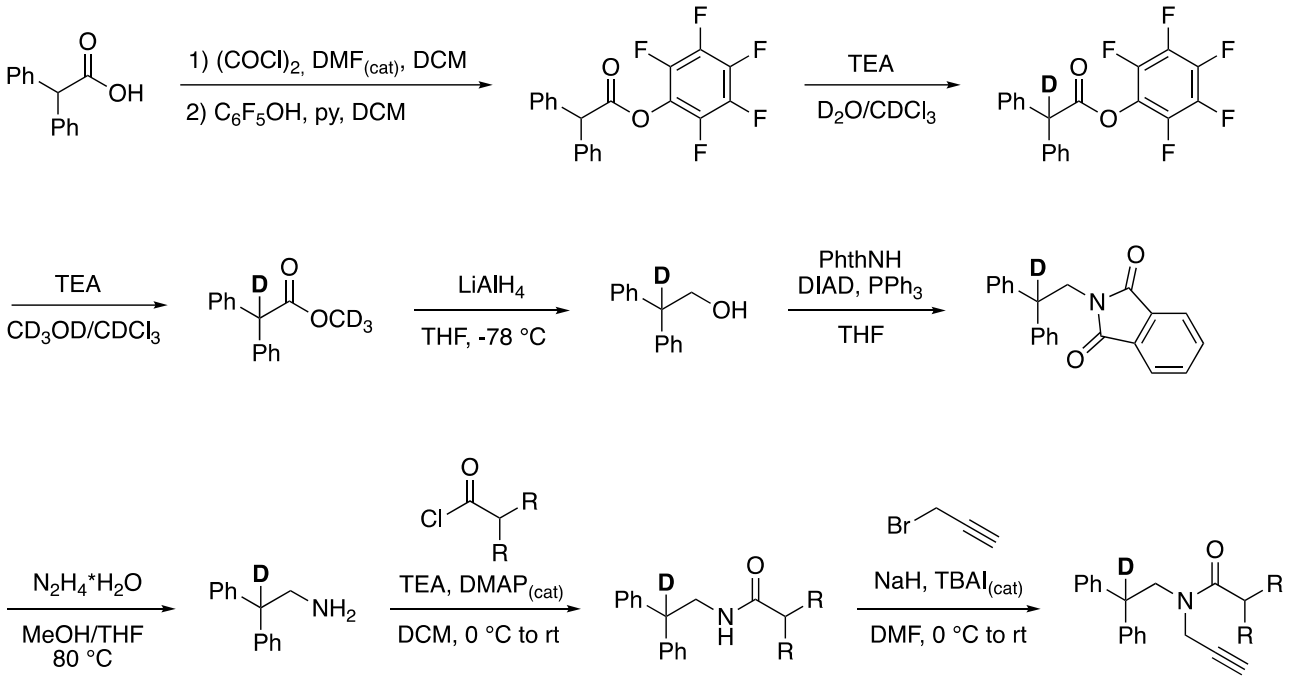

Highly deuterated precursors **[D]-66v** has been prepared adapting a procedure reported in the literature.[78]

To a solution of diphenylacetic acid (2.12 g, 10 mmol, 1 equiv.) in DCM (30 mL) a few drops of DMF and $(COCl)_2$ (1.11 mL, 13 mmol, 1.3 equiv.) were added at 0 °C. The reaction was stirred at rt for 2 hours, and then a solution of pentafluorophenol (2.02 g, 11 mmol, 1.1 equiv.) and pyridine (0.89 mL, 11 mmol, 1.1 equiv.) in DCM (10 mL) was slowly added. The reaction was stirred overnight and then quenched with a saturated NH_4Cl aqueous solution (20 mL) and extracted with DCM (3x20 mL). The combined organic layers were washed with brine, dried over sodium sulfate, and concentrated under reduced pressure. The crude was purified by chromatography on silica gel (*n*-hexane/EtOAc 30:1), affording perfluorophenyl 2,2-diphenylacetate as a white solid (3.77 g, 99% yield).

The pentafluorophenyl ester obtained was subjected to deuteration by vigorously stirring a solution of D_2O (5 mL) and $CDCl_3$ (3.5 mL) in the presence of TEA (0.28 mL, 2 mmol, 0.2 equiv.). After 24 hours the organic layer was separated, and the aqueous phase was extracted with DCM (2x20 mL). The combined organic layers were washed with brine, dried over sodium sulfate, and concentrated under

reduced pressure. The crude was purified by chromatography on silica gel (*n*-hexane/EtOAc 30:1), affording perfluorophenyl 2,2-diphenylacetate-*d* as a white solid (3.45 g, 91% yield, 95% D).

The deuterated pentafluorophenyl ester was then transesterificated by vigorously stirring in a solution of CD_3OD (6 mL) and $CDCl_3$ (4 mL) in the presence of TEA (1.27 mL, 9.1 mmol, 1 equiv.). After 24 hours the solvent was evaporated. The crude was purified by chromatography on silica gel (*n*-hexane/EtOAc 20:1), affording methyl-d_3 2,2-diphenylacetate-*d* as a white solid (3.17 g, 92% yield, 95% D).

The deuterated methyl ester (1.15 g, 5 mmol, 1 equiv.) was dissolved in THF (23 mL) and the solution was added dropwise to a solution of $LiAlH_4$ (0.57 g, 15 mmol, 3 equiv.) in THF (15 mL), under nitrogen atmosphere at -78 °C. The reaction was stirred at the same temperature for 1 hour, then allowed to warm to rt and quenched by the addition of a saturated aqueous solution of sodium/potassium tartrate. The mixture was extracted with EtOAc (3x20 mL) and the combined organic layers were washed with brine, dried over sodium sulfate, and concentrated under reduced pressure. The crude was purified by chromatography on silica gel (*n*-hexane/EtOAc 4:1), affording 2,2-diphenylethan-2-*d*-1-ol as a white solid (0.99 g, 99% yield, >90% D).

To a solution of deuterated alcohol (0.99 g, 5 mmol, 1 equiv.), phthalimide (1.84 g, 12.5 mmol, 2.5 equiv.) and PPh_3 (3.27 g, 12.5 mmol, 2.5 equiv.) in THF (50 mL), DIAD (2.46 mL, 12.5 mmol, 2.5 equiv.) was added dropwise at 0 °C under nitrogen atmosphere, and the reaction mixture was stirred at rt overnight. The reaction was quenched with water (40 mL), extracted with EtOAc (3x20 mL) and the combined organic layers were washed with brine, dried over sodium sulfate, and concentrated under reduced pressure. The crude was purified by chromatography on silica gel (*n*-hexane/EtOAc 6:1), affording 2-(2,2-diphenylethyl-2-*d*)isoindoline-1,3-dione as a white solid (1.38 g, 84% yield, >95% D).

The phthalimide was removed by refluxing the deuterated imide (1.2 g, 3.66 mmol, 1 equiv.) in a solution of THF (20 mL) and MeOH (30 mL) in the presence of hydrazine hydrated (1.1 mL, 21.96 mmol, 6 equiv.) for 2 hours. The resulting mixture was filtered on a celite pad, the solution obtained was concentrated under reduced pressure, washed with a saturated $NaHCO_3$ aqueous solution and extracted with DCM (3x20 mL), affording the crude primary amine which was used in the following step without further purification.

To a solution of crude 2,2-diphenylethan-2-*d*-1-amine (356 mg, 1.8 mmol, 1 equiv.), TEA (0.5 mL, 3.6 mmol 2 equiv.) and a catalytic amount of DMAP in DCM (9 mL), the desired acyl chloride (2.7 mmol, 1.5 equiv.) was added at 0 °C, and the reaction was stirred at rt for 1 hour. The reaction was quenched by the addition of water and extracted with DCM (3x10 mL). The combined organic layers were washed with brine, dried over sodium sulfate, and concentrated under reduced pressure. The crude was purified by chromatography on silica gel (*n*-hexane/EtOAc), affording the deuterated secondary amide.

To a solution of the desired amide (1.3 mmol, 1 equiv.) in DMF (6 mL) a catalytic amount of TBAI and NaH (60% dispersion, 63 mg, 1.6 mmol, 1.2 equiv.) were added at 0 °C under nitrogen atmosphere. After stirring at the same temperature for 30 min, propargyl bromide (80% in toluene, 0.18 mL, 1.7 mmol, 1.3 equiv.) was added dropwise, and the reaction was allowed to stir at rt overnight. The reaction was quenched by the addition of water and extracted with EtOAc (3x10 mL). The combined organic layers were washed with brine, dried over sodium sulfate, and concentrated under reduced pressure. The crude was purified by chromatography on silica gel (*n*-hexane/EtOAc), affording the deuterated propargyl amide.

***N*-(2,2-diphenylethyl-2-d)-2,2-diphenyl-*N*-(propa-1,2-dien-1-yl)acetamide**

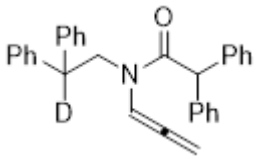

Allene **[D]-66v** was prepared following general procedure **GP-A** from the corresponding propargyl amide (430 mg, 1 mmol). Light-yellow oil (275 mg, 64% yield). Two rotamers were observed due to the dynamic amide group (70:30 mixture of rotamers). *d*- title 99%.

^{1}H NMR (600 MHz, $CDCl_3$) δ 7.66 (t, *J* = 6.5 Hz, 1H RotB), 7.37 – 7.34 (m, 2H RotA, 1H RotB), 7.31 – 7.21 (s, 12H RotA, 12H RotB), 6.95 – 6.93 (m, 4H RotA), 6.86 – 6.85 (m, 4H RotB), 6.52 (t, *J* = 6.2 Hz, 1H RotA), 5.31 – 5.30 (m, 2H RotA, 2H RotB), 5.19 (s, 1H RotA), 4.53 (s, 1H RotB), 4.28 (s, 2H RotA), 3.95 (s, 2H RotB). **^{13}C NMR** (151 MHz, $CDCl_3$) δ 202.4 (RotB), 202.2 (RotA), 170.5 (RotB), 170.3 (RotA), 141.9 (2C RotB), 141.7 (2C RotA), 139.04 (2C RotA), 138.97 (2C RotB), 129.1 (2C RotA), 129.02 (RotB), 128.97 (4C RotB), 128.67 (4C RotA), 128.65 (RotB), 128.63 (2C RotA, 2C RotB), 128.52 (4C RotA),

128.49 (4C RotB), 127.3 (4C RotB), 127.2 (4C RotB), 127.1 (4C RotA), 126.8 (4CRotA), 100.0 (RotA), 98.8 (RotB), 87.3 (RotB), 86.3 (RotA), 55.5 (RotA), 55.4 (RotB), 51.1 (RotB), 48.8 (RotA), 48.5 – 48.3 (m, RotA, RotB). **ESI-HRMS** calcd for $C_{31}H_{26}DNNaO$ $[M+Na]^+$ 453.2053, found 453.2050.

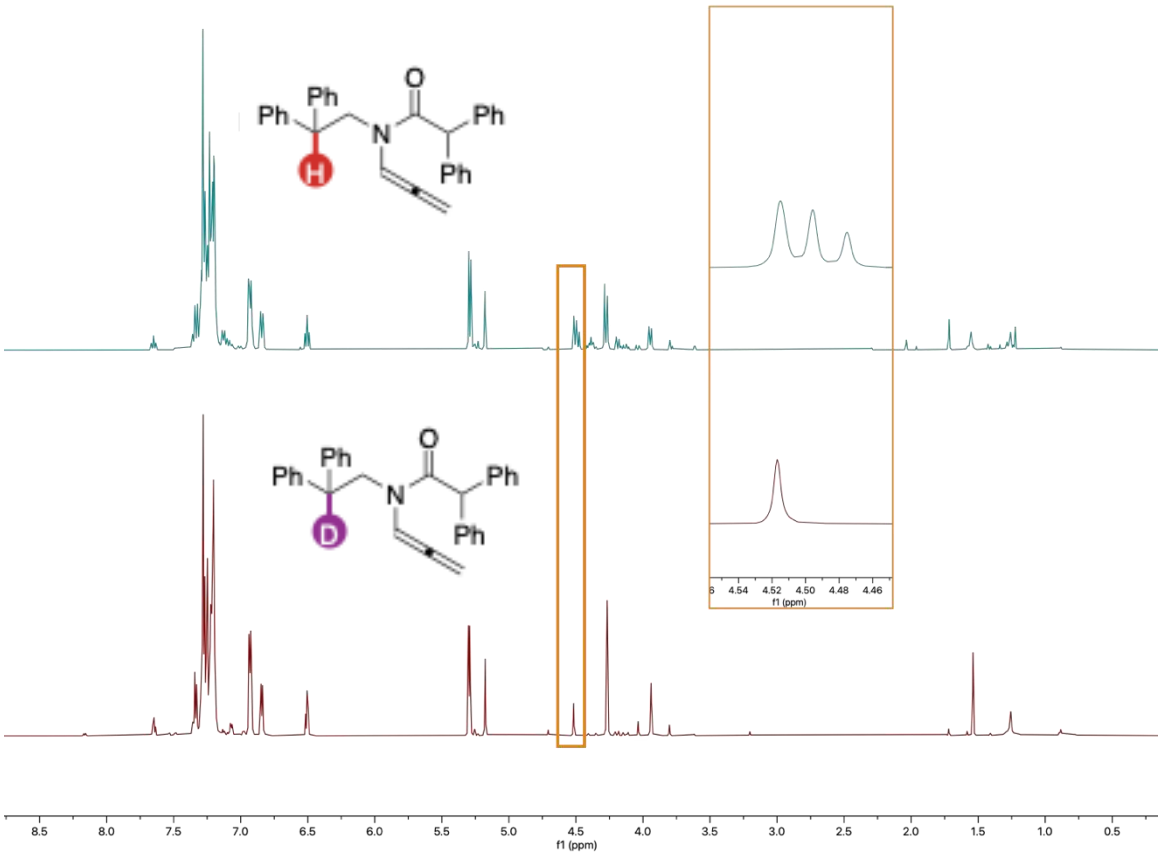
Ph
Ph
O
Ph
N
Ph
H
Ph
Ph
O
Ph
N
Ph
D
Ph
4.54
4.52
4.50
4.48
4.46
f1 (ppm)
8.5
8.0
7.5
7.0
6.5
6.0
5.5
5.0
4.5
4.0
3.5
3.0
2.5
2.0
1.5
1.0
0.5
f1 (ppm)

Kinetic studies

Kinetic profile of the photocatalytic synthesis of azetidine 67i

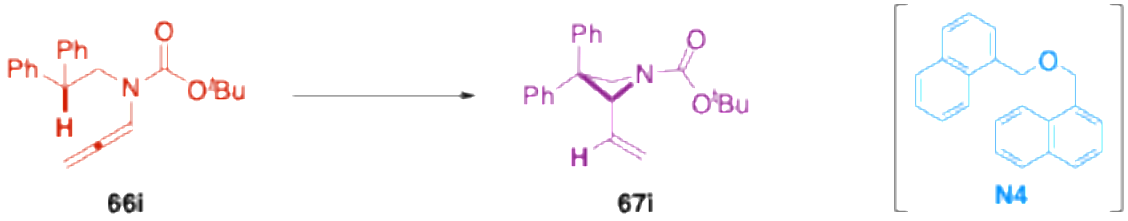

Allene **66i** was subjected to the HAT-cyclization sequence with and without co-catalyst **N4** (30 mol%). Two parallel runs were performed in a 8:2 toluene-d_8 / DCM-d_2 mixture employing the best conditions and monitored by **^{1}H NMR** regularly. The conversion of **66i** and yields of **67i** were evaluated by using the TMS (tetramethylsilane) residual peak as internal standard. Upon 36 hours of irradiation, 1,3,5-trimethoxybenzene was added to both the reaction mixtures as internal standard to confirm the final yield of **67i** and the final conversion of **66i**.

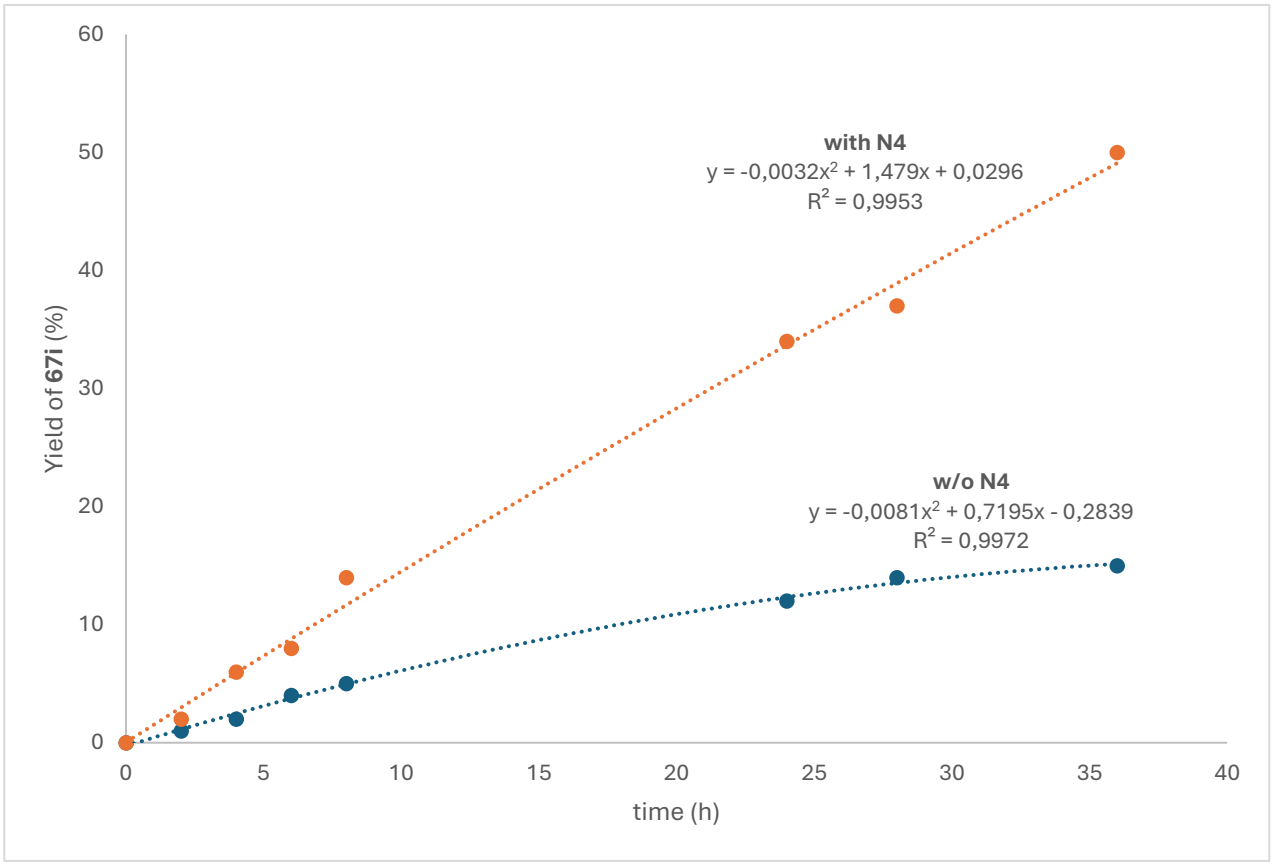
60
50
40
30
20
10
0
Yield of 67i (%)
0
5
10
15
20
25
30
35
40
time (h)
with N4
y = -0,0032x² + 1,479x + 0,0296
R² = 0,9953
w/o N4
y = -0,0081x² + 0,7195x - 0,2839
R² = 0,9972

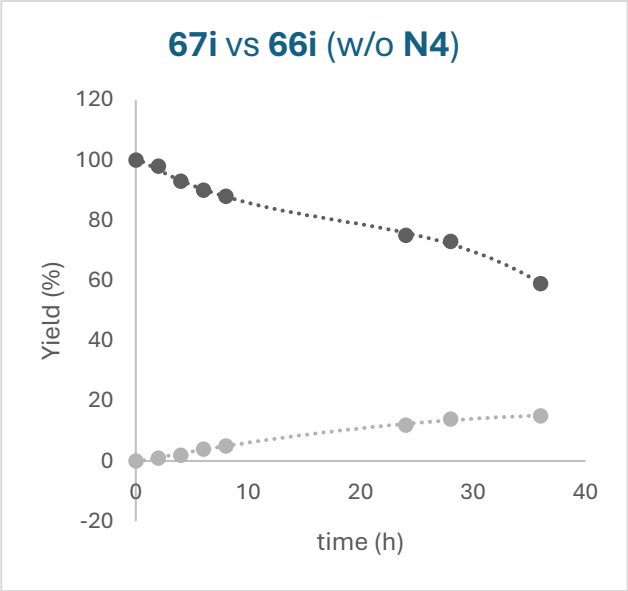

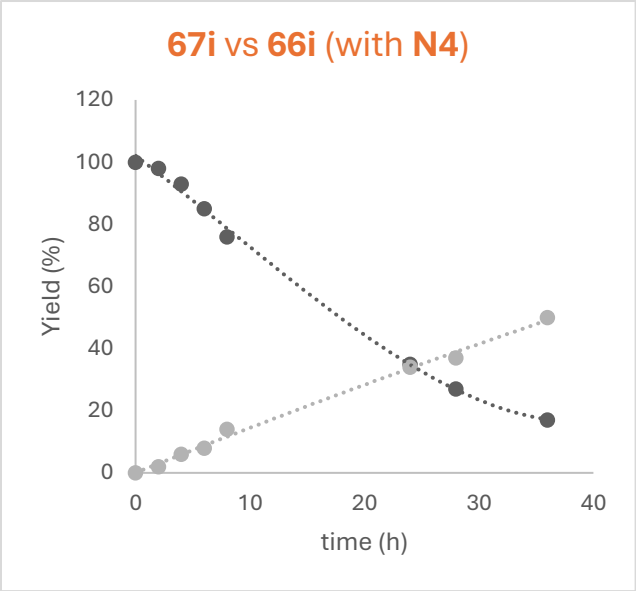

	w/o N4		with N4	
time	Y **66i** (%)	Y **67i** (%)	Y **66i** (%)	Y **67i** (%)
0	100	0	100	0
2	98	1	98	2
4	93	2	93	6
6	90	4	85	8
8	88	5	76	14
24	75	12	35	34
28	73	14	27	37
36	59	15	17	50

Stacking of the kinetic profile w/o N4

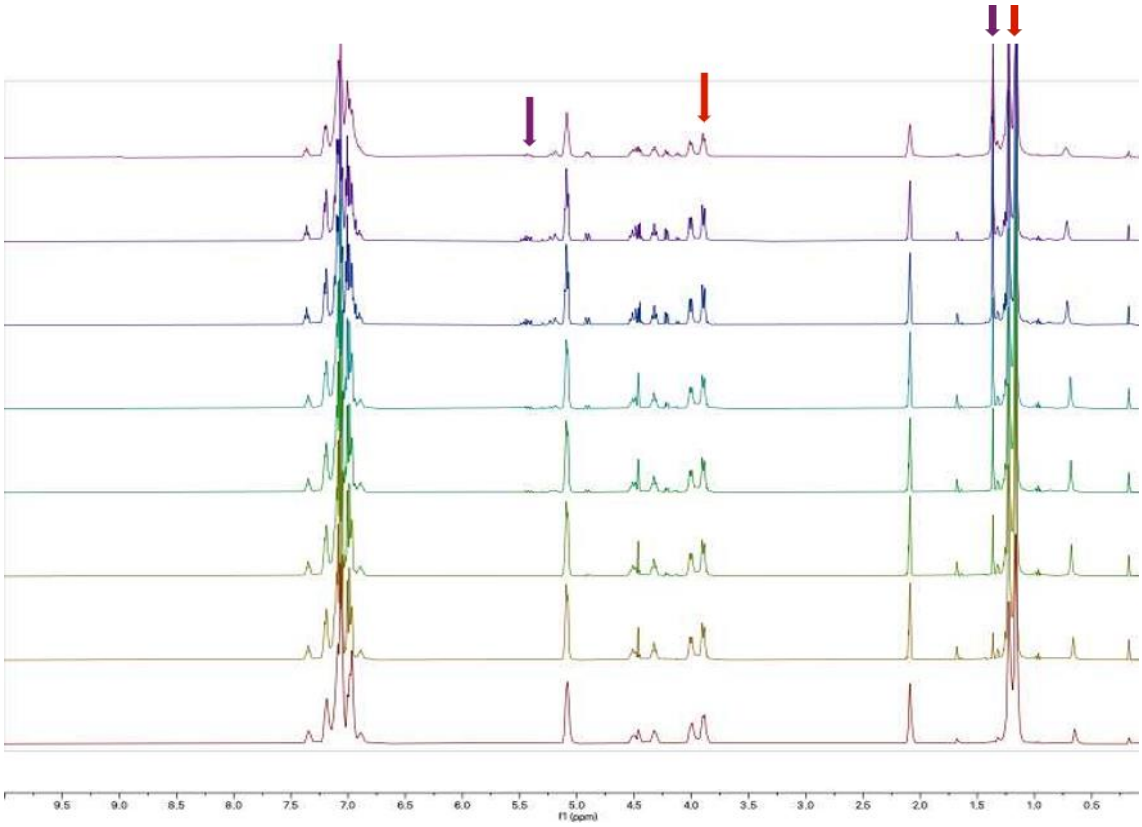

Enlarged stacking of the kinetic profile w/o N4

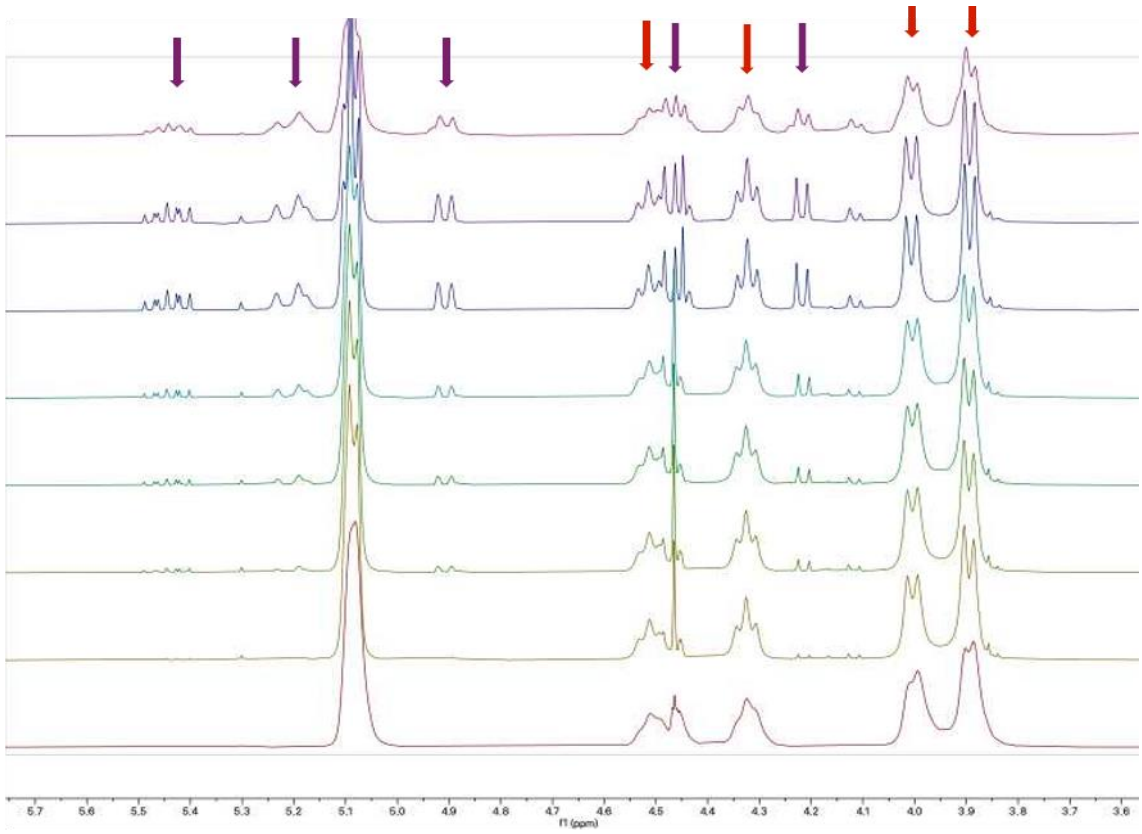

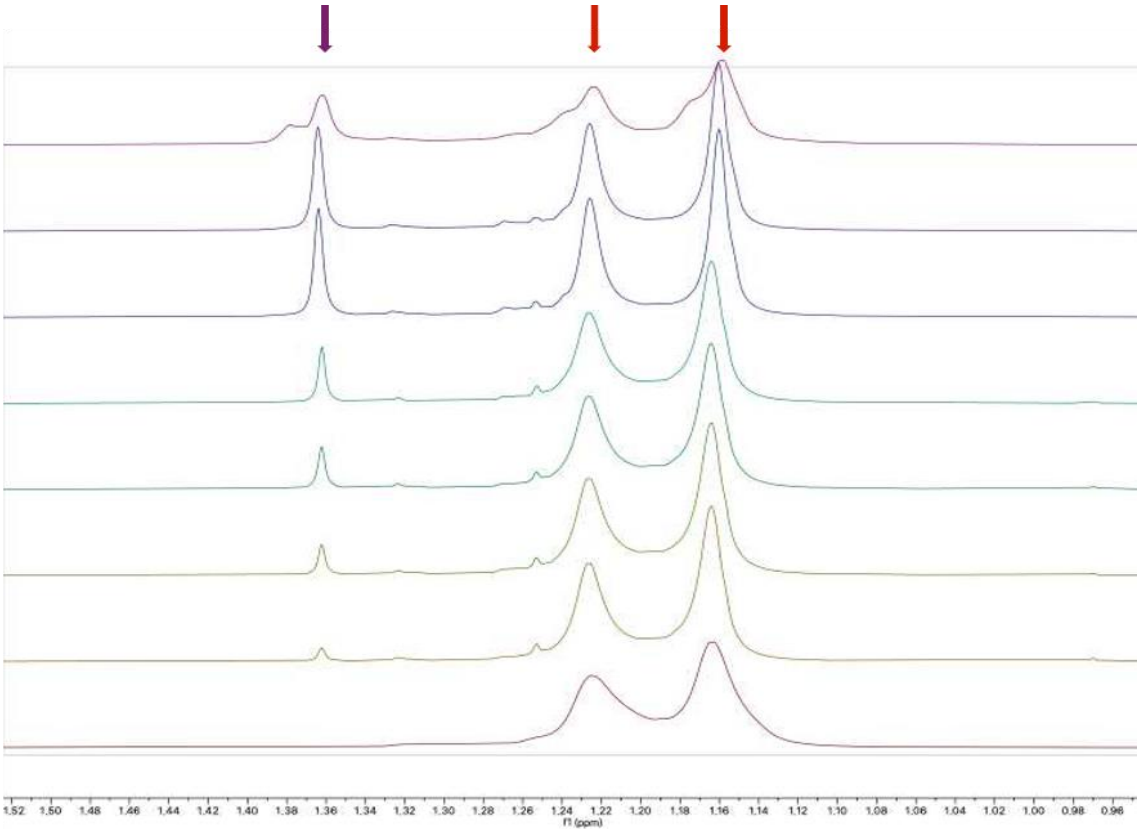

Control with TMB at 36 hours

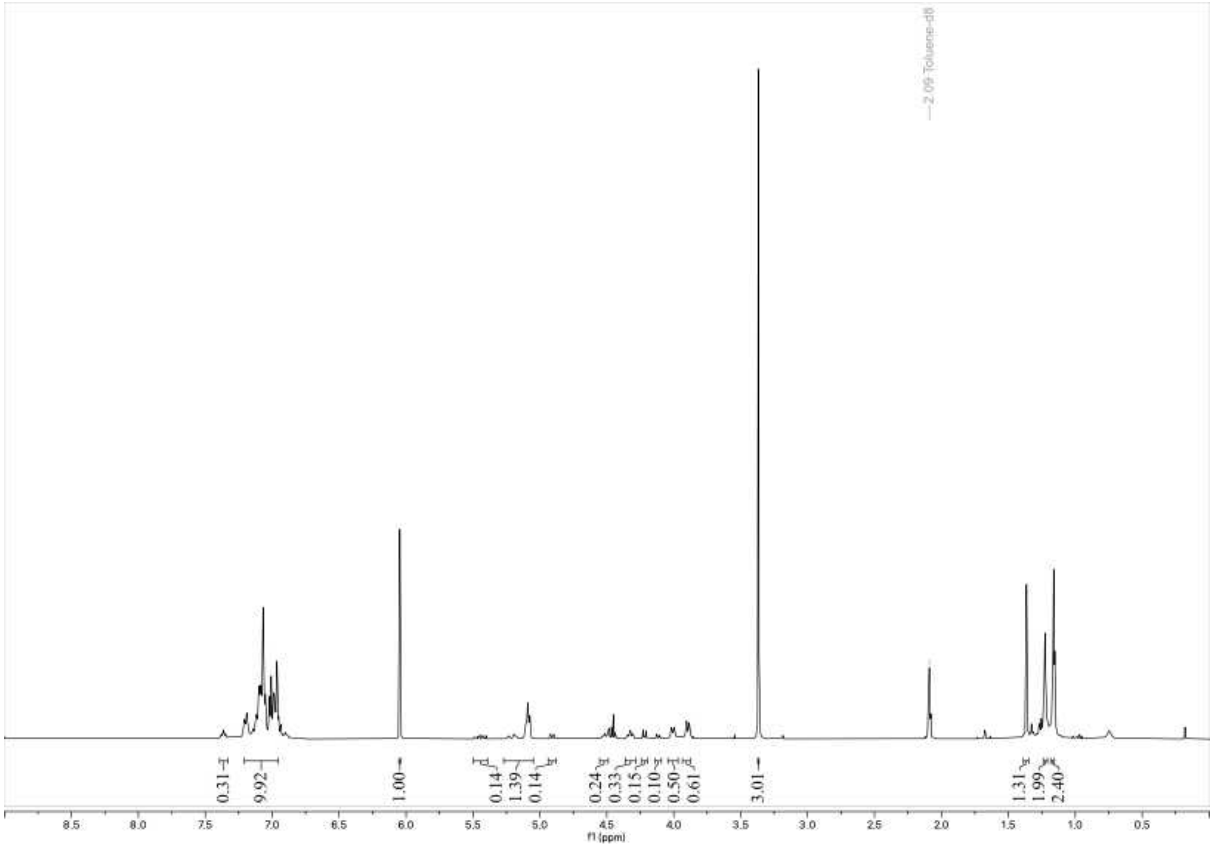

Stacking of the kinetic profile with N4

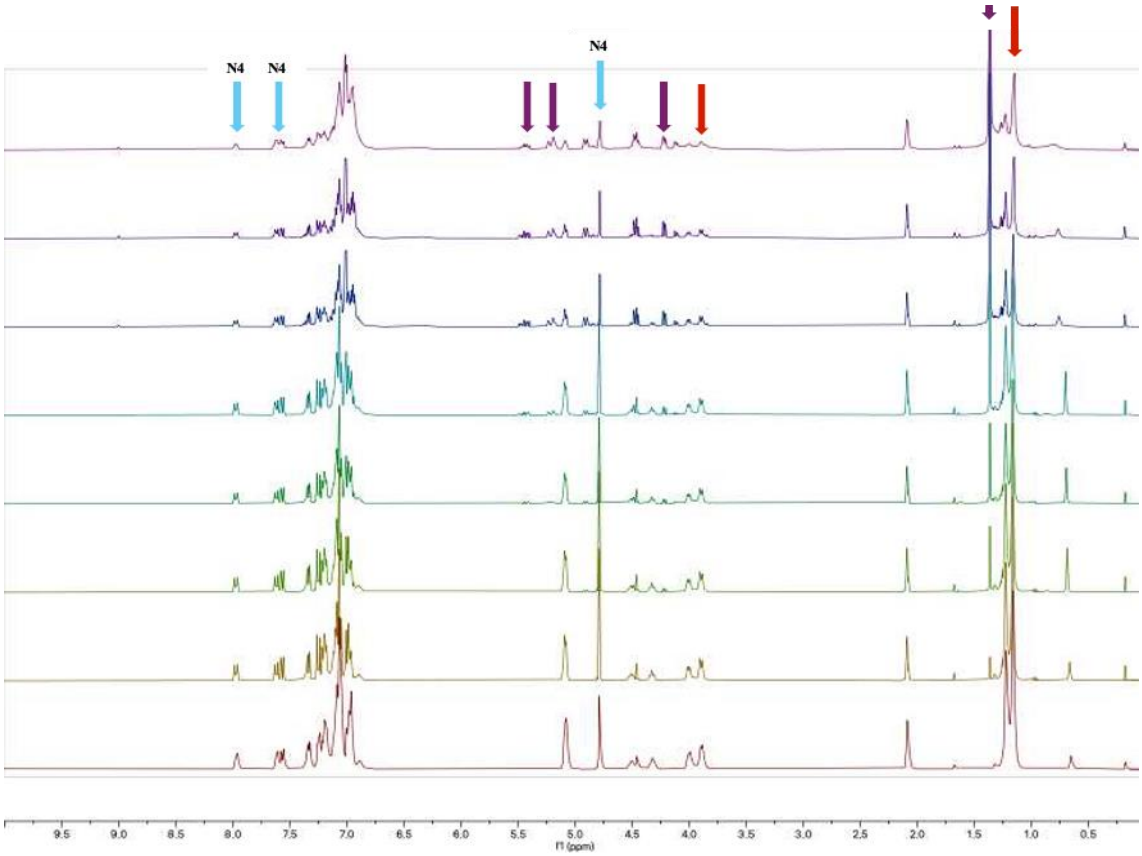

Enlarged stacking of the kinetic profile with N4

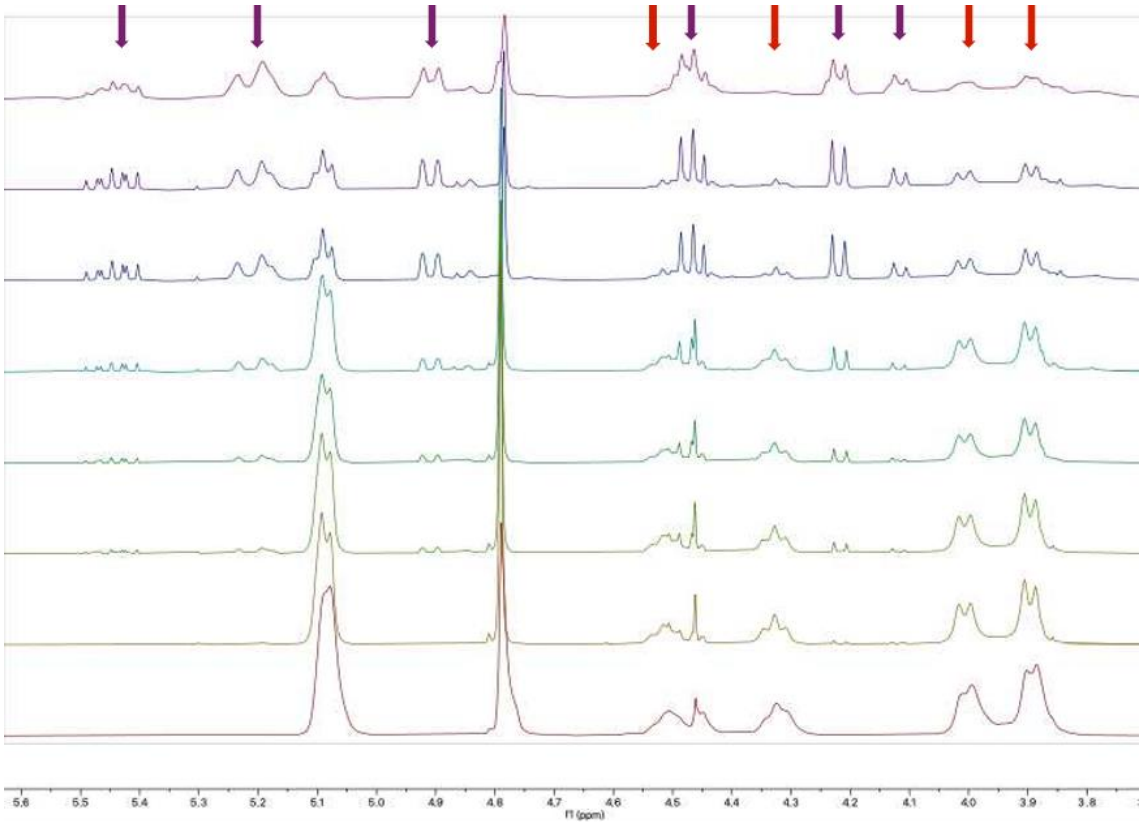

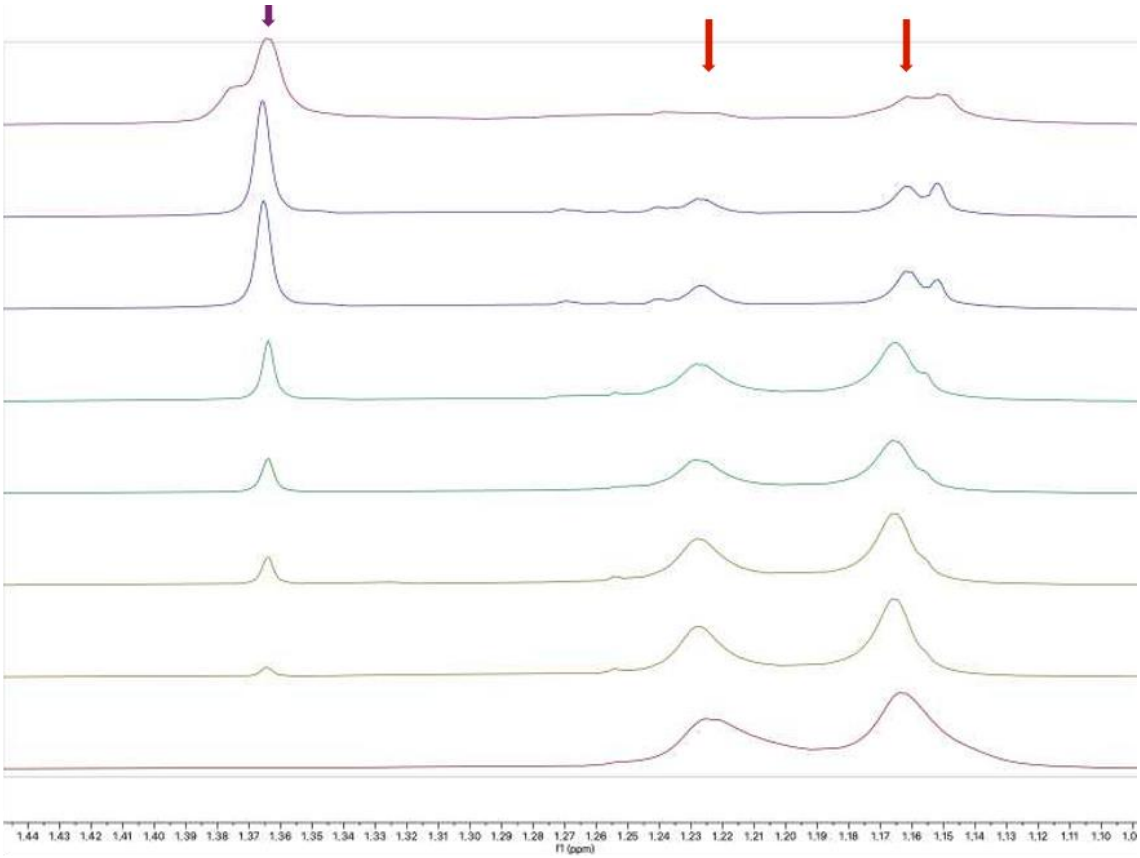

Control with TMB at 36 hours

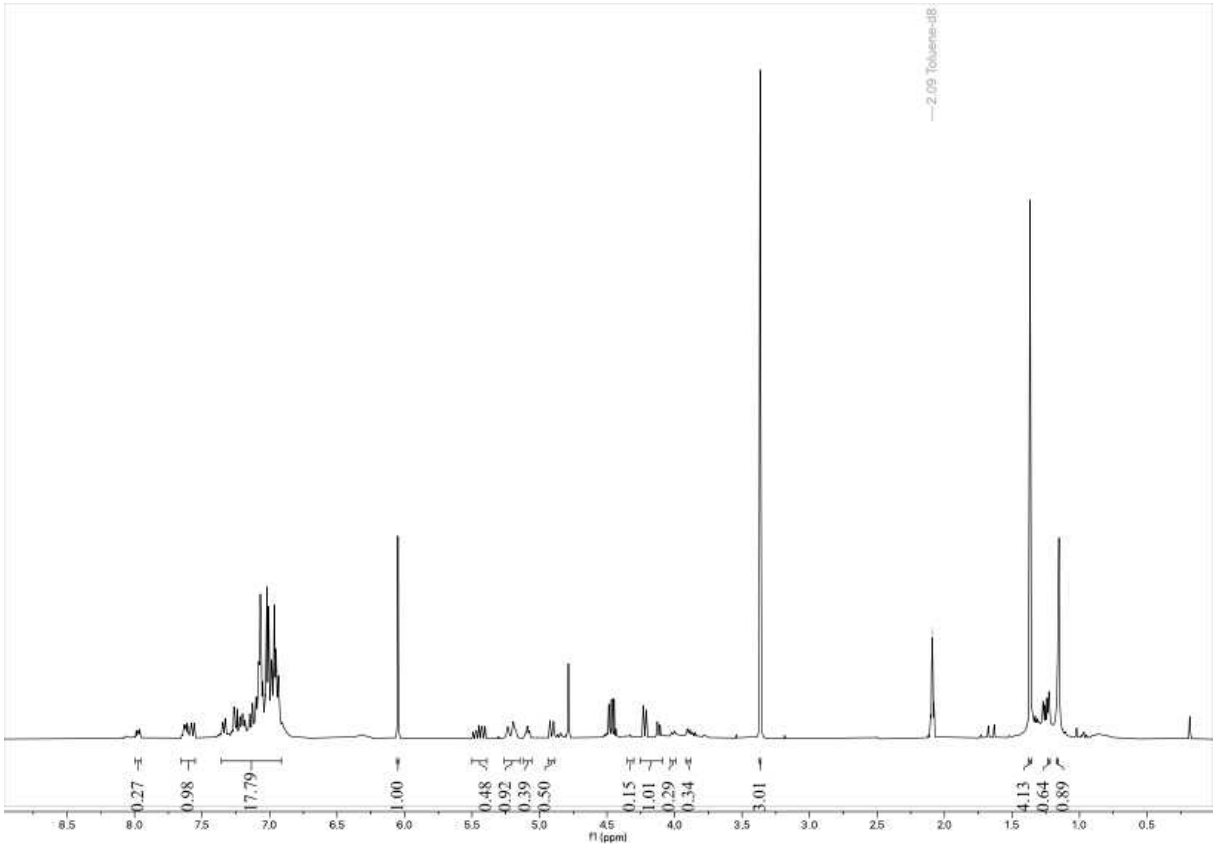

NMR titration assessing the ground-state interaction between N4 and allene 66h

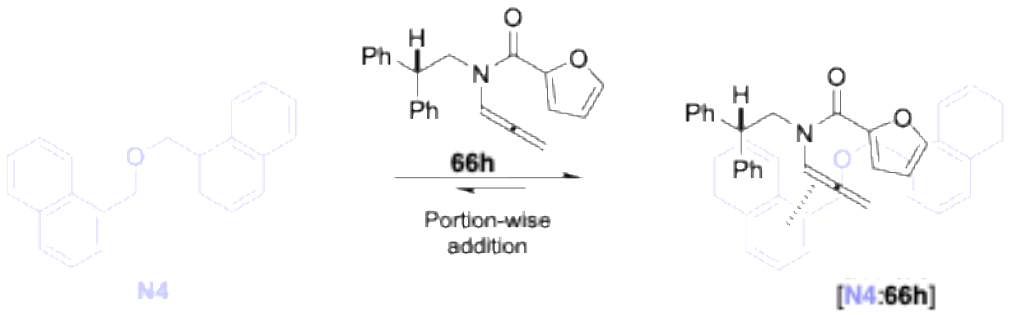

A solution of **N4** in an 8:2 mixture of toluene-d_8 and DCM-d_2 (17 mM, 0.5 mL) was prepared and its ^{1}H NMR spectrum was registered. Then, a solution of **66h** in toluene-d_8 (34 mM, 0.3 mL) was gradually added portion-wise, collecting four additional ^{1}H NMR spectra at various relative concentration of the two species. Various shifts to either lower or higher fields were observed both for resonances due to **N4** protons and for those of **66h** one, in different regions of the spectra. The shifts were proportional to the concentration of the titrating agent **66h**. In particular, stacking-like *p*-interaction between the two species were more evident for C(sp^2)-H protons derived from the allenylic and the aromatic arms of the two molecules, while shifts of the aliphatic protons were generally lower. The curve obtained by plotting the shifts vs the concentration of **66h** shows a quasi-logarithmic behavior, as predicted by literature examples for supramolecular adducts associated with a narrowly negative DG of formation. This is consistent with the values obtained by DFT that were presented in this manuscript. The Δδ values used for the titration plot presented hereafter were obtained by observing the shifts of the spectra of **N4** for the signal at 7.98 ppm and the one at 7.36 ppm.

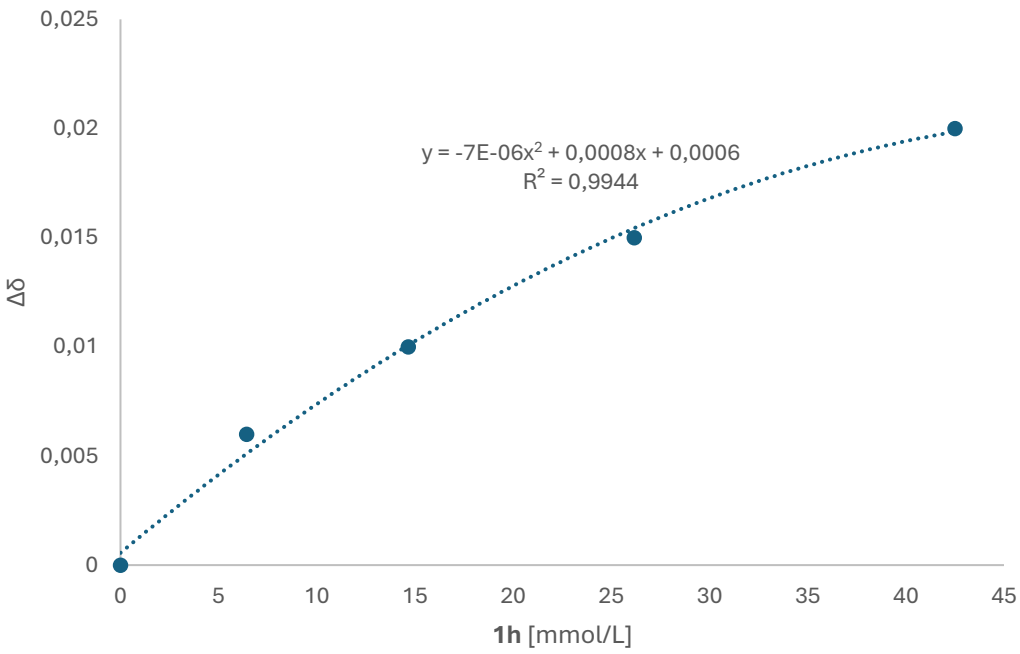

Titration plot showing the relative averaged shift of two **N4** resonances increasing the concentration of **66h**.

[66**h**] (mmol/L)	Δδ (ppm)
0	0
6,41509434	0,006
14,6551724	0,010
26,1538462	0,015
42,5000000	0,020

Stacking of the NMR spectra collected during the titration experiment

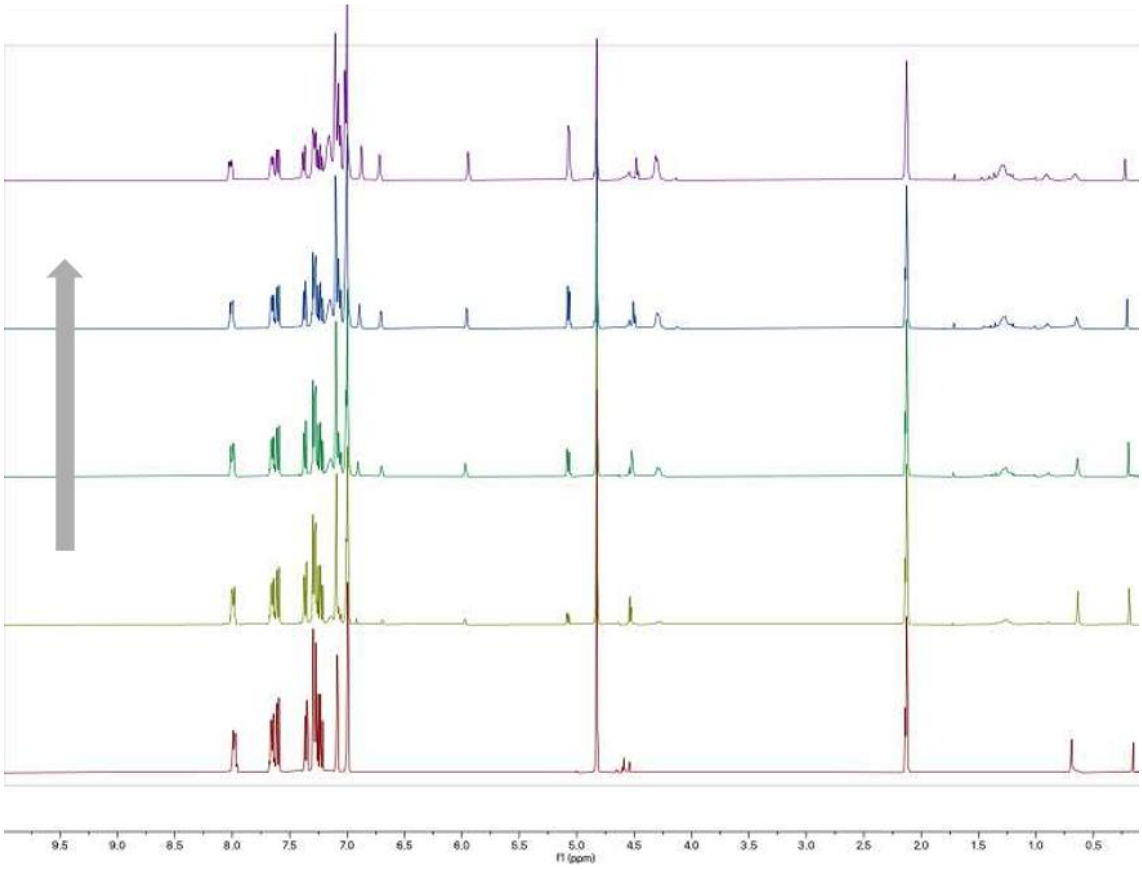

Enlarged stacking of spectra showing shifted signals of aromatic protons of N4 during the titration

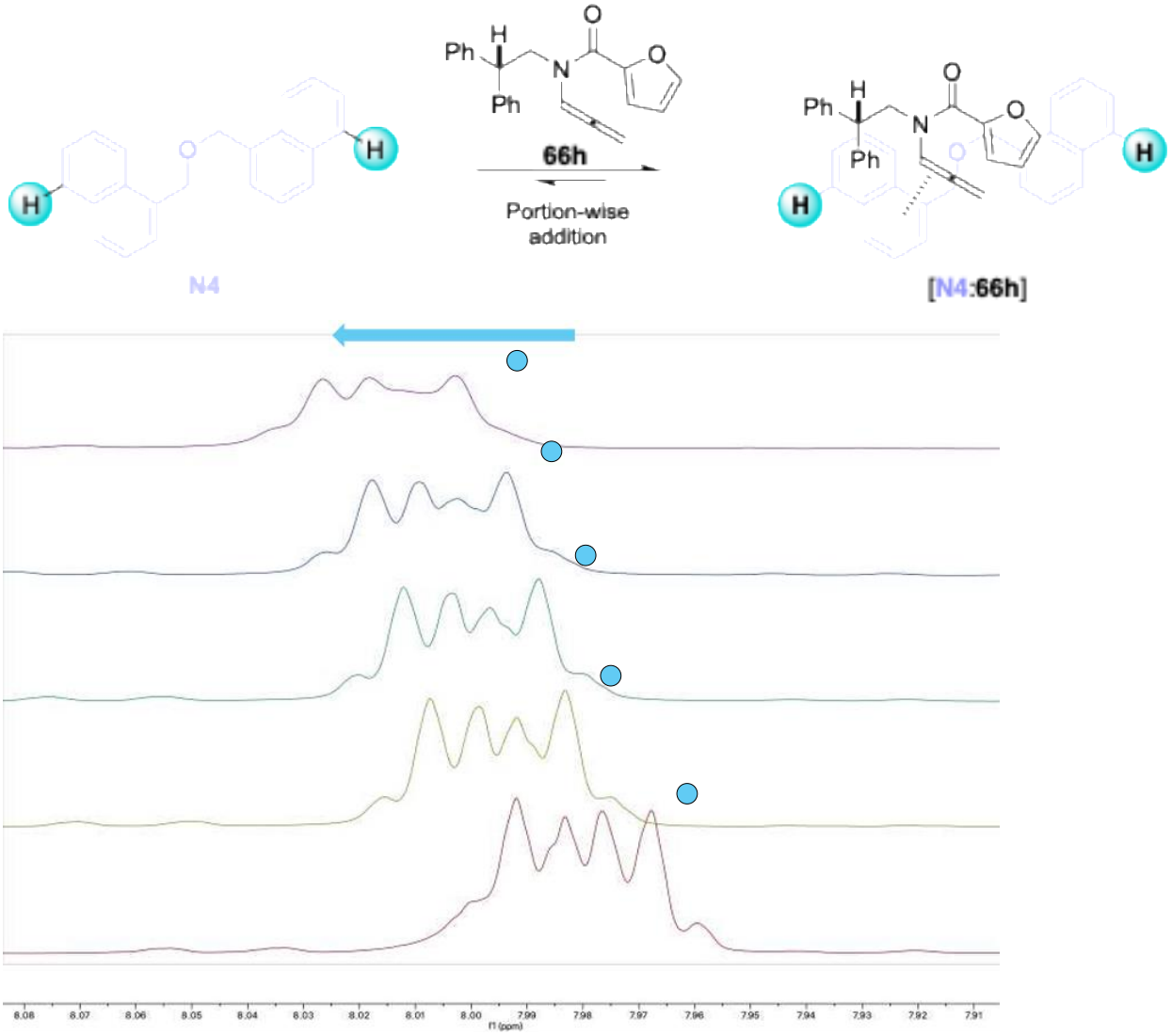

Δδ (cyan H) = 0.035 ppm

From bottom to top, effect of the addition of **66h** on the chemical shift of the cyan-labelled protons of **N4**. These resonances showed a meaningful de-shielding effect during the titration.

Enlarged stacking of spectra showing shifted signals of α-allenylic, green, and furyl, red, protons of 66h during the titration

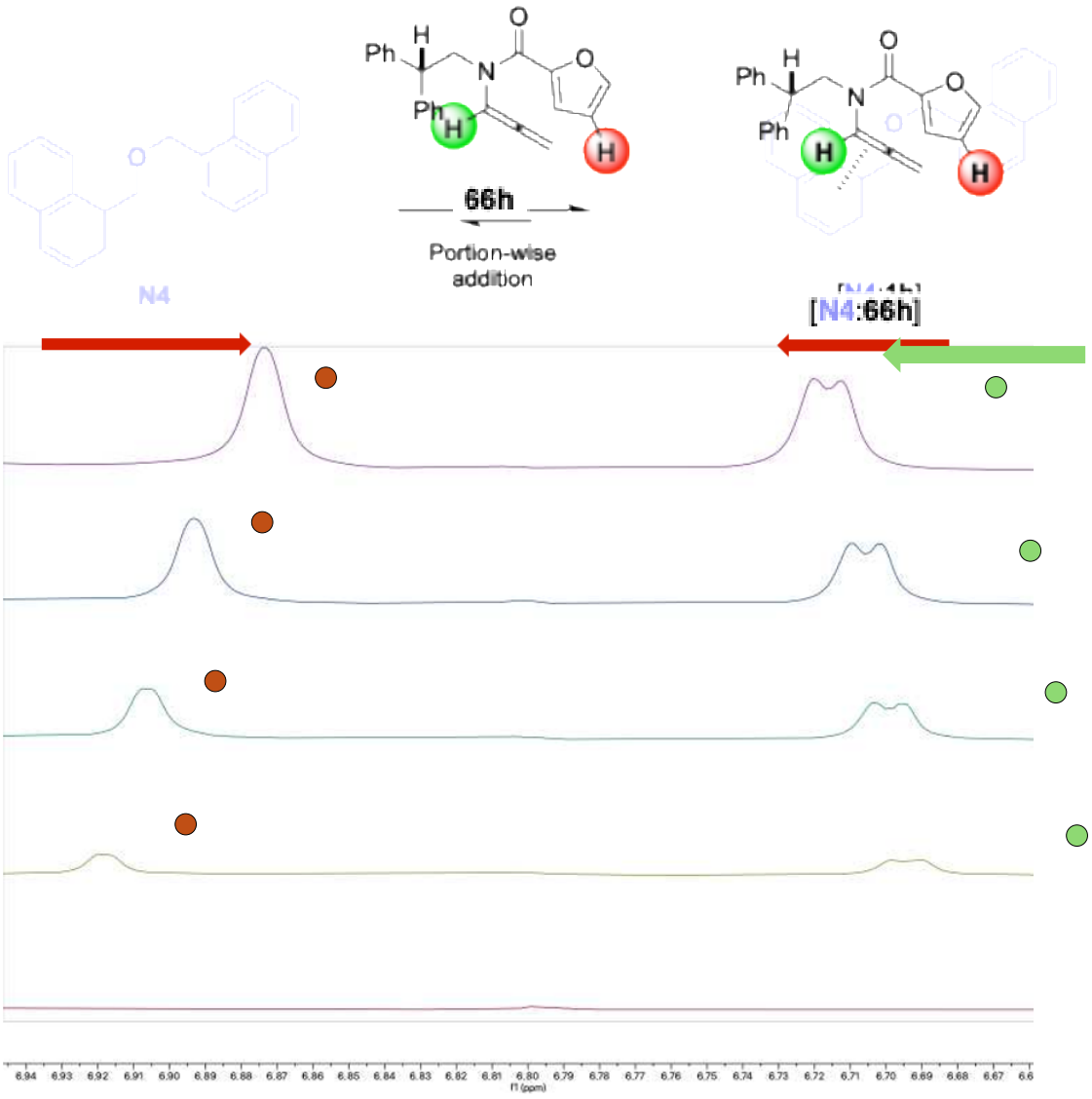

Δδ (green H) = 0.022 ppm

Δδ (red H) = 0.045 ppm

From bottom to top, effect of the addition of **66h** on the chemical shift of the red- and green-labelled protons of the substrate in the presence of **N4**. These resonances showed a meaningful shift during the titration. Indeed, a de-shielding of the a-allenyl resonance (green dots) was accompanied by a shielding of furyl resonances (red dots). It is worth noting that this opposite behavior ensures that the overall shifts observed cannot be due to the bare variation of the diamagnetic field of the sample.

Enlarged stacking of spectra showing shifted signals of γ-allenylic protons of 66h during the titration

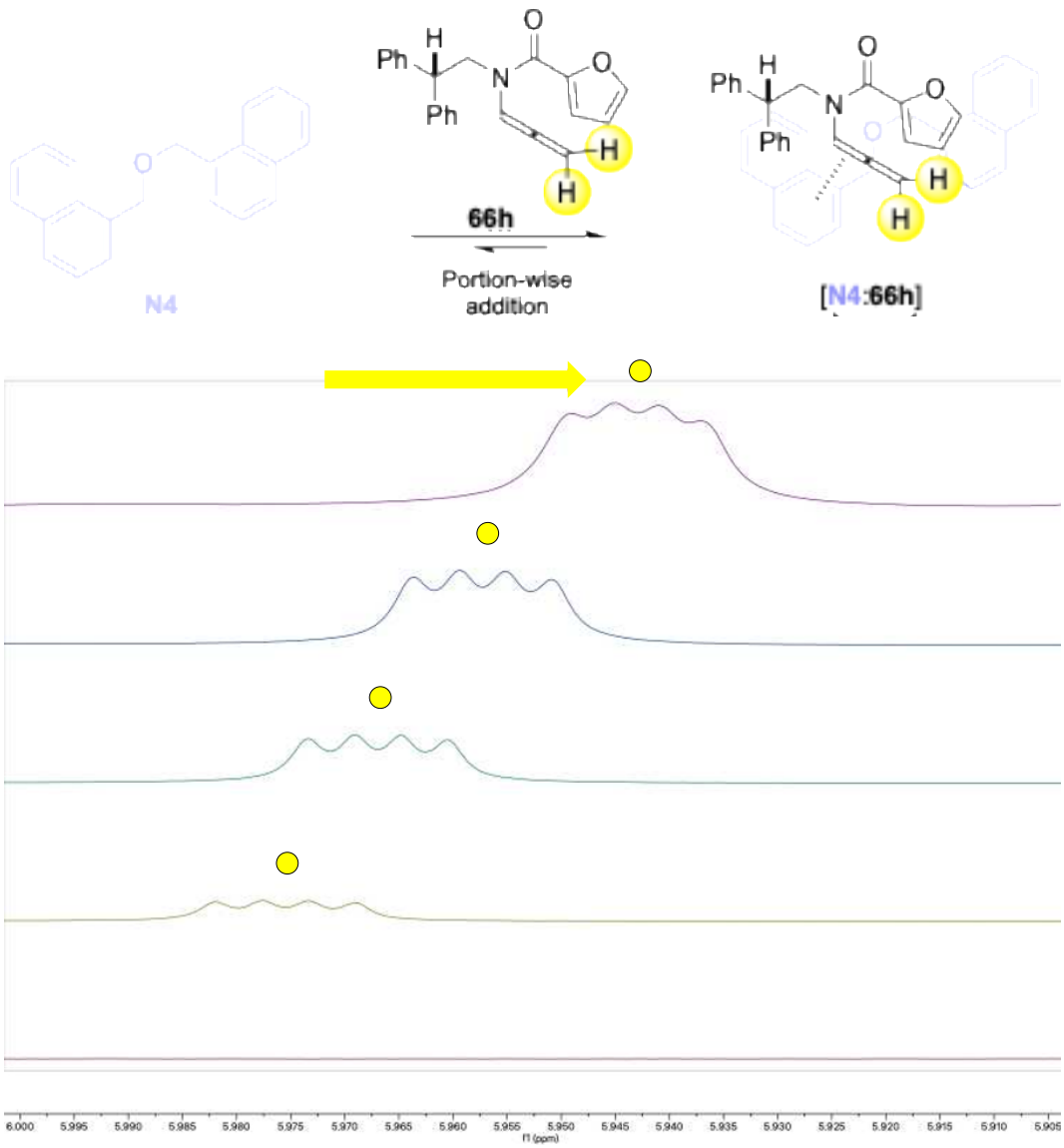

Δδ (yellow H) = 0.032 ppm

From bottom to top, effect of the addition of **66h** on the chemical shift of the yellow-labelled protons of the substrate in the presence of **N4**. Increasing the concentration of **66h** with respect to **N4** leads to an evident downfield shift of the γ-allenyl protons of the substrate.

Enlarged stacking of spectra showing shifted signals of the benzylic proton of 66h during the titration

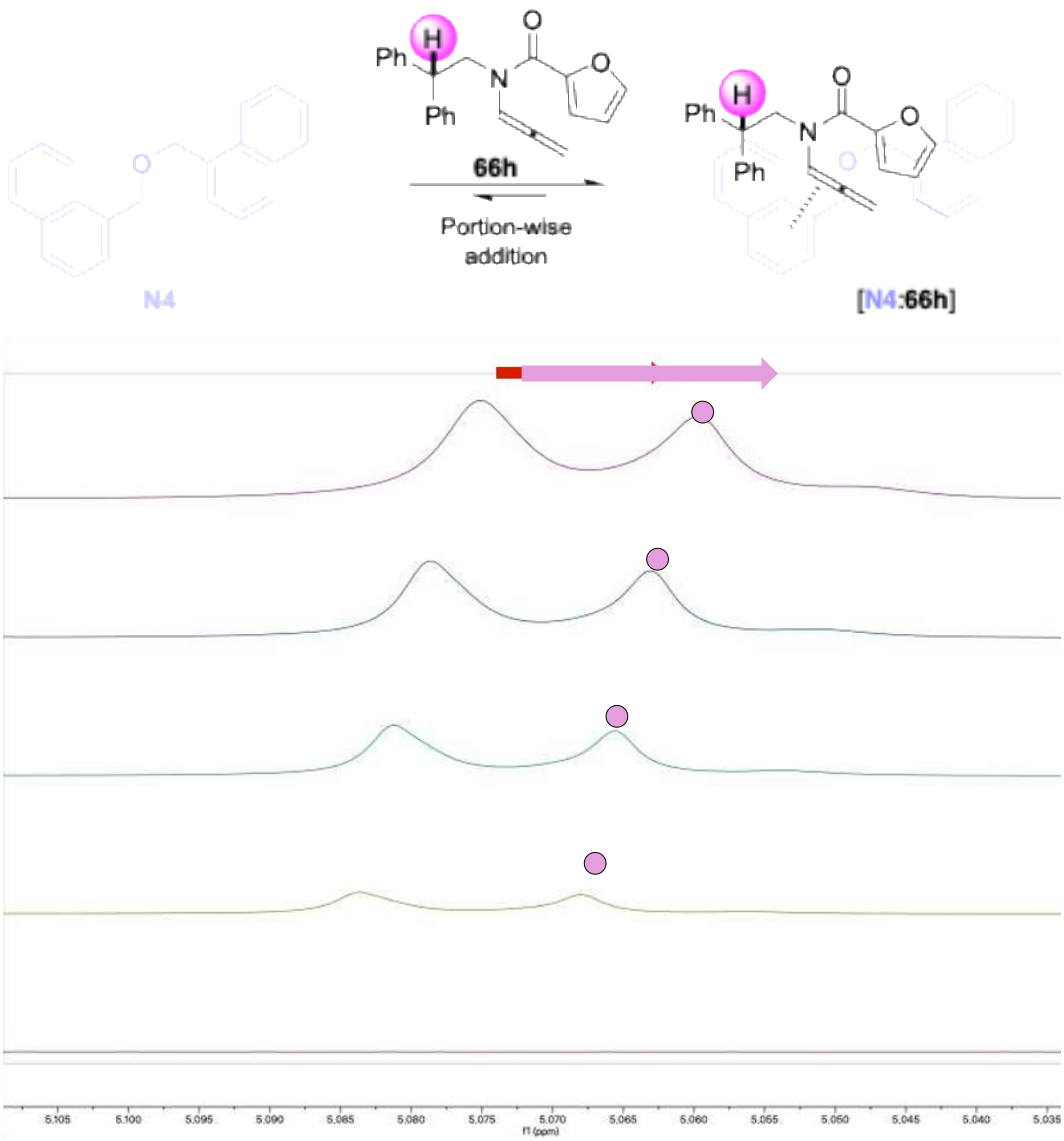

Δδ (purple H) = 0.009 ppm

From bottom to top, effect of the addition of **66h** on the chemical shift of the purple-labelled benzylic proton of the substrate in the presence of **N4**. Increasing the concentration of **66h** respect to **N4** leads to a lower, but still observable, shift of this resonance compared to those of other C(sp^2)-H ones. We speculate that this behavior could be due to the different arrangement of the aliphatic proton, because the C(sp^3)-H bond is not coplanar with the π-networks of the binaphthyl derivative **N4**.

Enlarged stacking of spectra showing shifted signals of the α-amido protons of 66h during the titration

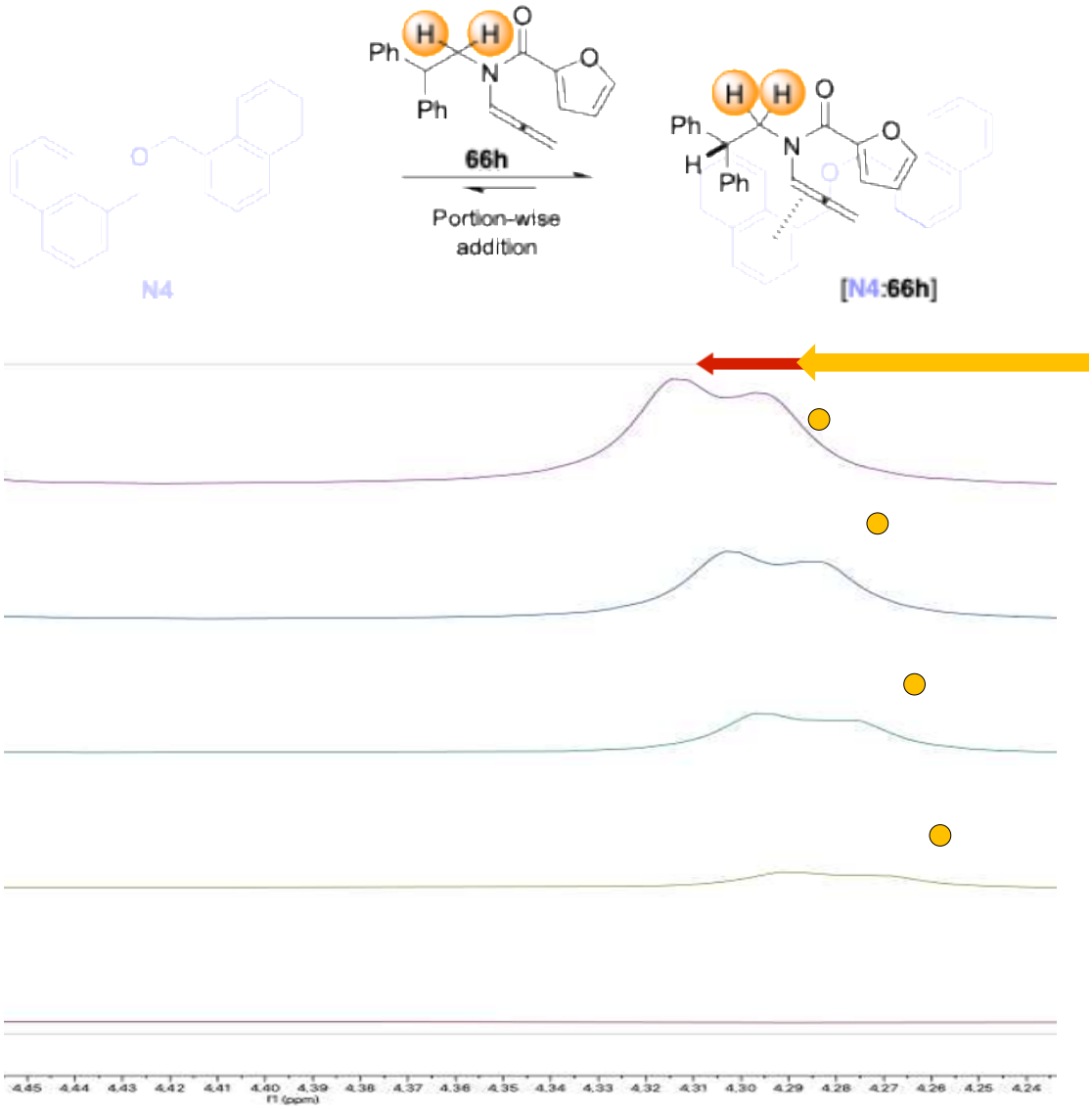

Δδ (orange H) = 0.023 ppm

From bottom to top, effect of the addition of **66h** on the chemical shift of the orange-labelled a-amido protons of the substrate in the presence of **N4**. Increasing the concentration of **66h** respect to **N4** leads to a de-shielding effect on the resonance of the CH_2 unit. Additionally, it can be observed that the resolution of this signal increased throughout the titration experiment. This can be consistent with the proposed rationale on the formation of a supramolecular adduct between the two entities because the [**N4**:**66h**] complex would reduce the rotational flexibility of the *N*- arm of the substrate, resulting in sharper signals for these otherwise broad resonances.

Optical spectroscopic data

Excitation and fluorescence analyses

UV/vis absorption and emission measurements were performed on a UV/Vis/NIR Lambda 750 spectrophotometer. The samples were measured in fluorescence quartz cuvettes.

(a)

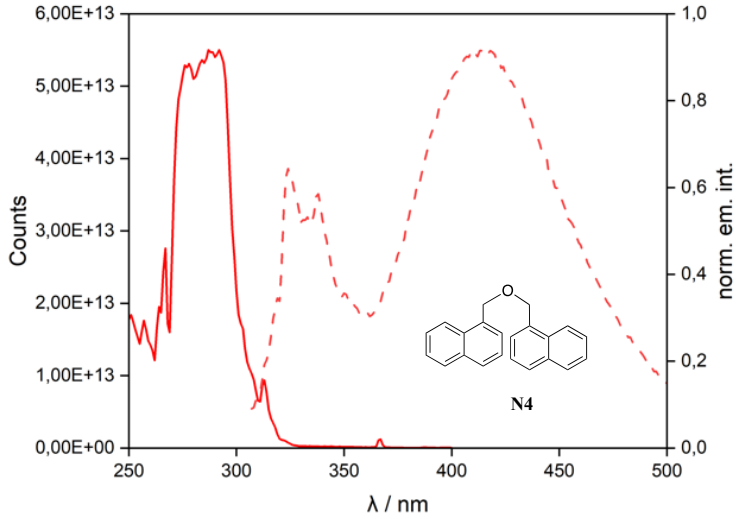

(b)

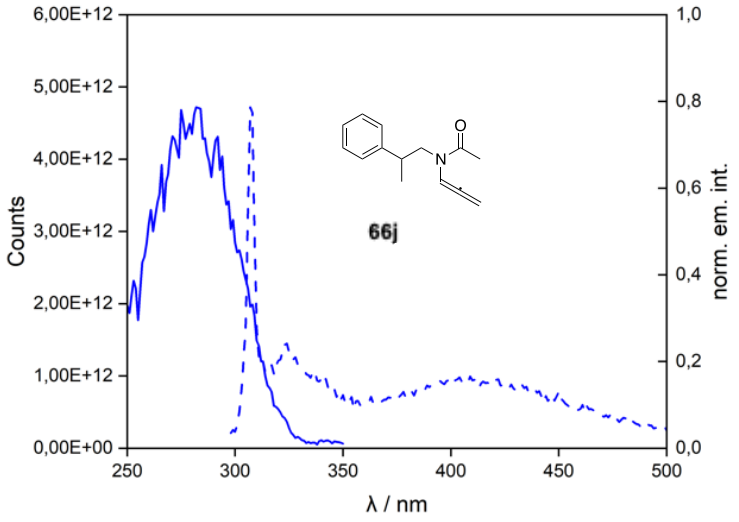

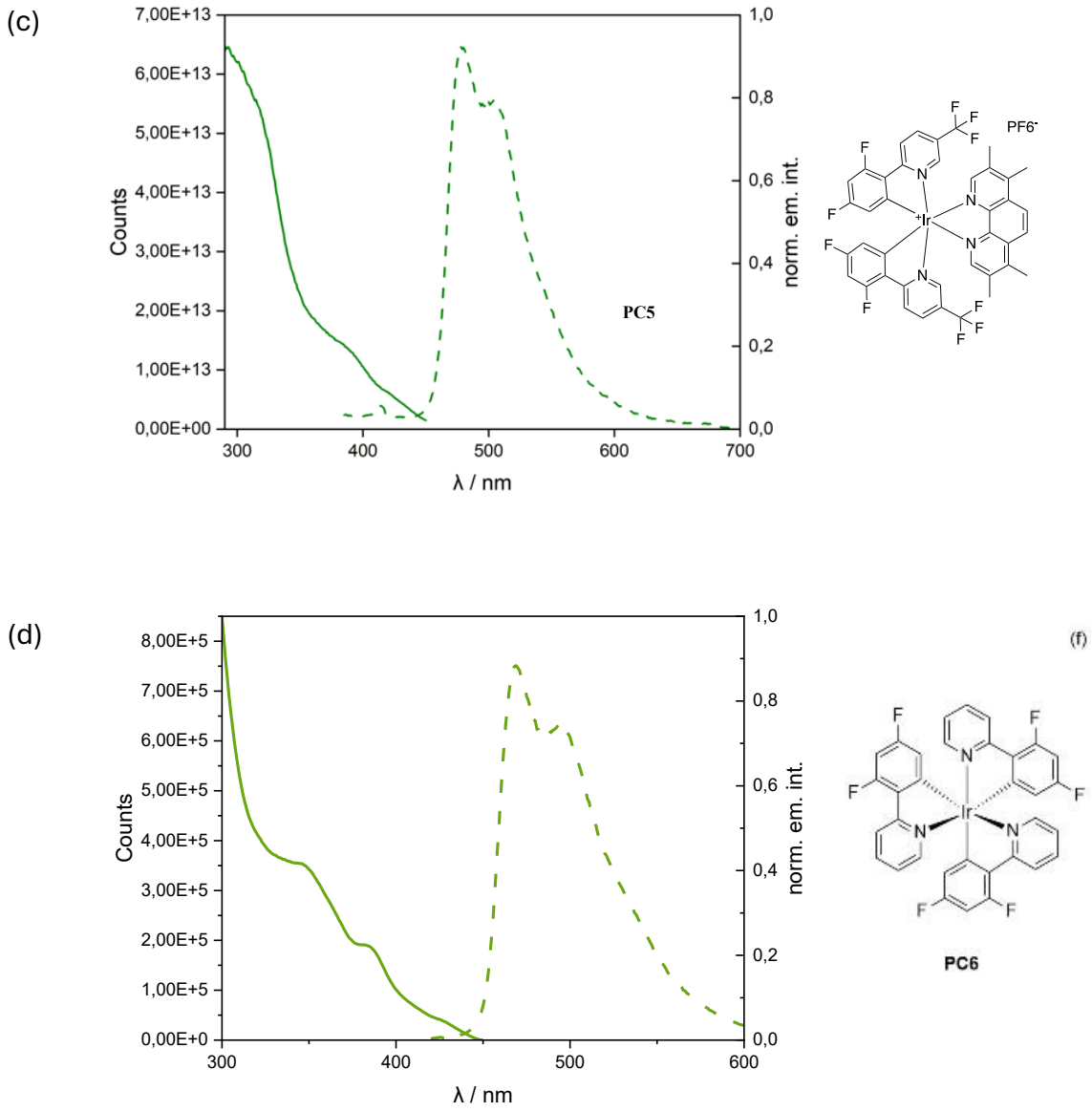

Figure S1. Absorption spectra (solid traces) and emission spectra (dashed traces) of **N4** (10^{-4} M in toluene/DCM 8:2), (b) **66j** (10^{-4} M in toluene/DCM 8:2), (c) **PC5** (10^{-5} M in toluene/DCM 8:2), and (d) **PC6** (10^{-5} M in toluene/DCM 8:2); all these spectra were collected at 293 K. The measured absorption and emission spectra of **PC5** and **PC6** are in accordance with previously reported data (*Inorg. Chim. Acta* **2021**, *527*, 120554 and *Dalton Trans*., **2013**, *42*, 4539, respectively). Excitations were induced at 283 nm for (b), at 313 nm for (a), at 370 nm for (c), and at 365 nm for (d).

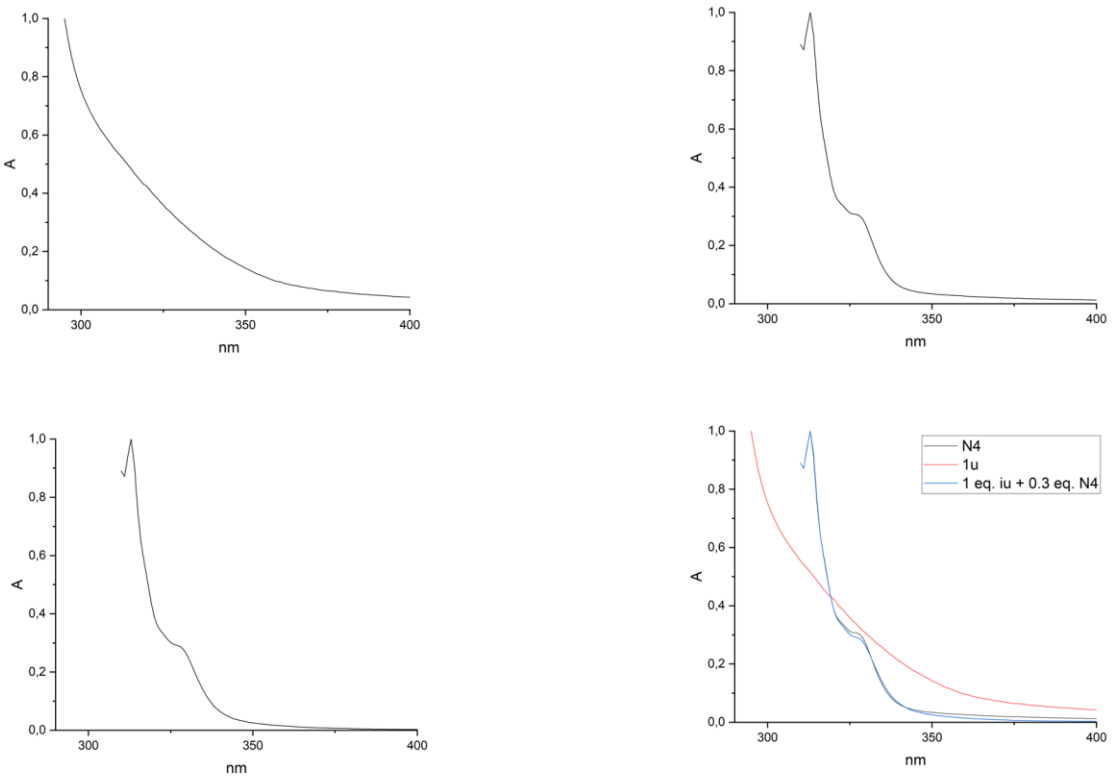

Figure S2. Absorption spectra of allene **66u** in *iso*-octane/DCM 9:1 (10^{-3} M, top left), **N4** (10^{-3} M, top right), **66u** + **N4** (1 eq., 10^{-3} M, and 0.3 eq., respectively, bottom left), the three stacked spectra (bottom right). No significant shift in bands and intensities were observed, suggesting that the formation of [**66u**:**N4**] adducts observed via NMR spectroscopy does not form a species with significantly altered UV-vis properties, such as a non-emitting or differently emitting entities that would be responsible for the static quenching of the fluorescence of **N4** by quencher **66**. These observations thus suggests that the observed quenching is a dynamic process.

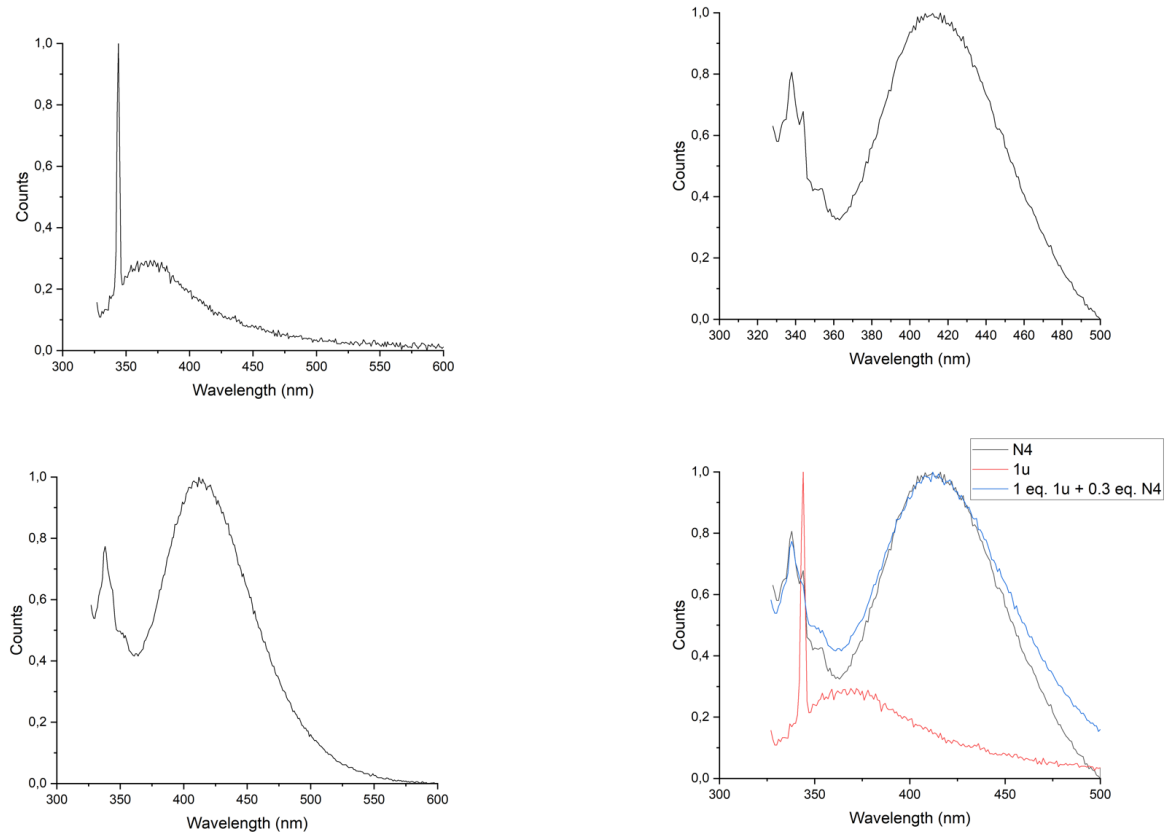

Figure S3. Emission spectra of allene **66u** in *iso*-octane/DCM 9:1 (10^{-3} M, top left), **N4** (10^{-3} M, top right), **66u** + **N4** (1 eq., 10^{-3} M, and 0.3 eq., respectively, bottom left), the three stacked spectra (bottom right), upon excitation at 313 nm. The emission band ascribed to the excimer of **N4** remains visible analyzing the **66u** + **N4** mixture. This indicates that the quenching of this band through the addition of the substrate mentioned in the main manuscript is not due to the formation of a non-emitting species between the two molecules.

Photoluminescence lifetimes

The measurements of the photoluminescence lifetime for **PC5** and **PC6** were carried out with a FLS1000 Edinburgh fluorometer. Photoluminescence decays for **PC5** and **PC6** were collected by exciting two samples for **PC5** and one sample for **PC6** with an EPL picosecond pulsed diode laser at a repetition rate of 50 KHz; the exciting wavelength was set at 293 nm, corresponding to the maximum absorption of the bis(α-naphtylmethyl) ether (**N4**). The emission was collected at 412 nm. All the data was processed with the Fluorescence Analysis Software Technology (FAST) package supplied by Edinburgh Instruments. A quartz cuvette (optical path = 1 cm) capped with a rubber septum was used. This provided the functions for the Stern-Volmer plot, from which the values of k_d were obtained. The first **PC5** sample was dissolved in CH_3CN, giving as a result a lifetime of τ = 3.8 µs, which corresponds to the result previously reported by our group the literature.[2] The second **PC5** sample was dissolved in a 8:2 toluene/DCM mixture, which reproduces the reaction conditions; the fitting of this decay analysis gave as a result a lifetime of τ = 1.6 µs. The **PC6** sample was dissolved in a 8:2 toluene/DCM mixture, which reproduces the reaction conditions; the fitting of this decay analysis gave as a result a lifetime of τ = 748 ns.

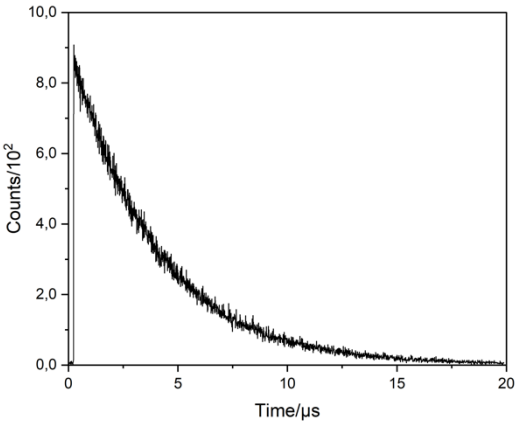

Measured phosphorescence decay of **PC5** in CH_3CN.

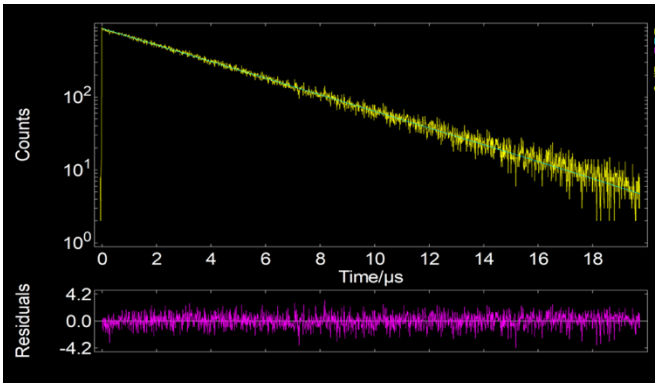

Fit result for the decay of **PC5** in CH_3CN

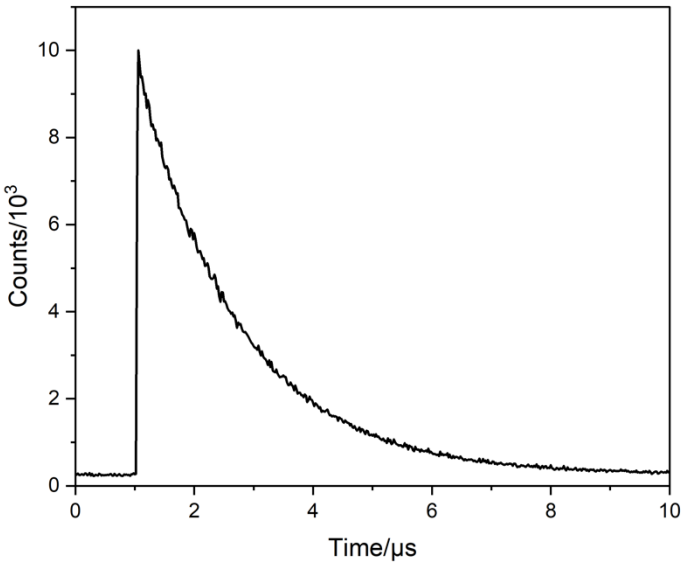

Measured phosphorescence decay of **PC5** in toluene/DCM 8:2

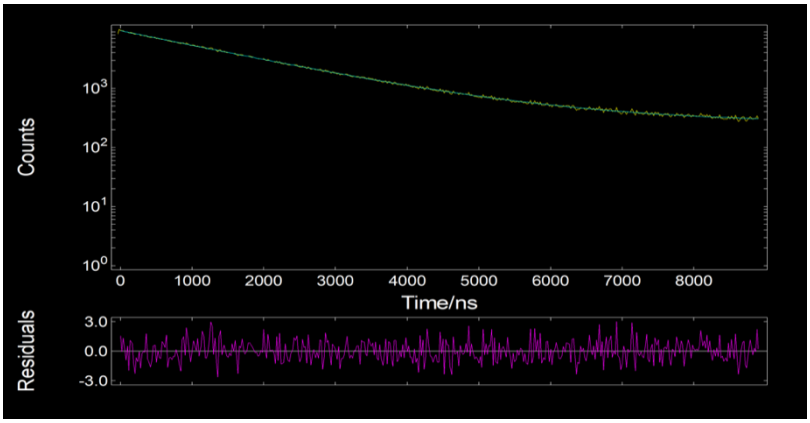

Fit result of the decay of **PC5** in toluene/DCM 8:2

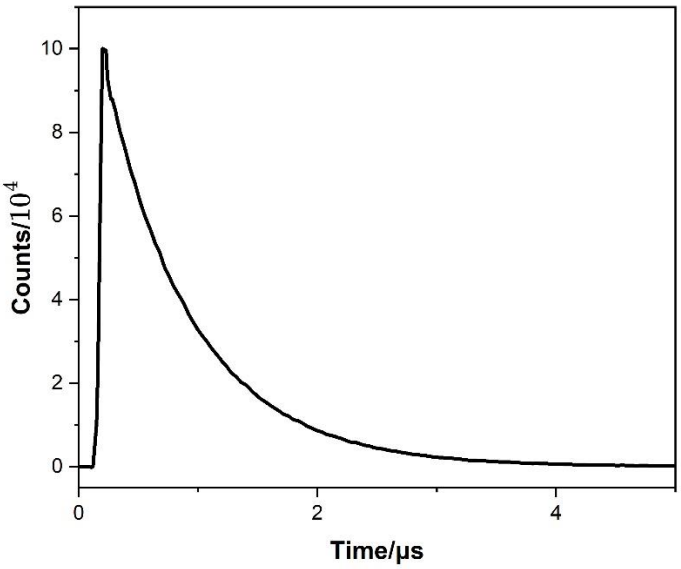

Measured phosphorescence decay of **PC6** in toluene/DCM 8:2

Fluorescence lifetime and phosphorescence lifetime of N4

All the analyses performed in glassy matrixes at 77 K on **N4** were carried out with a FLS1000 Edinburgh fluorometer, using the LP980KS setup as a cryostat; moreover, the standard cuvette holder was replaced by a dewar that holds a 4 mm glass tube surrounded by liquid nitrogen (setup shown in the depicted figure). The N4 derivative was tested in two different solvents, 2-MeTHF and absolute EtOH, and samples were prepared at a 10^{-4} M concentration.

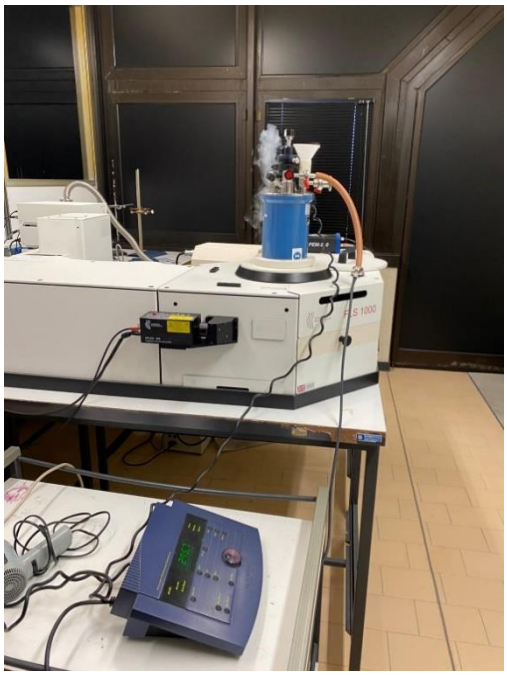

Cryostat setup to conduct the analysis at 77 K.

.

Firstly, emission spectra were collected by exciting the **N4** sample with a Xenon lamp at 295 nm.

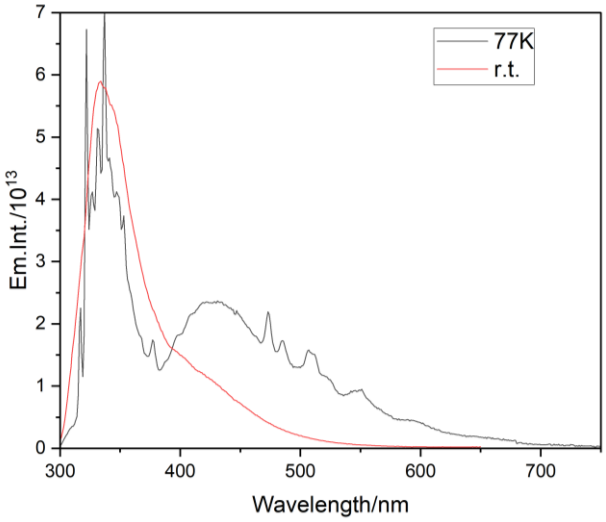

Comparison of emission spectra in 2-MeTHF upon 295 nm excitation (grey) and emission spectra at RT (red).

Subsequently, with the aim of better understanding the photophysical processes, time-resolved emission spectroscopy (TRES) was examined. The TRES allows to achieve curves whose intensities at different wavelengths are presented as functions of time. As shown in Figure below, the luminescence emission spectra were obtained at markedly different timeframes during the fluorescence and phosphorescence decays, respectively. The emission spectra of **N4** was measured in the range of 100-1700 ms.

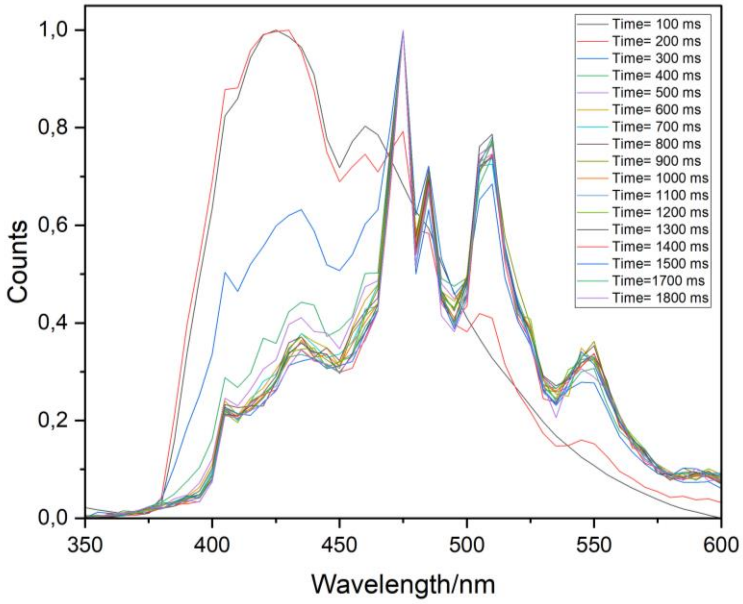

The TRES analysis graphical overlay shows different peaks profiles: at shorter times, the emission of excimer species ^{exc}**N4** is described, while at longer times (over 500 ms), the emission spectra is dominated by the phosphorescence decay. To confirm these findings, the phosphorescence decay

was measured with the TCSP (Time-Correlated Single Photon Counting) analysis, giving as a result a lifetime of τ = 1.5 s.

Fluorescence lifetimes were investigated by exciting the **N4** sample in *iso*-octane with an EPL picosecond pulsed diode laser at a repetition rate of 50 KHz; the exciting wavelength was set at 293 nm, corresponding to the maximum absorption of **N4**. The decay can be accurately modelled with two exponential components, τ_{fl} = 6.7 ns and τ_{exc} = 2.1 ns which correspond to the fluorescence and excimer decays, respectively.

The comprehensive set of radiative decays is presented through the following Jablonski diagram.

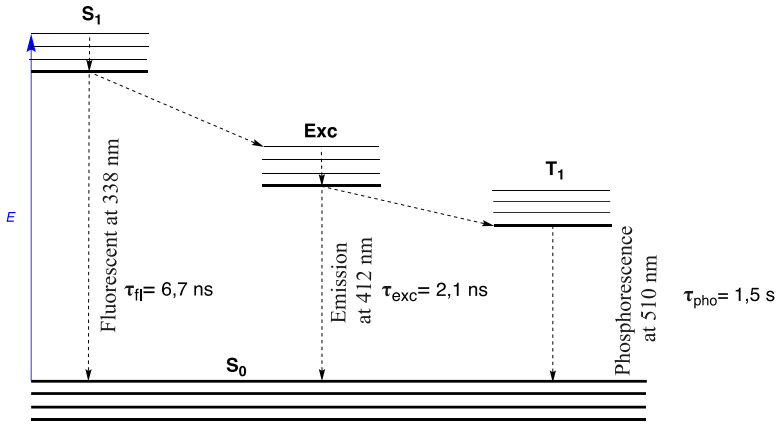

Jablonski diagram of **N4**

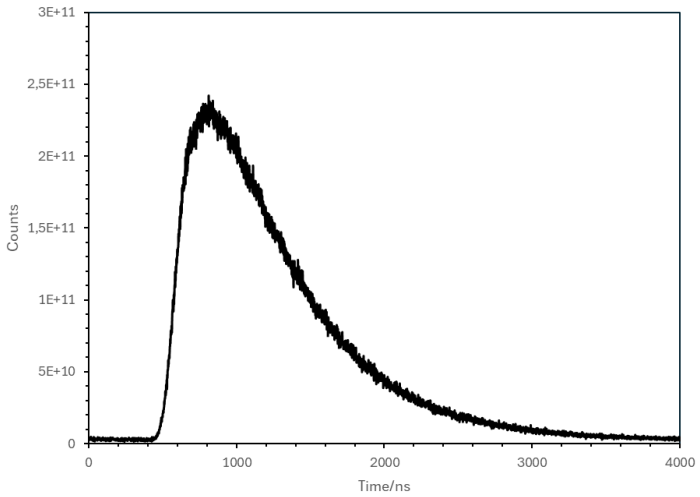

Fluorescence decay of **N4** in *iso*-octane, room temperature.

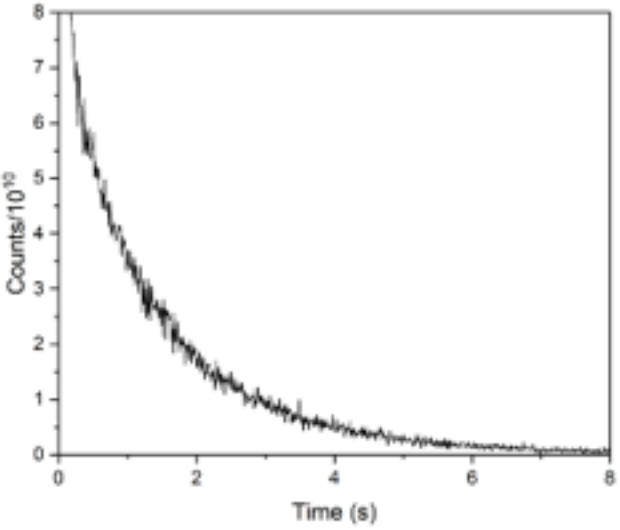

Kinetic Scan of **N4** in *iso*-octane at 77 K.

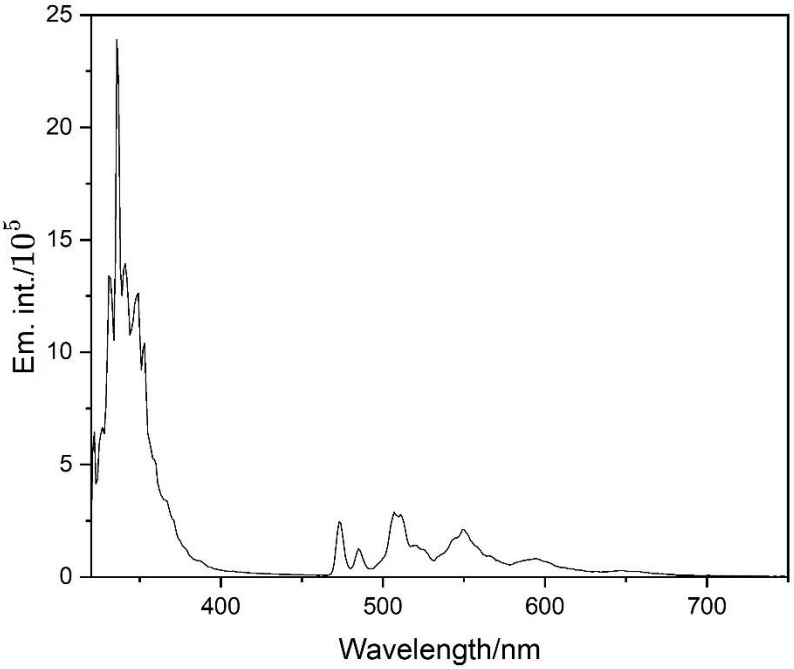

Emission spectra of **N4** in absolute EtOH upon 295 nm excitation at 77 K; under these conditions, the emission from the excimer of **N4** is hindered while phosphorescence bands remain visible.

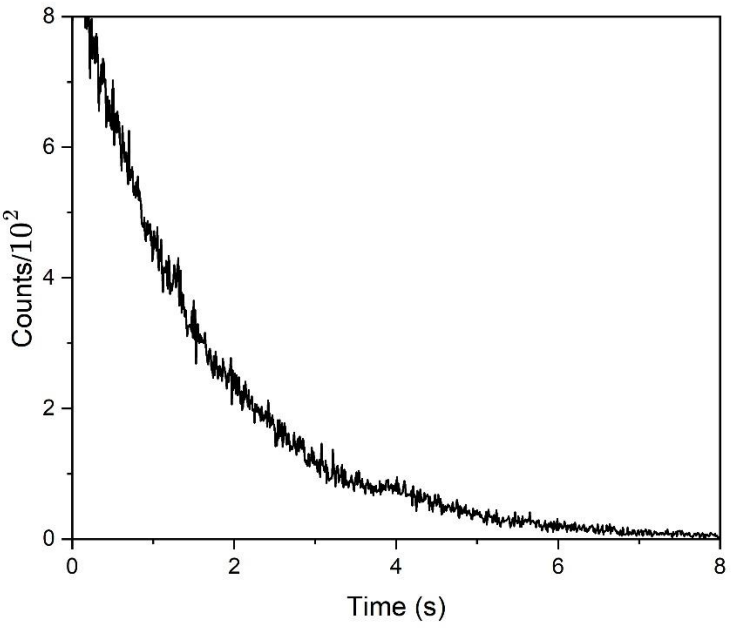

Kinetic Scan of **N4** in absolute EtOH at 77 K; the spectrum is comparable to that obtained in 2-MeTHF.

Stern-Volmer quenching studies

The measurements were carried out with a FLS1000 Edinburgh Fluorometer, equipped with automatic polarizers. Emissions have been collected by exciting samples with a Xenon lamp at 293 nm and the luminescence was measured at 412 nm. Luminescence spectra are corrected for the excitation intensity and the detector sensitivity.

Analyses on PC5

Stern – Vollmer quenching studies were carried out using a 10^{-5} M solution of **PC5** in toluene/DCM 8:2 and variable concentrations of **66j** and **N4** from 0 to 9.1 mM. 2.5 mL of the **PC5** solution were transferred into a 3.5 mL quartz cuvette and degassed twice for 5 minutes (with a 30 second break in between) before collecting the first spectrum. Then, after each addition of the quencher, the samples were degassed for 2 minutes, and the next spectrum was rapidly recorded.
Stern – Vollmer plots were obtained at varying concentrations of the quencher, and K_{SV} constants were extracted according to the equation $I_0/I = 1 + K_{SV}[Q]$. K_q constants were obtained according to the equation $K_q = Ksv/\tau_0$.

Comprehensive table of Stern – Vollmer constants and bimolecular kinetic quenching constants.

QUENCHER	K_{SV}	R^2	K_q [$mol^{-1} \cdot L \cdot sec^{-1}$] x 10^8
66j	346	0.99	2.2
N4	5120	0.97	32.0

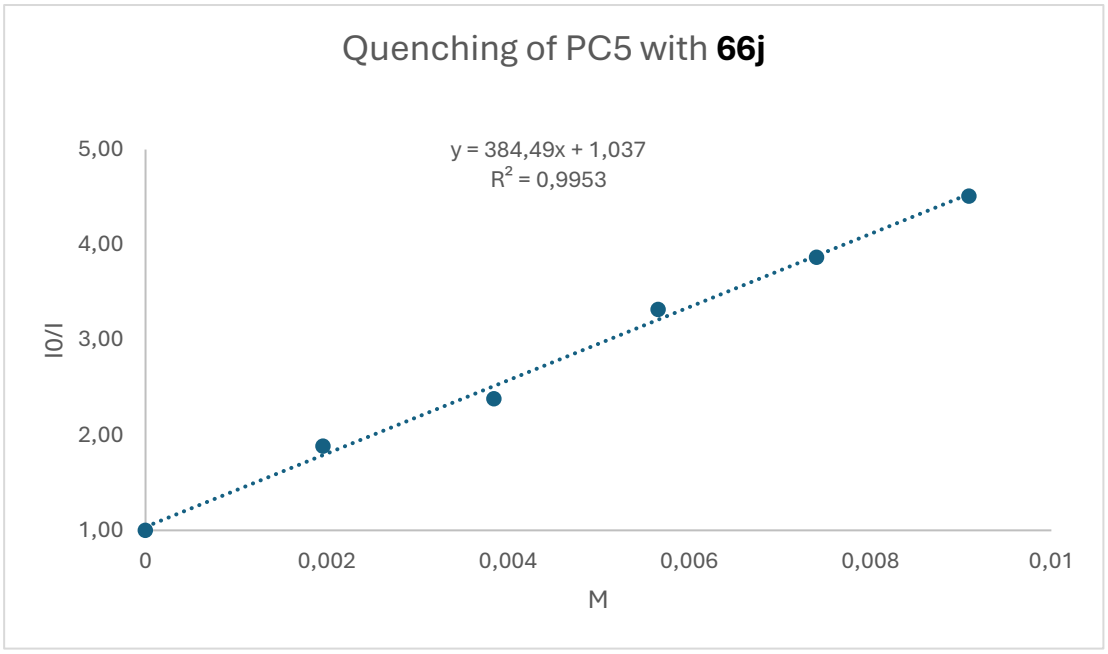

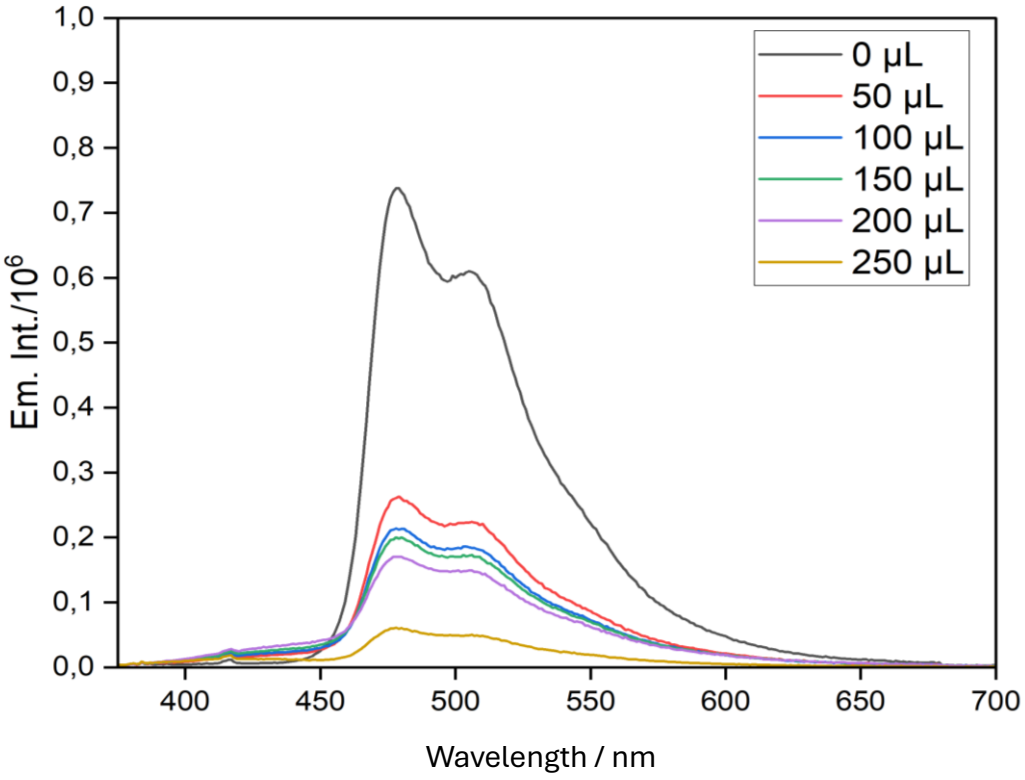

Measured emissions for the quench of excited **PC5** with 50µL, 100µL, 150µL, 200µL, and 250µL of **66j.**

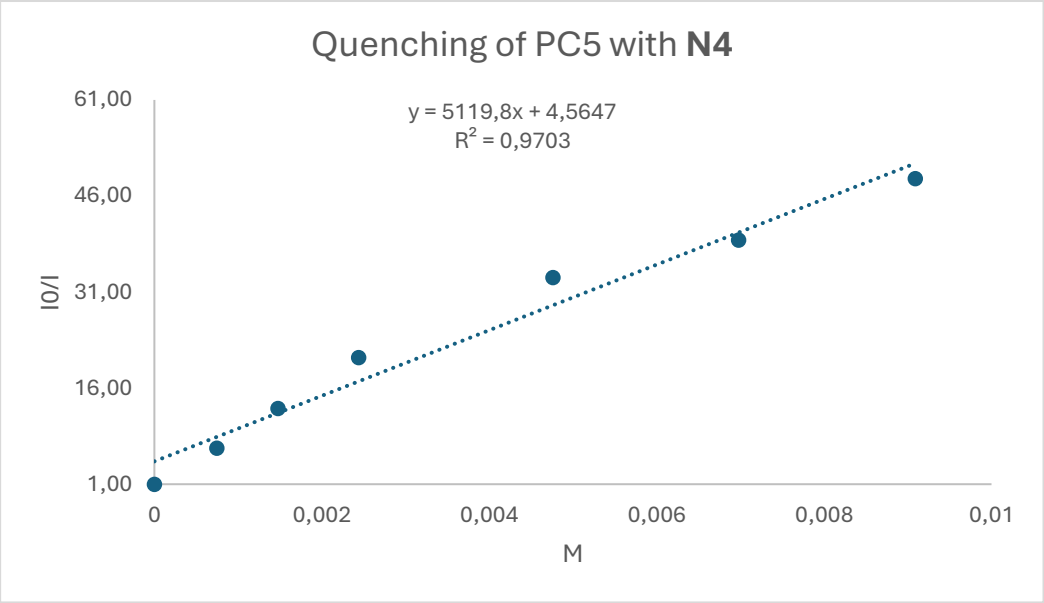

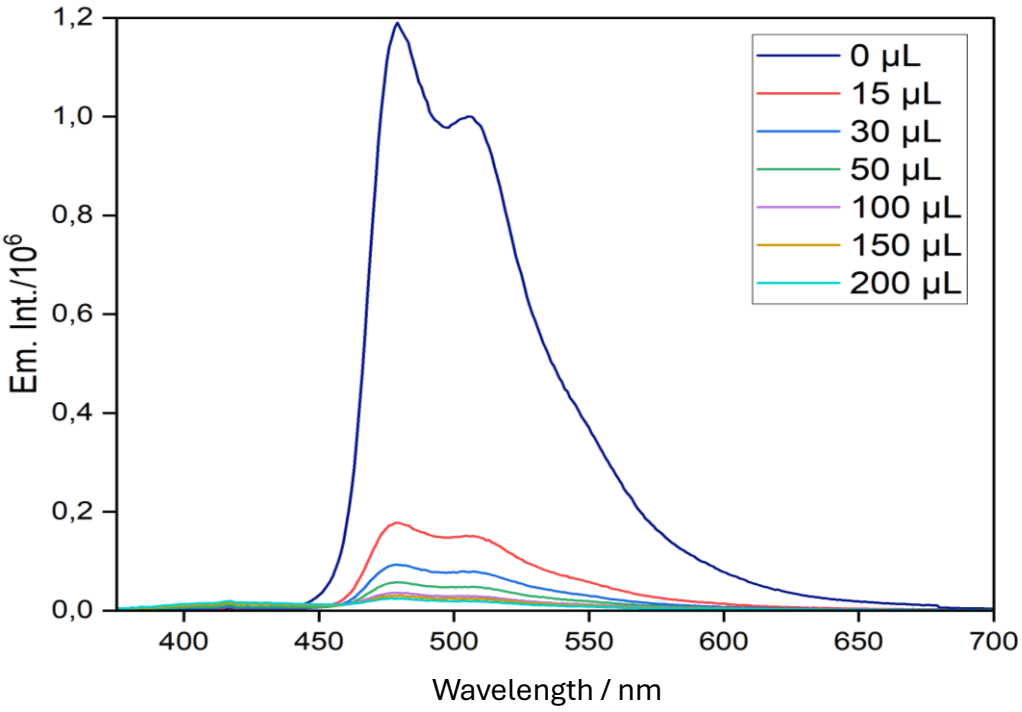

Measured emissions for the quench of the excited **PC5** with 15 µL, 30 µL, 50µL, 100µL, 150µL and 200µL of **N4**.

Analyses on PC6

Stern – Vollmer quenching studies were carried out using a 10^{-5} M solution of **PC6** in toluene/DCM 8:2 and variable concentrations of **66j** and **N4** from 0 to 11.7 mM. 2.5 mL of the **PC6** solution were transferred into a 3.5 mL quartz cuvette and degassed twice for 5 minutes (with a 30 second break in between) before collecting the first spectrum. Then, after each addition of the quencher, the samples were degassed for 2 minutes and the next spectrum was rapidly recorded.
Stern – Vollmer plots were obtained at varying concentrations of the quencher, and K_{SV} constants were extracted according to the equation $I_0/I = 1 + K_{SV}[Q]$. K_q constants were obtained according to the equation $K_q = Ksv/\tau_0$.

Comprehensive table of Stern–Vollmer constants and bimolecular kinetic quenching constants:

QUENCHER	**K_{SV}**	**R^2**	**K_q [$mol^{-1} \cdot L \cdot sec^{-1}$] x 10^8**
66j	290	0.98	3.9
N4	3749	0.99	50.1

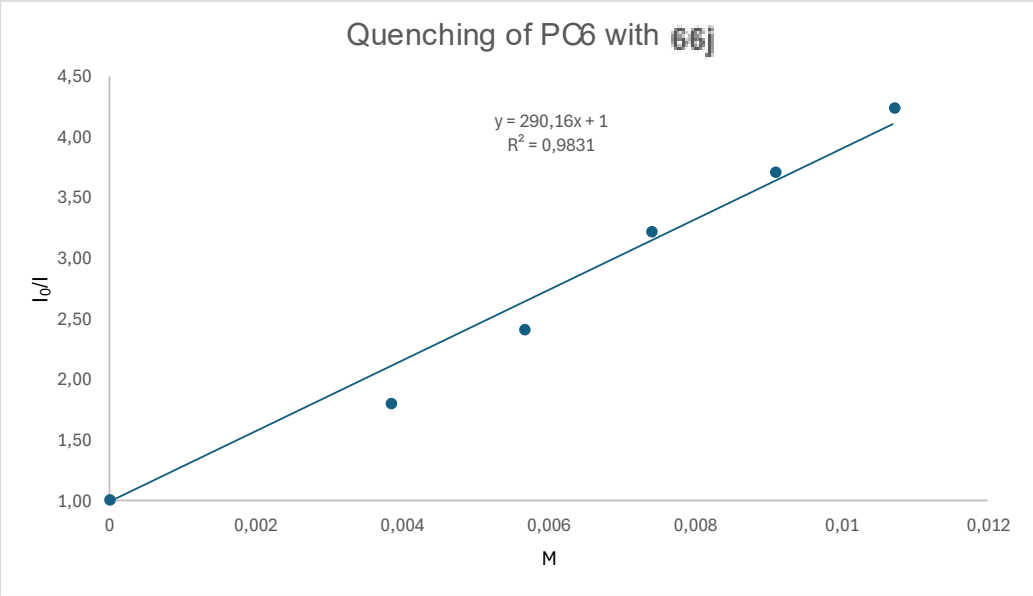

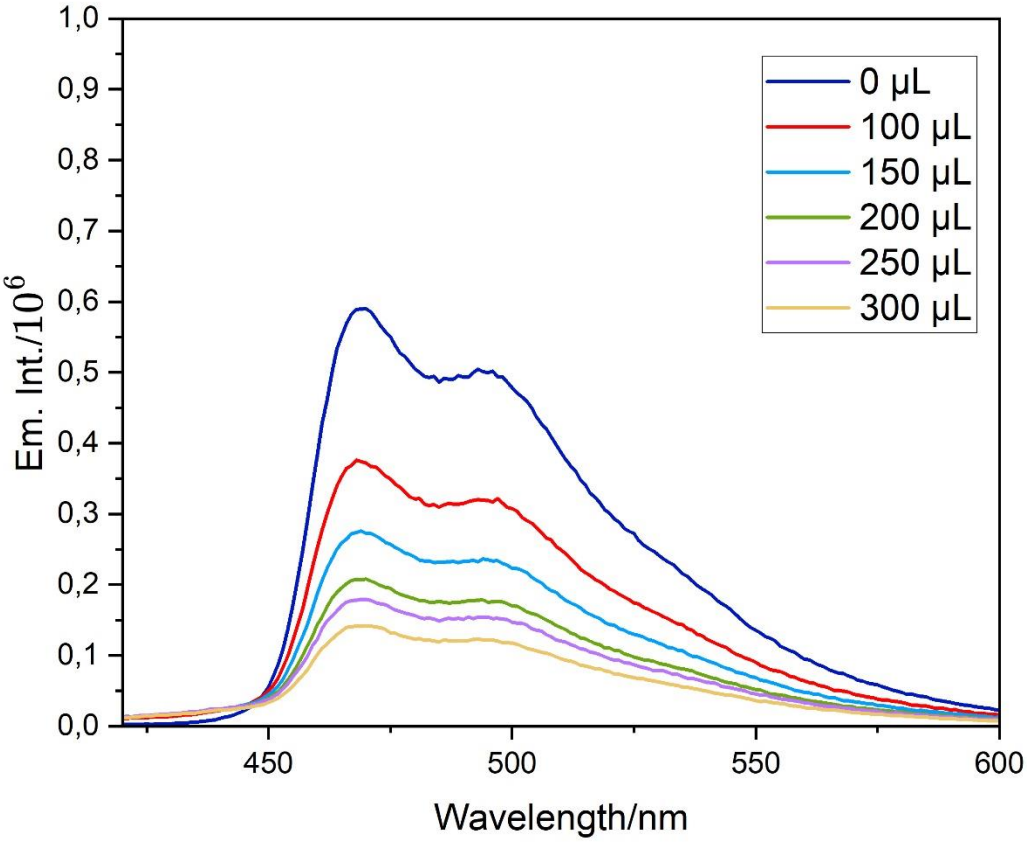

Measured emissions for the quench of excited **PC6** with 100 µL, 150 µL, 200 µL, 250 µL, and 300 µL of **66j**.

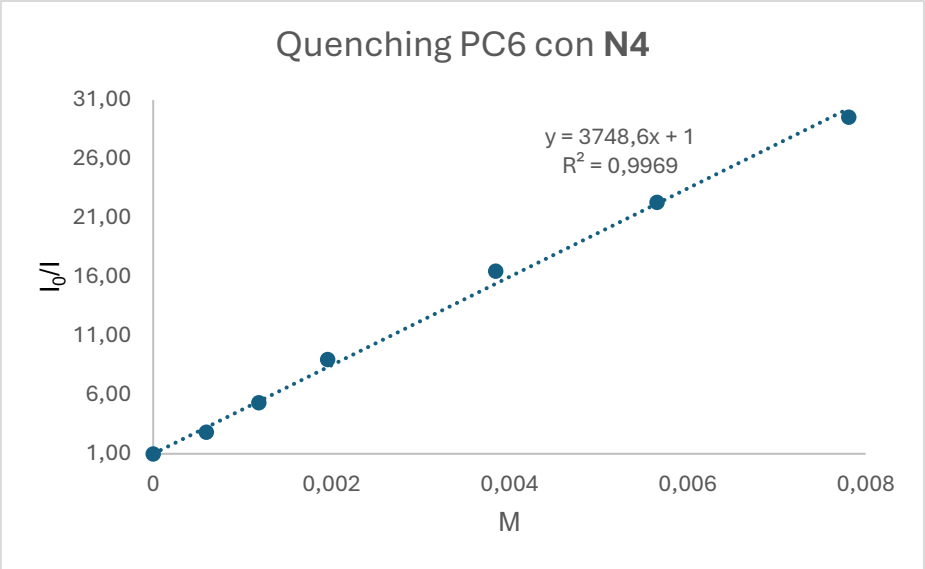

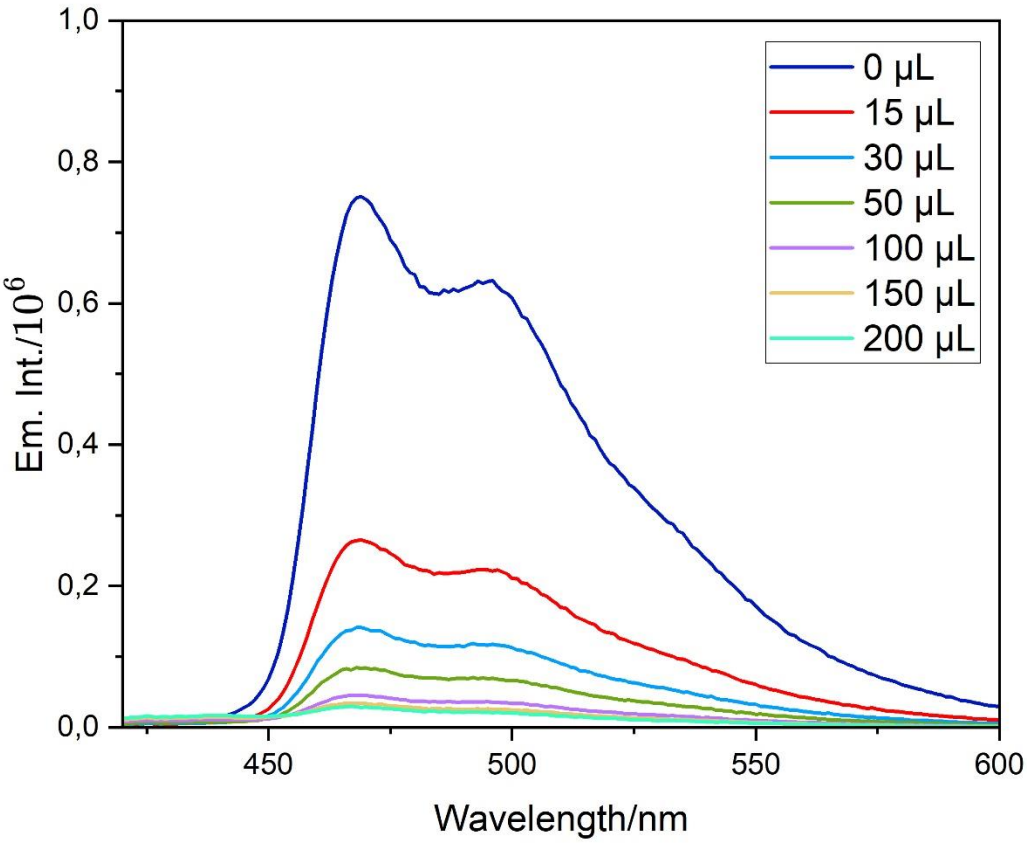

Measured emissions for the quench of the excited **PC6** with 15 µL, 30 µL, 50 µL, 100 µL, 150 µL and 200 µL of **N4**.

Analyses on N4

Another Stern – Vollmer quenching study was carried out using a 10^{-4} M solution of **N4** in *iso*-octane and variable concentrations of **1j** from 0 to 9.1 mM. 2.5 mL of the **N4** solution were transferred into a 3.5 mL quartz cuvette and degassed twice for 5 minutes (with a 30 second break in between) before collecting the first spectra. Then, after each addition of quencher, the samples were degassed for 2 minutes and spectra were rapidly recorded.

The Stern – Vollmer plot was obtained at varying concentrations of the quencher, and the K_{SV} constant was extracted according to the equation $I_0/I = 1 + K_{SV}[Q]$. The K_q constant was obtained according to the equation $K_q = Ksv/\tau_0$.

Comprehensive table of Stern – Vollmer and bimolecular kinetic quenching constants.

QUENCHER	**K_{SV}**	**R^2**	**K_q [$mol^{-1} \cdot L \cdot sec^{-1}$] x 10^8**
66j	106	0.98	158.2

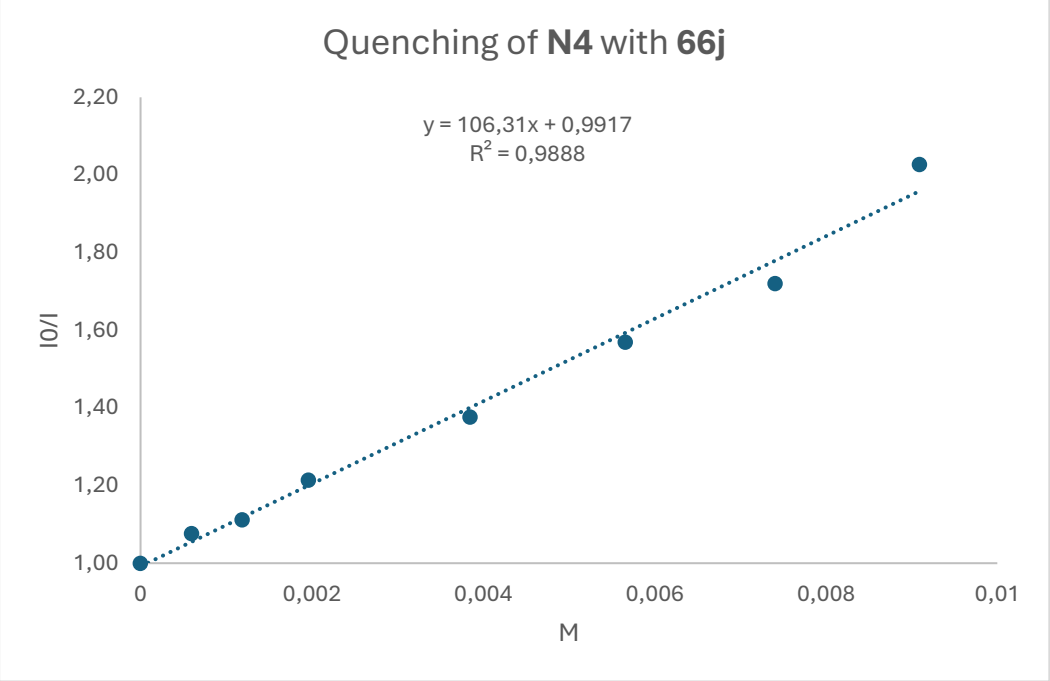

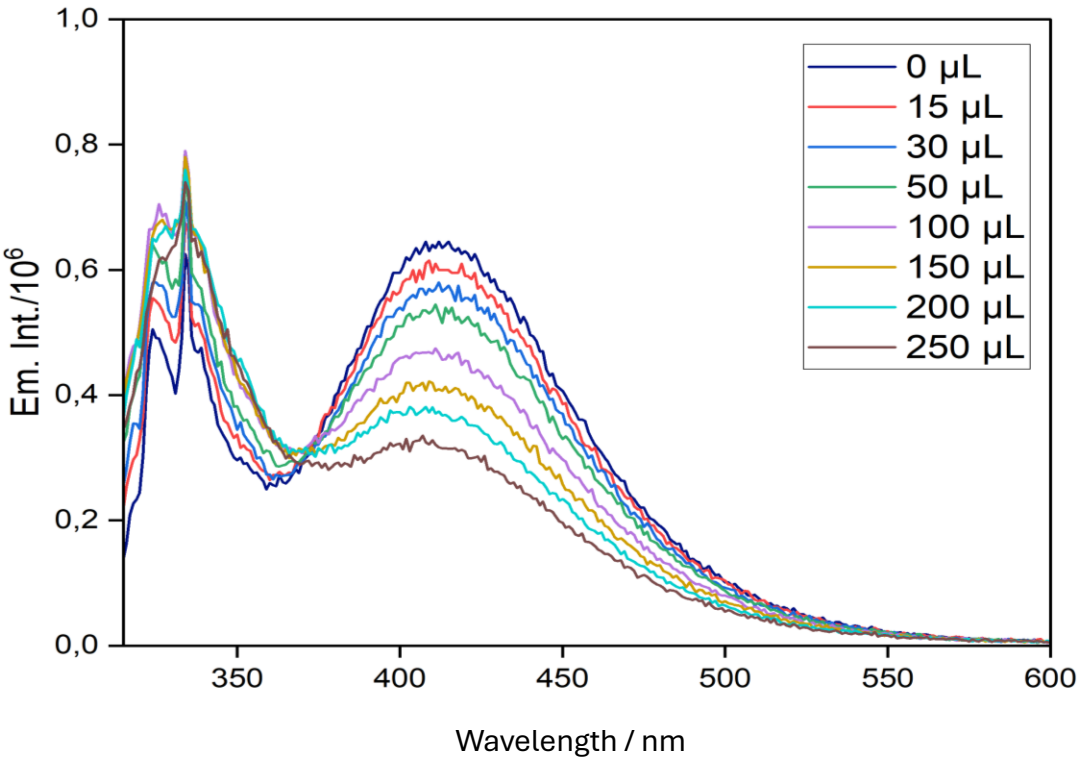

Measured emissions for the quench of **N4** with 15 µL, 30 µL, 50µL, 100µL, 150µL, 200µL, and 250µL **66j**.

DFT Calculations

Calculations were performed at the DFT level using Gaussian16.[79] The hybrid exchange/correlation M06 functional, as described by Zhao and Truhlar, was used for geometry optimization.[80] This broadly used functional has already proved to be reliable in related photochemical cascades, such as those described in refs 14 and 16 of the manuscript. Optimizations were performed without any constraint using the Def2-SVP basis set described by Weigend and Ahlrichs,[81] using toluene as implicit solvent through the CPCM method introduced by Barone and Cossi.[82] Free optimization was then performed again using the Def2-TZVP basis set to achieve more precise results.[83] In both cases, the model was used in combination with D3 corrections, as described by Grimme,[84] in order to consider dispersion interactions.

All values and geometries reported hereafter are those of freely optimized solvated structures, calculated at the M06/Def2-TZVP level. All intermediates, both in their ground and higher spin states were characterized by the absence of any imaginary frequency in their Hessian matrix. All transition states were characterized by the presence of a single imaginary frequency in their Hessian matrix, which corresponds to the molecular vibration connecting the reactant with the product.

In order to exclude that the present theoretical model delivered biased results, the triplet energy of model substrate **66j** was calculated using six different combinations of DFT functionals, including both exchange/correlation and orthodox hybrid ones, and basis sets (data refer to freely optimized structures in all cases); overall, all of these models provided values within a few kcal/mol compared to those presented in the main manuscript, as summarized in the following summary.

B3LYP/Def2-TZVP, CPCM = toluene

	H (Hartrees)	**S** (cal/K*mol)	**G** (kcal/mol)
^{1}66j	-672.89829	131.294	
^{3}66j	-672.83393	133.926	39.60

PBE1PBE/Def2-TZVP, CPCM = toluene

	H (Hartrees)	**S** (cal/K*mol)	**G** (kcal/mol)
^{1}66j	-672.1052	131.166	
^{3}66j	-672.04319	133.771	38.14

WB97D/Def2-TZVP, CPCM = toluene

	H (Hartrees)	**S** (cal/K*mol)	**G** (kcal/mol)
^{1}66j	-672.68336	130.266	
^{3}66j	-672.61678	133.405	40.84

M11/Def2-TZVP, CPCM = toluene

	H (Hartrees)	**S** (cal/K*mol)	**G** (kcal/mol)
^{1}66j	-672.45642	131.135	
^{3}66j	-672.38729	132.739	42.90

M06-2X/Def2-TZVP, CPCM = toluene

	H (Hartrees)	**S** (cal/K*mol)	**G** (kcal/mol)
^{1}66j	-672.58352	130.585	
^{3}66j	-672.51202	132.811	44.21

WB97D3/Grimme's 2DZ-ecp, CPCM = toluene

	H	**S**	**G**
	(Hartrees)	(cal/K*mol)	(kcal/mol)
^{1}66j	-115.48351	131.936	
^{3}66j	-115.41834	133.266	40.50

Comprehensive Table in AU for azetidine synthesis

M06/Def2-TZVP, CPCM = toluene, G3 dispersion corrections

	H (Hartrees)	**S** (cal/K*mol)	**imaginary frequency** (cm^{-1})
^{1}N4	-923.708729	140.503	
^{3}N4	-923.616183	143.891	
^{1}66j	-673.140802	130.968	
^{3}66j	-673.075014	132.121	
TS(66-A)	-673.057455	129.984	-1882.1890
^{3}66jA	-673.107247	133.067	
^{1}67j	-673.153121	125.273	
^{1}[66j:N4]	-1596.878489	224.402	
[66j:^{3}N4]	-1596.815134	221.189	
[^{3}66j: N4]	-1596.788638	226.308	
TS(66-A:N4)	-1596.798189	217.557	-1797.9256
^{3}[66jA:N4]	-1596.851416	220.177	
^{1}[67j:N4]	-1596.894057	214.114	

Study of rotamers

To confirm the presence of rotamers of **67a**, ^{1}H NMR were measured at different temperatures in DMSO-d_6, (298 K, 323 K and 348 K). The series of spectra do not provide significant variation of the ratio between the two species.

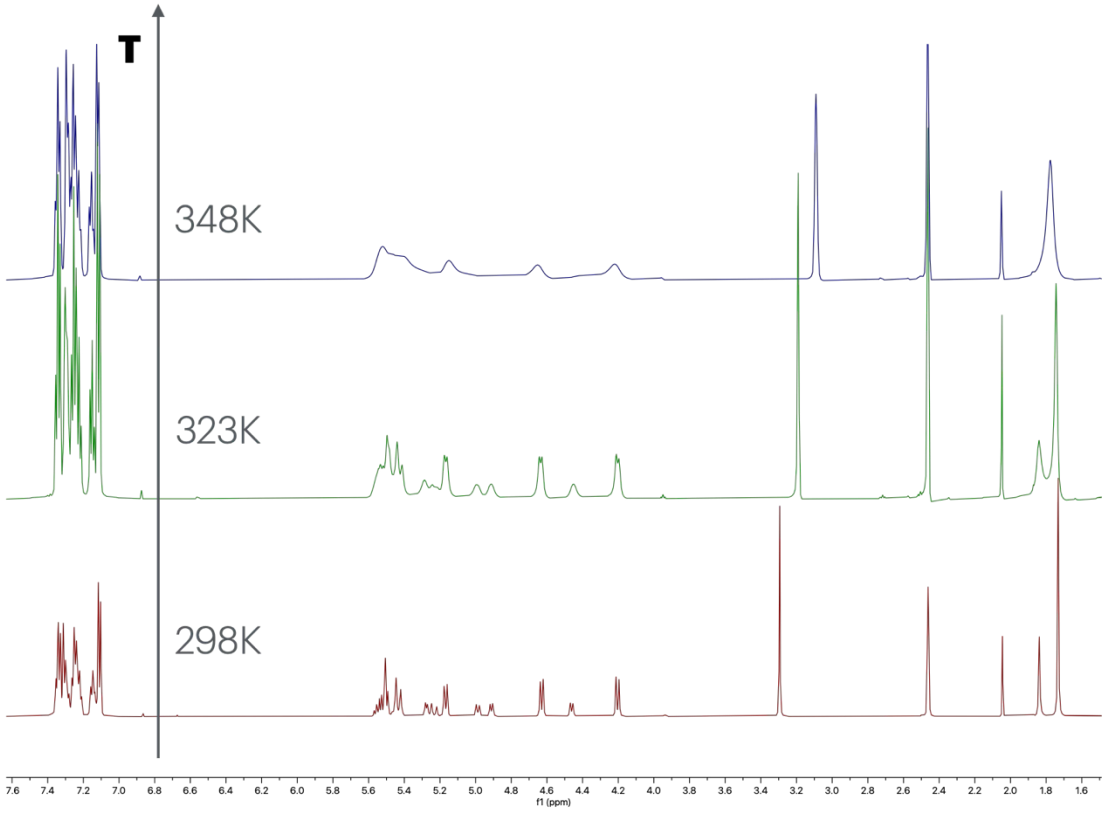

Copies of spectra of 2a in DMSO-d_6.

To confirm the presence of rotamers **67a**, ^{1}H NMR spectra were measured in $CDCl_3$ and DMF-d_7. The ratio between the species is modified by the nature of the deuterated solvent, thus confirming that the two species are rotamers. **Green line**: $CDCl_3$ (ROTa:ROTb 79:19); **Red line**: DMF-d_7 (ROTa:ROTb 69:31).

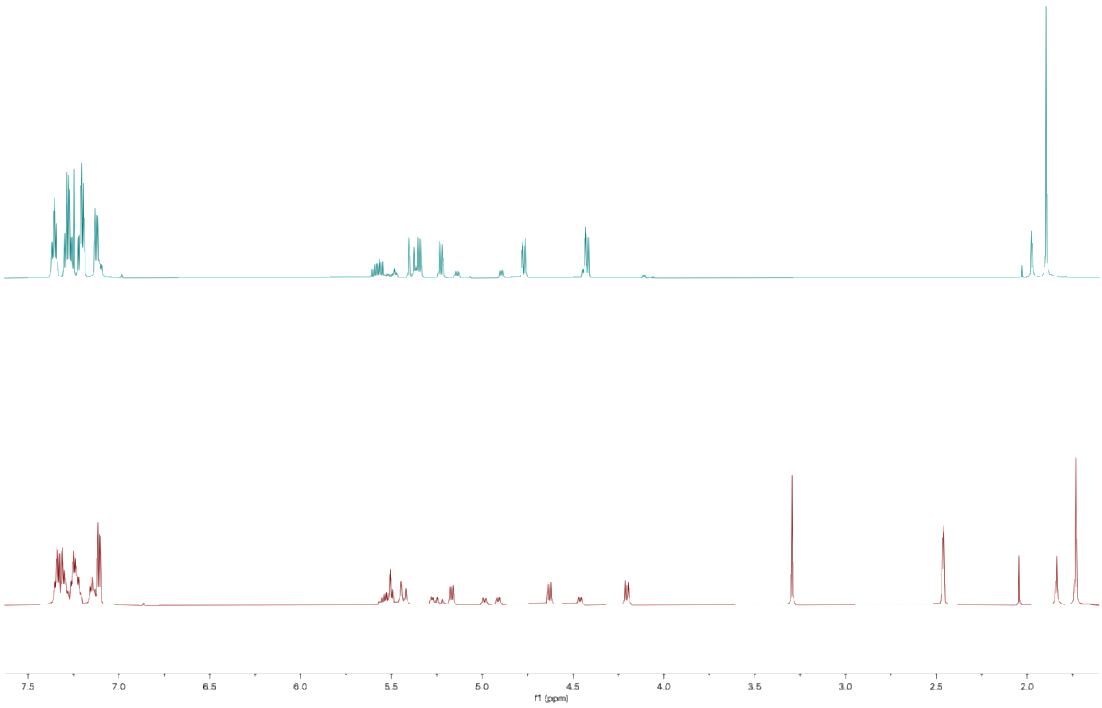

Chapter III

Visible Light-promoted Direct O-H activation and C(sp^3)-O Bond Formation via Intermolecular Hydrogen Atom Transfer from Allenamides

Preliminary results

3.1 Intermolecular HAT from C-centered radicals: an underdeveloped tool

Protocols based on intramolecular (1,n)-Hydrogen Atom Transfer mediated by C-centered radicals flourished numerously in the last decades, as an alternative more atom-economic and milder strategy to form new C-X bonds.[1,85] On the contrary, their intermolecular counterparts remains thus far severely underdeveloped,[86] especially when compared to intermolecular HATs mediated by heteroatom-based radicals (*e.g.* O-, N-, S-centered, and halogen radicals).[87] Indeed, the only precedents of Carbon radical-mediated intermolecular HATs are limited to alkyl – which often do not have sufficiently high BDEs - and aryl radicals – whose extreme instability makes them less efficient HAT agents. Hydrogen Atom abstraction by alkyl radicals remains limited to the use of tetrahalogenated methanes,[88] N-Hydroxyphtalimide esters,[89] alkyl bromides,[90] and acetic acid[91] as simple alkyl radical precursors. On the other hand, commonly employed aryl radical precursors for intermolecular HATs are aryl diazonium salts[92] or aryl azosulfones,[93] diaryliodonium salts,[94] O-benzoyl oximes,[95] aryl sulfonium salts,[96] aryl thioesters,[97] and aryl bromides/iodides,[98] usually employed as solvents or co-solvents. For instance, in Schemes 49-53, a few catalytic methods for the formation of C-X (X = N, S, O) bonds *via* intermolecular HAT mediated by aryl-radicals are illustrated.

In 2018, Toste's group[94b] reported the formation of a C-O bond at the α-position of cyclic ethers **73** *via* photoactivation of diaryliodonium salts **74** or **75** with chiral phosphate anion phase-transfer catalyst to impart stereoselectivity (Scheme 49). In this reaction, the reactive species is generated through photolytic excitation of the diaryliodonium salt **77**, which affords an aryl radical and an aryl iodonium radical after homolytic cleavage. The aryl radical abstracts a hydrogen atom from tetrahydrofuran **73**, forming a tetrahydrofuran radical, which then recombines with the aryl iodonium radical formed in the previous step to form intermediate **73A**, which eventually undergoes elimination and subsequent nucleophilic attack by alcohol **72**, to furnish enantioenriched acetal product **76**.

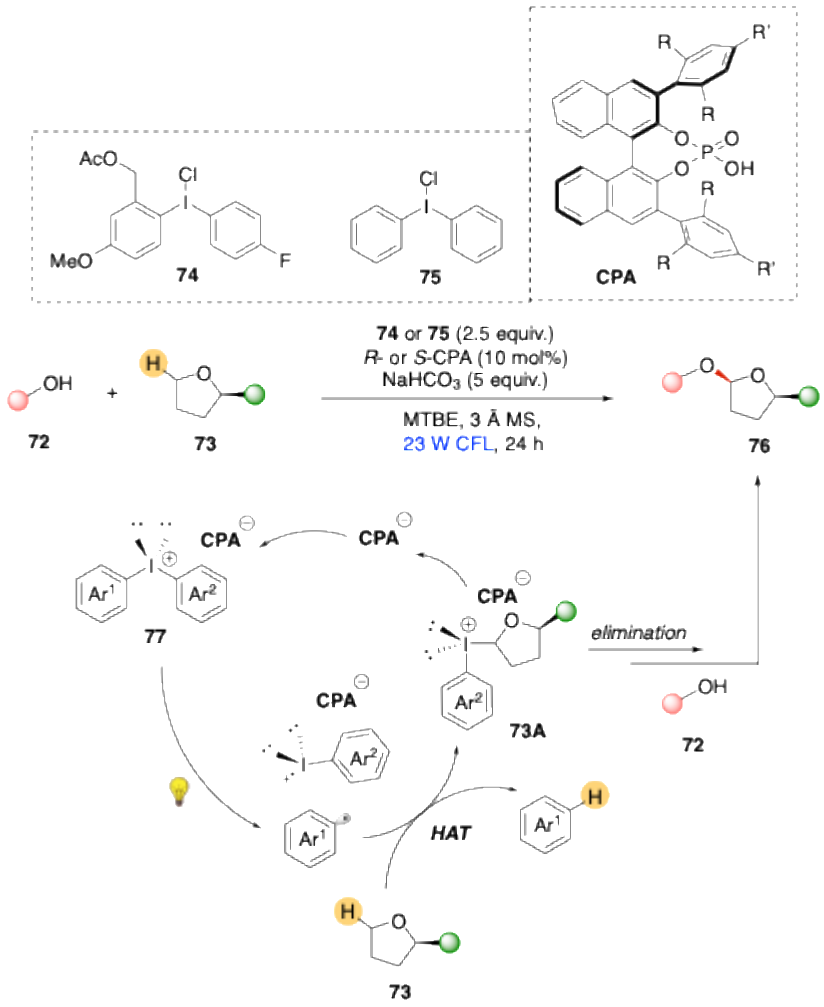

Scheme 49. C-O bond formation *via* intermolecular HAT by aryl radical from diaryliodonium salts.

In 2022, Gevorgyan's group developed a visible light-promoted, Pd-catalyzed allylic C-H amination of alkenes *via* indirect intermolecular HAT, employing aryl bromide **80** as the aryl radical precursor (Scheme 50).[98b] In addition, the authors also developed an asymmetric version of this protocol.[98b] In this mechanism, the generation of the aryl radical occurs through reduction of aryl bromide **80** by the photoexcited palladium catalyst. This aryl radical abstracts the allylic hydrogen from alkene **78** to form intermediate **78A**. Interaction of intermediate **78A** and $Pd(I)L_n$ generates a closed-shell π-allyl Pd(II) complex **78B**, which is eventually trapped by amine **79** to afford the desired product **81**, regenerating the initial redox state Pd-catalyst.

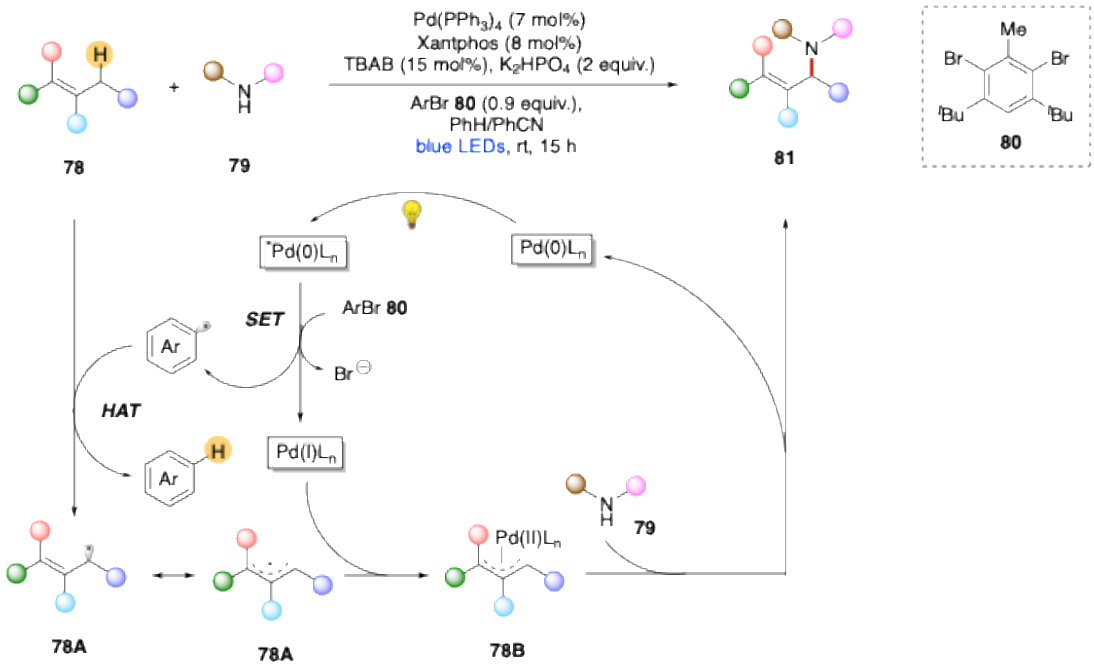

Scheme 50. Visible-light-induced, palladium-catalyzed C-N bond formation *via* aryl radical-mediated HAT.

With a similar mechanism, Gong, Han and co-workers[98c] reported a photo-induced Pd-catalyzed enantioselective three-component carboamination reaction for the synthesis of allylamines **86** (Scheme 51). Aryl bromide **85** is used as HAT agent, performing the abstraction on the weaker aliphatic C-H bond of **82**, which then adds to diene **83**, forming an allyl radical intermediate **83A**. The latter undergoes recombination with $Pd(I)L_n$ to form intermediate π-allyl Pd(II) complex **83B**, which eventually goes through nucleophilic attack by amine **84** to afford the desired product **86**.

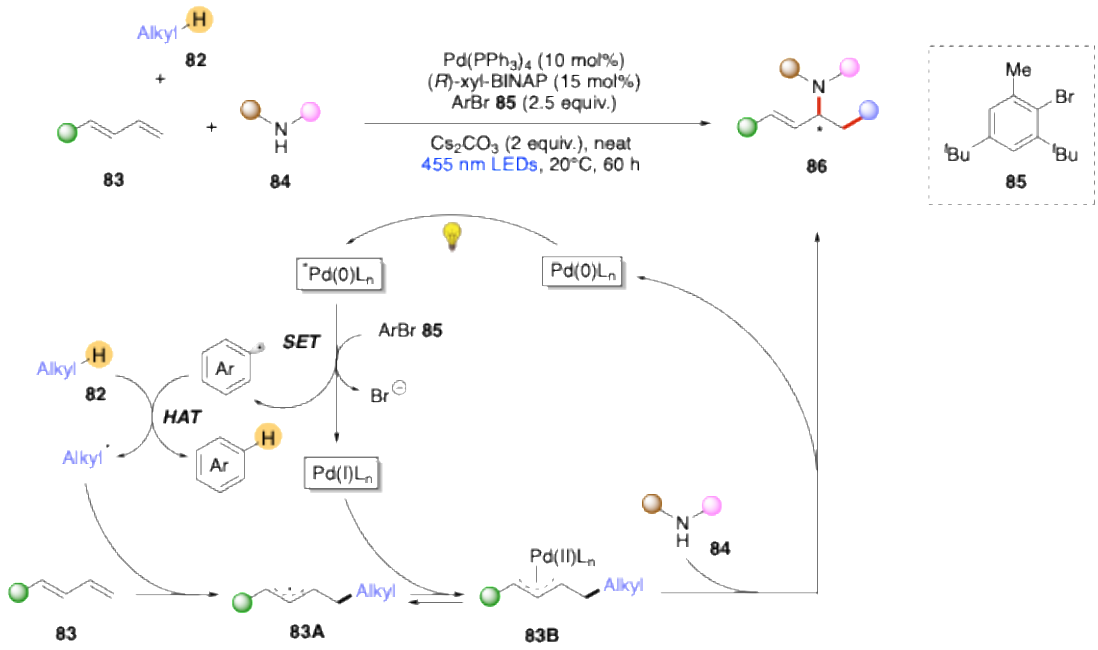

Scheme 51. Photo-induced, palladium-catalyzed enantioselective C-N bond formation *via* aryl radical-mediated HAT.

Another reported example of how intermolecular HAT can be exploited to form a new C-O bond is the visible light-induced Au-catalyzed α-C(sp^3)-H acetalization of saturated heterocycles.[98e] In this case, an EnT event occurs between the photoexcited Au-complex and aryl iodides **89** or **93**, to generate the correspondent excited state of the aryl iodide. The homolytic cleavage of the latter generates the HAT reagent aryl radical, which abstracts a Hydrogen from the α-C(sp^3)-H bond of heterocyclic compound **88** or **92**. This resulting radical undergoes radical–radical recombination with the iodine radical, leading to α-iodinated heterocycles as the reactive intermediate. Eventually, such α-halogenated heterocycles can easily be attacked by alcohols to deliver the corresponding acetals (Scheme 52).

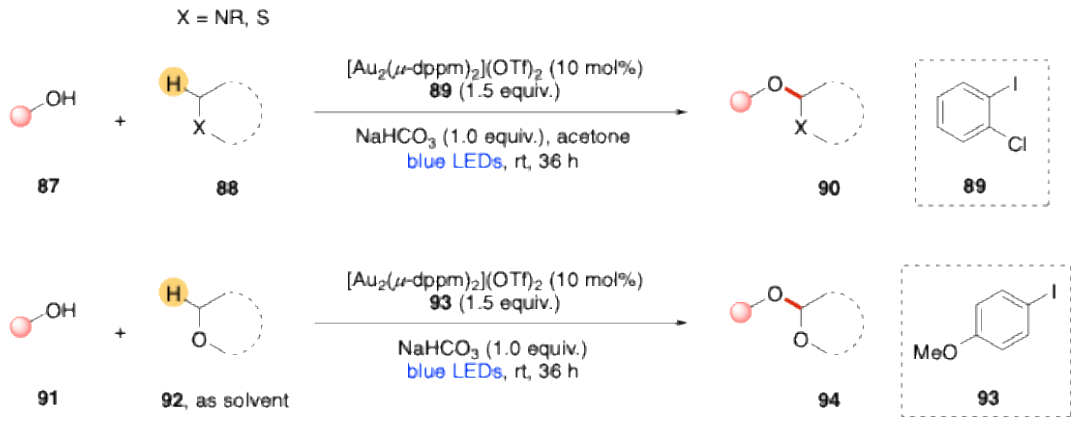

Scheme 52. Visible light-promoted α-C(sp^3)-H acetalization of saturated heterocycles *via* intermolecular HAT.

A visible light-induced intermolecular HAT approach has recently been used for C(sp^3)-H bond sulfurization.[98f] In this protocol, aryl iodide **97**, which is also used as the Hydrogen atom abstractor, is able to form an EDA complex **97A** with thiophenolate anion **96A** through halogen bonding interactions. Visible light irradiation causes a SET from EDA complex **97A**, generating an aryl radical and sulfur radical **96B**. The newly formed aryl radical plays the role of Hydrogen atom abstractor from an aliphatic C-H bond of substrate **95**, to form intermediate **95A**, which recombines with sulfur radical **96B**, allowing C(sp^3)-S bond formation.

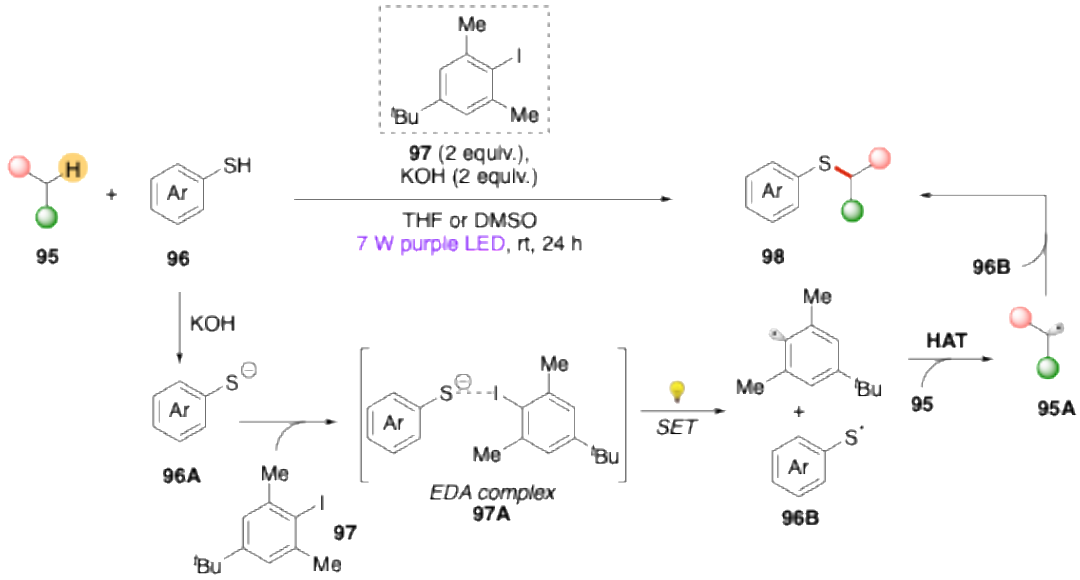

Scheme 53. Photocatalytic C(sp^3)–H sulfurization *via* intermolecular HAT.

Despite all the efforts that have been made in the last two decades to fill the gap between intramolecular and intermolecular HAT,[86] hitherto, none of the reported methodologies exploits the high reactivity of vinyl radicals as intermolecular Hydrogen abstractors.

3.2 Results and Discussion

To begin our journey, we decided to start our investigation by testing allenamide **99** - which we already employed in our previous work on intermolecular dearomatization of naphthalene[68] - as the Hydrogen abstractor precursor, and easily synthesized 2,2-diphenylethan-1-ol **100** as the Hydrogen donor. Alcohol substrate **100** has a very labile C(sp^3)-H bond (predicted BDE = 84.5 kcal/mol)[65b] in a di-benzylic position. We decided to employ our tailor-made Ir(III) complex (**PC5** as in Chapter II), and a binaphthyl (**N4** as in Chapter II) as this duo photosensitizer-co-catalyst proved to be extremely effective in increasing the reactivity of similar allenamides, and enhancing the rate of our previously reported intramolecular 1,5-HAT reaction for the synthesis of azetidines,[99] thanks to stabilizing radical-π LD interactions. Our ideal mechanism would have been the following: similarly to our previous work,[99] the photosensitization of allenamide **99**, in presence of **PC5** and **N4** would have brought to the formation of adduct **[99:N4]**. The first EnT event between photoexcited **^{3}PC5** and **N4**, would have brought to the formation of **[99:^{3}N4]**; the second intramolecular EnT process would have occurred between **^{3}N4** and **99**, delivering intermediate **[^{3}99A:N4]** with its other resonance form **[^{3}99B:N4]**. [**^{3}99A:N4]** has a reactive vinyl-radical site, and a secondary allylic C-radical one; [**^{3}99B:N4]** has a primary allylic C-radical site, and a reactive vinyl-radical one. Subsequently, an intermolecular HAT event with alcohol **100** would have occurred, delivering intermediate **100A**, which has a more stable tertiary di-benzylic radical site, and intermediates **^{3}[99C:N4]** or **^{3}[99D:N4]** - depending on which resonance form is involved in the HAT process - left with a secondary alkyl radical, and a primary alkyl radical site respectively. Eventually, radical recombination between radical intermediate **100A** and intermediate **^{3}[99C:N4]** and **^{3}[99D:N4]** would have afforded the desired products, **101** and **102**, respectively (Scheme 54).

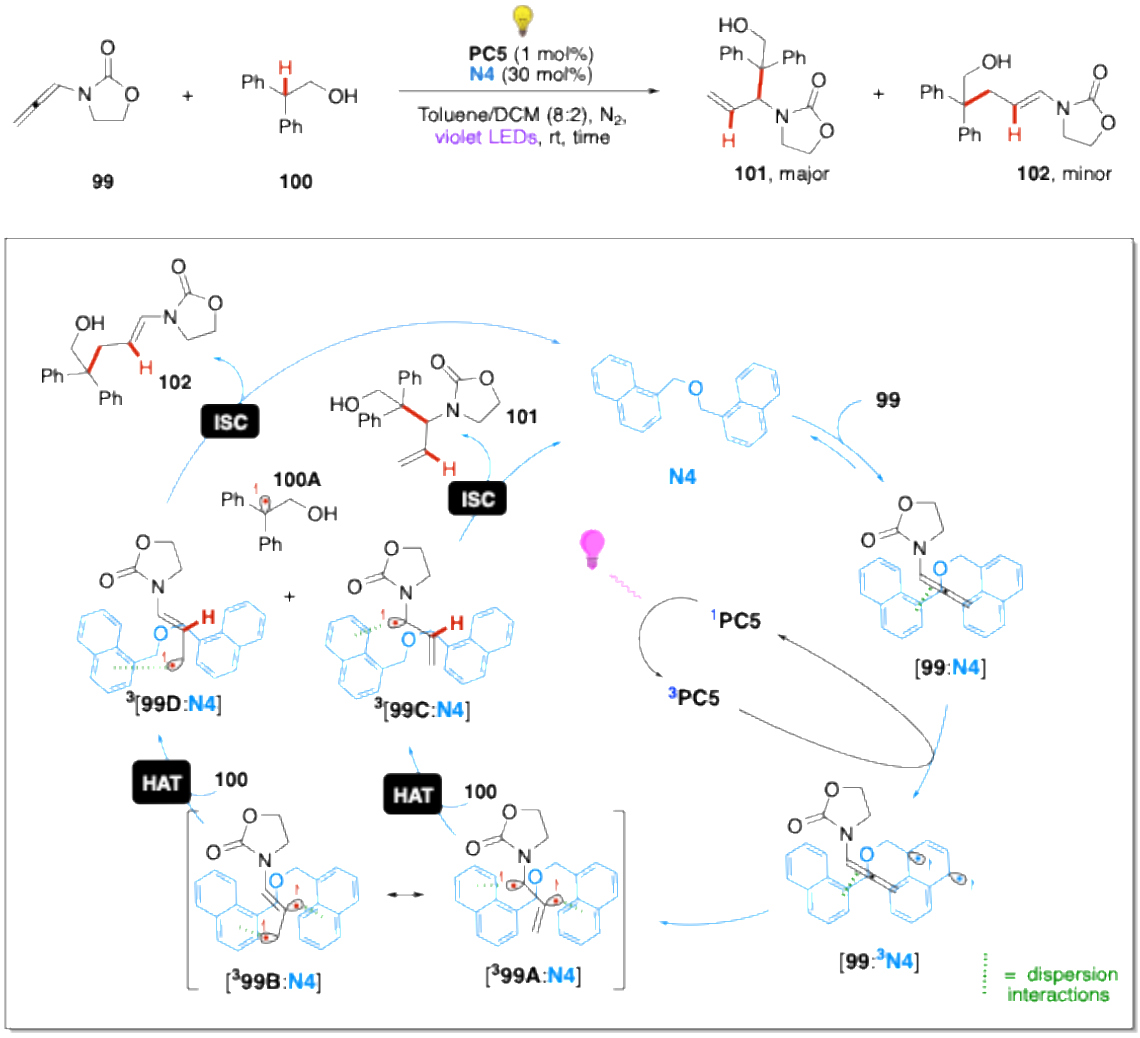

Scheme 54. Visible Light-promoted Direct C-H activation and C(sp^3)-C(sp^3) Bond Formation via Intermolecular Hydrogen Atom Transfer from Allenamides – expected mechanism.

We would have expected products **101** and **102** to form in different ratios, since intermediate **99D** is at a higher energy than intermediate **99C**, due to the minor stability of the primary alkyl radical site of **99D** compared to the secondary and in α-position to the Nitrogen alkyl radical site of **99C**. Thus, we would have expected product **101** to be the major product of our intermolecular HAT/radical recombination sequence.

With our great surprise, the photosensitization of allenamide **99**, in presence of **PC5** and **N4** afforded products **103** and **104** in 25% and 15% yield respectively, with full conversion of allenamide **99** after 72 hours of irradiation with violet LEDs (Scheme 55).

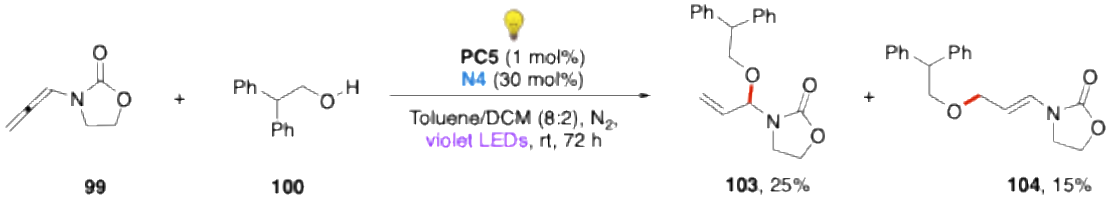

Scheme 55. Formation of unexpected ether products from photosensitization of an allenamide *via* HAT.

This was very surprising, as the exclusive presence of products **103** and **104** made us postulate that our photosensitized allenamide was capable of direct activation of unfunctionalized O-H bond, abstracting its Hydrogen despite its quite high BDE (predicted BDE = 103.1 kcal/mol),[65b] especially when compared to much labile C(sp^3)-H bonds available for HAT in the same molecule (Scheme 56).

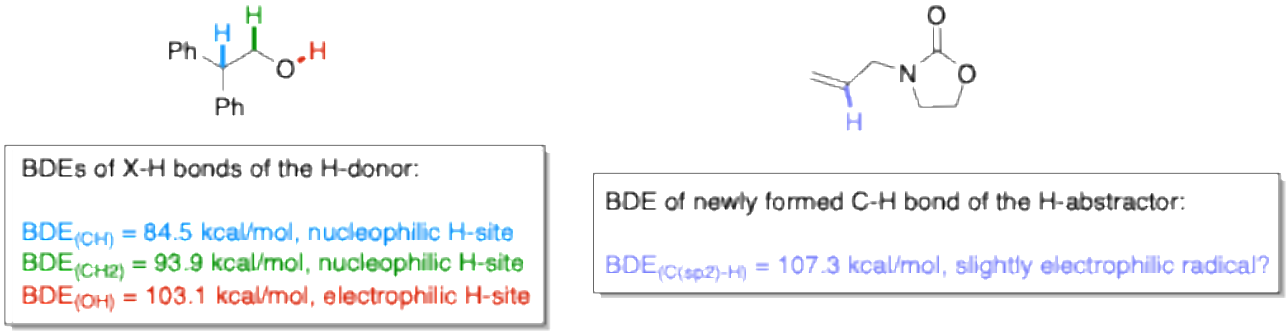

Scheme 56. Predicted BDEs for different C(sp^3)-H bonds and O-H bond of alcohol **100** and the newly formed C(sp^2)-H bond of **99**.

Indeed, generation of O-centered radicals through homolytic cleavage of unfunctionalized aliphatic O-H sites is intrinsically challenging due to their high Bond Dissociation free energies. Moreover, the ubiquitous presence of much weaker aliphatic C-H bonds in most of organic molecules, makes direct homolytic cleavage of O-H bonds extremely unlikely. To bypass those issues, several strategies based on indirect homolytic cleavage of pre-installed weak oxygen-heteroatom bonds were developed, such as peroxides,[100] nitrite esters,[101] hypohalites,[102] sulfenates,[103] and N-alkoxyphtalimides.[104] However, pre-functionalization of free alcohols comes with inevitable incorporation of additional chemo- and regioselective synthetic steps, loss of atom-economy and the use of often non-innocent thermolysis or UV photolysis techniques to cleave those O-X bonds. On the other hand, most of recent direct O-H activation approaches require the formation of an intermediate alkyliodo[105] or a metal-alkoxide species[106] to weaken the targeted O-H bond. From 2016, Knowles' group and Zhu's group developed several protocols based on proton-coupled

electron transfer (PCET),[107] as an alternative to classical HAT for direct O-H bond homolysis, where an oxidant catalyst/base pair serves together as a multisite formal H-atom acceptor. However, direct HAT from hydroxy group of alcohols remains elusive thus far. Indeed, the use of most common Hydrogen abstractors is precluded due to the very high BDEs of such O-H bonds ($BDE_{(O-H)} \approx 105$ kcal/mol), as well as for the electrophilic nature of mostly employed Hydrogen acceptors, which would bring to polarity-mismatched unfavored HAT from these protic O-H sites (Scheme 57).[107]

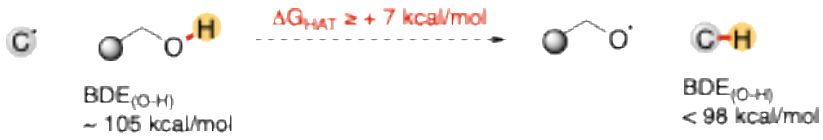

Scheme 57. Challenges of classical HAT from O-H sites.

Despite all, the chemoselectivity of our reaction, even if with low efficiency, seemed to be completely directed to the strongest – non-aromatic – (O-H) bond of the Hydrogen donor. Hereinafter some preliminary results on our visible light-promoted intermolecular Hydrogen Atom Transfer from allenamides, with new C(sp^3)-O bond formation are reported.

We doubted that our initially designed HAT reaction (Scheme 54) was so unfavored - for some unknown reason - that even an unfavored and low efficiency reactivity (Scheme 55) – at least at first glance - was possible. Indeed, HAT mostly depends on the BDE of the X-H bond of the abstraction site, but radical philicity also plays a key role in the rate and efficiency of this process.[1]

To understand something more about the mechanism of our reaction we started varying the nature of the Hydrogen abstractor and donor. We thus performed our reaction in the same conditions but employed malononitrile **105** as the hydrogen donor (Scheme 58), perhaps attributing the unfeasibility of our initially designed HAT to the nucleophilicity of the (C-)H-source of substrate **100**. Indeed, the C-radical originated from the HAT event on malononitrile **105** has an electrophilic nature - due to the presence of electron-withdrawing nitrile groups - but differently from alcohol **100**, **105** also has a labile C(sp^3)-H abstraction site (predicted $BDE_{(CH2)}$ = 87.9 kcal/mol),[65b] hoping that this could have had significantly increased the efficiency and rate of the HAT process. Photosensitization of allenamide **99** in presence of malononitrile **105** did not afford any of the desired product (Scheme 57).

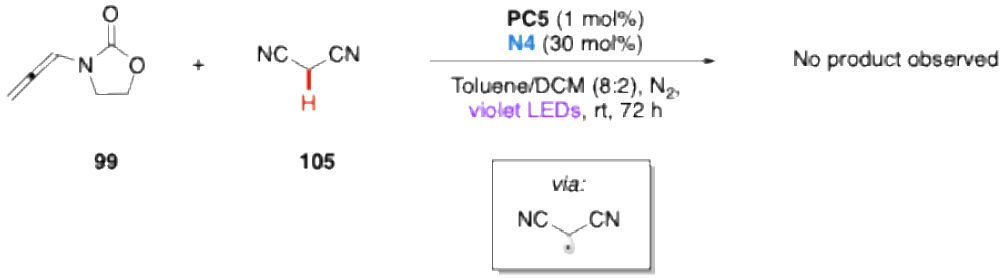

Scheme 58. Photosensitization of allene **99** in presence of malononitrile **105**.

We could also presume that, at an intermolecular level, the steric hindrance could play a major role on the success of our HAT event, thus, despite the low BDE of two C(sp^3)-H bonds in alcohol **100**, our desired HAT would still be unfavored due to destabilizing repulsive forces between our allenamide **99** and the phenyl rings of alcohol **100**. Thus, we evaluated the effect of the steric hindrance on the intermolecular HAT process. For this purpose, we decided to use a scaffold similar to that of alcohol **100**, but removing the -OH group to avoid reactivity toward that site, replacing it with an aldehyde, and reduce the steric hindrance around the putative hydrogen abstraction site, replacing one phenyl ring with a methyl group (Scheme 59). Photosensitization of allenamide **99** in presence of aldehyde **106** gave no results after 72 hours of irradiation with violet LEDs.

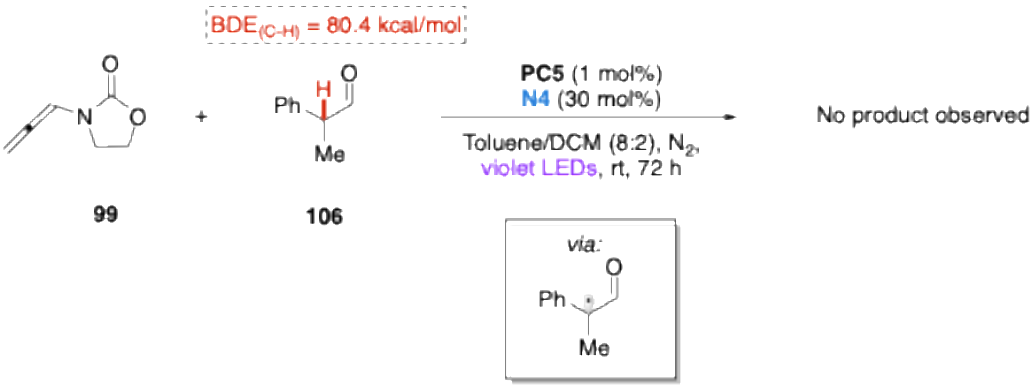

Scheme 59. Photosensitization of allene **99** in presence of aldehyde **106**.

At this point, we began to suspect that the presence of an -OH functionality on the hydrogen donor was crucial for the reactivity, as it could perhaps be involved in a hydrogen-bonding interaction with allenamide

99. This H-bonding could be facilitating the reaction mechanism by keeping the two HAT partners close to each other, giving a pseudo intramolecular HAT, or even by weakening the O-H bond of alcohol **100**, explaining why intrinsically weaker native C(sp^3)-H bonds of the hydrogen donor are unreactive in these conditions (Scheme 60).

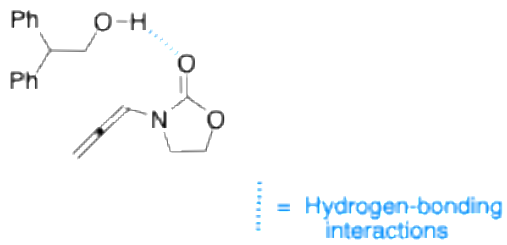

Scheme 60. Hydrogen bonding interaction between allenamide **99** and alcohol **100**.

MacMillan *et al*. already reported an example showing the power of H-bonding in a synthetic protocol based on a key HAT event.[109] In their work, an H-bonding catalyst, binding the hydroxyl group of an alcohol, is employed to achieve selective α-activation of alcohols' C-H bonds.

To support our hypothesis, we registered the IR spectra of a pure sample of allenamide **99**, a pure sample of alcohol **100**, and a mixture 1:1 of these two (Figure 12). In the IR spectrum of the mixture (**99** + **100**), we could clearly see a red shift (ca. 250 cm^{-1}) of the absorption band corresponding to the stretching of the O-H group of **100**. This could be an effect of a hydrogen-bonding interaction, as the O-H bond involved is weakened - resulting in a lower vibrational frequency – and with a distribution of bond strengths rather than a single frequency -resulting in a broad signal or band in the IR spectrum;[110] surprisingly, we didn't observe any significant variation in the stretching band of the C=O bond of the carbamate group of **99**. In addition to that, the band corresponding to the C-H stretching of the allene group in allenamide **99** completely disappears in the IR spectrum of the mixture **99** + **100** (for IR spectra, see the experimental section of this chapter), perhaps suggesting a strong interaction of this functionality with the -OH group of alcohol **100**.

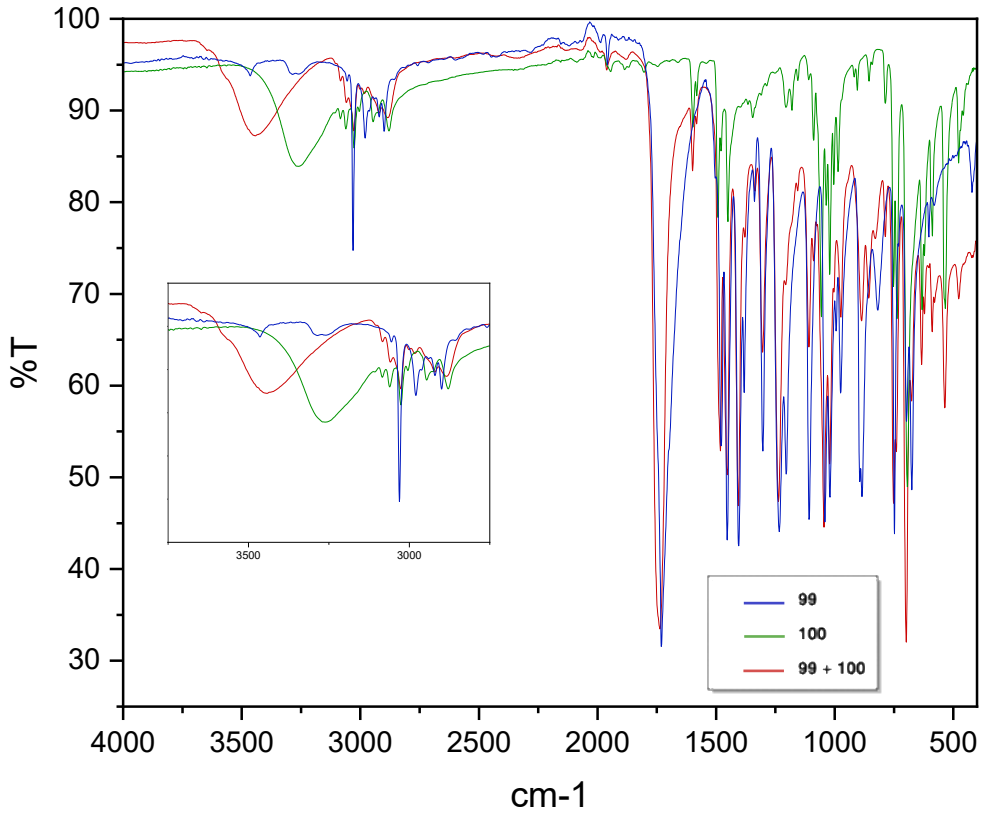

Figure 12. Layering of IR-spectra of allenamide **99** (blue line), alcohol **100** (green line) and a mixture 1:1 of **99** and **100** (red line).

We thus decided to test carboxylic acid **107**, as it should have still been able to form a H-bonding interaction, but the much higher BDE of its O-H bond (predicted $BDE_{(COO-H)}$ = 111.7 kcal/mol)[65b] should prevent HAT reactivity toward that -OH site (Scheme 61). Once again, photosensitization of allenamide **99** in presence of carboxylic acid **107** gave no results after 72 hours of irradiation with violet LEDs.

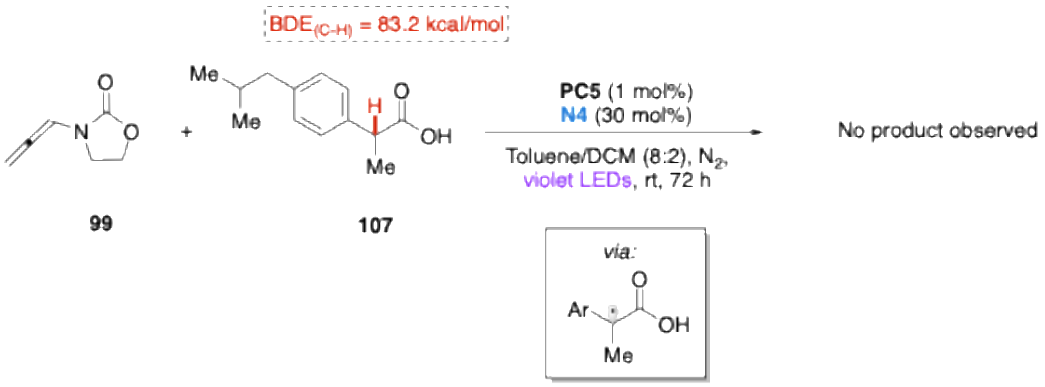

Scheme 10. Photosensitization of allenamide **99** in presence of carboxylic acid **107**.

If we tried to remove the carbamate group of allenamide **99**, by replacing it with an amido- group of substrate **108**, our reaction did not succeed (Scheme 62).

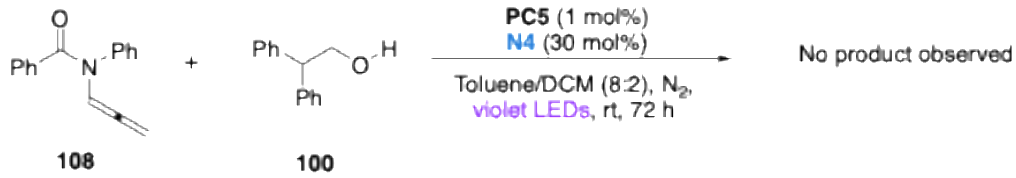

Scheme 62. Photosensitization of allenamide **108** in presence of alcohol **100**.

Protecting the -OH group of alcohol **100** by etherification also seemed to completely inhibit the reactivity (Scheme 63).

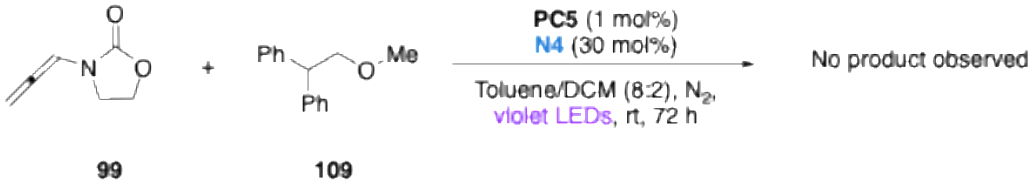

Scheme 63. Photosensitization of allenamide **99** in presence of ether **109**.

This made us realize that the reactivity we observed following the photosensitization of allenamide **99** in presence of alcohol **100** was a "privileged" pathway, as no other intermolecular HAT event took place with an even slight variation on the hydrogen donor/abstractor.

We then began our optimization study, aiming to find more suitable conditions to enhance efficiency and rate of our HAT/radical recombination sequence. Switching to a protic solvent, completely inhibited the reactivity (Table 2a, entry 2).

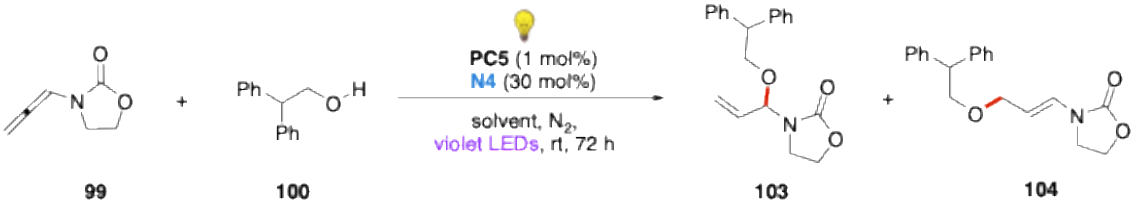

99 100 103 104

Entry	Solvent (0.1 M)	Conversion of **99** [%]	Yield of **103** [%]	Yield of **104** [%]
1	Toluene:DCM (8:2)	>99	25	15
2	MeOH	>99	0	0

Table 2a. Effect of solvent.

In our first attempt (Table 2a, entry 1), we noticed that a competitive side reaction was taking place: the intermolecular dearomatization reaction involving allenamide **99** and the naphthalene units of co-catalyst **N4**,[68] thus eroding the final yield of both products **103** and **104**. Thus, we decided to perform our reaction without **N4**. Indeed, we saw a slight increase of the overall yield (50% yield of products **103** + **104**), but a significant decrease of the reaction rate, with only 78% of conversion of allenamide **99** after 7 days of irradiation with violet LEDs (Table 2b, entry 3). Decreasing the loading of the co-catalyst from 30 to 10 mol% had a similar effect (entry 4).

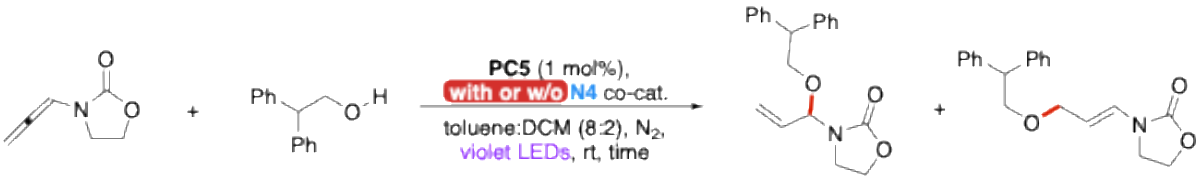

99 100 103 104

Entry	**N4** co-cat.	Time (h)	Conversion of **99** [%]	Yield of **103** [%]	Yield of **104** [%]
1	30 mol%	72	>99	25	15
3	--	168	78	40	10
4	10 mol%	144	73	34	18

Table 2b. Effect of additive **N4** and co-catalyst loading.

Employing 2 equiv. of alcohol **100**, did not prove beneficial, indeed a drop of efficiency and final yield was observed (Table 2c, entry 6). Increasing the concentration of the reaction mixture did not provide better

results (Table 2c, entry 7). A similar outcome was observed when **PC6** (see Chapter II) was tested as an alternative photosensitizer (Table 2c, entry 5).

99 **100** **103** **104**

Entry	**PC** cat.	**100** (equiv.)	Time (h)	Conversion of **99** [%]	Yield of **103** [%]	Yield of **104** [%]
5	**PC6**, Ir(d-F-ppy)$_3$	1.0	60	95	17	0
6	**PC5**, [Ir[dF(CF$_3$)ppy]$_2$(Me$_4$phen)]BF$_4$	2.0	72	91	6	0
7[a]	**PC5**, [Ir[dF(CF$_3$)ppy]$_2$(Me$_4$phen)]BF$_4$	1.0	60	>99	23	11

a) 0.3 M concentration.

Table 2c. Effect of a different Ir(III) photocatalyst, increased loading of **100**, and concentration.

Eventually, we tested several different bi-naphthyl co-catalyst, but unfortunately, none of them afforded better yields of products **103** and **104** (Table 2d, entries 9-11, for extended optimization study on co-catalysts see the experimental section of this chapter).

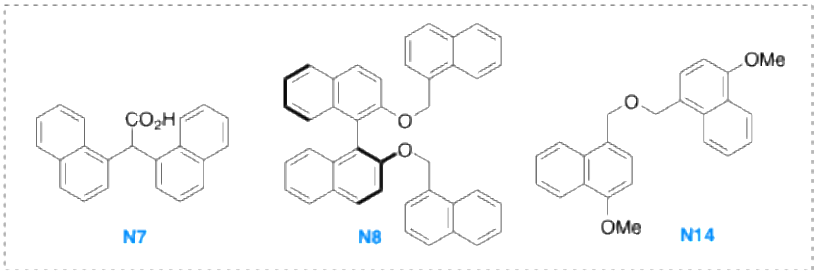

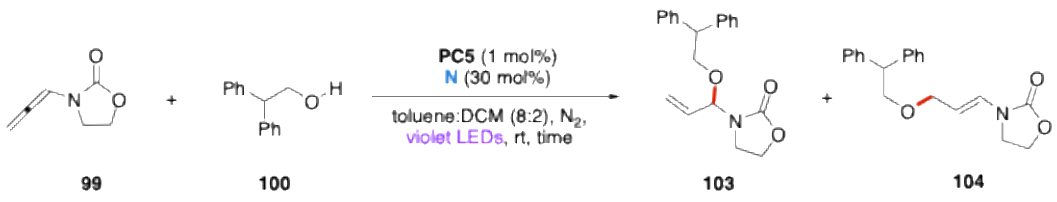

99 **100** **103** **104**

Entry	**N** co-cat. (30 mol%)	Time (h)	Conversion of **99** [%]	Yield of **103** [%]	Yield of **104** [%]
8	**N7**	84	>99	22	11
9	**N8**	84	30	0	0
10	**N14**	84	>99	33	0

Table 2d. Effect of different **N** co-catalysts.

Intrigued by this reactivity, we decided to test the homologous series of alcohol **100**, studying the effect of longer aliphatic C-chains. We thus tested alcohol **110** and **112**, as hydrogen donors. In these conditions, our reaction still proceeds, as we obtained products **111**, and **113**, in 20%, and 12% yield respectively (Scheme 64).

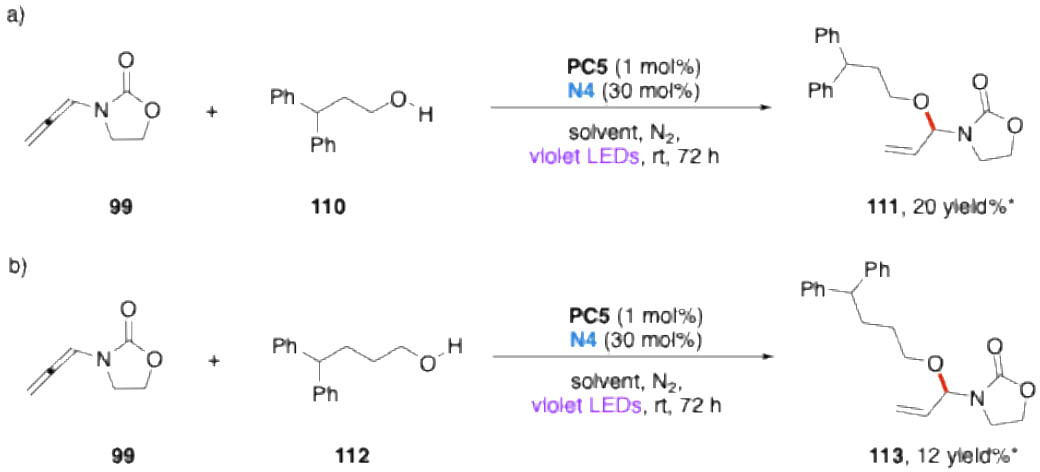

*) ^{1}H-NMR yield determined adding 2,2'-bipyridine as internal standard. In these conditions it was not possible to isolate pure products **111** and **113**.

Scheme 64. a) Photosensitization of allenamide **99** in presence of alcohol **110** and b) alcohol **112**.

Lastly, we wanted to preliminarily evaluate the possibility to discriminate between primary and secondary alcohols. We thus tested diols **114** and **119**, which have a primary and a secondary -OH site, and two secondary -OH sites, respectively. In these conditions, our reaction showed a selectivity towards primary -OH sites; indeed, we observed the formation of product **115** and **116** only, where the secondary -OH site is left untouched, while products **117** and **118** were not observed (Scheme 65a); with vicinal diol **119**, which only has secondary -OH sites, no product formation was observed (Scheme 65b).

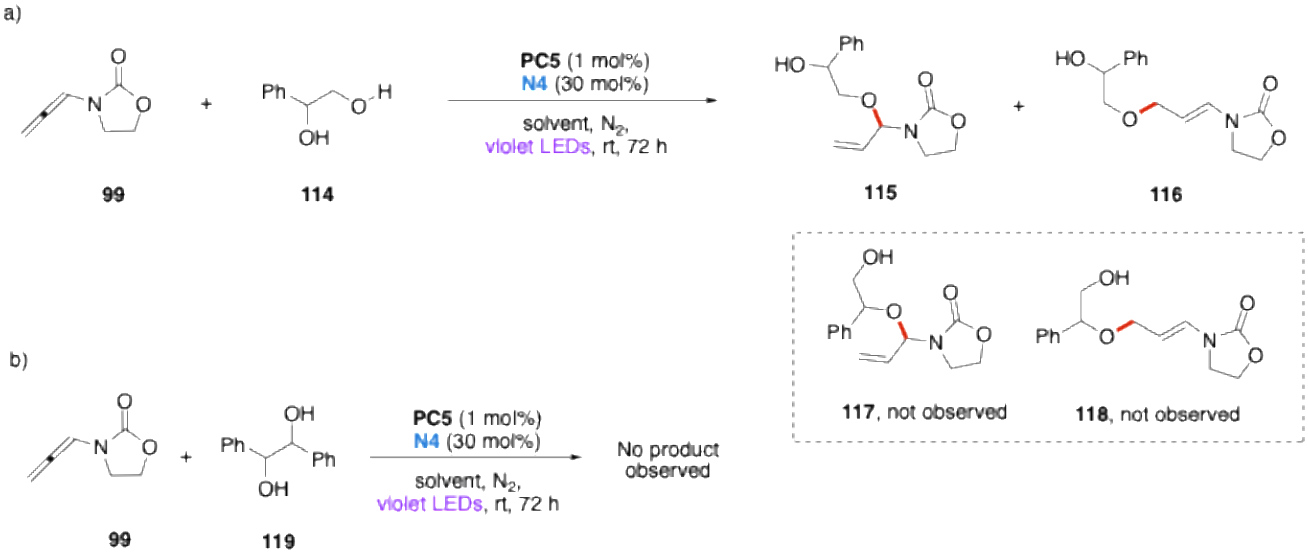

*) ^{1}H-NMR yield determined adding 2,2'-bipyridine as internal standard. In these conditions it was not possible to isolate pure products **115** and **116**.

Scheme 65. a) Photosensitization of allenamide **99** in presence of diol **114** and b) vicinal diol **119**.

3.3 Conclusions and Future perspectives

These preliminary results disclose an original intermolecular HAT reactivity from a typically inert unactivated -OH site. The reactive vinylic radical of the biradical species originated from the photosensitization of an allenamide could be the key to unlock the extremely challenging conventional direct HAT from aliphatic O-H bonds.

In the foreseeable future, studies on the mechanism of our reaction will have to be carried out, to better understand how our reaction works, and thus identify the main issues of this reactivity. Indeed, a mechanistic insight could really offer some hints to identify better conditions, allowing to enhance the reaction rate and achieve better yields of all products observed, as well as to develop a full scope for this intermolecular HAT/radical recombination sequence. For this purpose, Deuterium-labeling experiments could be very helpful in defining the exact mechanism, confirming or refuting our current hypothesis. Labeling the -OH site of alcohol **100**, could allow one to follow the Deuterium shifting; indeed, as the result of the intermolecular HAT event, the Deuterium will be located on the D-abstracting site – on the substituted C(sp^2) of the alkene in product **103**-*d*, and on the β-C(sp^2) of ether **104**-*d* (Scheme 66).

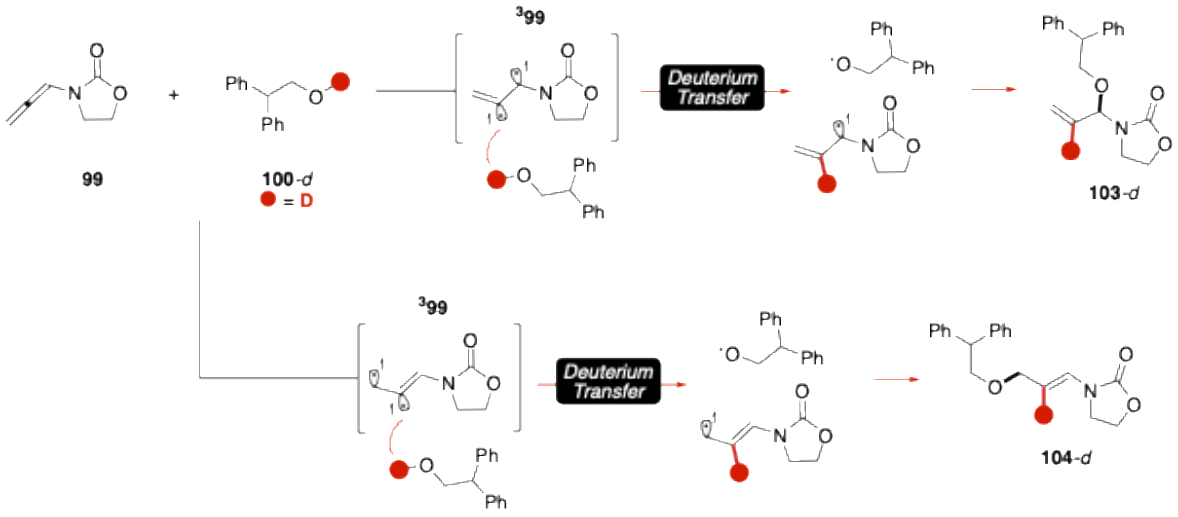

Scheme 66. Deuterium-labeling experiments – expected results.

The addition of good H-bond acceptors (*i.e.* tetra-*n*-butylammonium salts of phosphate, trifluoroacetate, diphenyl phosphate, *etc.*)[109] could also be evaluated, in order to confirm or refute our current hypothesis on the O-H bond weakening effect of H-bonding on the -OH abstraction site of alcohol **100**.

3.4 Experimental section

General remarks

All the chemicals whereby the syntheses are not reported here after were purchased from commercial sources and used as received. Solvents were dried passing through alumina columns using an Inert® system and were stored under nitrogen. Chromatographic purifications were performed under gradient using a Combiflash® system and prepacked disposable silica cartridges or through isocratic flash chromatography using commercial 60 Å silica gel. All reactions that required heating were performed with the use of high-vacuum grade silicon oil.

Present visible light promoted reactions required the use of degassed solvents as the presence of molecular oxygen exerts a negative effect on their rate. Reactions promoted by visible light were performed into standard 5 mm NMR tubes, which were placed inside a 500 mL glass beaker equipped with a commercial strip of 300 RGB household LEDs (12V, 14W) on its internal surface. The temperature of the tubes was checked with a thermometer. During warmer seasons, cooling was ensured by two fans recovered by outdated PCs to avoid overheating due to LEDs emission.

^{1}H and ^{13}C NMR spectra were recorded at 300 K on a Bruker 400 MHz or a Jeol 600 MHz spectrometers using residual non-deuterated solvents as internal standards (7.26 ppm for ^{1}H NMR and 77.00 ppm for ^{13}C-NMR for $CDCl_3$, 2.05 ppm for ^{1}H NMR and 29.84 ppm for ^{13}C NMR for acetone-d6). ^{19}F-NMR spectra were recorded in $CDCl_3$ at 298 K on a Jeol 600 spectrometer fitted with a BBFO probe head at 565 MHz. The terms m, s, d, t, q and quint represent multiplet, singlet, doublet, triplet, quadruplet and quintuplet respectively, and the term br and h mean respectively a broad signal and a heptuplet. Reported assignments were based on decoupling, COSY, NOESY, HSQC and HMBC correlation experiments.

Mass analyses were recorded on an Infusion Water Acquity Ultra Performance LC HO6UPS-823M instrument equipped with a SQ detector (Electrospray source); high-resolution mass analyses were recorded on a LTQ ORBITRAP XL Thermo Mass Spectrometer (Electrospray source).

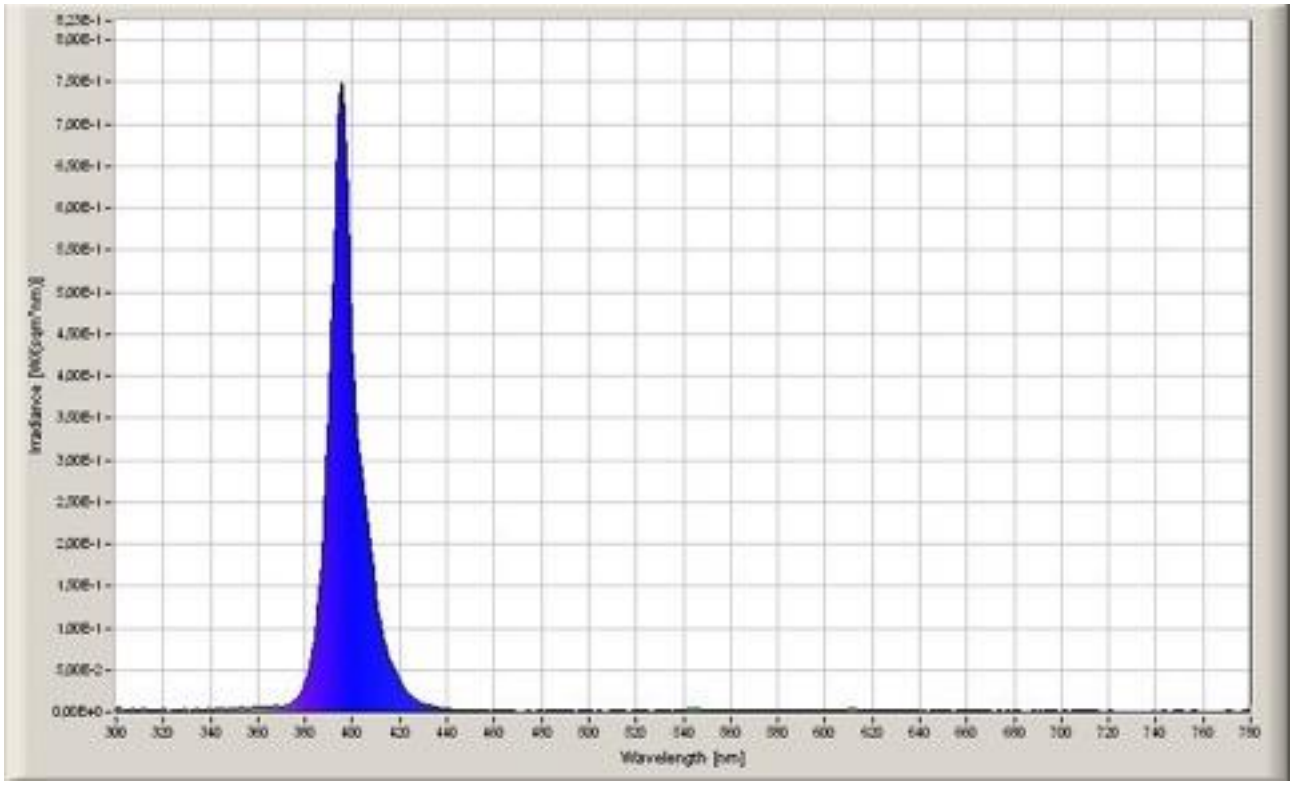

Measured emission spectrum of the purple LEDs used in this study.

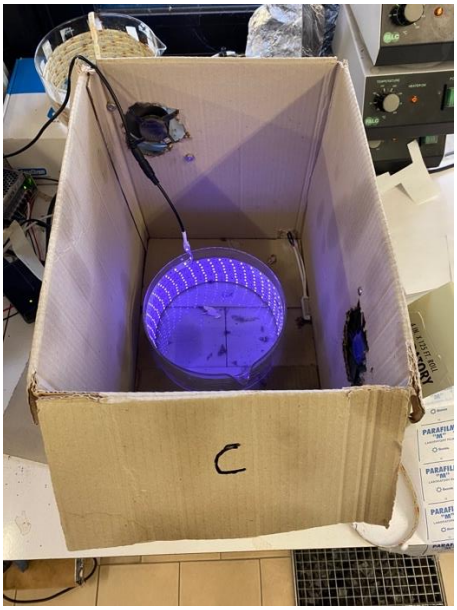

Representative setup using purple LEDs.

Synthesis of substrates and photocatalysts

3-(propa-1,2-dien-1-yl)oxazolidin-2-one (99)

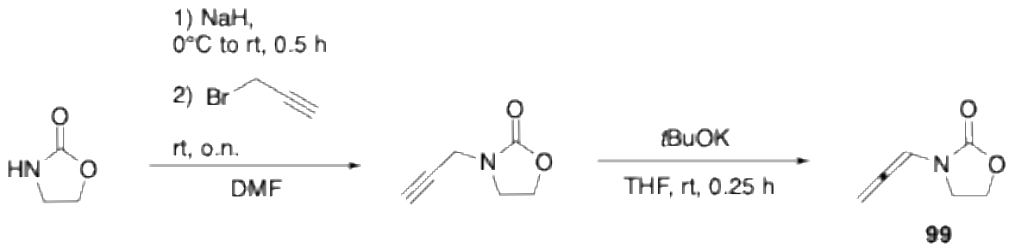

Step 1: To a solution of oxazolidin-2-one (1 equiv.) in DMF (0.6 M) at 0° C, NaH (60% in paraffine oil, 1.3 equiv.) was slowly added and the mixture was stirred for 0.5 h. Propargyl bromide (1.5 equiv.) was then slowly added, and the reaction was stirred at room temperature for 18 h. After complete conversion as monitored by TLC, the mixture was quenched with a saturated NH_4Cl solution and extracted with EtOAc (3 times). The combined organic layers were washed with brine (3 times), dried over Na_2SO_4 and concentrated under reduced pressure. The crude was purified by chromatography on silica gel (*n*-hexane/EtOAc gradient) to afford the desired product 3-(prop-2-yn-1-yl)oxazolidin-2-one (77% yield). *Data consistent with literature* (*Eur. J. Org. Chem.,* **2023**, 26, e202300135).

Step 2: 3-(prop-2-yn-1-yl)oxazolidin-2-one (1 equiv.) and THF (0.20 M) were sequentially added to a Schlenk tube equipped with a magnetic stirring bar. *t*BuOK (0.2 equiv.) was added and the resulting mixture was stirred at room temperature for 15 minutes. After complete conversion as monitored by TLC, 5 ml of a saturated NH_4Cl solution were added. The mixture was extracted with EtOAc (3 x 15 ml), the organic layers separated and dried over Na_2SO_4. The solution was concentrated under reduced pressure and the crude purified by chromatography on silica gel (*n*-hexane/EtOAc gradient) to afford the corresponding allene 3-(propa-1,2-dien-1-yl)oxazolidin-2-one (**99**), as a white solid (61% yield).

^{1}H NMR (400 MHz, $CDCl_3$) δ 6.86 (t, *J* = 6.4 Hz, 1H), 5.42 (d, *J* = 6.3 Hz, 2H), 4.45 – 4.37 (m, 2H), 3.63 – 3.56 (m, 2H). **^{13}C NMR** (101 MHz, $CDCl_3$) δ 201.4, 155.3, 97.0, 87.9, 62.3, 43.1. **ESI-MS** calcd for $C_6H_7NNaO_2$ $[M+Na]^+$, 148.04 found 148.16.

***N*-phenyl-*N*-(propa-1,2-dien-1-yl)benzamide (108)**

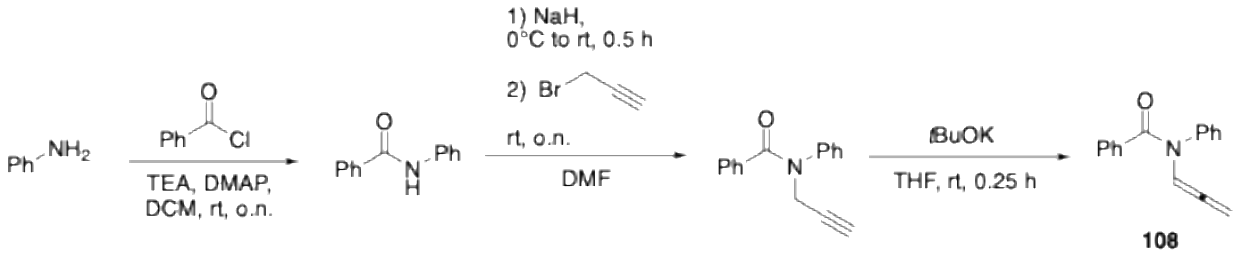

Step 1: In a round bottom flask equipped with a magnetic stirring bar, aniline (1 equiv.), DMAP (0.02 equiv.) and TEA (1 equiv.) were dissolved in DCM (0.25 M). The solution was cooled to 0 °C and benzoyl chloride (1 equiv.) was then added. The mixture was stirred at room temperature until completion, monitoring the process by TLC. The solution was then quenched with saturated NH_4Cl solution and diluted with DCM. The organic phase was then washed with brine, dried over Na_2SO_4 and concentrated under reduced pressure. The crude was finally purified by chromatography on silica gel (*n*-hexane/EtOAc gradient) to afford *N*-phenylbenzamide (99% yield). *Data consistent with literature* (*Tetrahedron Chem*., **2023**, 8, 100053).

Step 2: To a solution of *N*-phenylbenzamide (1 equiv.) in DMF (0.6 M) at 0° C, NaH (60% in paraffine oil, 1.3 equiv.) was slowly added and the mixture was stirred for 0.5 h. Propargyl bromide (1.5 equiv.) was then slowly added, and the reaction was stirred at room temperature for 18 h. After complete conversion as monitored by TLC, the mixture was quenched with a saturated NH_4Cl solution and extracted with EtOAc (3 times). The combined organic layers were washed with brine (3 times), dried over Na_2SO_4 and concentrated under reduced pressure. The crude was purified by chromatography on silica gel (*n*-hexane/EtOAc gradient) to afford *N*-phenyl-*N*-(prop-2-yn-1-yl)benzamide (99% yield). *Data consistent with literature* (Synthesis, **2023**, 55 (2), 315-332).

Step 3: *N*-phenyl-*N*-(prop-2-yn-1-yl)benzamide (1 equiv.) and THF (0.20 M) were sequentially added to a Schlenk tube equipped with a magnetic stirring bar. *t*BuOK (0.2 equiv.) was added and the resulting mixture was stirred at room temperature for 15 minutes. After complete conversion as monitored by TLC, 5 ml of a saturated NH_4Cl solution were added. The mixture was extracted with EtOAc (3 x 15 ml), the organic layers separated and dried over Na_2SO_4. The solution was concentrated under reduced pressure and the crude purified by chromatography on silica gel (*n*-hexane/EtOAc gradient) to afford the

corresponding allene *N*-phenyl-*N*-(propa-1,2-dien-1-yl)benzamide (**108**), as a pale orange solid (70% yield).

^{1}H NMR (400 MHz, $CDCl_3$) δ 7.68 (t, *J* = 6.4 Hz, 1H), 7.44 – 7.32 (m, 2H), 7.38 – 7.10 (m, 6H), 7.11 (dd, *J* = 7.4, 1.8 Hz, 2H), 5.10 (d, *J* = 6.3 Hz, 2H). **^{13}C NMR** (101 MHz, $CDCl_3$) δ 202.7, 168.5, 140.3, 135.1, 130.0, 128.85, 128.82, 128.5, 127.8, 127.5, 102.0, 86.8. **ESI-MS** calcd for $C_{16}H_{14}NO$ $[M+H]^+$ 236.11, found 236.23.

2,2-diphenylethan-1-ol (100)

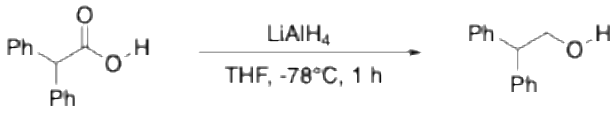

100

Dihenylacetic acid (1 equiv.) was dissolved in THF (0.2 M), and the solution was added dropwise to a solution of $LiAlH_4$ (3 equiv.) in THF (1 M), under nitrogen atmosphere at -78 °C. The reaction was stirred at the same temperature for 1 hour, then allowed to warm to room temperature and quenched by the addition of a saturated aqueous solution of sodium/potassium tartrate. The mixture was extracted with EtOAc (3x20 mL), and the combined organic layers were washed with brine, dried over sodium sulfate, and concentrated under reduced pressure. The crude was purified by chromatography on silica gel (*n*-hexane/EtOAc 4:1), affording 2,2-diphenylethan-1-ol (**100**), as a white solid (99% yield).

^{1}H NMR (400 MHz, $CDCl_3$) δ 7.37 – 7.20 (m, 10H), 4.25 – 4.20 (m, 1H), 4.20 – 4.15 (m, 2H), 1.48 (t, *J* = 6.1 Hz, 1H). *Data consistent with literature* (*The Journal of Organic Chemistry*, **2012**, *77* (16), 7071-7075).

(2-methoxyethane-1,1-diyl)dibenzene (109)

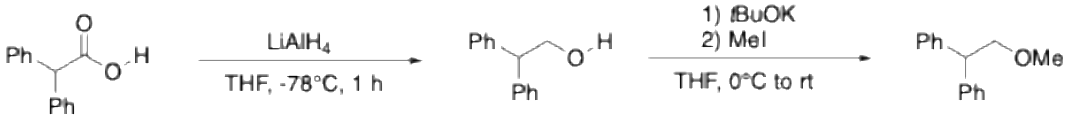

109

2,2-diphenylethan-1-ol (**100**) (1 equiv.) was dissolved in THF (0.5 M) and *t*BuOK (2 equiv.) was added at 0 °C. The reaction mixture stirred at room temperature for 5 mins and MeI (2 equiv.) was added dropwise at 0 °C. The reaction was stirred at room temperature for 2 hours. After complete conversion as monitored

by TLC, 5 ml of a saturated NH_4Cl solution were added. The mixture was extracted with EtOAc (3 x 15 ml), the organic layers separated and dried over Na_2SO_4. The solution was concentrated under reduced pressure and the crude purified by chromatography on silica gel (*n*-hexane/EtOAc gradient) to afford the corresponding ether (2-methoxyethane-1,1-diyl)dibenzene **(109)**, as a colorless oil (70% yield).

^{1}H NMR (400 MHz, $CDCl_3$) δ 7.34 – 7.17 (m, 11H), 4.29 (t, *J* = 7.3 Hz, 1H), 3.93 (d, *J* = 7.3 Hz, 2H), 3.38 (s, 3H). *Data consistent with literature* (*Angew. Chem. Int. Ed.* **2017**, *56*, 1120).

3,3-diphenylpropan-1-ol (110)

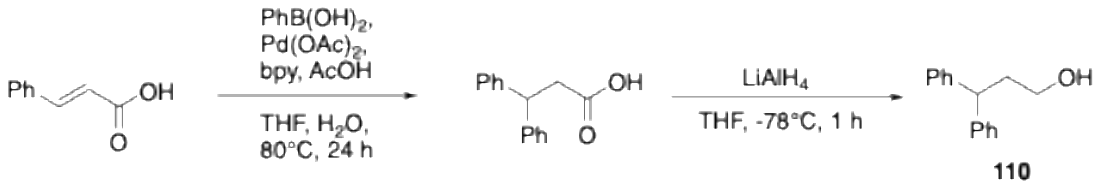

110

Step 1: To a Schlenk tube phenylboronic acid (2 equiv.), cinnamic acid (1 equiv.), $Pd(OAc)_2$ (5 mol%), bpy (0.1 equiv.), HOAc (1.0 mL/mmol), THF (2.0 mL/mmol), and H_2O (0.6 mL/mmol) were added, under air atmosphere. The mixture was stirred and heated at 80 °C for 24 hours, until the substrate disappeared as monitored by TLC. The solution was transferred into a flask, and the solvent was removed under vacuum. 5 mL of water was added to the crude product, the mixture was heated to 60 °C for 5 min with stirring, and then water was removed by filtration. This process was repeated, and then the product was dissolved in 10 mL of $CHCl_3$, dried with Na_2SO_4, filtered, and concentrated under vacuum. The crude product was used without further purification in step 2.

Step 2: crude product obtained in step 1 was dissolved in THF (0.2 M), and the solution was added dropwise to a solution of $LiAlH_4$ (3 equiv.) in THF (1 M), under nitrogen atmosphere at -78 °C. The reaction was stirred at the same temperature for 1 hour, then allowed to warm to room temperature and quenched by the addition of a saturated aqueous solution of sodium/potassium tartrate. The mixture was extracted with EtOAc (3x20 mL), and the combined organic layers were washed with brine, dried over sodium sulfate, and concentrated under reduced pressure. The crude was purified by chromatography on silica gel (*n*-hexane/EtOAc 4:1), affording 3,3-diphenylpropan-1-ol (**110**), as a colorless oil (87% yield over 2 steps).

^{1}H NMR (600 MHz, $CDCl_3$) δ 7.31 – 7.25 (m, 8H), 7.21 – 7.17 (m, 2H), 4.14 (t, *J* = 7.9 Hz, 1H), 3.62 (t, *J* = 6.4 Hz, 2H), 2.33 (dt, *J* = 7.8, 6.5 Hz, 2H). *Data consistent with literature* (Angew. Chem. Int. Ed., **2014**, 53, 6546-6549).

4,4-diphenylbutan-1-ol (112)

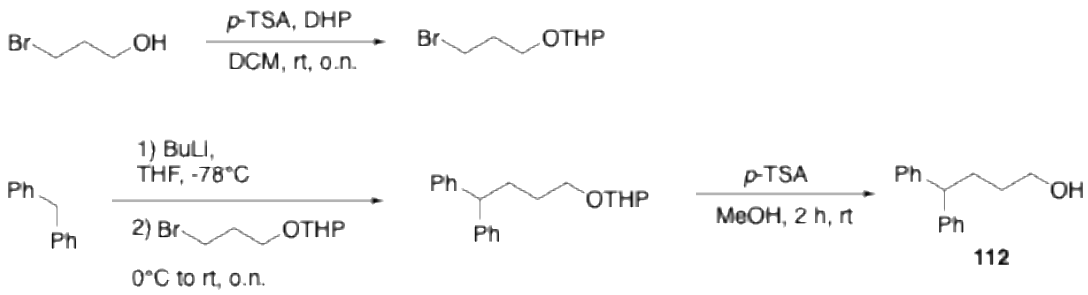

Step 1: In a round bottom flask, a solution of 3-bromopropanol (1 equiv.) and 3,4-dihydro-2*H*-pyran (1.5 equiv.) in dichloromethane (0.5 M) containing *p*-toluenesulfonic acid mono hydrate (0.1 equiv.) was stirred overnight at room temperature. The solution was diluted with *n*-hexane and washed with H_2O. The aqueous layer was extracted with n-hexane (2 x 50 mL). Combined organic layers were dried with anhydrous Na_2SO_4, filtered, and concentrated under reduced pressure. The crude product was used without further purification in step 2.

Step 2: diphenylmethane (1 equiv.) was dissolved in dry THF (0.3 M) in a Schlenk, under nitrogen atmosphere. *n*-BuLi (2.0 equiv.) was slowly added at -78 °C, and the reaction was allowed to stir for 1 hour at 0 °C. Crude product (1.3 equiv.) obtained in step 1 was slowly added, and the reaction was stirred overnight at room temperature. After complete conversion as monitored by TLC, 5 ml of a saturated NH_4Cl solution were added. The mixture was extracted with EtOAc (3 x 15 ml), the organic layers separated and dried over Na_2SO_4. The crude product was used without further purification in step 3.

Step 3: crude product obtained in step 2 was dissolved in MeOH (0.2 M) under nitrogen atmosphere, and *p*-toluenesulfonic acid mono hydrate (0.1 equiv.) was added. The reaction was stirred at room temperature for 2 hours. After complete conversion as monitored by TLC, the solvent was removed under reduced pressure and the residue was suspended in H_2O. The resulting suspension was extracted with EtOAc (3 times), washed with brine, dried over Na_2SO_4, filtered, and concentrated under reduced pressure. The

crude product was purified by chromatography on silica gel (*n*-hexane/EtOAc gradient) to afford the corresponding 3,3-diphenylpropan-1-ol (**110**), as a colorless oil (25% yield over 3 steps).

^{1}H NMR (600 MHz, $CDCl_3$) δ 7.29 – 7.23 (m, 9H), 7.19 – 7.15 (m, 2H), 3.91 (t, *J* = 7.9 Hz, 1H), 3.66 (t, *J* = 6.5 Hz, 2H), 2.13 (q, *J* = 7.9 Hz, 2H), 1.55 (dt, *J* = 14.3, 6.6 Hz, 2H). *Data consistent with literature* (*Angew. Chem. Int. Ed.* **2016**, *55*, 6315).

Synthesis of N derivatives

2,2-di(naphthalen-1-yl)acetic acid (N7)

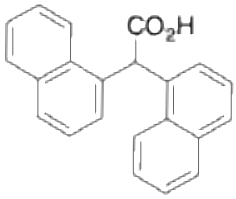

N7 was synthesized following a reported literature procedure (*Chem. Eur. J.* **2025**, 31, e202403309). From 1-bromo-methyl-naphthalene, over 3 steps, **N7** was recovered as a white solid (30% yield for the third step from di(naphthalen-1-yl)methane).

^{1}H NMR (400 MHz, $CDCl_3$) δ 12.64 (brs, 1H) 8.01 – 7.93 (m, 2H), 7.91 (dd, *J* = 7.4, 2.0 Hz, 2H), 7.83 (d, *J* = 8.1 Hz, 2H), 7.56 – 7.44 (m, 4H), 7.40 (t, *J* = 7.7 Hz, 2H), 7.33 (dd, *J* = 7.2, 1.2 Hz, 2H), 6.55 (s, 1H). *Data consistent with literature.*

(*S*)-2,2'-bis(naphthalen-1-ylmeth oxy)-1,1'-binaphthalene (N8)

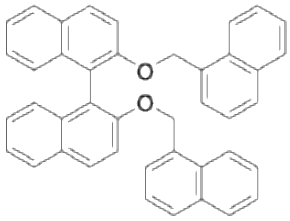

N8 was synthesized following a reported literature procedure (*Chem. Eur. J.* **2024**, 30, e202304010). From L-BINOL, **N8** was recovered as a white solid (48% yield).

^{1}HNMR (400 MHz, $CDCl_3$) δ 7.92 (d, *J* = 9.0 Hz, 2H), 7.87 (d, *J* = 8.2 Hz, 2H), 7.77–7.72 (m, 2H), 7.61 (d, *J* = 8.1 Hz, 2H), 7.50 (d, *J* = 8.5 Hz, 2H), 7.45 (d, *J* = 9.0 Hz, 2H), 7.39–7.30 (m, 4H), 7.21 (d, *J* = 3.9 Hz, 4H), 7.12 (ddd, *J* = 8.3, 6.9, 1.3 Hz, 4H), 7.08–7.00 (m, 2H), 5.58–5.12 (m, 4H). *Data consistent with literature.*

4,4'-(oxybis(methylene))bis(1-methoxynaphthalene) (N14)

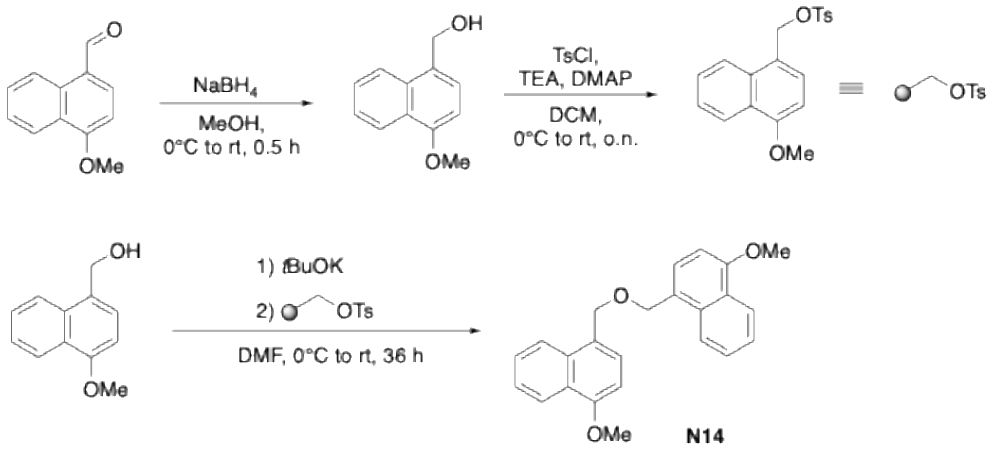

Step 1: 4-Methoxy-1-naphthaldehyde (1 equiv.) was dissolved in MeOH (0.2 M). $NaBH_4$ (2.5 equiv.) was added at 0 °C, and the reaction was stirred at room temperature for 30 minutes. After complete conversion as monitored by TLC, the solvent was removed under reduced pressure and the residue was suspended in H_2O. The resulting suspension was extracted with EtOAc (3 times), washed with brine, dried over Na_2SO_4, filtered, and concentrated under reduced pressure. The crude product was used without further purification in step 2.

Step 2: the crude product obtained in step 1, DMAP (0.02 equiv.) and TEA (1 equiv.) were dissolved in dry DCM (0.25 M) **i**n a round bottom flask equipped with a magnetic stirring bar. The solution was cooled to 0 °C and tosyl chloride (1 equiv.) was then added. The mixture was stirred at room temperature until completion, monitoring the process by TLC. The solution was then quenched with saturated NH_4Cl solution and diluted with DCM. The organic phase was then washed with brine, dried over Na_2SO_4 and concentrated under reduced pressure. The crude product was used without further purification in step 3.

Step 3: the crude product obtained in step 1 was dissolved in dry DMF (0.6 M). *t*BuOK (1.5 equiv.) was slowly added at 0 °C, and the mixture was stirred at room temperature for 0.5 h. Crude product obtained in step 2 (1.5 equiv.) was then slowly added, and the reaction was stirred at room temperature for 36 h. After complete conversion as monitored by TLC, the mixture was quenched with a saturated NH_4Cl solution and extracted with EtOAc (3 times). The combined organic layers were washed with brine (3 times), dried over Na_2SO_4 and concentrated under reduced pressure. The crude was purified by

chromatography on silica gel (*n*-hexane/EtOAc gradient) to afford 4,4'-(oxybis(methylene))bis(1-methoxynaphthalene) (**N14**), as a white crystalline solid (50% yield for step 3).

^{1}H NMR (600 MHz, $CDCl_3$) δ 8.37 – 8.33 (m, 1H), 8.11 – 8.07 (m, 1H), 7.51 (dtd, *J* = 13.4, 6.8, 3.3 Hz, 2H), 7.43 (d, *J* = 7.8 Hz, 1H), 6.77 (d, *J* = 7.8 Hz, 1H), 4.97 (s, 2H), 4.02 (s, 3H). **^{13}C NMR** (151 MHz, $CDCl_3$) δ 155.94, 133.07, 127.60, 126.75, 126.08, 126.03, 125.25, 124.41, 122.45, 102.89, 70.46, 55.59. **ESI-MS** calcd for $C_{24}H_{23}O_3$ $[M+H]^+$ 359.16, found 359.23.

(4*R*,5*R*)-4,5-bis(methoxydi(naphthalen-1-yl)methyl)-2,2-dimethyl-1,3-dioxolane (N15)

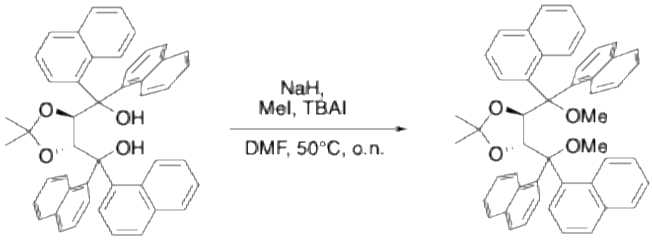

N15

To a solution of TADDOL (1 equiv.) and TBAI (1 mol%) in DMF (0.2 M) at 0 °C, NaH (3 equiv.) was added, and the mixture was stirred for 20 min at room temperature. Then iodomethane (4 equiv.) was added dropwise at 0 °C, and the reaction was heated to 50 °C until complete consumption of the starting material (monitored by TLC). The reaction was quenched with water, extracted with EtOAc (3 times), and the organic layers were washed with brine (20 mL x 2) and dried over Na_2SO_4. The crude was purified by chromatography on silica gel (*n-h*exane:EtOAc 8:1), affording (4*R*,5*R*)-4,5-bis(methoxydi(naphthalen-1-yl)methyl)-2,2-dimethyl-1,3-dioxolane (**N15**) as a white solid (94% yield).

^{1}H NMR (400 MHz, $CDCl_3$) δ 8.78 (d, *J* = 6.1 Hz, 2H), 8.26 (d, *J* = 6.5 Hz, 2H), 8.08 (d, *J* = 8.7 Hz, 2H), 7.92 (dd, *J* = 8.1, 4.7 Hz, 4H), 7.84 – 7.75 (m, 4H), 7.69 – 7.62 (m, 4H), 7.46 (d, *J* = 9.0 Hz, 2H), 7.23 (t, *J* = 7.5 Hz, 2H), 7.09 (t, *J* = 6.9 Hz, 2H), 6.98 (t, *J* = 8.6 Hz, 2H), 6.75 – 6.62 (m, 2H), 5.88 (s, 2H), 3.43 (s, 6H), -0.12 (s, 6H). **^{13}C NMR** (101 MHz, $CDCl_3$) δ 140.7 (2C), 138.9 (2C), 134.2 (2C), 134.1 (2C), 133.7 (2C), 132.7 (2C), 129.5 (2C), 129.2 (2C), 128.7 (2C), 128.5 (2C), 127.9 (2C), 127.5 (2C), 126.7 (2C), 125.7 (2C), 125.4 (2C), 125.4 (2C), 125.0 (2C), 124.5 (2C), 124.4 (2C), 123.8 (2C), 110.6, 84.6 (2C), 78.4 (2C), 53.1 (2C), 27.0 (2C). **ESI-MS** calcd for $C_{49}H_{43}O_4$ $[M+H]^+$ 695.87, found 695.89.

1,2-bis(naphthalen-1-ylmethoxy)ethane (N17)

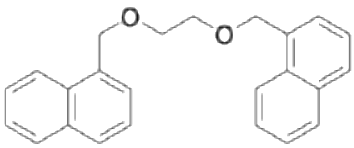

In a Schlenk, ethylene glycole (1 equiv.) and a catalytic amount of TBAI were dissolved in THF (0.5 M). The resulting solution was cooled to 0 °C and NaH (3 equiv.) was added portion wise. After 30 min, a solution of 1-chloromethyl naphthalene (3 equiv.) in THF (1.5 M) was added dropwise. The solution was stirred at room temperature for 30 hours, then the solvent removed under reduce pressure. The residue was suspended in water and was extracted with EtOAc (15 mLx3), the organic phase was dried with Na_2SO_4, and the solvent was removed under reduced pressure. The solid residue was purified by chromatography on silica gel (*n*-hexane:EtOAc) to afford 1,2-bis(naphthalen-1-ylmethoxy)ethane **N17** as a colorless oil (602 mg, 1.67 mmol, 88% yield). **^{1}H NMR**(600 MHz, $CDCl_3$) δ 1H NMR (400 MHz, $CDCl_3$) δ 8.36 (d, J = 8.4 Hz, 2H), 8.00 (dd, J = 24.0, 7.3 Hz, 4H), 7.70–7.64 (m, 6H), 7.59 (t, J = 7.6 Hz, 2H), 5.16 (s, 4H), 3.87 (s, 4H).**^{13}C NMR**(151 MHz, $CDCl_3$) δ 134.1 (2C), 134.1 (2C), 132.1 (2C), 128.8 (4C), 126.7 (2C), 126.5 (2C), 126.0 (2C), 125.5 (2C), 124.5 (2C), 72.0 (2C), 69.9 (2C). **ESI–MS** calcd for $C_{24}H_{23}O_2^+$ $[M + H]^+$ 343.17, found 343.27.

Synthesis of PC5

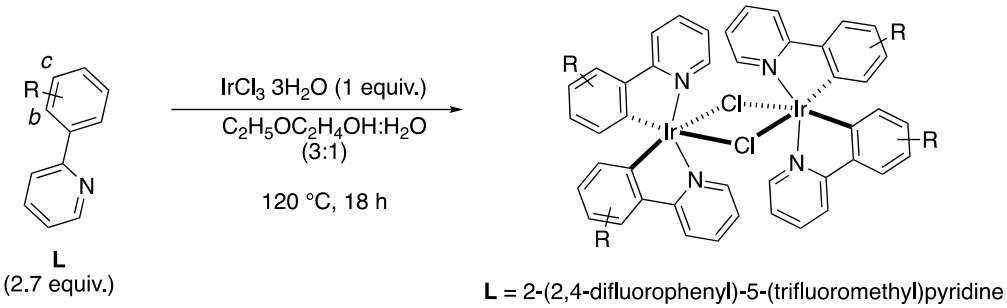

The Iridium dimer was synthetized adapting a literature procedure by Sun (*RSC Adv.* ***2016****, 6, 41214*). Iridium (III) chloride hydrate (200 mg, 0.63 mmol, 1 equiv.) and **L** (334 mg, 1.30 mmol, 2.05 equiv.) were placed in a sealed Schlenk, equipped with a stirring bar, under a nitrogen atmosphere. A degassed 2:1 solution of 2-ethoxyethanol and water (12 mL) was added, the mixture was stirred at 120 °C for 48 h and then cooled to room temperature. Water was added (10 mL) and the resulting mixture stirred for 0.5 h. The resulting yellow precipitate was filtered under vacuum, washed with water and hexane, and finally dried under reduced pressure affording the pure dimer as a yellow solid (341 mg, 0.23 mmol, 72% yield), which was used without further purification.

^{1}H NMR (600 MHz, $CDCl_3$) δ 9.51 (s, 4H), 8.46 (dd, *J* = 8.7, 2.9 Hz, 4H), 8.04 (dd, *J* = 8.7, 2.2 Hz, 4H), 6.43 (ddd, *J* = 12.4, 8.8, 2.3 Hz, 4H), 5.07 (dd, *J* = 8.8, 2.3 Hz, 4H). *Data consistent with the literature.*

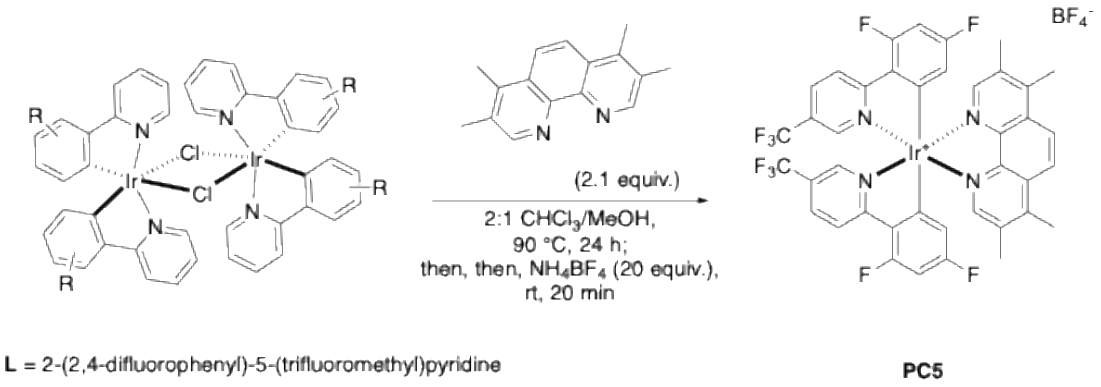

The heteroleptic Iridium complex **PC5** was synthetized adapting a literature procedure by Böttcher (*Inorg. Chim. Acta* ***2021****, 527, 120554*). To a vial equipped with a stirring bar, the Iridium dimer (1 equiv.) and the

desired bidentate *N-N'* ligand (2.2 equiv.) were charged under nitrogen. A degassed solution of $CHCl_3$ and MeOH (0.005 M, 2:1 v/v) was added, and the resulting mixture was stirred at 90 °C for 24 hours. After cooling the solution to room temperature, NH_4BF_4 (20 equiv.) was added. The mixture was stirred for further 20 minutes. Solvents were removed under reduced pressure and the crude product was purified by chromatography on silica gel (DCM:MeOH 30:1 to 9:1). Yellow crystalline solid (70 mg, 86% yield).

^{1}H NMR (400 MHz, CD_2Cl_2) δ 8.56 (dd, *J* = 8.8, 3.1 Hz, 2H), 8.45 (s, 2H), 8.15 – 8.05 (m, 2H), 8.04 (s, 2H), 7.54 – 7.44 (m, 2H), 6.76 (ddd, *J* = 12.5, 9.1, 2.3 Hz, 2H), 5.86 (dd, *J* = 8.1, 2.3 Hz, 3H), 2.93 (s, 6H), 2.51 (s, 6H). **^{13}C NMR** (101 MHz, CD_2Cl_2) δ 168.1 (d, *J* = 7.3 Hz), 166.2 (d, *J* = 12.6 Hz), 164.0 (d, *J* = 12.9 Hz), 163.6 (d, *J* = 12.7 Hz), 161.4 (d, *J* = 13.2 Hz), 154.4 (d, *J* = 7.1 Hz), 151.3, 148.4, 145.0 (d, *J* = 4.8 Hz), 144.8, 136.4 (d, *J* = 37.6 Hz), 130.5, 126.6, 125.8, 125.5, 124.9, 123.9 (d, *J* = 21.0 Hz), 123.0, 120.3, 114.5 (dd, *J* = 17.8, 3.1 Hz), 99.9 (t, *J* = 26.8 Hz), 18.0, 15.2. **^{19}F NMR** (565 MHz, CD_2Cl_2) δ -63.2, -99.2 – -104.1 (m), -106.2 (td, *J* = 12.4, 3.3 Hz), -153.2. **ESI-HRMS** calcd for $C_{40}H_{26}F_{10}IrN_4^+$ $[M\text{-}BF_4]^+$ 945.1621, found 945.1630. *Data consistent with the literature (Inorganica Chim. Acta **2021**, 527, 120554).*

Synthesis of PC6

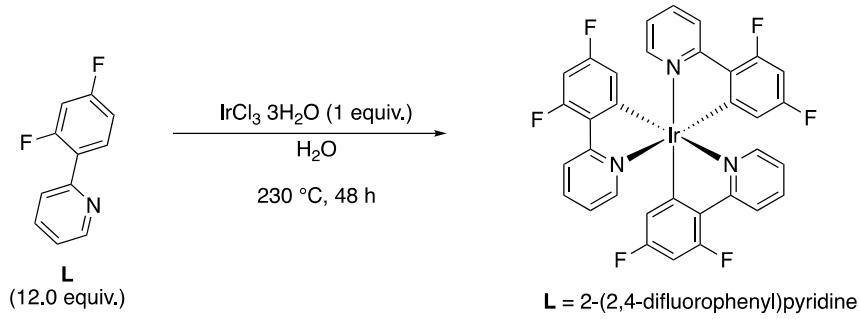

The homoleptic Iridium complex **PC6** was synthetized adapting a literature procedure (Organic Synth. **2018**, 95, 29-45). Iridium (III) chloride hydrate (65 mg, 0.20 mmol, 1.0 equiv.) and **L** (466 mg, 2.44 mmol, 12.0 equiv.) were added to a 45 mL autoclave. Distilled water (42 mL, 0.005 M) was bubbled with nitrogen for 15 minutes and then was added to the autoclave, which was immediately sealed. The reaction mixture was heated at 230 °C for 48 hours. The reactor was then allowed to cool to room temperature. After cooling, the reactor was opened revealing an insoluble yellow solid that was dispersed on the surfaces and in the aqueous phase. The content of the autoclave was transferred to a separatory funnel. The interior of the reactor was mechanically scraped to extract the yellow solid, with metal tongs, cotton balls and drops of dichloromethane; all the recovered contents were added to the separatory funnel. The aqueous phase was extracted with DCM (3 x 20 mL). The combined organic layers were washed with HCl 1M (3 x 20 mL), dried over Na_2SO_4 and concentrated under reduced pressure. The crude was purified by column chromatography on silica gel (DCM) to afford the Iridium complex **PC6** as a bright yellow solid (85 mg, 0.11 mmol, 56% yield).

^{1}H NMR (600 MHz, $CDCl_3$) δ 8.32 – 8.29 (m, 3H), 7.70 – 7.67 (m, 3H), 7.46 – 7.45 (m, 3H), 6.93 (ddd, *J* = 7.1, 5.6, 1.1 Hz, 3H), 6.40 (ddd, *J* = 12.9, 9.0, 2.4 Hz, 3H), 6.26 (dd, *J* = 9.1, 2.4 Hz, 3H). *Data consistent with the literature*.

Chart of the photocatalysts and N co-catalysts tested for the synthesis of ethers 103 and 104

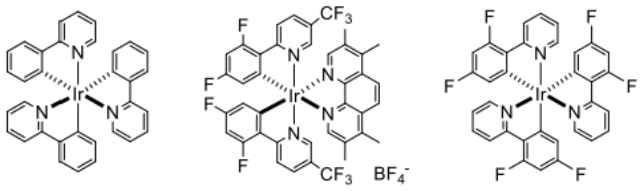

PC1 = $Ir(ppy)_3$, *58.1 kcal/mol*, 1.9 µsec

PC5 = $[Ir\{dFCF_3ppy\}_2(Me_4phen)]BF_4$, *63.0 kcal/mol*, **3.8 µsec**

PC6 = $Ir(dFppy)_3$, *63.5 kcal/mol*, 1.6 µsec

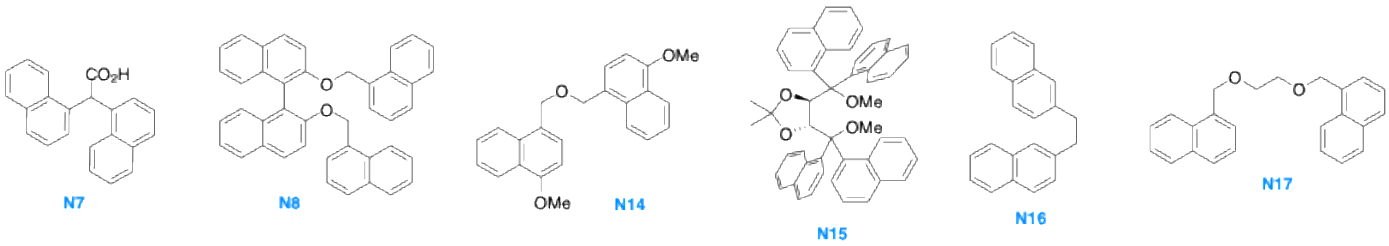

N7 N8 N14 N15 N16 N17

General procedure for the synthesis of ethers 103 and 104 (GP-1)

A vial was charged with the allene **99** (42 mg, 0.15 mmol, 1 equiv.), the desired photocatalyst (1 mol%), and the cocatalyst **N**. A freshly spilled dry solvent was added and the solution (0.1 M on substrate) was transferred into an NMR tube capped with a rubber septum. The mixture was degassed by freeze-pump-thaw (3 times) using a needle connected to a Schlenk line to pierce the septum, and then irradiated with either blue or purple LEDs. The reaction was monitored by TLC; once the conversion reached a plateau, the tube was recovered, the solvent removed under vacuum and 2,2'-dipyridine (11.7 mg, 0.075 mmol) was added as internal standard. A ^{1}H NMR was eventually collected to quantify the conversion **99** and the yield of **103** and **104**.

Optimization of reaction conditions for the synthesis of ethers 103 and 104

Preliminary experiments on the role of N4 on rate

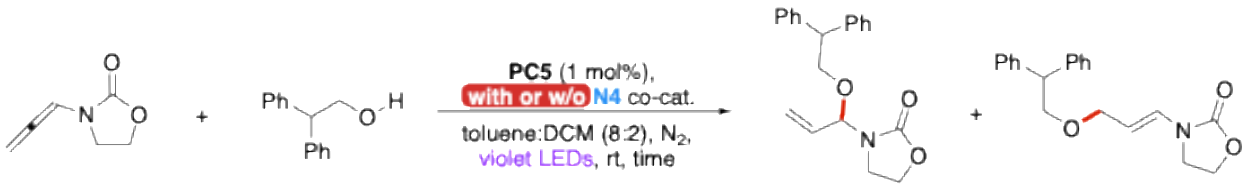

99 **100** **103** **104**

Entry	**N4** co-cat.	Time (h)	Conversion of **99** [%][a]	Yield of **103** [%][a]	Yield of **104** [%][a]
1[b]	30 mol%	72	>99	25	15
3	--	168	78	40	10
4[b]	10 mol%	144	73	34	18

Table S8a. [a]by ^{1}H NMR using 2,2'-dipyridine as internal standard. [b]intermolecular dearomatization side reaction between allene **99** and additive **N** was observed. Reactions performed with violet LEDs.

Effect of a different Ir(III) photocatalyst, increased loading of alcohol 100, and concentration.

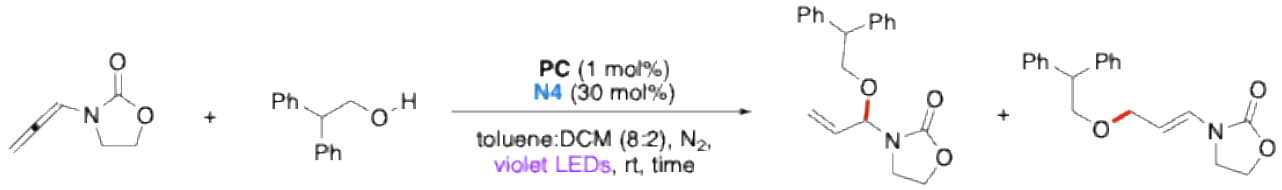

99 100 103 104

Entry	**PC** cat.	**100** (equiv.)	Time (h)	Conversion of **99** [%][a]	Yield of **103** [%][a]	Yield of **104** [%][a]
5[c]	**PC6**, Ir(d-F-ppy)$_3$	1.0	60	95	17	0
6[c]	**PC5**, [Ir[dF(CF$_3$)ppy]$_2$(Me$_4$phen)]BF$_4$	2.0	72	91	6	0
7[b,c]	**PC5**, [Ir[dF(CF$_3$)ppy]$_2$(Me$_4$phen)]BF$_4$	1.0	60	>99	23	11

Table S8b. [a]by ^{1}H NMR using 2,2'-dipyridine as internal standard. [b]0.3 M concentration. [c]intermolecular dearomatization side reaction between allene **99** and additive **N** was observed. Reactions performed with violet LEDs.

Effect of solvent

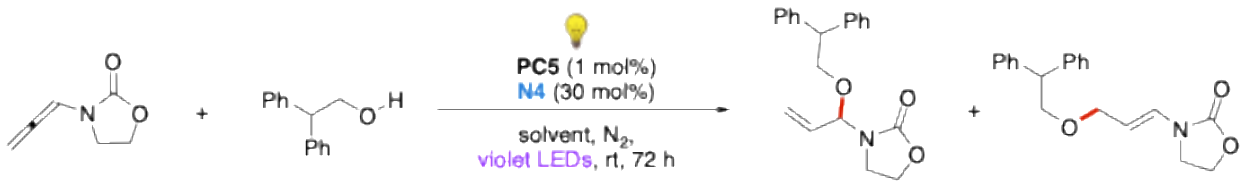

99 100 103 104

Entry	Solvent (0.1 M)	Conversion of **99** [%][a]	Yield of **103** [%][a]	Yield of **104** [%][a]
1[b]	Toluene:DCM (8:2)	>99	25	15
2	MeOH	>99	0	0

Table S8c. [a]by ^{1}H NMR using 2,2'-dipyridine as internal standard. [b]intermolecular dearomatization side reaction between allene **99** and additive **N** was observed. Reactions performed with violet LEDs.

Effect of different N co-catalysts

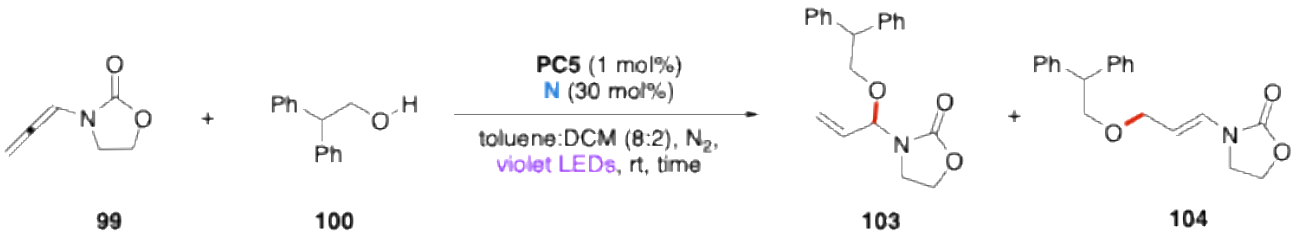

Entry	**N** co-cat. (30 mol%)	Time (h)	Conversion of **99** [%][a]	Yield of **103** [%][a]	Yield of **104** [%][a]
1[b]	**N4**	72	>99	25	15
8[b]	**N7**	84	>99	22	11
9	**N8**	84	30	0	0
10[b]	**N14**	84	>99	33	0
11	**N15**	84	82	3	0
12	**N16**	84	91	6	0
13[b]	**N17**	84	80	10	0

Table S8d. [a]by ^{1}H NMR using 2,2'-dipyridine as internal standard. Reactions performed with violet LEDs. [b]intermolecular dearomatization side reaction between allene **99** and additive **N** was observed.

Seven different poly-naphthyl derivatives were tested, varying principally the length and the rigidity of the tether between the two naphthyl arms, because this structural feature proved to be crucial in our recent studies on alkene-alkene [2+2] photocycloadditions and 1,5-HAT/cyclization sequence (see *Photochem. Photobio. Sci.* **2024**, *23*, 1543 and *ACS Catalysis*, **2025**, 15, 16, 13799-13809). In all of these cases, the rate of the reaction in the presence of the **N** species is significantly higher than that performed without a co-catalyst, which is presented in entry 3. Among all of the tested **N** species, **N4** (entry 1) granted the highest and fasted substrate conversion, followed by **N7** and **N14** (entries 8 and 10, respectively). However, the highest yield of **103** + **104** was observed in the reaction performed in the presence of 10 mol% of **N4** (entry 4). This derivative was thus adopted for the following iteration of the optimization process. Additive **N8** completely inhibited our reaction; indeed, only decomposition of the starting material was observed. Similar results were observed with **N15**, **N16**, and **N17** where we only observed formation of product **103** in 3%, 6%, and 10% yield respectively. Unfortunately, in most entries intermolecular dearomatization side reaction between allene **99** and additive **N** was observed (entries 1,4-8, 10, 13).

Characterization of ethers

3-(1-(2,2-diphenylethoxy)allyl)oxazolidin-2-one (103)

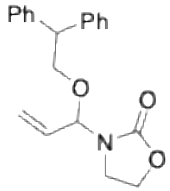

Product **103** was prepared following general procedure **GP-1** in 72 hours from allene **99** (25 mg, 0.2 mmol) and alcohol **100** (39.7 mg, 0.2 mmol). Light-yellow oil (16.2 mg, 25% yield).

^{1}H NMR (400 MHz, $CDCl_3$) δ 7.29 (ddd, *J* = 7.2, 5.3, 3.6 Hz, 7H), 7.21 (ddd, *J* = 15.5, 6.8, 1.9 Hz, 3H), 5.68 (ddd, *J* = 17.2, 10.6, 4.1 Hz, 1H), 5.59 – 5.56 (m, 1H), 5.38 (dt, *J* = 17.2, 1.4 Hz, 1H), 5.27 (dt, *J* = 10.6, 1.4 Hz, 1H), 4.29 (dd, *J* = 8.0, 6.3 Hz, 1H), 4.25 – 4.17 (m, 1H), 4.17 – 4.05 (m, 3H), 3.25 (td, *J* = 9.0, 6.3 Hz, 1H), 2.89 (td, *J* = 9.0, 7.7 Hz, 1H). **^{13}C NMR** (101 MHz, $CDCl_3$) δ 158.38, 142.43, 141.80, 133.12, 128.57, 128.55, 128.36, 126.70, 126.69, 119.00, 82.61, 71.76, 62.60, 51.01, 39.00. **ESI-MS** calcd for $C_{20}H_{21}NNaO_3$ $[M+Na]^+$ 346,14, found 346,09.

3-(3-(2,2-diphenylethoxy)prop-1-en-1-yl)oxazolidin-2-one (104)

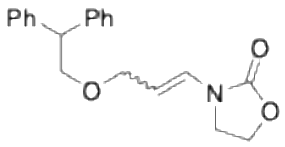

Product **104** was prepared following general procedure **GP-1** in 72 hours from allene **99** (25 mg, 0.2 mmol) and alcohol **100** (39.7 mg, 0.2 mmol). Light-yellow oil (9.7 mg, 15% yield).

^{1}H NMR (600 MHz, $CDCl_3$) δ 7.29 (t, *J* = 7.6 Hz, 4H), 7.25 – 7.19 (m, 6H), 6.86 (d, *J* = 14.3 Hz, 1H), 4.86 (dt, *J* = 14.1, 7.0 Hz, 1H), 4.43 (dd, *J* = 8.8, 7.4 Hz, 2H), 4.27 (t, *J* = 7.3 Hz, 1H), 4.04 – 4.02 (m, 2H), 3.95 (d, *J* = 7.3 Hz, 2H), 3.70 – 3.66 (m, 2H). **^{13}C NMR** (151 MHz, $CDCl_3$) δ 155.44, 142.32, 128.60, 128.42, 127.79, 126.66, 106.64, 73.15, 69.77, 62.33, 51.25, 42.54. **ESI-MS** calcd for $C_{20}H_{21}NNaO_3$ $[M+Na]^+$ 346,14, found 346,02.

IR-spectra

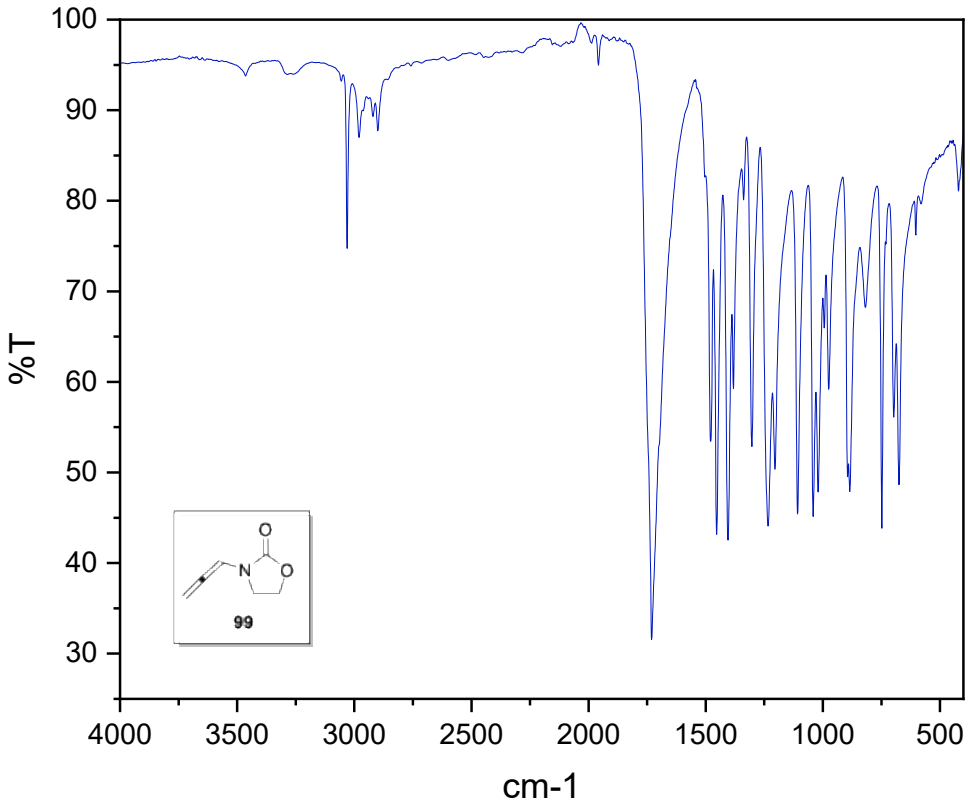

*IR-spectrum of allene **99**.*

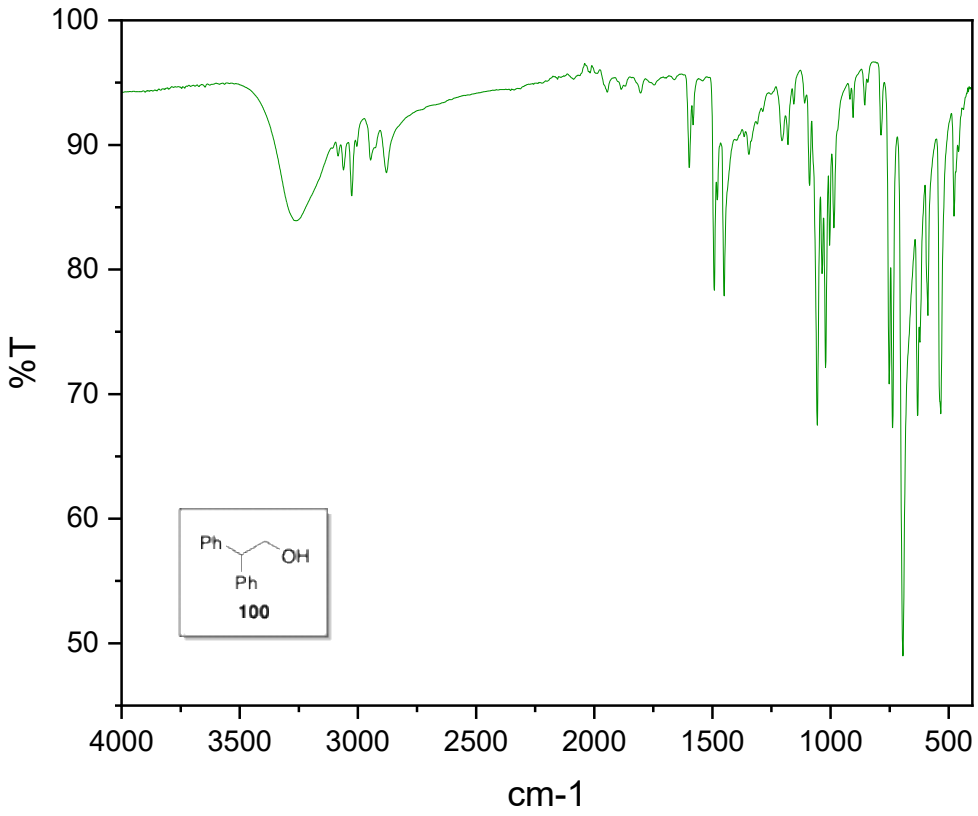

*IR-spectrum of alcohol **100**.*

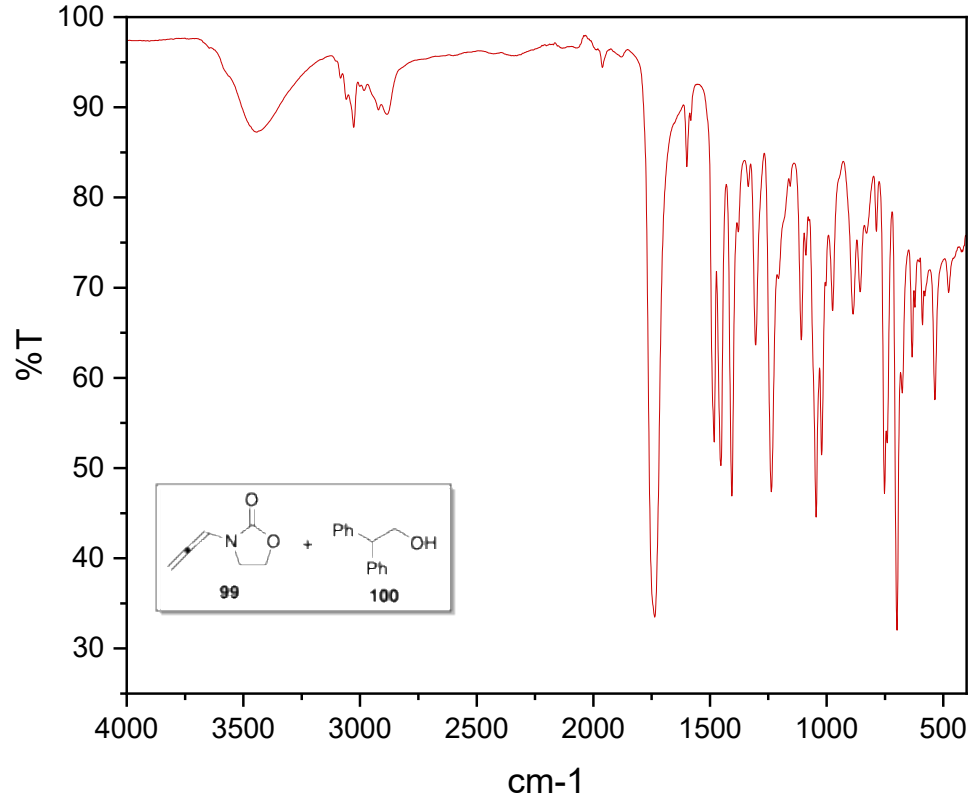

*IR-spectrum of a mixture 1:1 of allene **99** and alcohol **100**. Note that both **99** and **100** are white solids when pure; Mixing them together immediately liquifies both solids into a colorless liquid.*

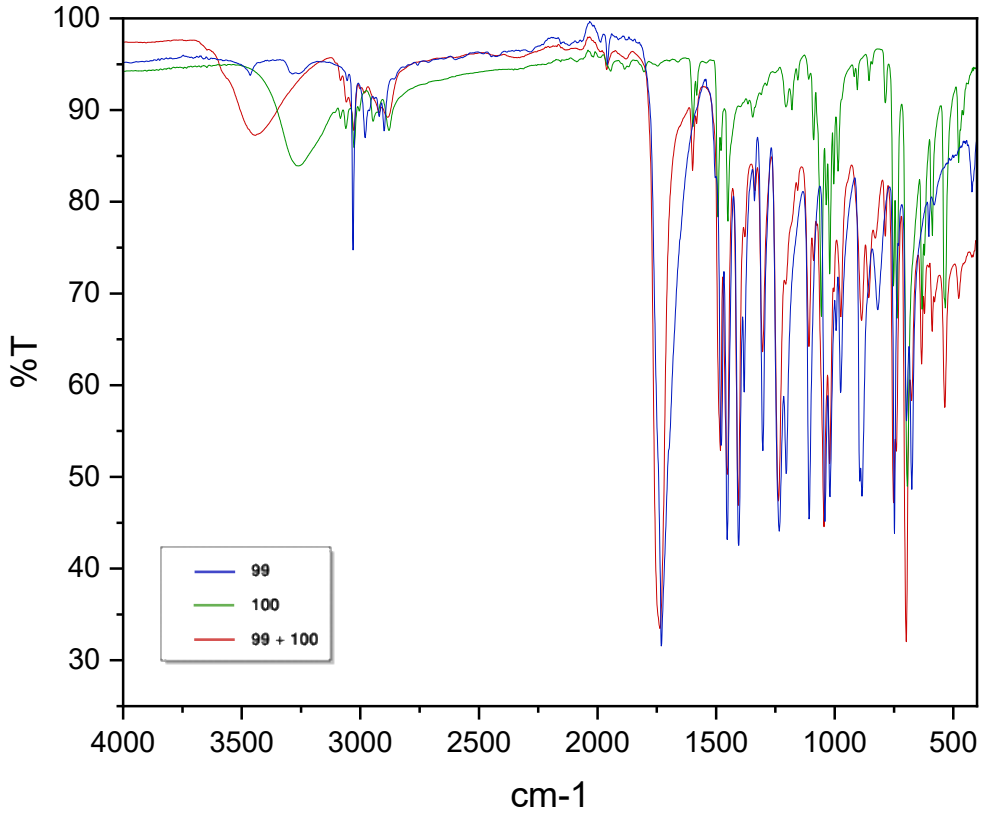

Layering of IR-spectra.

Chapter IV

Boosting Energy-Transfer Processes via Dispersion Interactions

From this chapter:

Cerveri, A.; Scarica, G.; Sparascio, S.; Hoch, M.; Chiminelli, M.; Tegoni, M.; Protti, S.; Maestri, G. Boosting Energy-Transfer Processes via Dispersion Interactions. *Chem. Eur. J.***2024**, 30, e202304010.

4.1 The Importance of Dispersion Interactions in (Radical) Chemistry

Radicals are incredibly reactive species, often allowing to unlock otherwise unfeasible transformations with relatively mild conditions: an array of light-promoted approaches, exploiting the high synthetic potential of those species has been developed in the last decades.[111] Indeed, several applications for the mild generation of reactive radical species were found, exploiting the photoactivation of popular Iridium, Ruthenium, and organic photocatalysts.[112] Moreover, an array of protocols relying on the merger of photocatalysis and metal-catalysis - such as Ti-, Cu-, and Pd-based systems – has also been widely described.[113] Despite the advantages that the generation of incredibly reactive species, such as radicals, can bring, the main issue of those intermediates is their very low stability. Indeed, their high energy levels are responsible for their low concentration in solution,[114] often causing slow kinetics for the desired reaction, thus requiring a finely and structure-specific tuning of the reaction conditions. Numerous solutions to this issue relying on the addition of an additional catalytic cycle, which exploits the formation of relatively strong bonding interactions have been proposed (Scheme 67).

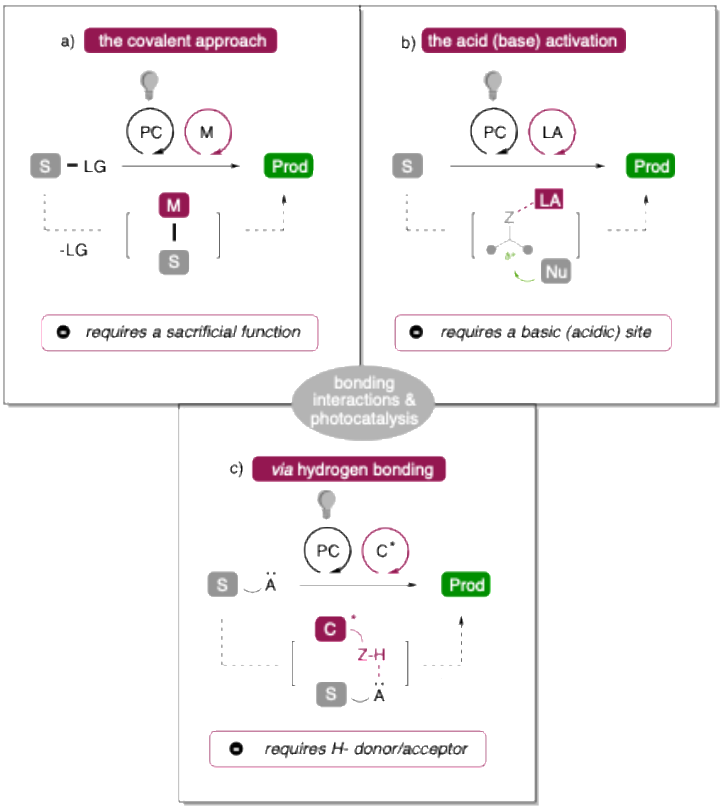

Scheme 67. Catalytic strategies in photocatalysis.

The covalent approach relies on the formation of transient covalent bonds, combining photo- with organo- and metal-catalysis (Scheme 67a).[115] The acid-base activation (Scheme 67b), along with the formation of H-bonding interactions (Scheme 67c) have also been coupled with photocatalysis.[116] However, these strategies require a dedicated optimization study of the experimental conditions for each substrate category (Scheme 67, purple boxes). In parallel, powerful Dispersion Energy Donors (DEDs)[44,117] groups were widely developed, decorating substrates and/or catalysts for the purpose of exploiting LD interactions to trap elusive entities or steer the stereocontrol of a catalytic reaction.[45b,50,118] Dispersion interactions are defined as fluctuations of the electron density, inducing instantaneous dipoles.[44,45b,50,117,118] Radicals are more polarizable as much the mono-occupied orbital is delocalized,[119] thus forming relatively strong dispersive interactions which were already observed in associated dimers of radical species.[120] Back in 1991, Miller *et al.* had already reported the formation of dimers (in water) and aggregates (in aqueous NaCl) of an imide anion radical in solution, thanks to π-π stacking interactions between the naphthalene units of the imide radical anion species (Scheme 68).[120c]

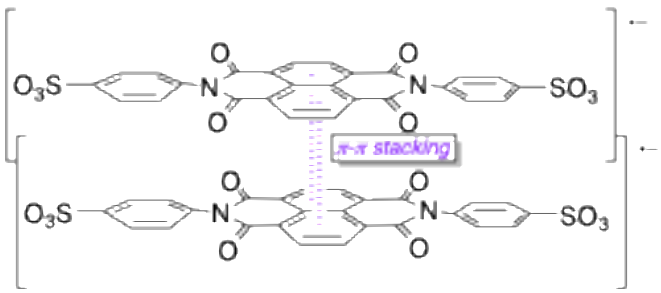

Scheme 68. π-π stacking in radical anion species aggregates.

More recently, Winter *et al.*[120b] systematically studied the effect of the viologen cation radical structure on the nature and the strength of the π-dimer (pimer) bond. What they found was surprising: the π-bond strength is unaffected by the substitution of electron-withdrawing or electron-donating groups or increased conjugation. Moreover, this π-interaction remains undiminished even when sterically bulky N-alkyl groups are introduced. The authors rationalized this, attributing to exceptionally strong dispersion forces a dominant role in the interaction between the radicals. The stacking of ultra-polarizable π-radicals generates attractive dispersion forces, strong enough to overcome the Coulombic repulsion that generates bringing two cationic species close to each other (Scheme 69).

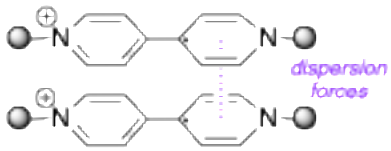

Scheme 69. Dispersion Forces in radical pimers.

Very recently, Dell'Amico's group[121] used light and steric parameters to steer the stereocontrol of the light-driven Paternò-Büchi reaction between indoles and ketones (Scheme 70). If UV light (370 nm) is used as the light source, the reaction proceeds *via* exciplex, in which radical-π interactions play a dominant role. When moving to visible light (456 nm), the formation of an electron-donor-acceptor (EDA) complex is progressively favored - where π-π stacking are crucial for its formation - enabling the switch of the diastereomeric ratio of the products from >99:<1 to 47:53. On the contrary, the switch from a methyl to *i*propyl substitution favors the exciplex intermediate, reversing the d.r. of the products.

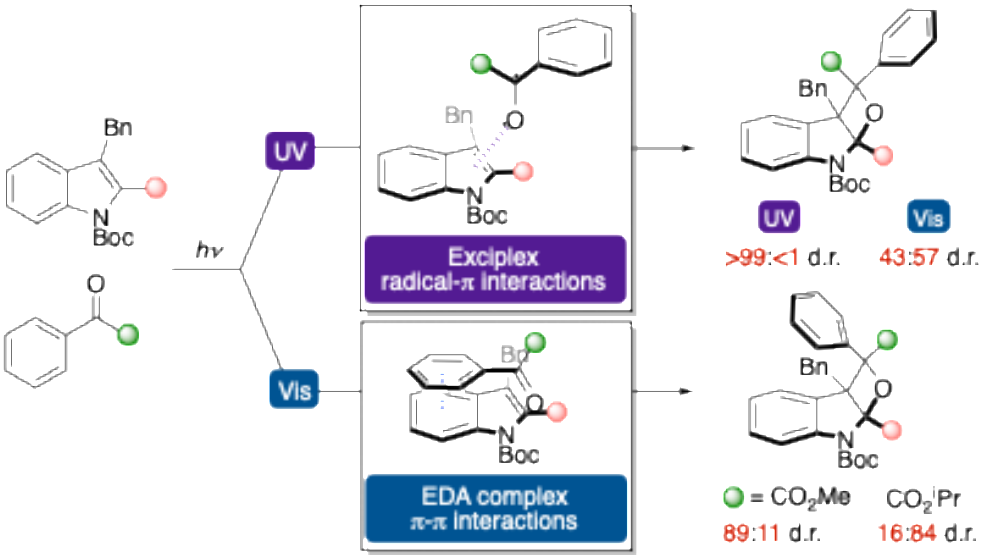

Scheme 70. Light and steric factors used to steer the stereocontrol of light-driven reactions.

Almost all visible light-promoted protocols proceed *via* open-shell intermediates,[112,115,116,122] nevertheless, a generalized approach taking advantage of dispersion interactions is still absent in this area.

Indeed, we already reported an example of visible light-promoted allene-arene *para*-cycloaddition,[61c] in which dispersive radical-π forces were crucial for the stabilization of unstable biradical intermediates.

4.2 Results and Discussion

In this work, we found that the use of Naphthalene (NP) (5-20 equiv.), or of tethered poly-naphthyl derivatives (poly-NPs, 10–30 mol %), significantly improves the efficiency of several EnT-promoted processes (Scheme 71).

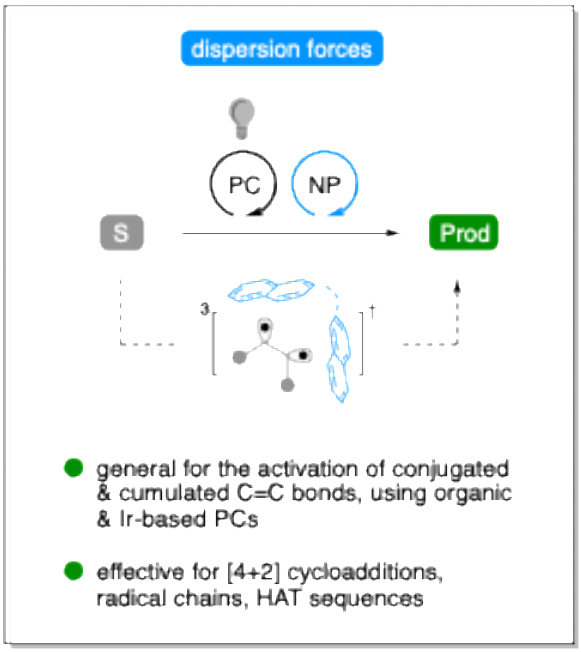

Scheme 71. Dispersive Interactions as rate enhancers of EnT-mediated processes.

We demonstrated that these additives can form reversible adducts with different ground-state substrates, thanks to π-π and CH-π dispersion interactions.[70] Plus, an extra stabilization of the triplet state of these adducts is provided by radical-π dispersion interactions.[119,120b] As a result, the EnT on the adduct is more favorable than that on the substrate as an isolated species, ensuring shortened irradiation times and/or higher yields for the desired products. The beneficial effect of NP and poly-NPs is general, and it was observed in six different model reactions, varying substrates, reactivities, solvents and photocatalysts.

Sulfonyl-radical chain

In our already reported formal [2+2]-cycloaddition/1,3-sulfonyl migration of 1,6-enallenes **120** (Scheme 72),[123] bicycles **121** are accessed through a EnT-induced radical chain reactivity. To evaluate the putative

positive effect of NP, we decided to test five different enallenes with $Ir(ppy)_3$ as the photosensitizer. For all the five substrates, a positive effect of NP (20 equiv.) was clearly observed, varying both the sulfonyl and the styryl fragments of the enallene substrate (Cond. A: 29–53 %, Cond. B: 48–68 %). For the anethole arm bearing substrate **120e** a weaker effect was reported. The strongest difference was observed with substrate **120c**, which has the least hindered sulfonyl group. We thus concluded that the presence of NP is beneficial for reactivities that involve the propagation of a radical chain, as its addition improved our reaction efficiency.

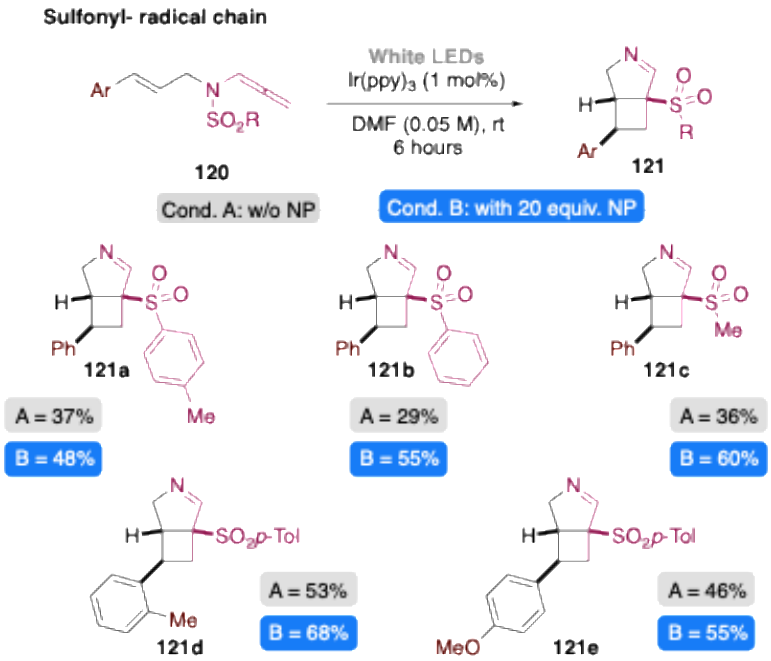

Scheme 72. Effect of NP on the synthesis of bicycles **121** from 1,6-enallenes **120** (0.2 mmol-scale), Cond. A described in ref. [121]; isolated yields upon chromatography.

Alkene-arene dearomative cycloaddition

Inspired by several works on EnT-triggered dearomatization reactions of naphthyl derivatives,[66a,124] we developed a novel intramolecular *para*-cycloaddition on a simple naphthyl group, triggered by the photosensitization of a cinnamyl functionality (Scheme 73, see the experimental section of this chapter for selected optimization tests and experimental details of this new synthetic method, with the variations of solvents and PCs, always comparing in parallel the results with and w/o additive). After a rapid screening of the reaction parameters, although products **123** were obtained in high yields employing 1 mol% of

$Ir(ppy)_3$ as photosensitizer, the time required to reach the full consumption of substrates **122d-f** was quite long (24 up to 48 hours). The addition of 20 equiv. of NP improved our reactivity and, on average, a three to four times shorter irradiation was sufficient to fully convert the starting materials. In addition to this, products **123d**, **123e**, and **123f** were also isolated in higher yields, although for the latter, in presence of NP, the reaction time remained unaltered. The lower reactivity of substrate **122f** could be addressed to the higher steric hindrance of its binaphthyl pendant, in this case balancing the positive stabilizing effect of dispersion interactions.

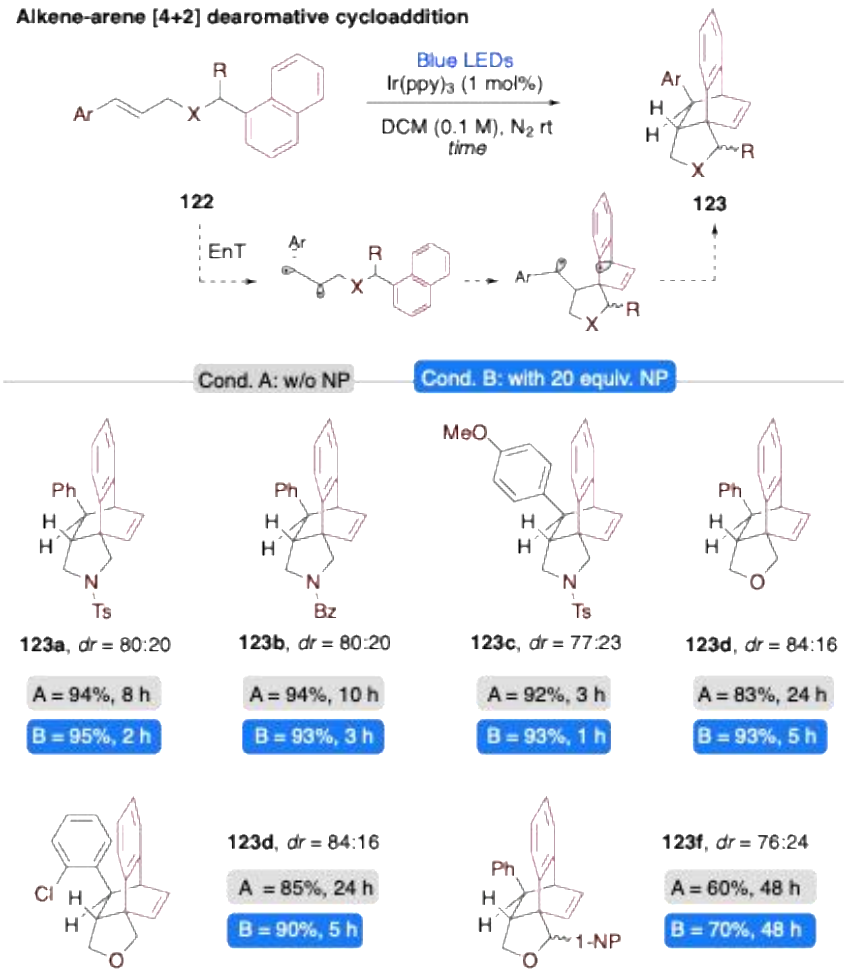

Scheme 73. Effect of NP on the dearomatization of **122** (0.2 mmol-scale) and working hypothesis for its mechanism; time required to fully consume **122** monitored by TLC, d.r. by ^{1}H NMR, isolated yields upon chromatography.

[1,5]-HAT/cyclization on allenamides

The photoactivation of allenamides *via* EnT[61b,c] was used to explore a new reactivity (Scheme 74). We were aiming to trigger a 1,5-Hydrogen atom abstraction from the labile C(sp^3)-H site at the α-position of the amido- group of allenamide **124**, mediated by the highly reactive vinyl radical site generated *via* photosensitization of the allene moiety. The triplet intermediate originated by this intramolecular HAT event, could form a 6-membered lactam **125** upon radical recombination and intersystem crossing. We screened the experimental conditions, changing solvents, photocatalysts and model substrate, but unfortunately we did not get satisfactory results (see the experimental section of this chapter for selected optimization tests and experimental details of this novel synthetic method, with variations of solvents and PCs, always comparing in parallel the outcome with and w/o additive). The best conditions found (1 mol% of $Ir(ppy)_3$, 0.1 M in DMF) gave product **125a** only in a moderate yield, and the other seven substrates tested did not provide good results without NP (Cond. A: 0-42%). Note that substrates **124c**, and **d** are more challenging for the intramolecular HAT step because of the higher bond dissociation energy (BDE) of the α-carbonyl C(sp^3)-H, and for the formation of a less stable α-carbonyl radical after the putative HAT has taken place, compared to the other substrates tested, which bring a tertiary C(sp^3)-H site with two aryl substituents at the abstraction site. Both factors limit the efficiency of the reaction and, indeed, no conversion of **124 c**, **d** was observed without NP. On the contrary, the addition of 20 equivalents of NP had a noticeable effect in all cases: products **125** were all delivered in good to excellent yields (Cond. A: 75–91 %), and the isolation of the otherwise inaccessible compounds **125c**, **d** (40–80 %) was also possible.

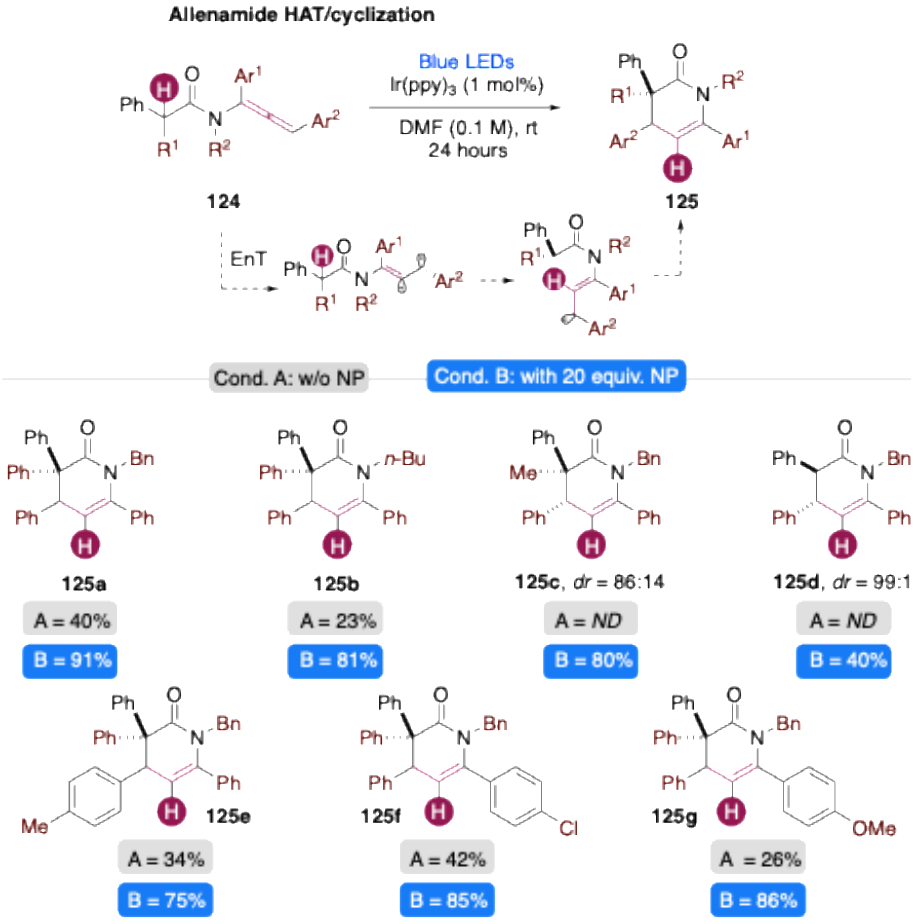

Scheme 74. Effect of NP on the cyclization of reagents **124** (0.2 mmol-scale) and working hypothesis for its mechanism; time required to fully consume **124** (Cond. B) monitored by TLC, d.r. by ^{1}H NMR, isolated yields upon chromatography.

Although the use of an excess of additive was required (5– 20 equiv., Schemes 72-74), it is worth noting that NP is a cheap, readily available species with a low molar cost, and can be recovered by column chromatography and thus reused at choice.

The effect of poly-NP derivatives on EnT processes

Poly-NP **N1–10** were prepared with a multivalent approach,[125] varying the presence of different functional groups in the tether (*i.e*. an -OH group in **N3**, an N-tosylamide in **N4** and **N5**, an L-proline derivative in **N6**, *etc.*), as well as its length and rigidity, with the purpose of evaluating the effect of these properties on the efficacy of the additive. Poly-NP **N1–10** were then tested in six different EnT-promoted reactions, identifying the best performing poly-NP candidate for each reactivity (Scheme 75). The use of 20 mol % of **N4** in the sulfonyl-radical chain providing bicycles **121** provided results that are comparable with those

using 20 equiv. of NP (**121b**, **c** = 51–56 %, Scheme 75a). The dearomatization of **122d** required the use of 1 equiv. of **N10** (Scheme 75b), which is not a proper catalytic amount, but nonetheless a 20-fold lower loading compared to that of NP. The relatively high amount of **N10** required to reach a satisfactory increase of the reaction efficiency could be explained by the high affinity observed between the additive and the product, which prevented the turnover of the poly-NP additive (^{1}H-NMR spectra showing the [**123d**:**N10**] interaction in the experimental section of this chapter). The use of 30 mol % of **N9** allowed us to isolate the 1,5-HAT product **125c** in 66 % yield (d.r. = 56:44, Scheme 75c), while no traces of **125c** were observed without **N9**. This difference indicates that **N9** is a co-catalyst of the reaction.[126] The dearomative [4 + 2] cycloaddition on simple aryl rings is challenging,[66a,124,127] as the conversion of **126a** is quite low without additives (Scheme 75d). On the contrary, the desired product is recovered in a very good yield when using 30 mol % of **N4** (15% vs 79% yield, respectively). The [2 + 2] cycloaddition on **128a** requires long irradiation times to reach full consumption of the substrate[128] and a low yield is observed upon four hours of irradiation (Scheme 75e). We attributed this low reactivity on the flexible tether present between the two alkenes, disfavoring the cyclization process, and on the terminal olefin arm that destabilizes the final triplet intermediate of the EnT process.[129] The reaction performed in the presence of 30 mol % of **N4** led to the complete consumption of substrate **128a** in four hours, affording **129a** in 96 % yield. Eventually, we also attempted the original dearomative [2 + 2] cycloaddition on electronically unbiased indoles, which cannot be directly activated by EnT (Scheme 75f).[35,130] A moderate yield of **131a** upon 24 hours of irradiation was observed without additives (37% yield). Once more, the use of 30 mol % of **N4** allowed us to dramatically improve the outcome of our reaction, delivering spiro-compound **131a** in 77 % yield within 6 hours of irradiation time.

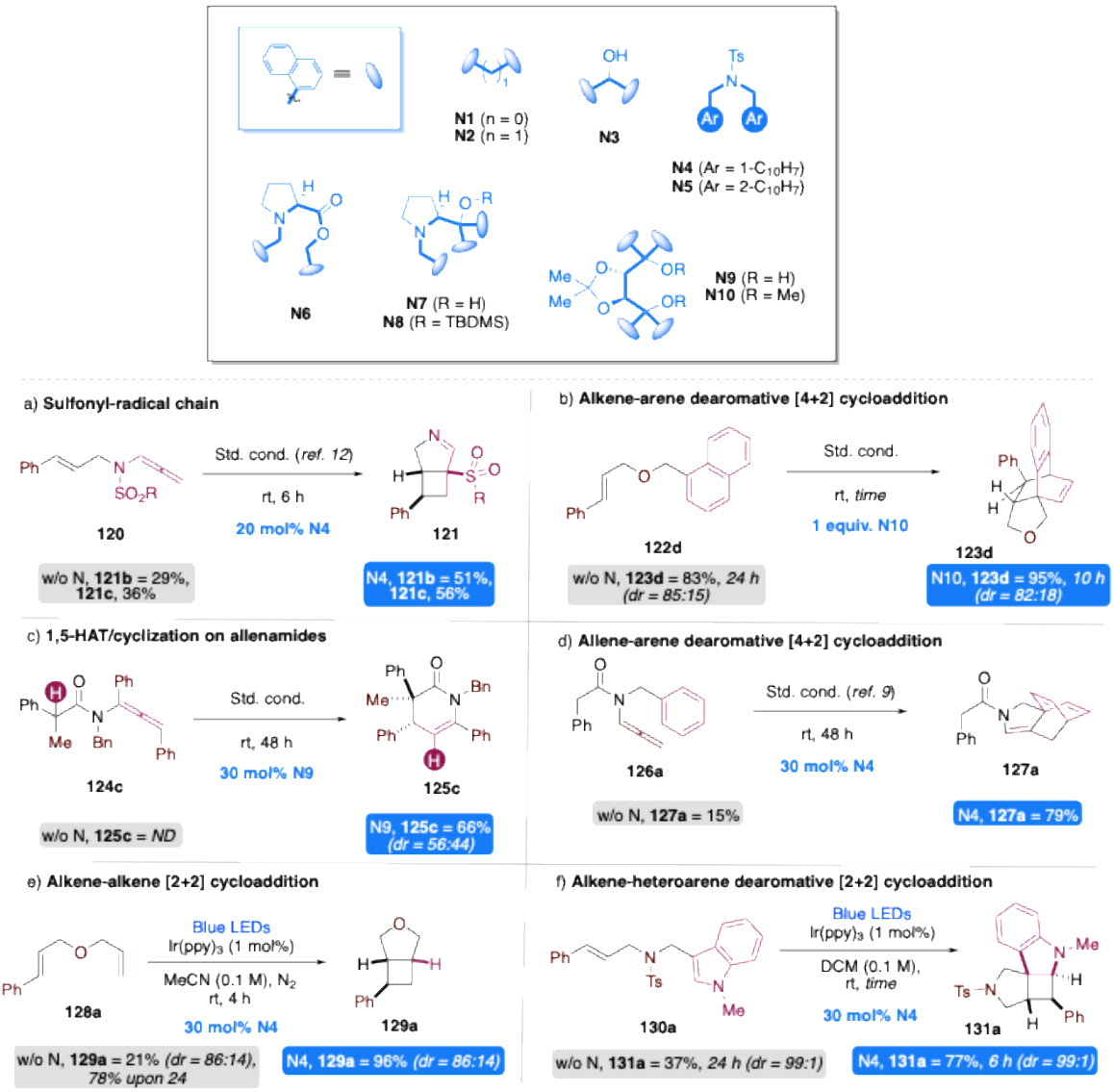

Scheme 75. Panel of synthetized poly-NPs and their effect on EnT-mediated processes.

NP and our poly-NPs **N1–10** could be efficiently recovered at the end of the reaction by column chromatography and reused at will. Furthermore, the possibility to tune the polarity of the poly-NP without hampering its performances ensures that its stereo-electronic properties could be adjusted to achieve a simple separation from the desired product, thus enhancing the practical viability of poly-NPs for future uses.

Several computational and ^{1}H-NMR experiments were carried out to rationalize the role of NPs and our poly-NPs in EnT processes.

First, we may exclude that NP and our poly-NPs can effectively quench the excited triplet state of the photosensitizer Ir(ppy)$_3$, since the latter has an energy of 58.1 kcal/mol,[112,122] which is lower than that of NP (60.7 kcal/mol);[131] on the contrary, this event is possible on **PC2** ([Ir(dFCF$_3$ppy)$_2$(bpy)]PF$_6$), which has a high enough triplet energy (62.4 kcal/mol)[131] to match that of NP and our poly-NPs (see the experimental section for Stern-Vollmer quenching studies of **PC2** with NP). These and our previous results and literature data on triplet energies suggest that NP-based additives have a positive effect as long as they do not quench the excited photocatalyst or, if activated by the excited photocatalyst, they can in turn activate the substrate for the desired reactivity. Indeed, the previously described EnT-relay phenomenon (see Chapter I) is only possible when a ground state [substrate:additive] adduct is generated, and the triplet energy of the NP-based additive matches that of the substrate, therefore this is not always possible in purely intermolecular EnT processes. The redox potentials of the NPs[132] do not match those of the excited PCs, reducing the likeliness of those events. The most likely explanation of the positive effect of our additives is the formation of [substrate:additive] adducts (Scheme 76a).[120] Indeed, an interaction between NP and substrates was observed by ^{1}H-NMR and it was particularly evident for substrates **120a** and **122a** (copies of spectra in the experimental section). A downfield shift by up to 0.2 ppm was observed, and the shift is larger for the signals of the π-groups of the substrate.[133] These results indicate that π–π stacking between NP and substrates is present in the ground state.

We studied by DFT calculations substrates **120**, **122**, **124**, **126**, and **130**, which have very different stereoelectronic properties, to confirm the generality of the concept. The triplet energies of the reagents and of 1:1 [substrate:**N2**] adducts were calculated (Scheme 76b, [substrate:NP] adducts and values for **128**, which is similar to **122**, in the experimental section). All the ^{1}[substrate:**N2**] adducts were more stable than the corresponding isolated species and a net stabilization of all the ^{3}[substrate:**N2**] adducts was observed (by 4.4–5.7 kcal/mol in ΔG). ^{3}[**120**:**N2**] adduct is 4.4 kcal/mol more stable than the corresponding triplet state isolated species. A 5.4 kcal/mol stabilization was calculated for the ^{3}[**122**:**N2**] adduct compared to ^{3}**122** as an isolated species. For ^{3}[**124:N2**] we calculated a stabilization of 4.7 kcal/mol compared to the corresponding triplet state isolated species. The highest stabilization of 5.7 kcal/mol was calculated for the ^{3}[**126**:**N2**] adduct. Lastly, for the ^{3}[**130**:**N2**] adduct, a 4.5 kcal/mol stabilization compared to ^{3}**130** was

calculated. The efficiency of poly-NPs additives can be explained by the geometries and spin-densities of the ^{3}[substrate:**N2**] adducts. The delocalized nature of the two mono-occupied orbitals (images in Scheme 76b) increases the strength of dispersion interactions.[119,120] In parallel, the structure of the additive makes it best suited to maximize the stabilizing interaction between its aryl π-networks and the two mono-occupied orbitals, which are in a nearly perpendicular arrangement to minimize the spin repulsion.

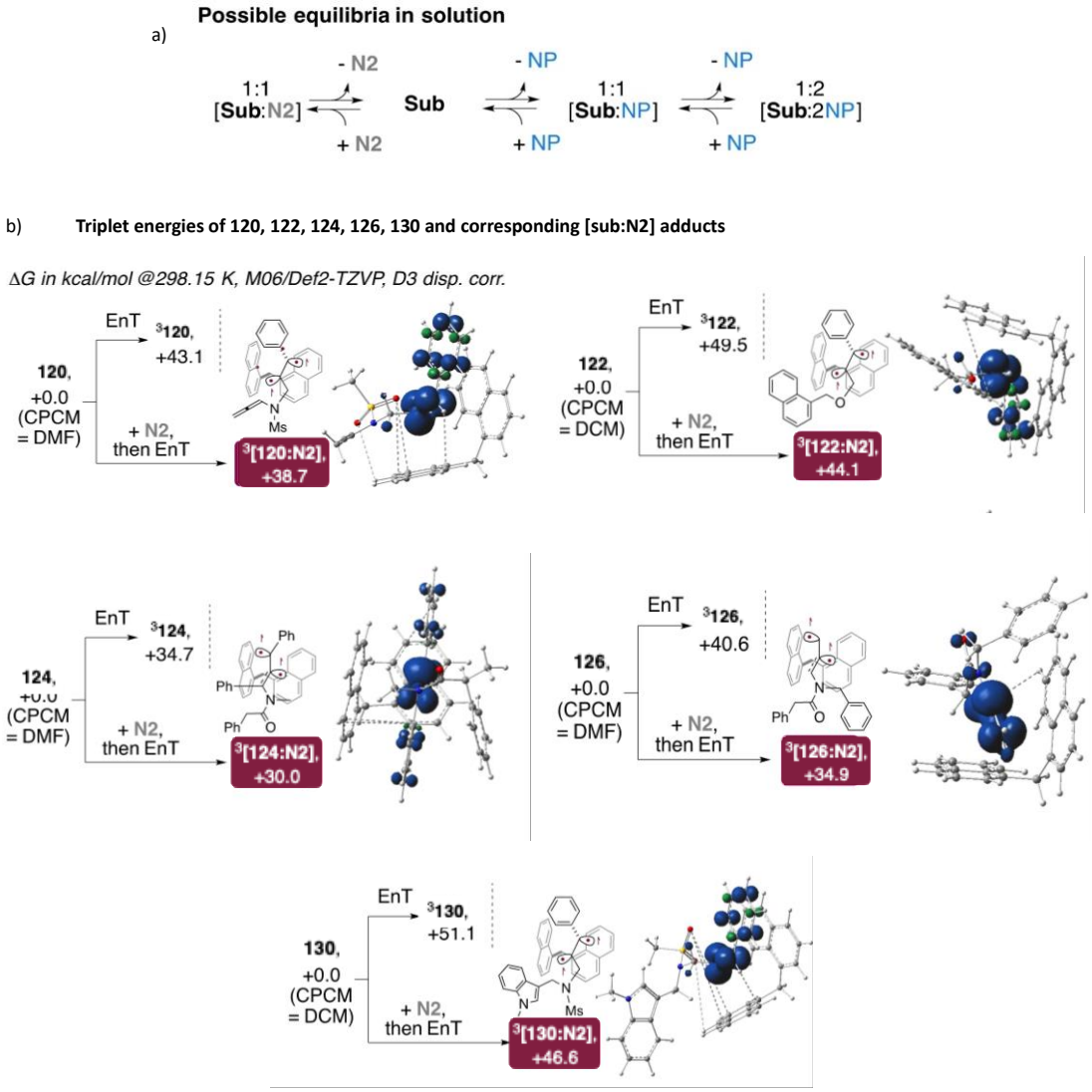

Scheme 76. a) possible equilibria in solution; b) DFT data comparing the triplet energy of substrates vs that of the corresponding [substrate:**N2**] adducts for **120**, **122**, **124**, **126** and **130** with calculated spin densities highlighting the stacking-like arrangement between the perpendicular mono-occupied molecular orbitals and the π-network of the naphthyl groups of **N2**.

4.3 Conclusions

In this chapter, a new strategy employing naphthalene and poly-NPs derivatives to improve the efficiency and rate of several EnT-induced processes was described. The beneficial effect of those additives was addressed to the stabilization of triplet reaction intermediates with radical-π dispersion interactions between mono-occupied molecular orbitals and the π-clouds of the NP or poly-NP additive. This concept will be further applicable in the design of new (photo)catalytic methods exploiting weak bonding interactions. From a synthetic point of view, these additives showed compatibility with most common photocatalysts (both Ir(III) and organic complexes), light sources (purple, blue and white LEDs), and different polarity organic solvents (DCM, $CHCl_3$, ACN and DMF). The most noticeable effect was observed when using a large excess (20 equiv.) of cheap NP or a catalytic amount (10-30 mol%) of one of our tethered poly-NPs. The additives reported a beneficial effect in several different visible light-promoted reactions, including sulfonyl radical chains, [2+2] cycloadditions, dearomative [2+2] and [4+2] cycloadditions, and a novel 1,5-HAT/cyclization cascade.

This novel strategy could be widely used to enhance the efficiency of already reported synthetic methods, to reduce the efforts required to optimize a new catalytic approach, and, eventually, to promote reactivities that would be unattainable otherwise.

4.4 Experimental Section

General remarks

All chemicals those syntheses are not reported hereafter were purchased from commercial sources and used as received. Solvents were dried passing through alumina columns using an Inert® system and were stored under nitrogen. Present visible light-promoted reactions did not require the use of dry solvents but the presence of molecular oxygen exerts a negative effect on their rate. Chromatographic purifications were performed under gradient using a Combiflash® system and prepacked disposable silica cartridges or through isocratic flash chromatography using commercial 60 Å silica gel. All reactions that required heating were performed with the use of high-vacuum grade silicon oil. Reactions promoted by visible light were performed into standard 5 mm NMR tubes, surrounded by a commercial strip of 300 RGB household leds (12V). These were put at a distance of ca 10 cm and irradiated with white light (model SMD5050-300 ip65, 12W), or blue light model (SMD5630-300 ip20, 14W), or purple light (SMD5630-300 ip20, 17W). Photos showing the experimental setup follows hereafter, together with spectra showing the emission of the different light sources. The tubes were inside an oil bath fitted with a thermometer to monitor the temperature. Cooling was ensured by two fans recovered by outdated PCs to avoid reproducibility issues. During summertime, solutions are kept at 25 °C through the addition of a rubber spire inside the silicon oil bath. The spire is linked to a chiller that keeps pumping a cooled water/ethylene glycol solution to maintain the desired temperature. ^{1}H and ^{13}C NMR spectra were recorded at 300 K on a Bruker 400 MHz spectrometer using residual non-deuterated solvents as internal standards (7.26 ppm for ^{1}H NMR and 77.00 ppm for ^{13}C-NMR for CDCl3, 2.05 ppm for ^{1} H NMR and 29.84 ppm for ^{13}C NMR for acetone-d6). ^{19}F-NMR spectra were recorded in CDCl3 at 298 K on a Jeol 600 spectrometer fitted with a BBFO probehead at 564 MHz. The terms m, s, d, t, q and quint represent multiplet, singlet, doublet, triplet, quadruplet and quintuplet respectively, and the term brs means a broad signal. Reported assignments were based on decoupling, COSY, NOESY, HSQC and HMBC correlation experiments. Mass analyses were recorded on an Infusion Water Acquity Ultra Performance LC HO6UPS-823M instrument equipped with a SQ detector (Electrospray source); high-resolution mass analyses were recorded on a LTQ ORBITRAP XL Thermo Mass Spectrometer (Electrospray source). Emission spectra have been measured by means of a PerkinElmer LS 55 Luminescence Spectrometer.

Optimization experiments

Photocatalysts used in this work

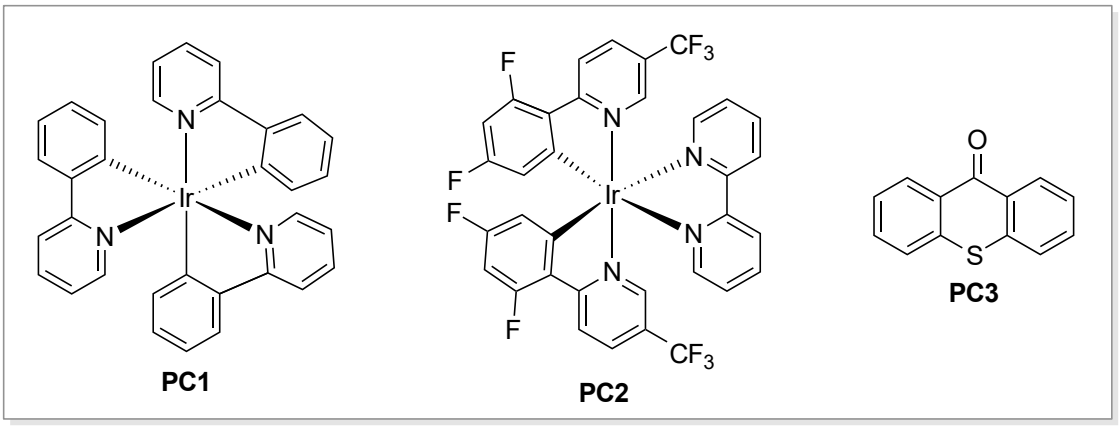

Setup adopted for the catalytic reactions

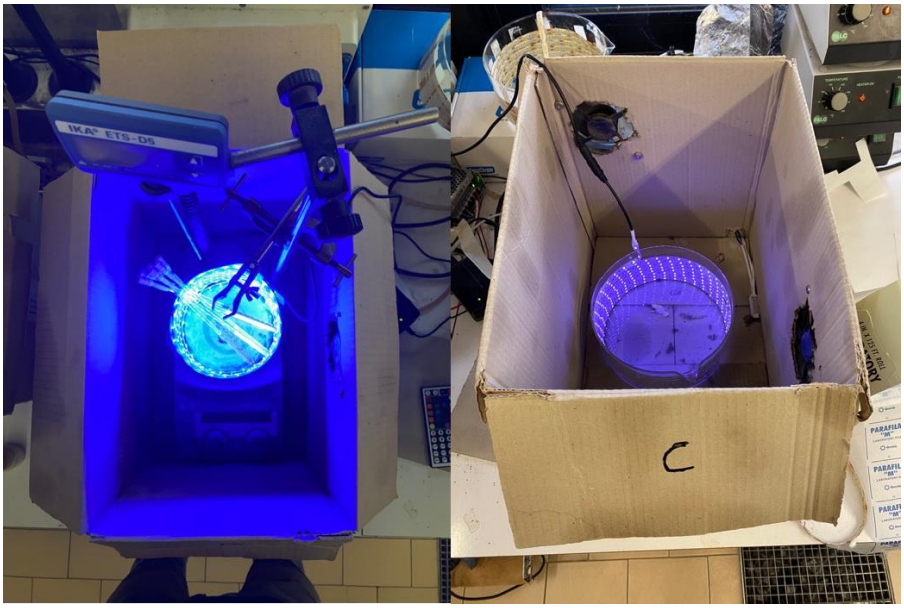

Left: setup using blue LEDs; right: setup using purple LEDs.

Emission spectra of the LEDs used in this work

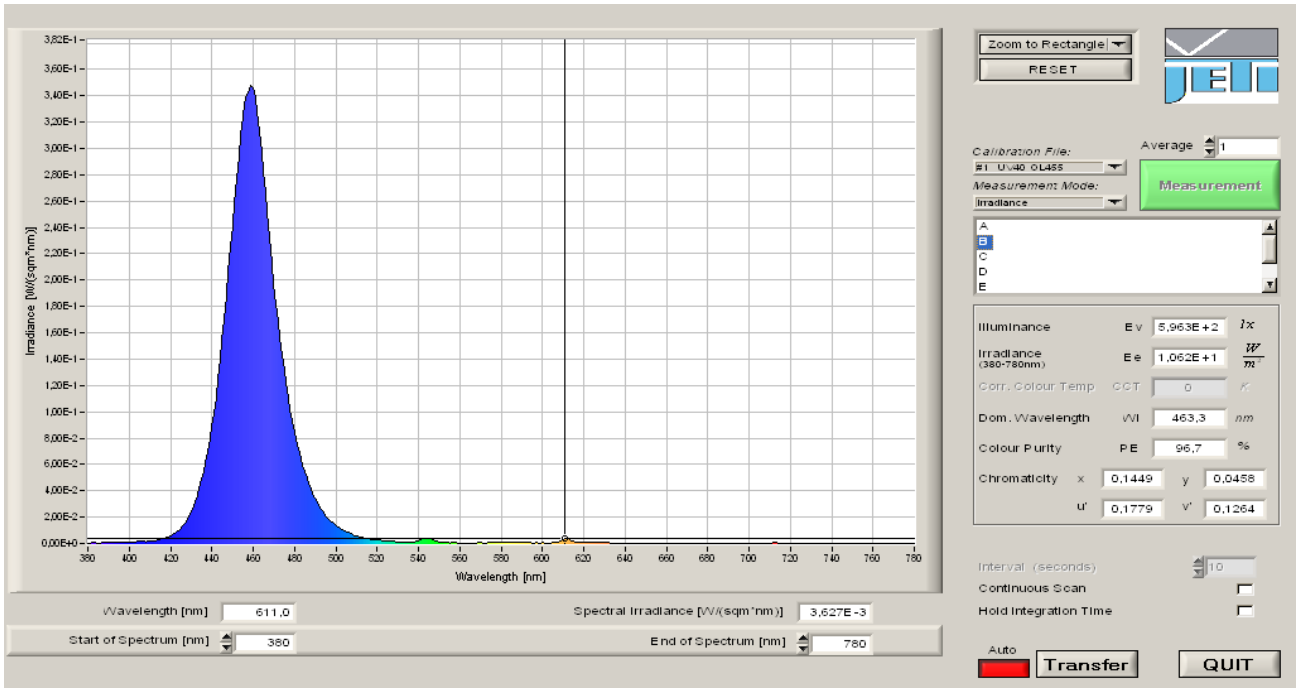

Emission of the blue LEDs, measured at 15 cm distance

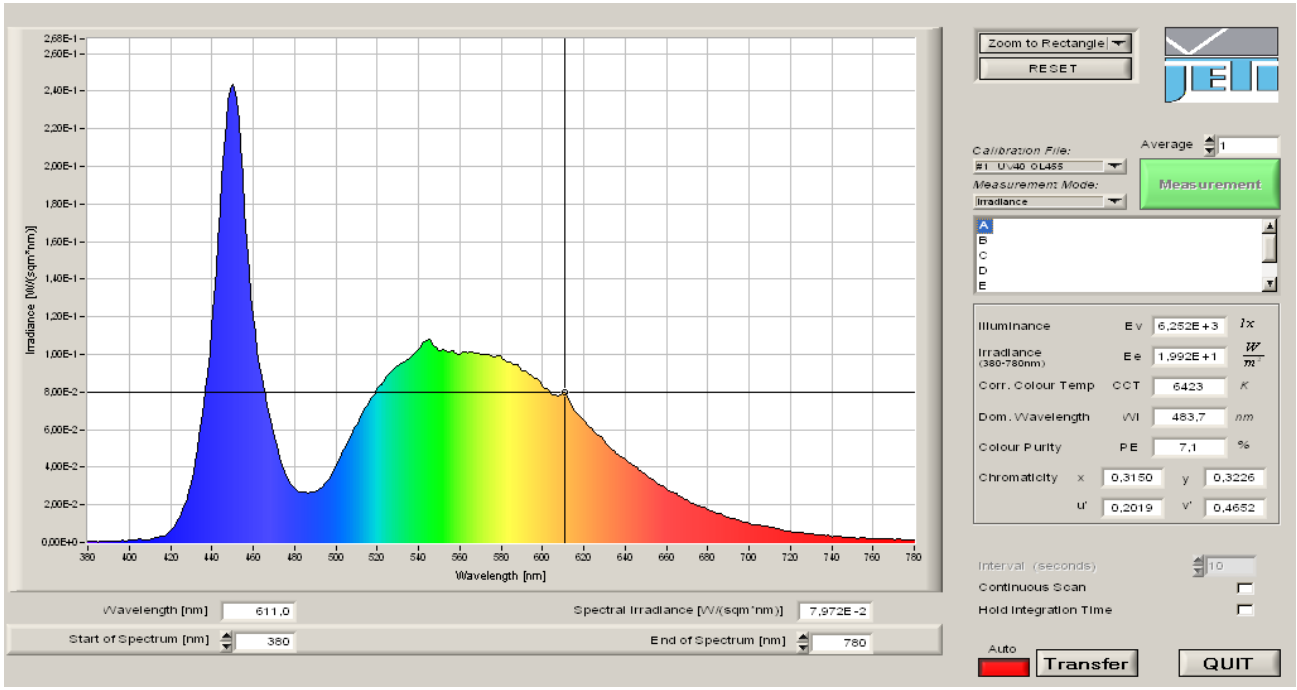

Emission of the white (RGB) LEDs, measured at 15 cm distance

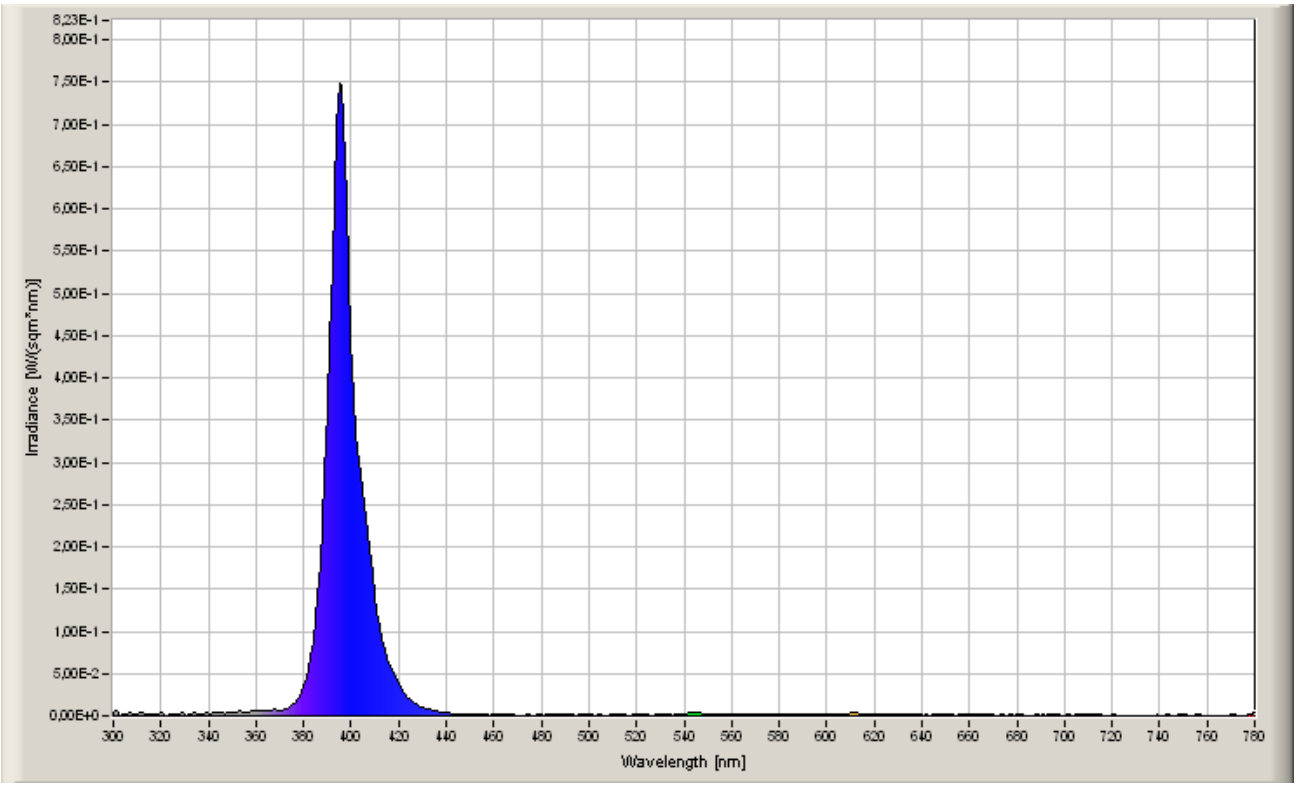

Emission of the purple LEDs, measured at 15 cm distance

Table S9: Photocatalytic [4+2]-dearomative cycloaddition

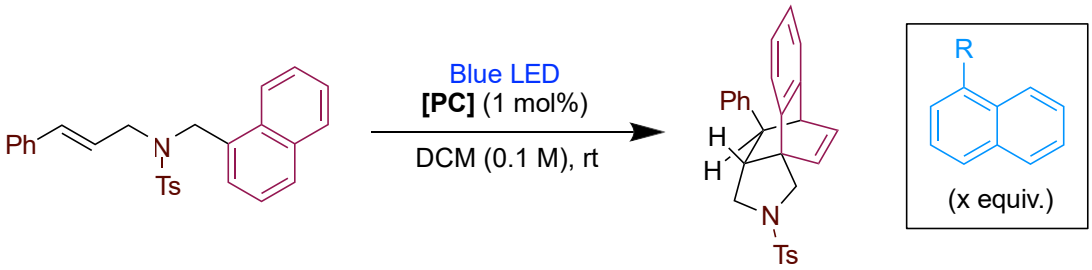

122a **123a**

Entry	[PC]	Naphthalene (equiv.)	R	Time (hours)	Yield (%) [a]	*dr* [b]
1	**PC1**	0	/	8	94	80:20
2	**PC1**	20	H	2	95	80:20
3	**PC2**	0	/	7	92	80:20
4	**PC2**	20	H	7	93	81:19
5 [c]	**PC3**	0	/	5	93	80:20
6 [c]	**PC3**	20	H	4	94	81:19
7	**PC1**	10	H	2	94	80:20
8	**PC1**	20	1-OMe	2	94	82:18
9	**PC1**	20	1-Ph	4	93	79:21
10 [d]	**PC1**	0 or 20	H	24	0	/
11	/	0 or 20	H	24	0	/

[a] Isolated yields, [b] determined by ^{1}H NMR on the reaction crude, [c] 20 mol% catalyst and violet LEDs, [d] without light.

Proposed mechanism of the photocatalytic [4+2]-dearomative cycloaddition

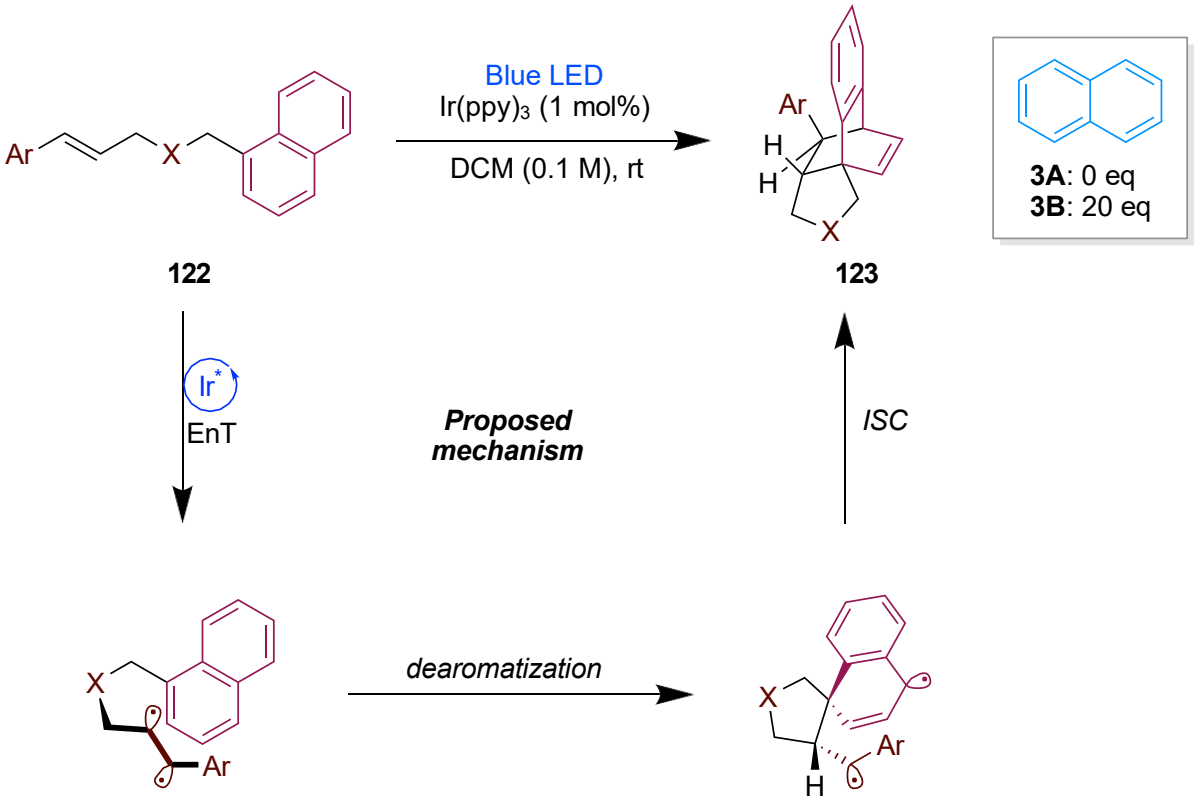

Table S10: Photocatalytic HAT-cyclization cascade

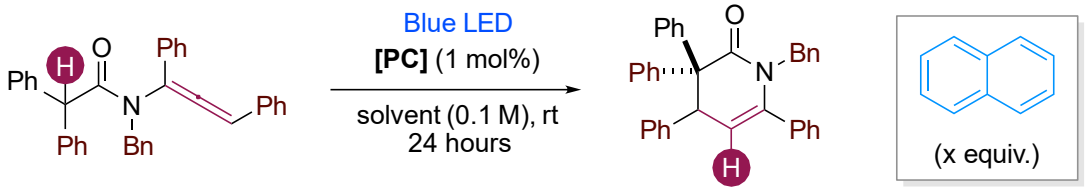

	124a		**125a**	
Entry	**[PC]**	**Naphthalene** (equiv.)	**Solvent**	**Yield** (%)
1	**PC1**	0	DMF	40
2	**PC1**	20	DMF	91
3	**PC2**	0	DMF	47
4	**PC2**	20	DMF	77
5 [b]	**PC3**	0	DMF	71
6 [b]	**PC3**	20	DMF	81
7	**PC1**	10	DMF	76
8	**PC1**	0	MeCN/CH_2Cl_2	36
9	**PC1**	20	MeCN/CH_2Cl_2	85
10	**PC1**	0	Toluene/CH_2Cl_2	37
11	**PC1**	20	Toluene/CH_2Cl_2	82
12 [c]	**PC1**	0 or 20	DMF	0
13	/	0 or 20	DMF	0

[a] Isolated yields, [b] 5 mol% catalyst and purple LEDs, [c] without light.

Proposed mechanism of the photocatalytic HAT-cyclization

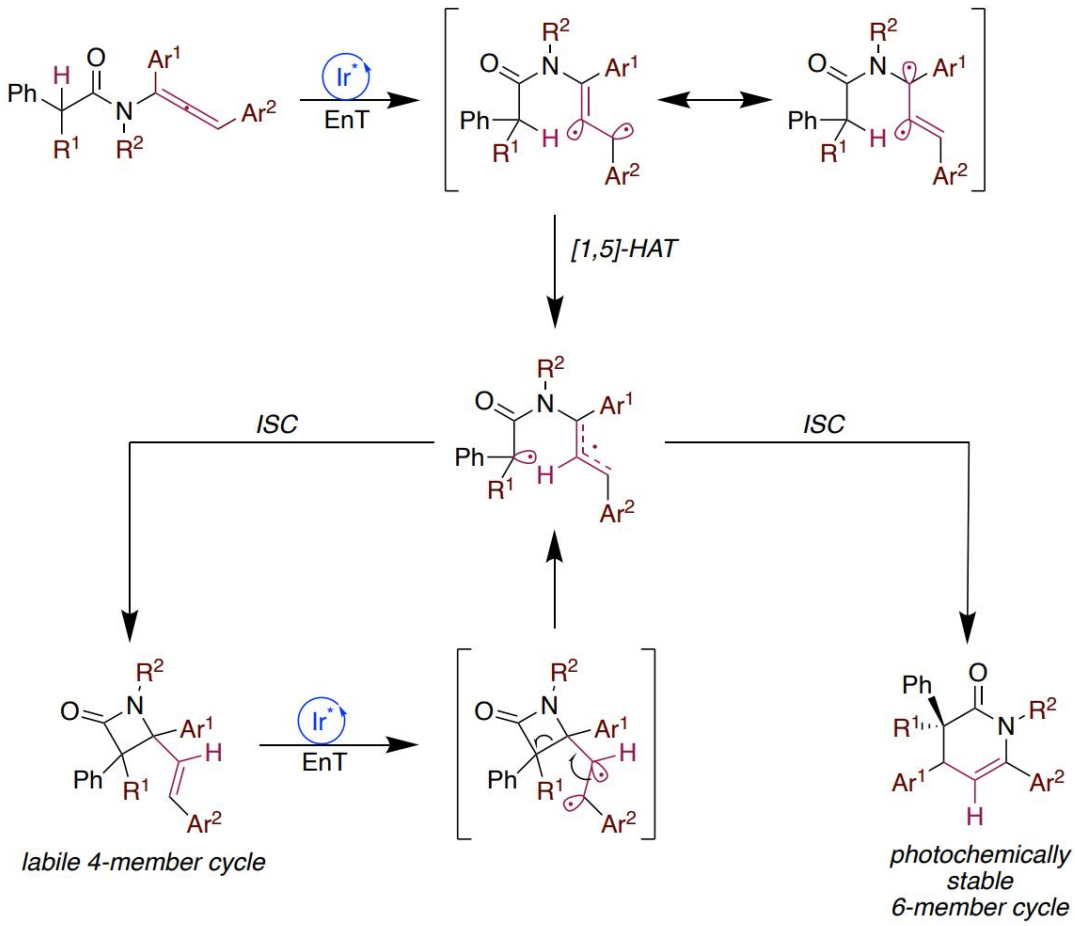

Photophysical experiments

Time-resolved laser flash spectroscopy

The laser pulse photolysis apparatus employed consists of a Flash lamp-pumped Q-switched SpitLight-100 Nd·YAG laser from InnoLas used at the fourth harmonic of its fundamental wavelength. The LP920-K monitor system (supplied by Edimburgh Instruments), arranged in a crossbeam configuration, consisted of a high intensity 450 W ozone free Xe arc lamp (operating in pulsed wave), a Czerny-Turner with triple grating turret monochromator, and a five-stage dynode photomultiplier. The signals were captured by means of a Tektronix TDS 3012C digital phosphor oscilloscope, and the data was processed using L900 software supplied by Edimburgh Instruments. Photoluminescence decays were collected by exciting the sample at 355 nm. The emission was collected at 525 nm. The same procedure was applied to **PC2**, by using its corresponding wavelengths. The 10 μM stock solution of the complex employed for the measurements was nitrogen saturated immediately prior to the use and then transferred into the capped cuvette by syringe. All solutions of the tested quenchers were similarly degassed by bubbling nitrogen into them immediately prior to use.

The linear regression for Stern-Vollmer plots provided the corresponding values of K_{sv} (= $K_{d\tau 0}$) and K_d, which were obtained through the following equation.

$I_0/I = 1 + K_{d\tau 0}[Q]$ (Equation 1)

Quenching of PC2 with Naphthalene

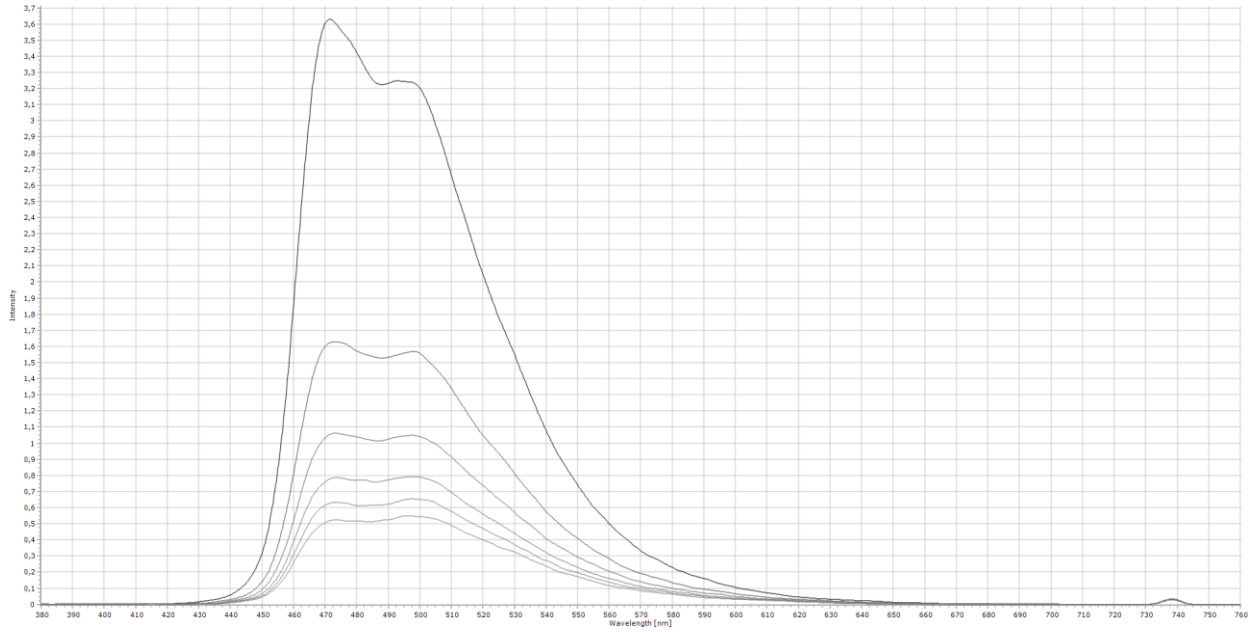

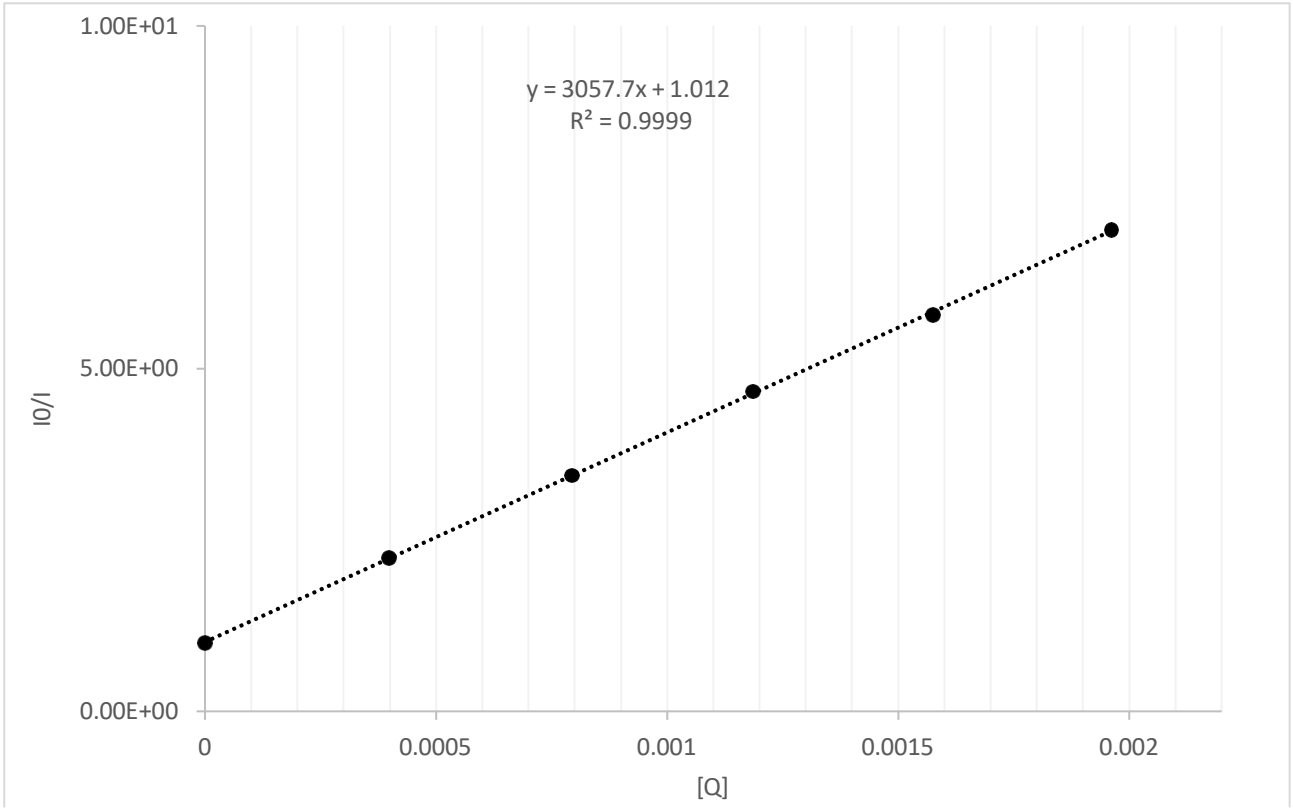

Stern-Volmer constant K_{SV} = 3057.8 M^{-1}

Quenching of PC2 with 1-Ph-Naphthalene

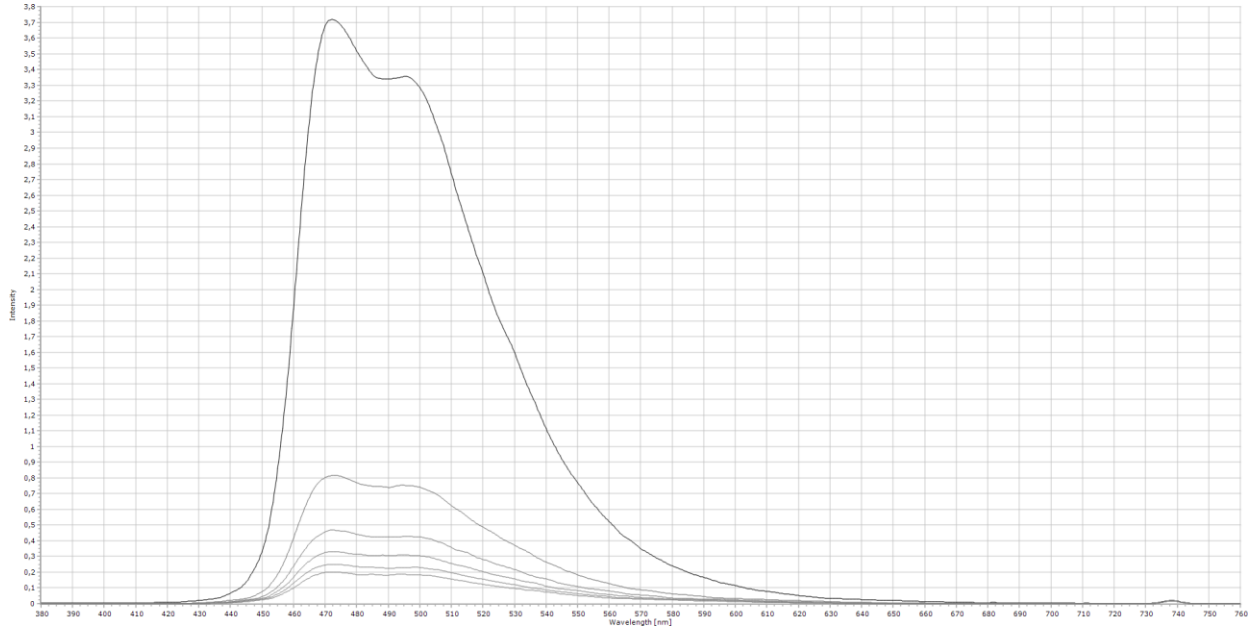

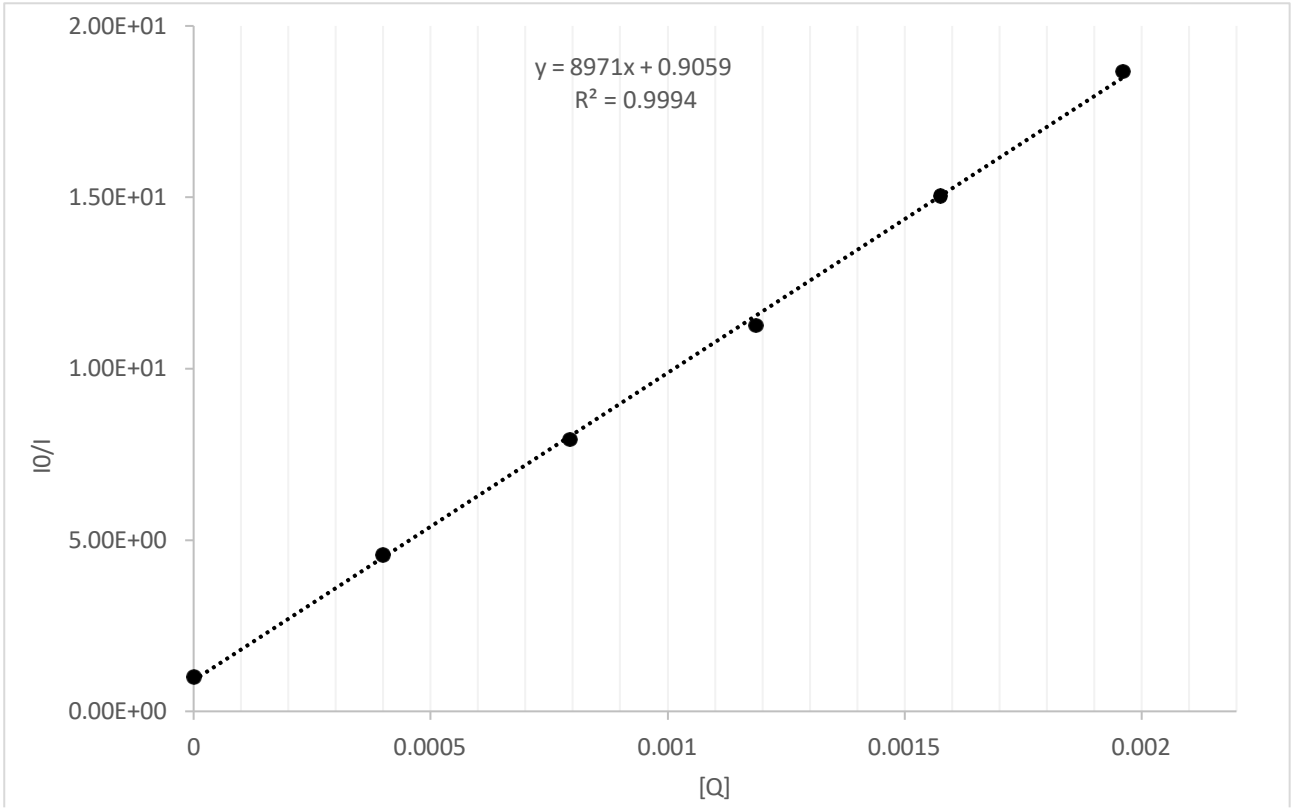

Stern-Volmer constant K_{SV} = 8971 M^{-1}

Quenching of PC1 with Naphthalene

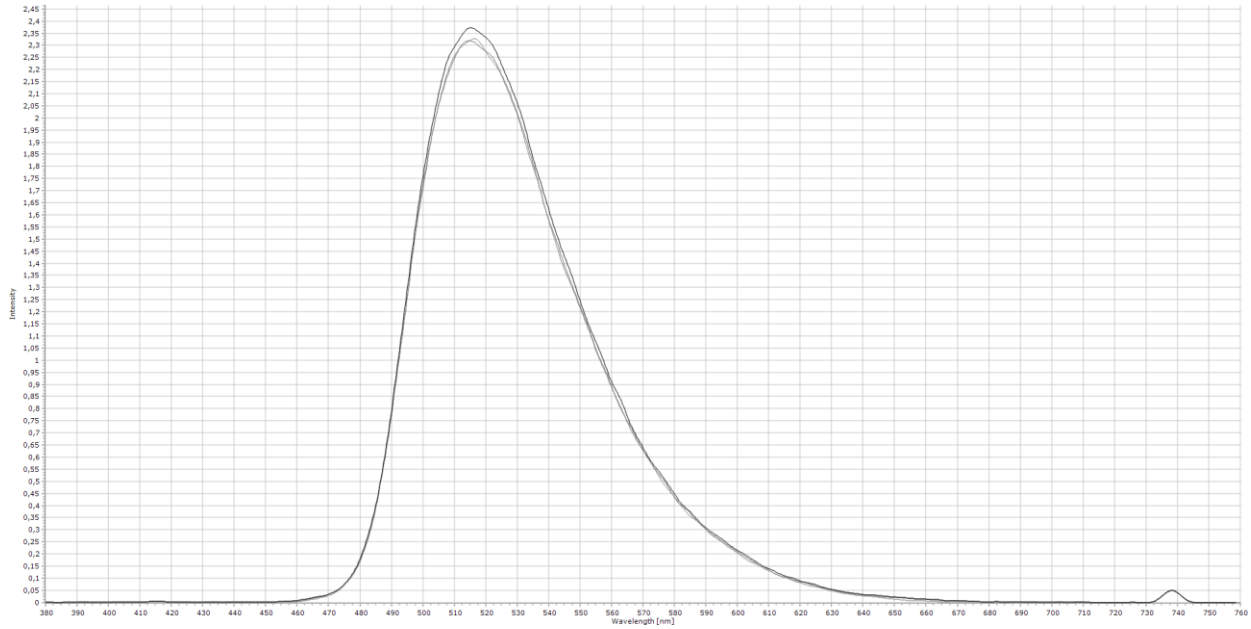

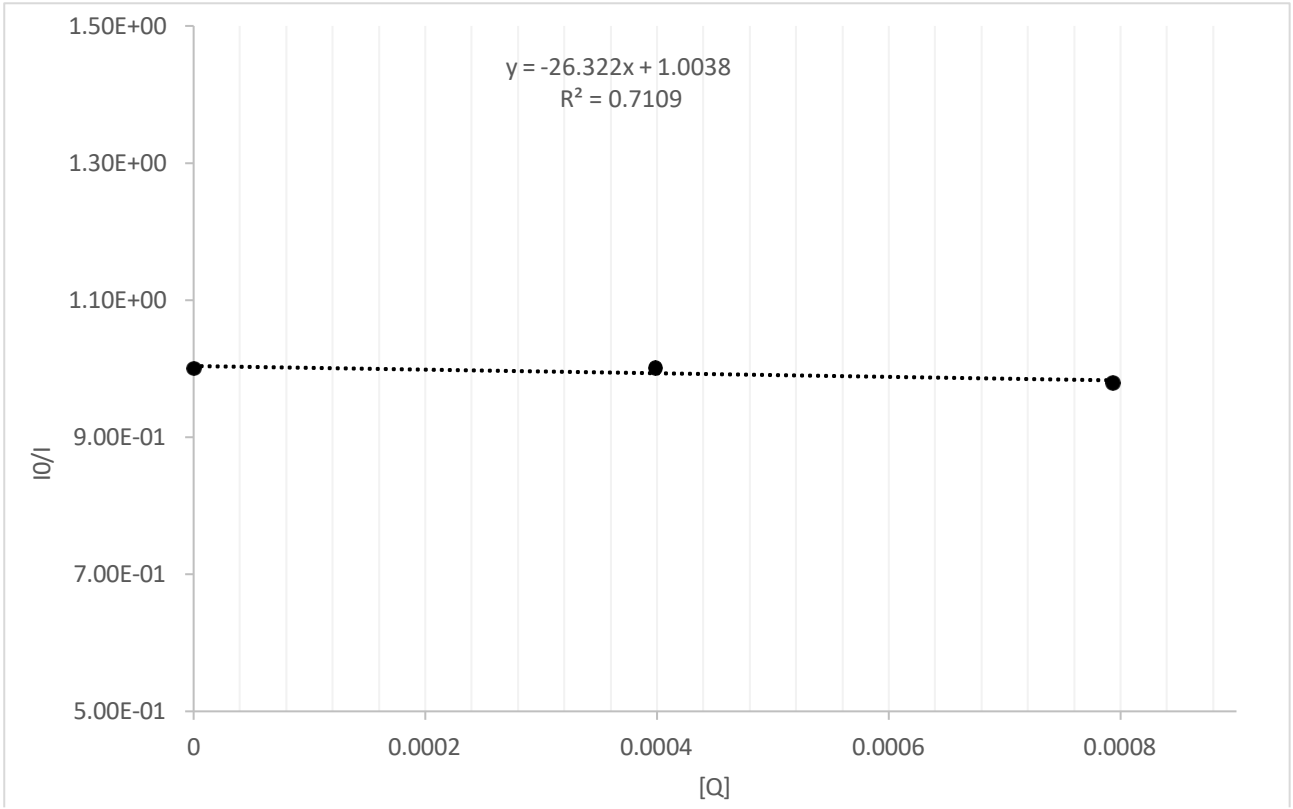

The value of the Stern-Volmer constant K_{SV} is ca. 0

Quenching of PC1 with 1-Ph-Naphthalene

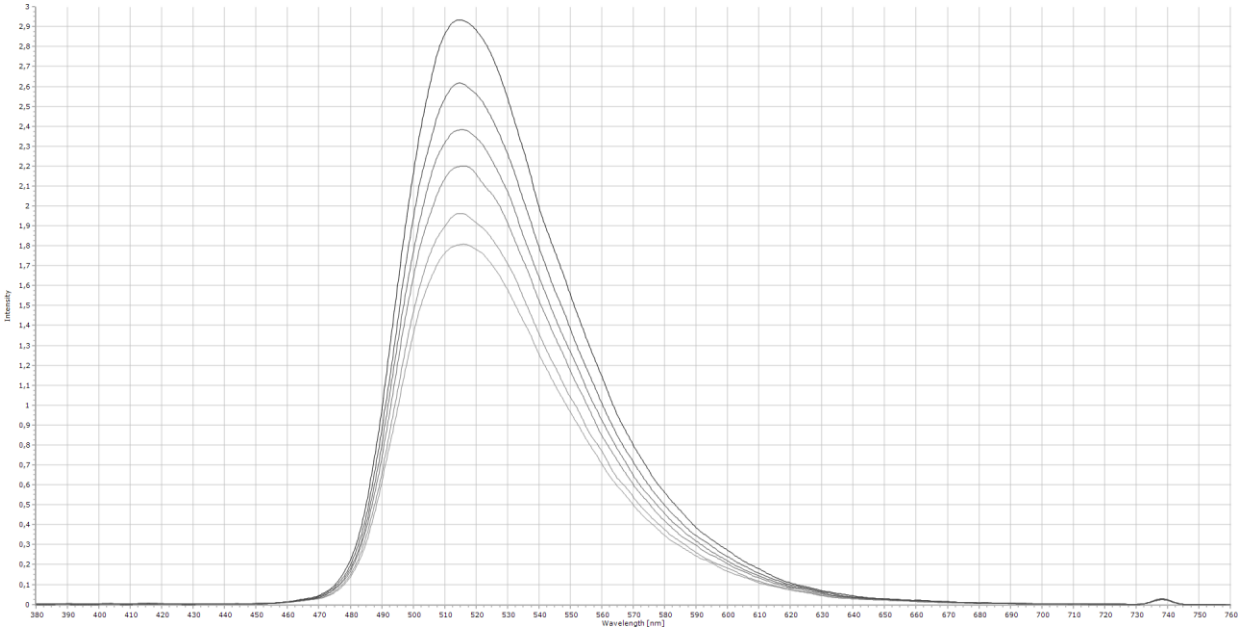

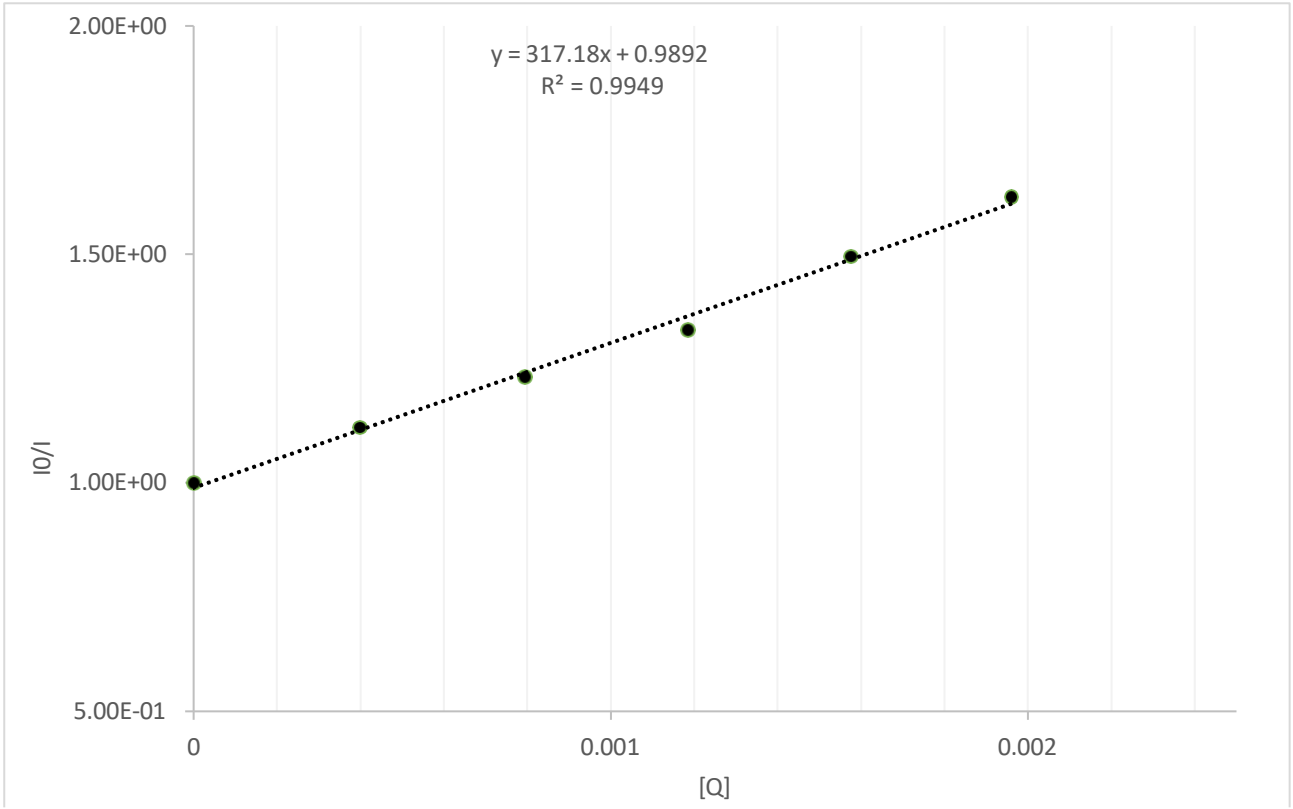

Stern-Volmer constant K_{SV} = 317.2 M^{-1} (notice the difference of more than one order of magnitude compared to values obtained using PC2).

Quenching of PC1 with N2

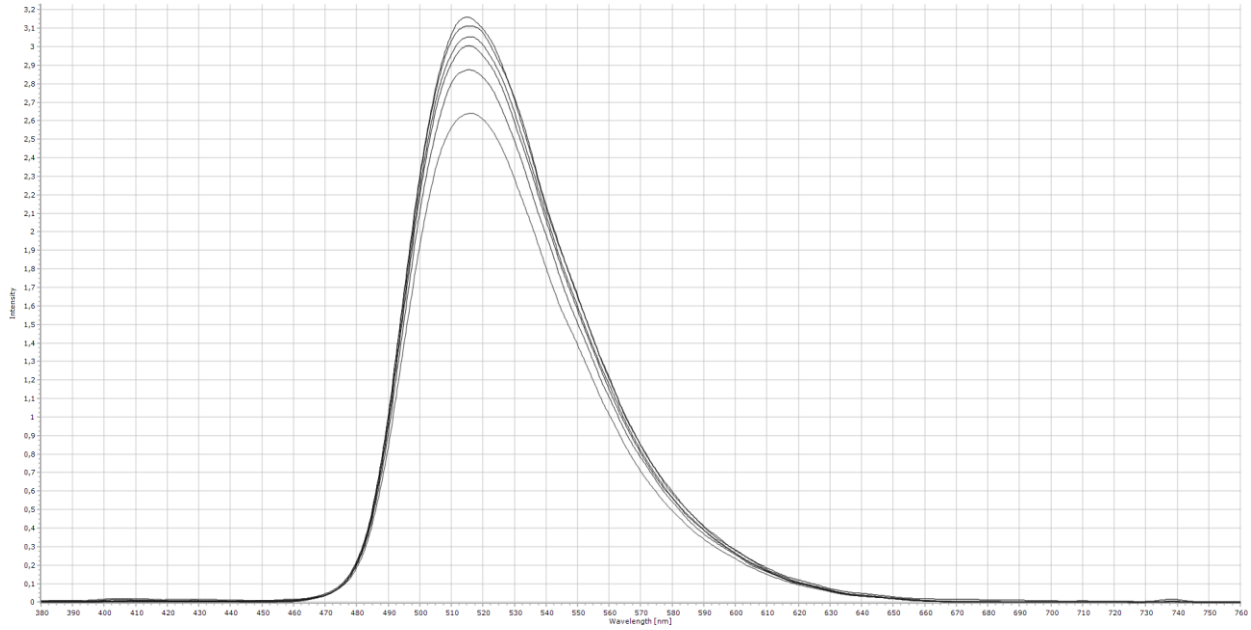

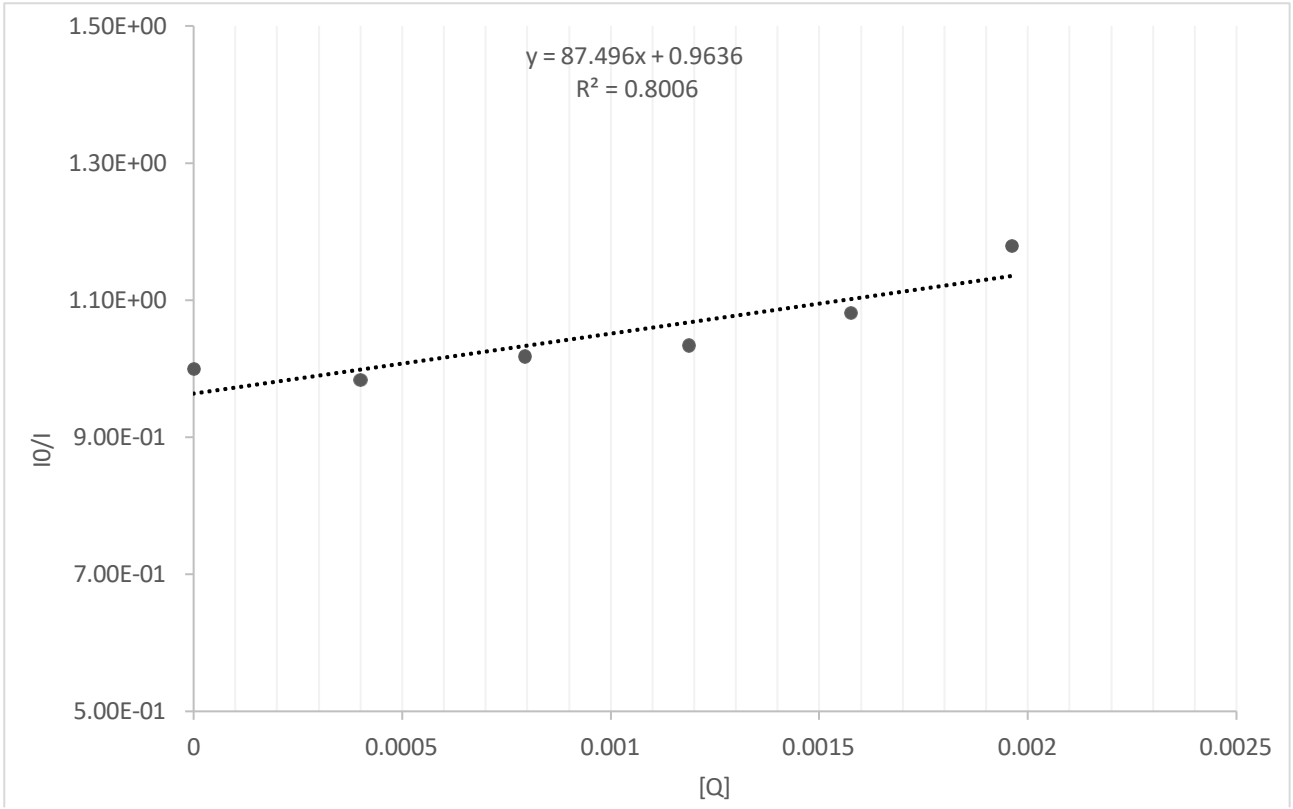

Stern-Volmer constant K_{SV} = 87.5 M^{-1}

UV-Vis absorption titrations

Absorption spectra of 120a + NP

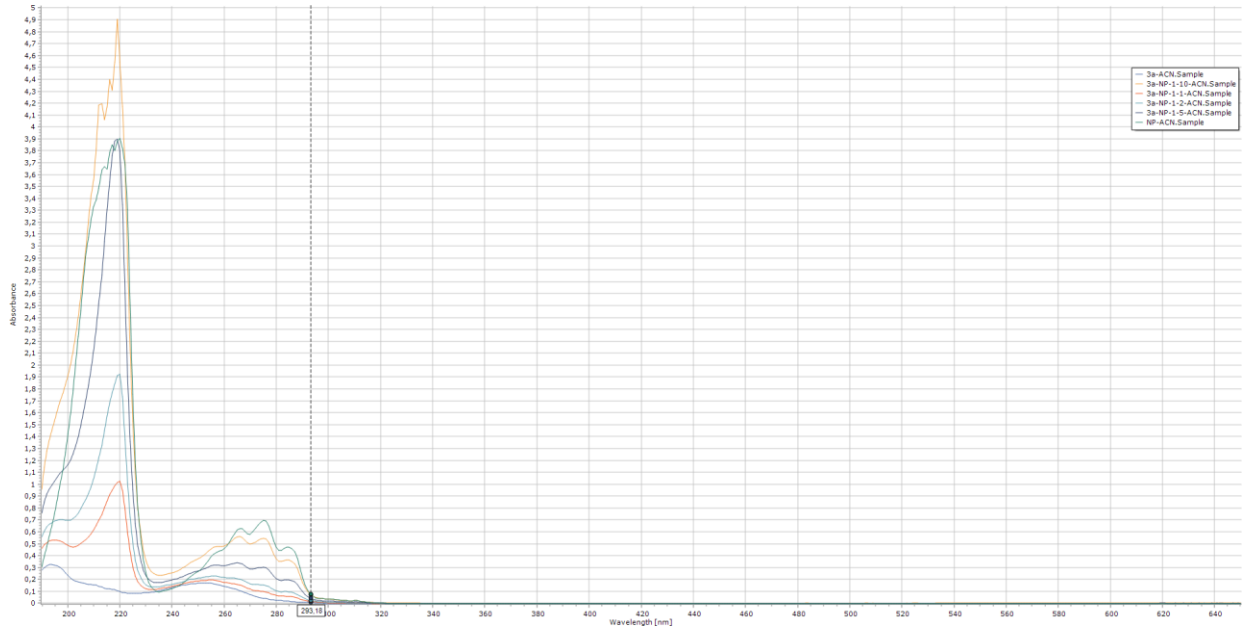

Absorption spectra of 120a + N4

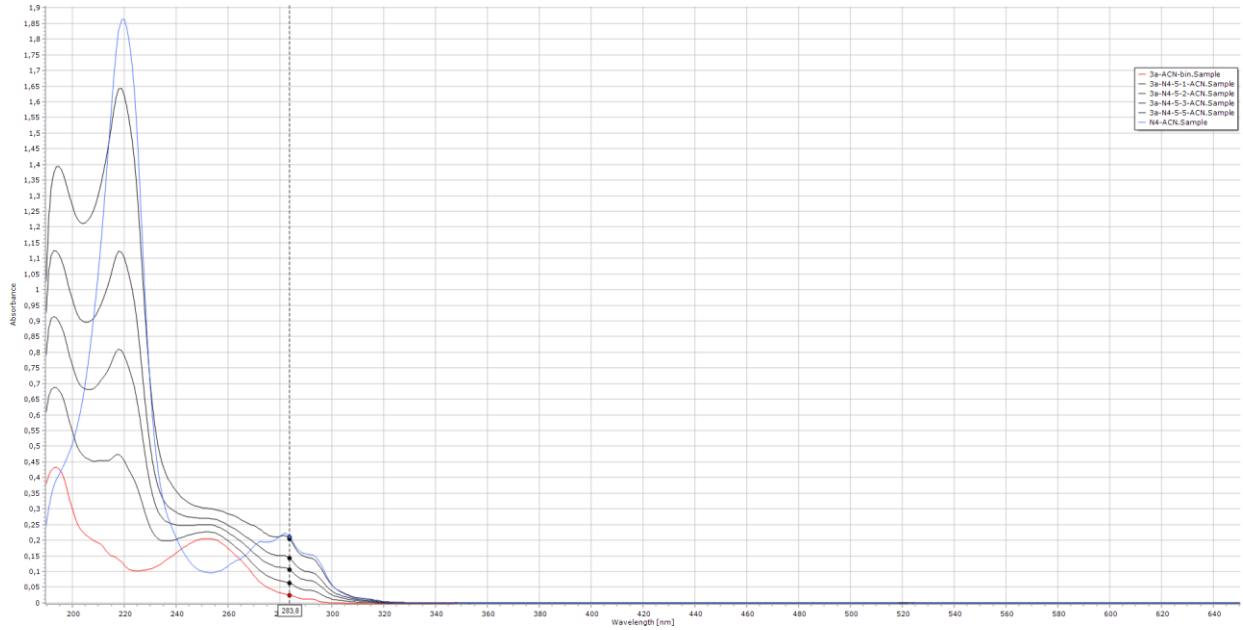

Absorption spectra of 122a + NP

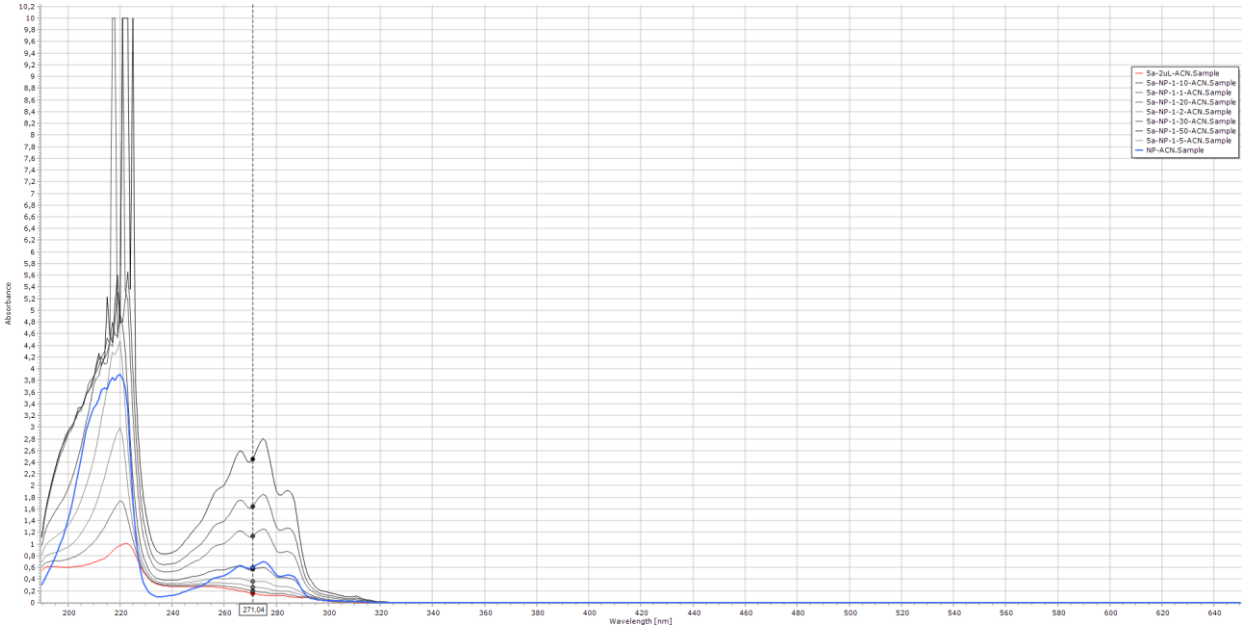

Absorption spectra of 122a + N4

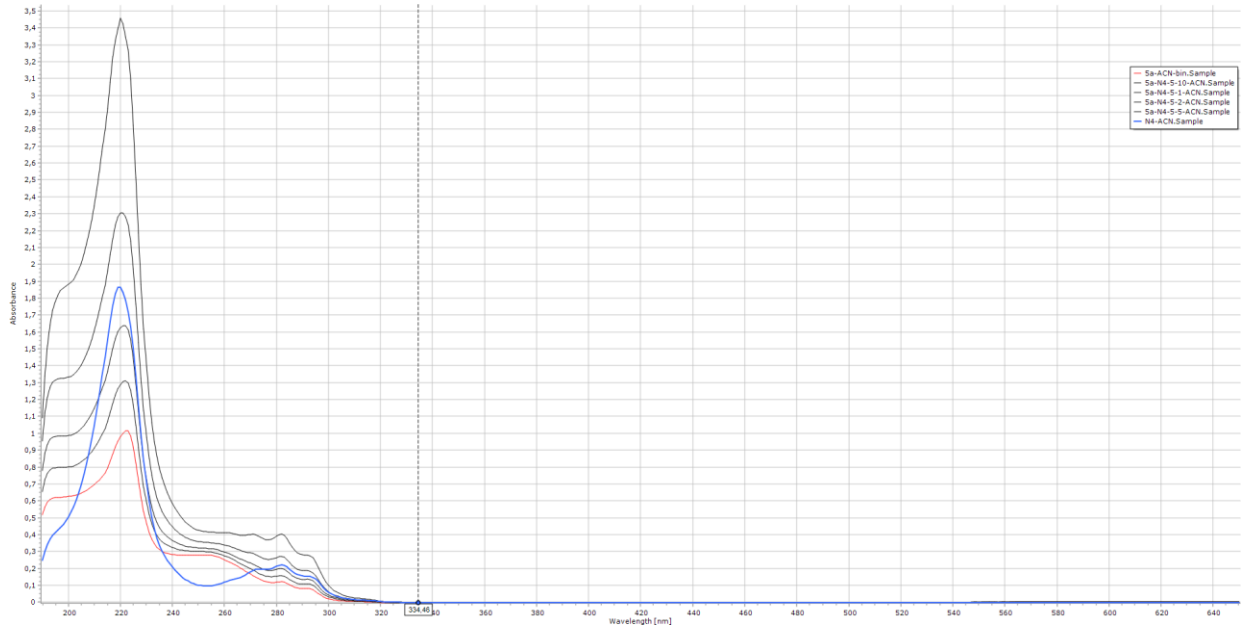

Absorption spectra of 124g + NP

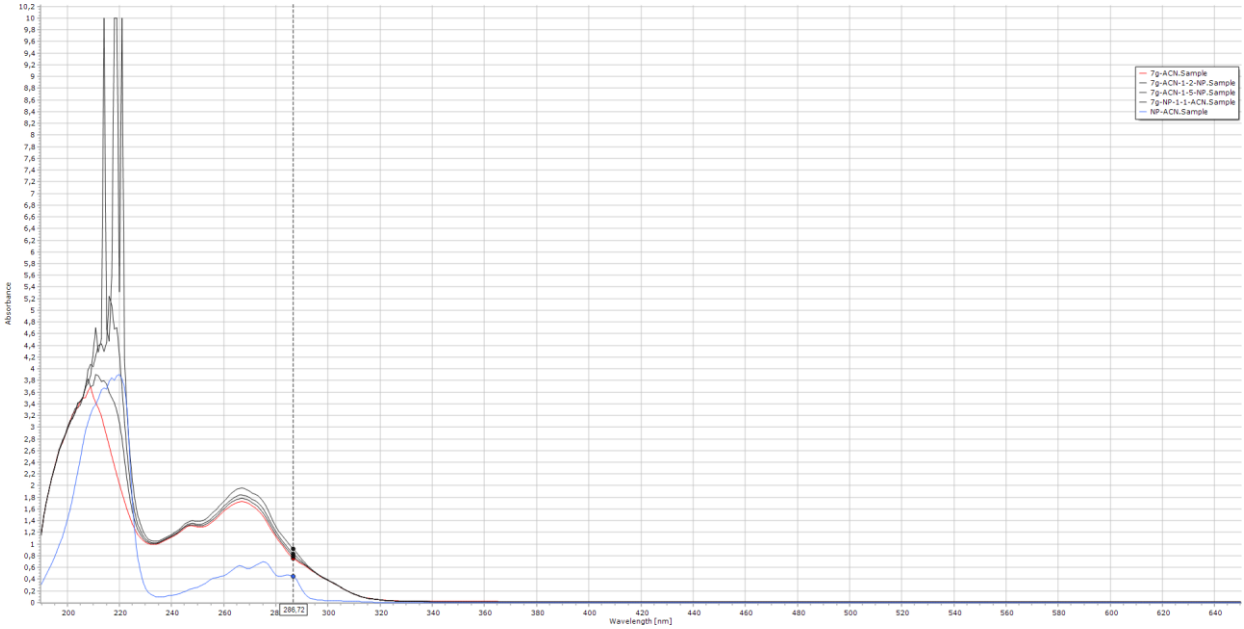

Absorption spectra of 124g + N4

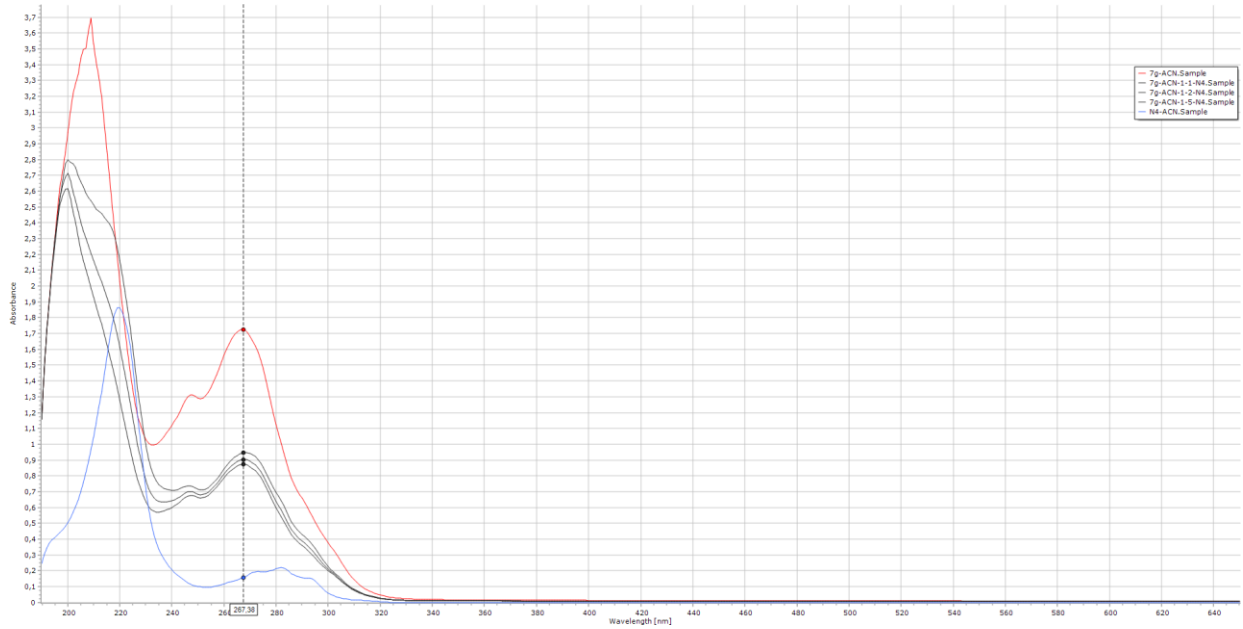

^{1}H NMR studies

Comparison for substrate **120b** with and without 20 equiv. of naphthalene

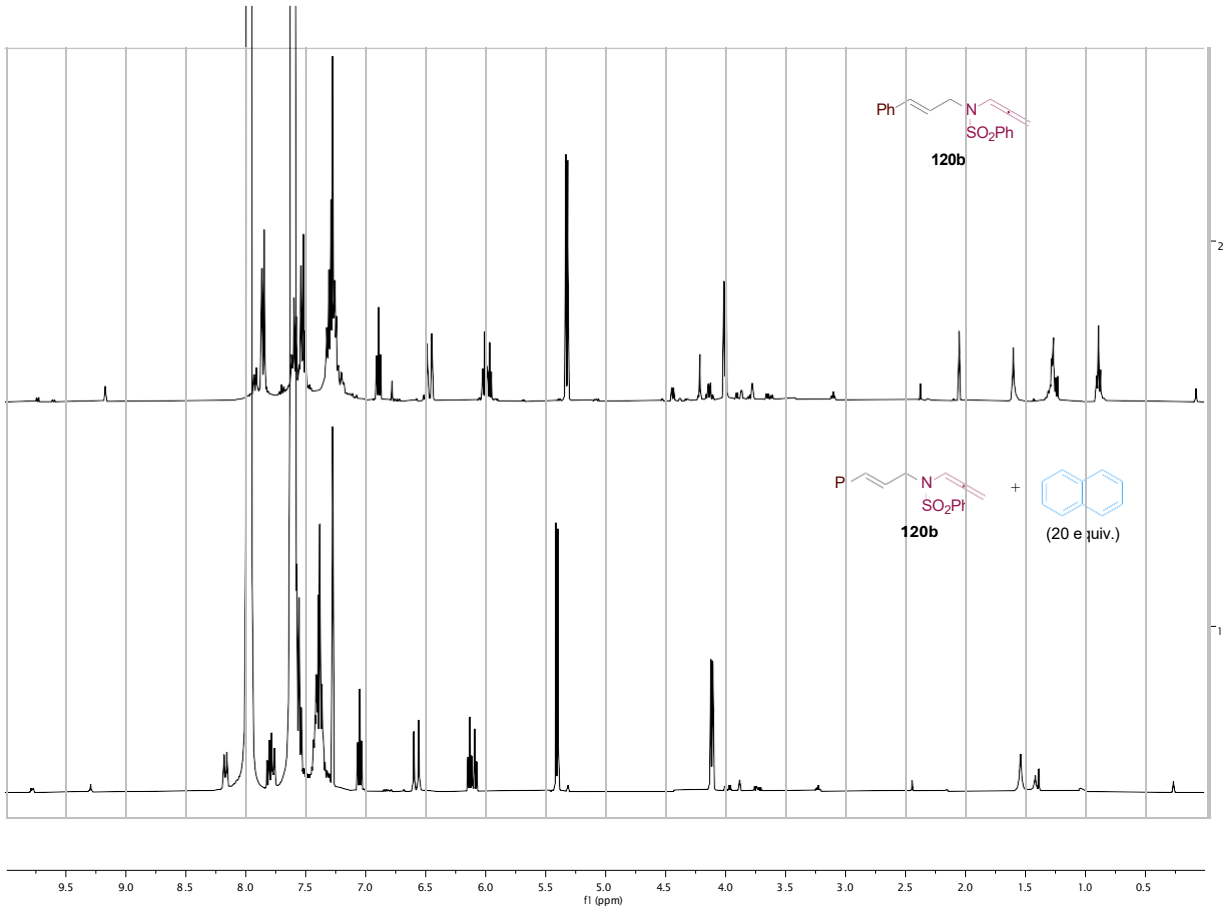

It is possible to observe how the presence of naphthalene leads to a deshielding of the protons of the substrate **120b**, more markedly involving the aromatic and alkenyl sites of the molecule. This is compatible with a dispersive π-π interaction between the substrate and the additive.

Enlargement of the aromatic and alkenyl zone

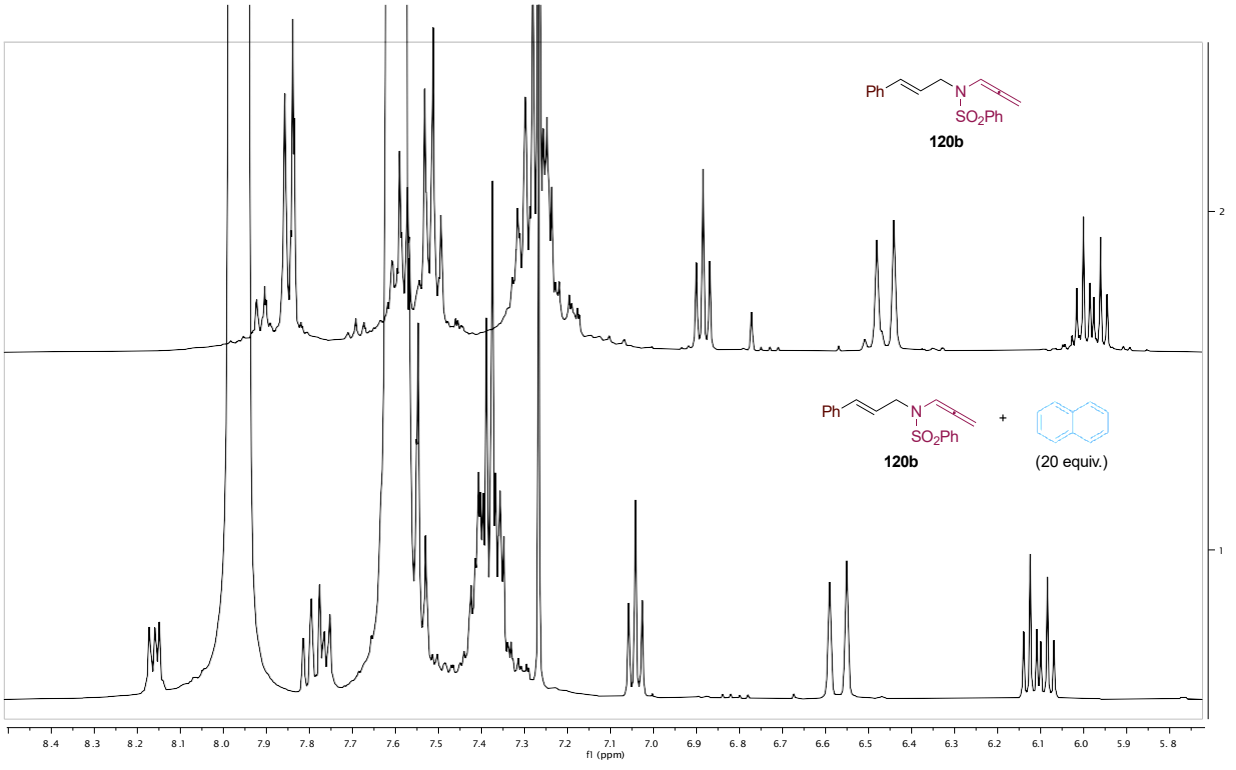

Enlargement of the aliphatic zone

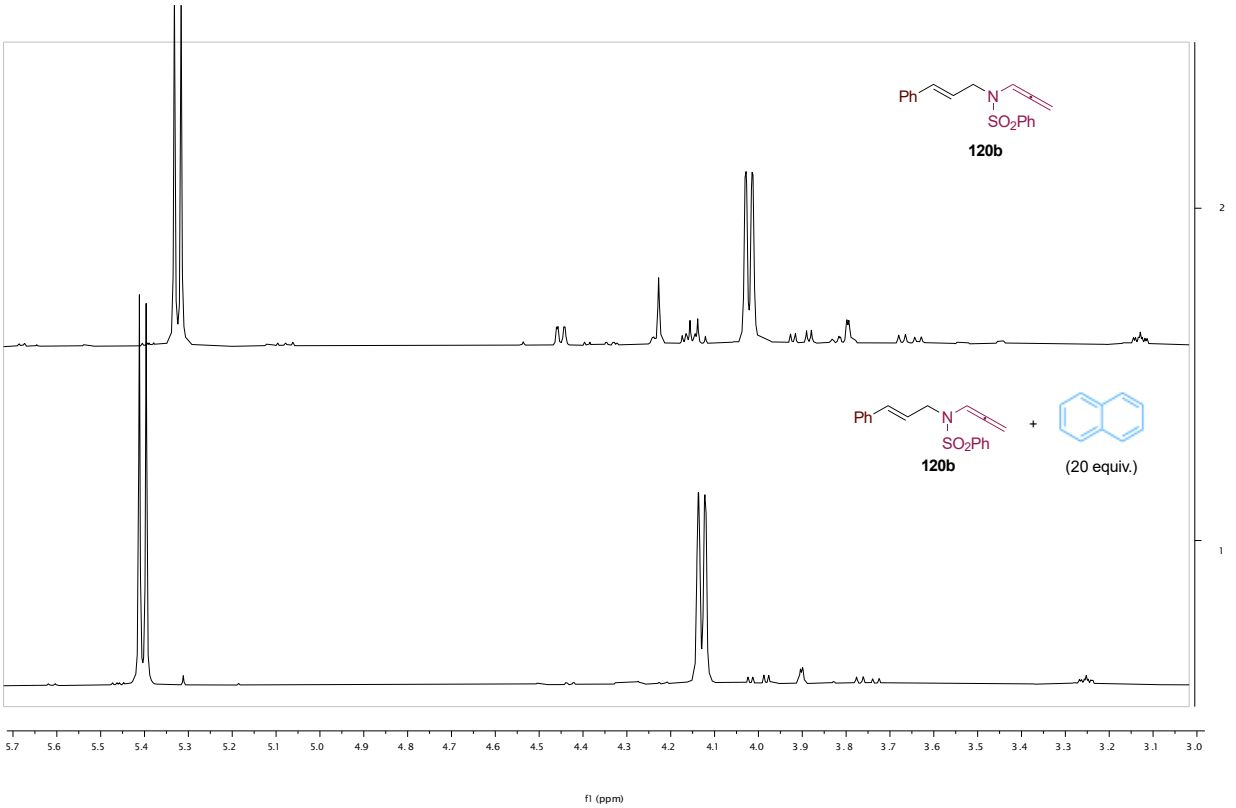

Partial decomposition of allenamide **120b** occurs through time, likely because of the acidity of chloroform; this process is slower in the presence of naphthalene (both NMR tubes were prepared in parallel from the same batch of substrate **120b**, and registered 1 hour later).

Comparison for substrate **122a** with and without 20 equiv. of naphthalene

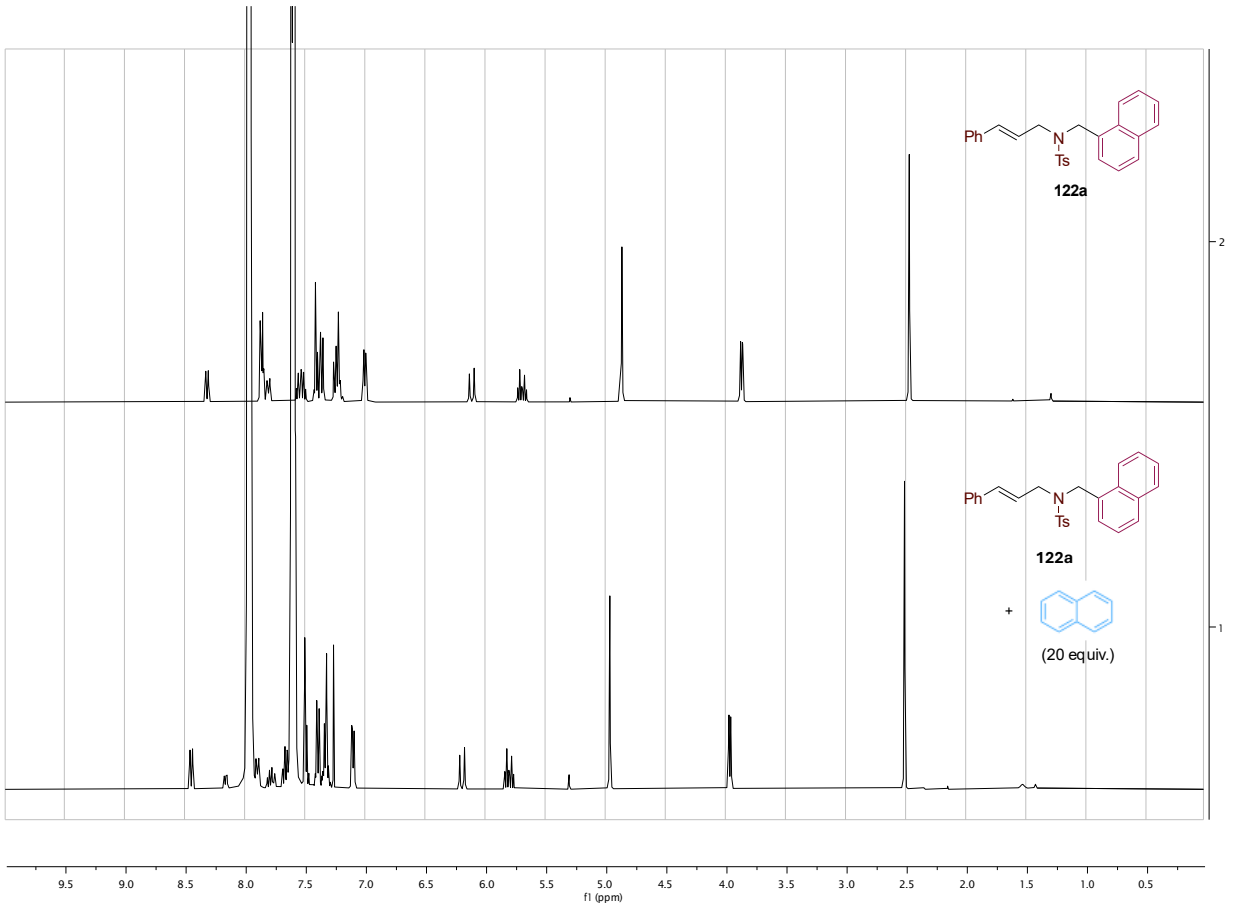

It is possible to observe how the presence of naphthalene leads to a deshielding of the protons of the substrate **122a**, more markedly involving the aromatic and alkenyl sites of the molecule. This is compatible with a dispersive π-π interaction between the substrate and the additive.

Enlargement of the aromatic zone

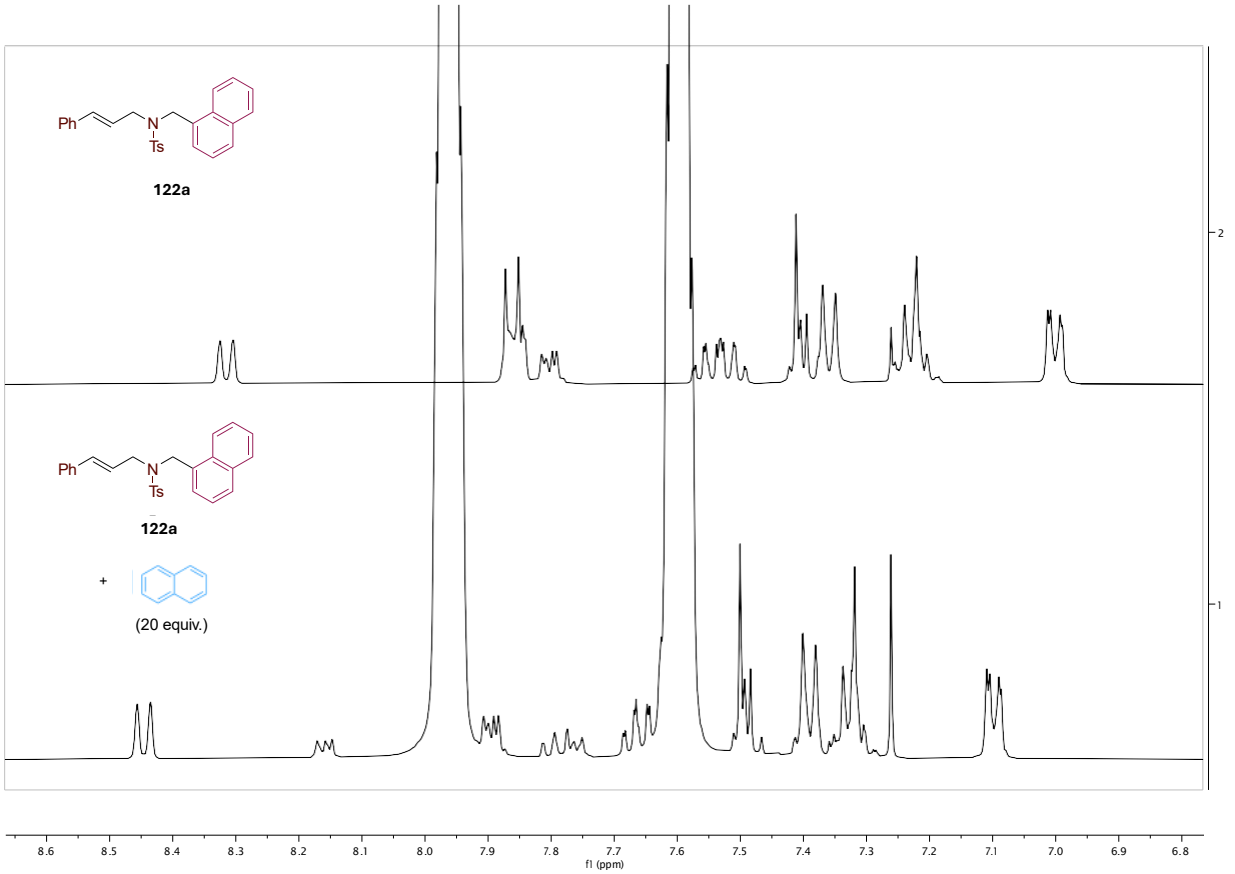

Enlargement of the alkenyl and benzylic zone

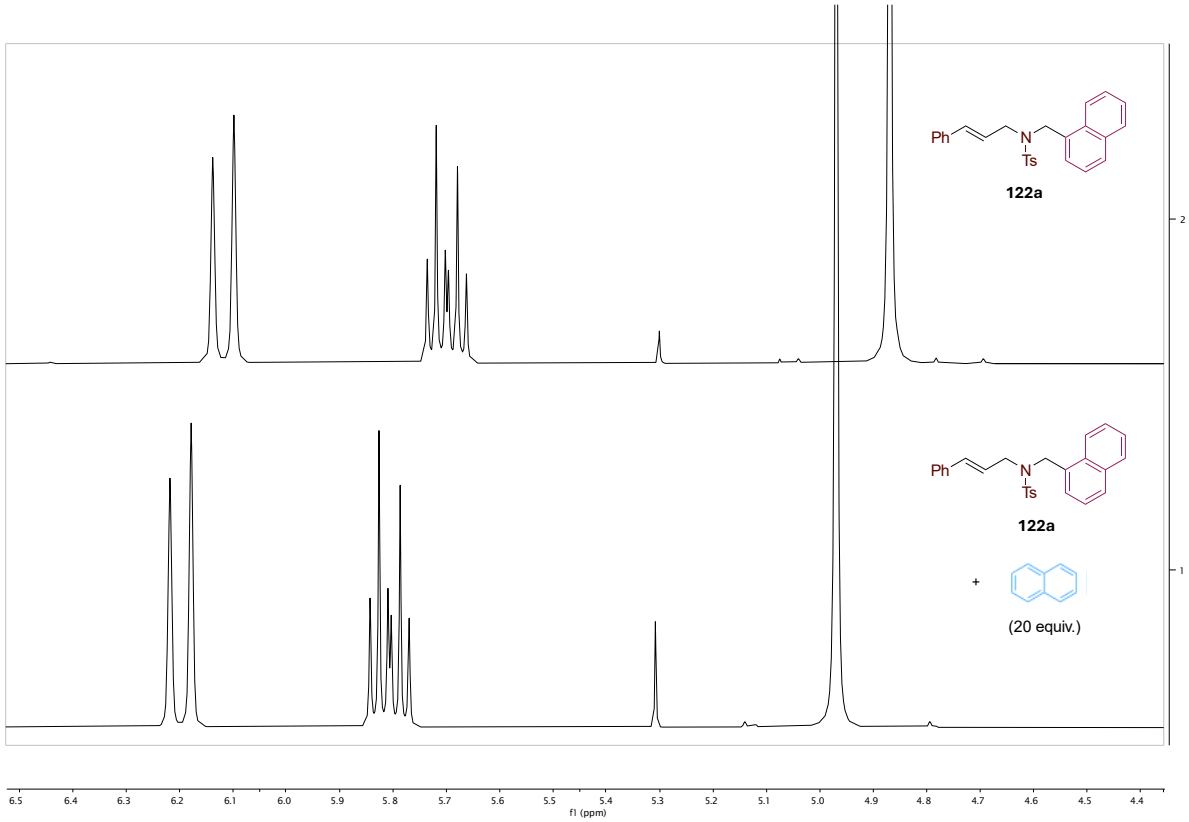

Enlargement of the aliphatic zone

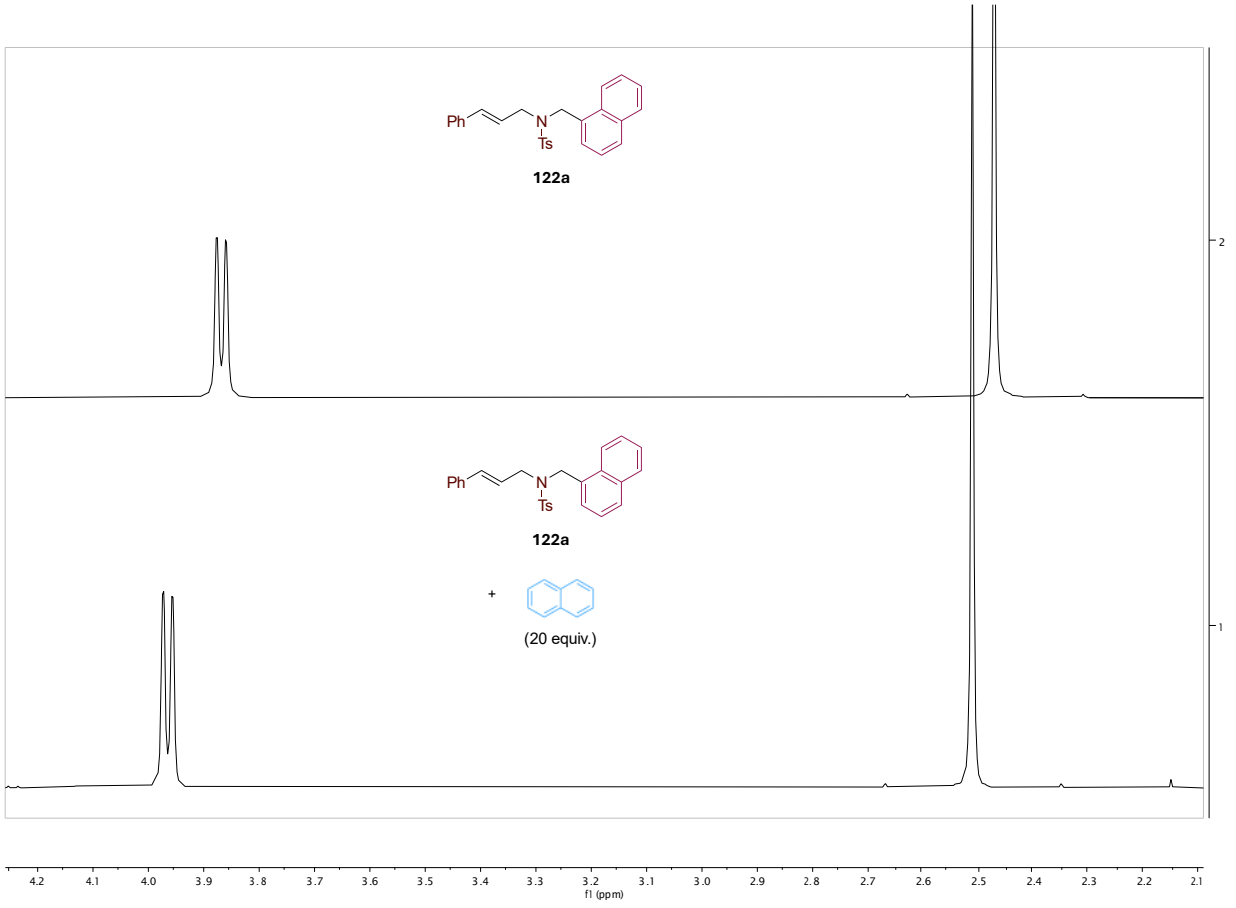

Comparison for product **123a** with and without 20 equiv. of naphthalene (reaction crude)

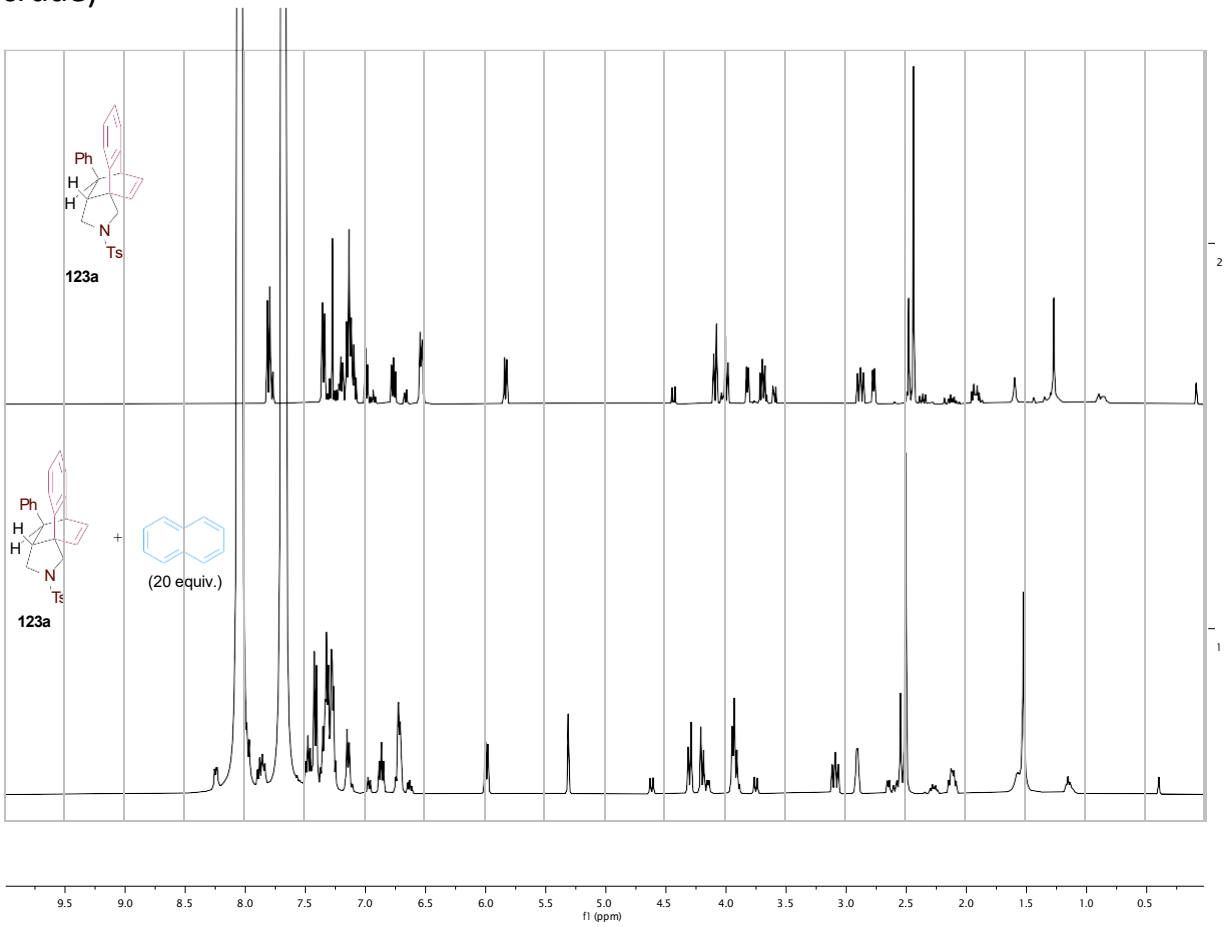

It is possible to observe how the presence of naphthalene leads to a deshielding of the protons of the product **123a**, more markedly involving the aromatic and alkenyl sites of the molecule. The shift of the various signal results to be even more evident than what was observed with the corresponding starting material **122a**. This could be consistent with a stronger interaction of **123a** with NP compared to that of **122a**. This would suggest that the use of NP or of a catalytic bi-NP would still require the presence of a stoichiometric amount of additive because the interaction with the product would hinder its turnover.

Enlargement of the aromatic and alkenyl zone

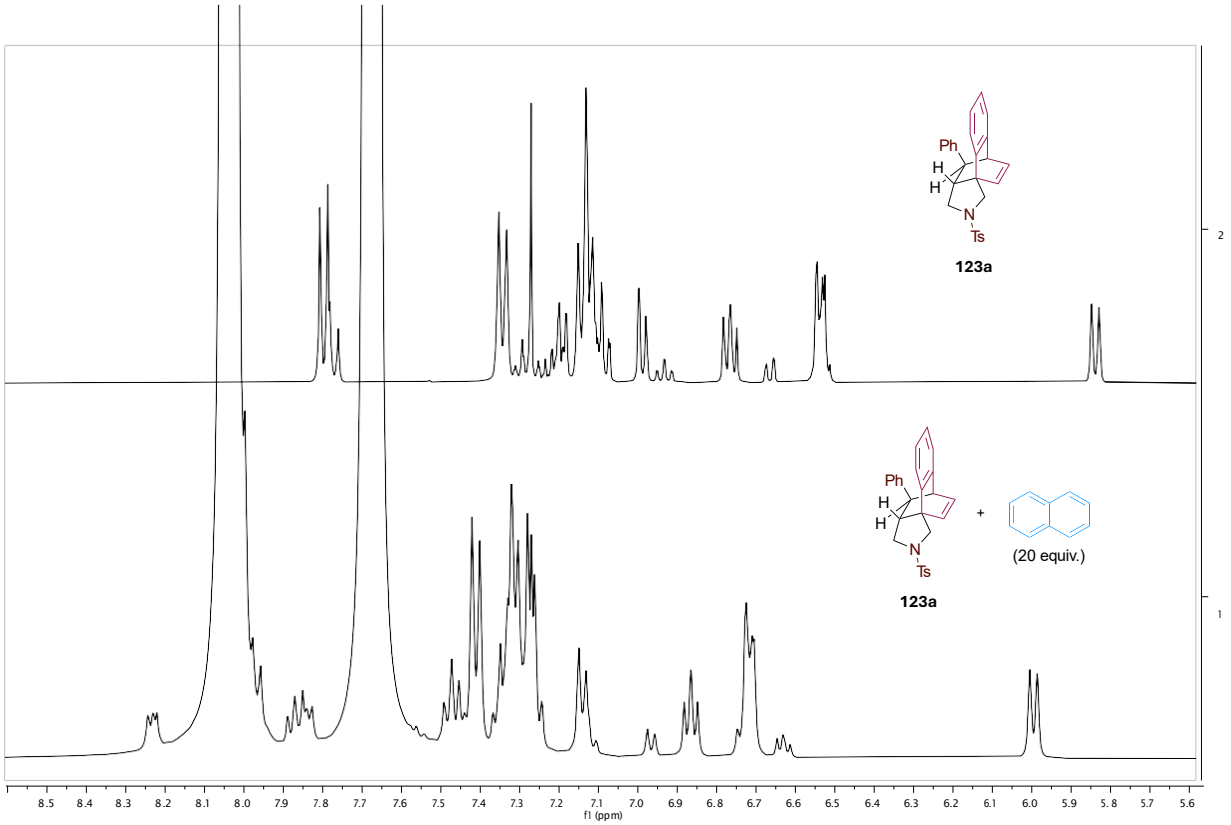

Enlargement of the aliphatic zone

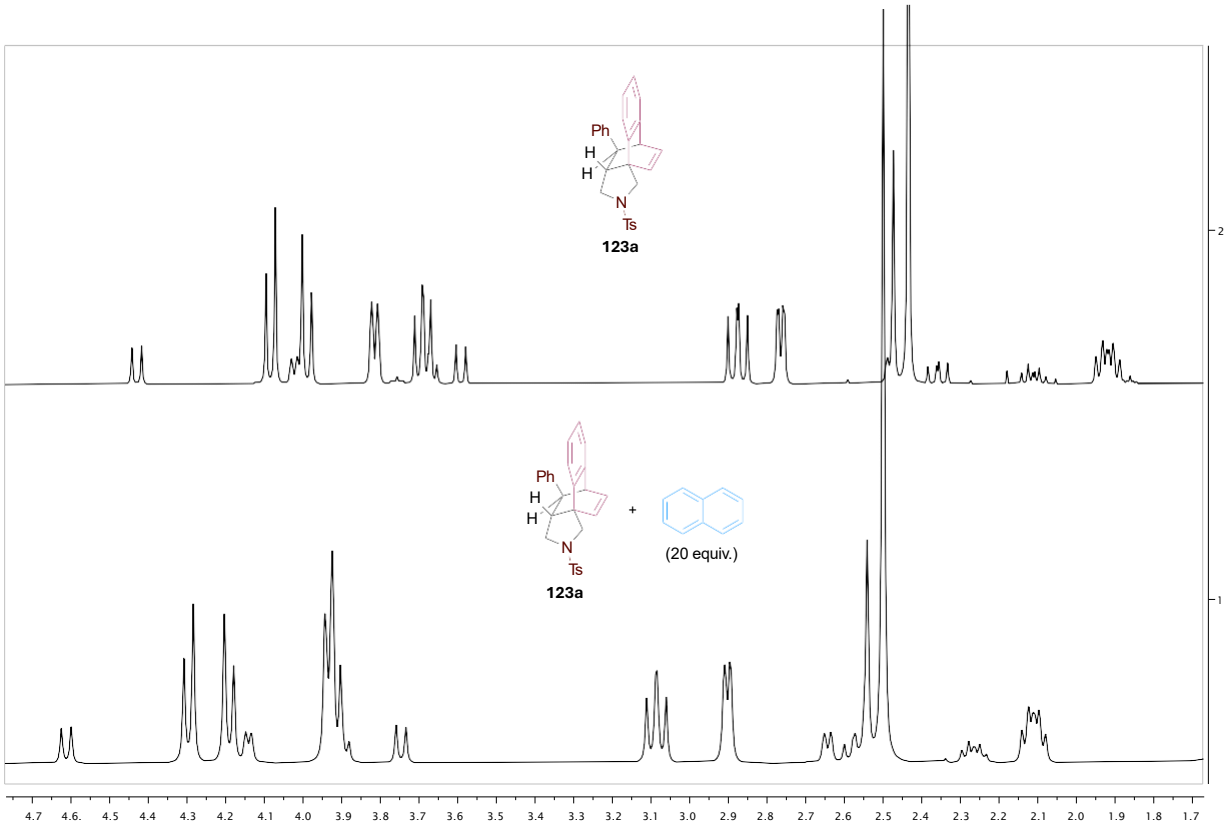

Synthesis and characterization of substrates

I. Synthesis of cinnamyl alcohols

Synthesis of **(*E*)-3-(2-chlorophenyl)prop-2-en-1-ol** (precursor of **120e**)

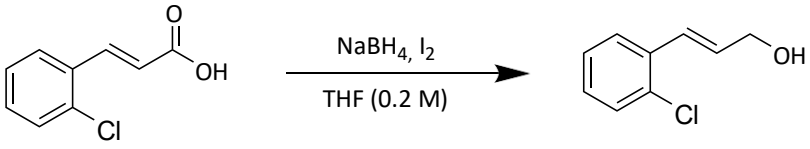

To a stirred mixture of 2-chlorocinnamic acid (915 mg, 5 mmol, 1 equiv.) in THF (9 mL) at 0 °C under nitrogen flow, $NaBH_4$ (228 mg, 6 mmol, 1.2 equiv.) dissolved in THF (7 mL) was added dropwise. Then a solution of I_2 (635 mg, 2.5 mmol, 0.5 eq) in THF (9 mL) was added dropwise over 30 minutes, and the reaction was stirred at rt for 12 h. The mixture was extracted with EtOAc (3x 10 mL) and the organic layer was dried over sodium sulfate and concentrated under reduced pressure. The crude was purified by chromatography on silica gel (*n*-hexane/EtOAc) affording the cinnamyl alcohol as a colorless oil (598 mg, 71% yield).

II. Synthesis of cinnamyl amines

Synthesis of N-cinnamyl-4-methyl-N-((1-methyl-1H-indol-3-yl)methyl)benzenesulfonamide (**128a**)

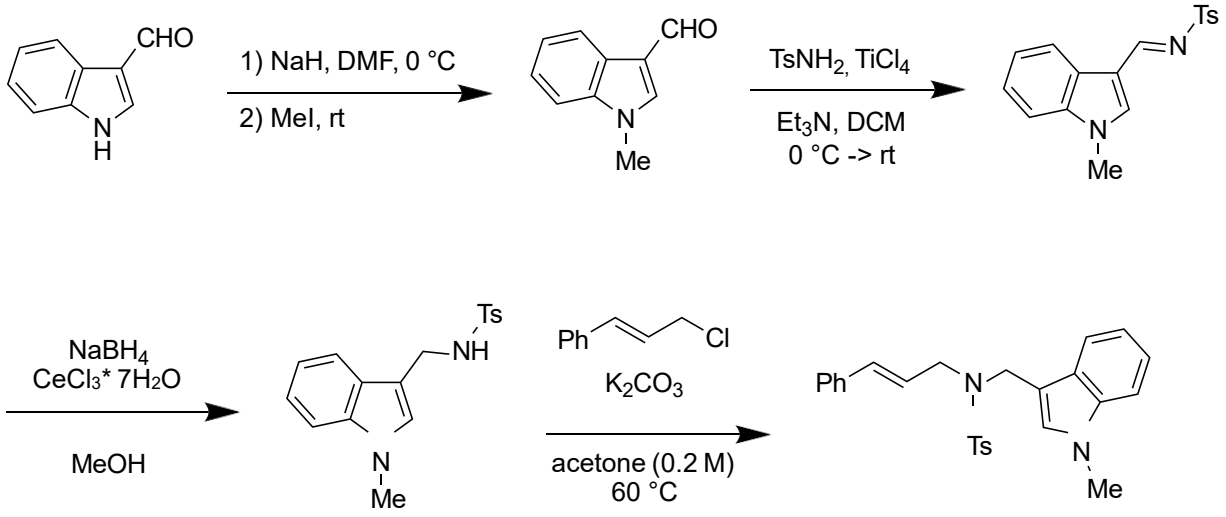

To a stirred mixture of 1H-indole-3-carbaldehyde (2.2 g, 15 mmol, 1 equiv.) in DMF (60 mL, 0.25 M) at 0 °C under nitrogen flow, NaH (60% in mineral oil, 780 mg, 19.5 mmol, 1.3 equiv.) was added. The mixture was allowed to stir at 0 °C for 45 minutes. Then CH_3I (1.9 mL, 30 mmol, 2 equiv.) dissolved in DMF (5 mL) was added dropwise over 15 minutes and the reaction was stirred at rt overnight. After complete conversion of the indole, the reaction was quenched with the addition of water (50 mL) and the mixture was extracted with diethyl ether (3x50 mL). The organic layer was dried over sodium sulphate and the solvent was removed under reduced pressure. The resulting crude was purified by flash chromatography on silica gel (*n*-hexane - EtOAc 4:1) affording the *N-Methyl- Indole-carbaldehyde* as a yellow solid (2.0 g, 84% yield).

To a stirred mixture of *N-Methyl-Indole-carbaldehyde* (2.0 g, 12.6 mmol, 1 equiv.) in DCM (63 mL, 0.2 M) at 0 °C under nitrogen flow, 4-methylbenzenesulfonamide (2.7 g, 15.6 mmol, 1.2 equiv.) was added. Then a solution of $TiCl_4$ 1M in DCM (6.93 mL, 6.9 mmol, 0.55 equiv.) was added over 5 minutes and the mixture was allowed to stir at 0 °C for 2 h and then overnight at r.t. After complete conversion of the *N-Methyl-Indole-carbaldehyde*, the reaction was filtered under vacuum to remove the solid, then the organic layer was washed with water and a saturated solution of NH_4Cl. The organic layer was dried over sodium sulphate and the solvent was removed under reduced pressure. The resulting crude was used without further purification. Yellow solid (12.6 mmol, 99% yield).

To a stirred mixture of the imine (2.0 g, 6.4 mmol, 1 equiv.) and $CeCl_3*H_2O$ (307.2 mg, 6.4 mmol, 1 equiv.) in MeOH (25 mL, 0.3 M) at 0 °C, $NaBH_4$ (242 mg, 6.4 mmol, 1.2 equiv.) was added. Then the reaction was stirred at rt overnight. After complete conversion of the substrate, the solvent was removed under reduced pressure and the solid residue was washed with water (30 mL) and extracted with EtOAc (3x 30 mL). The organic layer was dried over sodium sulfate and concentrated under reduced pressure. The resulting crude of *4-methyl-N-((1-methyl-1H-indol-3-yl)methyl)benzenesulfonamide* was used without further purification, white solid (1.3 g, 66% yield).

To a stirred mixture of *4-methyl-N-((1-methyl-1H-indol-3-yl)methyl)benzenesulfonamide* (500 mg, 1.6 mmol, 1 equiv.) and K_2CO_3 (663 mg, 4.8 mmol, 3 equiv.) in acetone (8 mL, 0.2 M) at 0 °C, cinnamyl chloride (293 mg, 270 µL, 1.92 mmol, 1.2 equiv.) was added. The reaction was allowed to stir at 60 °C overnight. After complete consumption of the amine, the mixture was cooled to room temperature,

diluted with water and extracted with EtOAc (3 x 30 mL). The organic layer was dried over Na_2SO_4, filtered, and concentrated under reduced pressure. The resulting crude was purified by chromatography on silica gel (*n*-hexane/EtOAc 8:1) affording *N-cinnamyl-4-methyl-N-((1-methyl- 1H-indol-3-yl)methyl)benzenesulfonamide* **128a** as a yellow solid (235 mg, 34% yield).

III. Synthesis of naphthyl-derivatives

Synthesis of ***N*-cinnamyl-4-methyl-*N*-(naphthalen-1-ylmethyl)benzenesulfonamide (122a)**

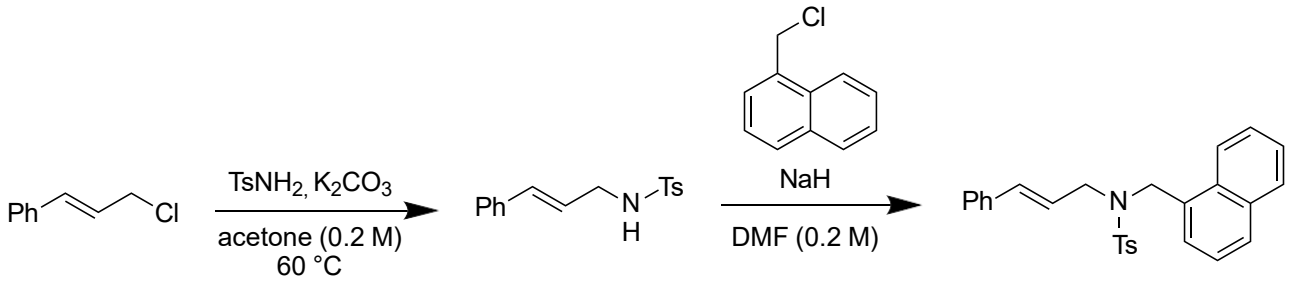

p-Toluenesulfonamide (1.30 g, 7.5 mmol, 1.5 equiv.) was added in a Schlenk tube equipped with a magnetic stirring bar and K_2CO_3 (1,28 g, 15 mmol, 3 equiv.). Acetone (25 mL, 0.2 M) was added, and the mixture was stirred at room temperature for 30 minutes. Cinnamyl chloride (763.1 mg, 5 mmol, 1.0 equiv.) was then added. The reaction mixture was stirred at 60 °C overnight. After complete consumption of the the cinnamyl chloride, the mixture was cooled to room temperature, diluted with water and extracted with EtOAc (3 x 30 mL). The organic layer was dried over Na_2SO_4, filtered and concentrated under reduced pressure. The resulting crude was purified by flash chromatography on silica gel (hexane/EtOAc 9:1) affording cinnamyltosylamide as a white solid (452 mg, 31% yield).

The cinnamyltosylamide (452 mg, 1.6 mmol, 1 equiv.) was dissolved in DMF (0.2 M). Then NaH (60% in mineral oil, 128 mg, 3.2 mmol, 2.0 equiv.) was added slowly at 0° C under vigorous stirring. The resulting mixture was stirred for 30 minutes at room temperature prior to the addition of 1-(chloromethyl)naphtalene (422 mg, 2.4 mmol, 1.5 equiv.). The resulting mixture was then stirred at room temperature overnight. After completion, the reaction mixture was quenched with water and a saturated solution of NH_4Cl. The mixture was extracted with EtOAc (3 x 30 mL) and the organic layers were dried over Na_2SO_4 and concentrated under reduced pressure. The resulting crude was purified by chromatography on silica gel (*n*-hexane/EtOAc 15:1) affording cinnamyltosylamide as a white solid (360 mg, 53% yield).

Synthesis of **N-cinnamyl-N-(naphthalen-1-ylmethyl)benzamide** (**122b**)

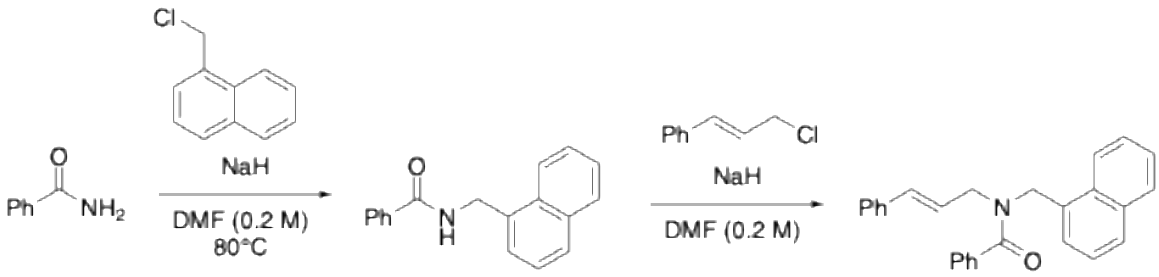

Benzamide (1.20 g, 10 mmol, 2 equiv.) was added in a Schlenk tube equipped with a magnetic stirring bar and dissolved in DMF (20 mL, 0.2 M). Then NaH (60% in mineral oil, 240 mg, 10 mmol, 2.0 equiv.) was added slowly at 0° C under vigorous stirring. The resulting mixture was stirred for 30 minutes at room temperature prior to the addition of 1-(chloromethyl)-naphtalene (880 mg, 5 mmol, 1.0 equiv.). The reaction mixture was stirred at 80 °C overnight. After completion of the reaction, the mixture was cooled to room temperature, quenched with a saturated solution of NH_4Cl and extracted with EtOAc (3 x 30 mL). The organic layer was dried over Na_2SO_4, filtered and concentrated under reduced pressure. The resulting crude was purified by flash chromatography on silica gel (*n*-hexane/EtOAc 9:1) affording the *N*-(naphthalen-1-ylmethyl)-benzamide as a white solid (236 mg, 0.9 mmol, 18% yield).

The resulting *N*-(naphthalen-1-ylmethyl)-benzamide (236 mg, 0.9 mmol, 1 equiv.) was dissolved in DMF (0.2 M). Then NaH (60% in mineral oil, 48 mg, 2 mmol, 2.1 equiv.) was added slowly at 0° C under vigorous stirring. The resulting mixture was stirred for 30 minutes at room temperature prior to the addition of cinnamyl chloride (229 mg, 1.45 mmol, 1.5 equiv.). The resulting mixture was then stirred at room temperature overnight. After completion, the reaction mixture quenched with water and a saturated solution of NH_4Cl. The resulting mixture was extracted with EtOAc (3 x 30 mL) and the organic layers were dried over Na_2SO_4 and concentrated under reduced pressure. The crude was purified by chromatography on silica gel (hexane/EtOAc 15:1) affording naphthyl derivative **122b** as a white solid (216 mg, 0.6 mmol, 63% yeld).

Synthesis of **(E)-N-(3-(4-methoxyphenyl)allyl)-4-methyl-N-(naphthalen-1-ylmethyl)benzenesulfonamide (122c)**

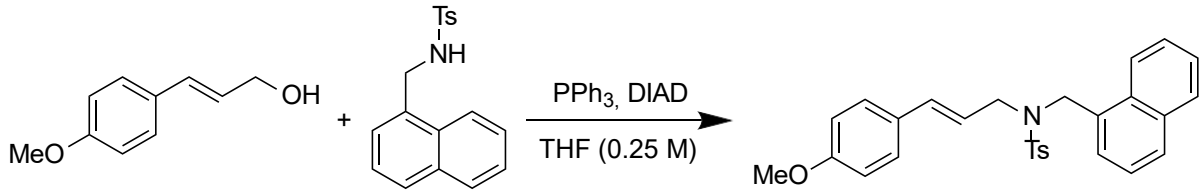

Under N_2 atmosphere, to a solution of naphthyl tosylamide (311 mg, 1.0 mmol, 1 equiv.), 4-methoxy cinnamyl alcohol (180 mg, 1.1 mmol, 1.1 equiv.), and Ph_3P (393 mg, 1.5 mmol, 1.5 equiv.) in THF (4 mL), DEAD (270 µL, 1.5 mmol, 1.5 equiv.) was added dropwise at 0 °C. The reaction was warmed to room temperature and stirred for 24 h. The volatiles were then removed under reduced pressure and the residue was purified by silica gel flash column chromatography (*n*-hexane/EtOAc 4:1) affording naphtyl derivative **122c** as a white solid (334 mg, 73% yeld).

General procedure **IIIa** for the preparation of naphthyl cinnamic ethers

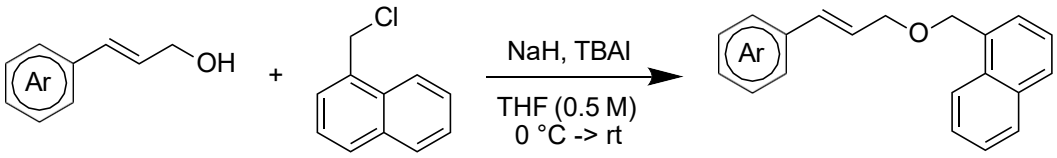

To a stirred mixture of cinnamyl alcohol (1.05 equiv.), TBAI (1 mol%) and NaH (1.4 equiv.) in THF (0.5 M), 1-(chloromethyl)naphthalene (1 equiv.) dissolved in THF (0.5 M, 25% of total volume) was added dropwise at 0 °C under nitrogen flow, and the reaction was stirred at rt for 12 h. The mixture was extracted with Et_2O (3x 10 mL) and the organic layer was dried over sodium sulfate and concentrated under reduced pressure. The crude was purified by chromatography on silica gel (*n*- hexane/EtOAc) affording the naphthyl derivative **122**.

Substrate	Ar	Yield (%)
122d	Ph	95
122e	2-Cl-C_6H_4	91

Synthesis of **1,1'-((cinnamyloxy)methylene)dinaphthalene** (**122f**)

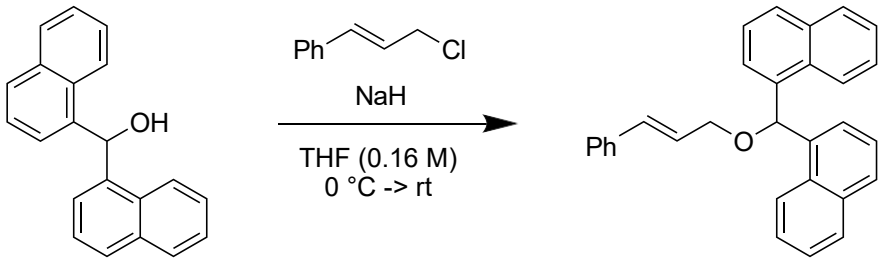

To a stirred mixture of di(naphthalen-1-yl)methanol (230 mg, 0.81 mmol, 1 equiv.) in THF (5 mL, 0.16 M), NaH (60% in mineral oil, 148 mg, 0.97 mmol, 1.4 equiv.) was added at 0 °C under nitrogen flow. The mixture was allowed to stir at 0 °C for 20 minutes. Then cinnamyl chloride (148 mg, 135 µL, 0.97 mmol, 1.2 equiv.) was added. The reaction was allowed to stir at 60 °C overnight. After complete conversion of the indole, the reaction was quenched with the addition of water (30 mL) and the THF was removed under reduced pressure. The mixture was extracted with EtOAc (3x 30 mL). The organic layer was dried over sodium sulphate and the solvent was removed under reduced pressure. The resulting crude was purified by chromatography on silica gel (*n*-hexane - EtOAc 59:1) affording 1,1'-((cinnamyloxy)methylene)dinaphthalene as a white solid (115 mg, 36% yield).

IV. Synthesis of propargyl amide precursors

General procedure **IVa** for the synthesis of 1,6-enynes

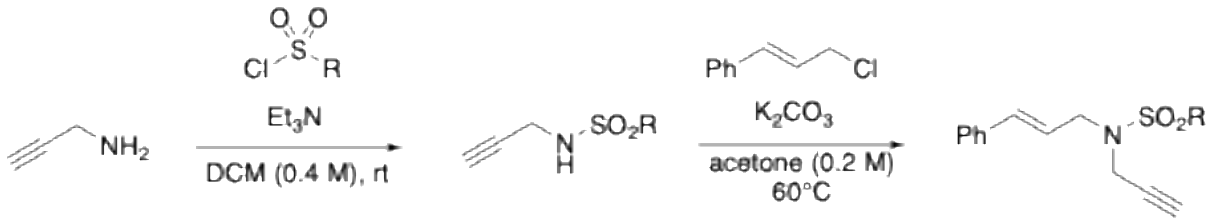

DCM (0.4 M), TEA (1.1 eq) and propargyl amine (1 equiv.) were added to a round bottom flask equipped with a magnetic stirring bar. The resulting mixture was stirred at 0 °C and sulfonyl halide (1.05 eq) was slowly added. The reaction mixture was stirred at room temperature for 12 hours, quenched with sat. NH_4Cl, diluted with DCM and washed with water. The organic layer was dried over Na_2SO_4, filtered and concentrated under reduced pressure.

Without isolation, propargyl tosylamide was transferred in a Schlenk tube equipped with a magnetic stirring bar and K_2CO_3 (1.5 equiv.). Acetone (0.33 M) and cinnamyl chloride (1.3 equiv.) were then added. The reaction mixture was stirred at 60 °C overnight. The mixture was cooled to room temperature, diluted with water and extracted three times with EtOAc. The combined organic layers were dried over Na_2SO_4, filtered and concentrated under reduced pressure. The resulting crude was purified by chromatography on silica gel (*n*-hexane/EtOAc 9:1).

Precursor of	R	Ar[1]	Yield (%)
120a	4-Me-C_6H_5	Ph	78
120b	Ph	Ph	70
120c	Me	Ph	75

General procedure **IVb** for the synthesis of 1,6-enynes via Heck coupling

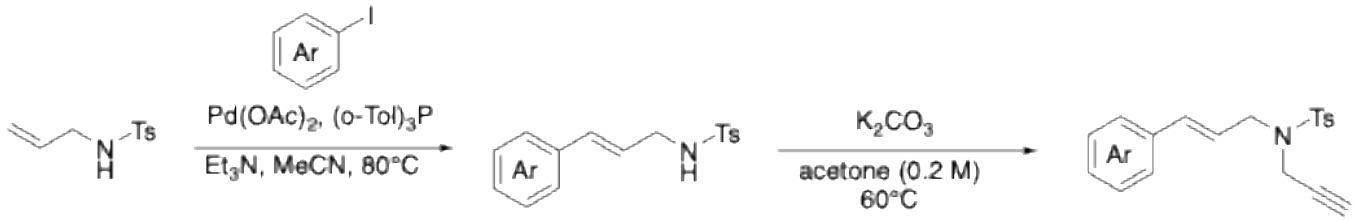

N-allyl-tosylamide (1 equiv.), (*o*-Tol)3P (0.1 equiv.) and $Pd(OAc)_2$ (0.05 equiv.) were sequentially added to a Schlenk tube equipped with a magnetic stirring bar. CH3CN (0.41 M), TEA (2 equiv.) and the desired aryl halide (1 equiv.) were added under N_2 atmosphere, and the mixture was stirred at 80 °C for 3 hours. A second batch of the desired aryl halide (0.42 equiv.), $Pd(OAc)_2$ (0.026 equiv.) and $(o\text{-}Tol)_3P$ (0.05 equiv.) were then added. The mixture was stirred at 80 °C for further 6 hours, allowed to cool to room temperature, diluted with water and extracted with EtOAc (3 x 30 mL). The combined organic layers were dried over Na_2SO_4, filtered and concentrated under reduced pressure. The resulting crude was purified by chromatography on silica gel (*n*-hexane/EtOAc 9:1).

The substituted cinnamyl tosylamide (1 equiv.) was dissolved in acetone (0.2 M). Then K_2CO_3 (3 equiv.) and propargyl bromide (85% in toluene, 1.5 equiv.) were added. The mixture was subsequently placed in a pre-heated oil bath at 60 °C and stirred overnight. After consumption of the starting material, the reaction mixture was cooled down to room temperature and water was added. The mixture was extracted with EtOAc (3 x 30 mL). The combined organic fractions were dried over Na_2SO_4 filtered and concentrated under reduced pressure. The resulting crude was purified by chromatography on silica gel (*n*-hexane/EtOAc 9:1).

Precursor of	**R**	**Ar[1]**	**Yield** (%)
120d	4-Me-C_6H_5	2-Me-C_6H_5	66
120e	4-Me-C_6H_5	4-MeO-C_6H_5	70

General procedure **IVc** for the three-component synthesis of propargyl amines

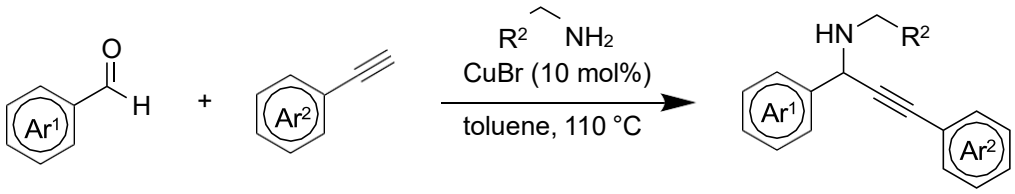

To a stirred mixture of aldehyde (1 equiv.), amine (1.5 equiv.) and phenylacetylene (1.5 equiv.) in toluene (0.5 M), CuBr (0.2 equiv.) was added under N_2 atmosphere and the reaction was refluxed for 2 h. The mixture was then cooled down to room temperature, quenched with NH_4Cl and stirred for an additional 2 hours. Then the mixture was extracted with Toluene (3 x 20 mL), the organic layer was dried over sodium sulfate and concentrated under reduced pressure. The crude was finally purified by chromatography on silica gel (*n*-hexane/EtOAc with 1 mol% of Et_3N).

Precursor of	R	Ar^1	R^2	Yield (%)
124a	Ph	Ph	Ph	67
124b	Ph	Ph	*n*Pr	51
124e	Ph	4-Me-C_6H_5	Ph	65
124f	4-Cl-C_6H_5	Ph	Ph	45
124g	4-OMe-C_6H_5	Ph	Ph	69

General procedure **IVd** for the synthesis of propargyl amides

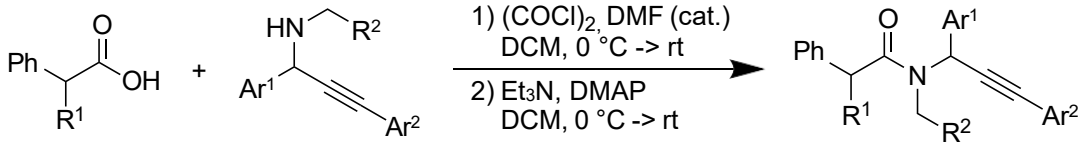

In a round bottom flask equipped with a magnetic stirring bar the correspondent acid was dissolved in CH_2Cl_2. The mixture was cooled down to 0 °C, and then oxalyl chloride (1.1 equiv.) was added dropwise, followed by the addition of one drop of DMF. The reaction was allowed to stir at 0 °C for 2 hours, then the mixture was carefully concentrated under reduced pressure and the resulting crude was used without further purification.

In a round bottom flask equipped with a magnetic stirring bar the correspondent amine was dissolved in CH_2Cl_2 (0.4 M) and Et_3N (1.5 equiv.). The mixture was then cooled to 0 °C, then a solution of the acyl chloride (1 equiv.) in CH_2Cl_2 was slowly added. After the addition, the reaction was slowly warmed to room temperature. After complete consumption of the substrate, the reaction mixture was quenched with a saturated solution of NH_4Cl, extracted with CH_2Cl_2 (3 x 20 mL) and the organic layer was dried over sodium sulfate and concentrated under reduced pressure. The crude was purified by precipitation (n-hexane/EtOAc).

Precursor of	R^1	Ar^1	Ar^2	R^2	Yield (%)
124a	Ph	Ph	Ph	Ph	66
124b	Ph	Ph	Ph	*n*Pr	69
124c	Me	Ph	Ph	Ph	64
124d	H	Ph	Ph	Ph	38
124e	Ph	Ph	4-Me-C_6H_5	Ph	55
124f	Ph	4-Me-C_6H_5	Ph	Ph	36
124g	Ph	4-Me-C_6H_5	Ph	Ph	53
126a	H	H	H	Ph	78

V. Synthesis of allenamides

General procedure **Va** for the isomerization of en-allenes

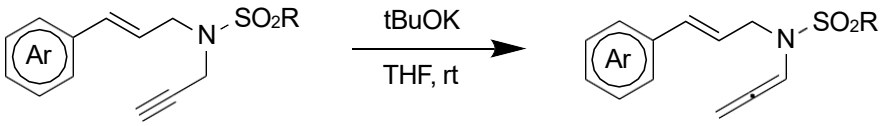

To a stirred solution of alkyne (1 equiv.) in THF (0.17 M), *t*-BuOK (0.3 equiv.) was added, and the resulting mixture was stirred at room temperature for 10-30 min. After complete conversion as monitored by TLC, a saturated NH_4Cl solution was added. The mixture was extracted three times with EtOAc, the organic layer was dried over sodium sulfate and concentrated under reduced pressure. The crude was purified by chromatography on silica gel (n-hexane/EtOAc).

Precursor of	R	Ar[1]	Yield (%)
3a	4-Me-C_6H_5	Ph	67
3b	Ph	Ph	68
3c	Me	Ph	50
3d	4-Me-C_6H_5	2-Me-C_6H_5	56
3e	4-Me-C_6H_5	4-MeO-C_6H_5	49

General procedure **Vb** for the synthesis of tri-substituted allenes

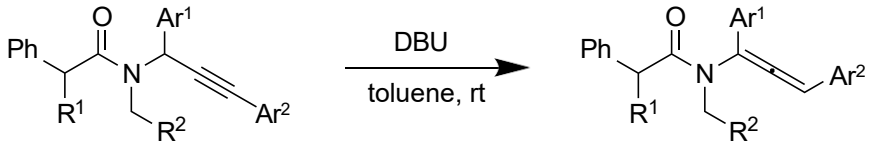

In a 50 mL Schlenk, equipped with a magnetic stirring bar, the amide (1 equiv.) was dissolved in toluene (0.05 M). The mixture was cooled to 0 °C and DBU (2 equiv.) was slowly added under N_2 atmosphere. After the addition, the mixture was slowly warmed to room temperature. After complete conversion, the reaction mixture was quenched with an aqueous solution of HCl (1 M) and extracted with EtOAc (3 x 15 mL). The organic layer was dried over sodium sulfate and concentrated under reduced pressure. The crude was purified by chromatography on silica gel (n-hexane/EtOAc).

Substrate	R^1	R^2	Ar^1	Ar^2	Yield (%)
124a	Ph	Ph	Ph	Ph	78
124b	Ph	*n*-Pr	Ph	Ph	58
124c	Me	Ph	Ph	Ph	82
124d	H	Ph	Ph	Ph	90
124e	Ph	Ph	Ph	4-Me-C_6H_5	96
124f	Ph	Ph	4-Cl-C_6H_5	Ph	90
124g	Ph	Ph	4-OMe-C_6H_5	Ph	93

Synthesis of ***N*-benzyl-2-phenyl-*N*-(propa-1,2-dien-1-yl)acetamide (126a)**

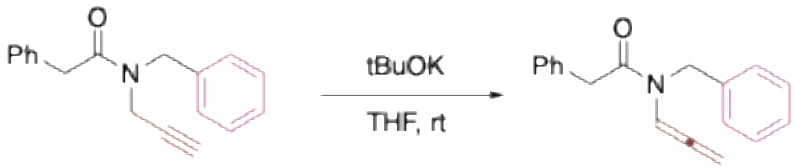

In a 25 mL Schlenk, equipped with a magnetic stirring bar, the propargyl amide (184 mg, 0.7 mmol) was dissolved in dry THF (0.18 M). t-ButOK (40 mg, 0.5 mmol) was slowly added to the reaction mixture at room temperature, under N2 atmosphere. After complete consumption of the substrate, the reaction mixture was quenched with a saturated solution of NH_4Cl and extracted with EtOAc (3 x 5 mL). The organic layer was dried over sodium sulfate and concentrated under reduced pressure. The crude was purified by chromatography on silica gel (n-hexane/EtOAc 9:1) affording the allenamide **126a** as a colorless oil (0.12 g, 67% yield).

VI. Synthesis of bi-naphthalenes

Synthesis of **di(naphthalen-1-yl)methanol** (**N3**) and of **di(naphthalen-1-yl)methane** (**N2**)

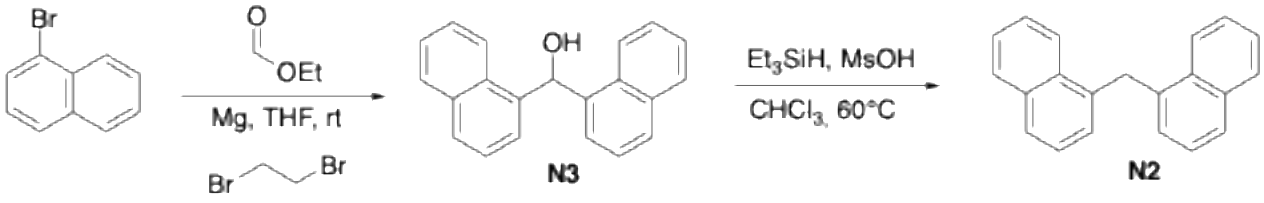

A two necked round bottom flask was charged with magnesium tunings (0.55 g, 23 mmol, 2.3 equiv.), 1-bromonaphthalene (3.10 mL, 22 mmol, 2.2 equiv.), dibromoethane (few drops) and dry THF (10 mL), under N_2 atmosfere. The suspension was stirred for 1 hour at rt, and then ethyl formate (0.85 mL, 10 mmol, 1 equiv.) was added dropwise, and the resulting mixture was stirred for an additional hour. The reaction was quenched with saturated ammonium chloride, extracted with EtOAc (15 mL x 3), washed with brine and dried over sodium sulphate. The crude was purified by chromatography on silica gel (n-exane/EtOAc 20:1) affording the carbinol as a white solid (2.58 g, 91% yield).

To a solution of bi-naphtalene **N3** (142 mg, 0.5 mmol, 1 equiv.), and MsOH (36 µL, 0.55 mmol, 1.1 equiv.) in $CHCl_3$ (3 mL) was added dropwise Et_3SiH (0.13 mL, 0.8 mmol, 1.6 equiv.). The mixture was heated to 60 °C, and stirred for 1 hour. A saturated solution of sodium bicarbonate was added, and the mixture was extracted with DCM (10 mL x3) and washed with brine. The organic layer was dried over sodium sulfate, and the crude was purified by chromatography on silica gel (n-hexane/EtOAc 40:1), affording the bi-naphthyl **N2** as a white solid (115 mg, 86% yield).

Synthesis of **4-methyl-*N*, *N*-bis(naphthalen-1-ylmethyl)benzenesulfonamide** (**N4**)

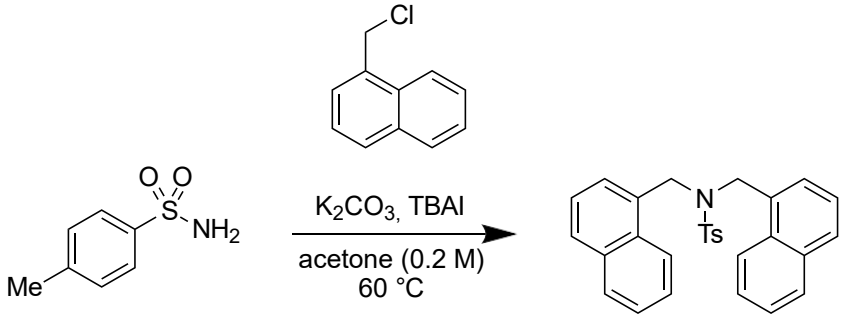

4-Methylbenzenesulfonamide (344 mg, 2 mmol, 1 equiv.) and K_2CO_3 (6 mmol, 3 equiv.) were added

to a round bottom flask equipped with a magnetic stirring bar. Acetone (10 mL, 0.2 M) was added, and the mixture was stirred at room temperature for 20 minutes. (1-(Chloromethyl)naphthalene (4.2 mmol, 2.1 equiv.) was added dropwise followed by a catalytic amount of TBAI (1 mol%). The reaction mixture was stirred at 60 °C overnight. After complete consumption of 4-methylbenzenesulfonamide, the reaction was cooled to room temperature and the solvent was removed under vacuum. The solid residue was then dissolved in water (30 mL) and extracted with ethyl acetate (3x 30 mL). The organic layer was dried over sodium sulphate and the solvent was removed under vacuum. The crude was purified with a chromatography on silica gel (exane:EtOAc 9:1) affording 4-Methyl-N, N-bis(naphthalen-1-ylmethyl)benzenesulfonamide **N4** as a white solid (640 mg, 72% yield).

Synthesis of **4-Methyl-N,N-bis(naphthalen-2-ylmethyl)benzenesulfonamide (N5)**

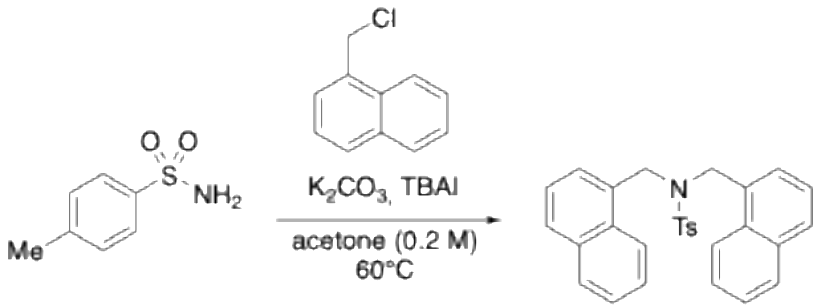

4-Methylbenzenesulfonamide (342 mg, 2 mmol, 1 equiv.) and K_2CO_3 (829 mg, 6 mmol, 3 equiv.) were added to a round bottom flask equipped with a magnetic stirring bar. Acetone (10 mL, 0.2 M) was added, then the mixture was stirred at room temperature for 20 minutes, followed by the addition of 2-(Bromomethyl)naphthalene (972 mg, 4.4 mmol, 2.1 equiv.). The reaction mixture was stirred at 60 °C overnight. After complete consumption of rìthe substrate, the reaction was cooled to room temperature and the solvent was removed under vacuum. The solid residue was then dissolved in water (30 mL) and extracted with ethyl acetate (3x 30 mL). The organic layer was dried over sodium sulphate and the solvent was removed under vacuum. The crude was purified by chromatography on silica gel (*n*-hexane:EtOAc 4:1) affording 4-methyl-N,N-bis(naphthalen-2-ylmethyl)benzenesulfonamide **N4** as a white solid (634 mg, 70% yield).

Synthesis of **Naphthalen-1-ylmethyl (naphthalen-1-ylmethyl)-L-prolinate (N6)**

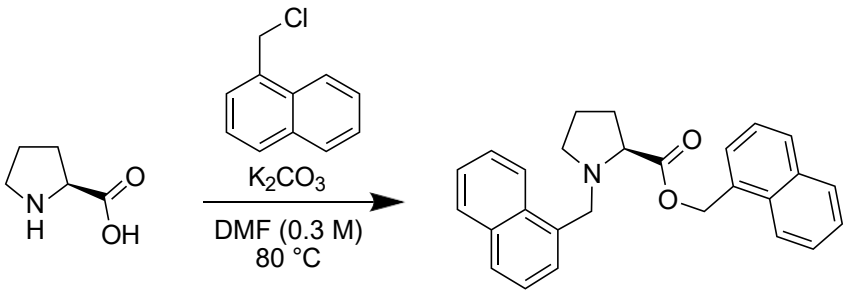

L-Proline (345 mg, 3 mmol, 1 equiv.) and K_2CO_3 (1.2 g, 9 mmol, 3 equiv) were added to a round bottom flask equipped with a magnetic stirring bar. DMF (10 mL, 0.3 M) was added and the mixture was stirred at room temperature for 20 minutes, followed by the addition of (1-(Chloromethyl)naphthalene (1.2 g, 6.6 mmol, 2.2 equiv.). The reaction mixture was stirred at 80 °C overnight. After complete consumption of the L-proline, the reaction was cooled to room temperature and the solvent was removed under vacuum. The solid residue was then dissolved in water (30 mL) and extracted with ethyl acetate (3x 30 mL). The organic layer was dried over sodium sulphate and the solvent was removed under vacuum. The crude was purified by chromatography on silica gel (*n*-hexane:EtOAc 15:1 to 6:1) affording naphthalen-1-ylmethyl (naphthalen-1-ylmethyl)-L-prolinate as an colorless oil (1.08g, 91% yield).

Synthesis of **(S)-di(naphthalen-1-yl)(1-(naphthalen-1-ylmethyl)pyrrolidin-2-yl)methanol (N7)**

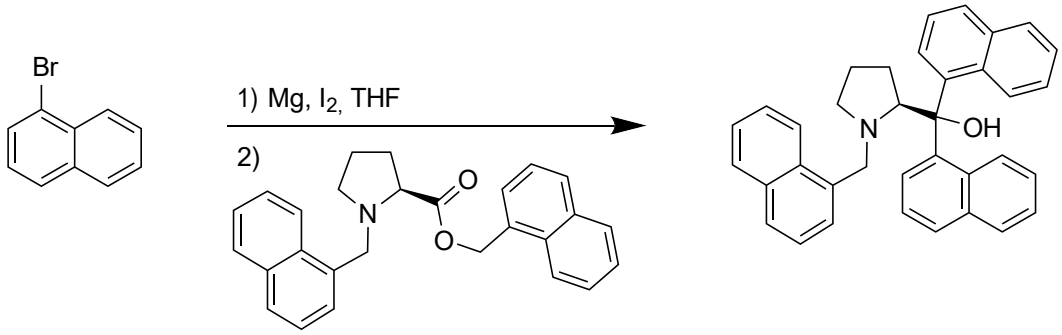

Iodine (1 mol%) and Magnesium (241 mg, 10.4 mmol, 1.02 equiv.) were added to a 3 necked round bottom flask equipped with magnetic stirring bar, condenser and dropping funnel. THF (4 mL) was added and the suspension was stirred for 20 minutes. Some drops of a solution of 1-bromo-naphthalene (2.04 g, 9.9 mmol, 4.8 equiv.) in THF (6 mL) were added to the suspension and heated to 50 °C. As soon as the colour changed from brown to pale yellow, the reaction was cooled to 0 °C and the remaining solution was added dropwise. The reaction mixture was refluxed for 30 minutes. A solution of the L-proline ester was prepared (800 mg, 2.03 mmol) in THF (4.5 mL) and added dropwise at 0 °C. The reaction mixture was refluxed for 1 h. Then the reaction mixture was cooled to 0 °C and quenched with a saturated solution of NH_4Cl and extracted with ethyl acetate (3x 50 mL). The organic layer was washed with brine and dried over Na_2SO_4. The crude was purified by chromatography on silica gel (*n*-hexane:TEA 100:1), affording the product as a white solid (161 mg, 16% yield).

Synthesis of **(S)-2-(((tert-butyldimethylsilyl)oxy)di(naphthalen-1-yl)methyl)-1-(naphthalen-1-ylmethyl)pyrrolidine (N8)**

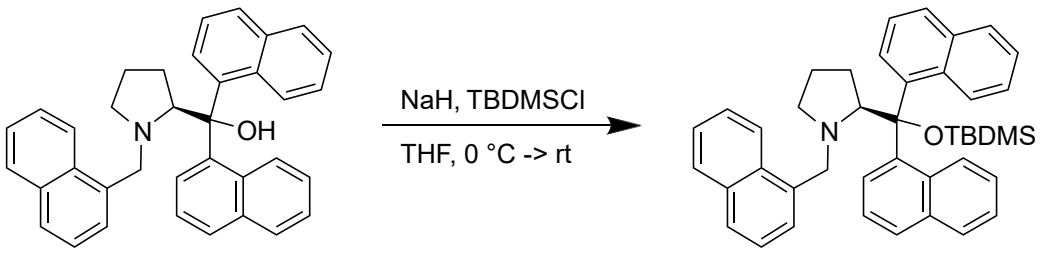

To a solution of (S)-di(naphthalen-1-yl)(1-(naphthalen-1-ylmethyl)pyrrolidin-2-yl)methanol (50 mg, 0.1 mmol, 1 equiv.) in dry THF (2 mL, 0.05 M), NaH (60% in mineral oil, 0.3 mmol, 3.0 equiv.) was added at 0° C. After 20 minutes of stirring, a solution of TBSCl (22.7 mg, 0.15 mmol, 1.5 equiv.) in THF (2 mL, 0.075 M) was added dropwise. After 12 hours the reaction was quenched with water and

extracted with diethyl ether (3x 30 mL). The organic layer was washed with 30 mL of brine, water and dried over Na_2SO_4 and the solvent was removed under reduce pressure. The crude was purified by chromatography on silica gel (*n*-hexane:EtOAc 8:1) affording the product as a yellow solid (161 mg, 80% yield).

Synthesis of **(4S,5S)-4,5-bis(methoxydi(naphthalen-1-yl)methyl)-2,2-dimethyl-1,3-dioxolane (N10)**

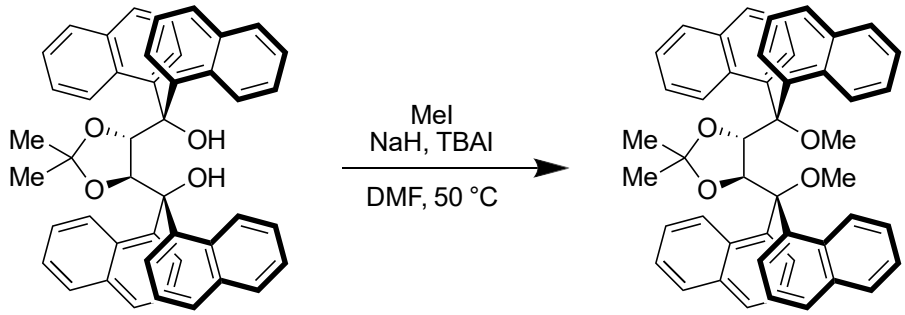

To a solution of TADDOL (333 mg, 0.5 mmol, 1 equiv.) and TBAI (1.8 mg, 5 µmol, 1 mol%) in DMF (3 mL) at 0 °C, NaH (60 mg, 1.5 mmol, 3 equiv.) was added, and the mixture was stirred for 20 min. Then iodomethane (0.12 mL, 2.0 mmol, 4 equiv.) was added dropwise, and the reaction was heated to 50 °C until complete consumption of the starting material (monitored by TLC). The reaction was quenched with water, extracted with EtOAc (10 mL x 3), and the organic layers were washed with brine (20 mL x 2) and dried over Na_2SO_4. The crude was purified by chromatography on silica gel (*n*-hexane:EtOAc 8:1), affording the product as a white solid (325 mg, 94%).

Calculated triplet energies for substrates **120**-**130**, [substrate:NP] and [substrate:**N2**] adducts

a) **DFT data on the activation of substrates 120, 122, 124, 126, 128, 130**

DG values in kcal/mol @298.15 K,
M06/Def2-TZVP, Grimme's D3 disp. corr., CPCM

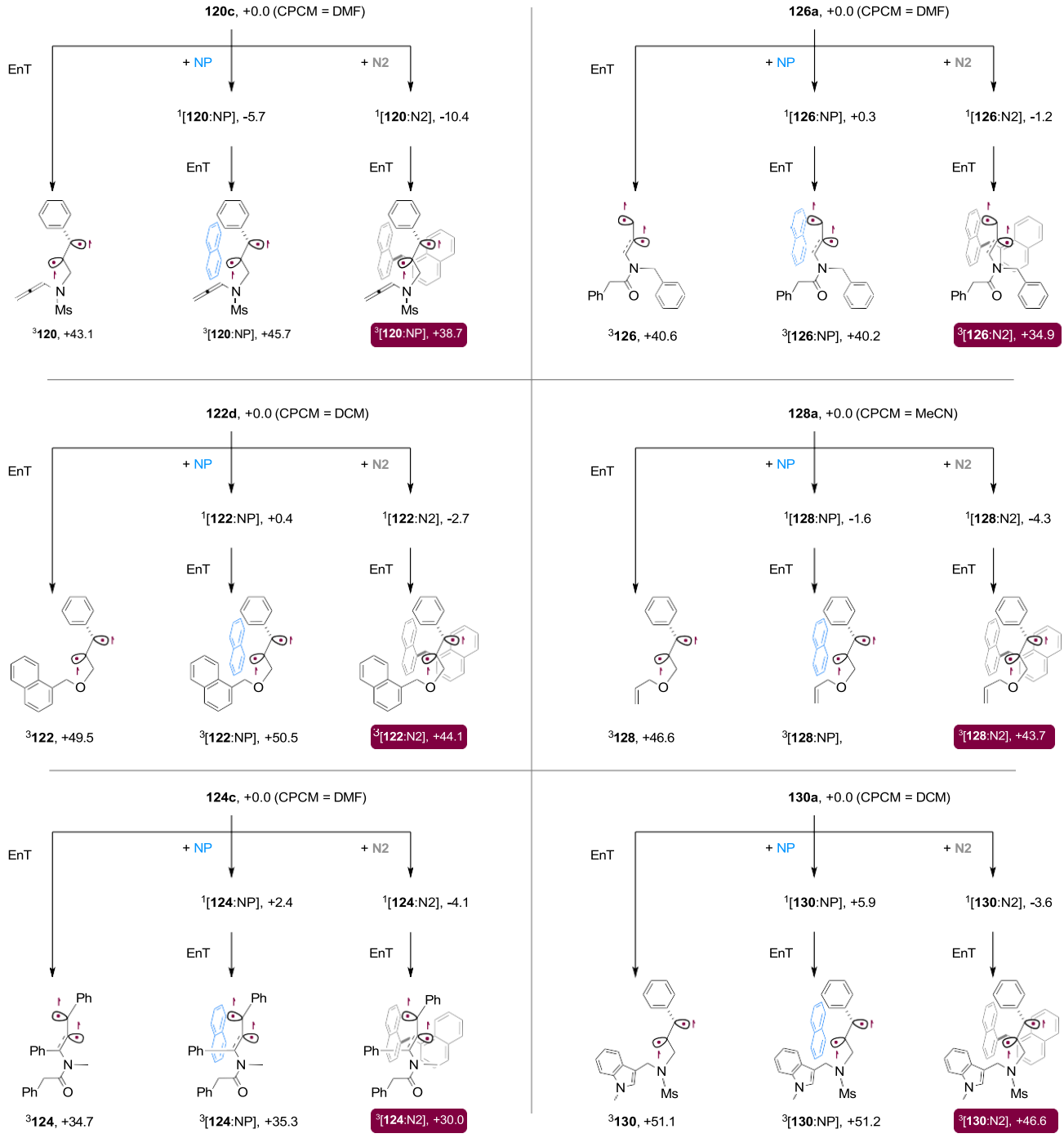

Characterization of Substrates

N-cinnamyl-4-methyl-N-(propa-1,2-dien-1-yl)benzenesulfonamide

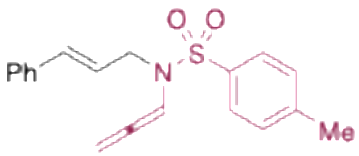

En-allene **120a** was prepared following general procedure **V-a** from the corresponding enyne (828 mg, 2.54 mmol). White solid (560 mg, 67%). **^{1}H NMR** (400 MHz, $CDCl_3$) δ 7.72 (d, *J* = 8.2 Hz, 2H), 7.38 – 7.20 (m, 7H), 6.89 (t, *J* = 6.2 Hz, 1H), 6.45 (d, *J* = 15.9 Hz, 1H), 5.98 (dt, *J* = 15.9, 6.2 Hz, 1H), 5.31 (d, *J* = 6.2 Hz, 2H), 3.98 (dd, *J* = 6.2, 1.4 Hz, 2H), 2.40 (s, 3H). **ESI-MS** calcd for $C_{19}H_{20}NO_2S$ $[M+H]^+$ 326.12, found 326.20. *Data are consistent with literature*.

N-cinnamyl-N-(propa-1,2-dien-1-yl)benzenesulfonamide

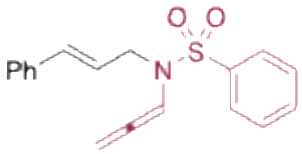

En-allene **120b** was prepared following general procedure **V-a** from the corresponding enyne (370 mg, 119 mmol). White solid (252.2 mg, 68%). **^{1}H NMR** (400 MHz, acetone-d6) δ 7.93 (d, *J* = 7.6 Hz, 2H), 7.82 – 7.56 (m, 3H), 7.40 – 7.22 (m, 5H), 6.91 (t, *J* = 6.3 Hz, 1H), 6.55 (d, *J* = 15.9 Hz, 1H), 6.09 (dt, *J* = 15.9, 6.1 Hz, 1H), 5.39 (d, *J* = 6.2 Hz, 2H), 4.04 (d, *J* = 6.1 Hz, 2H). **ESI-MS** calcd for $C_{18}H_{18}NO_2S$ $[M+H]^+$ 312.40, found 312.48. *Data are consistent with literature.*

***N*-cinnamyl-N-(propa-1,2-dien-1-yl)methanesulfonamide**

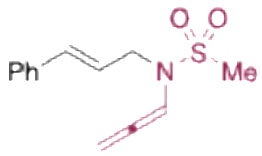

En-allene **120c** was prepared following general procedure **V-a** from the corresponding enyne (250 mg, 1 mmol). White solid (124.5 mg, 50%). **^{1}H NMR** (400 MHz, $CDCl_3$) δ 7.40 – 7.22 (m, 5H), 6.73 (tt, *J* = 6.2, 0.7 Hz, 1H), 6.63 (d, *J* = 15.8 Hz, 1H), 6.18 (dt, *J* = 15.9, 6.5 Hz, 1H), 5.44 (d, *J* = 6.3 Hz, 2H), 4.15 (ddd, *J* = 6.4, 1.4, 0.7 Hz, 2H), 2.93 (s, 3H). **ESI-MS** calcd for $C_{13}H_{16}NO_2S$ $[M+H]^+$ 250.33, found 250.36. *Data are consistent with literature.*

(E)-4-methyl-N-(propa-1,2-dien-1-yl)-N-(3-(o-tolyl)allyl)benzenesulfonamide

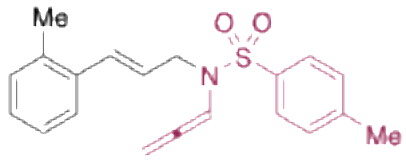

En-allene **120d** was prepared following general procedure **V-a** from the corresponding enyne (140 mg, 0.47 mmol). Viscous clear oil (78.7 mg, 56%). **^{1}H NMR** (400 MHz, acetone-d6) δ 7.80 (d, *J* = 8.2 Hz, 2H), 7.45 (d, *J* = 8.1 Hz, 2H), 7.35 – 7.27 (m, 1H), 7.18 – 7.09 (m, 3H), 6.92 (t, *J* = 6.3 Hz, 1H), 6.78 (d, *J* = 15.8 Hz, 1H), 5.92 (dt, *J* = 15.8, 6.1 Hz, 1H), 5.41 (d, *J* = 6.3 Hz, 2H), 4.05 (dd, *J* = 6.1, 1.5 Hz, 2H), 2.44 (s, 3H), 2.30 (s, 3H). **ESI-MS** calcd for $C_{20}H_{22}NO_2S$ $[M+H]^+$ 340.46, found 340.48. *Data are consistent with literature.*

(E)-N-(3-(4-methoxyphenyl)allyl)-4-methyl-N-(propa-1,2-dien-1-yl)benzenesulfonamide

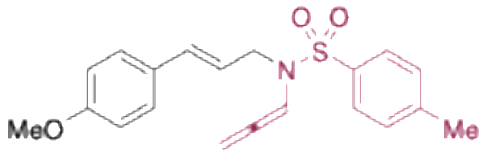

En-allene **120e** was prepared following general procedure **V-a** from the corresponding enyne (78.6 mg, 0.22 mmol). Viscous oil (38.6 mg, 49%). **^{1}H NMR** (400 MHz, acetone-d6) δ 7.78 (d, *J* = 8.3 Hz, 2H), 7.49 – 7.40 (m, 2H), 7.29 (d, *J* = 8.7 Hz, 2H), 6.95 – 6.83 (m, 3H), 6.47 (d, *J* = 15.9 Hz, 1H), 5.91 (dt, *J* =

15.9, 6.3 Hz, 1H), 5.38 (d, *J* = 6.3 Hz, 2H), 3.98 (d, *J* = 6.3 Hz, 2H), 3.80 (s, 3H), 2.43 (s, 3H). **ESI-MS** calcd for $C_{20}H_{22}NO_3S$ $[M+H]^+$ 356.46, found 356.49. *Data are consistent with literature.*

N-cinnamyl-4-methyl-N-(naphthalen-1-ylmethyl)benzenesulfonamide

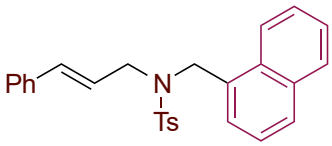

Naphthyl derivative **122a** was prepared by alkylation of the corresponding cinnamyl sulfonamide (460 mg, 1.6 mmol). White solid (350 mg, 80% yield). **^{1}H NMR** (400 MHz, $CDCl_3$) δ 8.31 (dd, *J* = 8.3, 1.4 Hz, 1H), 7.90 – 7.82 (m, 3H), 7.80 (dd, *J* = 6.6, 2.9 Hz, 1H), 7.60 – 7.47 (m, 2H), 7.45 – 7.33 (m, 4H), 7.30 – 7.16 (m, 3H), 7.00 (dd, *J* = 7.7, 1.8 Hz, 2H), 6.11 (d, *J* = 15.9 Hz, 1H), 5.69 (dt, *J* = 15.8, 6.7 Hz, 1H), 4.86 (s, 2H), 3.87 (dd, *J* = 6.8, 1.4 Hz, 2H), 2.47 (s, 3H). **^{13}C NMR** (101 MHz, $CDCl_3$) δ 143.8, 137.2, 136.5, 134.2, 134.2, 132.2, 131.1, 130.1 (2C), 129.3, 128.9, 128.7 (2C), 128.0, 127.9, 127.8 (2C), 126.9, 126.6 (2C), 126.3, 125.3, 124.2, 123.6, 49.5, 49.3, 21.8. **ESI-MS** calcd for $C_{27}H_{26}NO_2S$ $[M+H]^+$ 428.17, found 428.26.

N-cinnamyl-N-(naphthalen-1-ylmethyl)benzamide

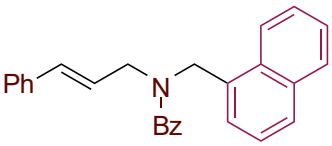

Naphthyl derivative **122b** was prepared by allylation of the corresponding naphthyl benzamide (236 mg, 0.9 mmol). White solid (216 mg, 63% yield). Two rotamers are observed due to the dynamic rotation of the amido group (66:34 mixture of rotamers). **^{1}H NMR** (400 MHz, $CDCl_3$) δ 8.25 (d, RotB *J* = 8.2 Hz, 1H), 8.06 – 7.79 (m, RotA 2H; RotB 2H), 7.79 – 6.98 (m, RotA 15H; RotB 15H), 6.42 – 6.35 (m, RotA 1H; RotB 1H), 6.04 – 5.98 (m, RotA 1H), 5.37 (s, RotA 2H), 5.03 (s, RotB 2H), 4.38 (s, RotB 2H), 4.06 – 3.81 (m, RotA 2H). **^{13}C NMR** (101 MHz, $CDCl_3$) δ 172.31, 171.97, 136.51, 136.26, 135.92, 134.03, 133.69, 132.97, 132.35, 132.14, 131.98, 130.91, 130.01, 129.68, 128.87, 128.71, 128.57, 128.24, 128.03, 127.33, 126.68, 126.59, 126.49, 126.11, 125.57, 125.29, 124.33, 123.95, 122.34, 49.72, 47.56, 45.32. **ESI-MS** calcd for $C_{27}H_{24}NO$ $[M+H]^+$ 378.19, found 378.27.

(E)-N-(3-(4-methoxyphenyl)allyl)-4-methyl-N-(naphthalen-1-ylmethyl)benzenesulfonamide

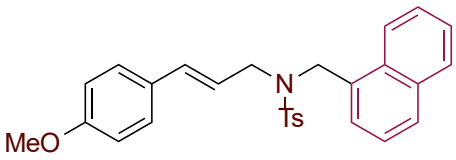

Naphthyl derivative **122c** was prepared by Mitsunobu reaction on the corresponding sulfonamide (311 mg, 1.0 mmol). White solid (334 mg, 73% yield). **^{1}H NMR** (400 MHz, $CDCl_3$) δ 8.31 (d, *J* = 8.3 Hz, 1H), 7.90 – 7.77 (m, 4H), 7.61 – 7.48 (m, 2H), 7.46 – 7.32 (m, 4H), 6.96 (d, *J* = 8.7 Hz, 2H), 6.79 (d, *J* = 8.7 Hz, 2H), 6.07 (d, *J* = 15.8 Hz, 1H), 5.57 (dt, *J* = 15.8, 6.8 Hz, 1H), 4.87 (s, 2H), 3.86 (d, *J* = 5.5 Hz, 2H), 3.81 (s, 3H), 2.49 (s, 3H). **^{13}C NMR** (101 MHz, $CDCl_3$) δ 159.3, 143.5, 137.0, 133.9, 133.6, 131.9, 130.9, 129.8 (2C), 129.0, 128.9, 128.6, 127.6 (2C), 127.5, 126.5 (2C), 126.0, 125.0, 123.9, 120.9, 113.8 (2C), 55.3, 49.1, 49.1, 21.6. **ESI-MS** calcd for $C_{28}H_{27}NNaO_3S$ $[M+Na]^+$ 480.16, found 480.22.

1-((cinnamyloxy)methyl)naphthalene

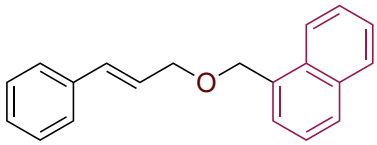

Naphthyl derivative **122d** was prepared following general procedure **III-a** from the corresponding cinnamyl alcohol (422 mg, 3.15 mmol). White sticky solid (820 mg, 95% yield). **^{1}H NMR** (400 MHz, $CDCl_3$) δ 8.18 (dd, *J* = 8.4, 1.2 Hz, 1H), 7.94 – 7.81 (m, 2H), 7.61 – 7.50 (m, 3H), 7.47 (dd, *J* = 8.2, 6.9 Hz, 1H), 7.44 – 7.40 (m, 2H), 7.34 (t, *J* = 7.4 Hz, 2H), 7.29 – 7.23 (m, 1H), 6.68 (d, *J* = 15.9 Hz, 1H), 6.39 (dt, *J* = 15.9, 6.0 Hz, 1H), 5.05 (s, 2H), 4.29 (dd, *J* = 6.1, 1.5 Hz, 2H). **^{13}C NMR** (101 MHz, $CDCl_3$) δ 137.0, 134.1, 134.0, 133.0, 132.1, 129.0, 128.9 (2C), 128.0, 126.8 (2C), 126.6, 126.4, 126.1, 125.6, 124.4, 71.2, 70.9. **ESI-MS** calcd for $C_{20}H_{18}NaO$ $[M+Na]^+$ 297.12, found 297.15.

(E)-1-(((3-(2-chlorophenyl)allyl)oxy)methyl)naphthalene

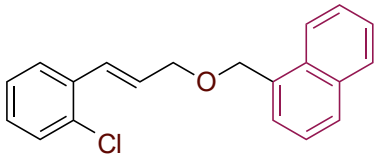

Naphthyl derivative **122e** was prepared following general procedure **III-a** from the corresponding cinnamyl alcohol (320 mg, 1.9 mmol). Colourless oil (533 mg, 91% yield). **^{1}H NMR** (400 MHz, $CDCl_3$) δ 8.23 (d, *J* = 8.3 Hz, 1H), 7.90 (dd, *J* = 20.1, 8.1 Hz, 2H), 7.63 – 7.47 (m, 5H), 7.40 (dd, *J* = 7.5, 1.8 Hz, 1H),

7.29 – 7.16 (m, 2H), 7.11 (d, *J* = 16.0 Hz, 1H), 6.38 (dt, *J* = 15.9, 6.0 Hz, 1H), 5.08 (s, 2H), 4.33 (dd, *J* = 6.0, 1.5 Hz, 2H). **^{13}C NMR** (101 MHz, $CDCl_3$) δ 135.2, 134.1, 133.9, 133.4, 132.1, 130.0, 129.4, 129.0 (2C), 128.8, 127.3, 127.1, 126.9, 126.6, 126.1, 125.5, 124.4, 71.0, 70.9. **ESI-MS** calcd for $C_{20}H_{17}ClNaO$ $[M+Na]^+$ 331.08, found 331.16.

1,1'-((cinnamyloxy)methylene)dinaphthalene

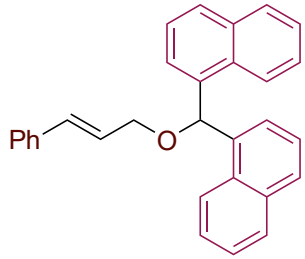

Naphthyl derivative **122f** was prepared from di(naphthalen-1-yl)methanol **N3** (230 mg, 0.81 mmol). White solid (115 mg, 36% yield). **^{1}H NMR** (400 MHz, $CDCl_3$) δ 8.18 (d, *J* = 9.8 Hz, 2H), 8.03 – 7.92 (m, 2H), 7.89 (d, *J* = 8.1 Hz, 2H), 7.63 – 7.42 (m, 10H), 7.40 – 7.34 (m, 2H), 7.33 – 7.27 (m, 1H), 7.06 (s, 1H), 6.70 (d, *J* = 16.0 Hz, 1H), 6.54 (dt, *J* = 15.9, 6.0 Hz, 1H), 4.49 (dd, *J* = 6.0, 1.5 Hz, 2H). **^{13}C NMR** (101 MHz, $CDCl_3$) δ 137.0, 136.5, 134.4, 133.2, 132.1, 129.2 (2C), 129.0 (3C), 128.9 (3C), 128.1, 126.9 (3C) 126.7 (2C), 126.3 (2C), 126.2, 126.0 (2C), 125.8 (2C), 124.1 (2C), 77.2, 70.9. **ESI-MS** calcd for $C_{30}H_{25}O[M+H]^+$ 401.19, found 401.32.

N-benzyl-N-(1,3-diphenylpropa-1,2-dien-1-yl)-2,2-diphenylacetamide

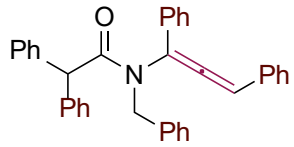

Allene **124a** was prepared following general procedure **V-b** from the corresponding propargyl amide (0.51 g, 1 mmol). White solid (0.38 g, 78% yield). **^{1}H NMR** (400 MHz, $CDCl_3$) δ 7.51 – 7.10 (m, 23H), 6.72 (d, *J* = 7.0 Hz, 2H), 5.95 (s, 1H), 5.55 (d, *J* = 14.6 Hz, 1H), 5.49 (s, 1H), 4.41 (d, *J* = 14.5 Hz, 1H). **^{13}C NMR** (101 MHz, $CDCl_3$) δ 207.14, 172.63, 140.21, 139.86, 137.42, 133.18, 131.84, 129.27 (2C), 129.21 (2C), 129.00 (2C), 128.74 (2C), 128.62, 128.58 (2C), 128.47 (4C), 128.38 (2C), 127.99, 127.55 (2C), 127.42, 127.04 (2C), 125.63 (2C), 114.54, 101.88, 55.49, 50.47. **ESI-MS** calcd for $C_{36}H_{29}NO$ $[M+H]^+$ 492.22, found 491.17.

N-butyl-N-(1,3-diphenylpropa-1,2-dien-1-yl)-2,2-diphenylacetamide

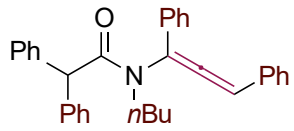

Allene **124b** was prepared following general procedure **V-b** from the corresponding propargyl amide. White solid (266.7 mg, 58% yield). **^{1}H NMR** (400 MHz, $CDCl_3$) δ 7.55 – 6.99 (m, 20H), 6.02 (s, 1H), 5.31 (s, 1H), 4.20 – 4.04 (dddd, 1H), 3.31 (dddd, *J* = 14.7, 9.9, 4.8 Hz, 1H), 1.83 – 1.66 (m, 1H), 1.66 – 1.51 (m, 1H), 1.33 (h, *J* = 7.4 Hz, 2H), 0.85 (t, *J* = 7.4 Hz, 3H). **^{13}C NMR** (101 MHz, $CDCl_3$) δ 206.76, 172.12, 140.29, 140.07, 138.89, 133.42, 132.60, 132.33, 130.15, 129.53, 129.27, 129.24, 129.06, 128.97, 128.92, 128.64, 128.58, 128.45, 128.33, 128.26, 127.80, 127.60, 127.29, 126.93, 126.90, 125.78, 125.52, 125.20, 115.06, 101.73, 77.48, 77.36, 77.16, 76.84, 58.25, 55.72, 53.52, 47.65, 31.04, 30.24, 29.79, 20.31, 20.14, 19.97, 13.82, 13.71. **ESI-MS** calcd for $C_{33}H_{31}NO$ $[M+H]^+$ 458.24, found 458.26.

N-benzyl-N-(1,3-diphenylpropa-1,2-dien-1-yl)-2-phenylpropanamide

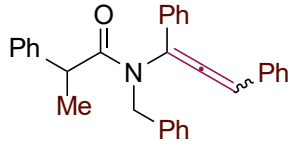

Allene **124c** was prepared following general procedure **V-b** from the corresponding propargyl amide (0.37 g, 0.86 mmol). Yellow solid (0.30 g, 82% yield, dr = 78:22). **^{1}H NMR** (400 MHz, $CDCl_3$) δ 7.51 – 7.01 (m, 26H), 6.83 – 6.75 (m, Dia 2, 2H), 6.79 – 6.60 (m, Dia 1, 2H), 5.77 (s, Dia 1, 1H), 5.48 (d, Dia 2, *J* = 14.3 Hz, 1H), 5.38 (d, Dia 1, 1H), 5.30 (s, Dia 2, *J* = 15.6 Hz, 1H), 4.39 (d, Dia 1, *J* = 15.8 Hz, 1H), 4.24 (q, Dia 2, *J* = 7.0 Hz, 1H), 4.14 (d, *J* = 14.7 Hz, 1H), 4.03 (q, Dia 1, *J* = 6.9 Hz, 1H), 1.55 (d, Dia 2, *J* = 7.0 Hz, 3H), 1.47 (d, Dia 1, *J* = 6.9 Hz, 3H). **^{13}C NMR** (101 MHz, $CDCl_3$) δ 207.28 (Dia 1), 206.87 (Dia 2), 175.21 (Dia 2), 174.71 (Dia 1), 142.51 (Dia 1), 141.45 (Dia 2), 137.54 (Dia 2), 137.37 (Dia 1), 133.05, 131.98 (Dia 2), 131.83 (Dia 1), 129.17 (2C), 128.79 (2C, Dia 2), 128.76 (2C, Dia 2), 128.68 (2C, Dia 2), 128.61 (2C, Dia 2), 128.50 (2C, Dia 1), 128.44 (2C, Dia 1), 128.38 (Dia 1), 128.33 (2C, Dia 1), 128.29 (2C, Dia 1), 128.12 (Dia 2), 128.04 (2C, Dia 2), 127.89 (Dia 1), 127.64 (2C, Dia 2), 127.59 (2C, Dia 1), 127.45 (2C, Dia 1), 127.37 (2C, Dia 2), 127.18 (Dia 1), 126.86 (Dia 2), 126.74 (Dia 1), 125.75 (2C, Dia 2), 125.32 (2C, Dia 1), 115.54 (Dia 2), 114.07 (Dia 1), 101.60, 50.44 (Dia 1), 49.91 (Dia 2),

44.29 (Dia 1), 43.19 (Dia 2), 21.30 (Dia 1), 19.95 (Dia 2). **ESI-MS** calcd for $C_{31}H_{27}NO$ $[M+H]^+$ 430.21, found 430.33.

N-benzyl-N-(1,3-diphenylpropa-1,2-dien-1-yl)-2-phenylacetamide

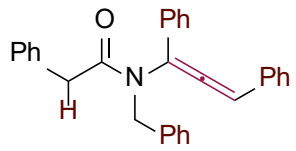

Allene **124d** was prepared following general procedure **V-b** from the corresponding propargyl amide (0.21 g, 0.51 mmol). Pale yellow solid (0.19 g, 90% yield). **^{1}H NMR** (400 MHz, $CDCl_3$) δ 7.61 – 7.04 (m, 18H), 6.85 (dd, *J* = 7.6, 1.9 Hz, 2H), 6.40 (s, 1H), 5.33 (d, *J* = 14.4 Hz, 1H), 4.40 (d, *J* = 14.5 Hz, 1H), 3.96 – 3.69 (m, 2H). **^{13}C NMR** (101 MHz, $CDCl_3$) δ 207.13, 171.81, 137.36, 135.40, 132.86, 131.85, 129.40 (2C), 129.11 (2C), 128.84 (2C), 128.70 (2C), 128.53, 128.45 (2C), 128.39 (2C), 128.15, 127.61 (2C), 127.41, 126.74, 125.59 (2C), 114.98, 101.81, 49.99, 41.04. **ESI-MS** calcd for $C_{30}H_{25}NO$ $[M+H]^+$ 416.19, found 415.90.

N-benzyl-2,2-diphenyl-N-(1-phenyl-3-(p-tolyl)propa-1,2-dien-1-yl)acetamide

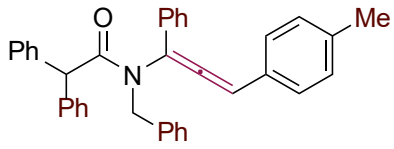

Allene **124e** was prepared following general procedure **V-b** from the corresponding propargyl amide (0.51 g, 1 mmol). Pale yellow solid (0.49 g, 96% yield). ^{1}H NMR (400 MHz, $CDCl_3$) δ 7.74 – 7.06 (m, 21H), 6.95 (d, *J* = 7.9 Hz, 2H), 6.59 (d, *J* = 7.9 Hz, 2H), 5.92 (s, 1H), 5.46 (m, 2H), 4.38 (d, *J* = 14.5 Hz, 1H), 2.33 (s, 3H). **^{13}C NMR** (101 MHz, $CDCl_3$) δ 207.07, 172.87, 140.45, 140.09, 138.23, 137.70, 133.61, 129.52 (2C), 129.50 (2C), 129.38 (2C), 129.21 (2C), 129.08, 128.98 (2C), 128.73, 128.69 (2C), 128.66 (2C), 128.58 (2C), 127.70 (2C), 127.62, 127.22 (2C), 125.85 (2C), 114.63, 101.99, 55.66, 50.71, 21.56. **ESI-MS** calcd for $C_{37}H_{31}NO$ $[M+H]^+$ 506.24, found 506.35.

N-benzyl-N-(1-(4-chlorophenyl)-3-phenylpropa-1,2-dien-1-yl)-2,2-diphenylacetamide

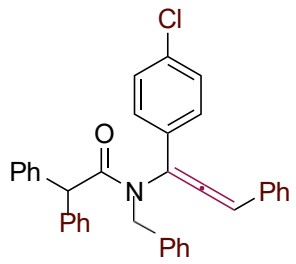

Allene **124f** was prepared following general procedure **V-b** from the corresponding propargyl amide (0.29 g, 0.55 mmol). Pale yellow solid (0.26 g, 90% yield). **^{1}H NMR** (400 MHz, $CDCl_3$) δ 7.67 – 7.04 (m, 22H), 6.84 – 6.54 (m, 2H), 5.97 (s, 1H), 5.48 (d, *J* = 15.8 Hz, 1H), 5.42 (s, 1H), 4.35 (d, *J* = 14.0 Hz, 1H). **^{13}C NMR** (101 MHz, $CDCl_3$) δ 206.32, 171.76, 139.18, 138.94, 136.44, 133.66, 131.01, 130.73, 128.60 (2C), 128.44 (2C), 128.16 (2C), 128.00 (2C), 127.89 (2C), 127.77 (4C), 127.68 (2C), 127.43, 126.82 (2C), 126.77, 126.38, 126.34, 126.11 (2C), 113.08, 101.41, 54.72, 49.66. **ESI-MS** calcd for $C_{36}H_{28}ClNO$ $[M+H]^+$ 526.19, found 525.94.

N-benzyl-N-(1-(4-methoxyphenyl)-3-phenylpropa-1,2-dien-1-yl)-2,2-diphenylacetamide

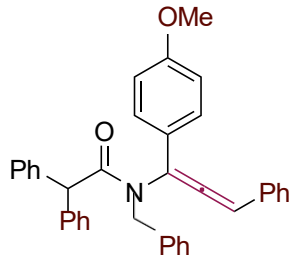

Allene **124g** was prepared following general procedure **V-b** from the corresponding propargyl amide (0.52 g, 1 mmol). White solid (0.49 g, 93% yield). **^{1}H NMR** (400 MHz, $CDCl_3$) δ 7.67 – 7.05 (m, 20H), 7.01 – 6.82 (m, 2H), 6.76 – 6.59 (m, 2H), 5.93 (s, 1H), 5.50 (m, 2H), 4.38 (d, *J* = 14.7 Hz, 1H), 3.88 (s, 3H). **^{13}C NMR** (101 MHz, $CDCl_3$) δ 206.74, 172.81, 160.27, 140.49, 140.13, 137.69, 132.39, 129.48, 129.18 (2C), 128.93 (2C), 128.75 (2C), 128.65 (4C), 128.57 (2C), 128.07, 127.69 (2C), 127.58, 127.20 (4C), 125.40, 114.86 (2C), 114.61, 101.97, 77.56, 55.69, 55.60, 50.60. **ESI-MS** calcd for $C_{37}H_{31}NO_2$ $[M+H]^+$ 522.24, found 522.36.

N-benzyl-2-phenyl-N-(propa-1,2-dien-1-yl)acetamide

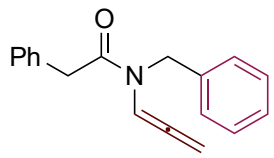

Allene **126a** was prepared from the corresponding propargyl amide (0.18 g, 0.70 mmol). Colorless oil (0.12 g, 67% yield). Two rotamers are observed due to the dynamic rotation of the amido group (48:52 mixture of rotamers). **^{1}H NMR** (400 MHz, $CDCl_3$) δ 7.71 (t, RotA, *J* = 6.4 Hz, 1H), 7.39 – 7.14 (m, 11H), 6.80 (t, RotB, *J* = 6.2 Hz, 1H), 5.28 (dd, *J* = 6.3, 4.9 Hz, 2H), 4.75 (s, 1H), 4.66 (s, 1H), 3.89 (s, 1H), 3.70 (s, 1H).**^{13}C NMR** (101 MHz, $CDCl_3$) 202.62 (RotA), 201.87 (RotB), 170.05 (RotA), 169.44 (RotB), 137.86 (RotB), 137.25 (RotA), 134.65 (RotA), 134.63 (RotB), 129.21, 129.15 (2C), 129.07, 128.63, 128.30, 127.74, 127.42, 127.37, 126.24, 100.83 (RotA), 100.06 (RotB), 87.99 (RotB), 87.36 (RotA), 49.58 (RotB), 47.86 (RotA), 41.62 (RotB), 41.43 (RotA). **ESI-MS** calcd for $C_{18}H_{17}NO$ $[M+H]^+$ 264.14, found 264.05.

N-cinnamyl-4-methyl-N-(propa-1,2-dien-1-yl)benzenesulfonamide

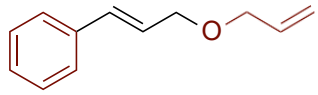

Diene **130a** was prepared by allylation of cinnamyl alcohol (373 mg, 2.78 mmol). Pale yellow oil (421 mg, 87%). **^{1}H NMR** (400 MHz, $CDCl_3$) δ 7.42 – 7.37 (m, 2H), 7.35 – 7.29 (m, 2H), 7.25 – 7.21 (m, 1H), 6.62 (dt, J = 15.9, 1.6 Hz, 1H), 6.31 (dt, J = 15.9, 6.0 Hz, 1H), 5.96 (ddt, J = 17.2, 10.4, 5.6 Hz, 1H), 5.32 (dd, J = 17.2, 1.7 Hz, 1H), 5.22 (dd, J = 10.4, 1.5 Hz, 1H), 4.17 (dd, J = 6.1, 1.5 Hz, 2H), 4.05 (dt, J = 5.6, 1.4 Hz, 2H). **ESI-MS** calcd for $C_{12}H_{15}O$ $[M+H]^+$ 175.11, found 175.20. *Data are consistent with the literature.*

N-cinnamyl-4-methyl-N-((1-methyl-1H-indol-3-yl)methyl)benzenesulfonamide

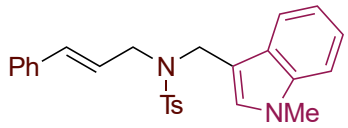

Naphthyl derivative **130a** was prepared the corresponding indolyl-sulfonamide (500 mg, 1.6 mmol). Yellow solid (235 mg, 34% yield). **^{1}H NMR** (400 MHz, $CDCl_3$) δ 7.80 (d, *J* = 8.3 Hz, 2H), 7.67 (d, *J* = 8.0 Hz, 1H), 7.35 – 7.20 (m, 7H), 7.14 – 7.08 (m, 3H), 6.91 (s, 1H), 6.24 (d, *J* = 15.9 Hz, 1H), 5.81 (dt, *J* = 15.8, 6.6 Hz, 1H), 4.59 (s, 2H), 3.93 (dd, *J* = 6.7, 1.4 Hz, 2H), 3.70 (s, 3H), 2.45 (s, 3H). **^{13}C NMR** (101 MHz, $CDCl_3$) δ 143.2, 137.7, 137.1, 136.4, 133.4, 129.7 (2C), 129.0, 128.5 (2C), 127.7, 127.6, 127.4 (2C), 126.3 (2C), 124.1, 122.0, 119.5, 119.5, 109.3, 108.8, 48.5, 42.1, 32.8, 21.5. **ESI-MS** calcd for $C_{26}H_{27}N_2O_2S$ $[M+H]^+$ 431.18, found 431.32.

di(naphthalen-1-yl)methane

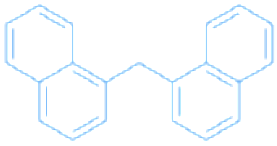

Bi-naphthalene **N2** was prepared from the corresponding bi-naphthyl methanol (142 mg, 0.5 mmol). White solid (115 mg, 86% yield). **^{1}H NMR** (400 MHz, $CDCl_3$) δ 8.07 (d, *J* = 7.3 Hz, 2H), 7.93 (d, *J* = 7.6 Hz, 2H), 7.79 (d, *J* = 8.2 Hz, 2H), 7.51 (t, *J* = 7.6 Hz, 4H), 7.36 (t, *J* = 7.6 Hz, 2H), 7.11 (d, *J* = 7.0 Hz, 2H), 4.91 (s, 2H). **ESI-MS** calcd for $C_{21}H_{17}$ $[M+H]^+$ 269.13, found 269.21. *Data are consistent with literature.*

di(naphthalen-1-yl)methanol

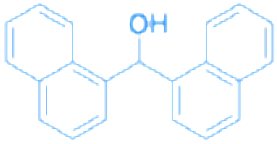

Bi-naphthalene **N3** was prepared from the corresponding ethyl formate (1.15 mL, 10 mmol). White solid (2.58 g, 91% yield). **^{1}H NMR** (400 MHz, $CDCl_3$) δ 8.05 (d, *J* = 8.3 Hz, 2H), 7.92 (d, *J* = 7.9 Hz, 2H), 7.84 (d, *J* = 8.0 Hz, 2H), 7.55 – 7.37 (m, 8H), 7.29 (d, *J* = 3.9 Hz, 1H), 2.47 (d, *J* = 4.1 Hz, 1H). **ESI-MS** calcd for $C_{21}H_{17}O$ $[M+H]^+$ 285.12, found 285.18. *Data are consistent with literature.*

4-methyl-N, N-bis(naphthalen-1-ylmethyl)benzenesulfonamide

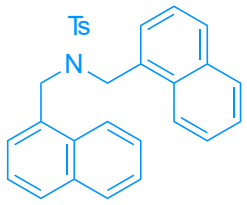

Bisnaphthalene derivative **N4** was prepared from 4-Methylbenzenesulfonamide (344 mg, 2 mmol). White solid (230 mg, 25% yield). **^{1}H NMR** (400 MHz, $CDCl_3$) δ 7.90 (d, *J* = 8.5 Hz, 2H), 7.80 (d, *J* = 8.3 Hz, 2H), 7.68 (d, *J* = 8.2, 2H), 7.50 (d, *J* = 8.2 Hz, 2H), 7.35 (m, 6H), 7.12 (m, 2H), 7.03 – 6.96 (m, 2H), 4.83 (s, 4H), 2.46 (s, 3H). **^{13}C NMR** (101 MHz, $CDCl_3$) δ 143.5, 135.9, 133.4 (2C), 131.2 (2C), 130.8 (2C), 129.7 (2C), 128.4 (2C), 128.2 (2C), 127.6 (2C), 127.0 (2C), 126.0 (2C), 125.5 (2C), 124.7 (2C), 123.3 (2C), 50.3 (2C), 21.6. **ESI-MS** calcd for $C_{29}H_{26}NO_2S$ $[M+H]^+$ 451.16, found 451.27.

4-methyl-N,N-bis(naphthalen-2-ylmethyl)benzenesulfonamide

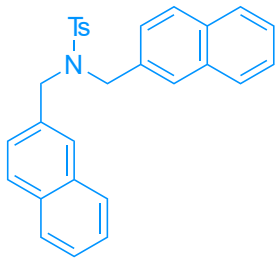

Bisnaphthalene derivative **N5** was prepared from 4-methylbenzenesulfonamide (344 mg, 2 mmol). White solid (230 mg, 25% yield). **^{1}H NMR** (400 MHz, $CDCl_3$) δ 7.84 (d, *J* = 8.4 Hz, 2H), 7.81 – 7.74 (m, 2H), 7.70 (d, *J* = 8.5 Hz, 2H), 7.65 – 7.60 (m, 2H), 7.51 – 7.42 (m, 4H), 7.39 (s, 2H), 7.33 (d, *J* = 8.0 Hz, 2H), 7.24 (dd, *J* = 8.5, 1.8 Hz, 2H), 4.55 (s, 4H), 2.47 (s, 3H). **^{13}C NMR** (101 MHz, $CDCl_3$) δ 143.7, 138.2, 133.3 (3C), 133.1 (2C), 130.1 (2C), 128.6 (2C), 128.0 (5C), 127.9 (2C), 127.6 (2C), 126.5 (2C), 126.4 (2C), 126.3 (2C), 50.9 (2C), 21.8. **ESI-MS** calcd for $C_{29}H_{26}NO_2S$ $[M+H]^+$ 451.16, found 451.27.

Naphthalen-1-ylmethyl (naphthalen-1-ylmethyl)-L-prolinate

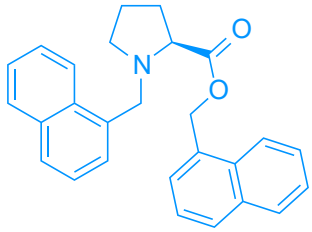

Naphthalene derivative **N6** was prepared from L-proline (345 mg, 3 mmol). Colourless sticky oil (1.08 g, 91% yield). **^{1}H NMR** (400 MHz, $CDCl_3$) δ 8.51 (d, *J* = 8.2 Hz, 1H), 8.10 – 8.04 (m, H), 7.94 – 7.88 (m, 3H), 7.82 (d, *J* = 7.9, 1H), 7.65 – 7.59 (m, 1H), 7.58 – 7.36 (m, 7H), 5.66 (s, 2H), 4.56 (d, *J* = 12.6 Hz, 1H), 3.90 (d, *J* = 12.6 Hz, 1H), 3.45 (dd, *J* = 8.9, 6.2 Hz, 1H), 2.98 (td, *J* = 7.8, 3.3 Hz, 1H), 2.48 (q, *J* = 8.4 Hz, 2H), 2.28 – 2.13 (m, 1H), 2.13 – 2.01 (m, 1H), 2.00 – 1.66 (m, 2H). **^{13}C NMR** (101 MHz, $CDCl_3$) δ174.2, 134.9, 133.8, 132.6, 131.8, 131.6, 129.4, 128.8, 128.3, 128.1, 127.7, 127.2, 126.7, 126.1 (2C), 126.0, 125.7, 125.4, 125.2, 125.0, 123.7, 65.9, 64.7, 57.0, 53.3, 29.6, 23.1. **ESI-MS** calcd for $C_{27}H_{26}NO_2$ $[M+H]^+$ 396.19, found 396.28.

(S)-di(naphthalen-1-yl)(1-(naphthalen-1-ylmethyl)pyrrolidin-2-yl)methanol

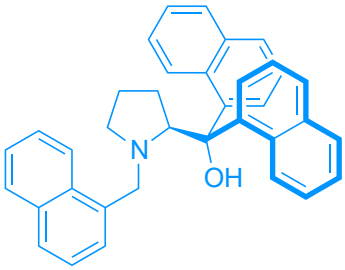

Naphthalene derivative **N7** was prepared from Naphthalen-1-ylmethyl (naphthalen-1-ylmethyl)-L-prolinate (800 mg, 2 mmol). White solid (160 mg, 16% yield). **^{1}H NMR** (400 MHz, Acetone-d6) δ 8.92 – 8.26 (bm, 4H), 7.90 – 7.53 (m, 8H), 7.52 – 7.12 (m, 8H), 4.79 (bs, 1H), 3.80 (s, 1H), 2.86 (m, 4H), 2.45 (bs, 2H), 1.73 (bs, 2H), 1.31 (bs, 1H).**^{13}C NMR** (101 MHz, Acetone-d6) δ 135.4, 135.0, 134.6, 133.6, 131.6, 128.9, 128.4 (3C), 128.2 (3C), 127.1, 126.5, 126.3, 125.3 (3C), 125.2 (2C), 124.8 (3C), 124.7 (3C), 124.5 (3C), 124.0 (3C), 58.3, 55.3, 29.7, 24.5. **ESI-MS** calcd for $C_{36}H_{32}NO$ $[M+H]^+$ 494.24, found 494.35.

(S)-2-(((tert-butyldimethylsilyl)oxy)di(naphthalen-1-yl)methyl)-1-(naphthalen-1- ylmethyl)pyrrolidine

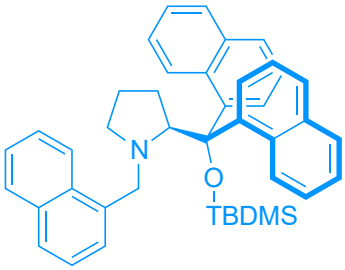

Naphthalene derivative **N8** was prepared from (S)-di(naphthalen-1-yl)(1-(naphthalen-1-ylmethyl)pyrrolidin-2-yl)methanol (50 mg,). Yellow solid (49 mg, 80% yield). Two conformers are observed (77:23 mixture). **^{1}H NMR** (400 MHz, Acetone-d6) δ 8.94 – 8.23 (RotA + RotB: bm, 4H), 8.17 (RotA: d, *J* = 7.2 Hz, 1H), 8.01 (RotA: s, 1H), 7.95 (RotA: d, *J* = 5.5 Hz, 1H), 7.90 – 7.17 (RotA: m, 13H, RotB: m, 11H), 6.67 (RotB: s, 1H), 4.76 (RotA: bm, 1H), 4.35 (RotB: bm, 1H), 2.88 – 2.77 (RotA: m, 3H), 2.49 – 2.37 (RotA: m, 2H), 1.70 (RotA + RotB: bm, 2H), 1.30 (RotA + RotB: s, 9H), 1.15 – 1.04 (RotA: m, 2H), 1.00 – 0.79 (RotA: m, 6H). **^{13}C NMR** (101 MHz, Acetone-d6) δ 145.1, 142.3, 140.0, 135.4, 135.0, 134.6, 134.0, 133.6, 132.6, 131.6, 131.4, 128.9, 128.7, 128.5, 128.4 (2C), 128.1 (2C), 128.0, 127.1 (2C), 126.5, 126.3, 126.0, 125.5, 125.4, 125.3 (2C), 125.2, 125.0, 124.8, 124.7, 124.6, 124.5, 124.0 (2C), 82.3 (RotA), 78.3, 71.5 (RotB), 58.4, 55.3, 29.9, 25.4. **ESI-MS** calcd for $C_{42}H_{45}NOSi$ $[M+H]^+$ 608.33, found 494.09 (M-TBS).

(4S,5S)-4,5-bis(methoxydi(naphthalen-1-yl)methyl)-2,2-dimethyl-1,3-dioxolane

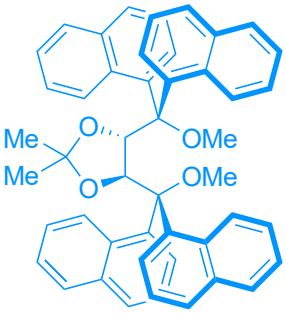

Bi-naphthalene **N10** was prepared from the corresponding tetra-naphthalene **N9** (333.4 mg, 0.5 mmol). White solid (325.4 mg, 94%). **^{1}H NMR** (400 MHz, $CDCl_3$) δ 8.78 (d, *J* = 6.1 Hz, 2H), 8.26 (d, *J* = 6.5 Hz, 2H), 8.08 (d, *J* = 8.7 Hz, 2H), 7.92 (dd, *J* = 8.1, 4.7 Hz, 4H), 7.84 – 7.75 (m, 4H), 7.69 – 7.62 (m,

4H), 7.46 (d, *J* = 9.0 Hz, 2H), 7.23 (t, *J* = 7.5 Hz, 2H), 7.09 (t, *J* = 6.9 Hz, 2H), 6.98 (t, *J* = 8.6 Hz, 2H), 6.75 – 6.62 (m, 2H), 5.88 (s, 2H), 3.43 (s, 6H), -0.12 (s, 6H). **^{13}C NMR** (101 MHz, $CDCl_3$) δ 140.7 (2C), 138.9 (2C), 134.2 (2C), 134.1 (2C), 133.7 (2C), 132.7 (2C), 129.5 (2C), 129.2 (2C), 128.7 (2C), 128.5 (2C), 127.9 (2C), 127.5 (2C), 126.7 (2C), 125.7 (2C), 125.4 (2C), 125.4 (2C), 125.0 (2C), 124.5 (2C), 124.4 (2C), 123.8 (2C), 110.6, 84.6 (2C), 78.4 (2C), 53.1 (2C), 27.0 (2C). **ESI-MS** calcd for $C_{49}H_{43}O_4$ $[M+H]^+$ 695.87, found 695.89.

Characterization of Products

- **Photocatalytic intramolecular [2+2]-cycloaddition [GP-2]:**

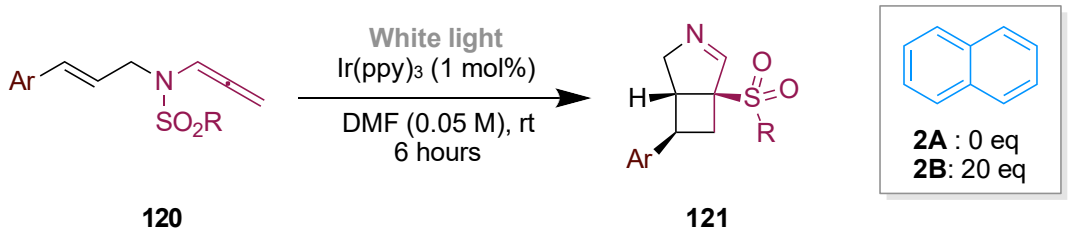

120 **121**

To a vial charged with substrate **120** (1 equiv., 0.15 mmol), $Ir(ppy)_3$ (1 mg, 1.5 µmol, 1 mol%), and naphthalene (**GP-2B**: 384 mg, 3 mmol, 20 equiv.), a dry and degassed mixture of DMF (0.05 M) was added through a syringe. Then the solution was transferred into an NMR tube capped with a rubber septum and it was placed in an oil bath kept at 25 °C and irradiated with white LED stripes for 6 hours. The mixture was then concentrated in vacuo and the residue was purified by chromatography on silica gel; the catalyst and naphthalene were removed using toluene as eluent prior to the separation of desired products (*n*-hexane/EtOAc/DCM).

6-phenyl-1-tosyl-3-azabicyclo[3.2.0]hept-2-ene

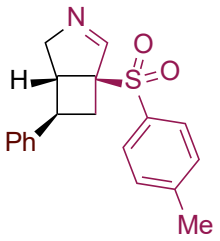

Product **121a** was prepared following general procedure **GP-2A** (18.1 mg, 37% yield, 13% *rsm*) or **GP-2B** (23.4 mg, 48% yield), from the corresponding enyne **120a** (48.8 mg, 0.15 mmol). Pale yellow solid. **^{1}H NMR** (400 MHz, $CDCl_3$) δ 7.74 (d, *J* = 7.5 Hz, 2H), 7.60 (s, 1H), 7.43 – 7.20 (m, 7H), 3.97 (d, *J* = 17.0 Hz, 1H), 3.53 (ddd, *J* = 16.9, 6.4, 2.9 Hz, 1H), 3.32 (t, *J* = 6.5 Hz, 1H), 3.20 (dd, *J* = 12.2, 8.9 Hz, 1H), 2.93 (q, *J* = 8.2 Hz, 1H), 2.73 – 2.62 (m, 1H), 2.45 (s, 3H). **ESI-HRMS** calcd for $C_{19}H_{20}NO_2S$ $[M+H]^+$ 326.4335, found 326.4326. *Data are consistent with literature.*

6-phenyl-1-(phenylsulfonyl)-3-azabicyclo[3.2.0]hept-2-ene

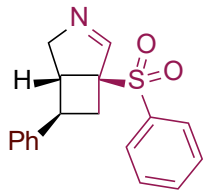

Product **121b** was prepared following general procedure **GP-2A** (13.4 mg, 29% yield, 20% *rsm*) or **GP-2B** (25.4 mg, 55% yield), from the corresponding enyne **120b** (46.3 mg, 0.15 mmol). Pale yellow solid. **^{1}H NMR** (400 MHz, $CDCl_3$) δ 7.97 – 7.84 (m, 2H), 7.79 – 7.53 (m, 4H), 7.45 – 7.20 (m, 5H), 4.00 (d, *J* = 17.0 Hz, 1H), 3.53 (ddd, *J* = 17.0, 6.3, 2.9 Hz, 1H), 3.36 (t, *J* = 6.4 Hz, 1H), 3.24 (dd, *J* = 12.1, 8.8 Hz, 1H), 2.97 (td, *J* = 8.6, 6.6 Hz, 1H), 2.72 (dd, *J* = 12.1, 8.5 Hz, 1H). **ESI-HRMS** calcd for $C_{18}H_{18}NO_2S$ $[M+H]^+$ 312.4065, found 312.4069. Data are consistent with literature.

1-(methylsulfonyl)-6-phenyl-3-azabicyclo[3.2.0]hept-2-ene

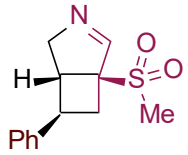

Product **121c** was prepared following general procedure **GP-2A** (13.6 mg, 36% yield, 5% *rsm*) or **GP-2B** (22.3 mg, 60% yield), from the corresponding enyne **120c** (37.4 mg, 0.15 mmol). Pale brown solid **^{1}H NMR** (400 MHz, $CDCl_3$) δ 7.80 (t, *J* = 2.6 Hz, 1H), 7.40 – 7.14 (m, 5H), 4.29 – 4.09 (m, 2H), 3.41 (t, *J* = 6.2 Hz, 1H), 3.18 – 3.00 (m, 2H), 2.80 – 2.69 (m, 4H). **ESI-HRMS** calcd for $C_{13}H_{16}NO_2S$ $[M+H]^+$ 250.3355, found 250.3347. *Data are consistent with literature.*

6-(o-tolyl)-1-tosyl-3-azabicyclo[3.2.0]hept-2-ene

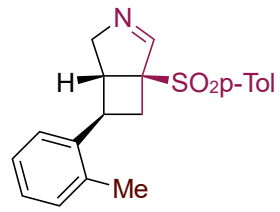

Product **121d** was prepared following general procedure **GP-2A** (27.2 mg, 53% yield, 10% *rsm*) or **GP-2B** (34.4 mg, 68% yield), from the corresponding enyne **120d** (50.9 mg, 0.15 mmol). White solid. **^{1}H NMR** (400 MHz, $CDCl_3$) δ 7.74 (d, *J* = 8.0 Hz, 2H), 7.64 (s, 1H), 7.49 (d, *J* = 7.8 Hz, 1H), 7.35 (d, *J* = 8.0

Hz, 2H), 7.31 – 7.24 (m, 1H), 7.22 – 7.08 (m, 2H), 3.98 (d, *J* = 17.0 Hz, 1H), 3.58 (ddd, *J* = 17.0, 6.4, 2.9 Hz, 1H), 3.39 (t, *J* = 6.3 Hz, 1H), 3.24 – 3.15 (m, 2H), 2.74 – 2.61 (m, 1H), 2.45 (s, 3H), 2.21 (s, 3H). **ESI-HRMS** calcd for $C_{20}H_{22}NO_2S$ $[M+H]^+$ 340.4605, found 340.4612. *Data are consistent with literature.*

6-(4-methoxyphenyl)-1-tosyl-3-azabicyclo[3.2.0]hept-2-ene

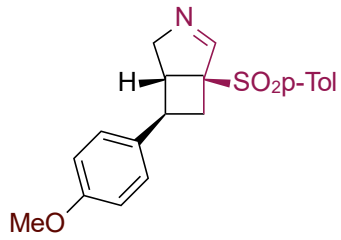

Product **121e** was prepared following general procedure **GP-2A** (24.5 mg, 46% yield, 5% *rsm*) or **GP-2B** (29.3 mg, 55% yield), from the corresponding enyne **120e** (53.2 mg, 0.15 mmol). Yellow solid. **^{1}H NMR** (400 MHz, $CDCl_3$) δ 7.74 (d, *J* = 8.3 Hz, 2H), 7.60 (s, 1H), 7.35 (d, *J* = 8.0 Hz, 2H), 7.29 – 7.17 (m, 2H), 6.88 (d, *J* = 8.6 Hz, 2H), 3.96 (d, *J* = 16.7 Hz, 1H), 3.80 (s, 3H), 3.53 (ddd, *J* = 16.8, 6.3, 2.5 Hz, 1H), 3.27 (t, *J* = 6.4 Hz, 1H), 3.15 (dd, *J* = 12.1, 8.7 Hz, 1H), 2.88 (td, *J* = 8.6, 6.6 Hz, 1H), 2.66 (dd, *J* = 12.1, 8.6 Hz, 1H), 2.45 (s, 3H). **ESI-HRMS** calcd for $C_{20}H_{22}NO_3S$ $[M+H]^+$ 356.4595, found 356.4589. *Data are consistent with literature.*

- **Photocatalytic [4+2]-dearomative cycloaddition [GP-3]:**

To a vial charged with substrate **122** (1 equiv., 0.1 mmol), Ir(ppy)3 (0.7 mg, 1 µmol, 1 mol%), and naphthalene (**GP-3B**: 256 mg, 2 mmol, 20 equiv.), dry and degassed CH_2Cl_2 (0.1 M) was added through a syringe. The solution was transferred into an NMR tube capped with a rubber septum and it was placed in an oil bath kept at 25 °C and irradiated with blue LED stripes for 1-24 hours. Conversion was monitored by TLC and the mixture was then concentrated in vacuo. The residue was purified by chromatography on silica gel; the catalyst and naphthalene were removed using toluene as eluent prior to the separation of desired products (*n*-hexane/EtOAc).

(5S,9bS)-4-phenyl-2-tosyl-1,2,3,3a,4,5-hexahydro-5,9b-ethenobenzo[e]isoindole

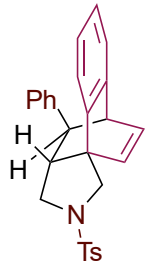

Product **123a** was prepared following general procedure **GP-3A** (40.1 mg, 94% yield, *dr* = 80:20, 8 hrs) or **GP-3B** (40.5 mg, 95% yield, *dr* = 80:20, 2 hrs), from the corresponding naphtyl amide **122a** (42.7 mg, 0.1 mmol). White solid. **^{1}H NMR** (400 MHz, $CDCl_3$) δ 7.83 – 7.72 (m, Dia1, 2H; Dia2, 2H), 7.33 (d, *J* = 8.1 Hz, Dia1, 2H; Dia2, 2H), 7.29 – 7.04 (m, Dia1, 6H; Dia2, 7H), 6.98 (dd, *J* = 7.3, 1.2 Hz, Dia1, 1H), 6.92 (td, *J* = 7.5, 1.3 Hz, Dia2, 1H), 6.75 (dd, *J* = 7.6, 6.0 Hz, Dia1, 1H; Dia2, 1H), 6.65 (dd, *J* = 7.8, 1.2 Hz, Dia2, 1H), 6.52 (dt, *J* = 7.5, 3.3 Hz, Dia1, 2H; Dia2, 1H), 5.82 (dt, *J* = 7.6, 1.2 Hz, Dia1, 1H), 4.42 (d, *J* = 10.0 Hz, Dia2, 1H), 4.08 (d, *J* = 9.6 Hz, Dia1, 1H), 4.04 – 3.93 (m, Dia1, 1H; Dia2, 1H), 3.81 (d, *J* = 6.3 Hz, Dia1, 1H), 3.69 (dd, *J* = 9.1, 7.5 Hz, Dia1, 1H; Dia2, 1H), 3.59 (d, *J* = 10.1 Hz, Dia2, 1H), 2.87 (dd, *J* = 11.0, 9.1 Hz, Dia1, 1H), 2.76 (dd, *J* = 6.0, 1.9 Hz, Dia1, 1H), 2.47 (s, Dia2, 3H), 2.43 (s, Dia1, 3H), 2.36 (dd, *J* = 11.4, 9.0 Hz, Dia2, 1H), 2.11 (dt, *J* = 11.5, 6.9 Hz, Dia2, 1H), 1.97 – 1.82 (m, Dia1, 1H). **^{13}C NMR** (101 MHz, $CDCl_3$, Dia1) δ 143.9, 143.8, 143.0, 139.9, 139.2, 135.2, 135.0, 130.1 (2C), 128.5 (2C), 127.9 (2C), 127.6 (2C), 126.9, 126.6, 126.0, 125.7, 119.0, 53.7, 53.4, 53.2, 51.1, 49.8, 48.5, 21.9. **ESI-HRMS** calcd for $C_{27}H_{26}NO_2S$ $[M+H]^+$ 428.1679, found 428.1685.

Phenyl((5S,9bS)-4-phenyl-3,3a,4,5-tetrahydro-5,9b-ethenobenzo[e]isoindol-2(1H)- yl)methanone

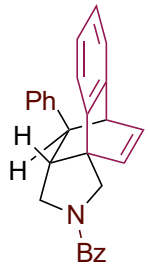

Product **123b** was prepared following general procedure **GP-3A** (35.8 mg, 94% yield, *dr* = 80:20, 10 hrs) or **GP-3B** (35.0 mg, 93% yield, *dr* = 81:19, 3 hrs), from the corresponding naphtyl amide **122b** (37.7 mg, 0.1 mmol). White solid. Two rotamers are observed due to the dynamic rotation of the amido group (Dia1 65:35 mixture of rotamers, Dia2 64:36 mixture of rotamers). **^{1}H NMR** (400 MHz, CD_2Cl_2) δ 7.67 – 7.56 (m, Dia1 RotA, 1H; Dia2 RotA, 1H; Dia2 RotB, 1H), 7.54 – 7.45 (m, Dia1 RotA, 2H; Dia1 RotB, 1H; Dia2 RotA, 2H; Dia2 RotB, 2H), 7.44 – 6.97 (m, Dia1 RotA, 11H; Dia1 RotB, 11H; Dia2 RotA, 11H; Dia2 RotB, 12H), 6.94 – 6.85 (m, Dia1 RotA, 1H; Dia1 RotB, 1H; Dia2 RotA, 1H; Dia2 RotB, 1H), 6.83 (dd, *J* = 7.7, 1.2 Hz, ,Dia2 RotA, 1H), 6.74 – 6.62 (m, Dia1 RotB, 1H; Dia2 RotB, 1H), 6.60 – 6.51 (m, Dia1 RotA, 1H; Dia2 RotA, 1H; Dia2 RotB, 1H), 6.38 (dt, *J* = 7.6, 1.2 Hz, Dia1 RotA, 1H), 6.17 (dt, *J* = 7.6 Hz, Dia1 RotB, 1H), 4.82 (d, *J* = 12.4 Hz, Dia2 RotA, 1H), 4.38 – 4.30 (m, Dia1 RotA, 1H; Dia2 RotA, 1H, Dia2 RotB 1H), 4.24 (d, *J* = 10.3 Hz, Dia1 RotB, 1H; Dia2 RotB 1H), 4.10 (d, *J* = 6.2 Hz, Dia2 RotA 1H), 4.10 – 4.00 (m, Dia2 RotB, 1H), 4.00 – 3.83 (m, Dia1 RotA, 1H; Dia1 RotB, 1H; Dia2 RotA, 1H), 3.64 (dd, *J* = 9.8, 7.3 Hz, Dia1 RotA, 1H), 3.52 (dd, *J* = 9.7, 7.0 Hz, Dia1 RotB, 1H), 3.23 – 3.10 (m, Dia1 RotA, 1H; Dia1 RotB, 1H), 2.96 (dd, *J* = 6.0, 1.9 Hz, Dia1 RotB 1H), 2.77 (dd, *J* = 6.0, 1.9 Hz, Dia1 RotA, 1H), 2.65 (dd, *J* = 6.6, 1.7 Hz, Dia2 RotB, 1H), 2.59 – 2.44 (m, Dia1RotB 1H; Dia2 RotA 1H), 2.33 (m, Dia2 RotA, 1H; Dia2 RotB, 1H), 2.20 – 2.01 (m, Dia1 RotA, 1H; Dia1 RotB, 1H). **^{13}C NMR** (101 MHz, CD_2Cl2, Dia_1) δ 170.1, 144.5, 143.2, 139.4, 139.2, 135.9, 135.1, 129.9, 128.5, 128.3 (2C), 128.1 (2C), 127.7 (3C), 127.2 (2C), 126.5, 125.2, 119.1, 55.4, 54.0, 51.9, 49.7, 47.8, 29.8. **ESI-HRMS** calcd for $C_{27}H_{24}NO$ $[M+H]^+$ 378.1932, found 378.1925.

(5S,9bS)-4-(4-methoxyphenyl)-2-tosyl-1,2,3,3a,4,5-hexahydro-5,9b-ethenobenzo[e]isoindole

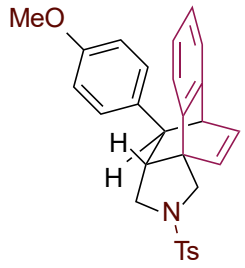

Product **123c** was prepared following general procedure **GP-3A** (42.3 mg, 92% yield, *dr* = 77:23, 3 hrs) or **GP-3B** (42.5 mg, 93% yield, *dr* = 77:23, 1 hrs), from the corresponding naphtyl amide **122c** (45.7 mg, 0.1 mmol). White solid. **^{1}H NMR** (400 MHz, $CDCl_3$) δ 7.79 (d, *J* = 8.1 Hz, Dia1, 2H; Dia2, 2H), 7.33 (d, *J* = 8.2 Hz, Dia1, 2H; Dia2, 2H), 7.29 – 7.23 (m, Dia2, 1H), 7.18 (d, *J* = 7.2 Hz, Dia1, 1H; Dia2, 2H), 7.14 – 7.03 (m, Dia1, 3H, Dia2, 1H), 6.98 (d, *J* = 7.3 Hz, Dia1, 1H), 6.91 (t, *J* = 7.5 Hz, Dia2, 1H), 6.82 (d, *J* = 8.7 Hz, Dia2, 2H), 6.74 (t, *J* = 6.8 Hz, Dia1, 1H; Dia2, 1H), 6.65 (d, *J* = 8.7 Hz, Dia1, 2H; Dia2, 1H), 6.52 – 6.47 (m, Dia2, 1H), 6.43 (d, *J* = 8.5 Hz, Dia1, 2H), 5.79 (d, *J* = 7.6 Hz, Dia1, 1H), 4.42 (d, *J* = 10.0 Hz, Dia2, 1H), 4.07 (d, *J* = 9.6 Hz, Dia1, 1H), 3.98 (d, *J* = 9.6 Hz, Dia1, 1H; Dia2, 1H), 3.85 – 3.74 (m, Dia1, 1H, Dia2, 4H), 3.72 (s, Dia1, 3H), 3.67 (d, *J* = 8.3 Hz, Dia1, 1H; Dia2, 1H), 3.58 (d, *J* = 10.1 Hz, Dia2, 1H), 2.90 – 2.81 (m, Dia1, 1H), 2.72 (d, *J* = 5.1 Hz, Dia1, 1H), 2.47 (s, Dia2, 3H), 2.43 (s, Dia1, 3H), 2.35 – 2.29 (m, Dia2, 1H), 2.09 (d, *J* = 6.8 Hz, Dia2, 1H), 1.92 – 1.81 (m, Dia1, 1H). **^{13}C NMR** (101 MHz, $CDCl_3$, Dia1) δ 158.6, 143.9, 143.8, 140.0, 139.2, 137.7, 135.1, 135.0, 130.1 (2C), 128.8 (2C), 127.6 (2C), 126.6, 126.0, 125.6, 118.9, 113.8 (2C), 55.5, 53.9, 53.4, 53.1, 51.1, 50.1, 47.7, 21.9. **ESI-HRMS** calcd for $C_{28}H_{27}NNaO_3S$ $[M+Na]^+$ 480.1609, found 480.1615.

(5S,9bS)-4-phenyl-3,3a,4,5-tetrahydro-1H-5,9b-ethenonaphtho[1,2-c]furan

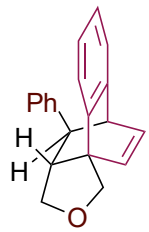

Product **123d** was prepared following general procedure **GP-3A** (23.2 mg, 83% yield, *dr* = 85:15, 24 hrs) or **GP-3B** (25.5 mg, 93% yield, *dr* = 83:17, 5 hrs), from the corresponding naphtyl ether **122d** (27.4 mg, 0.1 mmol). Colourless oil. **^{1}H NMR** (400 MHz, $CDCl_3$) δ 7.43 (m, Dia2, 1H), 7.33 (m, Dia2, 2H),

7.28 – 7.06 (m, Dia1, 7H; Dia2, 6H), 6.91 (dd, *J* = 7.6, 6.2 Hz, Dia1, 1H), 6.79 (dd, *J* = 7.7, 1.2 Hz, Dia2, 1H), 6.64 (m, Dia1, 2H; Dia2, 1H), 6.38 (d, *J* = 7.6 Hz, Dia1, 1H), 4.96 (d, *J* = 8.7 Hz Dia2, 1H), 4.52 (s, Dia1, 2H), 4.16 – 4.03 (m, Dia1, 1H; Dia2, 2H), 3.93 (d, *J* = 6.1 Hz, Dia1, 1H), 3.36 (dd, *J* = 11.0, 7.4 Hz, Dia1, 1H), 2.88 – 2.81 (m, Dia1 1H; Dia2, 2H), 2.56 (dd, *J* = 6.9, 1.6 Hz, Dia2, 1H), 2.41 (dt, *J* = 11.3, 7.1 Hz, Dia2, 1H), 2.21 (dddd, *J* = 11.0, 7.5, 6.3, 1.1 Hz, Dia1, 1H). **^{13}C NMR** (101 MHz, $CDCl_3$, Dia1) δ 144.2, 143.4, 140.3, 138.7, 136.0, 128.2 (2C), 127.6 (2C), 126.5, 126.3, 125.6, 125.1, 118.7, 72.7, 70.1, 55.5, 54.7, 50.0, 47.2. **ESI-HRMS** calcd for $C_{20}H_{18}O$ $[M+H]^+$ 275.3650, found 275.3663.

(5S,9bS)-4-(2-chlorophenyl)-3,3a,4,5-tetrahydro-1H-5,9b-ethenonaphtho[1,2-c]furan

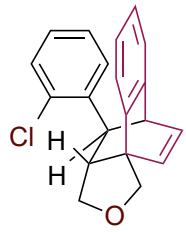

Product **123e** was prepared following general procedure **GP-3A** (26.2 mg, 85% yield, *dr* = 84:16, 24 hrs) or **GP-3B** (27.7 mg, 90% yield, *dr* = 83:17, 5 hrs), from the corresponding naphtyl ether **122e** (30.8 mg, 0.1 mmol). White solid. **^{1}H NMR** (400 MHz, $CDCl_3$) δ 7.42 – 7.39 (m, Dia2, 1H), 7.34 (dd, *J* = 8.0, 1.4 Hz, Dia1, 1H; Dia2, 2H), 7.28 (dd, *J* = 6.6, 1.9 Hz, Dia2, 2H), 7.24 – 7.15 (m, Dia1, 2H, Dia2, 3H), 7.08 (dtd, *J* = 9.6, 7.6, 1.6 Hz, Dia1, 2H), 6.99 (d, *J* = 7.3 Hz, Dia1, 1H), 6.96 – 6.87 (m, Dia1, 2H), 6.78 (dd, *J* = 7.7, 1.2 Hz, Dia2, 1H), 6.59 (dd, *J* = 7.7, 5.7 Hz, Dia2, 1H), 6.38 (d, *J* = 7.6 Hz, Dia1, 1H), 6.11 (dd, *J* = 7.9, 1.6 Hz, Dia1, 1H), 4.93 (d, *J* = 8.7 Hz, Dia2, 1H), 4.50 (d, *J* = 1.1 Hz, Dia1, 2H), 4.16 – 4.02 (m, Dia1, 1H; Dia2, 3H), 3.86 (d, *J* = 6.2 Hz, Dia1, 1H), 3.44 (dd, *J* = 6.4, 1.7 Hz, Dia1, 1H), 3.37 (dd, *J* = 10.9, 7.6 Hz, Dia1, 1H), 3.07 (dd, *J* = 7.0, 1.5 Hz, Dia2, 1H), 2.88 (dd, *J* = 11.3, 7.7 Hz, Dia2, 1H), 2.31 (d, *J* = 11.3 Hz, Dia2, 1H), 2.22 – 2.11 (m, Dia1, 1H). **^{13}C NMR** (101 MHz, $CDCl_3$, Dia1) δ 144.1, 140.2, 138.7, 136.2, 134.3, 129.4, 127.7, 127.6, 127.5, 126.5, 126.2, 125.7, 125.1, 118.8, 72.6, 69.9, 54.7, 54.4, 48.7, 42.3. **ESI-HRMS** calcd for $C_{20}H_{18}ClO$ $[M+H]^+$ 309.1046, found 309.1051.

(5S,9bS)-1-(naphthalen-1-yl)-4-phenyl-3,3a,4,5-tetrahydro-1H-5,9b-ethenonaphtho[1,2- c]furan

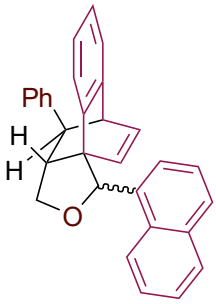

Product **123f** was prepared following general procedure **GP-3A** [24 mg, 60, yield, *dr* (Dia1:Dia2:Min1:Min2)= 44:44:12:2, 48 hrs] or **GP-3B** [28 mg, 70% yield, *dr* (Dia1:Dia2:Min1:Min2)= 44:44:12:2, 48 hrs], from the corresponding bisnaphtyl ether **122f** (40 mg, 0.1 mmol). White solid. Four products were observed, namely Dia1, Dia2, Min1 and Min2. **^{1}H NMR** (400 MHz, $CDCl_3$) δ 8.67 (d, *J* = 8.6 Hz, Dia1 1H), 8.60 – 8.55 (m, Min1 1H), 8.14 – 8.09 (bm, Min2 1H), 8.08 – 7.97 (m, Min1 2H, Min2 2H), 7.99 – 7.79 (m, Dia1 3H, Dia2 3H, Min1 3H, Min2 3H), 7.77 – 7.43 (m, Dia1 4H, Dia2 5H, Min1 4H, Min2 5H), 7.42 – 7.03 (m, Dia1 6H, Dia2 8H, Min1 6H, Min2 3H), 6.98 – 6.90 (m, Dia2 2H), 6.89 – 6.85 (m, Dia1 1H, Min1 1H, Min2 1H), 6.79 (d, *J* = 7.7 Hz, Dia2 1H), 6.69 – 6.64 (m, Dia1 1H, Min1 1H), 6.26 (dd, *J* = 8.1, 5.7 Hz, Dia1 1H, Min1 1H), 6.19 (s, Dia1 1H), 6.13 (d, *J* = 7.9 Hz, Min2 1H), 6.09 (s, Min2 1H), 6.03 (dd, *J* = 8.0, 1.2 Hz, Dia1 1H), 5.93 (d, *J* = 8.9 Hz, Min2 1H), 5.05 (dd, *J* = 9.2, 7.8 Hz, Min1 1H), 4.97 – 4.91 (m, Min2 1H), 4.82 – 4.67 (m, Min1 1H), 4.50 – 4.37 (m, Dia1 2H, , Min1 1H), 4.32 (t, *J* = 7.4 Hz, Min2 1H), 4.28 (dd, *J* = 5.3, 2.6 Hz, Min2 1H), 4.25 (d, *J* = 2.7 Hz, Min2 1H), 4.20 – 4.17 (m, Min1 1H, Min2 1H), 4.03 (t, *J* = 5.1 Hz, Dia2 2H), 3.57 (dd, *J* = 10.6, 7.6 Hz, Dia1 1H), 3.13 (dd, *J* = 11.4, 7.7 Hz, Dia2 1H), 3.00 – 2.89 (m, Dia1 1H), 2.87 (dd, *J* = 6.4, 1.8 Hz, Min2 1H), 2.65 – 2.52 (m, Dia1 1H, Dia2 2H, Min1 1H). **^{13}C NMR** (101 MHz, $CDCl_3$) 146.95, 144.63, 144.22, 143.63, 140.57, 140.50, 137.94, 137.73, 137.52, 134.61, 133.69, 133.44, 133.24, 133.17, 131.86, 131.03, 129.30, 129.19, 128.87, 128.74, 128.54, 128.25, 128.08, 127.83, 127.74, 126.90, 126.84, 126.77, 126.72, 126.59, 126.45, 126.36, 126.14, 126.09, 125.97, 125.80, 125.63, 125.11, 124.49, 123.60, 123.12, 122.48, 120.48, 81.61, 79.42, 75.93, 73.92, 72.40, 71.93, 58.32, 57.86, 56.73, 56.54, 53.26, 50.19, 49.29, 48.76, 48.45, 47.42. **ESI-HRMS** calcd for $C_{27}H_{24}NO$ $[M+H]^+$ 401.1987, found 401.2001.

- Photocatalytic HAT-cyclization cascade [GP-4]:

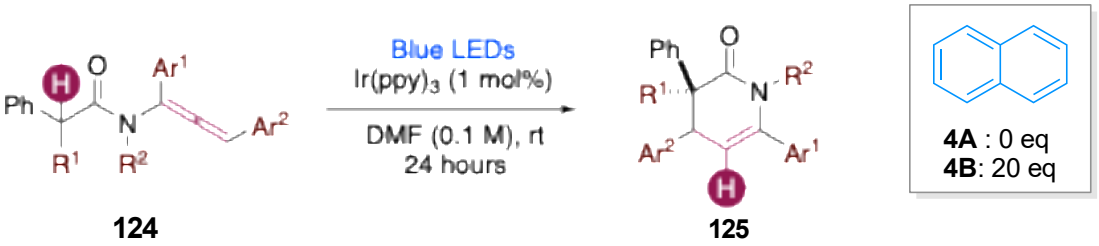

124 **125**

To a vial charged with substrate **124** (1 equiv., 0.15 mmol), $Ir(ppy)_3$ (1 mg, 1.5 µmol, 1 mol%), and naphthalene (**GP-4B**: 384 mg, 3 mmol, 20 equiv.) a dry and degassed mixture of DMF (0.1 M) was added through a syringe. Then the solution was transferred into an NMR tube capped with a rubber septum and it was placed in an oil bath kept at 25 °C and irradiated with blue LED stripes for 1 day. The mixture was then concentrated in vacuo and the residue was purified by chromatography on silica gel; the catalyst and the naphthalene were removed using toluene as eluent prior to the separation of desired products (*n*-hexane/EtOAc).

1-benzyl-3,3,4,6-tetraphenyl-3,4-dihydropyridin-2(1H)-one

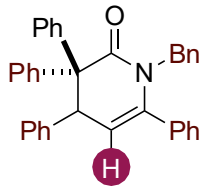

Product **125a** was prepared following general procedure **GP-4A** (39 mg, 40% yield) or **GP-4B** (68 mg, 91% yield), from the corresponding N-benzyl-N-(1,3-diphenylpropa-1,2-dien-1-yl)-2,2-diphenylacetamide (74 mg, 0.15 mmol). White solid. **^{1}H NMR** (400 MHz, $CDCl_3$) δ 7.64 (dd, *J* 7.8, 2.0 Hz, 1H), 7.50 – 7.35 (m, 2H), 7.35 – 7.25 (m, 4H), 7.14 – 6.93 (m, 5H), 6.89 (t, *J* = 7.7 Hz, 1H), 6.71 – 6.61 (m, 1H), 6.58 – 6.42 (m, 1H), 5.68 (d, *J* = 6.9 Hz, 1H), 5.27 (d, *J* = 14.5 Hz, 1H), 4.37 (d, *J* = 14.5 Hz, 1H), 4.18 (d, *J* = 6.9 Hz, 1H). **^{13}C NMR** (101 MHz, $CDCl_3$) δ 171.86, 142.60, 141.91, 141.09, 137.79, 136.47, 130.84 (2C), 129.80 (2C), 129.57 (2C), 129.13 (2C), 128.64 (2C), 128.60 (2C), 128.48 (2C), 128.36 (2C), 128.27 (2C), 128.16 (2C), 127.68 (2C), 127.09, 126.80 (2C), 126.06, 114.06, 61.11, 48.82, 47.52. **ESI-HRMS** calcd for $C_{36}H_{30}NO$ $[M+H]^+$ 492.2322, found 492.2332.

1-butyl-3,3,4,6-tetraphenyl-3,4-dihydropyridin-2(1H)-one

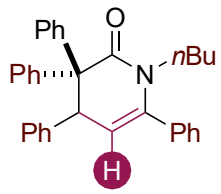

Product **125b** was prepared following general procedure **GP-4A** (15.8 mg, 23% yield) or **GP-4B** (55.6 mg, 81% yield), from the corresponding N-butyl-N-(1,3-diphenylpropa-1,2-dien-1-yl)-2,2-diphenylacetamide (68.6 mg, 0.15 mmol). White solid. **^{1}H NMR** (400 MHz, $CDCl_3$) δ 7.67 – 7.56 (m, 2H), 7.43 – 7.24 (m, 6H), 7.23 – 7.08 (m, 3H), 7.08 – 6.92 (m, 5H), 6.92 – 6.84 (m, 2H), 6.68 (dd, *J* = 7.5, 1.8 Hz, 2H), 5.65 (d, *J* = 6.8 Hz, 1H), 4.23 (d, *J* = 6.9 Hz, 1H), 3.85 (ddd, *J* = 13.5, 9.9, 5.9 Hz, 1H), 3.20 (ddd, *J* = 13.6, 9.8, 5.6 Hz, 1H), 1.58 (dtd, *J* = 19.3, 9.6, 8.1, 4.9 Hz, 2H), 1.17 (ddt, *J* = 14.0, 11.1, 7.1 Hz, 2H), 0.79 (t, *J* = 7.4 Hz, 3H). **^{13}C NMR** (101 MHz, $CDCl_3$) δ 171.27, 142.20, 141.87, 141.20, 138.13, 136.30, 130.73, 129.58, 128.78, 128.33, 128.00, 127.34, 127.10, 126.57, 125.86, 112.91, 60.78, 48.46, 44.27, 30.47, 20.27, 13.64. **ESI-HRMS** calcd for $C_{33}H_{32}NO$ $[M+H]^+$ 458.6245, found 458.6238.

(3R)-1-benzyl-3-methyl-3,4,6-triphenyl-3,4-dihydropyridin-2(1H)-one

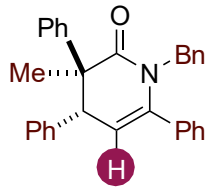

Product **125c** was prepared following general procedure **GP-4B** (44 mg, 80% yield, dr = 86:14), from the corresponding N-benzyl-N-(1,3-diphenylpropa-1,2-dien-1-yl)-2-phenylpropanamide (64 mg, 0.15 mmol). Yellow solid. Dia maj **^{1}H NMR** (400 MHz, $CDCl_3$) δ 7.48 – 7.45 (m, 2H), 7.39 – 7.23 (m, 10H), 7.19 – 7.00 (m, 6H), 6.90 – 6.83 (m, 2H), 5.43 (d, *J* = 6.7 Hz, 1H), 5.24 (d, *J* = 14.3 Hz, 1H), 4.48 (d, *J* = 14.3 Hz, 1H), 4.02 (d, *J* = 6.6 Hz, 1H), 1.28 (s, 3H). Dia maj **^{13}C NMR** (101 MHz, $CDCl_3$) δ 174.33, 144.65, 141.70, 138.37, 137.49, 136.37, 129.92 (2C), 129.57 (2C), 128.72 (2C), 128.63 (3C), 128.57 (4C), 128.31 (2C), 127.81, 127.36, 127.19, 126.41 (2C), 114.29, 51.65, 48.53, 47.39, 24.67. **ESI-HRMS** calcd for $C_{31}H_{28}NO$ $[M+H]^+$ 430.2165, found 430.2171.

1-benzyl-3,4,6-triphenyl-3,4-dihydropyridin-2(1H)-one

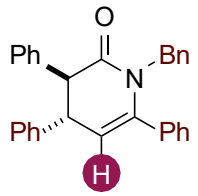

Product **125d** was prepared following general procedure **GP-4B** (25 mg, 40% yield), from the corresponding N-benzyl-N-(1,3-diphenylpropa-1,2-dien-1-yl)-2-phenylacetamide (62 mg, 0.15 mmol). Yellow solid. **^{1}H NMR** (400 MHz, $CDCl_3$) δ 7.40 – 7.14 (m, 16H), 7.05 (dd, *J* = 6.6, 3.0 Hz, 2H), 6.97 – 6.87 (m, 2H), 5.46 (d, *J* = 5.3 Hz, 1H), 5.01 (d, *J* = 14.8 Hz, 1H), 4.70 (d, *J* = 14.8 Hz, 1H), 4.06 (d, *J* = 6.1 Hz, 1H), 3.94 (t, *J* = 5.8 Hz, 1H). **^{13}C NMR** (101 MHz, $CDCl_3$) δ 171.10, 142.51, 141.68, 138.97, 137.92, 136.15, 128.94 (2C), 128.87 (2C), 128.83 (2C), 128.79 (2C), 128.74 (2C), 128.49 (2C), 128.47 (2C), 128.44 (2C), 128.01, 127.53, 127.47, 127.18, 113.14, 55.59, 46.86, 45.21. **ESI-HRMS** calcd for $C_{30}H_{26}NO$ $[M+H]^+$ 416.2009, found 416.2014.

1-benzyl-3,3,6-triphenyl-4-(p-tolyl)-3,4-dihydropyridin-2(1H)-one

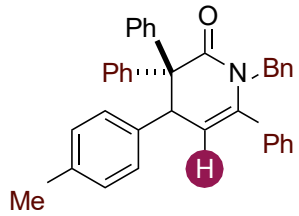

Product **125e** was prepared following general procedure **GP-4A** (41 mg, 34% yield) or **GP-4B** (57 mg, 75% yield), from the corresponding N-benzyl-2,2-diphenyl-N-(1-phenyl-3-(p-tolyl)propa-1,2-dien-1-yl)acetamide (76 mg, 0.15 mmol). Orange solid. **^{1}H NMR** (400 MHz, $CDCl_3$) δ 7.63 (dd, *J* = 7.8, 1.9 Hz, 2H), 7.46 – 7.22 (m, 9H), 7.12 – 6.85 (m, 7H), 6.76 – 6.63 (m, 4H), 6.41 (d, *J* = 8.0 Hz, 2H), 5.66 (d, *J* = 6.9 Hz, 1H), 5.26 (d, *J* = 14.5 Hz, 1H), 4.36 (d, *J* = 14.5 Hz, 1H), 4.15 (d, *J* = 7.0 Hz, 1H), 2.25 (s, 3H). **^{13}C NMR** (101 MHz, $CDCl_3$) δ 171.96, 142.62, 142.02, 140.88, 137.84, 136.71, 136.52, 134.62, 130.90 (2C), 129.70 (2C), 129.56 (2C), 129.13 (2C), 128.86 (2C), 128.61 (2C), 128.55, 128.45 (2C), 128.36 (2C), 128.25 (2C), 127.66, 127.63, 126.78 (2C), 126.02, 114.35, 61.10, 48.42, 47.51, 21.32. **ESI-HRMS** calcd for $C_{37}H_{32}NO$ $[M+H]^+$ 506.2478, found 506.2468.

1-benzyl-6-(4-chlorophenyl)-3,3,4-triphenyl-3,4-dihydropyridin-2(1H)-one

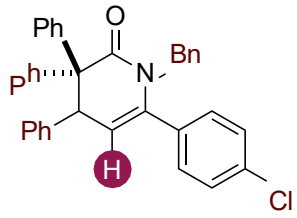

Product **125f** was prepared following general procedure **GP-4A** (42 mg, 39% yield) or **GP-4B** (68 mg, 85% yield), from the corresponding N-benzyl-N-(1-(4-chlorophenyl)-3-phenylpropa-1,2-dien-1-yl)-2,2-diphenylacetamide (79 mg, 0.15). Pale yellow solid. **^{1}H NMR** (400 MHz, $CDCl_3$) δ 7.64 (dd, *J* = 7.7, 2.1 Hz, 2H), 7.49 – 7.18 (m, 8H), 7.17 – 6.80 (m, 10H), 6.66 (dd, *J* = 7.2, 1.6 Hz, 2H), 6.53 – 6.50 (m, 2H), 5.68 (d, *J* = 6.9 Hz, 1H), 5.27 (d, *J* = 14.6 Hz, 1H), 4.36 (d, *J* = 14.6 Hz, 1H), 4.20 (d, *J* = 7.0 Hz, 1H). **^{13}C NMR** (101 MHz, $CDCl_3$) δ 171.83, 142.39, 141.78, 140.09, 137.59, 137.51, 134.91, 134.54, 130.81 (2C), 129.74 (2C), 129.60 (2C), 129.44 (2C), 129.06 (2C), 128.90 (2C), 128.59 (2C), 128.33 (2C), 128.21 (2C), 127.82, 127.77, 127.19, 126.84 (2C), 126.15, 114.67, 61.09, 48.77, 47.53. **ESI-HRMS** calcd for $C_{36}H_{28}ClNNaO$ $[M+Na]^+$ 548.1752, found 548.1755.

1-benzyl-6-(4-methoxyphenyl)-3,3,4-triphenyl-3,4-dihydropyridin-2(1H)-one

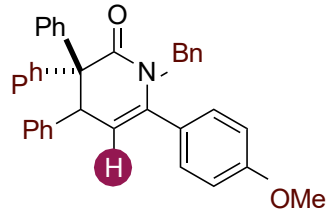

Product **125g** was prepared following general procedure **GP-4A** (38 mg, 27% yield) or **GP-4B** (68 mg, 86% yield), from the corresponding N-benzyl-N-(1-(4-methoxyphenyl)-3-phenylpropa-1,2-dien-1-yl)-2,2-diphenylacetamide (78 mg, 0.15 mmol). White solid. **^{1}H NMR** (400 MHz, $CDCl_3$) δ 7.63 (dd, *J* = 7.8, 1.9 Hz, 2H), 7.47 – 7.22 (m, 6H), 7.14 – 6.75 (m, 12H), 6.66 – 6.61 (m, 2H), 6.53 – 6.46 (m, 2H), 5.62 (d, *J* = 6.9 Hz, 1H), 5.24 (d, *J* = 14.5 Hz, 1H), 4.38 (d, *J* = 14.5 Hz, 1H), 4.15 (d, *J* = 7.0 Hz, 1H), 3.81 (s, 3H). **^{13}C NMR** (101 MHz, $CDCl_3$) δ 171.86, 159.86, 142.68, 141.97, 140.73, 137.92 (2C), 130.85 (2C), 129.80 (2C), 129.65 (2C), 129.51 (2C), 129.16 (2C), 128.89, 128.46 (2C), 128.24 (2C), 128.14 (2C), 127.64 (2C), 127.04, 126.78 (2C), 126.03, 113.98 (2C), 113.50, 61.13, 55.61, 48.79, 47.48. **ESI-HRMS** calcd for $C_{37}H_{32}NO_2$ $[M+H]^+$ 522.2428, found 522.2421.

●Bi-naphthalene catalyzed intramolecular [2+2]-cycloaddition [GP-5]:

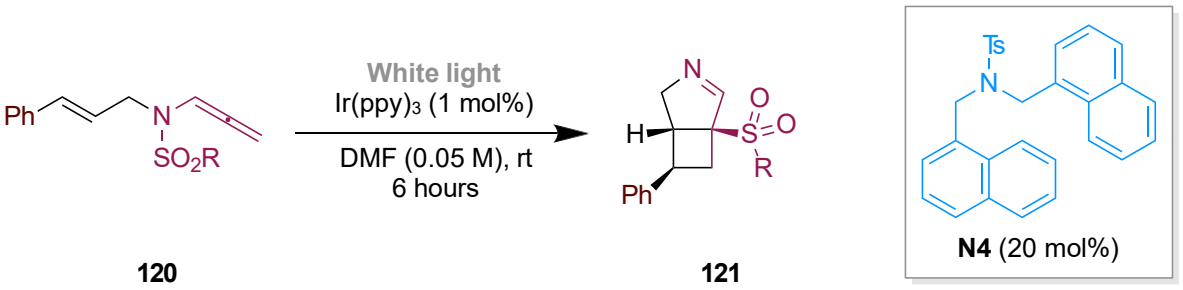

120 **121**

To a vial charged with substrate **120** (1 equiv., 0.15 mmol), $Ir(ppy)_3$ (1 mg, 1.5 µmol, 1 mol%), and bi-naphthalene **N4** (13.5 mg, 30 µmol, 20 mol%) a dry and degassed mixture of DMF (0.05 M) was added through a syringe. Then the solution was transferred into an NMR tube capped with a rubber septum and it was placed in an oil bath kept at 25 °C and irradiated with white LED stripes for 6 hours. The mixture was then concentrated in vacuo and the residue was purified by chromatography on silica gel (*n*-hexane/EtOAc/DCM).

Product	R	Yield (%)
121b	Ph	51
121c	Me	56

●Bi-naphthalene promoted [4+2]-dearomative cycloaddition [GP-6]:

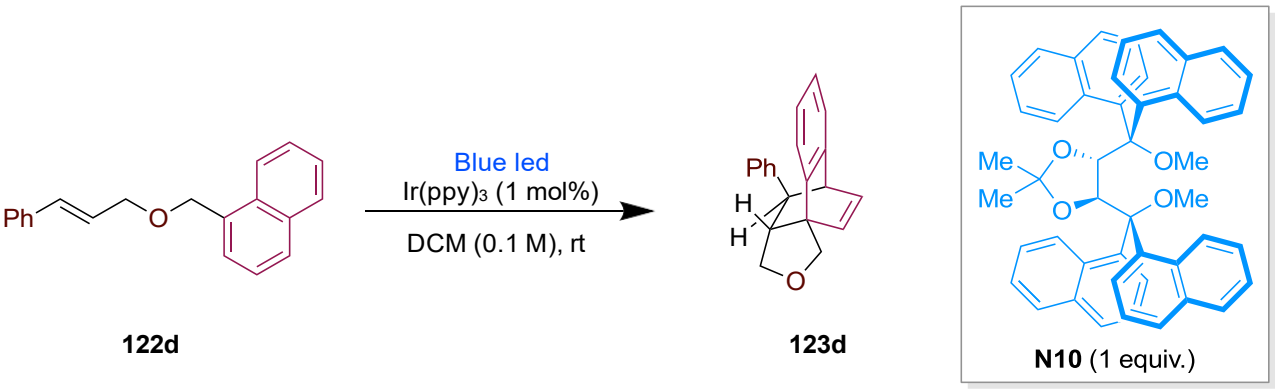

122d **123d**

To a vial charged with substrate **122d** (1 equiv., 0.1 mmol), $Ir(ppy)_3$ (0.7 mg, 1 µmol, 1 mol%), and tetra-naphthalene **N10** (69.5 mg, 0.1 mmol, 1 equiv.), dry and degassed CH_2Cl_2 (0.1 M) was added through a syringe. The solution was transferred into an NMR tube capped with a rubber septum and it was placed in an oil bath kept at 25 °C and irradiated with blue LED stripes until complete

consumption of the starting material. Conversion was monitored by TLC and the mixture was then concentrated in vacuo. The residue was purified by chromatography on silica gel (*n*-hexane/EtOAc 20:1), affording the cycloadduct **123d** as a colourless oil (26.1 mg, 95% yield, *dr* = 82:18, 10 hrs).

- **Bi-naphthalene catalyzed HAT-cyclization cascade [GP-7]:**

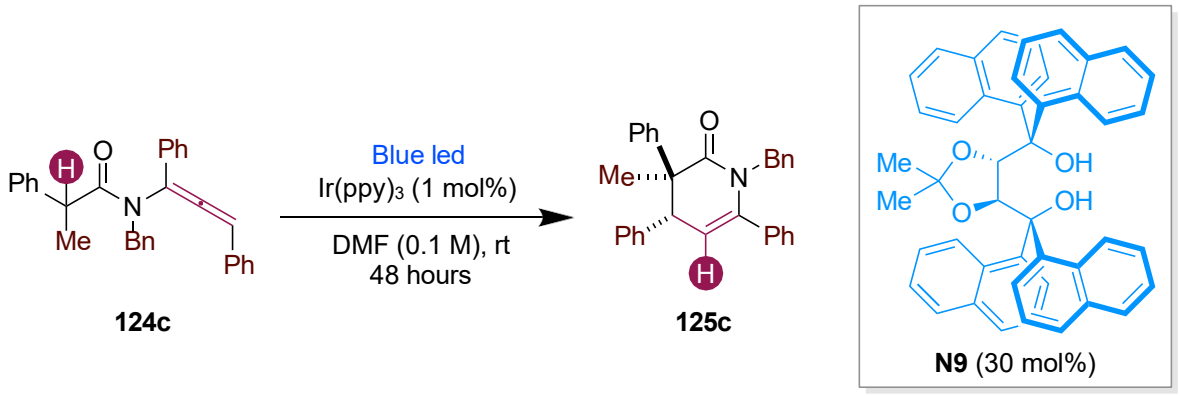

To a vial charged with substrate **124c** (1 equiv., 0.15 mmol), $Ir(ppy)_3$ (1 mg, 1.5 µmol, 1 mol%), and tetra-naphthalene **N9** (30.0 mg, 45 µmol, 30 mol%) a dry and degassed mixture of DMF (0.1 M) was added through a syringe. Then the solution was transferred into an NMR tube capped with a rubber septum and it was placed in an oil bath kept at 25 °C and irradiated with blue LED stripes for 2 days. The mixture was then concentrated in vacuo and the residue was purified by chromatography on silica gel; the catalyst and naphthalene were removed using toluene as eluent prior to the separation of desired products (*n*-hexane/EtOAc 9:1), affording the cycloadduct **125c** as a white solid (42.5 mg, 66% yield, *dr* = 56:44).

- **Bi-naphthalene catalyzed intramolecular benzyl-dearomatization [GP-8]:**

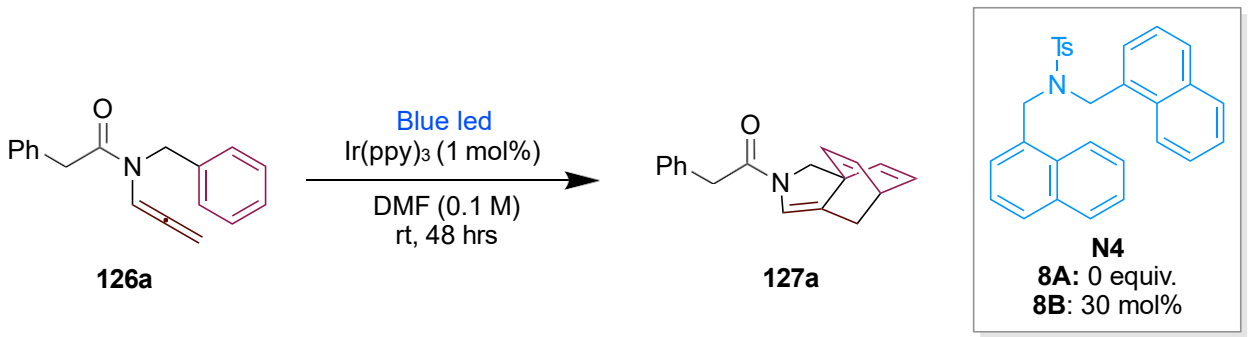

To a vial charged with substrate **126a** (26 mg, 0.1 mmol), $Ir(ppy)_3$ (1 mg, 1.5 µmol, 1 mol%), and bi-

naphthalene **N4** (**GP-8B**: 13.5 mg, 30 µmol, 30 mol%) a dry and degassed mixture of DMF (0.1 M) was added through a syringe. Then the solution was transferred into an NMR tube capped with a rubber septum and it was placed in an oil bath kept at 25 °C and irradiated with blue LED stripes for 2 days. The mixture was then concentrated in vacuo and the residue was purified by chromatography on silica gel (*n*-hexane/EtOAc 9:1).

1-((3as,6s)-6,7-dihydro-3a,6-ethenoisoindol-2(3H)-yl)-2-phenylethan-1-one

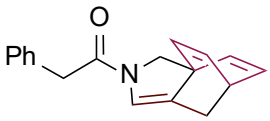

Product **127a** was prepared following general procedure **GP-8A** (3.8 mg, 15% yield) or **GP-8B** (21 mg, 79% yield), from the corresponding N-benzyl-2-phenyl-N-(propa-1,2-dien-1-yl)acetamide (26 mg, 0.1 mmol). Yellow solid. Two rotamers are observed due to the dynamic rotation of the amido group (65:35 mixture of rotamers). **^{1}H NMR** (400 MHz, $CDCl_3$) δ 7.44 – 7.10 (m, 5H), 6.65 (t, RotB, *J* 1.9 Hz, 1H), 6.34 – 6.26 (m, 4H), 6.21 (t, RotA *J* = 1.9 Hz, 1H), 4.29 (s, RotA 2H), 4.21 (s, RotB, 2H), 3.89 (dq, *J* = 5.3, 2.7, 2.2 Hz, 1H), 3.73 (s, RotB, 1H), 3.71 (s, RotA, 1H), 2.06 (t, RotB, *J* = 2.3 Hz, 2H), 2.05 (t, RotA, *J* = 2.2 Hz, 2H). **^{13}C NMR** (101 MHz, $CDCl_3$) δ 166.72 (RotA), 166.40 (RotB), 138.70 (2C, RotA), 138.28 (2C, RotB), 134.22 (2C, RotB), 134.17 (2C, RotA), 129.97 (2C, RotB), 129.30 (2C, RotB), 129.18 (2C, RotA), 129.05 (RotA) 129.01 (2C, RotA), 127.24 (RotB), 127.17 (Rot A), 117.35 (RotB), 117.06 (RotA), 58.30 (RotB), 56.19 (RotA), 54.83 (RotB), 53.99 (RotA), 42.28 (RotB), 41.87 (RotA), 40.32 (RotB), 40.27 (RotA), 30.03 (RotB), 28.39 (RotA), 28.08 (RotB). **ESI-HRMS** calcd for $C_{18}H_{18}NO$ $[M+H]^+$ 264.1383, found 264.1377.

- **Bi-naphthalene catalyzed intramolecular [2+2]-cycloaddition [GP-8]:**

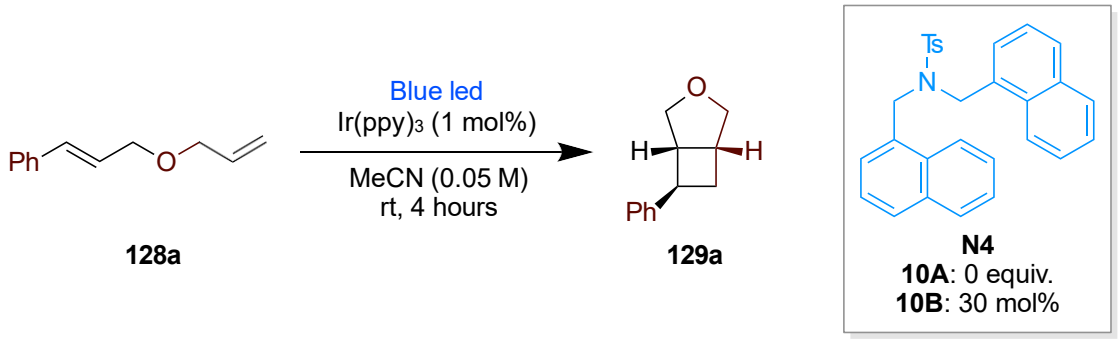

To a vial charged with substrate **128a** (17.4 mg, 0.1 mmol), $Ir(ppy)_3$ (0.7 mg, 1 µmol, 1 mol%), and bi-naphthalene **N4** (**GP-10B**: 13.5 mg, 30 µmol, 30 mol%) a dry and degassed mixture of MeCN (0.05 M) was added through a syringe. Then the solution was transferred into an NMR tube capped with a rubber septum and it was placed in an oil bath kept at 25 °C and irradiated with blue LED stripes for 4 hours. The mixture was then concentrated in vacuo and the residue was purified by chromatography on silica gel (*n*-hexane/EtOAc 20:1).

6-phenyl-3-oxabicyclo[3.2.0]heptane

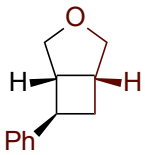

Product **129a** was prepared following general procedure **GP-10A** (3.6 mg, 21% yield, *dr* = 86:14) or **GP-10B** (16.7 mg, 96% yield, *dr* = 86:14), from the corresponding cinnamyl ether (17.4 mg, 0.1 mmol). Yellow oil. **^{1}H NMR** (400 MHz, $CDCl_3$) δ 7.37 – 7.31 (m, Dia1, 2H; Dia2, 2H), 7.30 – 7.26 (m, Dia1, 2H), 7.24 – 7.19 (m, Dia1, 1H; Dia2, 3H), 4.01 (dd, J = 9.3, 7.3 Hz, Dia1, 2H), 3.86 (d, J = 9.0 Hz, Dia2, 1H), 3.72 (dd, J = 9.8, 1.6 Hz, Dia2, 2H), 3.63 (dd, J = 9.3, 5.7 Hz, Dia1, 1H), 3.53 (dd, J = 9.3, 4.6 Hz, Dia1, 1H), 3.45 (dd, J = 9.0, 4.4 Hz, Dia2, 1H), 3.38 (dd, J = 10.0, 6.7 Hz, Dia2, 1H), 3.30 – 3.17 (m, Dia1, 1H; Dia2, 1H), 3.07 – 2.93 (m, Dia1, 2H; Dia2, 1H), 2.45 (dddd, J = 12.4, 10.4, 8.2, 2.4 Hz, Dia2, 1H), 2.32 (dt, J = 12.4, 8.1 Hz, Dia1, 1H), 2.23 – 2.15 (m, Dia1, 1H; Dia2, 1H). **^{13}C NMR** (101 MHz, $CDCl_3$) δ 146.2, 128.5 (2C), 126.5 (2C), 126.0, 74.5, 74.1, 47.3, 42.0, 35.4, 31.9. **ESI-HRMS** calcd for $C_{12}H_{14}O$ $[M+H]^+$ 175.1045, found 175.1050. *Data is consistent with the literature.*

- **Bi-naphthalene catalyzed [2+2]-dearomative cycloaddition [GP-9]:**

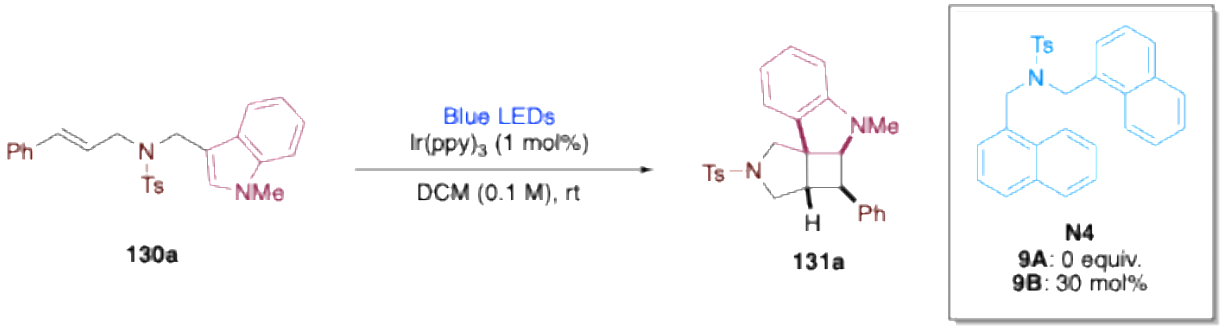

To a vial charged with substrate **130a** (43,0 mg, 1 equiv., 0.1 mmol), $Ir(ppy)_3$ (0.7 mg, 1 µmol, 1 mol%), and bi-naphthalene **N4** (**GP-9B**: 13.5 mg, 30 µmol, 30 mol%), dry and degassed CH_2Cl_2 (0.1 M) was added through a syringe. The solution was transferred into an NMR tube capped with a rubber septum and it was placed in an oil bath kept at 25 °C and irradiated with blue LED stripes until complete consumption of the starting material (monitored by TLC). Conversion was monitored by TLC and the mixture was then concentrated in vacuo. The residue was purified by chromatography on silica gel (*n*-hexane/EtOAc 20:1 + Et_3N 1 %), affording the cycloadduct **131a** as a colourless oil (*the product was found to be unstable in acid environments, and tends to undergo retro [2+2] reforming the starting material*).

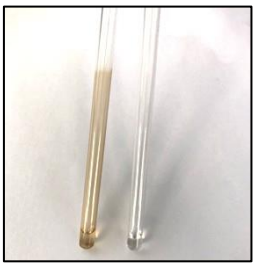

Comparison of the decomposition residue in the reaction tubes following **GP- 9A** (left) and **GP-9B** (right).

(3aS,4R,4aS,9bS)-5-methyl-4-phenyl-2-tosyl-2,3,3a,4,4a,5-hexahydro-1H-pyrrolo[3',4':2,3]cyclobuta[1,2-b]indole

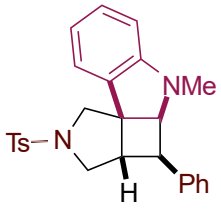

Product **131a** was prepared following general procedure **GP-9A** (15.9 mg, 37% yield, *dr* = 99:1, 24 hours) or **GP-9B** (33.1 mg, 77% yield, *dr* = 99:1, 6 hours), from the corresponding indolyl- sulfonamide (43 mg, 0.1 mmol). White solid. Two rotamers are observed due to the dynamic rotation of the amido group (65:35 mixture of rotamers). **^{1}H NMR** (400 MHz, Acetone-d6) δ 7.71 (d, *J* = 8.3 Hz, 2H), 7.47 (d, *J* = 7.8 Hz, 2H), 7.39 – 7.32 (m, 4H), 7.26 (t, *J* = 6.8 Hz, 1H), 7.09 (td, *J* = 7.6, 1.2 Hz, 1H), 6.96 (dd, *J* = 7.3, 1.5 Hz, 1H), 6.56 (td, *J* = 7.4, 1.0 Hz, 1H), 6.46 (d, *J* = 7.9 Hz, 1H), 4.46 (d, *J* = 6.2 Hz, 1H), 3.78 (dd, *J* = 8.2, 5.3 Hz, 1H), 3.71 (d, *J* = 9.7 Hz, 1H), 3.20 (dd, *J* = 10.5, 1.6 Hz, 1H), 3.14 (t, *J* = 8.7 Hz, 1H), 2.94 (d, *J* = 9.8 Hz, 1H), 2.86 (dd, *J* = 10.6, 8.1 Hz, 1H), 2.75 (s, 3H), 2.47 (s, 3H). **^{13}C NMR** (101 MHz, Acetone-d6) δ 154.1, 143.8, 138.9, 132.6, 129.7 (2C), 129.2, 128.9, 128.5 (2C), 128.1 (2C), 127.9 (2C), 126.5, 123.7, 117.1, 107.2, 69.9, 55.0, 54.0, 49.1, 48.3, 44.5, 30.8, 20.6. **ESI-HRMS** calcd for $C_{26}H_{27}N_2O_2S$ $[M+H]^+$ 431.5735, found 431.5741.

Comprehensive Table in AU

M06/Def2TZVP D3 disp. corr. CPCM=MeCN for 128, DMF for 120, 124, 126, DCM for 122 and 130	H (Hartrees)	S (cal/K*mol)
NP (MeCN)	-385.572690	82.020
N2 (MeCN)	-809.241669	125.535
NP (DCM)	-385.572152	81.998
NP (DMF)	-385.572651	81.99
N2 (DCM)	-809.240709	125.819
N2 (DMF)	-809.241713	125.686
^{1}120c (DMF)	-1107.22342	137.144
^{3}120c	-1107.152578	141.664
^{1}[120c:NP$_L$]	-1492.825461	176.393
^{3}[120c:NP$_L$]	-1492.739783	184.053
^{1}[120c:N2]	-1916.505518	212.834
^{3}[120c:N2]	-1916.424724	218.138
^{1}122d (DCM)	-847.51334	141.402
^{3}122d	-847.432885	144.85
^{1}[122d:NP$_L$]	-1233.103385	184.361
^{3}[122d:NP$_L$]	-1233.021305	187.526
^{1}[122d:N2]	-1656.784369	212.54
^{3}[122d:N2]	-1656.706439	219.505
^{1}124’a (DMF)	-1095.631632	171.426

^{3}124’a	-1095.574694	174.9
^{1}[124’a:NP$_{L}$]	-1481.223245	205.428
^{3}[124’a:NP$_{L}$]	-1481.165512	216.573
^{1}[124’a:N2]	-1904.906963	239.988
^{3}[124’a:N2]	-1904.849186	247.448
^{1}126a (DMF)	-825.478498	139.779
^{3}126a	-825.412676	142.078
^{1}[126a:NP$_{L}$]	-1211.066098	189.158
^{3}[126a:NP$_{L}$]	-1211.001769	190.585
^{1}[126a:N2]	-1634.744309	218.955
^{3}[126a:N2]	-1634.68625	219.844
^{1}128a (MeCN)	-540.437548	113.563
^{3}128a	-540.359433	121.819
^{1}[128a:NP$_{L}$]	-926.028933	161.504
^{3}[128a:NP$_{L}$]	-925.945416	165.467
^{1}[128a:N2]	-1349.708257	189.504
^{3}[128a:N2]	-1349.628325	199.748
^{1}130a (DCM)	-1432.76989	160.488
^{3}130a	-1432.682816	172.254
^{1}[130a:NP$_{L}$]	-1818.349747	206.289
^{3}[130a:NP$_{L}$]	-1818.273253	212.17
^{1}[130a:N2]	-2242.038736	239.104
^{3}[130a:N2]	-2241.953927	249.086

	H (Hartrees)	S (cal/K*mol)	Imaginary freq. (cm^{-1})
TS-NPc1	-809.349615	136.602	-398.3604
tdearo_c1	-809.377909	136.369	
TS-NPc2	-809.344970	137.566	-491.3116
tdearo_c2	-809.370081	137.705	
TS-N2c2	-1233.022687	175.568	-564.9527
tdearoN2_c2	-1233.052801	176.675	
TS-N2c4	-1233.024016	172.808	-574.5163
tdearoN2_c4	-1233.059064	173.555	
TS-N2c8	-1233.026103	173.660	-563.2265
tdearoN2_c8	-1233.054538	170.271	

References

1. a) Sarkar, S.; Pak Shing Cheung, K.; Gevorgyan, V. *Chem. Sci.*, **2020**, 11, 12974-12993; b) Yamaguchi, J.; Yamaguchi, A.D.; Itami, K. *Angew. Chem. Int. Ed*., **2012**, 51: 8960-9009.
2. a) Chu, J. C. K.; Rovis, T. *Angew. Chem. Int. Ed.* **2018**, *57*, 62; b) White, M. C. *Science*, **2012**, 335, 807-809.
3. Siegbahn, P. E. M. *J. Phys. Chem.* **1995**, 99, 12723–12729.
4. Zhang, S.; He, G.; Nack, W. A.; Zhao, Y.; Li, Q.; Chen, G. *J. Am. Chem. Soc*. **2013**, 135, 6, 2124–2127.
5. Wasa, M.; Engle, K. M.; Yu, J.-Q. *J. Am. Chem. Soc.* **2010**, 132, 3680–3681.
6. Taber, D. F.; Petty, E. H. *J. Org. Chem.* **1982**, 47, 4808–4809.
7. Roizen, J.; Harvey, M. E.; Du Bois, J. *Acc. Chem. Res.* **2012**, 45, 911–922.
8. a) Hofmann, A. W. *Chem. Ber*., **1883**, 16, 558–560; b) Löffler, K.; Freytag, C. *Chem. Ber*., **1909**, 42, 3427–3431; c) Barton, D. H. R.; Beaton, J. M.; Geller, L. E.; Pechet, M. M. *J. Am. Chem. Soc*., **1961**, 83, 4076–4083.
9. Vleeschouwer, F. D.; Speybroeck, V. V.; Waroquier, M.; Geerlings, P.; Proft, F. D. *J. Org. Chem*., **2008**, 73, 9109–9120.
10. Salamone, M.; Bietti, M. *Acc. Chem. Res*. **2015**, 48, 11, 2895–2903.
11. Roberts, B. P. *Chem. Soc. Rev*., **1999**, 28, 25–35.
12. Forbes, M. D. E.; Patton, J. T.; Myers, T. L.; Maynard, H. D.; Smith Jr., D. W.; Schulz, G. R.; Wagener, K. B. *J. Am. Chem. Soc*. **1992**, 114, 27, 10978–10980.
13. Huang, X. L.; Dannenberg, J. J. *J. Org. Chem*., **1991**, 56, 5421–5424.
14. Lathbury, D. C.; Parsons, P. J.; Pinto, I. *J. Chem. Soc., Chem. Commun*., **1988**, 81–82.
15. Bosch, E.; Bachi, M.D. *J. Org. Chem*., **1993**, 58, 5581–5582.
16. Vitaku, E.; Smith, D. t.; Njardason, J. t. *J. Med. Chem*. **2014**, 57, 24, 10257–10274.
17. Bogen, S.; Gulea, M.; Fensterbank, L.; and Malacria, M. *J. Org. Chem*., **1999**, 64, 4920–4925.
18. a) Margrey, K. A.; Czaplyski, W. L.; Nicewicz, D. A.; Alexanian, E. J. J. *Am. Chem. Soc*., **2018**, 140, 4213–4217; b) Mukherjee, S.; Maji, B.; Tlahuext-Aca, A.; Glorius, F. *J. Am. Chem. Soc*., **2016**, 138, 16200–16203; c) Zhu, J. L.; Schull, C. R.; Tam, A. T.; Rentería-Gómez, Á.; Gogoi, A. R.; Gutierrez, O.; Scheidt, K. A. *J. Am. Chem. Soc*. **2023**, 145, 3, 1535–1541.
19. Xie, X.; Qiao, K.; Shao, B.; Jiang, W.; Shi, L. *Org. Lett.*, **2023**, *25*, 23, 4264-4269.

20. Yang, S.; Hu, H.; Li, J.; Chen, M. *ACS Catalysis*, **2023**, *13,* 24, 15652-15662.
21. Pak Shing Cheung, K.; Fang, J.; Mukherjee, K.; Mihranyan, A.; Gevorgyan, V. *Science,* **2022**, *378*, 1207-1213.
22. Klan, P.; Wirz, J. *Photochemistry of Organic Compounds: From Concepts to Practice*, Wiley-Blackwell: Oxford, **2009**.
23. Ciamician, G. *Science*, **1912**, *36*, 385.
24. Schultz, D. M.; Yoon, T. P. *Science*, **2014**, *3*43, 1239176.
25. Nicewicz, D. A.; MacMillan, D. W. C. *Science* **2008**, *322*, 77.
26. Pitre, S. P.; Overman, L. E. *Chemical Reviews*, **2022**, 122, 2, 1717-1751.
27. Marzo, L.; Pagire, S. K.; Reiser, O.; König, B. *Angew. Chem. Int. Ed.* **2018**, *57*, 10034.
28. a) Guo, W.; Wang, Q.; Zhu, J. *Chem. Soc. Rev.*, **2021**, 50, 7359-7377; b) Xu, G.; Wang, W. D.; Xu, P. *J. Am. Chem. Soc*. **2024**, 146, 2, 1209–1223; c) Fan, H.; Fang, Y.; Yu, J. *Chem. Commun.*, **2024**, 60, 13796-13818; d) Chang, L.; Wang, S.; An, Q.; Liu, L.; Wang, H.; Li, Y.; Feng, K.; Zuo, Z. *Chem. Sci.*, **2023**, 14, 6841-6859.
29. Hasegawa, T.; Watabe, M.; Aoyama, H.; Omote, Y. *Tetrahedron*, **1977**, *33*, 485−488.
30. Peez, T.; Schmalz, V.; Harms, K.; Koert, U. *Org. Lett.* **2019**, *21*, 4365−4369.
31. Liu, J.; Hao, T.; Qian, L.; Shi, M.; Wei, Y. *Angew. Chem. Int. Ed.* **2022**, *61*, e202204515.
32. Norrish, R. G. W.; Bamford, C. H. *Nature*, **1937**, 140, 195–196.
33. Hu, Y.; Liu, Q.; Zhou, X.; Huang, Y.; Fernández, I.; Xiong, Y. *Org. Lett.* **2024**, *26*, 8005−8010.
34. Gu, X.; Shen, J.; Xu, Z.; Liu, J.; Shi, M.; Wei, Y. *Angew. Chem., Int. Ed.* **2024**, *63*, e202409463.
35. Xiong, Y.; Grosskopf, J.; Jandl, C.; Bach, T. *Angew. Chem., Int. Ed.* **2022**, *61*, e202200555.
36. Oddy, M. J.; Kusza, D. A.; Epton, R. G.; Lynam, J. M.; Unsworth, W. P.; Petersen, W. F. *Angew. Chem., Int. Ed.* **2022**, *61*, e202213086.
37. Li, H.-Y.; Zhang, S.-Z.; Niu, X.; Meng, Q.-Y.; Yang, X.-L. *Adv. Synth. Catal.* **2025**, *367*, e202400976.
38. a) Lovering, F.; Bikker, J.; Humblet, C. *J. Med. Chem.* **2009**, *52*, 6752; b) Lovering, F. *Med. Chem. Comm.* **2013**, *4*, 515.
39. Wertjes, W. C.; Southgate, E. H.; Sarlah, D. *Chem. Soc. Rev*. **2018**, *47*, 7996.

40. Liu, D.-H.; Nagashima, K.; Liang, H.; Yue, X.-L.; Chu, Y.-P.; Chen, S.; Ma, J. *Angew. Chem. Int. Ed.* **2023**, 62, e202312203.
41. Birch, A. J. *Pure Appl. Chem.* **1996**, 68, 553–556.
42. Xu, Z.-Y.; Gu, X.-T.; Wei, Y.; Shi, M. *Angew. Chem. Int. Ed.* **2025**, 64, e202506073.
43. 'van der Waals forces' in *IUPAC Compendium of Chemical Terminology*, 5th ed. International Union of Pure and Applied Chemistry; 2025. Online version 5.0.0, 2025. doi.org/10.1351/goldbook.V06597.
44. Rummel, L.; Schreiner, P. R. *Angew. Chem. Int. Ed.* **2024**, 63, e202316364.
45. a) Gomberg, M. *Ber. Dtsch. Chem. Ges.* **1900**, *33*, 3150–3163; b) Rösel, S.; Schreiner, P. R. *Isr. J. Chem.* **2022**, *62*, e202200002; c) Rummel, L.; Schümann, J. M.; Schreiner, P. R. *Chem. Eur. J.* **2021**, *27*, 13699–13702.
46. Ishigaki, Y.; Shimajiri, T.; Kawakami, Y.; Kawaguchi, S.; Hayashi, Y.; Hada, K.; Suzuki, T. *Synlett.* **2023**, 34, 1147–1152.
47. a) Šponer, J.; Riley, K. E.; Hobza, P. *Phys. Chem. Chem. Phys.* **2008**, *10*, 2595-2610; b) Altun, A.; Garcia-Ratés, M.; Neese, F.; Bistoni, G. *Chem. Sci.* **2021**, *12*, 12785–12793.
48. Dakin, H. D.; West, R. *J. Biol. Chem.* **1928**, 78, 91-104.
49. Wende, R. C.; Seitz, A.; Niedek, D.; Schuler, S. M. M.; Hofmann, C.; Becker, J.; Schreiner, P. R. *Angew. Chem. Int. Ed.* **2016**, *55*, 2719.
50. Lu, G.; Liu, R. Y.; Yang, Y.; Fang, C.; Lambrecht, D. S.; Buchwald, S. L.; Liu, P. *J. Am. Chem. Soc*. **2017**, 139, 46, 16548–16555.
51. Du, Y.; Krenske, E. H.; Antoline, J. E.; Lohse, A. G.; Houk, K. N.; Hsung, R. P. *J. Org. Chem*. **2013**, 78, 5, 1753–1759.
52. Hejna, B. G.; Ganley, J. M.; Shao, H.; Tian, H.; Ellefsen, J. D.; Fastuca, N. J.; Houk, K. N.; Miller, S. J.; Knowles, R. R. *J. Am. Chem. Soc.* **2023**, *145*, 16118–16129.
53. a) Lescop, C.; Birker, M.; Brotschi, C.; Bürki, C.; Morrison, K.; Froidevaux, S.; Delahaye, S.; Nayler, O.; Bolli, M. H. *J. Med. Chem.* **2024**, 67, 2397−2424; b) Maetani, M.; Zoller, J.; Melillo, B.; Verho, O.; Kato, N.; Pu, J.; Comer, E.; Schreiber, S. L. *J. Am. Chem. Soc.* **2017**, 139, 11300−11306; c) Oizumi, K.; Nishino, H.; Koike, H.; Sana, T.; Miyamoto, M.; Kimura, T. *Japan. J. Pharm.*, **1989**, 51, 1, 57-64; d) Candel, F. J.; Peñuelas, M. *Drug. Des. Devel. Ther*. **2017**, 11, 881-891.
54. St. Jean Jr., D. J.; Fotsch, C. *J. Med. Chem.,* **2012**, *55*, 13, 6002-6020.

55. a) Ju, Y.; Varma, R. S. *J. Org. Chem.* **2006**, 71, 135−141; b) Fritz, S. P.; Moya, J. F.; Unthank, M. G.; McGarrigle, E. M.; Aggarwal, V. K. *Synthesis,* **2012**, 44, 1584−1590; c) Betz, K. N.; Chiappini, N. D.; Du Bois, J. *Org. Lett.* **2020**, 22, 1687−1691; d) Xu, P.; Zhang, M.; Ingoglia, B.; Allais, C.; Dechert-Schmitt, A.-M. R.; Singer, R. A.; Morken, J. P. *Org. Lett.* **2021**, 23, 3379−3383.

56. a) Fawcett, A.; Murtaza, A.; Gregson, C. H. U.; Aggarwal, V. K. *J. Am. Chem. Soc.* **2019**, 141, 4573−4578; b) Tyler, J. L.; Noble, A.; Aggarwal, V. K. *Angew. Chem., Int. Ed.* **2021**, 60, 11824−11829; c) Jaiswal, V.; Mondal, S.; Singh, B.; Singh, V. P.; Saha, J. *Angew. Chem., Int. Ed.* **2023**, 62, e202304471; d) Hsu, C.-M.; Lin, H.-B.; Hou, X.-Z.; Tapales, R. V. P. P.; Shih, C.-K.; Miñoza, S.; Tsai, Y.-S.; Tsai, Z.-N.; Chan, C.-L.; Liao, H.-H. *J. Am. Chem. Soc.* **2023**, 145, 19049− 19059.

57. Rodríguez, R. I.; Corti, V.; Rizzo, L.; Visentini, S.; Bortolus, M.; Amati, A.; Natali, M.; Pelosi, G.; Costa, P.; Dell'Amico, L. *Nat. Catalysis,* **2024**, 7, 1223−1231.

58. Wearing, E. R.; Yeh, Y.-C.; Terrones, G. G.; Parikh, S. G.; Kevlishvili, I.; Kulik, H. J.; Schindler, C. S. *Science*, **2024**, 384, 1468−1476.

59. a) Rivero, A. R.; Fernandez, I.; Sierra, M. A. *Chem. Eur. J.* **2014**, 20, 1359−1366; b) Aoki, T.; Koya, S.; Yamasaki, R.; Saito, S. *Org. Lett.* **2012**, 14, 4506−4509; c) Couty, F.; Durrat, F.; Evano, G.; Marrot, J. *Eur. J. Org. Chem.* **2006**, 4214−4223; d) Satake, A.; Ishii, H.; Shimizu, I.; Inoue, Y.; Hasegawa, H.; Yamamoto, A. *Tetrahedron*, **1995**, 51, 5331−5340.

60. a) Dolle, R. E.; Li, C.-S.; Shaw, A. N. *Tetrahedron Lett.* **1989**, 30, 4723−4726; b) Hassner, A.; Weigand, N. *J. Org. Chem.* **1986**, 51, 3652−3656.

61. For EnT on C-allenyl amides, see a) Plaza, M.; Großkopf, J.; Breitenlechner, S.; Bannwarth, C.; Bach, T. *J. Am. Chem. Soc.* **2021**, 143, 11209; for EnT on acyl allenamides, see b) Serafino, A.; Chiminelli, M.; Balestri, D.; Marchiò, L.; Bigi, F.; Maggi, R.; Malacria, M.; Maestri, G. *Chem. Sci*. **2022**, 13, 2632; c) Chiminelli, M.; Serafino, A.; Ruggeri, D.; Marchiò, L.; Bigi, F.; Maggi, R.; Malacria, M.; Maestri, G. *Angew. Chem., Int. Ed*. **2023**, 62, e202216817; for EnT on sulfonyl allenamides, see d) Guo, J.-D.; Korsaye, F.-A.; Schutz, D.; Ciofini, I.; Miesch, L. *Chem. Sci.* **2024**, 15, 17962.

62. a) Ning, Y.; Chen, H.; Ning, Y.; Zhang, J.; Bi, X. *Angew. Chem. Int. Ed*. **2024**, 63, e202318072; b) Jacob, C.; Baguia, H.; Dubart, A.; Oger, S.; Thilmany, P.; Beaudelot, J.;

Deldaele, C.; Peruško, S.; Landrain, Y.; Michelet, B.; Neale, N.; Romero, E.; Moucheron, C.; Van Speybroeck, V.; Theunissen, C.; Evano, G. *Nat. Commun.* **2022**, 13, 560.

63. a) Stutz, A. *Angew. Chem. Int. Ed.* **1987**, 26, 320; b) Johannsen, M.; Jørgensen, K. A. *Chem. Rev.* **1998**, 98, 1689; c) Candeias, N. R.; Montalbano, F.; Cal, P. M. S. D.; Gois, P. M. P. *Chem. Rev.* **2010**, 110, 6169; d) Nag, S.; Batra, S. *Tetrahedron,* **2011**, 67, 8959; e) Skoda, E. M.; Davis, G. C.; Wipf, P. *Org. Process Res. Dev.* **2012**, 16, 26.
64. For reviews on photochemical HATs, see a) Capaldo, L.; Ravelli, D.; Fagnoni, M. *Chem. Rev.* **2022**, 122, 1875; b) Cao, H.; Tang, X.; Tang, H.; Yuan, Y.; Wu, J. *Chem Catal.* **2021**, 1, 523.
65. a) Blanksby, S. J.; Ellison, G. B. *Acc. Chem. Res.* **2003**, 36, 255; an online practical tool for the calculation of BDE and BD free energies, based on the article b) St. John, P. C.; Guan, Y.; Kim, Y.; Kim, S.; Paton, R. S. *Nat. Commun.* **2020**, 11, 2328, can be freely accessed at https://bde.ml.nrel.gov/.
66. a) Wang, W.; Cai, Y.; Guo, R.; Brown, M. K. *Chem. Sci.* **2022**, 13, 13582-13587; b) Guo, R.; Chang, Y.-C.; Herter, L.; Salome, C.; Braley, S. E.; Fessard, T. C.; Brown, M. K. *J. Am. Chem. Soc.* **2022**, 144, 7988; c) Chang, Y.-C.; Salome, C.; Fessard, T. C.; Brown, M. K. *Angew. Chem. Int. Ed*. **2023**, 62, e202314700.
67. a) Coppo, P.; Plummer, E. A.; De Cola, L. *Chem. Commun.* **2004**, 1774; b) Di Luzio, S.; Mdluli, V.; Connell, T. U.; Lewis, J.; VanBenschoten, V.; Bernhard, S. *J. Am. Chem. Soc.* **2021**, 143, 1179.
68. Chiminelli, M.; Scarica, G.; Balestri, D.; Marchiò, L.; Della Ca', N.; Maestri, G. *Tetrahedron Chem*., **2023**, 8, 100053.
69. Dispersion corrections were applied according to the method by Grimme, see a) Grimme, S. *WIREs Comput. Mol. Sci.* **2011**, *1*, 211; b) Grimme, S.; Ehrlich, S.; Goerigk, L. *J. Comput. Chem.* **2011**, *32*, 1456.
70. For selected studies on π–π stacking and C-H-π interactions, see a) Bravin, C.; Piekos, J. A.; Licini, G.; Hunter, C. A.; Zonta, C. *Angew. Chem. Int. Ed.* **2021**, 60, 23871; b) Fatima, M.; Steber, A. L.; Poblotzki, A.; Pérez, C.; Zinn, S.; Schnell, M. *Angew. Chem. Int. Ed.* **2019**, 58, 3108; c) Hwang, J.; Dial, B. E.; Li, P.; Kozik, M. E.; Smith, M. D.; Shimizu, K. D. *Chem. Sci.* **2015**, 6, 4358.

71. We were unable to measure a lifetime for **^{3}N4** at room temperature in various media, but Davidson reported lifetimes of 14.0 msec for **^{3}N4** at room temperature, in cyclohexane; these values are compatible with a role of triplet-state reservoir because they are much longer than the lifetime of excited Ir(III) photosensitizers, see Beecroft, R. A.; Davidson, R. S.; Goodwin, D. *Tetrahedron* **1984**, 40, 4497.
72. Todesco, B.; Gelan, J.; Martens, H.; Put, J.; Boens, N.; De Schryver, F. C. *Tetrahedron Lett.* **1978**, 19, 2815.
73. The emission of the ***N4** excimer does not overlap with the absorption **1**, suggesting that a Förster-type EnT should not occur; the limited overlap between the emission of the ***N4** excimer and the emission of **1** reduces the likeliness that a singlet-singlet EnT might be responsible for the luminesence quenching of ***N4** by the substrate; the feasibility of the ***Nn**-to-^{3}**Nn** intersystem crossing, which is required prior to a **^{3}N4**-**1** EnT, is described in refs. 28 and 29b; similarly to the approach described herein for **N4**, the assessment of triplet-triplet EnT *via* Stern-Vollmer titration quenching a fluorescence band, rather than a phosphorescence one, is routinely carried out for thioxanthone, which is a popular photosensitizer; see, for instance, a) Kleinmans, R.; Katzenburg, F.; Daniliuc, C.; Glorius, F. *Nat. Catal.* **2022**, 5, 1120; b) Tan, G.; Das, M.; Keum, H.; Belotti, P.; Daniliuc, C.; Glorius, F. *Nat. Chem.* **2022**, 14, 1174.
74. Elliot, J.; McCraken, D. R.; Buxton, G. V.; Wood, N. D. *J. Chem. Soc., Faraday Trans.* **1990**, 86, 1539.
75. Contreras-García, J.; Johnson, E. R.; Keinan, S.; Chaudret, R.; Piquemal, J.-P.; Beratan, D.; Yang, W. *J. Chem. Theory Comput.* **2011**, 7, 625.
76. Hoch, M.; Sparascio, S.; Cerveri, A.; Bigi, F.; Maggi, R.; Viscardi, R.; Maestri, G. *Photochem. Photobio. Sci.* **2024**, 23, 1543.
77. For the photoactivation of phenylglyoxylates, see Hu, S.; Neckers, D. C. *J. Org. Chem.* **1996**, 61, 6407.
78. Peng, M.; Li, H.; Qin, Z.; Li, J.; Sun, Y.; Zhang, X.; Jiang, L.; Do, H.; An, J. *Adv. Synth. Catal.* **2022**, 364, 2184.
79. Gaussian 16, Revision B.01, Frisch, M. J.; Trucks, G. W.; Schlegel, H. B.; Scuseria, G. E.; Robb, M. A.; Cheeseman, J. R.; Scalmani, G.; Barone, V.; Petersson, G. A.; Nakatsuji, H.; Li, X.; Caricato, M.; Marenich, A. V.; Bloino, J.; Janesko, B. G.; Gomperts, R.; Mennucci,

B.; Hratchian, H. P.; Ortiz, J. V.; Izmaylov, A. F.; Sonnenberg, J. L.; Williams-Young, D.; Ding, F.; Lipparini, F.; Egidi, F.; Goings, J.; Peng, B.; Petrone, A.; Henderson, T.; Ranasinghe, D.; Zakrzewski, V. G.; Gao, J.; Rega, N.; Zheng, G.; Liang, W.; Hada, M.; Ehara, M.; Toyota, K.; Fukuda, R.; Hasegawa, J.; Ishida, M.; Nakajima, T.; Honda, Y.; Kitao, O.; Nakai, H.; Vreven, T.; Throssell, K.; Montgomery, J. A., Jr.; Peralta, J. E.; Ogliaro, F.; Bearpark, M. J.; Heyd, J. J.; Brothers, E. N.; Kudin, K. N.; Staroverov, V. N.;Keith, T. A.; Kobayashi, R.; Normand, J.; Raghavachari, K.; Rendell, A. P.; Burant, J. C.;Iyengar, S. S.; Tomasi, J.; Cossi, M.; Millam, J. M.; Klene, M.; Adamo, C.; Cammi, R.; Ochterski, J. W.; Martin, R. L.; Morokuma, K.; Farkas, O.; Foresman, J. B.; Fox, D. J. Gaussian, Inc., Wallingford CT, **2016**.

80. Zhao, Y.; Truhlar, D. G. *Theor. Chem. Acc*. **2008**, 120, 215.
81. Weigend, F.; Ahlrichs, R. *Phys. Chem. Chem. Phys.* **2005**, 7, 3297.
82. a) Barone, V.; Cossi, M. *J. Phys. Chem. A* **1998**, 102, 1995. b) Cossi, M.; Rega, N.; Scalmani, G.; Barone, V. *J. Comput. Chem.* **2003**, 24, 669.
83. Deng, G.; Luo, J. *Tetr.* **2013**, 69, 5937.
84. Grimme, S.; Antony, J.; Ehrlich, S.; Krieg, H. *J. Chem. Phys.* **2010**, 132, 154104.
85. a) Meger, F. S.; Murphy, J. A. *Molecules*, **2023**, *28*, 6127; b) Capaldo, L.; Ravelli, D. *Eur. J. Org. Chem*., **2017**, 15, 2056-2071; c) Li, L.-X.; Hu, K. *Tetr.*, **2023**, 130, 133172.
86. a) Tu, J.-L.; Huang, B. *Chem. Comm*. **2024**,60, 11450; b) Cao, H.; Tang, X.; Tang, H.; Yuan, Y.; Wu, J. *Chem. Cat.* **2021**, 1, 3, 523-598.
87. a) Sanjoś e-Orduna, J.; Silva, R. C.; Raymenants, F.; Reus, B.; Thaens, J.; de Oliveira, K. T.; Nöel, T. *Chem. Sci*., **2022**, 13, 12527–12532; b) Perry, I. B.; Brewer, T. F.; Sarver, P. J.; Schultz, D. M.; DiRocco, D. A.; MacMillan, D. W. C. *Nature*, **2018**, 560, 70–75; c) Cao, H.; Kong, D.; Yang, L.-C.; Chanmungkalakul, S.; Liu, T.; Piper, J. L.; Peng, Z.; Gao, L.; Liu, X.; Hong, X.; Wu, J. *Nat. Synth*., **2022**, 1, 794–803; d) Tu, J.-L.; Hu, A.-M.; Guo, L.; Xia, W. *J. Am. Chem. Soc.*, **2023**, 145, 7600–7611; e) Cuthbertson, J. D.; MacMillan, D. W. C. *Nature*, **2015**, 519, 74–77; f) Hu, A.; Guo, J.-J.; Pan, H.; Zuo, Z. *Science*, **2018**, 361, 668–672; g) Li, N.; Li, J.; Qin, M.; Li, J.;Han, J.; Zhu, C.; Li, W.; Xie, J. *Nat. Commun*., **2022**, 13, 4224.
88. a) Lu, P.; Hou, T.; Gu, X.; Li, P. *Org. Lett*., **2015**, 17, 1954–1957; b) Wang, D.; Mück-Lichtenfeld, C.; Studer, A. *J. Am. Chem. Soc*., **2019**, 141, 14126–14130.

89. Leibler, I. N.-M.; Tekle-Smith, M. A.; Doyle, A. G. *Nat. Commun*., **2021**, 12, 6950.

90. Yang, S.; Hu, H.; Li, J.-H. Chen, M. *ACS Catal*., **2023**, 13, 15652–15662.

91. Morii, Y.; Watanabe, T.; Saga, Y.; Kambe, T.; Kondo, M.; Masaoka, S. *ChemElectroChem*, **2024**, 11, e202400061.

92. a) Clerici, A.; Cannella, R.; Panzeri, W.; Pastori, N.; Regolini, E.; Porta, O. *Tetrahedron Lett.*, **2005**, 46, 8351–8354; b) Anselmo, M.; Basso, A.; Protti, S.; Ravelli, D. *ACS Catal*., **2019**, 9, 2493–2500.

93. a) Capurro, P.; Ricciardiello, V.; Lova, P.; Lambruschini, C.; Protti, S.; Basso, A. *ACS Omega*, **2022**, 7, 48564–48571; b) Russo, C.; Volpe, C.; Santoro, F.; Brancaccio, D.; Di Porzio, A.; Carotenuto, A.; Randazzo, A.; Grimaud, L.; Vitale, M. R.; Protti, S.; Giustiniano, M. *Chem. Eur. J*., **2024**, e202401997.

94. a) Lu, M.-Z.; Loh, T.-P. *Org. Lett*., **2014**, 16, 4698–4701; b) Ye, B.; Zhao, J.; Zhao, K.; McKenna, J. M.; Toste, F. D. *J. Am. Chem. Soc*., **2018**, 140, 8350–8356.

95. Kang, J.; Hwang, H. S.; Soni, V. K.; Cho, E. J. *Org. Lett*., **2020**, 22, 6112–6116.

96. Wang, J.; Ye, Y.; Sang, T.; Zhou, C.; Bao, X.; Yuan, Y.; Huo, C. *Org. Lett*., **2022**, 24, 7577–7582.

97. Kang, B.; Hong, S. H. *Chem. Sci*., **2017**, 8, 6613–6618.

98. a) Uchikura, T.; Hara, Y.; Tsubono, K.; Akiyama. *ACS Org. Inorg. Au*, **2021**, 1, 23–28; b) Cheung, K. P. S.; Fang, J.; Mukherjee, K.; Mihranyan, A.; Gevorgyan, A. *Science*, **2022**, 378, 1207–1213; c) Ruan, X.-Y.; Wu, D.-X.; Li, W.-A.; Lin, Z.; Sayed, M.; Han, Z.-Y.; Gong, L.-Z. *J. Am. Chem. Soc*., **2024**, 146, 12053–12062; d) Liu, Z.; Li, M.; Deng, G.; Wei, W.; Feng, P.; Zi, Q.; Li, T.; Zhang, H.; Yang, X.; Walsh, P. J. *Chem. Sci.*, **2020**, 11, 7619–7625; e) Si, X; Zhang, L.; Wu, Z.; Rudolph, M.; Asiri, A. M.; Hashmi, A. S. K. *Org. Lett.,* **2020**, 22, 5844–5849; f) Li, T.; Liang, K.; Tang, J.; Ding, Y.; Tong, X.; Xia, C. *Chem. Sci.,* **2021**, 12, 15655–15661; g) Uchikura, T.; Tsubono, K.; Hara, Y.; Akiyama, T. *J. Org. Chem*., **2022**, 87, 15499–15510; h) Liu, X.; Wang, D.; Garo, J.; Sotiropoulos, J.-M.; Taillefer, M. *Org. Chem. Front*., **2024**, 11, 775–780.

99. Sparascio, S.; Scarica, G.; Cerveri, A.; Russo, G.; Spataro, D.; Marchiò, L.; Lanzi, M.; Maestri, G. *ACS Catalysis*, **2025**, 15, 16, 13799-13809.

100. a) Kochi, J. K.; *J. Am. Chem. Soc.*, **1962**, 84, 1193–1197; b) Čeković, Z.; Cvetković, M. *Tetrahedron Lett.*, **1982**, 23, 3791–3794; c) Kundu, R.; Ball, Z. T. *Org. Lett.*, **2010**, 12,

2460–2463; d) Guan, H.; Sun, S.; Mao, Y.; Chen, L.; Lu, R.; Huang, J.; Liu, L. *Angew. Chem., Int. Ed.*, **2018**, 57, 11413–11417.

101. a) Barton, D. H. R.; Beaton, J. M.; Geller, L. E.; Pechet, M. M. *J. Am. Chem. Soc.*, **1960**, 82, 2640–2641; b) Barton, D. H. R.; Beaton, J. M. *J. Am. Chem. Soc.*, **1960**, 82, 2641; c) Barton, D. H. R.; Beaton, J. M.; Geller, L. E.; Pechet, M. M. *J. Am. Chem. Soc.*, **1961**, 83, 4076–4083; d) Surzur, J. M.; Bertrand, M. P.; Nouguier, R. *Tetrahedron Lett.*, **1969**, 48, 4197–4200.

102. a) Walling, C.; Clark, R. T. *J. Am. Chem. Soc.*, **1974**, 96, 4530–4534; b) Walling, C.; Padwa, A. *J. Am. Chem. Soc.*, **1961**, 83, 2207–2208; c) Walling, C.; Bristol, D. *J. Org. Chem.*, **1972**, 37, 3514–3516; d) Walling, C.; Mcguinness, J. A. *J. Am. Chem. Soc.*, **1969**, 91, 2053–2058; e) Heusler, K.; Kalvoda, J. *Angew. Chem., Int. Ed.*, **1964**, 3, 525–538.

103. a) Beckwith, A. L. J.; Hay, B. P.; Williams, G. M. *J. Chem. Soc., Chem. Commun.*, **1989**, 1202–1203; b) Pasto, D. J.; Cottard, F. *Tetrahedron Lett.*, **1994**, 35, 4303–4306; c) Petrović, G.; Saičić, R. N.; Čeković, Ž. *Synlett*, **1999**, 635–637.

104. a) Kim, S.; Lee, T. A.; Song, Y. *Synlett*, **1998**, 471–472; b) Zlotorzynska, M.; Zhai, H.; Sammis, G. M. *Org. Lett.*, **2008**, 10, 5083–5086.

105. a) Jia, K.; Zhang, F.; Huang, H.; Chen, Y. *J. Am. Chem. Soc.*, **2016**, 138, 1514–1517; b) Jia, K.; Pan, Y.; Chen, Y. *Angew. Chem., Int. Ed.*, **2017**, 56, 2478–2481; c) Wang, D.; Mao, J.; Zhu, C. *Chem. Sci.*, **2018**, 9, 5805–5809; d) Wu, X.; Zhang, H.; Tang, N.; Wu, Z.; Wang, D.; Ji, M.; Xu, Y.; Wang, M.; Zhu, C. *Nat. Commun.*, **2018**, 9, 3343; e) Li, G.-X.; Hu, X.; He, G.; Chen, G. *Chem. Sci.*, **2019**, 10, 688–693.

106. a) Zhao, H.; Fan, X.; Yu, J.; Zhu, C. *J. Am. Chem. Soc.*, **2015**, 137, 3490–3493; b) Zhou, X.; Ding, H.; Chen, P.; Liu, L.; Sun, Q.; Wang, X.; Wang, P.; Lv, Z.; Li, M. *Angew. Chem., Int. Ed.*, **2020**, 59, 4138–4144; c) Ren, R.; Zhao, H.; Huan, L.; Zhu, C. *Angew. Chem., Int. Ed.*, **2015**, 54, 12692–12696; d) Zhu, Y. ; Huang, K.; Pan, J.; Qiu, X.; Luo, X.; Qin, Q.; Wei, J.; Wen, X.; Zhang, L.; Jiao, N. *Nat. Commun.*, **2018**, 9, 2625; e) Ren, H.; Song, J.-R.; Li, Z.-Y.; Pan, W.-D. *Org. Lett.*, **2019**, 21, 6774–6778; f) Guo, J.-J.; Hu, A.; Chen, Y.; Sun, J.; Tang, H.; Zuo, Z. *Angew. Chem., Int. Ed.*, **2016**, 55, 15319–15322; g) Hu, A.; Chen, Y.; Guo, J. J.; Yu, N.; An, Q.; Zuo, Z. *J. Am. Chem. Soc.*, **2018**, 140, 13580–13585; h) Zhang, K.; Chang, L.; An, Q.; Wang, X.; Zuo, Z. *J. Am. Chem. Soc.*, **2019**, 141, 10556–10564; i) Hu, A.; Guo,

J.-J.; Pan, H.; Tang, H.; Gao, Z.; Zuo, Z. *J. Am. Chem. Soc.*, **2018**, 140, 1612–1616; j) Hu, A.; Guo, J.-J.; Pan, H.; Zuo, Z. *Science*, **2018**, 361, 668–672; k) An, Q.; Wang, Z.; Chen, Y.; Wang, X.; Zhang, K.; Pan, H.; Liu, W.; Zuo, Z. *J. Am. Chem. Soc.*, **2020**, 142, 6216–6226.

107. a) Yayla, H. G.; Wang, H.; Tarantino, K. T.; Orbe, H. S.; Knowles, R. R. *J. Am. Chem. Soc.*, **2016**, 138, 10794–10797; b) Ota, E.; Wang, H.; Frye, N. L.; Knowles, R. R. *J. Am. Chem. Soc.*, **2019**, 141, 1457–1462; c) Zhao, K.; Yamashita, K.; Carpenter, J. E.; Sherwood, T. C.; Ewing, W. R.; Cheng, P. T. W.; Knowles, R. R. *J. Am. Chem. Soc.*, **2019**, 141, 8752–8757; d) Wu, X.; Wang, M.; Huan, L.; Wang, D.; Wang, J.; Zhu, C. *Angew. Chem., Int. Ed.*, **2018**, 57, 1640–1644; e) Wang, M.; Huan, L.; Zhu, C. *Org. Lett.*, **2019**, 21, 821–825; f) Tsui, E.; Metrano, A. J.; Tsuchiya, Y.; Knowles, R. R. *Angew. Chem., Int. Ed.*, **2020**, 59, 11845–11849.

108. Tsui, E.; Wang, H.; Knowles, R. R. *Chem. Sci*., **2020**, 11, 11124.

109. Jeffrey, J. L.; Terrett, J. A.; MacMillan, D. W. C. *Science*, **2015**, 349, 1532-1536.

110. a) Nibbering, E. T. J.; Elsaesser, T. *Chem. Rev.,* **2004**, 104, 4, 1887-1914; b) Giese, K.; Petković, M.; Naundorf, H.; Kühn, O. *Phys. Rep.*, **2006**, 430, 4, 211-276.

111. For selected reviews, see a) Wang, H.; Tian, Y. M.; König, B. *Nat. Chem. Rev.* **2022**, 6, 745–755; b) Chan, A. Y.; Perry, I. B.; Bissonette, N. B.; Buksh, B. F.; Edwards, G. A.; Frye, L. I.; Garry, O. L.; Lavagnino, M. N.; Li, B. X.; Liang, Y.; Mao, E.; Millet, A.; Oakley, J. V.; Reed, N. L.; Sakai, H. A.; Seath, C. P; MacMillan, D. W. C. *Chem. Rev.* **2022**, 122, 1485–1542; c) Amos, S. G. E; Garreau, M.; Buzzetti, L.; Waser, J. *Beilstein J. Org. Chem.* **2020**, 16, 1163–1187; d) Leifert, D.; Studer, A. *Angew. Chem. Int. Ed*. **2020**, 59, 74–108.

112. For recent general reviews, see: a) McAtee, R. C.; McClain, E. J.; Stephenson, C. R. J. *Trends Chem.* **2019**, 1, 111–125; b) Marzo, L.; Pagire, S. K.; Reiser, O.; König, B. *Angew. Chem. Int. Ed. Engl*. **2018**, 57, 10034–10072.

113. For reviews, see a) Huo, H.; Shen, X.; Wang, C.; Zhang, L.; Röse, P.; Chen, L-A.; Harms, K.; Marsch, M.; Hilt, G.; Meggers, E. *Nature*, **2014**, 515, 100–103; b) Hossain, A.; Bhattacharyya, A.; Reiser, O.; *Science*, **2019**, 364, eaav9713; c) Sarkar, S.; Cheung, K. P. S.; Gevorgyan, V. *Angew. Chem. Int. Ed.* **2024**, 63, e202311972; for a recent example of enantioselective Ti-promoted photoredox cascade, see d) Calogero, F.; Magagnano, G.; Potenti, S.; Pasca, F.; Fermi, A.; Gualandi, A.; Ceroni, P.; Bergamini, G.; Cozzi, P. G. *Chem. Sci.,* **2022**, 13, 5973–5981.

114. a) Shree Sowndarya, S. V.; St. John, P. C.; Paton, R. S. *Chem. Sci.*, **2021**, 12, 13158–13166; b) Studer, A.; Curran, D. P. *Angew. Chem. Int. Ed*., **2016**, 55, 58–102; c) Griller, A.; Ingold, K. U. *Acc. Chem. Res*., **1976**, 9, 13–19.

115. For seminal reports, see a) Nicewicz, D. A.; MacMillan, D. W. C. *Science*, **2008**, 322, 77–80; b) Rueping, M.; Vila, C.; Koenigs, R. M.; Poscharny, K; Fabry, D. C. *Chem.Commun*., **2011**, 47, 2360–2362; c) Sahoo, B.; Hopkinson, M. N.; Glorius, F. *J. Am. Chem. Soc.,* **2013**, 135, 5505–5508; d) Kalyani, D.; McMurtrey, K. B.; Neufeldt, S. R.; Sanford, M. S. *J. Am. Chem. Soc.,* **2013**, 135, 18566–18569; e) Zuo, Z.; Ahneman, D. T.; Chu, L.; Terrett, J. A; Doyle, A. G.; MacMillan, D. W. C. *Science*, **2014**, 345, 437–440; f) for a review, see Silvi, M.; Melchiorre, P. *Nature*, **2018**, 554, 41–49.

116. For reviews on dual catalysis, see a) Sherbrook, E. M.; Jung, H.; Cho, D; Baik, M.-H.; Yoon, T. P. *Chem. Sci.,* **2020**, 11, 856–861; b) Fabry, D. C.; Rueping, M. *Acc. Chem. Res.,* **2016**, 49, 1969–1979; c) Hopkinson, M. N.; Sahoo, B.; Li, J.-L.; Glorius, F. *Chem. Eur. J.,* **2014**, 20, 3874–3886.

117. Wagner, J. P.; Schreiner, P. R. *Angew. Chem. Int. Ed.,* **2015**, 54, 12274–12296.

118. Fore selected examples, see a) Li, B.; Xu, H.; Dang, Y.; Houk, K. N. *J. Am. Chem. Soc.,* **2022**, 144, 1971–1985; b) Xu, E. Y.; Werth, J.; Roos, C. B. Bendelsmith, A. J.; Sigman, M. S.; Knowles, R. R. *J. Am. Chem. Soc.,* **2022**, 144, 18948–18958; c) Mears, K. L.; Power, P. P. *Acc. Chem. Res.,* **2022**, 55, 1337–1348; d) Polloth, B.; Sibi, M. P.; Zipse, H. *Angew. Chem. Int. Ed*., **2021**, 60, 774–778; e) Eschmann, C.; Song, L.; Schreiner, P. R. *Angew. Chem. Int. Ed*., **2021**, 60, 4823–4832; f) Schreiner, P. R.; Chernish, L. V.; Gunchenko, P. A.; Tikhonchuk, E. Y.; Hausmann, H.; Serafin, M.; Schlecht, S.; Dahl, J. E. P.; Carlson, R. M. K.; Fokin, A. A. *Nature*, **2011**, 477, 308–311.

119. a) Gryn'ova, G.; Coote, M. L. *J. Am. Chem. Soc*., **2013**, 135, 15392–15403; b) Van Lommel, R.; Verschueren, R. H.; De Borggraeve, W. M.; De Vlee-schouwer, F.; Stuyver, T. *Org. Lett.*, **2022**, 24, 1–5.

120. a) Peterson, J. P.; Ellern, A.; Winter, A. H. *J. Am. Chem. Soc*., **2020**, 142, 5304–5313; b) Geraskina, M. R.; Dutton, A. S.; Juetten, M. J.; Wood, S. A; Winter, A. H. *Angew. Chem. Int. Ed.*, **2017**, 56, 9435–9439; c) Penneau, J. F; Stallman, B. J.; Kasai, P. H.; Miller, L. L. *Chem. Mater*., **1991**, 3, 791–796.

121. Mateos, J.; Rigodanza, F.; Costa, P.; Natali, M.; Vega-Peñaloza, A.; Fresch, E.; Collini, E.; Bonchio, M.; Sartorel, A.; Dell'Amico, L. *Nature synthesis*, **2023**, 962, 1, 26–36.

122. For reviews on EnT, see a) Großkopf, J.; Kratz, T.; Rigotti, T.; Bach, T. *Chem. Rev.*, **2022**, 122, 1626–1653; b) Neveselý, T.; Wienhold, M.; Molloy, J. J.; Gilmour, R. *Chem. Rev.*, **2022**, 122, 2650–2694; c) Strieth-Kalthoff, F.; Glorius, F.; *Chem*, **2020**, 6, 1888–1903; d) Strieth-Kalthoff, F.; James, M. J.; Teders, M.; Pitzer, L.; Glorius, F. *Chem. Soc. Rev*., **2018**, 47, 7190–7202.

123. Serafino, A.; Balestri, D.; Marchiò, L.; Malacria, M.; Derat, E.; Maestri, G. *Org. Lett.,* **2020**, 22, 6354–6359.

124. a) Cheng, Y.-Z.; Feng, Z.; Zhang, X.; You, S.-L. *Chem. Soc. Rev*., **2022**, 51, 2145–2170; b) Huck, C. J.; Boyko, Y. D.; x Sarlah, Y. D. *Nat. Prod. Rep*., **2022**, 39, 2231–2291.

125. For representative reviews, see a) Baldini, L.; Casnati, A.; Sansone, F.; Ungaro, R. *Chem. Soc. Rev.*, **2007**, 36, 254–266; b) Mulder, A.; Huskens, J.; Reinhoudt, D. N. *Org. Biomol. Chem.*, **2004**, 2, 3409–3424.

126. **N9** increased the rate of the reaction, which does not occur without it, and it was not altered upon the series of elementary steps that converted **124c** into the product **125c**, fulfilling the definition of catalyst.

127. For a review on dearomative cycloadditions, see Remy, R.; Bochet, C. G. *Chem. Rev.,* **2016**, 116, 9816–9849.

128. Lu, Z.; Yoon, T. P. *Angew. Chem. Int. Ed.*, **2012**, 51, 10329–10332.

129. For a review on [2 + 2] photocycloadditions, see Poplata, S.; Troster, A.; Zou, Y.-Q.; Bach, T. *Chem. Rev*., **2016**, 116, 9748–9815.

130. The direct sensitization of indoles requires a conjugated auxiliary group on the N1- or C2- position, see: a) Zhu, M.; Zhang, X.; Zheng, C.; You, S.-L. *Acc. Chem. Res*., **2022**, 55, 2510–2525; b) Zhang, Z.; Dong, Y.; Zhang, M.; Wei, J.; Lu, J.; Yang, L.; Wang, J.; Hao, N.; Pan, X.; Zhang, S; Wei, S.; Fu, Q. *ACS Catal*., **2020**, 10, 10149–10156.

131. For the triplet energies of NPs, see Handbook of Photochemistry, 3rd ed. (Eds.: M. Montaldi, A. Credi, L. Prodi, M. T. Gandolfi), Taylor & Francis: Boca Raton, **2006**.

132. a) Sioda, R. E.; Frankowska, B. *J. Electroanal. Chem.,* **2008**, 612, 147–150; b) Heinis, T.; Chowdhury, S.; Kebarle, P. *J. Mass Spectrom*., **1993**, 28, 358–365.

133. The uneven shift of the substrate resonances excludes that the effect is due to the diamagnetic contribution of the additive, see: Evans, D. F. *J. Chem. Soc*., **1959**, 2003–2005.